CLIMATE SERVICES FOR ADAPTATION TO SEA-LEVEL RISE

EDITED BY: Jing Li, Michael Dylan Sparrow, Julie Billy, Roderik Van De Wal, Robert James Nicholls and Goneri Le Cozannet

PUBLISHED IN: Frontiers in Marine Science

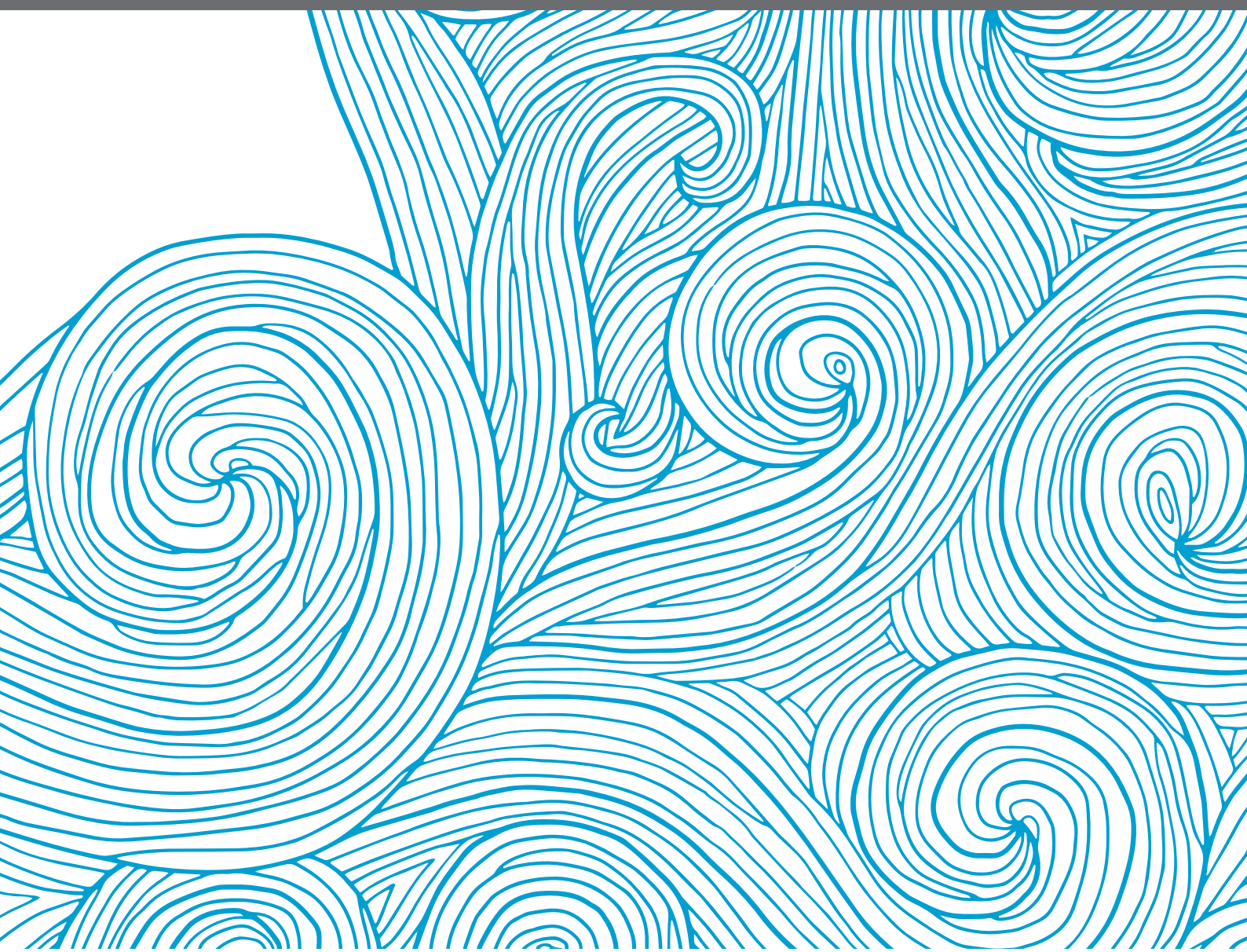

frontiers Research Topics

Frontiers eBook Copyright Statement

The copyright in the text of individual articles in this eBook is the property of their respective authors or their respective institutions or funders. The copyright in graphics and images within each article may be subject to copyright of other parties. In both cases this is subject to a license granted to Frontiers.

The compilation of articles constituting this eBook is the property of Frontiers.

Each article within this eBook, and the eBook itself, are published under the most recent version of the Creative Commons CC-BY licence. The version current at the date of publication of this eBook is CC-BY 4.0. If the CC-BY licence is updated, the licence granted by Frontiers is automatically updated to the new version.

When exercising any right under the CC-BY licence, Frontiers must be attributed as the original publisher of the article or eBook, as applicable.

Authors have the responsibility of ensuring that any graphics or other materials which are the property of others may be included in the CC-BY licence, but this should be checked before relying on the CC-BY licence to reproduce those materials. Any copyright notices relating to those materials must be complied with.

Copyright and source acknowledgement notices may not be removed and must be displayed in any copy, derivative work or partial copy which includes the elements in question.

All copyright, and all rights therein, are protected by national and international copyright laws. The above represents a summary only. For further information please read Frontiers' Conditions for Website Use and Copyright Statement, and the applicable CC-BY licence.

ISSN 1664-8714
ISBN 978-2-88976-493-8
DOI 10.3389/978-2-88976-493-8

About Frontiers

Frontiers is more than just an open-access publisher of scholarly articles: it is a pioneering approach to the world of academia, radically improving the way scholarly research is managed. The grand vision of Frontiers is a world where all people have an equal opportunity to seek, share and generate knowledge. Frontiers provides immediate and permanent online open access to all its publications, but this alone is not enough to realize our grand goals.

Frontiers Journal Series

The Frontiers Journal Series is a multi-tier and interdisciplinary set of open-access, online journals, promising a paradigm shift from the current review, selection and dissemination processes in academic publishing. All Frontiers journals are driven by researchers for researchers; therefore, they constitute a service to the scholarly community. At the same time, the Frontiers Journal Series operates on a revolutionary invention, the tiered publishing system, initially addressing specific communities of scholars, and gradually climbing up to broader public understanding, thus serving the interests of the lay society, too.

Dedication to Quality

Each Frontiers article is a landmark of the highest quality, thanks to genuinely collaborative interactions between authors and review editors, who include some of the world's best academicians. Research must be certified by peers before entering a stream of knowledge that may eventually reach the public - and shape society; therefore, Frontiers only applies the most rigorous and unbiased reviews.
Frontiers revolutionizes research publishing by freely delivering the most outstanding research, evaluated with no bias from both the academic and social point of view. By applying the most advanced information technologies, Frontiers is catapulting scholarly publishing into a new generation.

What are Frontiers Research Topics?

Frontiers Research Topics are very popular trademarks of the Frontiers Journals Series: they are collections of at least ten articles, all centered on a particular subject. With their unique mix of varied contributions from Original Research to Review Articles, Frontiers Research Topics unify the most influential researchers, the latest key findings and historical advances in a hot research area! Find out more on how to host your own Frontiers Research Topic or contribute to one as an author by contacting the Frontiers Editorial Office: frontiersin.org/about/contact

CLIMATE SERVICES FOR ADAPTATION TO SEA-LEVEL RISE

Topic Editors:
Jing Li, Other, China
Michael Dylan Sparrow, World Meteorological Organization, Switzerland
Julie Billy, Bureau de Recherches Géologiques et Minières, France
Roderik Van De Wal, Utrecht University, Netherlands
Robert James Nicholls, University of East Anglia, United Kingdom
Goneri Le Cozannet, Bureau de Recherches Géologiques et Minières, France

Citation: Li, J., Sparrow, M. D., Billy, J., Van De Wal, R., Nicholls, R. J., Le Cozannet, G., eds. (2022). Climate Services for Adaptation to Sea-Level Rise. Lausanne: Frontiers Media SA. doi: 10.3389/978-2-88976-493-8

Table of Contents

05 ***Editorial: Climate Services for Adaptation to Sea-Level Rise***
Gonéri Le Cozannet, Robert James Nicholls, Roderik van de Wal, Michael Dylan Sparrow, Jing Li and Julie Billy

08 ***A Regional Frequency Analysis of Tide Gauges to Assess Pacific Coast Flood Risk***
William V. Sweet, Ayesha S. Genz, Jayantha Obeysekera and John J. Marra

23 ***Impact Assessment and Management Challenges of Key Rural Human Health Infrastructure Under Sea Level Rise***
Molly Mitchell, Robert E. Isdell, Julie Herman and Christine Tombleson

31 ***Sea Level Projections From IPCC Special Report on the Ocean and Cryosphere Call for a New Climate Adaptation Strategy in the Skagerrak-Kattegat Seas***
Jian Su, Elin Andrée, Jacob W. Nielsen, Steffen M. Olsen and Kristine S. Madsen

43 ***Coastal Flooding in the Maldives Induced by Mean Sea-Level Rise and Wind-Waves: From Global to Local Coastal Modelling***
Angel Amores, Marta Marcos, Rodrigo Pedreros, Gonéri Le Cozannet, Sophie Lecacheux, Jérémy Rohmer, Jochen Hinkel, Geronimo Gussmann, Thomas van der Pol, Ali Shareef and Zammath Khaleel

61 ***Visualising the Uncertainty Cascade in Multi-Ensemble Probabilistic Coastal Erosion Projections***
Alexandra Toimil, Paula Camus, Iñigo J. Losada and Moises Alvarez-Cuesta

80 ***A Roadmap for Policy-Relevant Sea-Level Rise Research in the United Arab Emirates***
Hannah Melville-Rea, Clare Eayrs, Nasser Anwahi, John A. Burt, Denise Holland, Fatin Samara, Francesco Paparella, Ahmed Hassan Al Murshidi, Maryam Rashed Al-Shehhi and David M. Holland

88 ***Climate Services Transformed: Decision-Making Practice for the Coast in a Changing Climate***
Judy Lawrence, Scott Stephens, Paula Blackett, Robert G. Bell and Rebecca Priestley

102 ***Coastal Flooding in the Balearic Islands During the Twenty-First Century Caused by Sea-Level Rise and Extreme Events***
Pau Luque, Lluís Gómez-Pujol, Marta Marcos and Alejandro Orfila

123 ***Effective Coastal Climate Services—An End-User Perspective for Resilient Infrastructure***
Jonathan Simm, Ben Gouldby, Darren Lumbroso and Tom Matthewson

130 ***European Copernicus Services to Inform on Sea-Level Rise Adaptation: Current Status and Perspectives***
Angélique Melet, Carlo Buontempo, Matteo Mattiuzzi, Peter Salamon, Pierre Bahurel, George Breyiannis, Samantha Burgess, Laurence Crosnier, Pierre-Yves Le Traon, Lorenzo Mentaschi, Julien Nicolas, Lorenzo Solari, Freja Vamborg and Evangelos Voukouvalas

156 ***Coastal Landfills and Rising Sea Levels: A Challenge for the 21st Century***
Robert J. Nicholls, Richard P. Beaven, Anne Stringfellow, Daniel Monfort, Gonéri Le Cozannet, Thomas Wahl, Julia Gebert, Matthew Wadey, Arne Arns, Kate L. Spencer, Debra Reinhart, Timo Heimovaara, Víctor M. Santos, Alejandra R. Enríquez and Samantha Cope

179 ***Copernicus Sea Level Space Observations: A Basis for Assessing Mitigation and Developing Adaptation Strategies to Sea Level Rise***
Jean-François Legeais, Benoît Meyssignac, Yannice Faugère, Adrien Guerou, Michaël Ablain, Marie-Isabelle Pujol, Claire Dufau and Gérald Dibarboure

193 ***Local Sea-Level Rise Caused by Climate Change in the Northwest Pacific Marginal Seas Using Dynamical Downscaling***
Yong-Yub Kim, Bong-Gwan Kim, Kwang Young Jeong, Eunil Lee, Do-Seong Byun and Yang-Ki Cho

208 ***Global Climate Services: A Typology of Global Decisions Influenced by Climate Risk***
Alexander Bisaro, Jochen Hinkel, Gonéri Le Cozannet, Thomas van der Pol and Armin Haas

223 ***Sea-Level Rise: From Global Perspectives to Local Services***
Gaël Durand, Michiel R. van den Broeke, Goneri Le Cozannet, Tamsin L. Edwards, Paul R. Holland, Nicolas C. Jourdain, Ben Marzeion, Ruth Mottram, Robert J. Nicholls, Frank Pattyn, Frank Paul, Aimée B. A. Slangen, Ricarda Winkelmann, Clara Burgard, Caroline J. van Calcar, Jean-Baptiste Barré, Amélie Bataille and Anne Chapuis

231 ***Coastal Flood Modeling to Explore Adaptive Coastal Management Scenarios and Land-Use Changes Under Sea Level Rise***
Jessie Louisor, Olivier Brivois, Paloma Mouillon, Aurelie Maspataud, Patrice Belz and Jean-Michel Laloue

frontiers | Frontiers in Marine Science

EDITORIAL
published: 09 June 2022
doi: 10.3389/fmars.2022.943079

Editorial: Climate Services for Adaptation to Sea-Level Rise

Gonéri Le Cozannet[1], Robert James Nicholls[2], Roderik van de Wal[3], Michael Dylan Sparrow[4], Jing Li[5] and Julie Billy[1]*

[1] Risk and Prevention Department, Bureau de Recherches Géologiques et Minières (BRGM), Orléans, France, [2] Tyndall Centre of Climate Change Research, University of East Anglia, Norwich, United Kingdom, [3] Institute for Marine and Atmospheric Research Utrecht, Utrecht University, Utrecht, Netherlands, [4] World Climate Research Programme (WCRP) Secretariat, World Meteorological Organisation, Geneva, Switzerland, [5] International Climate and Ocean: Variability, Predictability and Change (CLIVAR) Project Office, Qingdao, China

Keywords: climate change, sea-level rise (SLR), adaptation, climate services, coastal risks

Editorial on the Research Topic:

Climate Services for Adaptation to Sea-Level Rise

OPEN ACCESS

Edited and reviewed by:
Marta Marcos, University of the Balearic Islands, Spain

****Correspondence:***
Gonéri Le Cozannet
g.lecozannet@brgm.fr

Specialty section:
This article was submitted to Coastal Ocean Processes, a section of the journal Frontiers in Marine Science

Received: *13 May 2022*
Accepted: *23 May 2022*
Published: *09 June 2022*

Citation:
Le Cozannet G, Nicholls RJ, van de Wal R, Sparrow MD, Li J and Billy J (2022) Editorial: Climate Services for Adaptation to Sea-Level Rise. Front. Mar. Sci. 9:943079. doi: 10.3389/fmars.2022.943079

INTRODUCTION

We are committed to sea-level rise of at least 4mm/year over the coming century, contributing to increases in extreme flooding, coastal erosion and shoreline changes, as well as the salinization of estuaries, soils and coastal aquifers. Adaptation will be required to manage these hazards and their consequences for human activities, coastal infrastructure and ecosystems.

The latest report of the Intergovernmental Panel on Climate Change (IPCC) shows that adaptation to sea-level rise can be supported efficiently by tailored climate services (Cooley et al., 2022). Climate services can be defined as the operationalization of climate and climate impacts science, in order to support the diverse adaptation needs in the public and private sectors. Within this broad area, climate services supporting coastal adaptation to sea-level rise are developing in a distinctive manner: besides large authoritative services such as Copernicus in Europe (Melet et al.; Legais et al.), many activities that do not identify themselves as climate services, are in fact supporting coastal adaptation and contribute to the uptake of coastal climate services (Le Cozannet et al., 2017; Lawrence et al.).

This Research Topic contributes to better understanding of the status of climate services for coastal adaptation. It builds upon a workshop organized by the Regional Sea-level Change and Coastal Impacts Grand Challenge of the World Climate Research Programme in Orléans in November 2019, where scientists working with coastal adaptation practitioners around the world shared their views about current developments and needs for information and services to support adaptation to sea-level rise. The 16 resulting papers provide evidence of progress in this area.

MEAN AND EXTREME SEA-LEVEL CHANGES

A most obvious need is sea-level projections that are applicable locally. Regional sea-level projections presented in IPCC reports since AR5 are available for scientists and practitioners (Oppenheimer et al., 2019; Fox-Kemper et al., 2021; https://sealevel.nasa.gov/ipcc-ar6-sea-level-projection-tool). Yet, they do not resolve two important regional and local components: (1) vertical ground motions, and (2) the meso-scale oceanic processes at the coast. In this Research Topic, Su et al. examined enhanced SROCC projections using local data such as precise national-wide land-rise and subsidence information in Denmark. Similarly, Kim et al. provide new evidence that high resolution oceanic models resolving currents, eddies, and tides, and considering the influence of the bathymetry, can modify broad scale sea-level scenarios by more than 15 cm. On the practical side, the slight increases in sea-level rise projections since AR5 mean that protection standards need to be revised upwards, as shown in Danish municipalities by Su et al. More generally, both papers highlight how regional sea-level scenarios can be taken forward to inform adaptation strategies in specific countries and regions.

Extreme sea levels are changing consistently with mean sea-level rise, including small changes in storminess, surges and waves at each location. Using a regional frequency analysis of tide gauge records, Sweet et al. re-assess risks of flooding in the Pacific. This technique uses many tide gauge records in the region in order to improve the sampling of rare events. This leads to 100-year extreme sea-levels that are revised upwards by 0.15m (median). Furthermore, damaging floods whose return periods are currently 20 to 25 years are projected to occur annually by the mid-21st century in that region.

Where no tide gauge observations are available, the only possible approach to evaluate flood risks is modeling. For example, in low-lying atoll settings such as the Maldives, swell is a major driver of flooding, but information is lacking to assess risks ahead of development projects. Amores et al. model regional waves along the oceanward Maldivian coastlines with a spatial resolution down to 500 m, which can be used to assess local flood risks as illustrated in the case of a new airport on an atoll island. Luque et al. assess future flooding and beach losses in the Balearic islands due to sea-level rise and extreme events. They show that the resulting recreational services could represent up to 7% of the 2019 Gross Domestic Product by 2100. Flood modeling can also be used to evaluate adaptation strategies, such as the implementation of dikes to protect cities in areas where softer shoreline management strategies are being implemented (Louisor et al.). Such studies can help support the identification, planning and sequencing of adaptation options over time.

MANAGING AND COMMUNICATING COMPLEXITY

Future coastal risks assessments often come with large uncertainties resulting from different climate scenarios that cascade across the chain of coastal models from regional to local scales. Toimil et al. present an approach to decompose and visualize uncertainties in future coastal erosion. They show that climate variability can have substantial effects on coastal erosion prediction, and that ignoring their impact may lead to poor decision making. More generally, Simm et al. argue that more attention should be given to the form in which climate services are provided. In this context, official institutions have the challenge to deliver consistent and transparent guidance on climate information and its use.

The Research Topic demonstrates that climate services supporting coastal adaptation to sea-level rise are addressing increasingly complex management issues. For example, Mitchell et al. assess the challenges related to the maintenance and installation of septic systems affected by ongoing and future sea-level rise in low-lying rural areas of coastal Virginia (USA). Yet, systematic guidance is lacking to define climate service requirements. Similarly, Nicholls et al. assess how the large legacy of coastal landfills can be managed as they are increasingly threatened by sea-level rise across Europe and the United States. Yet, financial resources to manage such issues are limited. This raises the need for initial screening services, assessing the scale and characteristics of the problems, and then assessing management options and priorities with careful consideration of acceptance and legal aspects.

Climate services are generally addressing local to regional issues and therefore require consideration of local land use and attitudes toward risks (Durand et al.). However, there are also other adaptation decisions that consider bigger scales up to global (Bisaro et al.). This includes, for example, large private companies assessing the vulnerability of their supply chains, of their geographical presence in multiple countries or governments negotiating greenhouse gas emission targets and their impacts for adaptation aid. Bisaro et al. provide a typology of such adaptation decisions that require climate services addressing larger to global scales.

ADDRESSING RESEARCH GAPS

This Research Topic shows that sea-level adaptation science is progressing rapidly. Yet, there remain key unknowns such as the rate of ice-sheet melting in Greenland and Antarctica over the coming decades and centuries (Durand et al.). A key challenge of climate services is to deliver information that recognizes the committed impacts and adaptation needs on the short term, as well as the deep uncertainties on the long term (Lawrence et al., 2021; Durand et al.).

A regional or national research strategy supporting coastal adaptation can bring substantial benefits to countries exposed to sea-level rise and where research gaps are identified. Melville-Rea et al. proposes such a strategy, with the aim to improve the use of climate and sea-level science in the United Arab Emirates. The strategy considers science and policy coordination, data collection and sharing and funding aspects.

As climate services for coastal adaptation are being developed, people, the institutional frameworks and the environment are changing. Lawrence et al. invite us to rethink how current or projected climate services fit within the evolving decision making, policy and governance contexts. Together with Durand et al., they show that co-production efforts involving scientists, decision makers and communities can enable the transformation of climate services into benefits for society.

The Copernicus services using satellite altimetry monitor global and regional mean sea-level changes with increasing accuracy (Legeais et al.). Early detection of accelerating signals is identified as a potential benefit of this service for adaptation. The wider services of Copernicus cover information on mean and extreme sea level observations and projections, of exposure and vulnerability, notably using digital elevation models and the ground motion service (Melet et al.). In the coming decades, a challenge will be to better connect these authoritative services with the flourishing diversity of activities supporting coastal adaptation on the ground.

We hope that the papers in this Research Topic contribute to the discussion on climate services and indicate the wide range of problems encountered in the development of adaptation strategies to reduce risk caused by sea-level rise.

AUTHOR CONTRIBUTIONS

GC, RN, RW, MS and JL contributed to the ideas development and writing. All authors contributed to the article and approved the submitted version.

FUNDING

GC, RN, RW were supported by PROTECT. This project has received funding from the European Union's Horizon 2020 research and innovation programme under grant agreement No 869304, PROTECT contribution number 37.

ACKNOWLEDGMENTS

We thank Ricardo Briganti, Juan Jose Munoz-Perez, João Canning-Clode and Ivica Vilibic for editing papers involving editors of this Research Topic. We thank the WRCP Grand Challenge on Regional Sea level and Coastal Impacts, Clivar and BRGM for organizing the workshop and US-Clivar, UNESCO/IOC for sponsorship.

REFERENCES

Cooley, S., Schoeman, D., Bopp, L., Boyd, P., Donner, S., Ghebrehiwet, D. Y., et al. (2022). "Ocean and Coastal Ecosystems and Their Services," in *Climate Change 2022: Impacts, Adaptation, and Vulnerability. Contribution of Working Group II to the Sixth Assessment Report of the Intergovernmental Panel on Climate Change*. Eds. H.-O. Pörtner, D. C. Roberts, M. Tignor, E. S. Poloczanska, K. Mintenbeck, A. Alegría, M. Craig, S. Langsdorf, S. Löschke, V. Möller, A. Okem and B. Rama (Cambridge, United Kingdom and New York, NY, USA: Cambridge University Press. In Press).

Fox-Kemper, B., Hewitt, H. T., Xiao, C., Aðalgeirsdóttir, G., Drijfhout, S. S., Edwards, T. L., et al. (2021). "Ocean, Cryosphere and Sea Level Change," in *Climate Change 2021: The Physical Science Basis. Contribution of Working Group I to the Sixth Assessment Report of the Intergovernmental Panel on Climate Change*. Eds. V. Masson-Delmotte, P. Zhai, A. Pirani, S. L. Connors, C. Péan, S. Berger, N. Caud, Y. Chen, L. Goldfarb, M. I. Gomis, M. Huang, K. Leitzell, E. Lonnoy, J. B. R. Matthews, T. K. Maycock, T. Waterfield, O. Yelekçi, R. Yu and B. Zhou (Cambridge, United Kingdom and New York, NY, USA: Cambridge University Press), 1211–1362. doi: 10.1017/9781009157896.011

Le Cozannet, G., Nicholls, R. J., Hinkel, J., Sweet, W. V., McInnes, K. L., Van de Wal, R. S. W., et al. (2017). Sea Level Change and Coastal Climate Services: The Way Forward. *J. Mar. Sci. Engi.* 5 (4), 49. doi: 10.3390/jmse5040049

Oppenheimer, M., Glavovic, B. C., Hinkel, J., van de Wal, R., Magnan, A. K., Abd-Elgawad, A., et al. (2019). "Sea Level Rise and Implications for Low-Lying Islands, Coasts and Communities," in *IPCC Special Report on the Ocean and Cryosphere in a Changing Climate*. Eds. H.-O. Pörtner, D. C. Roberts, V. Masson-Delmotte, P. Zhai, M. Tignor, E. Poloczanska, K. Mintenbeck, A. Alegría, M. Nicolai, A. Okem, J. Petzold, B. Rama and N. M. Weyer (Cambridge, UK and New York, NY, USA: Cambridge University Press), 321–445. doi: 10.1017/9781009157964.006

Conflict of Interest: The authors declare that the research was conducted in the absence of any commercial or financial relationships that could be construed as a potential conflict of interest.

Publisher's Note: All claims expressed in this article are solely those of the authors and do not necessarily represent those of their affiliated organizations, or those of the publisher, the editors and the reviewers. Any product that may be evaluated in this article, or claim that may be made by its manufacturer, is not guaranteed or endorsed by the publisher.

Copyright © 2022 Le Cozannet, Nicholls, van de Wal, Sparrow, Li and Billy. This is an open-access article distributed under the terms of the Creative Commons Attribution License (CC BY). The use, distribution or reproduction in other forums is permitted, provided the original author(s) and the copyright owner(s) are credited and that the original publication in this journal is cited, in accordance with accepted academic practice. No use, distribution or reproduction is permitted which does not comply with these terms.

frontiers in Marine Science

ORIGINAL RESEARCH
published: 23 October 2020
doi: 10.3389/fmars.2020.581769

A Regional Frequency Analysis of Tide Gauges to Assess Pacific Coast Flood Risk

William V. Sweet[1], Ayesha S. Genz[2], Jayantha Obeysekera[3] and John J. Marra[4]*

[1] National Oceanic and Atmospheric Administration, National Ocean Service, Silver Spring, MD, United States, [2] Joint Institute for Marine and Atmospheric Research, University of Hawai'i at Mānoa, Honolulu, HI, United States, [3] Sea Level Solutions Center, Florida International University, Miami, FL, United States, [4] National Oceanic and Atmospheric Administration, National Centers for Environmental Information, Inouye Regional Center, Honolulu, HI, United States

A regional frequency analysis (RFA) of tide gauge (TG) data fit with a Generalized Pareto Distribution (GPD) is used to estimate contemporary extreme sea level (ESL) probabilities and the risk of a damaging flood along Pacific Basin coastlines. Methods to localize and spatially granulate the regional ESL (sub-annual to 500-year) probabilities and their uncertainties are presented to help planners of often-remote Pacific Basin communities assess (ocean) flood risk of various threshold severities under current and future sea levels. Downscaling methods include use of local TG observations of various record lengths (e.g., 1–19+ years), and if no *in situ* data exist, tide range information. Low-probability RFA ESLs localized at TG locations are higher than other recent assessments and generally more precise (narrower confidence intervals). This is due to increased rare-event sampling as measured by numerous TGs regionally. For example, the 100-year ESLs (1% annual chance event) are 0.15 m and 0.25 higher (median at-site difference) than a single-TG based analysis that is closely aligned to those supporting recent Intergovernmental Panel on Climate Change (IPCC) assessments and a third-generation global tide and surge model, respectively. Height thresholds for *damaging* flood levels along Pacific Basin coastlines are proposed. These floods vary between about 0.6–1.2 m or more above the average highest tide and are associated with warning levels of the U.S. National Oceanic and Atmospheric Administration (NOAA). The risk of a damaging flood assessed by the RFA ESL probabilities under contemporary sea levels have about a (median) 20–25-year return interval (4–5% annual chance) for TG locations along Pacific coastlines. Considering localized sea level rise projections of the IPCC associated with a global rise of about 0.5 m by 2100 under a reduced emissions scenario, damaging floods are projected to occur annually by 2055 and >10 times/year by 2100 at the majority of TG locations.

Keywords: flood risk, tide gauges, extreme sea levels, sea level rise, regional frequency analysis

OPEN ACCESS

Edited by:
Goneri Le Cozannet, Bureau de Recherches Géologiques et Minières, France

Reviewed by:
Thomas Wahl, University of South Florida, United States
Jeremy Rohmer, Bureau de Recherches Géologiques et Minières, France

****Correspondence:***
William V. Sweet
william.sweet@noaa.gov

Specialty section:
This article was submitted to Coastal Ocean Processes, a section of the journal Frontiers in Marine Science

Received: *09 July 2020*
Accepted: *29 September 2020*
Published: *23 October 2020*

Citation:
Sweet WV, Genz AS, Obeysekera J and Marra JJ (2020) A Regional Frequency Analysis of Tide Gauges to Assess Pacific Coast Flood Risk. Front. Mar. Sci. 7:581769. doi: 10.3389/fmars.2020.581769

INTRODUCTION

Coastal flood risk is on the rise along many coastlines. Along the densely populated coastlines of the U.S that are well-monitored by tide gauges (TGs), the annual rate of high tide flooding impacting roadways, storm and wastewater systems, and commerce is accelerating and has doubled nationally since 2000 (Sweet and Park, 2014; Sweet et al., 2020). Here, and elsewhere, the primary reason is sea

level rise, with >9 cm occurring globally since the early 1990s (Hamlington et al., 2019; Thompson et al., 2019) and even higher rise of relative sea levels (RSL) from regional variability and land subsidence (Kopp et al., 2015).

Across the Pacific Basin and its vast coastlines, decision makers are also facing mounting impacts from rising seas and they need flood risk information to plan and implement well-timed adaptation solutions (Keener et al., 2018). Unfortunately, risk quantification at space scales useful for decision-making is challenging across the Pacific Basin. Extreme events like tropical cyclones are common, extreme climatic variability is constantly occurring [e.g., from the El Nino Southern Oscillation (ENSO)], bathymetries are complex (e.g., islands), and TGs needed to support risk assessments are relatively sparse. With a global sea level rise of 0.5 m (or more) projected by 2100 under a reduced emissions scenario (Church et al., 2013; Oppenheimer et al., 2019) and impacts and expenditures mounting (Moftakhari et al., 2017), the need for contemporary and future projected estimates of coastal flood risk by decision makers here and elsewhere is growing (Le Cozannet et al., 2017; Hall et al., 2019; Kopp et al., 2019).

The basis for assessing contemporary coastal (ocean) flood risk depends upon local extreme sea level (ESL) probabilities from TGs (**Figure 1A**) to map associated exposure (Kulp and Strauss, 2019) as shown in **Figure 1B**. Future estimates typically include localized RSL projections (e.g., Hunter, 2012; Tebaldi et al., 2012; Church et al., 2013; Kopp et al., 2014; Sweet and Park, 2014; Buchanan et al., 2017; Wahl et al., 2017; Ghanbari et al., 2019; Oppenheimer et al., 2019; Frederikse et al., 2020; Taherkhani et al., 2020). Most of these studies use the 100-year ESL (1% annual chance level) as a suitable flood threshold to assess impacts and communicate risk, though empirically derived height thresholds for flooding of various severities is preferable as to align with actual infrastructure vulnerabilities and weather warnings affecting daily decision making (Sweet and Park, 2014; Sweet et al., 2018). A drawback is that singular TG records suffer from record-length bias (e.g., short records), and from the perspective of a particular location, under-sample regionally significant rare events like land-falling tropical cyclones leading to large uncertainties in important (e.g., 100-year) ESLs (Hall et al., 2016; Wahl et al., 2017; **Figure 1C**). Assessments using dynamical models increase spatial coverage and inclusion of synthetic storms are capable of lengthening the record-length of rare event sampling (Lin et al., 2012, 2019; Haigh et al., 2014a,b; Nadal-Caraballo et al., 2015; Vitousek et al., 2017; Vousdoukas et al., 2018; Muis et al., 2020). However, dynamical models usually perform poorly in areas with high TC activity with complex bathymetries (Muis et al., 2016). Recent studies using satellite altimeter (Lobeto et al., 2018) and Bayesian hierarchical models of TG data (Calafat and Marcos, 2020) show promise, but neither have been applied along Pacific Basin coastlines to our knowledge.

In this study, we estimate ESL probabilities and those specifically for *damaging* flood heights along Pacific coastlines. Our criteria for a damaging flood are calibrated to U.S. National Oceanic and Atmospheric Administration (NOAA) coastal flood thresholds for weather-related hazards along a variety of U.S. Pacific coastlines. We use a regional frequency analysis (RFA) of TG data building upon efforts of Hall et al. (2016), who supported a flood risk assessment of U.S. Department of Defense coastal installations worldwide. In our usage, the RFA method is used to aggregate sets of TG threshold exceedances across particular Pacific basin regions and fit the data with a Generalized Pareto Distribution (GPD) to form a regional ESL probability distribution. A RFA-based assessment provides three key advantages as compared to a single-TG analysis only (Hosking and Wallis, 1997). (1) Rare-event sampling is increased by combining data within a region to provide a more robust parameterization. (2) Shorter TG records are lengthened by regional data to reduce record length bias. (3) Regional ESL probabilities can be downscaled even where there are no TGs if a reasonable localization factor is available.

Our paper has four main components. First, we identify statistically homogeneous regions and for the RFA and fit Pacific TG threshold exceedances with a GPD to estimate regional ESL probabilities (subannual to 500-year). Next, methods to obtain the necessary localization factor to downscale the regional ESL probabilities are presented with results compared to recent sets of foundational results using both TGs and advanced tide and storm surge modeling. Then, we define a Pacific-wide height threshold for a damaging flood. Lastly, we assess the current risk of the damaging flood heights under current sea levels and show how this risk will change under current flood defenses using RSL rise projected by the Intergovernmental Panel of Climate Change (IPCC, Oppenheimer et al., 2019) under Representative Concentration Pathways (RCP) 4.5 (IPCC, 2014).

MATERIALS AND METHODS

The RFA method (Hosking and Wallis, 1997) is based upon the assumption that regional environments with similar forcing attributes experience a similar event frequency and (extreme) probability density up to a local flood index (u), which is a local scaling factor that captures response peculiarities (Dalrymple, 1960). A RFA uses regional sets of data locally normalized by their respective u with a statistical heterogeneity test (H value) to assess the extent that the data are sufficiently similar. Using statistical L-moments, heterogeneity is a measure of the variation between sites of a location's summary distribution statistics relative to the amount of dispersion expected if the locations were indeed a homogeneous region (Hosking and Wallis, 1997). If $H < 1$, the region is considered acceptably homogeneous. If $1 \leq H < 2$, the region is considered possibly heterogeneous, but acceptable for our study. If $H \geq 2$, then the TG group is definitely heterogeneous and not suitable for analysis. Where $H \geq 2$, a discordancy measure that also uses L-moments is used to pinpoint and remove individual locations whose sample L-moment ratios are an outlier within a region (Hosking and Wallis, 1997). Once the regional bounds are established whose data is acceptably homogeneous, the aggregated data is fit with an extreme value distribution. RFA has been useful in river (Michele and Rosso, 2001; Smith et al., 2015), rainfall (Roth et al., 2012; Carreau et al., 2017; Perica et al., 2018), wave height (Weiss et al., 2014), tsunami (Hosking, 2012),

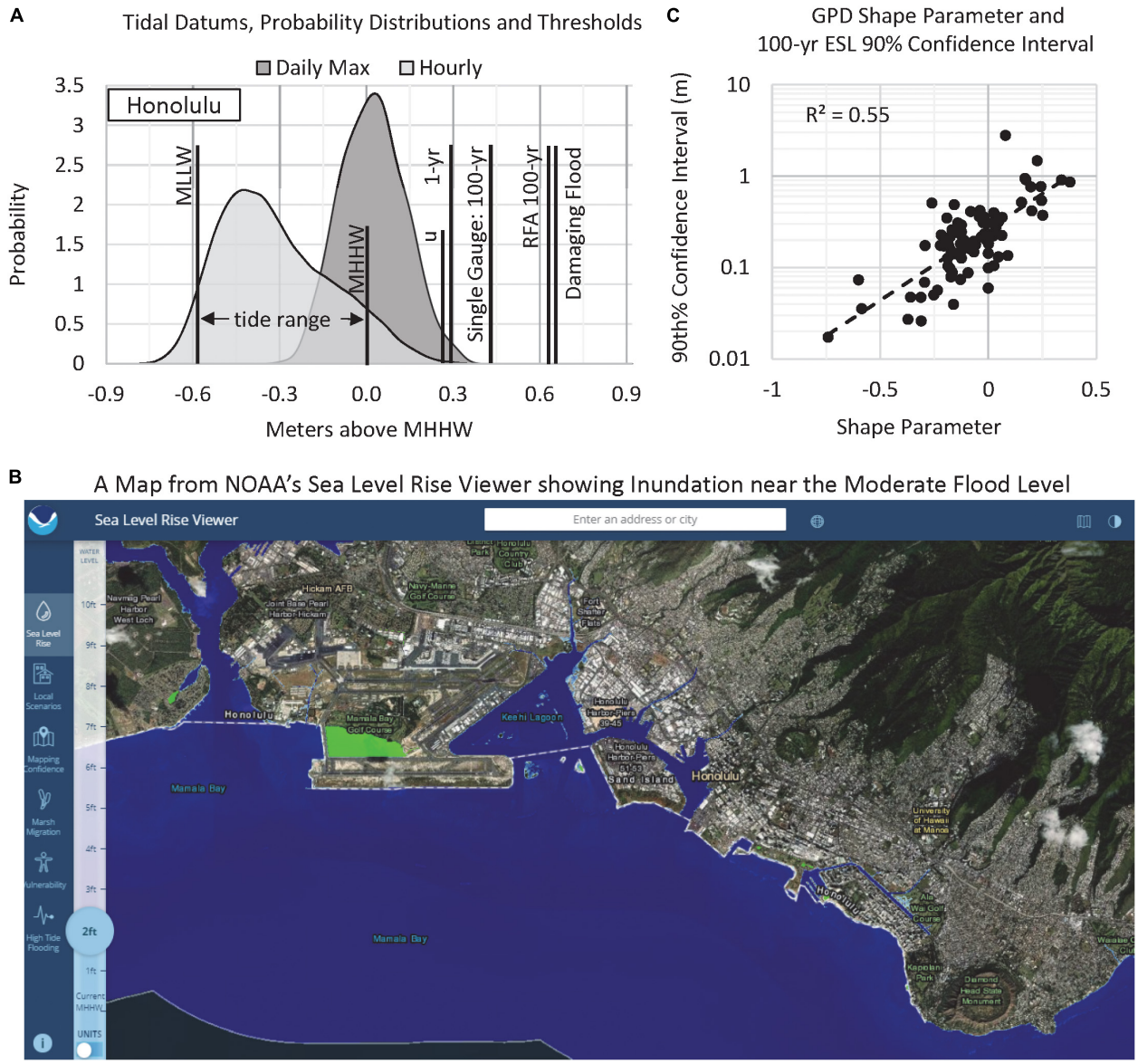

FIGURE 1 | (A) Empirical probability distributions of hourly and daily highest water levels at the NOAA TG in Honolulu with tidal datums [mean lower low water (MLLW), mean higher high water (MHHW) and tide range], the 1- and 100-year extreme sea level probabilities and a proposed Pacific damaging flood threshold for Honolulu. In **(B)** is a map from NOAA's Sea Level Rise Viewer for Honolulu (https://coast.noaa.gov/slr/#/layer/slr) showing 0.6 m (2 feet) of inundation that is slightly below the damaging flood level. In **(C)** is the GPD shape parameter values based upon a single TG analysis from this study and the spread of the 90% confidence interval from all TGs with an exponential fit. Positive shape parameters generally occur where extreme outliers (e.g., tropical storm surges) tend to occur.

and coastal storm surge (Bardet et al., 2011; Bernardara et al., 2011; Weiss and Bernardara, 2013; Frau et al., 2018) studies.

In our study, hourly TG observations with >10 years of record archived by the University of Hawaii Sea Level Center are used and referenced to mean higher high water (MHHW; NOAA, 2003) to help normalize for tide range differences. MHHW is approximated as a 19-year (or record length if < 19 years of data; **Supplementary Table 1**) average of daily highest water levels. Also used is tide range defined as the difference between MHHW and mean lower low water (MLLW), which is approximated as a 19-year average of daily lowest water levels (NOAA, 2003). Observations from TGs with >20 years of record are linearly detrended and centered with respect to 1992 (i.e., the trend line intercepts the x-axis at the year 1992) similar to methods of NOAA (Zervas, 2013) to align with the midpoint of the current (1983–2001) national tidal datum epoch. Alignment is important as NOAA's real-time observations and tide predictions along the U.S. West Coast and coastlines of Alaska, Hawaii and the US Pacific Affiliated Islands currently reference the 1983–2001 epoch[1]. From the hourly data, daily highest water levels are

[1]https://tidesandcurrents.noaa.gov/tide_predictions.html

declustered at each TG using a 4-day storm window to ensure event independence. The 98th percentile of the declustered daily highest levels at each TG is both the threshold to assess exceedances and is also the flood index to localize the RFA ESL probabilities (described below; henceforth, both are referred to as "u" and are the same quantity).

To identify RFA homogeneous regions, we start with the classifications of Rueda et al. (2017) for the Pacific, who divide the global ocean in terms of physical processes (storm surge, tides and wave effects) and their influence inherent within ESL probabilities (**Figure 2** and **Supplementary Table 1**). Within our Pacific study region are Rueda et al. (2017) Tide-dominated (T), Tropical Cyclone (TC), Extratropical (ET), Wave-dominated (W), and Transition (TR) regional classifications. The first step is to regionally aggregate the normalized (by local u value) set of TG threshold exceedances within each of Rueda et al. (2017) classifications. Next, the regional data are spatially declustered with an additional 4-day storm window to ensure that only the maximum water level across TGs within a region is retained (removes any lesser peak water levels from the same event). Then, the statistical heterogeneity measure (H) is estimated and where H $\geq$2, the TG groups were further subdivided based on the following: sub-classifications from Rueda et al. (2017), geographic divisions (e.g., northern latitude vs. southern latitude stations), and/or the Discordancy measure of a particular TG. In some instances, a TG fit multiple regions and the choice was to keep island groups together as long as the group's H value was <2 (e.g., Hawaiian Islands).

For example, Rueda et al. (2017) identified two sub-classifications in the Wave region: one that is wave-tide dominant and one that is wave dominant. Within the Pacific, the Wave regions (yellow and whitish-yellow hue colored regions in **Figure 2**) were located in two areas—one north of the equator and one south of the equator. The main Hawaiian Islands straddle two groups—the wave-tide dominant sub-classification (yellow region in **Figure 2**) of the Wave region and two sub-classifications (greenish colored regions in **Figure 2**) within the Transition Region (wave-tide dominant and tide dominant). In order to keep the Island groupings together, we included the main Hawaiian Islands in the Wave Region. We initially grouped TGs from all sub-classifications and the HI stations as one region within the Pacific (13 stations), but the H value was not resolvable. We further separated this group (W1 and W2) based on geographic location (one group north of the equator and one south of the equator). For the southern group (W1), we included Rarotonga, Cook Islands (#23). Technically this station sits in the Tide (T1) region, but it borders the Wave (W1) region and when included within the T1 region its high discordancy resulted in an H value > 2. This region (W1) resulted in an H value of -0.28, which is considered homogeneous. The northern group including the Hawaiian Island stations (W2) resulted in an H value of 1.67, which is considered possibly (acceptably) homogeneous.

With the TG regions established (**Figure 2**), the aggregated and normalized sets of TG threshold exceedances are fit with a GPD (Coles, 2001) using the penalized maximum likelihood method (Coles and Dixon, 1999; Frau et al., 2018) to estimate

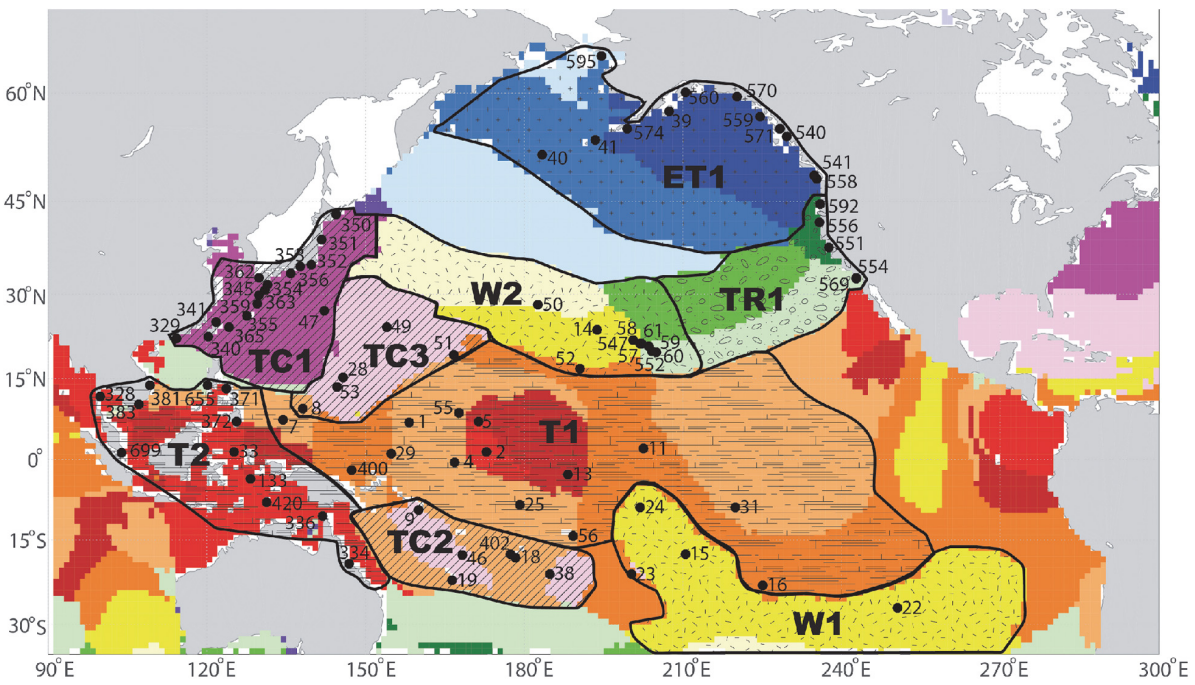

FIGURE 2 | TGs with the University of Hawaii Sea Level Center numbering designation and the RFA homogeneous Tide-dominated (T), Tropical Cyclone (TC), Extratropical (ET), Wave-dominated (W), and Transition (TR) regions delineated in this study based upon the color-shaded classifications of Rueda et al. (2017). The Rueda et al. (2017) shape-file classifications were shared by the authors as licensed under CC BY 4.0.

(median) regional ESL (RESL) probabilities and the 5th and 95th% levels (90% confidence interval) defined as:

$$G\ (Z;\ u,\ \alpha, \xi) = \lambda \left[1 + \xi \left(\frac{z - u}{\alpha}\right)\right]^{-\frac{1}{\xi}}, \qquad (1)$$

where G is the exceedance probability (P[Z > z]), λ is the probability of an individual (normalized) observation exceeding the threshold (u), α is the scale parameter, and ξ is the shape parameter. It is assumed that the distribution of the number of exceedances per year follows a Poisson distribution and the return level (e.g., 100-year) for an ESL of height (z) is given by

$$Z_N = u + \frac{\alpha}{\xi}\left[(Nn_y\lambda)^{\xi} - 1\right], \qquad (2)$$

where N is the annual return interval (~0.3–500-year level), n_y is number days per year (365.25) and λ is the average number of event exceedances/year (about 3.15 on average across all TGs in the study).

In our RFA approach using GPD, the local ESLs (LESLs) including the model of expected values and their 90% confidence interval at a particular location is given as

$$LESL = RESL^{*}u + u, \qquad (3)$$

where RESL is the regional return level for a particular homogeneous TG region and u is the local flood index. The RESLs are first multiplied by u to localize the values (i.e., LESLs relative to the local u value), which is then added to u to put the LESL results onto MHHW (u is a height above MHHW; **Figure 1A**). The uncertainty of RESL, as determined from RFA is assumed to be σ_{RESL}. When localized at any of the TGs used in our study (LESL), u is assumed to have no uncertainty. It is recognized that values of u will have time-dependent characteristics, e.g., similar to those identified in the location parameter of the Generalized Extreme Value (GEV) distribution (e.g., Menéndez and Woodworth, 2010). To our knowledge, no other studies consider or include uncertainties of u within GDP-based estimates of ESL probabilities.

Methods to obtain a prediction or estimate of u and its uncertainty [i.e., root mean squared error (RMSE)] are provided to localize the RESL probabilities and confidence intervals for coastlines (**Figure 2**) without existing TG data or perhaps a few years of data only. The first method provides a prediction of u and its uncertainty based upon a linear dependence that exists between tide range and u at the Pacific TGs. Tide range information is readily available along most coastlines and islands, e.g., from models calibrated by the global set of TGs and/or satellite altimetry (e.g., https://www.aviso.altimetry.fr/data/products/auxiliary-products/global-tide-fes.html; https://vdatum.noaa.gov/; https://tidesandcurrents.noaa.gov/tide_predictions.html).

The other option provides an estimate of the uncertainty in u as a function of a 1–19 record length. For simplicity, an RMSE estimate of u is assessed for the set of Pacific TGs as a whole. To compute the RMSE, we first find the maximum absolute differences between u derived over the entire record (**Supplementary Table 1**) and for progressively longer consecutive record lengths between 2001 and 2019 at each TG (e.g., 19 discrete 1-year records; 18 overlapping 2-year records, etc.). We use the maximum (absolute) difference at each TG to account for potential interannual variability that can be extreme (e.g., due to phases of ENSO). This difference is considered the error in estimating u for shorter records and the average of the absolute differences across all TGs is considered the bias. The standard deviation of the absolute differences is also computed across all TGs and an estimate of the RMSE is then computed as the square root of the sum of the square of the bias and the standard deviation (variance).

When using predicted values or short-record estimates of u, the uncertainty estimates of LESL will include additional uncertainty in $u\ (\sigma_u)$. For simplicity, we assume that RESL (estimated from the regional return level curve) and u are independent and derive an expression for variance of LESL (σ^2_{LESL})as follows:

First, using Eq. (3), $\sigma^2_{LESL} = Var[RESL^{*}u] + Var[u] + 2Cov[RESL^{*}u, u]$ where Var and Cov represent the variance and the covariance, respectively, of terms inside the square brackets. It may be shown (Mood et al., 1974) that $Var[RESL^{*}u] = \mu^2_u\sigma^2_{RESL} + \mu^2_{RESL}\sigma^2_u + \sigma^2_u\sigma^2_{RESL}$ where μ and σ^2 are the expected value and the variance of the variable indicated in the subscript. Also, the covariance term above simplifies to: $Cov[RESL^{*}u, u] = \mu_u\sigma^2_u$. Combining the above expressions, we obtain:

$$\sigma^2_{LESL} = \left[(1 + \mu_{RESL})^2 + \sigma^2_{RESL}\right]\sigma^2_u + \mu^2_u\sigma^2_{RESL} \qquad (4)$$

where μ_{RESL} and μ_u are the expected values of the regional return levels and the expected value of u, for example, predicted by the tide-range and u dependency, respectively, and σ^2_u is the uncertainty inherent to any u-prediction relationship (e.g., RMSE). It should be noted that the added uncertainty in u as estimated from this relationship would introduce additional uncertainty in estimates of LESL.

Derivation of a threshold defining a damaging flood height builds upon patterns found by Sweet et al. (2018) between discrete coastal flood thresholds of NOAA's National Weather Service and local tide range. NOAA's National Weather Service[2] coastal flood thresholds are empirically calibrated over years of impact monitoring, define infrastructure vulnerabilities and used to warn emergency managers of forecasted impacts. Projections of RSL rise under RCP4.5 used to assess future changes in flood risk come from the IPCC Special Report on the Ocean and Cryosphere in a Changing Climate (SROCC; Oppenheimer et al., 2019). To estimate LESLs with return intervals down to a 0.1-year event frequency, we extrapolate our GPD model with a logarithmic fit for return levels between 2 years and the ~0.3 years ($1/\lambda$) limit, with results that are in agreement with those of Sweet et al. (2018).

FINDINGS

The RESL probabilities span from about 0.3- to 500-year levels and are shown in **Figure 3** (values also listed in **Supplementary Table 2**) as return level curves following

[2]https://water.weather.gov/ahps/

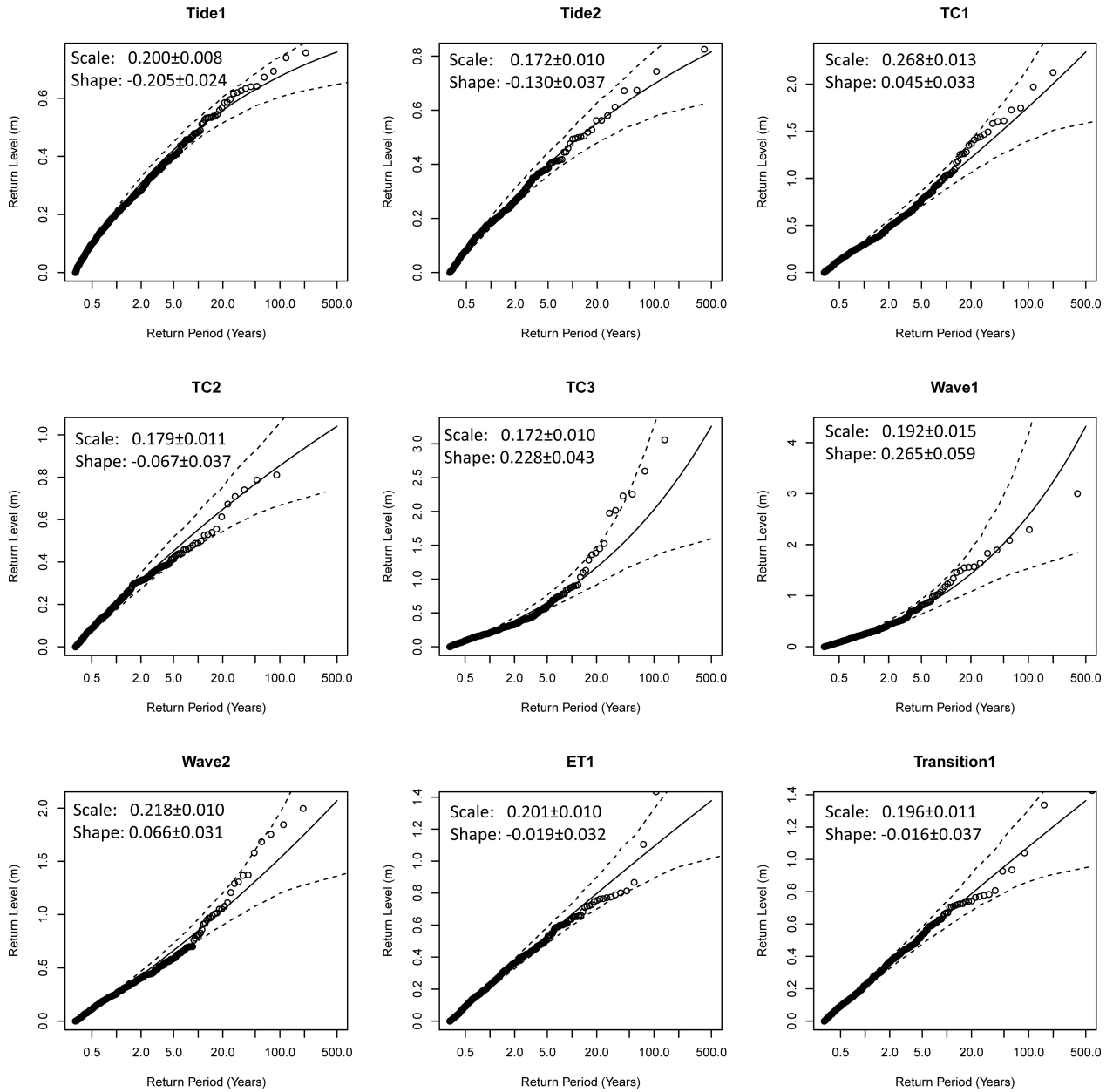

FIGURE 3 | Normalized TG data and the regional extreme sea level (RESL) return level curves with 90% confidence intervals (5th and 95th% levels) as mapped in **Figure 2**. The y-axes are in meters above MHHW.

common engineering practice along with the GPD model parameters and their uncertainties. The regional return level curves show where RESL probabilities are limited (bounded) or not (unbounded) as quantified by either a negative or positive shape parameter, respectively. Unbounded regions include TC regions 1 and 3 and W regions 1 and 2. Visual inspection of the regional return level curves show a satisfactory fit to the data, though outliers within the extreme tails are noticeable mainly within regions TC3 and W2 (**Figure 3**). These outliers (data near/above the 90% confidence interval) suggest a mixed response from tropical and extratropical cyclones (Haigh et al., 2014a), which is reflected in their higher heterogeneity measure (H values in TC3 and W2 of 1.39 and 1.67, respectively in **Supplementary Table 2**). Indeed, outlier data in region TC3 include several tropical storm surges measured at Saipan (TG #28), Yap (TG #8), and Wake Island (TG #51). Region W2 contains tropical storm surges measured at Johnston Atoll (TG #52) and a record-setting event in response to Hurricane Iniki, which hit Hawaii in 1992 and whose surge (e.g., 0.96 m above MHHW at Kauai–TG #58) produced highest TG-measured water levels ever along the Hawaiian Islands.

Factors affecting the fit of the regional models (**Figure 3**), and hence LESLs (Eq. 3) include methodological choices of the RFA local flood index (u), the threshold (also u in our case) or time block to assess local TG exceedances or block maxima and the extreme value distribution (e.g., GEV or GPD) fit to the regional data. As discussed by Wahl et al. (2017) for single-gauge analyzes, 100-year LESLs can vary by 10's of centimeters in some unbounded locations depending upon methodological choices and the extreme value distribution used to fit TG data, though GPD fits to threshold exceedances are less likely to be biased high or low. Specific to the RFA is the selection of an optimal flood index as discussed by Weiss and Bernardara (2013) who show that RFA-based LESLs can vary (<10 cm per their GEV-based examples) depending upon regional heterogeneity and on the nature of treatment to the local flood index (e.g., using the mean or median value of annual maxima or threshold exceedances) used within a particular region. In both studies (Weiss and Bernardara, 2013; Wahl et al., 2017), nuances in model choice mostly affect the tail of the distribution (e.g., 100-year LESLs). Our usage of the TG exceedance threshold directly as the local flood index is the equivalent to the location parameter, which Weiss and Bernardara (2013) find as an optimal index in some circumstances and follows other studies (Roth et al., 2012; Frau et al., 2018).

For method consistency and application simplicity across all the Pacific study regions (**Figure 2**), we compute LESLs (i.e., Eq. 3) keeping to a constant definition of u (98th percentile of a TG's 4-day declustered daily highest levels). However, we compute several sets of LESL results using alternate methods to estimate u values and their uncertainties (Eq. 4) and compare them to those based upon the entire TG record (**Supplementary Table 1**). These alternative methods may be of interest to coastal communities that are not co-located to a TG used in this study, but have predictions of tide range or have access to or be planning deployments to collect *in situ* water level records. Applicable for where tide range predictions exist, a set of LESLs are based upon predicted values of u and their uncertainties from an underlying linear dependence between tide range and u across the Pacific TGs (**Figure 4A**). The underlying high correlation between tide range and u (R^2 = 0.86 with a 0.074 m RMSE) is similar to findings of Merrifield et al. (2013) who found a high correlation between the range in water level variability and average annual highest water level. Two exceptions not included in the linear regression are Nome, Alaska (TG #595; **Supplementary Table 1**) and the Japanese coral atoll of Minamito (TG #49) that have extremely small tide ranges compared to their u values (>two standard deviation outliers).

Another set of LESLs are based upon u values estimated using short data records and utilize an uncertainty estimate (RMSE) in u which is record-length dependent (**Figure 4B**). For simplicity (as in **Figure 4A**), the RMSE in u is estimated across the entire Pacific study region (64 of 84 TGs included), but only those with complete 2001–2019 records and also excluding Ofunato (TG #351) and Yakutat (TG #570) due to significant non-linear vertical land motion in the time series. The RMSE as a function of consecutive record length is plotted in **Figure 4B** and fit using a best-fit logarithmic function. With about 4 years of data, the RMSE in u (7–8 cm) is about the same as those based upon the tide range (**Figure 4A**). After 19 years, the RMSE is about 1 cm (not shown), but has been reduced to zero across the 1–19 year range.

Our 1- and 100-year RFA LESLs (**Figure 5**) based upon record-length values of u (**Supplementary Table 1**) have median values of 0.47 and 0.83 m above MHHW, respectively. Higher 100-year LESLs (e.g., >1.2 m) generally occur along the continental margins where larger variability occurs from extreme astronomical tides or tropical and extratropical storm exposure such as is the case for Nagasaki, Townsville and Ketchikan (**Table 1**). In terms of the 1-year LESLs and higher probability events, a similar spatial pattern emerges, but tide range becomes more of a dominant factor as expressed by the tight coupling between u and tide range across the Pacific TG locations (**Figure 4A**). For example, smaller 1-year levels at Papeete,

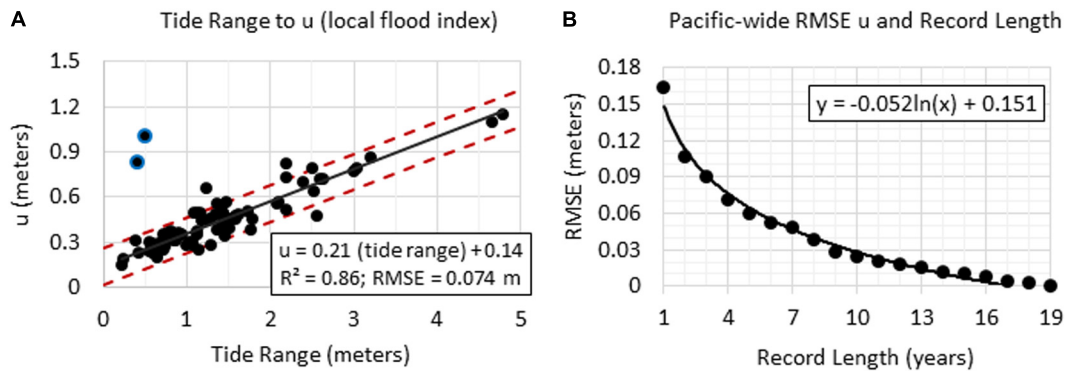

FIGURE 4 | (A) Tide range and u (local RFA local flood index and TG exceedance threshold) and linear regression fit statistics with two outlier TGs (Nome and Minamito > 2 stdev) not included in the regression. In **(B)** is the root mean square error (RMSE) for estimates of u based upon 1–19 years of consecutive data over the 2001–2019 period based upon 64 of the 84 TGs used in this study.

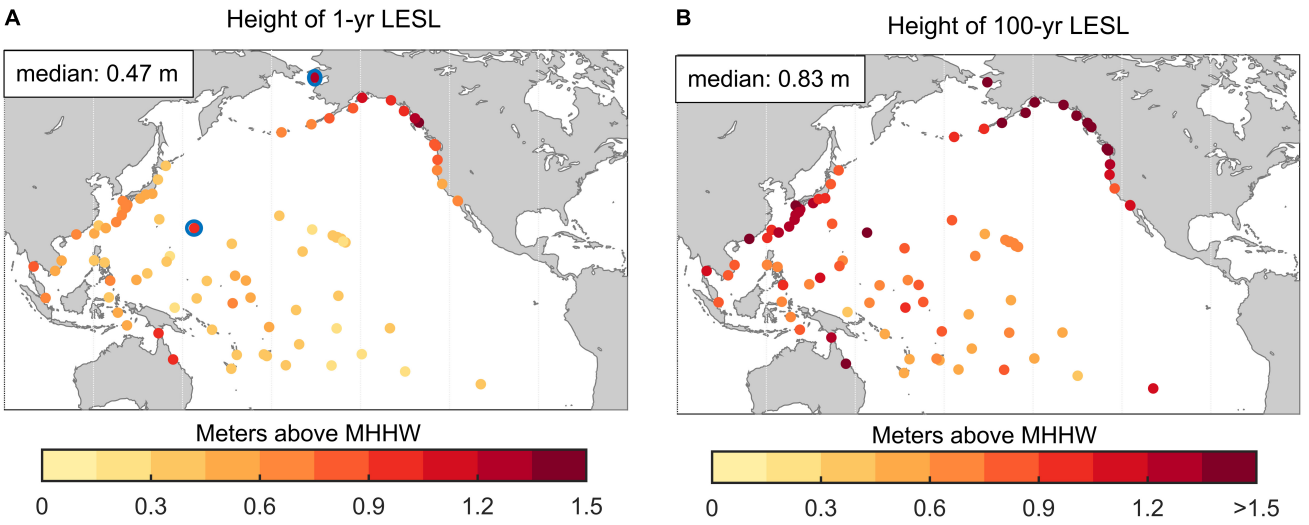

FIGURE 5 | (A) 1-year and **(B)** 100-year LESLs with the two outlier TGs shown with blue circles. The ">" in the last tick label in the legend (in this figure and similarly in others) indicate at least one value exceeds 1.5 m.

TABLE 1 | An example of 1-, 10-, and 100-year return levels (meters above MHHW) with 90% confidence intervals (CI: spread of the 5th and 95th% levels) from regional frequency analysis (RFA) highlighting a subset of tide gauges (TG) within each homogeneous region and its H value.

Region	H Value	TG #	Location	Tide Range (m)	u (m)	1-year (m)	90% CI	10-year (m)	90% CI	100-year (m)	90% CI
ET1	1.37	571	Ketchikan	4.65	1.10	1.35	1.33–1.36	1.83	1.77–1.89	2.30	2.14–2.46
T1	0.73	55	Kwajalein	1.17	0.45	0.54	0.53–0.54	0.67	0.66–0.68	0.75	0.73–0.77
T2	-2.37	334	Townsville	2.18	0.82	0.98	0.96–0.99	1.22	1.19–1.25	1.40	1.33–1.47
TC1	0.53	362	Nagasaki	2.09	0.56	0.74	0.73–0.75	1.13	1.08–1.17	1.56	1.41–1.70
TC2	-0.96	18	Suva	1.28	0.29	0.34	0.34–0.35	0.44	0.43–0.46	0.53	0.49–0.57
TC3	1.39	53	Guam	0.71	0.25	0.30	0.30–0.31	0.47	0.44–0.50	0.75	0.63–0.88
TR1	0.21	569	San Diego	1.73	0.51	0.62	0.61–0.63	0.84	0.81–0.87	1.05	0.97–1.14
W1	-0.28	15	Papeete	0.22	0.15	0.19	0.18–0.19	0.31	0.28–0.34	0.54	0.40–0.67
W2	1.67	57	Honolulu	0.58	0.25	0.31	0.31–0.32	0.46	0.44–0.48	0.63	0.57–0.68

Also shown is the TG's tide range and u value (98th% of daily highest water levels, which is both the TG exceedance threshold and the RFA local flood index).

Honolulu and Guam (**Table 1**) occur largely in response to smaller tide ranges.

Result Comparisons

When compared to a single-gauge GPD estimate of LESLs using the same TG data, the RFA-based LESLs show some important distinctions. At the 1-year LESL (**Figure 6A**), the two approaches yield similar results with RFA estimates only slightly higher (median value is 2 cm higher). However, the 100-year LESLs are very different (**Figure 6B**), with the RFA LESLs much higher in many locations (0.3–0.6 m) such as along the Japan and U.S. Pacific Northwest coastlines and 0.11 m higher overall (median value). In terms of a broad regional comparison (**Figure 6C**), the single-gauge LESLs are 87% of those from the RFA based upon linear regression coefficient (or RFA is about 13% higher), which about the ratio of the median of the single gauge (0.76 m) to RFA (0.83 m) 100-year LESLs. Higher LESLs is a typical artifact of the RFA (Hall et al., 2016) and a primary purpose of the RFA process–to quantify ESL probabilities and exposure locally from a regional perspective. There are a few exceptions where the RFA 100-year LESLs are much smaller (∼1 m, **Figure 6B**), e.g., Nome, which may be partly attributed to its short record length (bias) of 23 years (**Supplementary Table 1**).

Sensitivity of LESLs localized by various methods to estimate u are the focus of **Figures 6D–F**. Comparisons between the RFA 100-year LESLs and those with u values from 9 years of data (2011–2019, which is an arbitrary record length, but represents half of a tidal nodal cycle) and predicted by tide range (**Figures 6D,F**, respectively) reveal little inherent bias with (median) differences of ≤1 cm. Linear regression shows a tight coupling (R^2 = 0.98) between the LESLs based upon record-length and 9-year estimates of u (**Figure 6F**). Differences using a tide-range predicted u (**Figure 6E**) are more pronounced due to its underlying predictive relationship (**Figure 4A**), with the two outliers (Nome and Minamito) >1 m apart and reducing the overall goodness-of-fit (**Figure 6F**; R^2 = 0.47).

Comparison of the spread in 100-year 90% confidence intervals (**Figure 7**) show that the (median) RFA LESLs spread

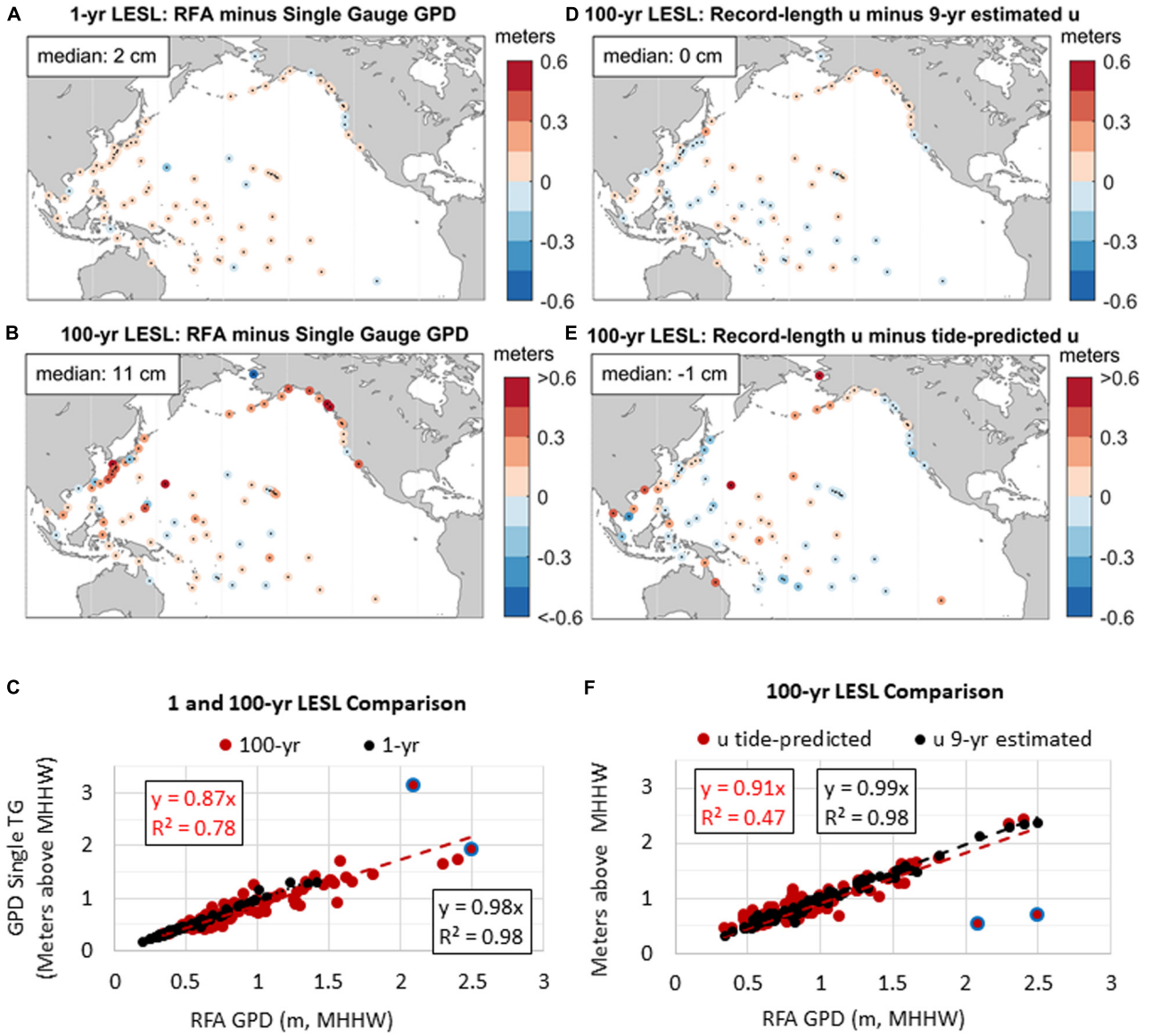

FIGURE 6 | Differences in the RFA LESLs and those computed using a single TG only at the **(A)** 1-year and **(B)** 100-year levels and **(C)** linear regression between the sets in **(A,B)**. Mapped differences in the 100-year LESLs using record length u and **(D)** 9-year (2011–2019) estimates and **(E)** a tide-range based predictions of u plotted with linear regression statistics in **(F)**. The outliers (blue circles) are included in the regressions in plot **(C,F)**.

is 14 cm (**Figure 7A**) and is 8 cm tighter (**Figure 7B**; negative values illustrate where RFA values are less) than those based upon a single-gauge (GPD) analysis. The locations with much tighter (<-0.6 m) RFA 100-year 90% confidence intervals are mostly within regions prone to rare (outlier) extremes and with unbounded tails (positive shape parameters in **Figure 3**), namely TC Regions 1 and 3 and Wave Regions 1 and 2. Comparison of the 100-year 90% confidence intervals using u predicted by tide range as the local index flood (**Figure 7C**) shows the additional inflation due to method uncertainty (Eq. 4), which is persistent spatially (median difference of -0.35 m). Of note is that some of the location-specific peculiarities are less than those based upon a single-gauge approach (**Figure 7B**) due to the RFA process (standard deviation of 10 vs. 34 cm by single-gauge estimate). The inflation in the 100-year 90% confidence interval when using a 9-year estimate of u (**Figure 7D**) is less than those from a tide-range predicted u (**Figure 7C**) and closer to those using u values based upon the complete TG record (median difference = -0.09 m in **Figure 7D**).

The RFA LESLs are next compared to recent foundational sets of LESLs derived from both TGs and advanced tide and storm surge modeling. A comparison in **Figure 8** is made to the results of a single-gauge GPD analysis (Rasmussen et al., 2018) that are closely aligned (similar methodology and results) to those supporting the IPCC Global Warming of

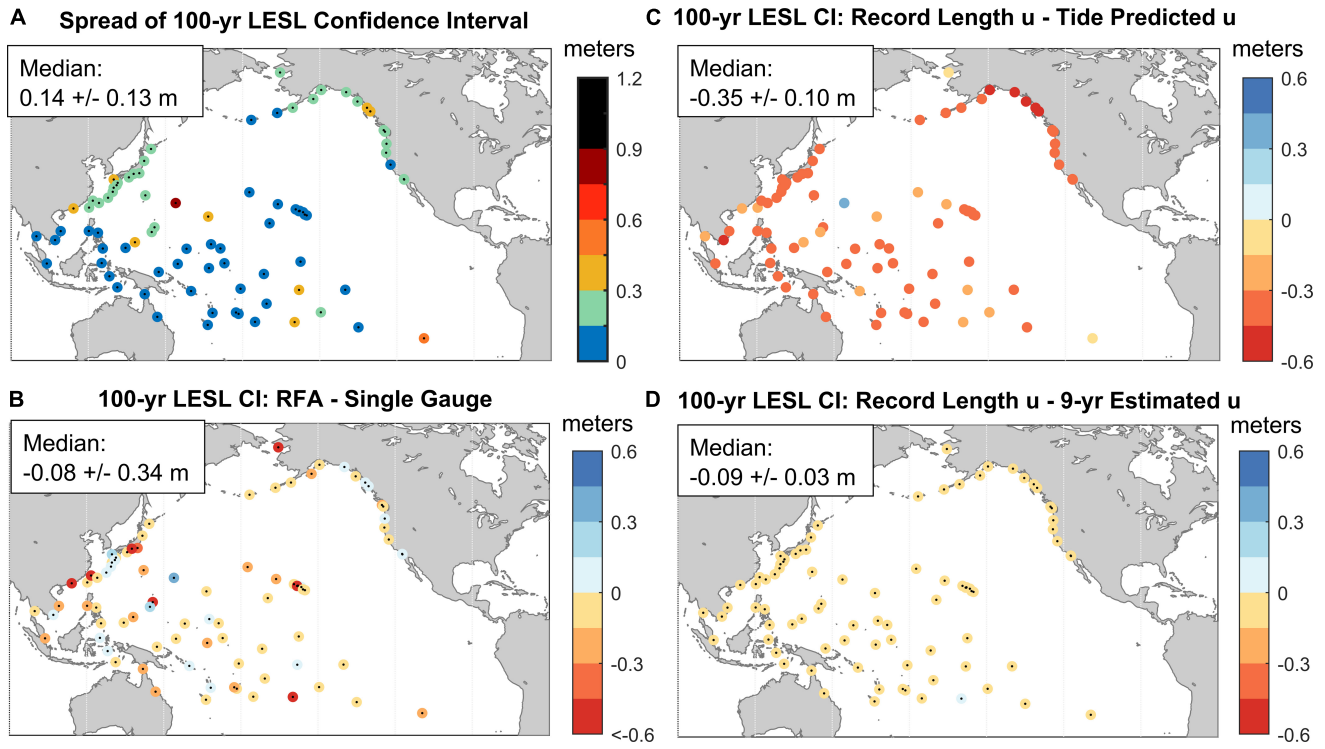

FIGURE 7 | The spread of the 100-year LESL 90% confidence interval using **(A)** the RFA values and the differences with those computed using **(B)** a single TG GPD analysis, **(C)** RFA estimates predicted from tide range (**Figure 4A**) and **(D)** 9-year estimates of u (**Figure 4B**).

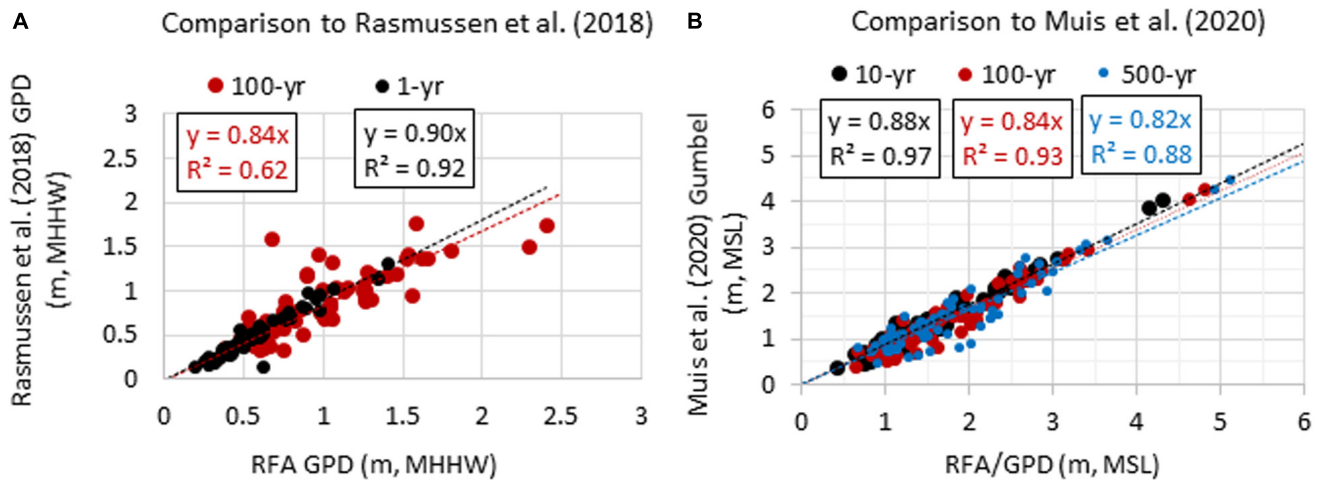

FIGURE 8 | Comparison of our RFA GPD **(A)** 1- and 100-year LESLs to those from a single-gauge GPD of Rasmussen et al. (2018) and **(B)** 10-, 100-, and 500-year LESLs to those with a Gumbel fit for global tide and surge model output of Muis et al. (2020) with linear regression fit and statistics.

1.5°C (Hoegh-Guldberg et al., 2018) and SROCC (Oppenheimer et al., 2019) assessments. The comparison with Rasmussen et al. (2018) results is made at 61 of the 84 TGs in our study. The RFA 1- and 100-year LESLs are both higher overall, by about 10 and 16%, respectively based upon linear regression (**Figure 8A**). For context, the median (±1 SD) TG difference of the 1- and 100-year LESLs being compared in **Figure 8A** is 0.06 and 0.15 m (±0.07 and 0.26 m), respectively, with the higher values from the RFA LESLs. Comparison of a 100-year LESLs based on a single-gauge GPD analysis using data in this study (e.g., same data set compared in **Figure 6B**) to the Rasmussen et al. (2018) are quite similar as would be expected since both use the same data set (regression slope of 1.01; not shown).

LESLs are also compared to those from a third-generation global tide and surge model forced by ERA5 climate reanalysis from 1979 to 2017 (Muis et al., 2020). The RFA LESLs, once adjusted to a comparable mean sea level datum, are also higher overall to the modeled results of Muis et al. (2020), who fit a Gumbel distribution to the annual maxima (**Figure 8B**). Comparing the 10-, 100-, and 500-year LESLs at 74 of the 84 TGs, the RFA estimates are about 12, 16, and 18% higher based upon linear regression with good agreement (small variability) between the two sets of results (R^2 of 0.97, 0.93, 0.88), respectively (**Figure 8B**). For context, the median (±1 SD) differences are 0.20, 0.25, and 0.31 m (±0.14, 0.21, 0.30 m), respectively. The RFA result comparison to Muis et al. (2020) could also reflect inherent differences in data utilization (threshold exceedances vs. annual maxima) and fitted extreme value distribution (GPD vs. Gumbel) and not necessarily model biases (Wahl et al., 2017). However, the large discrepancies between results, even down to the 2-year LESL (median difference of 0.17 m, not shown), would suggest some underlying response and/or possible tidal datum bias.

A Damaging Flood Threshold and Its Current Risk

Local flood risk varies according to many factors such as elevation, topography, urbanization and flood proofing. Instead of using probabilistic thresholds like the 100-year LESL (e.g., Oppenheimer et al., 2019), which may or may not cause significant or even noticeable impacts, we utilize NOAA's flood severity thresholds. Following methods of Sweet et al. (2018), we first regionalize all TGs with NOAA minor flood thresholds along U.S. Pacific coastlines (**Figure 9A**; median value of 0.58 m above MHHW) and then plot relative to tide range (**Figure 9B**) as the initial basis for deriving a Pacific Basin flood threshold/infrastructure vulnerability definition. NOAA-defined minor flooding typically is more disruptive (e.g., flooding of some roadways, stormwater system infiltration), whereas NOAA-defined moderate flooding is damaging to public and private infrastructure. When a moderate (and/or major) flood is imminent, NOAA issues a coastal flood warning for conditions posing a serious risk to life and property (Sweet et al., 2018). To define a moderate flood threshold throughout the Pacific Basin (henceforth called a *damaging* flood), we add 0.3 m to this quadratic fit/threshold, which is about the median offset between the U.S. NOAA minor and moderate flood thresholds (Sweet et al., 2018) and apply this relationship at all TGs within our study. We do this because there are many more TGs with NOAA minor flood thresholds than with NOAA moderate threshold defined along the U.S. Pacific coastline. An important distinction between this study's approach broadly defining infrastructure flood thresholds and that of Sweet et al. (2018) is the inclusion of Alaska NOAA thresholds and the usage of a quadratic fit.

Applying this definition across our study's TGs, the median height of the Pacific damaging flood threshold is 0.69 m above MHHW and spans from about 0.6 and 1.2 m above

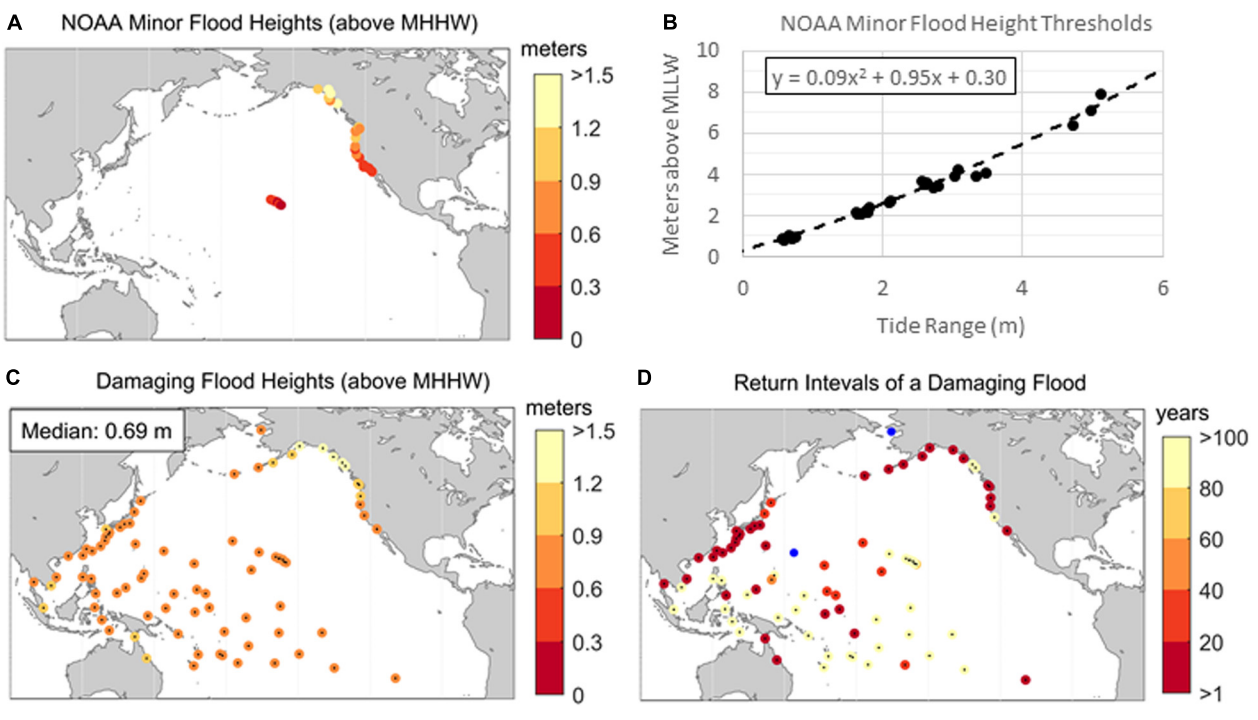

FIGURE 9 | (A) NOAA coastal thresholds for minor flooding along U.S. Pacific coastlines, **(B)** regression of NOAA minor flood threshold heights along Pacific coastlines shown in **(A)** with tide range, **(C)** proposed heights of a Pacific damaging flood level (minor flood threshold +0.3 m) at TGs in this study and **(D)** return intervals of the damaging flood level based upon the RFA LESLs. The two outlier TGs in blue have return intervals less than 0.1 years.

MHHW (**Figure 9C**) depending upon local tide range. As a whole, damaging floods have a median (not shown) return interval (**Figure 9D**) of about 20–25 years, which equates to about a 4–5% annual chance of occurring. Longer return intervals (i.e., >100 years) occur where extreme variability is less (where LESL probabilities tend to be bounded: **Figure 3**) and there is a spatial pattern resembling that of the heights of the 100-year LESLs (**Figure 5B**). At the two outlier TGs where non-tidal variability is relatively extreme (**Figure 4A**), damaging floods occur >10 times per year (blue dots in **Figure 9D**) and local vulnerability and impacts are likely not adequately defined by this threshold level. For context, a damaging flood in Honolulu is defined here as 0.66 m above MHHW (**Figure 9C**), which is 0.3 m higher than the regression fit to NOAA minor flood heights along Pacific coastlines (**Figure 9B**) that locally cause impacts (Habel et al., 2020), 0.03 m higher than its RFA 100-year LESL, and about 0.24 m higher than the 100-year LESL quantified using a single-gauge GPD analysis (**Figure 1A**).

Future Flood Risk

To quantify future risk of a damaging flood event, the median RSL projections of RCP4.5 developed under the IPCC SROCC (Oppenheimer et al., 2019), which equate to about a 0.5 m global rise by 2100 are used with our LESL probabilities. We note that the 1983–2001 reference frame is about the same as the RSL projection baseline (1986–2005). Under such a scenario and assuming flood defenses do not change, by 2055 (**Figure 10A**), the damaging flood level is (median value) only 0.44 m above MHHW and occurs about once/year (median value). This finding is supportive of the findings of Oppenheimer et al. (2019), though their metric to assess flood risk is their 100-year LESL, which is generally less than our RFA LESLs (e.g., as in Honolulu, **Figure 1A**). Damaging floods in 2055 are projected to occur less often along many island coastlines (dark blue dots in **Figure 10A**) where flood levels have contemporary return intervals closer to the 100-year level (**Figure 9D**). By 2100, the damaging flood level is only 0.14 m above MHHW (median value) and events occur more than 10 times/year in most locations (**Figure 10B**).

SUMMARY REMARKS

The risk of disruptive-to-destructive flooding (e.g., from "king tides" to tropical cyclone storm surge) is a serious concern within Pacific Basin coastal communities (Keener et al., 2018). Especially in light of rising seas, there is a need for data and mapped (e.g., **Figure 1**) information regarding current and future LESL probabilities along all populated coastlines—not just where TGs exist—for planning and preparedness purposes. Modeling and reanalysis of storm tides can help spatially granulate LESL probabilities, but their results often do not capture the response (e.g., surge/set up) peculiarities in some locations, especially those exposed to tropical cyclones. Even where TGs exist, measurements often are not long enough to capture historically significant events at a particular location or miss those completely that are of regional significance. Regional aggregation of TG data via the RFA process and its ability to support localization of RESL probabilities is a method that can help in both regards. Here, we suggest usage of short-term water level observations (either existing or future efforts) or tide-range information to augment estimates of LESL probabilities and flood risk for Pacific coastal communities without long-term TG observations. Ideally, output from high-resolution tide models would be employed to localize the RESLs and produce high-resolution LESLs estimates along coastlines.

A consequence of the RFA's data aggregation is that uncertainties of low-probability LESLs are better constrained

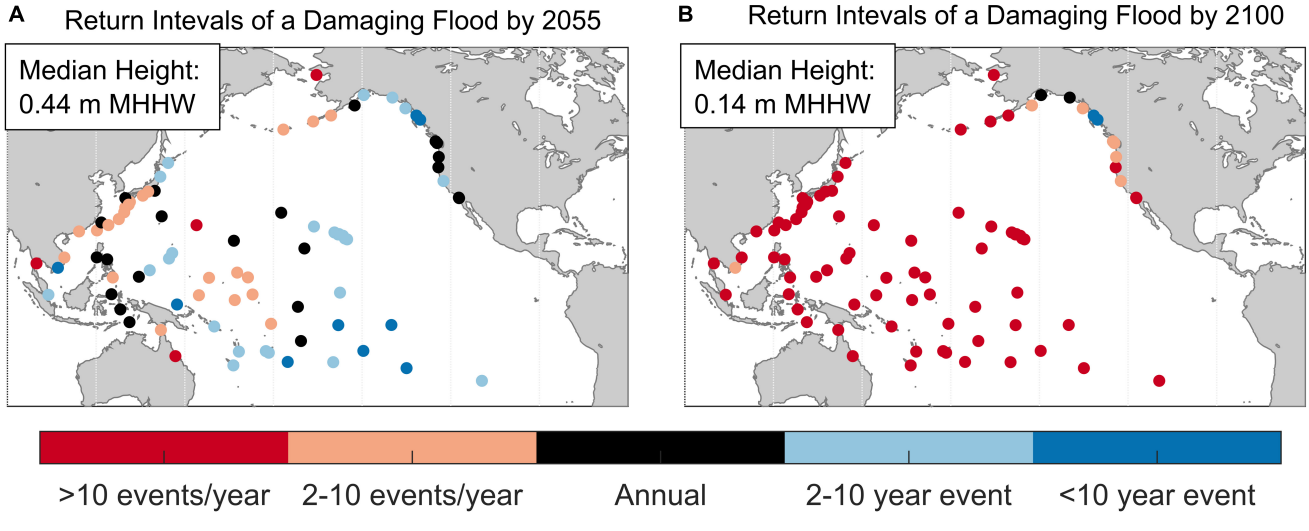

FIGURE 10 | Change in return intervals of a damaging flood in **(A)** 2055 and by **(B)** 2100 under median RSL projections of the SROCC RCP4.5.

(i.e., narrower 90% confidence interval) and their magnitudes are generally higher. This is particularly important from the perspective of an individual TG location where rare (outlier) events may be a (hidden) threat since occurrences are under-sampled. Using a RFA, the probability of occurrence for the same water level is more probable than recognized by conventional (single gauge or dynamical model) statistics. By extension, the risk of consequential flooding along Pacific coastlines is also likely under-estimated by these same conventional methods. There may be locations that due to topography and/or coastline orientation are afforded some level of natural protection and the RFA process produces a positive bias in LESL estimates.

Narrower confidence intervals of the RFA, though implying greater precision, do not necessarily imply greater accuracy. Accuracy measures such as reduced high or low bias of LESL probabilities from GPD fits (Wahl et al., 2017) and minimizing record-length biases and regionalizing risk through the RFA process, however, would suggest that the RFA results are more accurate than those from single-gauge analysis or a 40–50 year reanalysis from dynamical storm-tide modeling. In a practical sense, the storm surge associated with Hurricane Iniki in 1992, which caused record-setting water levels along the Hawaiian Island of Kauai (e.g., 0.96 m above MHHW at Nawiliwili: TG #58) offers a lens to evaluate the robustness of results. By chance, this hurricane narrowly missed Oahu Island and the nearby TG in Honolulu (TG #57) where water levels were more than a 0.5 m less (about 0.41 m above MHHW). From a probabilistic standpoint, Hurricane Iniki's water levels represent about a 5-year and a 100-year LESL at Honolulu (**Figure 1** and **Table 1**) and are about 0.1 and 0.25 m above the 500-year LESL 90% confidence interval at Nawiliwili from a RFA and both a single-gauge analysis/storm-tide reanalysis, respectively. Though this event and its surge are still an outlier, its occurrence is captured via the RFA process and transferred to all TGs across the Hawaiian Islands. We would argue that the results from the RFA process, if not more accurate, are a more sensible result for risk management and robust decision making under current and future LESLs (Hall et al., 2016).

LESL event probabilities themselves do not necessarily imply a certain severity of damage or impacts, although the 100-year event is a common proxy for severe or consequential flooding (Oppenheimer et al., 2019). Instead, a height threshold is proposed for a damaging flood to broadly establish infrastructure vulnerabilities along the Pacific Basin (**Figure 9C**). The height for a damaging flood varies according to the underlying relationship between tide range and NOAA coastal flood severity thresholds along the U.S. Pacific coastline used for weather impact forecasting and communication purposes. Along U.S. coastlines, NOAA moderate (damaging) floods pose a serious risk to life and property. As defined for the Pacific Basin region in this study, damaging floods currently have about a (median value) 20–25 year return interval (4–5% annual chance). However, that risk continues to grow with RSL rise. In fact, damaging floods are likely to occur on an annual basis in the next 35 years (2055) considering RCP4.5 projections at a majority of TGs if flood defenses or other adaptive measures are not enacted. They will become a common occurrence (>10 events/year) by 2100 largely in response to tidal forcing alone as the gap or freeboard between average high tide and damaging flood levels closes.

One flood risk threshold does not fit all circumstances and other locally important thresholds should be examined as appropriate. Likewise, no one model will definitively provide the "true probability" of rare and often-compounding events leading to damaging floods. As discussed here, a host of factors can affect estimates of rare-event probabilities (e.g., the 100-year LESL), but methodological differences may be indistinguishable relative to the uncertainties imposed by mapping for decision-support purposes (Kulp and Strauss, 2019)[3]. On the other hand, most extreme value model estimates converge and their uncertainties close at the higher probability portion of the distribution nearing the annual (1-year) event. In this context, and with knowledge of a realistic damaging flood height threshold, an examination of remaining freeboard can be made and future projections of its loss under RSL projections leading to chronic flooding can be performed with relative certainty. A strength of the RFA approach is the ability to spatially define LESLs across regions affording coastal communities with or without long-term TGs tools they need to assess current flood risk and make informed decisions in the face of RSL rise and an uncertain future.

DATA AVAILABILITY STATEMENT

Publicly available datasets were analyzed in this study. This data can be found at the University of Hawaii Sea Level Center (https://uhslc.soest.hawaii.edu/datainfo/).

AUTHOR CONTRIBUTIONS

WS, AG, and JO were responsible for data processing and analysis. WS wrote the manuscript, with contributions from AG, JO, and JM. All authors contributed to the article and approved the submitted version.

FUNDING

Support was provided from the US Department of Defense (DoD) Strategic Environmental Research and Development Program (SERDP) through work carried out under Project RC-2644.

SUPPLEMENTARY MATERIAL

The Supplementary Material for this article can be found online at: https://www.frontiersin.org/articles/10.3389/fmars.2020.581769/full#supplementary-material

[3]https://coast.noaa.gov/slr/#/layer/slr

REFERENCES

Bardet, L., Duluc, C. M., Rebour, V., and L'her, J. (2011). Regional frequency analysis of extreme storm surges along the French coast. *Nat. Hazards Earth Syst. Sci.* 11, 1627–1639. doi: 10.5194/nhess-11-1627-2011

Bernardara, P., Andreewsky, M., and Benoit, M. (2011). Application of regional frequency analysis to the estimation of extreme storm surges. *J. Geophys. Res.* 116:C02008. doi: 10.5194/nhess-11-1627-2011

Buchanan, M. K., Oppenheimer, M., and Kopp, R. E. (2017). Amplification of flood frequencies with local sea level rise and emerging flood regimes. *Environ. Res. Lett.* 12:064009. doi: 10.1088/1748-9326/aa6cb3

Calafat, F. M., and Marcos, M. (2020). Probabilistic reanalysis of storm surge extremes in Europe. *Proc. Natl. Acad. Sci. U.S.A.* 117, 1877–1883. doi: 10.1073/pnas.1913049117

Carreau, J., Naveau, P., and Neppel, L. (2017). Partitioning into hazard subregions for regional peaks-over-threshold modeling of heavy precipitation. *Water Resour. Res.* 53, 4407–4426. doi: 10.1002/2017wr020758

Church, J. A., Clark, U., Cazenave, A., Gregory, J. M., Jevrejeva, S., Levermann, A., et al. (2013). "Sea Level Change," in *Climate Change 2013: The Physical Science Basis. Contribution of Working Group I to the Fifth Assessment Report of the Intergovernmental Panel on Climate Change*, eds T. F. Stocker, D. Qin, G.-K. Plattner, M. Tignor, S. K. Allen, J. Boschung, et al. (Cambridge: Cambridge University Press), 1137–1216.

Coles, S., and Dixon, M. (1999). Likelihood-based inference for extreme value models. *Extremes* 2, 5–23. doi: 10.1023/A:1009905222644

Coles, S. G. (2001). *An Introduction to Statistical Modeling of Extreme Values*. London: Springer, 208.

Dalrymple, T. (1960). *Flood Frequency Analysis. U.S. Geological Survey Water-Supply Paper 1543-A*. Washington, D.C: U.S. Government Printing Office.

Frau, R., Andreewsky, M., and Bernardara, P. (2018). The use of historical information for regional frequency analysis of extreme skew surge. *Nat. Hazards Earth Syst. Sci.* 18, 949–962. doi: 10.5194/nhess-18-949-2018

Frederikse, T., Buchanan, M. K., Lambert, E., Kopp, R. E., Oppenheimer, M., Rasmussen, D. J., et al. (2020). Antarctic Ice Sheet and emission scenario controls on 21st-century extreme sea-level changes. *Nat. Commun.* 11, 1–11. doi: 10.1029/ar077p0001

Ghanbari, M., Arabi, M., Obeysekera, J., and Sweet, W. (2019). A coherent statistical model for coastal flood frequency analysis under nonstationary sea level conditions. *Earth's Future* 7, 162–177. doi: 10.1029/2018ef001089

Habel, S., Fletcher, C. H., Anderson, T. R., and Thompson, P. R. (2020). Sea-Level Rise induced Multi-Mechanism flooding and contribution to Urban infrastructure failure. *Sci. Rep.* 10, 1–12.

Haigh, I. D., MacPherson, L. R., Mason, M. S., Wijeratne, E. M. S., Pattiaratchi, C. B., Crompton, R. P., et al. (2014a). Estimating present day extreme water level exceedance probabilities around the coastline of Australia: tropical cyclone-induced storm surges. *Clim. Dyn.* 42, 139–157. doi: 10.1007/s00382-012-1653-0

Haigh, I. D., Wijeratne, E. M. S., MacPherson, L. R., Pattiaratchi, C. B., Mason, M. S., Crompton, R. P., et al. (2014b). Estimating present day extreme water level exceedance probabilities around the coastline of Australia: tides, extra-tropical storm surges and mean sea level. *Clim. Dyn.* 42, 121–138. doi: 10.1007/s00382-012-1652-1

Hall, J. A., Gill, S., Obeysekera, J., Sweet, W., Knuuti, K., and Marburger, J. (2016). *Regional Sea Level Scenarios for Coastal Risk Management: Managing the Uncertainty of Future Sea Level Change and Extreme Water Levels for Department of Defense Coastal Sites Worldwide*. Virginia: U.S. Department of Defense, 224.

Hall, J. A., Weaver, C. P., Obeysekera, J., Crowell, M., Horton, R. M., Kopp, R. E., et al. (2019). Rising sea levels: helping decision-makers confront the inevitable. *Coast. Manag.* 47, 127–150. doi: 10.1080/08920753.2019.1551012

Hamlington, B. D., Fasullo, J. T., Nerem, R. S., Kim, K. Y., and Landerer, F. W. (2019). Uncovering the pattern of forced sea level rise in the satellite altimeter record. *Geophys. Res. Lett.* 46, 4844–4853. doi: 10.1029/2018gl081386

Hoegh-Guldberg, O., Jacob, D., Taylor, M., Bindi, M., Brown, S., Camilloni, I., et al. (2018).*Impacts of 1.5°C Global Warming on Natural and Human Systems. Global Warming of 1.5ř C°C.* An IPCC Special Report.

Hosking, J. R. M. (2012). Towards statistical modeling of tsunami occurrence with regional frequency analysis. *J. Math Ind.* 4, 41–48.

Hosking, J. R. M., and Wallis, J. R. (1997). *Regional Frequency Analysis: An Approach Based on L-Moments*. Cambridge: Cambridge Univ. Press.

Hunter, J. (2012). A Simple Technique for Estimating an Allowance for Uncertain Sea-Level Rise. *Clim. Change* 113, 239–252. doi: 10.1007/s10584-011-0332-1

IPCC (2014). "Climate change 2014: synthesis report," in *Contribution of Working Groups I, II and III to the Fifth Assessment Report of the Intergovernmental Panel on Climate Change*, eds Core Writing Team, R. K. Pachauri, and L. A. Meyer (Geneva: IPCC), 151.

Keener, V., Helweg, D., Asam, S., Balwani, S., Burkett, M., Fletcher, C., et al. (2018). "Hawai'i and U.S.-affiliated pacific Islands," in *Impacts, Risks, and Adaptation in the United States: Fourth National Climate Assessment*, Vol. II, eds D. R. Reidmiller, C. W. Avery, D. R. Easterling, K. E. Kunkel, K. L. M. Lewis, T. K. Maycock, et al. (Washington, DC: U.S. Global Change Research Program), 1242–1308. doi: 10.7930/NCA4.2018.CH27

Kopp, R. E., Gilmore, E. A., Little, C. M., Lorenzo-Trueba, J., Ramenzoni, V. C., and Sweet, W. V. (2019). Usable science for managing the risks of sea-level rise. *Earth's Future* 7, 1235–1269. doi: 10.1029/2018ef001145

Kopp, R. E., Hay, C. C., Little, C. M., and Mitrovica, J. X. (2015). Geographic variability of sea-level change. *Curr. Clim. Change Rep.* 1, 192–204. doi: 10.1007/s40641-015-0015-5

Kopp, R. E., Horton, R. M., Little, C. M., Mitrovica, J. X., Oppenheimer, M., Rasmussen, D. J., et al. (2014). Probabilistic 21st and 22nd century sea-level projections at a global network of tide- gauge sites. *Earth's Future* 2, 383–406. doi: 10.1002/2014ef000239

Kulp, S. A., and Strauss, B. H. (2019). New elevation data triple estimates of global vulnerability to sea-level rise and coastal flooding. *Nat. Commun.* 10, 1–12.

Le Cozannet, G., Nicholls, R. J., Hinkel, J., Sweet, W. V., McInnes, K. L., Van de Wal, R. S., et al. (2017). Sea level change and coastal climate services: the way forward. *J. Mar. Sci. Eng.* 5:49. doi: 10.3390/jmse5040049

Lin, N., Emanuel, K., Oppenheimer, M., and Vanmarcke, E. (2012). Physically based assessment of hurricane surge threat under climate change. *Nat. Clim. Change* 2, 462–467. doi: 10.1038/Nclimate1389

Lin, N., Marsooli, R., and Colle, B. (2019). Storm surge return levels induced by the mid-to-late-twenty-first-century extratropical cyclones in the Northeastern United States. *Clim. Change* 154, 143–158. doi: 10.1007/s10584-019-02431-8

Lobeto, H., Menendez, M., and Losada, I. J. (2018). Toward a methodology for estimating coastal extreme sea levels from satellite altimetry. *J. Geophys. Res.* 123, 8284–8298. doi: 10.1029/2018jc014487

Menéndez, M., and Woodworth, P. L. (2010). Changes in extreme high water levels based on a quasi-global tide-gauge data set. *J. Geophys. Res.* 115:C10011. doi: 10.1029/2009JC005997

Merrifield, M. A., Genz, A. S., Kontoes, C. P., and Marra, J. J. (2013). Annual maximum water levels from tide gauges: contributing factors and geographic patterns. *J. Geophys. Res. Oceans* 118, 2535–2546. doi: 10.1002/jgrc.20173

Michele, C. D., and Rosso, R. (2001). Uncertainty assessment of regionalized flood frequency estimates. *J. Hydrol. Eng.* 6, 453–459. doi: 10.1061/(asce)1084-0699(2001)6:6(453)

Moftakhari, H. R., AghaKouchak, A., Sanders, B. F., and Matthew, R. A. (2017). Cumulative hazard: the case of nuisance flooding. *Earth's Future* 5, 214–223. doi: 10.1002/2016ef000494

Mood, A., Graybill, F. A., and Boes, D. C. (1974). *Introduction to the Theory of Statistics*. New York, NY: McGraw-Hill.

Muis, S., Apecechea, M. I., Dullaart, J., de Lima Rego, J., Madsen, K. S., Su, J., et al. (2020). A High-resolution global dataset of extreme sea levels, tides, and storm surges, including future projections. *Front. Mar. Sci.* 7:263. doi: 10.3389/fmars.2020.00263

Muis, S., Verlaan, M., Winsemius, H. C., Aerts, J. C., and Ward, P. J. (2016). A global reanalysis of storm surges and extreme sea levels. *Nat. Commun.* 7, 1–12.

Nadal-Caraballo, N. C., Melby, J. A., Gonzalez, V. M., and Cox, A. T. (2015). *Coastal storm hazards from Virginia to Maine (No. ERDC/CHL-TR-15-5)*. Vicksburg, MS: Engineer research and development center.

NOAA (2003). *Computational Techniques for Tidal Datums Handbook. NOAA Special Publication NOS CO-OPS 2*. Silver Spring, MA: U.S. Department of Commerce.

Oppenheimer, M., Glavovic, B. C., Hinkel, J., van de Wal, R., Magnan, A. K., Abd-Elgawad, A., et al. (2019). "Sea level rise and implications for low-lying islands,

coasts and communities," in *IPCC Special Report on the Ocean and Cryosphere in a Changing Climate*, eds H.-O. Pörtner, D. C. Roberts, V. Masson-Delmotte, P. Zhai, M. Tignor, E. Poloczanska, et al.

Perica, S., Pavlovic, S., St Laurent, M., Trypaluk, C., Unruh, D., and Wilhite, O. (2018). *Precipitation-Frequency Atlas of the United States. Texas: Version 2.0, 11*. Silver Spring, MD: National Oceanic and Atmospheric Administration, National Weather Service.

Rasmussen, D. J., Bittermann, K., Buchanan, M. K., Kulp, S., Strauss, B. H., Kopp, R. E., et al. (2018). Extreme sea level implications of 1.5 C, 2.0 C, and 2.5 C temperature stabilization targets in the 21st and 22nd centuries. *Environ. Res. Lett.* 13:034040. doi: 10.1088/1748-9326/aaac87

Roth, M., Buishand, T. A., Jongbloed, G., Klein Tank, A. M. G., and Van Zanten, J. H. (2012). A regional peaks-over-threshold model in a nonstationary climate. *Water Resour. Res.* 48:W11533.

Rueda, A., Vitousek, S., Camus, P., Tomás, A., Espejo, A., Losada, I. J., et al. (2017). A global classification of coastal flood hazard climates associated with large-scale oceanographic forcing. *Sci. Rep.* 7, 1–8.

Smith, A., Sampson, C., and Bates, P. (2015). Regional flood frequency analysis at the global scale. *Water Resour. Res.* 51, 539–553. doi: 10.1002/2014WR015814

Sweet, W. V., Dusek, G., Carbin, G., Marra, J. J., Marcy, D., and Simon, S. (2020). *2019 State of US High Tide Flooding With a 2020 Outlook. NOAA Tech. Rep. NOS CO-OPS.*, Vol. 92. Silver Spring, MD: National Oceanic and Atmospheric Administration, 17.

Sweet, W., Dusek, G., Obeysekera, J., and Marra, J. (2018). *Patterns and Projections of High Tide Flooding Along the U.S. Coastline using a Common Impact Threshold. NOAA Technical Report NOS CO-OPS*, Vol. 86. Silver Spring, MD: National Oceanic and Atmospheric Administration.

Sweet, W. V., and Park, J. (2014). From the extreme and the mean: acceleration and tipping point of coastal inundation from sea level rise. *Earth Futures* 2, 579–600. doi: 10.1002/2014EF000272

Taherkhani, M., Vitousek, S., Barnard, P. L., Frazer, N., Anderson, T. R., and Fletcher, C. H. (2020). Sea-level rise exponentially increases coastal flood frequency. *Sci. Rep.* 10, 1–17.

Tebaldi, C., Strauss, B. H., and Zervas, C. E. (2012). Modelling sea level rise impacts on storm surges along US coasts. *Environ. Res. Lett.* 7:014032. doi: 10.1088/1748-9326/7/1/014032

Thompson, P. R., Widlansky, M. J., Leuliette, E., Sweet, W., Chambers, D. P., Hamlington, B. D., et al. (2019). Sea level variability and change [in "State of the Climate in 2018"]. *Bull. Amer. Meteor. Soc.* 100, S181–S185. doi: 10.1175/2019BAMSStateoftheClimate.1

Vitousek, S., Barnard, P. L., Fletcher, C. H., Frazer, N., Erikson, L., and Storlazzi, C. D. (2017). Doubling of coastal flooding frequency within decades due to sea-level rise. *Sci. Rep.* 7, 1–9.

Vousdoukas, M. I., Mentaschi, L., Voukouvalas, E., Verlaan, M., Jevrejeva, S., Jackson, L. P., et al. (2018). Global probabilistic projections of extreme sea levels show intensification of coastal flood hazard. *Nat. Commun.* 9, 1–12.

Wahl, T., Haigh, I. D., Nicholls, R. J., Arns, A., Dangendorf, S., Hinkel, J., et al. (2017). Understanding extreme sea levels for broad-scale coastal impact and adaptation analysis. *Nat. Commun.* 8, 1–12. doi: 10.2112/jcoastres-d-12-00127.1

Weiss, J., and Bernardara, P. (2013). Comparison of local indices for regional frequency analysis with an application to extreme skew surges. *Water Resour. Res.* 49, 2940–2951. doi: 10.1002/wrcr.20225

Weiss, J., Bernardara, P., and Benoit, M. (2014). Formation of homogeneous regions for regional frequency analysis of extreme significant wave heights. *J. Geophys. Res.* 119, 2906–2922. doi: 10.1002/2013jc009668

Zervas, C. (2013). *NOAA Technical Report NOS Co-OPS 067: Extreme Water Levels of the United States 1893–2010*. Silver Spring, MD: National Ocean Service.

Conflict of Interest: The authors declare that the research was conducted in the absence of any commercial or financial relationships that could be construed as a potential conflict of interest.

Copyright © 2020 Sweet, Genz, Obeysekera and Marra. This is an open-access article distributed under the terms of the Creative Commons Attribution License (CC BY). The use, distribution or reproduction in other forums is permitted, provided the original author(s) and the copyright owner(s) are credited and that the original publication in this journal is cited, in accordance with accepted academic practice. No use, distribution or reproduction is permitted which does not comply with these terms.

frontiers in Marine Science

BRIEF RESEARCH REPORT
published: 22 March 2021
doi: 10.3389/fmars.2021.631757

Impact Assessment and Management Challenges of Key Rural Human Health Infrastructure Under Sea Level Rise

Molly Mitchell, Robert E. Isdell, Julie Herman and Christine Tombleson*

Virginia Institute of Marine Science, William & Mary, Gloucester Point, VA, United States

Accelerating sea level rise in Virginia, United States, will significantly increase the flooding threat to low-lying roads, residences, and critical infrastructure as well as raise the water table, allowing saltwater intrusion into well water and threatening the function of septic fields. Although most of the adaptation work in Virginia has focused on urban economic centers, the majority of the coastline is rural and faces different threats and opportunities to address them compared to urban areas due to their reduced economic assets and their reliance on private infrastructure. In this case study, we assess the potential for geospatially quantifying impact to septic systems and adjacent water ways due to sea level rise. The case study found that the data necessary to reliably quantify these impacts on a state-wide scale are lacking and collection of that information needs to be prioritized given the potential for extensive sea level impacts.

Keywords: sea level rise, human health, risk assessment, adaptation, climate change, septic, resilience

OPEN ACCESS

Edited by:
Robert James Nicholls, University of East Anglia, United Kingdom

Reviewed by:
Helena Granja, University of Minho, Portugal
Rodolfo Silva, National Autonomous University of Mexico, Mexico

****Correspondence:***
Molly Mitchell
molly@vims.edu

Specialty section:
This article was submitted to Coastal Ocean Processes, a section of the journal Frontiers in Marine Science

Received: *20 November 2020*
Accepted: *04 March 2021*
Published: *22 March 2021*

Citation:
Mitchell M, Isdell RE, Herman J and Tombleson C (2021) Impact Assessment and Management Challenges of Key Rural Human Health Infrastructure Under Sea Level Rise. Front. Mar. Sci. 8:631757. doi: 10.3389/fmars.2021.631757

INTRODUCTION

Among long-term tide gage records, Virginia has one of the highest rates of sea level rise of any station on the East Coast, making the entire coastal area vulnerable to an increasing risk of "sunny day flooding" (flooding associated with high astronomic tides, rather than storm surge) and storm flooding. The shoreline of the mid-Atlantic coast of the United States is highly vulnerable to the effects of relative sea level rise (RSLR) due to changes in global sea level combined with regional and local land subsidence (Boon, 2012; Eggleston and Pope, 2013; Campbell and Wang, 2020) and shifts in the Gulf Stream current location and speed (Ezer, 2013). Sea level is rising in Norfolk, VA at a rate of 5.1 mm/year (compared to global sea level rise rates ∼3.2 mm/year; Church and White, 2011; Ezer, 2013) and that rate is accelerating at 0.119 mm/year^2 (Boon et al., 2018). This rate of acceleration has led to a 577% increase in flooding time in downtown Norfolk since the 1970s (Ezer and Atkinson, 2014). With these high rates of RSLR, and with evidence that those rates are accelerating (Sallenger et al., 2012; Boon and Mitchell, 2015; Boon et al., 2018), inundation is becoming an increasing concern both to ecological systems and built infrastructure. Currently, the impacts of storm-induced flooding added to long term RSLR on the natural landscape, local population, and built infrastructure are readily observable during nor'easters, hurricanes and even

nuisance storms (Miller et al., 2013; Mitchell et al., 2013). Sea level rise will significantly increase the flooding threat to low-lying roads, residences, and critical infrastructure. It will also raise the water table, allowing saltwater intrusion into well water and threatening the function of septic fields. A study in Rhode Island found that groundwater levels were increasing 14–17 mm/year (Cox et al., 2019), which is far faster than sea level rise rates in that region (Boon et al., 2018).

In rural areas, an increased groundwater table will interfere with the function of the ubiquitous septic systems, causing serious damage to public health, water quality (WQ), and local fisheries (e.g., Katz et al., 2011; Macintosh et al., 2011; Withers et al., 2014). Failing septic systems result in an increased loading of bacteria, viruses, nitrogen and possibly phosphorus to adjacent waterways and are believed to represent about 6% of the total nitrogen load from the Chesapeake watershed (Bay Watershed Model 2009 Scenario, Chesapeake Bay TMDL). In small waterbodies, the local impact can be much higher. For example, in Buttermilk Bay, MA, United States 74% of the nitrogen was attributed to septic systems (Horsley Witten Hegeman Inc, 1991). Although, it has been suggested that a properly functioning septic system may remove phosphorus more effectively than a sewage treatment plant and might be a better option in areas where phosphorus contamination is an issue, and the water table is sufficiently low (Robertson et al., 2019). Where septic systems are at risk from high water tables, accelerating rates of sea level rise can cause impacts to increase dramatically. For example, in Miami (which currently has a lower rate of sea level rise than Virginia; Boon and Mitchell, 2015), approximately 1,000 properties with septic systems are already impacted by high water tables and they expect over 67,000 systems to be periodically compromised due to storms by 2040 (Miami Dade County, 2018). With accelerating sea level rise, failing septic systems will become a significant stressor to individual property owners, and may force them to retreat from the coastline, disrupting communities and creating significant economic losses both to the relocating population and the deserted localities.

Much consideration has been given to the impacts of sea level rise on urban areas and the significant costs associated with resilience efforts. However, globally, the majority of coastal populations live in rural areas, but have received limited attention (Small and Nicholls, 2003). To enhance resilience in these rural regions, we first need to understand the geospatial distribution of vulnerable septic systems and how those vulnerabilities may change overtime. Available data on the locations of existing septic systems are limited, due to the historical use of paper records. Only about 10 years of digital data currently exist in the Virginia Department of Health database on locations of installed septic systems.

CONTEXT

This study focused on rural areas in Virginia, United States (**Figure 1**). The Chesapeake Bay is located on the mid-Atlantic coast in Virginia (south) and Maryland (north) and is the largest estuary in the United States. There are approximately 11,500 kilometers of tidal shoreline in the Virginia portion of Chesapeake Bay. Coastal Virginia has 44 localities, with some urban centers, but a predominance of rural land use (residential, forested, and agriculture). Topography is low relief along much of the shoreline, but there are stretches of higher bluffs up the Bay tributaries.

The coastal region is underlain by marine sediments that are unconsolidated but well compacted. Soil types range from well-drained to poorly drained and primarily sand to primarily clay, depending upon location. In low-lying areas, the water table is relatively high.

METHODS

Analysis of Septic Failures

The first step of the case study analysis was to statistically analyze the geospatial distribution of septic system repair permits to find underlying patterns that could help inform decision-making using the Emerging Hot Spot Analysis tool in ArcGIS (ESRI, 2020). This tool looks at patterns across both spatial and temporal scales simultaneously. It can identify continuous hot spots (where there are constant and high numbers of repair permits) and emerging hot spots (locations representing new, intensifying, or diminishing clusters of repair permits). A full description of all types of hot spot classifications is available from ESRI[1]. Repair permit data for the years 2008–2018 were used, with a single temporal scale of one year. Data were aggregated within grid cells at a spatial scale of 1 km. This spatial scale was selected as an appropriate management scale because the grids typically contained >1 house, so could show clusters, but were small enough for targeted management actions. Of the 19,753 grid cells that contained at least 1 house, the median number of houses was 17 (95% of the cells had between 1 and 816 addresses, 7.8% of the cells had exactly 1 house/address).

The analysis was performed on both (1) the total number of repair permits within a cell and (2) the number of repair permits standardized to the total number of houses. These two approaches answer slightly different questions. The first approach locates the areas with the most repair permits recorded and tends to identify areas with a relatively high density of housing. Targeting these areas for mitigation measures would reduce overall issues under current conditions. The second approach highlights areas where there are unusually high failures relative to the housing density. It helps identify where failures are likely due to aging infrastructure, high groundwater tables, or other factors. Additional analyses to identify linkages between septic system failures and underlying geologic conditions were attempted using a maximum entropy machine learning approach implemented in the MaxEnt software (Phillips et al., 2021). Geologic data was obtained from the United States Department of Agriculture's National Resources Conservation Service Soil Service Geographic (SSURGO) soils database (Soil Survey Staff et al., 2012) and included features such as composition (percentages of sand,

[1]https://bit.ly/EHSA_ESRI

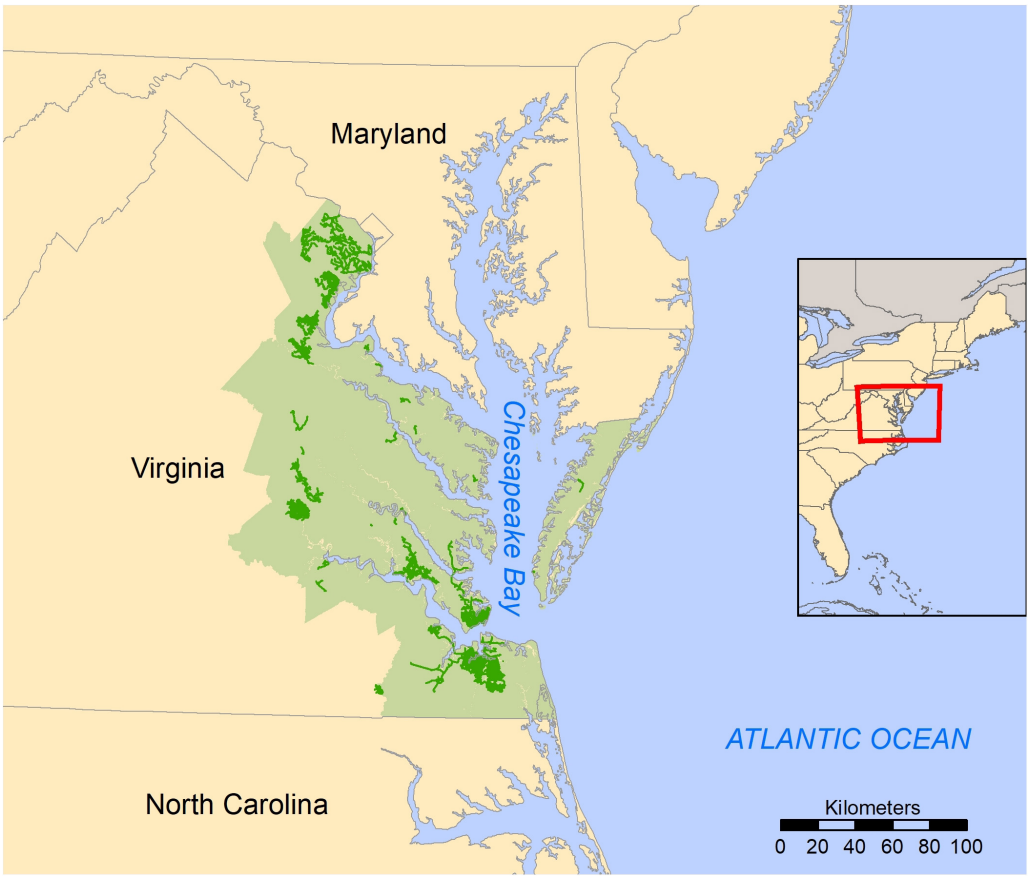

FIGURE 1 | Map of the study area, Virginia United States. Urban areas are designated by the sewer lines (shown in dark green) and were excluded from the study. All light green areas were included in the study.

silt, and clay), septic suitability, sediment saturation, and depth to water table. All factors were hypothesized to have a potential impact on the drainage efficiency and functionality of a septic system. Study-area-wide application of this analysis was abandoned after initial tests in subsets of the study area resulted in very poor predictive ability, with reduced predictive power as the size of the area under consideration increased. This was likely a result of the myriad and undocumented reasons for septic failure, chief among them being human error (e.g., putting things down their drains that they should not), combined with fairly coarse spatial resolutions in both the geologic and septic system data causing too much noise for the model to sort through and identify any clear correlations among septic failures and the underlying geology.

The results of analysis 1 (Tidewater hot spot results) suggest three basic issues are occurring. First, there are several areas where hotspots of septic failures occur annually (continuous hot spots). These may be areas with high groundwater tables that have low suitability for septic systems. Second, there are also several areas that have been hot spots in some years, but not others (sporadic hot spots). This may be due to high annual water tables associated with heavy rain or sea level variability or periodic episodes of aging septic systems. These areas are good targets for monitoring, particularly in heavy precipitation years and under sea level rise. Last, there are emerging hot spots, areas that should be investigated to see if conditions have changed or if systems are beginning to reach the end of their lifespan. Overall, 1,148 1-km grid cells were identified as hot spots of some kind. Hot spots were identified in most of the Tidewater localities where sewer is limited or unavailable and were prevalent in the areas surrounding the City of Richmond and in Gloucester County (**Supplementary Figure 1**).

The results of analysis two (high density failure areas) highlight 1 km grid cells where >25% of the houses in the grid (minimum of five houses within the cell) had repair permits during the time of the analysis. High density failures were less common than hot spots, with a total of 72 grid cells. However, these areas are frequently located near water bodies or at the tops of creeks, where they have the potential to impact WQ in the immediate area. This proximity to the water is the only apparent pattern in the geographic dispersion of the high-density failure grids. This might suggest a connection between high groundwater tables and higher than expected need for repairs. This hypothesis would need to be tested specifically with data looking at groundwater tables in areas of high-density failures relative to surrounding areas to validate the connection.

Connection to Human Health and Fishery Safety

To highlight areas where septic failures might be impacting human health and fisheries safety, or where repairs to septic systems might improve local WQ, we examined the results from the hot spot analysis in conjunction with WQ data from Virginia Department of Health's Division of Shellfish Safety.

Shellfish harvesting closure criteria were determined using WQ data and standard criteria for closure. This approach was used because it calculates a threshold of WQ at which shellfish in these waters are considered unsafe for human consumption. These levels would also indicate the potential for other environmental and human health issues. Two different metrics were calculated: the number of years in a 9-year period when the criteria for closure were met, and the annual trend in colony forming units (CFUs) of *Escherichia coli* in areas where the criteria for closure were met.

Years of closure were calculated using the Division of Shellfish Safety closure criteria where if the geometric mean of the previous 30 WQ measurements (approximately monthly) exceeds 14.0 CFUs or the 90th percentile exceeds 31.5 CFUs, the station and its surrounding waters are closed for shellfish harvest. The analysis was run on an annual interval from March 2012 to March 2020. After each run, the WQ station was classified as open or closed, and the number of all years in which the station was classified as closed were summed. Of the 2,254 stations, 2,121 stations had enough data to run the analysis. The number of stations that were closed for *N out of nine* possible years are provided in **Table 1**.

The annual trend in CFUs looked at the trend in WQ at a station over a 9-year period. Based on the calculated geometric mean CFU values for each station, we ran a simple linear regression in R [function lm(), R Development Core Team, 2019] for each station through time (2012–2020) to see if there was a significant ($\alpha = 0.05$) positive trend in the number of CFUs. Among the 2,121 stations, 1,370 had significant positive trends (increasing annual CFUs) and 22 had significant negative trends (decreasing annual CFUs). Stations which were both classified as closed in 2020 and had significant positive trends in CFUs ($n = 471$; subset in **Figure 2**) were selected for a geospatial overlap analysis (intersect in ArcGIS Pro). Results of the analysis identifies only one incident where a low WQ region overlapped directly with a septic hot spot in Tidewater Virginia. This emphasizes the difficulty in trying to correlate septic repair permits and potential environmental impacts. Neither dataset was collected specifically for the purpose of making these types of connections and therefore any correlation should be viewed with extreme caution.

TABLE 1 | The 2,121 water quality monitoring stations from the Virginia Division of Shellfish Safety were classified as closed or open for shellfish harvesting each year from 2012 to 2020 and the total number of years they were closed were summed.

Years closed	Stations
0	1087
1	138
2	103
3	80
4	70
5	83
6	60
7	59
8	75
9	366

Consideration of Future Conditions

As sea level rises, so too will the groundwater. As groundwater is typically at or above sea level unless there is significant withdrawal, increases in groundwater table elevation as a result of sea level rise are likely to negatively impact the efficiency of septic drain fields long before direct inundation. Since there are no large spatial models of groundwater in Virginia nor its potential to change with sea level rise, we instead mapped the areas whose elevations are less than three feet (∼1 m) above mean sea level (MSL) at the current time and under projected sea level rise (Sweet et al., 2017, Intermediate Scenario). The Intermediate Scenario was chosen because it most closely aligns with historic tide-gage data analysis and projections for coastal Virginia (Boon et al., 2018). Elevations used were:

$$\text{Current} = 0\text{ft NAVD88} + 3\text{ft}$$

$$2040 = 1.4\text{ft NAVD88} + 3\text{ft}$$

$$2080 = 3.16\text{ ft NAVD88} + 3\text{ft}$$

Hot spots were geographically analyzed for overlap with MSL + 3 feet in the current time frame to identify areas where hot spots might be driven by high water tables.

Results (**Table 2**) show that between a quarter and a third of Consecutive and Sporadic hot spots are located in areas with potentially high-water tables. Interestingly, a similar number of diminishing hot spots are also located in these areas, making it difficult to draw any firm conclusions about the connection of groundwater to the different types of hot spots.

DISCUSSION

The key limitation in assessing the vulnerability of septic systems to failure was a lack of data collected specifically for this purpose. Important information, such as system age, siting, design and maintenance history were essentially unknown, an issue not limited to Virginia or the United States (Withers et al., 2012, 2014). Most information that exists on septic systems is collected for permitting or regulatory purposes. For this case study, we utilized a septic repair permit database from the Virginia Department of Health. This dataset allowed us to analyze clusters of failures; however, it was created for regulatory purposes and conclusions drawn from it require some critical caveats:

- The data do not necessarily represent the total number of septic failures because there may be currently unidentified issues. This means that repair permits could underestimate the total problem. This also could lead to geographic

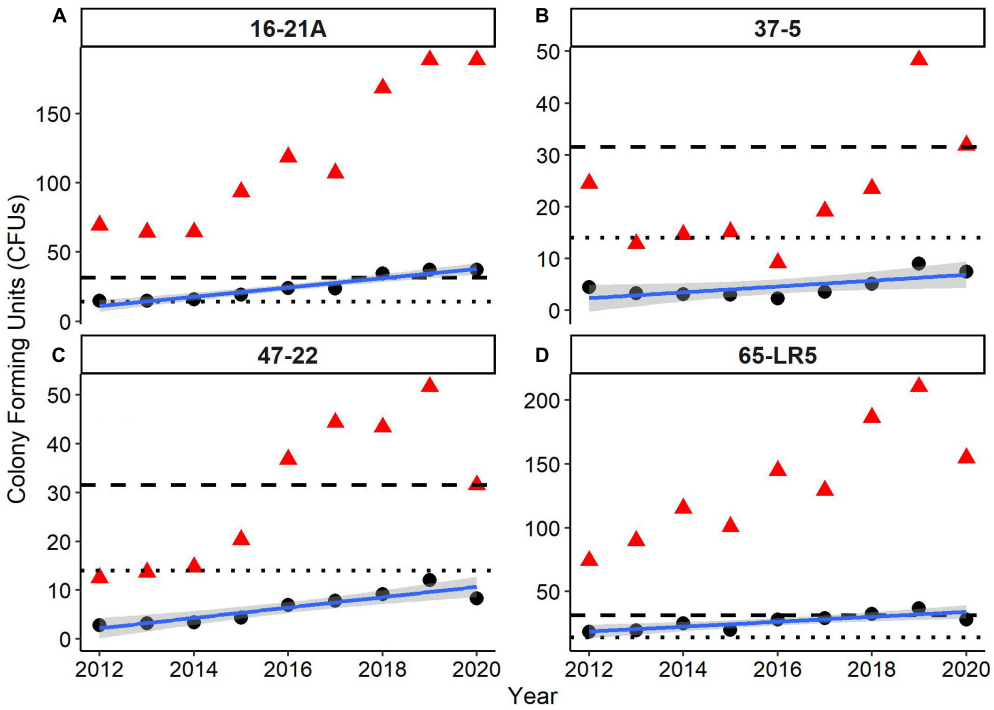

FIGURE 2 | The number of *Escherichia coli* colony forming units (CFUs) for four water quality monitoring sites spread throughout the Chesapeake Bay from 2012 to 2020. The annual geometric mean (black circle) and its trend line (solid blue line) along with the estimated 90th percentile (red triangle) are provided with horizontal lines representing the closure thresholds for an annual geometric mean (dotted; 14 CFUs) and the 90th percentile (dashed; 31.5 CFUs). Station names are provided above each plot. Each of the displayed stations had significant ($\alpha = 0.05$) positive trends and were closed in 2020. Panels **(A)** and **(D)** exceeded both thresholds, while panels **(B)** and **(C)** only exceeded the 90th percentile.

discrepancies in spatial patterns of failures if socio-economic factors affect the likelihood that a septic issue is identified and repaired.

- The data does not necessarily represent the total number of septic failures because it does not record the degree of severity of the problem resulting in the repair. This could mean that the repair permits are equally counting minor issues and severe drain field failures, which means the data could overestimate the total problem. This leads to an additional caveat, that the repair permits do not distinguish the reason for the repair. Areas with high numbers of septic failures could be due to all of the systems aging simultaneously or could be due to rising groundwater tables. In areas in close proximity to the waterfront, we believe it is reasonable to assume that these clusters of failures could be related to groundwater tables, and that these areas should be targets for environmental monitoring.
- Repair permits are attached to street addresses. On large parcels, the actual drain field can be some distance from the spatially located street address. Therefore, potential explanatory variables (such as the underlying soil conditions, groundwater levels, and proximity to waterways) cannot be extracted from other data sets and connected with repair permits with a high level of confidence. Broad generalizations can be made but should be used cautiously.
- Dates on repair permits reflect an ambiguous time between when the issue occurred and when the issue was fixed. Temporal connections between septic issues and environmental impacts (such as adjacent WQ) cannot be made with a high level of confidence due to the time lag between contamination and potential for detection (Katz et al., 2011, Withers et al., 2012). Broad generalizations can be made but should be used cautiously.
- The age of septic systems is known to be a factor in septic system failure. Construction permits for systems often occur prior to house or neighborhood construction and use tax parcel and lot numbers for permit location rather than addresses. Although this information can be used to locate the parcel the septic is on, it must be done individually, and a researcher cannot take advantage of the automated geocoding processes. Locating these sites individually is time-intensive; therefore, incorporating septic system age into an analysis would be very expensive. Detailed information about the hydraulic networks, such as the vertical distance of the septic tanks above the groundwater table at the time of installation, is not always known. This measure is one of the key variables affecting nutrient and pathogen contamination of groundwater, and by extension, adjacent waterways (Harris, 1995). Newly saturated septic drain fields, associated with sea level rise, have been shown to increase fecal coliform bacteria in

TABLE 2 | Hot spots potentially related to high groundwater table.

Pattern	Total number	Number in MSL + 3ft	% in MSL + 3ft
Consecutive hot spot	265	78	29.43
Diminishing hot spot	54	13	24.07
Historical hot spot	83	2	9.38
Intensifying hot spot	32	3	9.38
Persistent hot spot	172	23	13.37
Sporadic hot spot	542	146	26.94
Overall	1148	265	23.08

output waters (Cooper et al., 2016) and could result in decreasing creek WQ over time. Coastal properties where septic tanks only met minimum standards (3ft above the water table) at the time of installation have a higher probability of impacts from rising groundwater than tanks installed with more vertical space.

Although is it critical to understand the impacts of future sea level rise and increased rainfall intensity, duration, and frequency on septic system failure, the caveats listed above preclude the use of predictive modeling in the region of this case study. In addition, the regulatory structure of both the septic repair database and the shellfish closure database limit analyses to correlative measures, restricting conclusions that can be drawn from the analyses. Previous studies have shown that septic systems cause bacterial contamination of groundwater (e.g., Stewart and Reneau, 1981; Arnade, 1999), but that definitively connecting bacterial concentrations in estuarine creeks to failing septic systems on a broad scale can be difficult (Cahoon et al., 2006) perhaps in part due to tidal flushing or the prevalence of tidal marshes (Giordano et al., 2011). We suspect the limited existence of data necessary to connect septic systems with human health risks is a wide-spread issue throughout coastal areas. We recommend concerted efforts to build datasets specific to understanding changes in rural infrastructure and connections to the critical issues such as human and ecological health to improve the resiliency of rural areas under sea level rise.

Understanding the geographical scope and the potential financial resources necessary to address rural septic issues under accelerating sea level rise will be critical to finding a solution. **Supplementary Figure 2** shows a DASIR (Driver-Activity-State-Impact-Responses) framework for coastal septic issues; these frameworks have been found to be a useful approach to analyze and explain human-environmental relationships and help lead to management actions (Patrício et al., 2016). In this framework, there is a basic need for waste management (Driving Force) that will continue. Management actions should focus on removing the waste management systems from potential interactions with groundwater. This can be addressed using alternative, aboveground, or mounded septic systems (Macintosh et al., 2011) or through centralized wastewater treatment systems (such as sewer systems or community septic systems). The best approach for managing this issue will depend on the financial resources available and the political and cultural aspects of the community.

Although this study focused on rising groundwater impacts to septic fields, the majority of the properties included also use private wells, so sea level rise impacts in rural areas may go beyond failing septic systems. Contamination from failing septic systems can be carried to adjacent wells, polluting the drinking water (e.g., Hickey and Duncan, 1966; Murphy et al., 2020). Salinization of drinking water is also a growing threat from sea level rise due to its serious effect on human health (Tully et al., 2019). Saltwater intrusion into well water requires water treatment or abandonment of the well and has been the documented cause for the closure of hundreds of drinking wells in coastal areas such as Cyprus, Mexico, Oman, and Israel (Barlow and Reichard, 2010). In Virginia, the extent of salinity intrusion into well water is not known; however, the information available suggests that it could be a significant issue. In 2019, sodium contamination was documented in approximately 30% of the 2,300 tested private water wells across Virginia (VAHWQP, 2019). In certain coastal localities those numbers are much higher. For example, in Isle of Wight County 83% of tested wells have sodium contamination and on the Eastern Shore of Virginia contamination was found in 43% of tested wells (VAHWQP, 2017). Sea level rise is expected to cause an increase in groundwater salinity throughout most of the Eastern Shore of Virginia, resulting in impacts to private drinking wells in multiple locations (Sanford et al., 2009).

CONCLUSION

Despite the limitations of this case study, this type of analysis can still inform decision making and improve rural resilience. In coastal Virginia, where rural governments typically have limited financial resources, rural homeowners are frequently responsible for any adaptation costs on their individual properties, including both installation of new septic systems and maintenance of existing systems. Analyses such as the ones in this project can position individual homeowners to potentially receive funding available for septic adaptations. In addition, if areas of high vulnerability for septic systems can be targeted, Virginia has state programs that can help to fund community adaptations. The development of more targeted datasets and enhanced sea level rise-groundwater models will allow for an improved understanding of the future vulnerabilities of the vast rural septic infrastructure at risk from sea level rise.

DATA AVAILABILITY STATEMENT

The raw data supporting the conclusions of this article will be made available by the authors, without undue reservation.

AUTHOR CONTRIBUTIONS

MM, RI, JH, and CT all contributed to the design of the case study, and analysis, and the final manuscript. RI and CT did the primary data cleaning and analysis. MM drafted the

manuscript. All authors contributed to the article and approved the submitted version.

FUNDING

The authors would like to acknowledge the Virginia Department of Health for funding of the project.

ACKNOWLEDGMENTS

The authors would like to acknowledge the Virginia Department of Health for collaboration in providing data for the analysis. This manuscript is Contribution No. 4000 of the Virginia Institute of Marine Science, William & Mary.

SUPPLEMENTARY MATERIAL

The Supplementary Material for this article can be found online at: https://www.frontiersin.org/articles/10.3389/fmars.2021.631757/full#supplementary-material

Supplementary Figure 1 | Example of results from the Tidewater Hot Spot analysis, focused on two areas with high concentration of repair permit hot spots. The different categories of hot spots are shown in the legend.

Supplementary Figure 2 | A DASIR (Driver-Activity-State-Impact-Responses) framework for septic issues under sea level rise.

REFERENCES

Arnade, L. J. (1999). Seasonal correlation of well contamination and septic tank distance. *Groundwater* 37, 920–923. doi: 10.1111/j.1745-6584.1999.tb01191.x

Barlow, P. M., and Reichard, E. G. (2010). Saltwater intrusion in coastal regions of North America. *Hydrogeology Journal* 18, 247–260. doi: 10.1007/s10040-009-0514-3

Boon, J. D. (2012). Evidence of sea-level acceleration at US and Canadian tide stations, Atlantic Coast, North America. *Journal of Coastal Research* 28, 1437–1445. doi: 10.2112/jcoastres-d-12-00102.1

Boon, J. D., and Mitchell, M. (2015). Nonlinear Change in Sea Level Observed at North American Tide Stations. *Journal of Coastal Research* 316, 1295–1305. doi: 10.2112/JCOASTRES-D-15-00041.1

Boon, J. D., Mitchell, M., Loftis, J. D., and Malmquist, D. M. (2018). *Anthropocene Sea Level Change: A History of Recent Trends Observed in the U.S. East, Gulf, and West Coast Regions, Special Report in Applied Marine Science and Ocean Engineering (SRAMSOE) No. 467*. Virginia Institute of Marine Science, William & Mary.

Cahoon, L. B., Hales, J. C., Carey, E. S., Loucaides, S., Rowland, K. R., and Nearhoof, J. E. (2006). Shellfishing closures in southwest Brunswick County, North Carolina: Septic tanks vs. storm-water runoff as fecal coliform sources. *Journal of Coastal Research* 22, 319–327. doi: 10.2112/03-0028.1

Campbell, A. D., and Wang, Y. (2020). Salt marsh monitoring along the mid-Atlantic coast by Google Earth Engine enabled time series. *PLoS ONE* 15:e0229605. doi: 10.1371/journal.pone.0229605

Church, J. A., and White, N. J. (2011). Sea-level rise from the late 19th to the early 21st century. *Surveys in geophysics* 32, 585–602. doi: 10.1007/978-94-007-2063-3_17

Cooper, J. A., Loomis, G. W., and Amador, J. A. (2016). Hell and high water: Diminished septic system performance in coastal regions due to climate change. *PloS one* 11:e0162104. doi: 10.1371/journal.pone.0162104

Cox, A. H., Loomis, G. W., and Amador, J. A. (2019). Preliminary evidence that rising groundwater tables threaten coastal septic systems. *Journal of Sustainable Water in the Built Environment* 5, 04019007. doi: 10.1061/jswbay.0000887

Eggleston, J., and Pope, J. (2013). *Land subsidence and relative sea-level rise in the southern Chesapeake Bay region: U.S. Geological Survey Circular*. 1392.

ESRI (2020). *ArcGIS Pro*. Redlands, CA: Environmental Systems Research Institute.

Ezer, T. (2013). Sea level rise, spatially uneven and temporally unsteady: Why the U.S. East Coast, the global tide gauge record, and the global altimeter data show different trends. *Geophys. Res. Lett.* 40, 5439–5444. doi: 10.1002/2013GL057952

Ezer, T., and Atkinson, L. P. (2014). Accelerated flooding along the US East Coast: on the impact of sea-level rise, tides, storms, the Gulf Stream, and the North Atlantic oscillations. *Earth's Future* 2, 362–382. doi: 10.1002/2014ef000252

Giordano, J. C. P., Brush, M. J., and Anderson, I. C. (2011). Quantifying annual nitrogen loads to Virginia's coastal lagoons: sources and water quality response. *Estuaries and Coasts* 34, 297–309. doi: 10.1007/s12237-010-9345-7

Harris, P. J. (1995). Water quality impacts from on-site waste disposal systems to coastal areas through groundwater discharge. *Environmental Geology* 26, 262–268. doi: 10.1007/bf00770477

Hickey, J. L., and Duncan, D. L. (1966). Performance of single family septic tank systems in Alaska. *Journal (Water Pollution Control Federation)* 1298–1309.

Horsley Witten Hegeman Inc (1991). *Quantification and control of nitrogen inputs to Buttermilk Bay*, Vol. Vol I. Barnstable, Massachusetts. Report: 32.

Katz, B. G., Eberts, S. M., and Kauffman, L. J. (2011). Using Cl/Br ratios and other indicators to assess potential impacts on groundwater quality from septic systems: a review and examples from principal aquifers in the United States. *J Hydrol* 397, 151–166. doi: 10.1016/j.jhydrol.2010.11.017

Macintosh, K. A., Jordan, P., Cassidy, R., Arnscheidt, J., and Ward, C. (2011). Low flow water quality in rivers: septic tank systems and high-resolution phosphorus signals. *Sci Total Environ* 412, 58–65. doi: 10.1016/j.scitotenv.2011.10.012

Miami Dade County (2018). *Septic Systems Vulnerable To Sea Level Rise. Report*. 66. https://www.miamidade.gov/green/library/vulnerability-septic-systems-sea-level-rise.pdf (accessed January 22, 2021).

Miller, K. G., Kopp, R. E., Horton, B. P., Browning, J. V., and Kemp, A. C. (2013). A geological perspective on sea-level rise and its impacts along the U.S.mid-Atlantic coast. *Earth's Future* 1, 3–18. doi: 10.1002/2013EF000135

Mitchell, M., Hershner, C., Herman, J., Schatt, D. E., Eggington, E., and Center for Coastal Resources Management (2013). *Recurrent flooding study for Tidewater Virginia*. Virginia Institute of Marine Science, William & Mary.

Murphy, H. M., McGinnis, S., Blunt, R., Stokdyk, J., Wu, J., Cagle, A., et al. (2020). Septic Systems and Rainfall Influence Human Fecal Marker and Indicator Organism Occurrence in Private Wells in Southeastern Pennsylvania. *Environmental Science & Technology* 54, 3159–3168. doi: 10.1021/acs.est.9b05405

Patrício, J., Elliott, M., Mazik, K., Papadopoulou, K. N., and Smith, C. J. (2016). DPSIR—two decades of trying to develop a unifying framework for marine environmental management? *Frontiers in Marine Science* 3:177.

Phillips, S. J., Dudík, M., and Schapire, R. E. (2021). *[Internet] Maxent software for modeling species niches and distributions (Version 3.4.1)*. Available from url: http://biodiversityinformatics.amnh.org/open_source/maxent/. Accessed on 2021-1-21

R Development Core Team (2019). *R: A language and environment for statistical computing*. Vienna, Austria: R Foundation for Statistical Computing. Available online at: http://www.R-project.org/ (accessed November 14, 2020).

Robertson, W. D., Van Stempvoort, D. R., and Schiff, S. L. (2019). Review of phosphorus attenuation in groundwater plumes from 24 septic systems. *Science of The Total Environment* 692, 640–652. doi: 10.1016/j.scitotenv.2019.07.198

Sallenger, A. H., Doran, K. S., and Howd, P. A. (2012). Hotspot of accelerated sea-level rise on the Atlantic coast of North America. *Nature Climate Change* 2, 884–888. doi: 10.1038/nclimate1597

Sanford, W. E., Pope, J. P., and Nelms, D. L. (2009). *Simulation of groundwater-level and salinity changes in the Eastern Shore, Virginia: U.S. Geological Survey Scientific Investigations Report 2009–5066*. 125.

Small, C., and Nicholls, R. J. (2003). A global analysis of human settlement in coastal zones. *Journal of coastal research* 584–599.

Soil Survey Staff, Natural Resources Conservation Service, and United States Department of Agriculture (2012). *Web Soil Survey*. Available online at https://websoilsurvey.nrcs.usda.gov/. Accessed [Jan/2021].

Stewart, L. W., and Reneau, R. B. Jr. (1981). Spatial and Temporal Variation of Fecal Coliform Movement Surrounding Septic Tank-Soil Absorption Systems in Two Atlantic Coastal Plain Soils. *Journal of Environmental Quality* 10, 528–531. doi: 10.2134/jeq1981.00472425001000040022x

Sweet, W. V., Kopp, R. E., Weaver, C. P., Obeysekera, J., Horton, R. M., Thieler, E. R., et al. (2017). *Global and Regional Sea Level Rise Scenarios for the United States. NOAA Technical Report NOS CO-OPS 083*. NOAA/NOS Center for Operational Oceanographic Products and Services.

Tully, K., Gedan, K., Epanchin-Niell, R., Strong, A., Bernhardt, E. S., BenDor, T., et al. (2019). The invisible flood: The chemistry, ecology, and social implications of coastal saltwater intrusion. *BioScience* 69, 368–378.

VAHWQP (2017). *Virginia Household Water Quality Program data 2011-2017*. https://www.wellwater.bse.vt.edu/resources.php (accessed January 15, 2021).

VAHWQP (2019). *Virginia Household Water Quality Program 2019 Annual Report*. https://www.wellwater.bse.vt.edu/files/2019VAHWQP-Annual-Report.pdf (accessed January 15, 2021).

Withers, P. J., Jordan, P., May, L., Jarvie, H. P., and Deal, N. E. (2014). Do septic tank systems pose a hidden threat to water quality? *Frontiers in Ecology and the Environment* 12:123–130. doi: 10.1890/130131

Withers, P. J. A., May, L., Jarvie, H. P., Jordan, P., Doody, D., Foy, R. H., et al. (2012). Nutrient emissions to water from septic tank systems in rural catchments: Uncertainties and implications for policy. *Environmental Science & Policy* 24, 71–82. doi: 10.1016/j.envsci.2012.07.023

Conflict of Interest: The authors declare that the research was conducted in the absence of any commercial or financial relationships that could be construed as a potential conflict of interest.

Copyright © 2021 Mitchell, Isdell, Herman and Tombleson. This is an open-access article distributed under the terms of the Creative Commons Attribution License (CC BY). The use, distribution or reproduction in other forums is permitted, provided the original author(s) and the copyright owner(s) are credited and that the original publication in this journal is cited, in accordance with accepted academic practice. No use, distribution or reproduction is permitted which does not comply with these terms.

frontiers in Marine Science

ORIGINAL RESEARCH
published: 12 May 2021
doi: 10.3389/fmars.2021.629470

Sea Level Projections From IPCC Special Report on the Ocean and Cryosphere Call for a New Climate Adaptation Strategy in the Skagerrak-Kattegat Seas

Jian Su[1]*, *Elin Andrée*[1,2], *Jacob W. Nielsen*[1], *Steffen M. Olsen*[1] and *Kristine S. Madsen*[1]

[1] Danish Meteorological Institute, Copenhagen, Denmark, [2] Department of Technology, Management and Economics, Technical University of Denmark, Lyngby, Denmark

Denmark has a long, complex coastline, connecting the North Sea in the west to the semi-enclosed Baltic Sea in the east, via the Skagerrak-Kattegat Seas. Historical sea level records indicate that relative sea level (RSL) has been increasing along the Danish North Sea coast, south of Skagerrak, following the global mean sea level (GMSL) rise. In the central Skagerrak-Kattegat Seas, RSL rise has been practically absent, due to the GMSL rise being off-set by the Fennoscandian post-glacial land-uplift. The new IPCC Special Report on the Ocean and Cryosphere in a Changing Climate (SROCC) reported that under RCP8.5 GMSL will increase more than the previous estimates in the IPCC Fifth Assessment Report (AR5) at the end of twenty-first century due to Antarctic ice sheet dynamics. We performed a regionalization of the SROCC sea level projections for the "Danish Climate Atlas" dataset, a nation-wide climate adaptation dataset based on IPCC and various national and international databases. In these complementary datasets, important local data have been considered, which have not been included in the IPCC SROCC GMSL rise estimates, i.e., more precise national-wide land-rise prediction and sets of sea level fingerprints. Our results indicate that sea level projections under RCP8.5 results in a $>$ 40 cm RSL rise at the end of the twenty-first century in the Skagerrak-Kattegat Seas, which might call for a new adaptation strategy in this region. The rate of mean sea level rise will exceed the rate of the land-rise earlier than the previous estimates by AR5 under the RCP8.5 scenario. In particular, we stress how these new estimates will affect future extreme sea levels in this region. Based on our results, we suggest this more recent GMSL projection needs to be considered in coastal risk assessments in the Skagerrak-Kattegat Seas also in this century.

Keywords: sea level rise, IPCC SROCC, North Sea, Baltic Sea, Denmark, storm surge

OPEN ACCESS

Edited by:
Michael Dylan Sparrow, World Meteorological Organization, Switzerland

Reviewed by:
Helena Granja, University of Minho, Portugal
Pushpa Dissanayake, University of Kiel, Germany

***Correspondence:**
Jian Su
jis@dmi.dk

Specialty section:
This article was submitted to Coastal Ocean Processes, a section of the journal Frontiers in Marine Science

Received: *14 November 2020*
Accepted: *09 April 2021*
Published: *12 May 2021*

Citation:
Su J, Andrée E, Nielsen JW, Olsen SM and Madsen KS (2021) Sea Level Projections From IPCC Special Report on the Ocean and Cryosphere Call for a New Climate Adaptation Strategy in the Skagerrak-Kattegat Seas. Front. Mar. Sci. 8:629470. doi: 10.3389/fmars.2021.629470

1. INTRODUCTION

Adapting to climate change, especially to sea level rise (SLR), in the coastal region is an ongoing challenge for policy-makers now and into the future (Moser and Ekstrom, 2010). Policy-makers are struggling to keep on-top of fast growing, up-to-date scientific data, such as global mean sea level (GMSL) projections from global climate models (Slangen et al., 2017), new land topography

and elevation data (key to translate SLR into potential exposure of population, Kulp and Strauss, 2019; Ludwigsen et al., 2020), new economic assessments of coastal flooding damage (Jevrejeva et al., 2018; Prahl et al., 2018; Vousdoukas et al., 2018a), and information on extreme sea level (Woodworth et al., 2016). The concept of "climate service", aiming to provide science-based information and advice for local adaptation decisions, was established to facilitate decision-making on climate mitigation and adaptation strategies (Hewitt et al., 2012; Swart et al., 2017; Hinkel et al., 2019). A variety of organizations currently develop and deliver climate services, including private consultancies, non-governmental organizations, universities, and government agencies (Gregory et al., 2019). On a national level, the Danish Climate Atlas project was designed to provide climate service by establishing a go-to platform for climate information, based on the production of a consistent, nation-wide and easily accessible data set, which is maintained and regularly updated.

Denmark is a low-lying country with a coastline totalling more than 7,000 km. The coastline extends from the North Sea to the Baltic Sea, where the islands constituting the Danish Straits forms part of the reason for the restricted oceanic influence on the Baltic Sea (**Figure 1**). Denmark has implemented national level requirements for municipalities to develop climate adaptation plans (Sørensen et al., 2016), while such efforts remain voluntary for many other EU countries (Keskitalo et al., 2016). Pioneering projects assessing the users' needs for sea level rise information within the Copernicus Climate Change Service framework, further accentuates that it is of vital importance for coastal planning and adaptation purposes that reliable and robust, up-to-date information on SLR, and the impacts of extreme sea level events, are updated regularly (1–5 years, Madsen et al., 2019b; Muis et al., 2020).

The Danish North Sea coasts are highly exposed to the large sea level variability of the North Sea, and therefore has a long coastal protection history, e.g., the Danish Wadden Sea Dikes (Sørensen, 2016). In this region, the observed relative sea level (RSL) rise has followed the GMSL rise (upwards triangles at the western coast of Denmark in **Figure 1** with an example of sea level time series in Esbjerg, Holgate et al., 2013; Wahl et al., 2013). On the east coast of the Jutland Peninsula (Skagerrak-Kattegat Seas in **Figure 1**), GMSL rise has had less of an impact on the RSL (**Figure 1** rightwards arrows with an example of sea level time series in Frederikshavn). Usually, RSL rise rate between −0.5 and 0.5 mm y^{-1} is considered as an area absent of SLR, i.e., a neutral SLR zone (the rightwards arrows in **Figure 1**). For example, the Danish capital Copenhagen, located in the inner Danish waters (even south of this neutral SLR zone) is generally considered not highly vulnerable to SLR (Hallegatte et al., 2011).

The major cause of the absence of RSL rise in the Skagerrak-Kattegat Seas is the cancelation between the GMSL rise and glacial isostatic adjustment (GIA, Hieronymus and Kalén, 2020). The whole northern tip of the Jutland Peninsula is a post-glacial, rising sea floor (Møller, 1997). Since GIA dominates the RSL change in the past century, detailed spatial GIA information is crucial for accurate, future estimates of RSL around Denmark (Madsen et al., 2019a). However, the GIA information used in the IPCC reports often has a coarse resolution or is not fully resolved in the global SLR estimates for our study area (Kopp et al., 2014; Jevrejeva et al., 2018). Recent developments in the land uplift modeling provided a detailed map for the study area (Spada, 2017; Vestøl et al., 2019). In addition, all the references mentioned above regarding the inner Danish waters, acknowledged that the local climate adaptation strategy might change as the extreme sea level (ESL) rise caused by GMSL rise may cause more economic loss in the region due to the absence of climate protection plans. Thus, detailed information on future climate change for climate adaptation strategy is highly desired.

Information on climate change is assessed by the Intergovernmental Panel on Climate Change (IPCC). In 2013, IPCC released their 5th assessment report (AR5), giving best estimates and likely ranges of sea level change on global and regional scales (Church J. et al., 2013). Based on this data, mean SLR has been estimated for Denmark as a whole (Olesen et al., 2014), however that report did not address the spatial inhomogeneities for individual municipalities, which means that a systematic understanding of SLR on regional to local scales for Danish coastlines is still lacking. In 2019, IPCC released a Special Report on the Ocean and Cryosphere in a Changing Climate (SROCC) (Oppenheimer et al., 2019). The new SROCC report updated two important aspects of sea level: climate change induced GMSL rise and ESL rise.

There are clear links between rising temperature and GMSL rise. Globally, SLR over the last centuries is well documented, including acceleration after the nineteenth century (Church J. A. et al., 2013; Bamber et al., 2018). Over the last two centuries, estimated SLR mostly relies on coastal tide-gauge measurements. The average estimate is 1.4 mm yr^{-1} for the period 1901–1990 based on two recent reconstructions by Hay et al. (2015) and Dangendorf et al. (2017). High precision satellite altimetry started in October 1992, providing altimetry-based ocean wide estimates of SLR. Average global SLR increased to 3.2 mm yr^{-1} over the period 1993–2015 (Watson et al., 2015; Nerem et al., 2018), reflecting an acceleration in recent decades. Observed and projected SLR has two major components, thermal expansion (increase in the volume of ocean water caused by additional heat uptake) and melt water input to the ocean from retreating land-ice (glaciers and ice-sheets). Other contributions include for example changes in land water storage. The thermal expansion effect is included in AR5 CMIP (Coupled Model Intercomparison Project) models. The melt water input from ice sheet is presently not included in the global climate models assessed in SROCC and AR5, but is added to the GMSL signal afterwards (Slangen et al., 2017). In the SROCC report, it is clear that Antarctica is a major joker in the estimation of future SLR, which has a positive net contribution on GMSL rise (Yu et al., 2018; Golledge et al., 2019). Therefore, a reliable sea level fingerprint of Antarctic ice-sheet collapse is essential to local estimation of SLR (Mitrovica et al., 2009; Kopp et al., 2014).

One of the main consequences of GMSL rise is an increase in the intensity and frequency of coastal ESL (Wahl et al., 2017). Many studies conclude that trends in future changes in storminess have large uncertainties which challenge the assessments of ESL (Marcos et al., 2015; Muis et al., 2016; Vousdoukas et al., 2018b; Kirezci et al., 2020). For the Danish

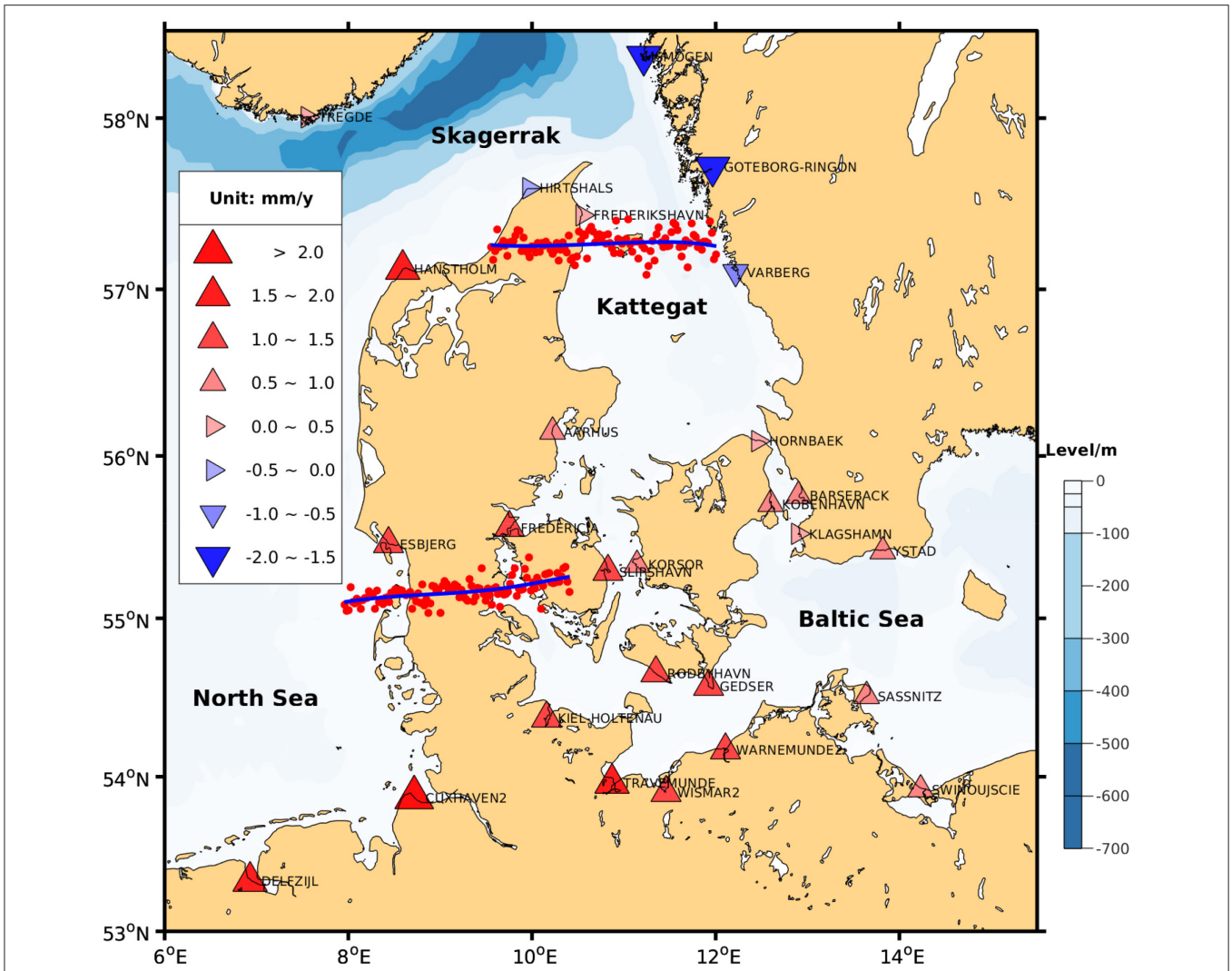

FIGURE 1 | Background shaded color: bathymetry (m) of the study area, the North Sea–Baltic Sea transition zone. Top symbols: relative sea level rise trends—the change rate (mm y^{-1}) of the long-term sea level (> 60 years) derived from monthly mean values of sea level records at tidal gauge stations in the PSMSL data set (Permanent Service for Mean Sea Level, 2020). The blue downwards and red upwards triangles indicate a decrease or increase of sea level, respectively. The rightwards arrow refers to small change rates of the sea level. For the methods to calculate the relative sea level rise trends, please refer to https://www.psmsl.org/products/trends/methods.php. Two sea level time series at Esbjerg and Frederikshavn stations are illustrated, original yearly data in red dots and blue lines are trends with polynomial fit to the original data.

coasts, even the ESL reanalysis based on observations has a very large uncertainty, attributed to the complexity of the coastlines (Calafat and Marcos, 2020). On top, RSL rise adds another dimension of uncertainty, leading to the estimates of recurrence high water level being non-stationary (Masina and Lamberti, 2013; Ghanbari et al., 2019). Despite the uncertainties, estimates of recurrence periods for extreme high waters is of critical interest to risk managers (Woodworth, 2006; Hinkel et al., 2014; Sørensen et al., 2016; Woodworth et al., 2016; Wahl et al., 2017). In this paper we quantify the impact of SLR projections under different scenarios in SROCC on the frequency of extreme high water levels. In particular, we discuss the possible future research advances that could affect the current state-of-the-art estimates of both future mean and extreme sea levels.

2. METHODS AND MATERIALS

2.1. Difference Between IPCC SROCC and AR5

The IPCC SROCC used the same quantification of the contributors to SLR as in the predecessor IPCC AR5, except for the Antarctic ice-sheet dynamics. IPCC AR5 only estimated the Antarctic ice sheet dynamics' contribution as a linear extrapolation of the observed ice discharge (Little et al., 2013), while IPCC SROCC projected the SLR projections based on some process-based numerical ice sheet models (detailed discussion see section 4, Shepherd et al., 2018). Therefore, SROCC results are very similar to the AR5 in 2100 except for the high emission scenario (RCP8.5), for which the contribution of Antarctica is

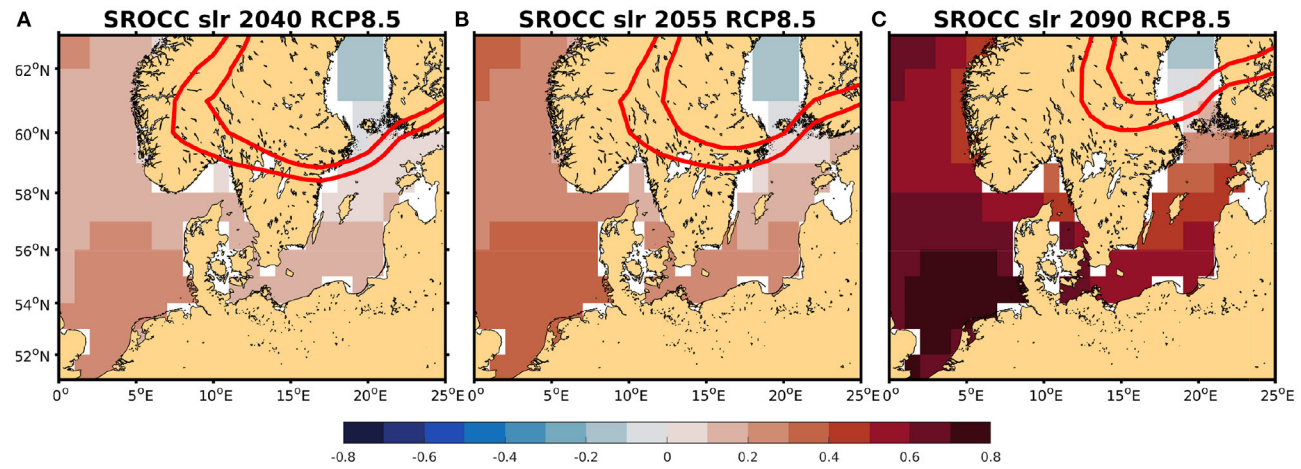

FIGURE 2 | Regional sea level rise (m, median value) in 2040 **(A)**, 2055 **(B)**, and 2090 **(C)** in IPCC SROCC for IPCC RCP 8.5 scenario. The position of near-neutral sea level rise zone are indicated by −0.5 mm y^{-1} (north red line) and 0.5 mm y^{-1} (south red line) lines. Data are from Oppenheimer et al. (2019).

tripled from a median of 4–12 cm. Finally, the SROCC estimate of GMSL rise is around 10 cm higher, with a median of 84 cm and a likely range (17–83rd percentile) of 61–110 cm (**Figure 2C**).

2.2. Land-Uplift and Reference Framework

The contribution of GIA to the RSL can be of the same magnitude as climate change induced GMSL in regions like Scandinavia (Kierulf et al., 2014) or North America (Sella et al., 2007). It is the primary source of spatial inhomogeneities in SLR for Denmark (Madsen et al., 2019a). To obtain a spatial map of the land uplift, a land uplift model is an obvious solution. The dataset in this study is assessed by DTU Space (National Space Institute, Technical University of Denmark) to provide the regional/local land rise in Denmark (Personal communication, Per Knudsen, DTU Space, 2016). This dataset is based on classic geodetic data for a 100 years period (1900–2000) combined with Global Navigation Satellite System (GNSS) data from varying time periods. As a final step, the spatial land-uplift data was interpolated to the stations representing each of the coastal stretches (**Figure 3**, red squares).

2.3. Fingerprints

Sea level change is not evenly distributed around the globe. Changes in the Earth's gravity field and elastic deformation of the solid Earth give rise to spatial differences in the sea level rise pattern (Mitrovica and Milne, 2003). For example, near the Antarctic ice-sheet, reduced gravitational attraction from ice-sheet mass loss between the ice and the nearby ocean causes sea level to fall, despite a contribution to global sea level rise (Mitrovica et al., 2011). In the Climate Atlas project, we adopted the factor of 1.1 for the sea level signal from the Antarctic ice sheet for the whole Denmark, following the sea level fingerprint from Mitrovica et al. (2009) and the new work from Mitrovica et al. (2018).

2.4. Methods for Regionalization of Global Mean Sea Level Change

In this section, we summarize the steps carried out to obtain the local sea level rise values. The localizing methodology follows the previous work in Olesen et al. (2014) after IPCC AR5, which has been widely used in the local municipalities for coastal protection planning. The main procedures are as listed below.

(1) Obtain the data for the regions around Denmark, i.e., North and Baltic Seas, from supplement materials in Church J. et al. (2013) and the new input of global SLR from Oppenheimer et al. (2019) (**Figure 2**). The data from IPCC include the median value (50%) and the likely range (upper 83% and lower 17%).

(2) It is evident that sea level change varies from the Danish North Sea coast to the Danish Baltic coast (**Figure 1**), and high resolution data are needed to resolve the Inner Danish Straits. After comparing the GIA data in SROCC (map in **Figure 2**) and better resolution GIA data (**Figure 3**), we found that the resolution of SROCC data is still not high enough for municipalities to use directly. Therefore, GIA should be deducted from the SROCC data, and we used a simple averaging method to obtain a SLR value for the entire Danish coastline (see next procedure). This way the spatial GIA information is filtered out.

(3) To obtain the sea level change for the entire Danish coastline without spurious effects of averaging, we averaged the values from two points; one point in the southern North Sea (54.5 °N, 4.5 °E) and one point in the southern Baltic Sea (56.6 °N, 18.5 °E). The high resolution GIA data (see section 2.2) is added to this value to obtain the local SLR values. Note that this method may be adjusted in the later release of Climate Atlas project, when the resolution of IPCC regional SLR data is at a satisfactory level for local usage.

(4) Scale to the Climate Atlas reference period. Often the reference periods and future time slices required in the local climate adaptation strategy are different for different purposes. IPCC SLR projections in AR5 and SROCC used the reference period 1986–2005 and 20 year time slices. Today, however, it is

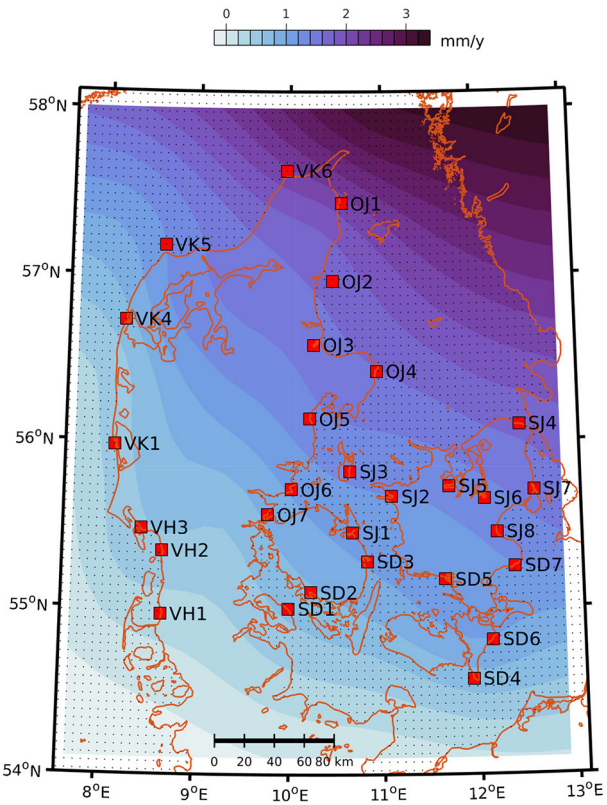

FIGURE 3 | Regional/local land rise (mm y^{-1}) in Denmark (Personal communication, Per Knudsen, DTU Space, 2016). The data is calculated based on land observations, and the ocean data is extrapolated (shaded with dots). Overall, all of Denmark is rising due to glacial isostatic land rise in Scandinavia after the last ice age. The land rise of northern Denmark is about 2 mm per year, decreasing toward south and west, to zero just south of the Danish-German border. We extracted the data at the stations (red squares) to represent the coastal stretches. The name lists of the stations and coastal stretches are in **Table 1**.

TABLE 1 | The names of the 34 coastal stretches and the observing stations that represent the coastal stretches.

KDI code	Name for coastal stretch	Name for stations
VH1	Vadehavskyst sydlig	Vidå
VH2	Vadehavskyst central	Ribe
VH3	Vadehavskyst nordlig	Esbjerg
VK1	Vestkyst central	Hvide Sande
VK4	Vestkysten ud for Limfjorden	Thyborøn
VK5	Skagerrakkyst sydlige	Hanstholm
VK6	Skagerrakkyst nordlig	Hirtshals
LF1	Limford østlig	Nr. Sundby
LF2	Limfjorden ved Skive	Skive
LF3	Limfjorden ved Lemvig	Lemvig
LF4	Limfjorden ved Thisted	Thisted
OJ1	Kattegatkyst nordlige	Frederikshavn
OJ2	Ålborg Bugt	Hals Barre
OJ3	Randers Fjord og Mariager Fjord	Randers
OJ4	Djurslands østkyst og Anholt	Grenå
OJ5	Åhus Bugt	Århus
OJ6	Lillebælt nordlig	Juelsminde
OJ7	Lillebælt central	Fredericia
SD1	Lillebælt sydlig	Fynshav
SD2	Sydfynske Øhav	Fåborg
SD3	Storebælt Sydvest	Slipshavn
SD4	Femern Bælt	Gedser
SD5	Smålandsfarvandet	Karrebæksminde
SD6	Falsters og Møns Østersøkyst	Hesnæs
SD7	Faxe Bugt	Rødvig
SJ1	Storebælt nordvest og Odense Fjord	Kerteminde
SJ2	Storebælt nordøst	Kalundborg
SJ3	Sejrø Bugt	Ballen
SJ4	Nordsjællands kyst	Hornbæk
SJ5	Isefjord	Holbæk
SJ6	Roskilde Fjord	Roskilde
SJ7	Øresunds kyst	København
SJ8	Køge Bugt	Køge
SJ9	Bornholms kyst	Tejn

The KDI code is the name of coastal stretch following the KDI definition.

not suitable for the municipalities for near-term and long-term future climate adaptation planning anymore, since 20 years is too short for extreme sea level analysis. In the Climate Atlas project, we choose the reference period as 1981–2010 and 30 year time slices, in line with previous studies like Meier et al. (2004). Therefore, projected SLR is scaled to the Climate Atlas reference period according to a quadratic formula. Since the national Danish height system DVR90 is designed to give almost-zero mean sea level in year 1990, just a few years before the center of our reference period, and the measured sea level may have a bias toward high sea level, we used 0 cm, relative to DVR90, as mean sea level for the reference period.

(5) Regional effects. The importance of mean sea level change caused by local ocean dynamics and steric effects has been evaluated by averaging 30 years of sea level data from the operational storm surge model at the Danish Meteorological Institute (DMI)—HBM (Hiromb-Boos Model, Berg and Poulsen, 2012) model simulations for each 30 year period. We found that this contribution at the end of the century (by subtracting the mean sea level values of the reference period from the future periods) varies between −1.5 and −0.4 cm. We therefore considered this change to be well within the uncertainty range, and thus too small to be significant. It has been left out of the further calculations.

(6) The likely range of the IPCC provides lower and upper limits (17 and 83%). Ten and 90 percentiles are calculated from the likely range of IPCC, based on a symmetric normal distribution. For the 10-percentile, this is considered a good approximation. For the 90 percentile, the method should give a lower limit estimation of the true uncertainty because of asymmetric distribution (Grinsted et al., 2015), especially for the RCP8.5 scenario, but the method is chosen because it is robust and well-described.

(7) All values were corrected for regional land rise, to provide the relative sea level signal for different coastal stretches (**Table 1**). Each coastal stretch is represented by one station, chosen to have the most reliable present day high water statistics for that coastal stretch (**Table 1**). The definition of coastal stretches is according to the extensive coastal risk management experience from the Danish Coastal Authority (KDI) and their climate adaptation plans (Auken, 2013).

3. RESULTS

3.1. Relative Sea Level Rise in the Skagerrak-Kattegat Seas

The resolution of SROCC GMSL information is too low to provide reliable information for local communities, e.g. in the Skagerrak-Kattegat Seas and even for the Baltic Sea, as shown in **Figure 2**. Nevertheless, SROCC estimates still provide the grounds for the quantification of local RSL.

One of the essential questions for SLR in the Skagerrak-Kattegat Seas is whether the location of the neutral SLR zone (defined as RSL rise rate between −0.5 and 0.5 mm y^{-1}) will remain, or else how it will shift in the future. One advantage of exploring the global SROCC SLR dataset is that the position of the neutral SLR zone can be easily depicted. **Figure 2** shows a general northwards movement of the neutral SLR zone under RCP8.5 scenario. In the middle of the twenty-first century, the median value of the rate of RSL rise already shows that the Skagerrak-Kattegat Seas are within the positive SLR zone, and it will accelerate in the next half of the twenty-first century.

The land rise of northern Denmark is about 2 mm per year, decreasing toward south and west, to zero just south of the Danish-German border (**Figure 3**). In the central Skagerrak-Kattegat Seas, the land rise (or sea-bed rise) is more than 2 mm per year. Overall, all of Denmark is rising after the last ice age, which has compensated for global SLR, giving an average RSL decrease in the northern-most part of the country in the twentieth century (Hansen, 2018). However, the rate of GMSL rise will in the coming decades outpace by a factor of two the rate of land rise (**Figure 4**, bars); under RCP8.5 the GMSL rise in the 2020's will reach 5 mm y^{-1}, and close to 10 mm y^{-1} around 2060. **Figure 4** shows time series for the different locations along the Danish coasts under RCP8.5 based on the IPCC SROCC dataset. The colors indicate location, and changes from dark red for the North Sea coast to dark blue for the Baltic coasts. It is apparent that locations with light colors, in the Skagerrak-Kattegat Seas (see named two stations in **Figure 4**), show slower SLR, especially in the first half of this century. In the next half of the twenty-first century, on the other hand, SLR will accelerate. By the end of the century, the sea level in the Skagerrak-Kattegat Seas already reaches 60–70 cm higher than the reference period.

3.2. SLR Under Different Scenarios

The coastal climate adaptation plan in Denmark is the responsibility of each municipality. Individual municipalities assess the flood risk in the future according to the vulnerability, RSL and ESL rise along their coastal stretches (Sørensen et al., 2016). RSL rise varies from one coastal stretch to the next, but the variability within one coastal stretch is rather small. Overall, the RSL changes are positive in all regions (**Figure 5**), with higher values toward south and west, where the compensation from land rise is smaller. Except for this, the major challenge for municipalities is which scenario to consider in the future. For example, the median value for mean SLR in the end of this century is much higher under the RCP8.5 scenario (∼ 44 cm) than the RCP4.5 scenario (∼ 23 cm) along the Skagerrak-Kattegat coasts. This implies that the choice of scenarios play a major part in what adaptation strategies might be deemed appropriate—possibly with very different climate adaptations plans as outcome.

3.3. 95 Percentile of GMSL

The uncertainty of the future RSL rise (figures not shown, but can be easily visualized online at https://www.dmi.dk/klimaatlas/) is of course very large, and has quite different sources (see the discussion of SROCC SLR uncertainty in Hieronymus and Kalén, 2020).

The present consensus on particularly the higher percentiles (95 percentile and above) is that they cannot be constructed meaningfully by statistical analysis of data from the existing climate model ensembles (Jevrejeva et al., 2016). This is in part due to the lack of interactive glacier and ice sheet modules in the applied climate models, and partly due to a limited physical understanding of the processes that have been suggested to lead to instabilities in the Antarctic Ice sheet as ocean and atmospheric temperatures increase (DeConto and Pollard, 2016; Bamber et al., 2019). After consultations with Danish experts, the expert elicitation of Bamber et al. (2019) is chosen as the basis for a 95 percentile estimate. This expert judgement concludes that for a five degree warming there is a 5% risk that global mean sea-level will exceed 2.4 m in the year 2100, where 1.8 m is directly linked to ice sheet melting. We use 2.4 m directly as the best estimate available for the 95 percentile for RCP8.5 2071–2100 period. As GMSL rise is both one of the most certain (the sea level will rise) and uncertain (with regards to the magnitude of the sea level rise) components of climate change, and subject to intense investigations, it can be expected that these numbers will be updated in future versions of the Climate Atlas.

3.4. Extreme Sea Level Rise

In Denmark, water levels which exceed the 20-year return level are defined as storm surges by the Danish Storm Council. A return level is often used in statistics for coastal engineering purposes to describe the level the water reaches on average once in a return period. There is a large variation of local 20-year return levels, due to e.g., variable tidal range and wind conditions between different locations. Here we examine the return level change at 5 tide gauge locations in the Skagerrak-Kattegat Seas. **Figure 6** shows a typical statistical graph to describe storm surge statistics with the return level on y-axis as function of the return period on x-axis.

The present day storm surge statistics used for the reference period in the Climate Atlas are from the authoritative statistics, which is provided by KDI (**Figure 6**, gray lines and uncertainty). KDI update the authoritative statistics reports approximately every 5 years, with the latest one published in 2018 and revised

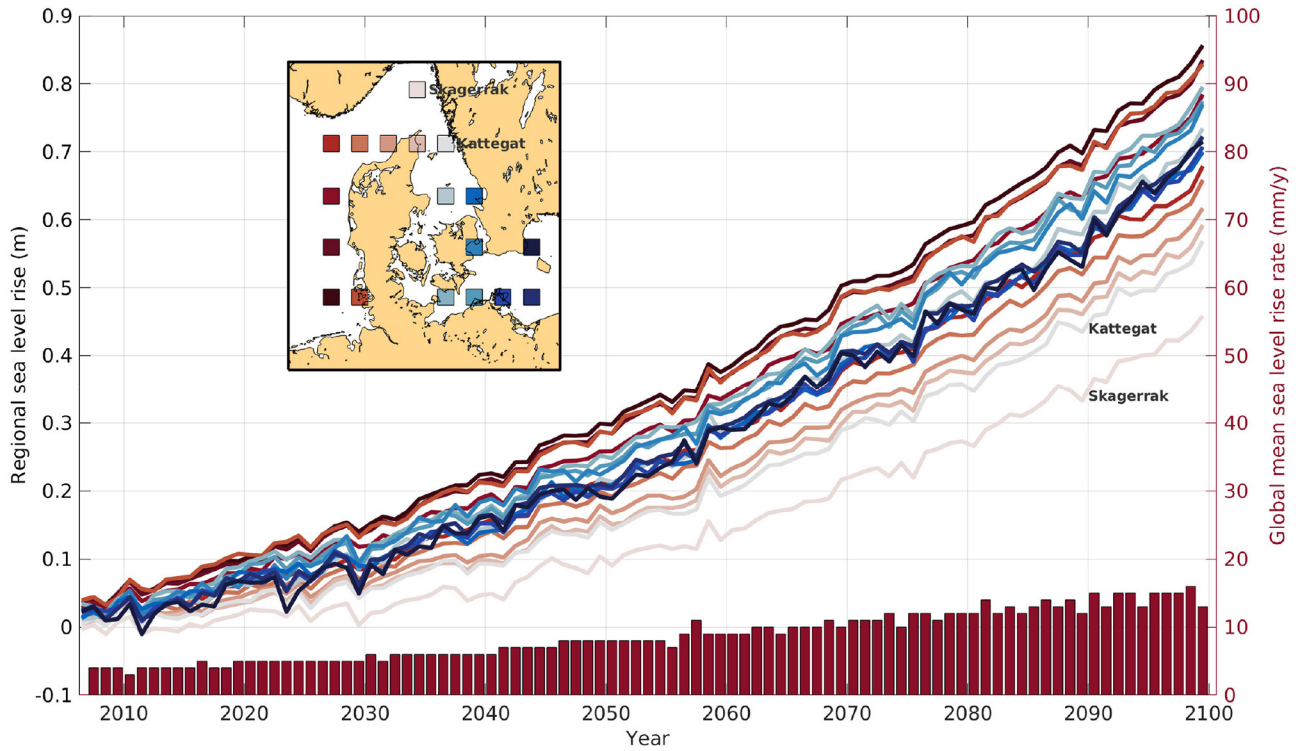

FIGURE 4 | Lines: time series of regional sea level rise projection (m, median value, 2006–2100) for RCP8.5 scenario at different areas around Denmark according to IPCC SROCC on the left y-axis. The locations corresponding to each of the time series are indicated by different colors in the map. The locations in Skagerrak and Kattegat with the slowest increasing trends are denoted Skagerrak and Kattegat, respectively, both in the map and time series lines. Bars: the global mean sea level rise rate (mm y^{-1}) on the right y axis. Data are from SROCC-Ch4ArticleSM.

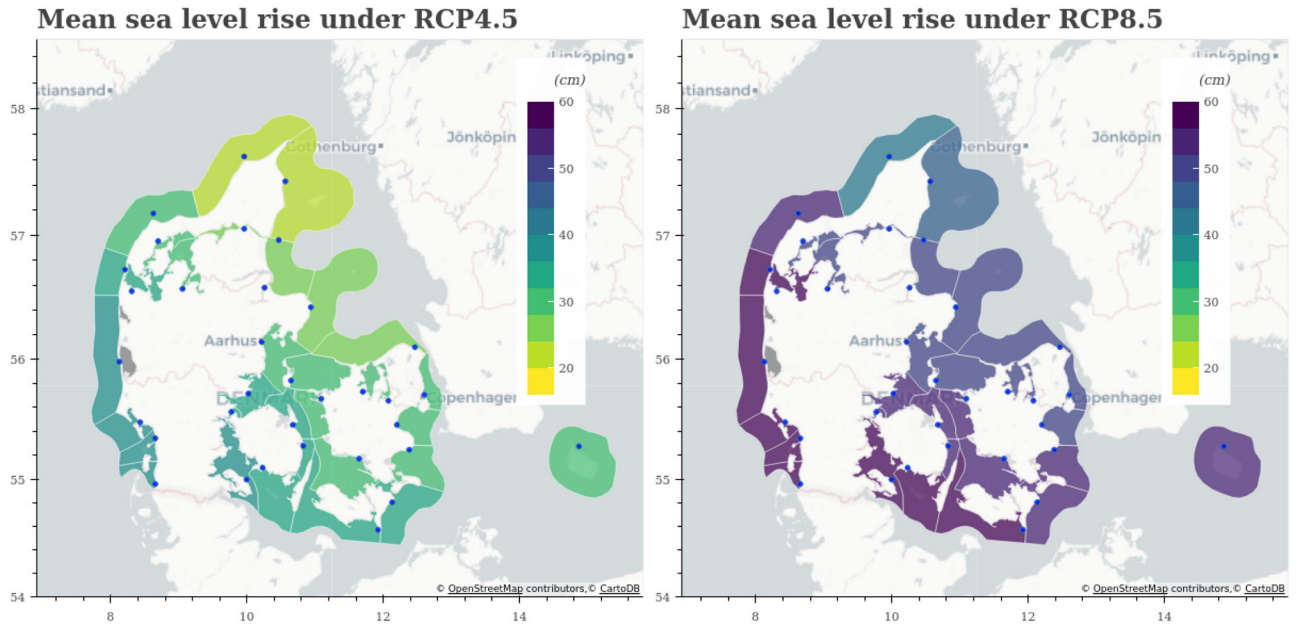

FIGURE 5 | Regional sea level rise (cm) in different coastal stretches for RCP4.5 **(left)** and RCP8.5 **(right)** scenarios in 2070–2100, relative to 1980–2010. The value at each stretch is calculated based on a representative tidal gauge station (blue dots). The name lists of the stations and coastal stretches are in **Table 1**.

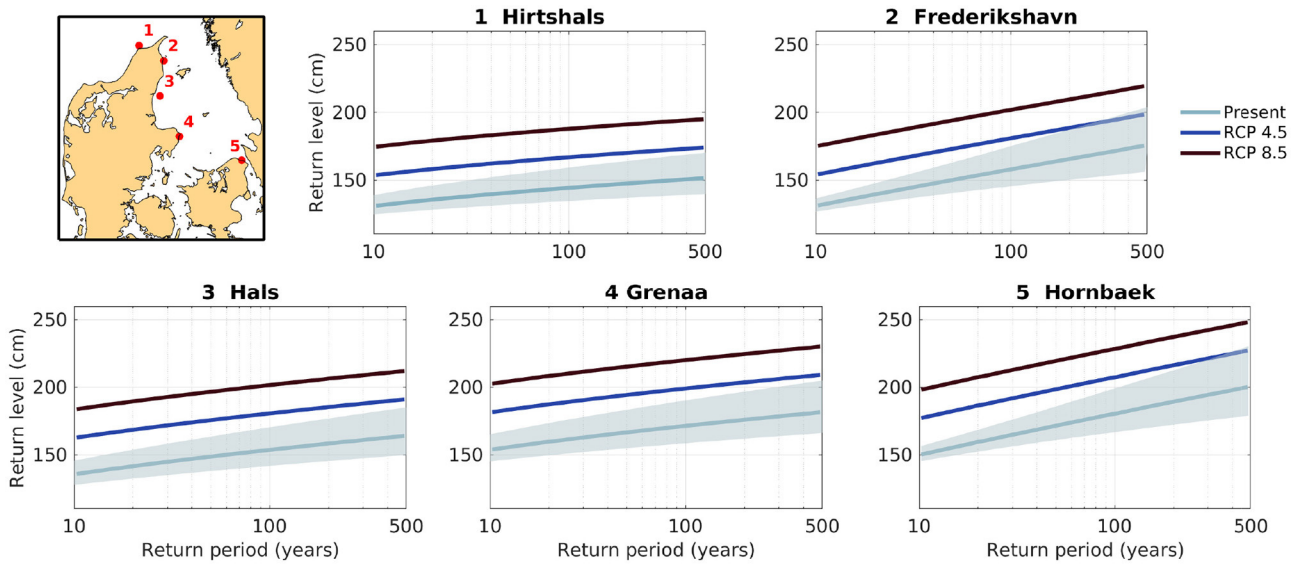

FIGURE 6 | The expected extreme sea level (ESL, cm) with the corresponding return period at x-axis at 5 tide gauge locations in Skagerrak-Kattegat (location in upper-left panel) in present and future conditions (in 2070–2100) under RCP4.5 (light blue lines) and RCP8.5 (red lines) scenarios. The mean sea levels added to the present day statistics are different values (in **Figure 5**) at 5 tide gauge locations. The gray lines are based on tide gauge observations, and the gray bands refer to the 5–95% uncertainty range in the fit of the extreme value distribution to observations from Ditlevsen et al. (2019).

in 2019 (Ditlevsen et al., 2019). The storm surge statistics are based on measured water levels at tide gauge stations along the Danish coasts with a sufficiently long time-series. The statistics report published in 2018, which is used for the Climate Atlas, includes measurements until the beginning of 2017. For individual stations, different statistical models (Weibull or Log-normal distribution) are applied, giving an assessment of how frequently extreme water levels are to be expected.

There is no doubt that adding the mean SLR (different SLR values at 5 locations in **Figure 5**) to the present day return level curve already provides us with a quite different image for what can be considered as an extreme event at the end of this century (**Figure 6**, blue and red curves). This combined presentation of present and future scenarios return level graphs can help to interpret the "amplification factor," referring to the multiplication factor by which the frequency of flooding of a given height increases (Buchanan et al., 2017). For example, in Frederikshavn, a 500 year storm surge event will become a 10 year event under the RCP8.5 only because of the mean SLR. In Kattegat, a 100 year storm surge event will become an annual event at the end of this century only under RCP8.5 scenario.

4. DISCUSSION AND CONCLUSION

The Danish Climate Atlas is not only a dataset, but also a climate information platform, since the municipalities can also obtain our interpretation of the data. Main concerns that users should be aware of when using output from the regionalized dataset presented in this study are summarized in the following.

- Ocean dynamics on local scale.

SLR varies from region to region. SROCC noted that regional changes in sea level associated with water temperature and salinity variations can be quite significant. The CMIP Phase 6 (CMIP6) will become available soon to assess the contribution of the regional ocean dynamics contribution to the SLR.

Regional ocean dynamics have a sea level signal associated (Bilbao et al., 2015). For instance, a change in the average local wind patterns on time scales up to some days are accountable for occasional strong sea level changes in the inner Danish waters lasting for up to a month, hence contributing to seasonal but also interannual variability of the Baltic Sea mean sea level (Mohrholz, 2018). The dynamic effects are included in ocean models of climate change and impacts depending on the scales resolved. Regional steric effects occur if the climate change signal of salinity or temperature is amplified. Studies of these effects are conducted by the author team with a fine scale regional ocean model (see section 2.4, item 5).

- Land-uplift in the future.

GIA is one of the known phenomena resulting in vertical land motion at decadal to millennia timescales. However, we can not neglect that many other natural and anthropogenic processes can also invoke vertical land motion at vastly different time scales (e.g., earthquake, groundwater depletion, or dam building), see the detailed discussion in Woodworth (2006) and Woodworth et al. (2019). Such a vertical land motion dataset on meso-scale is still missing.

For the Baltic Sea, the contribution of deceleration of GIA to the acceleration of RSL was rather small, and GIA alone can not fully explain the acceleration of RLS in the past century (Hünicke and Zorita, 2016). We only consider GIA in our local

dataset, while factors judged to have a significant influence on SLR in the future will be further updated when they become available, e.g., the component of nonlinear elastic uplift from present-day ice loading (Ludwigsen et al., 2020).

- Connecting mean SLR with ESL rise.

  Our ESL results are in line with SROCC that a 100 year storm surge event today will become an annual event for most coasts of the world in the mid of this century. Nevertheless, the milestone will only be reached at the second half of this century in the inner Danish waters. The precise timing of the milestone relies on the emission scenarios and a reliable sea level monitoring framework.

  In Denmark, the local sea level has been measured with tide gauges since the end of the nineteenth century. Long records exist at only 8–10 stations, while many locations have a rather short record. This makes the uncertainty of return level estimates highly variable. Moreover, these time series have data gaps and inconsistencies due to e.g., instrument malfunctions or replacements. Reconstruction work of monthly and annual mean sea level from 14 stations with more than 20 years of data was carried out by Madsen et al. (2019a), and available online in Hansen (2018). However, the gap-filling of the historical storm surge events, which in turn affects the high water statistics, is still ongoing work for the author teams.

  Changes in physical processes (e.g., tides, wind storms, waves) as well as their respective interactions can cause water level variability to become of an even higher concern in the future. Understanding the combined future impact of these physical processes is a big challenge. This is especially true for the local scales considered in the Climate Atlas. Therefore, a detailed hydrodynamical model has been developed and operated at DMI for operational storm surge modeling (Berg and Poulsen, 2012). This model serves to provide sufficient details and knowledge for the Climate Atlas, where the model is run with atmospheric forcing from climate models, and with the same high level of details in coastline and bathymetry as in the operational model setup. Finally, the ongoing build-up of an ensemble of ocean climate model simulations, based on this operational model, will further provide the Climate Atlas users with the ESL rise information and associated uncertainty estimates they require. A very similar modeling framework has already been established in Sweden for a similar initiative (Dieterich et al., 2019).

- Uncertainty and next centuries.

  The real barrier for translating uncertainty estimation to flood risk management is the extant communication challenge, i.e., the communication between scientists developing climate projections and those professional groups who are the recipients for flood risk estimates and warnings (Faulkner et al., 2007). After consultations with relevant stakeholders, the upper limit of the SLR projection by 2100 is of most concerns to them, i.e., the small but significant risk of rapid sea level rise outside the likely estimates which is mirrored in relatively high numbers for the upper percentiles for GMSL (Jevrejeva et al., 2014).

  Another uncertainty worth to communicate with the municipalities is that although the IPCC report is based on the publications of a large group of highly recognized researchers, other publications are critical of the IPCC assessments, and present sea level predictions resulting in both lower (Mörner, 2013) and higher (Rahmstorf, 2010) future sea level rise. More transparent essential climate variables data platforms, allowing users to extract past, current, and future climate data by themselves, are key for enabling open and evidence-based climate services (Bojinski et al., 2014). This emphasizes the need for regional climate data platforms such as the Danish Climate Atlas.

Beyond 2100, global sea level rise will continue to increase with high confidence primarily due to continued thermal expansion and loss of ice from both Greenland and Antarctic ice sheets, including contributions from both surface melting and dynamical mass loss. These two critical issues need to be taken into account when looking beyond year 2100.

First, for Antarctica, it is worthwhile to note that intense research on the ice-sheets' mass balance is ongoing, and it is expected that more precise knowledge will become available in the coming years. The dynamical ice loss may include new instabilities such as the so called Marine-Ice-Cliff-Instability (DeConto and Pollard, 2016), but our physical understanding is limited and confidence low for this contribution, as also reported in new studies (Edwards et al., 2019). At present, it is widely acknowledged that there is a small but not negligible risk of large and rapid changes in the ice sheet contributions to GMSL rise especially from the Antarctic ice sheet (DeConto and Pollard, 2016; Bamber et al., 2019), and that SLR will continue for centuries, with a speed that strongly depends on greenhouse gas emissions (Oppenheimer et al., 2019). Therefore, the difference between SROCC and AR5 is larger for longer time scales. SROCC estimates that the likely range of Antarctic mass loss in 2,300 translates into 7–37 cm GMSL rise for RCP2.6 and 60–289 cm for RCP8.5. That is a big change which further emphasizes the importance of mitigation.

For continued increase of global mean temperatures in the range of 1–4°C, consistent with unchecked emissions (RCP8.5 and its Extended Concentration Pathways beyond 2100), the Greenland ice sheet surface mass loss will increase and a complete mass loss is projected as a direct result over the next millennia or more. The exact path depends strongly on the emission scenario and there is medium confidence in the interval for the critical temperatures for irreversible and continued melt.

Since AR5 new knowledge of the Antarctic contribution in particular explains why SROCC estimates are significantly higher. For RCP8.5 in the year 2300 the likely range of global mean sea-level is 2.3–5.4 m. With a large Antarctic contribution, numbers corrected to the Danish Waters will be slightly higher. Considering the large uncertainty this has not been pursued and no attempt is made to describe the regional differences due to land rise, which would generally be a negative local correction. Therefore, areas like the Skagerrak-Kattegat Seas will keep the same accelerating rate as other places in the world. DMI suggests to use the global estimates directly for Denmark, and to be prepared for updates of

these multi-century numbers in the next years, as new knowledge appear.

After carefully considering above mentioned limitations of climate data, precise climate projections can go into decisions on spatial climate adaptation plans. In particular, for the study area in this paper, the Skagerrak-Kattegat Seas, the new SROCC projections should be adopted in the decision making plans to replace the previous ones based on AR5, since considerable research has been conducted on the sea-level problem since AR5. As a results of this transition, due to the new information from the SROCC projections, municipalities along the coastal stretches in the Skagerrak-Kattegat Seas may need to reconsider their protection levels against future risk of flooding under RCP8.5 scenario, since a 100 year storm surge event today will become an annual event as we approach the end of this century. More importantly, SLR along the Danish coasts will certainly accelerate beyond 2100 at the same rate as other places in the world.

DATA AVAILABILITY STATEMENT

The datasets presented in this study can be found in online repositories. The datasets for this study can be found in different data formats, like netcdf, excel, maps, and statistics graphs through the link from DMI home webpage https://www.dmi.dk/klimaatlas/.

AUTHOR CONTRIBUTIONS

JS: drafting of the manuscript and analysis and interpretation of data. EA: acquisition of data and analysis and interpretation of data. JN and SO: analysis and interpretation of data. KM: study conception and design and project coordinator. All authors contributed to the article and approved the submitted version.

FUNDING

This research was funded by the Danish State through the Danish Climate Atlas.

ACKNOWLEDGMENTS

We would like to acknowledge Per Knudsen for providing the land-uplift data and advice on how to interpret the data.

REFERENCES

Auken, I. (2013). *Forord. I Klimatilpasningsplaner og Klimalokalplaner Vejledning*. Technical report, Miljøministeriet, Naturstyrelsen.

Bamber, J. L., Oppenheimer, M., Kopp, R. E., Aspinall, W. P., and Cooke, R. M. (2019). Ice sheet contributions to future sea-level rise from structured expert judgment. *Proc. Natl. Acad. Sci. U.S.A.* 116, 11195–11200. doi: 10.1073/pnas.1817205116

Bamber, J. L., Westaway, R. M., Marzeion, B., and Wouters, B. (2018). The land ice contribution to sea level during the satellite era. *Environ. Res. Lett.* 13:063008. doi: 10.1088/1748-9326/aac2f0

Berg, P., and Poulsen, J. W. (2012). *Implementation Details for HBM*. Technical Report 12-11, Danish Meteorological Institute.

Bilbao, R. A. F., Gregory, J. M., and Bouttes, N. (2015). Analysis of the regional pattern of sea level change due to ocean dynamics and density change for 1993–2099 in observations and CMIP5 AOGCMs. *Clim. Dyn.* 45, 2647–2666. doi: 10.1007/s00382-015-2499-z

Bojinski, S., Verstraete, M., Peterson, T. C., Richter, C., Simmons, A., and Zemp, M. (2014). The concept of essential climate variables in support of climate research, applications, and policy. *Bull. Am. Meteorol. Soc.* 95, 1431–1443. doi: 10.1175/BAMS-D-13-00047.1

Buchanan, M. K., Oppenheimer, M., and Kopp, R. E. (2017). Amplification of flood frequencies with local sea level rise and emerging flood regimes. *Environ. Res. Lett.* 12:064009. doi: 10.1088/1748-9326/aa6cb3

Calafat, F. M., and Marcos, M. (2020). Probabilistic reanalysis of storm surge extremes in Europe. *Proc. Natl. Acad. Sci. U.S.A.* 117, 1877–1883. doi: 10.1073/pnas.1913049117

Church, J., Clark, P., Cazenave, A., Gregory, J., Jevrejeva, S., Levermann, A., et al. (2013). *Sea Level Change. Climate Change 2013: the Physical Science Basis. Contribution of Working Group I to the Fifth Assessment Report of the Intergovernmental Panel on Climate Change*. Cambridge; New York, NY: Cambridge University Press, 1137–1216.

Church, J. A., Clark, P. U., Cazenave, A., Gregory, J. M., Jevrejeva, S., Levermann, A., et al. (2013). Sea-level rise by 2100. *Science* 342:1445. doi: 10.1126/science.342.6165.1445-a

Dangendorf, S., Marcos, M., Wöppelmann, G., Conrad, C. P., Frederikse, T., and Riva, R. (2017). Reassessment of 20th century global mean sea level rise. *Proc. Natl. Acad. Sci. U.S.A.* 114, 5946–5951. doi: 10.1073/pnas.1616007114

DeConto, R. M., and Pollard, D. (2016). Contribution of Antarctica to past and future sea-level rise. *Nature* 531, 591–597. doi: 10.1038/nature17145

Dieterich, C., Gröger, M., Arneborg, L., and Andersson, H. C. (2019). Extreme sea levels in the Baltic Sea under climate change scenarios-Part 1: Model validation and sensitivity. *Ocean Sci.* 15, 1399–1418. doi: 10.5194/os-15-1399-2019

Ditlevsen, C., Ramos, M., Sørensen, C., Ciocan, U., and Piontkowitz, T. (2019). *Højvandsstatistikker 2017*. Technical report, Kystdirektoratet.

Edwards, T., Brandon, L., Durand, M. A. G., and Edwards, N. R. (2019). Revisiting Antarctic ice loss due to marine ice-cliff instability. *Nature* 566, 58–64. doi: 10.1038/s41586-019-0901-4

Faulkner, H., Parker, D., Green, C., and Beven, K. (2007). Developing a translational discourse to communicate uncertainty in flood risk between science and the practitioner. *AMBIO* 36, 692–704. doi: 10.1579/0044-7447(2007)36[692:DATDTC]2.0.CO;2

Ghanbari, M., Arabi, M., Obeysekera, J., and Sweet, W. (2019). A coherent statistical model for coastal flood frequency analysis under nonstationary sea level conditions. *Earth's Fut.* 7, 162–177. doi: 10.1029/2018EF001089

Golledge, N. R., Keller, E. D., Gomez, N., Naughten, K. A., Bernales, J., Trusel, L. D., et al. (2019). Global environmental consequences of twenty-first-century ice-sheet melt. *Nature* 566, 65–72. doi: 10.1038/s41586-019-0889-9

Gregory, J. M., Griffies, S. M., Hughes, C. W., Lowe, J. A., Church, J. A., Fukimori, I., et al. (2019). Concepts and terminology for sea level: mean, variability and change, both local and global. *Surv. Geophys.* 40, 1251–1289. doi: 10.1007/s10712-019-09525-z

Grinsted, A., Jevrejeva, S., Riva, R., and Dahl-Jensen, D. (2015). Sea level rise projections for northern Europe under RCP8.5. *Clim. Res.* 64, 15–23. doi: 10.3354/cr01309

Hallegatte, S., Ranger, N., Mestre, O., Dumas, P., Corfee-Morlot, J., Herweijer, C., et al. (2011). Assessing climate change impacts, sea level rise and storm surge risk in port cities: a case study on Copenhagen. *Clim. Change* 104, 113–137. doi: 10.1007/s10584-010-9978-3

Hansen, L. (2018). *Sea Level Data 1889-2017 From 14 Stations in Denmark Mean, Maximum and Minimum Values Calculated on Monthly and Yearly Basis Including Plots of Mean Values*. Technical Report 18-16, Danish Meteorological Institute.

Hay, C. C., Morrow, E., Kopp, R. E., and Mitrovica, J. X. (2015). Probabilistic reanalysis of twentieth-century sea-level rise. *Nature* 517:481. doi: 10.1038/nature14093

Hewitt, C., Mason, S., and Walland, D. (2012). The global framework for climate services. *Nat. Clim. Change* 2, 831–832. doi: 10.1038/nclimate1745

Hieronymus, M., and Kalén, O. (2020). Sea-level rise projections for Sweden based on the new IPCC special report: the ocean and cryosphere in a changing climate. *Ambio* 49, 1587–1600. doi: 10.1007/s13280-019-01313-8

Hinkel, J., Church, J. A., Gregory, J. M., Lambert, E., Le Cozannet, G., Lowe, J., et al. (2019). Meeting user needs for sea level rise information: a decision analysis perspective. *Earth's Fut*. 7, 320–337. doi: 10.1029/2018EF001071

Hinkel, J., Lincke, D., Vafeidis, A. T., Perrette, M., Nicholls, R. J., Tol, R. S. J., et al. (2014). Coastal flood damage and adaptation costs under 21st century sea-level rise. *Proc. Natl. Acad. Sci. U.S.A*. 111, 3292–3297. doi: 10.1073/pnas.1222469111

Holgate, S. J., Matthews, A., Woodworth, P. L., Rickards, L. J., Tamisiea, M. E., Bradshaw, E., et al. (2013). New data systems and products at the permanent service for mean sea level. *J. Coast. Res*. 29, 493–504. doi: 10.2112/JCOASTRES-D-12-00175.1

Hünicke, B., and Zorita, E. (2016). Statistical analysis of the acceleration of Baltic mean sea-level rise, 1900–2012. *Front. Mar. Sci*. 3:125. doi: 10.3389/fmars.2016.00125

Jevrejeva, S., Grinsted, A., and Moore, J. C. (2014). Upper limit for sea level projections by 2100. *Environ. Res. Lett*. 9:104008. doi: 10.1088/1748-9326/9/10/104008

Jevrejeva, S., Jackson, L. P., Grinsted, A., Lincke, D., and Marzeion, B. (2018). Flood damage costs under the sea level rise with warming of 1.5 °C and 2 °C. *Environ. Res. Lett*. 13:074014. doi: 10.1088/1748-9326/aacc76

Jevrejeva, S., Jackson, L. P., Riva, R. E. M., Grinsted, A., and Moore, J. C. (2016). Coastal sea level rise with warming above 2 °C. *Proc. Natl. Acad. Sci. U.S.A*. 113, 13342–13347. doi: 10.1073/pnas.1605312113

Keskitalo, E. C. H., Juhola, S., Baron, N., Fyhn, H., and Klein, J. (2016). Implementing local climate change adaptation and mitigation actions: the role of various policy instruments in a multi-level governance context. *Climate* 4:7. doi: 10.3390/cli4010007

Kierulf, H. P., Steffen, H., Simpson, M. J. R., Lidberg, M., Wu, P., and Wang, H. (2014). A GPS velocity field for Fennoscandia and a consistent comparison to glacial isostatic adjustment models. *J. Geophys. Res*. 119, 6613–6629. doi: 10.1002/2013JB010889

Kirezci, E., Young, I. R., Ranasinghe, R., Muis, S., Nicholls, R. J., Lincke, D., et al. (2020). Projections of global-scale extreme sea levels and resulting episodic coastal flooding over the 21st Century. *Sci. Rep*. 10:11629. doi: 10.1038/s41598-020-67736-6

Kopp, R. E., Horton, R. M., Little, C. M., Mitrovica, J. X., Oppenheimer, M., Rasmussen, D. J., et al. (2014). Probabilistic 21st and 22nd century sea-level projections at a global network of tide-gauge sites. *Earth's Fut*. 2, 383–406. doi: 10.1002/2014EF000239

Kulp, S. A., and Strauss, B. H. (2019). New elevation data triple estimates of global vulnerability to sea-level rise and coastal flooding. *Nat. Commun*. 10:4844. doi: 10.1038/s41467-019-13552-0

Little, C. M., Oppenheimer, M., and Urban, N. M. (2013). Upper bounds on twenty-first-century Antarctic ice loss assessed using a probabilistic framework. *Nat. Clim. Change* 3, 654–659. doi: 10.1038/nclimate1845

Ludwigsen, C. A., Khan, S. A., Andersen, O. B., and Marzeion, B. (2020). Vertical land motion from present-day deglaciation in the wider Arctic. *Geophys. Res. Lett*. 47:e2020GL088144. doi: 10.1029/2020GL088144

Madsen, K. S., Høyer, J. L., Suursaar, Ü., She, J., and Knudsen, P. (2019a). Sea level trends and variability of the Baltic sea from 2D statistical reconstruction and altimetry. *Front. Earth Sci*. 7:243. doi: 10.3389/feart.2019.00243

Madsen, K. S., Murawski, J., Blokhina, M., and Su, J. (2019b). Sea level change: mapping danish municipality needs for climate information. *Front. Earth Sci*. 7:81. doi: 10.3389/feart.2019.00081

Marcos, M., Calafat, F. M., Berihuete, Á., and Dangendorf, S. (2015). Long-term variations in global sea level extremes. *J. Geophys. Res*. 120, 8115–8134. doi: 10.1002/2015JC011173

Masina, M., and Lamberti, A. (2013). A nonstationary analysis for the Northern Adriatic extreme sea levels. *J. Geophys. Res*. 118, 3999–4016. doi: 10.1002/jgrc.20313

Meier, H. E. M., Broman, B., and Kjellström, E. (2004). Simulated sea level in past and future climates of the Baltic Sea. *Climate Res*. 27, 59–75. doi: 10.3354/cr027059

Mitrovica, J. X., Gomez, N., and Clark, P. U. (2009). The sea-level fingerprint of West Antarctic collapse. *Science* 323, 753–753. doi: 10.1126/science.1166510

Mitrovica, J. X., Gomez, N., Morrow, E., Hay, C., Latychev, K., and Tamisiea, M. (2011). On the robustness of predictions of sea level fingerprints. *Geophys. J. Int*. 187, 729–742. doi: 10.1111/j.1365-246X.2011.05090.x

Mitrovica, J. X., Hay, C. C., Kopp, R. E., Harig, C., and Latychev, K. (2018). Quantifying the sensitivity of sea level change in coastal localities to the geometry of polar ice mass flux. *J. Clim*. 31, 3701–3709. doi: 10.1175/JCLI-D-17-0465.1

Mitrovica, J. X., and Milne, G. A. (2003). On post-glacial sea level: I. General theory. *Geophys. J. Int*. 154, 253–267. doi: 10.1046/j.1365-246X.2003.01942.x

Mohrholz, V. (2018). Major Baltic inflow statistics?revised. *Front. Mar. Sci*. 5:384. doi: 10.3389/fmars.2018.00384

Møller, J. T. (1997). "Denmark," in *Geomorphological Hazards of Europe, Vol. 5 of Developments in Earth Surface Processes*, eds C. Embleton and C. Embleton-Hamann (Amsterdam: Elsevier), 91–98. doi: 10.1016/S0928-2025(97)80005-3

Mörner, N.-A. (2013). Sea level changes past records and future expectations. *Energy Environ*. 24, 509–536. doi: 10.1260/0958-305X.24.3-4.509

Moser, S. C., and Ekstrom, J. A. (2010). A framework to diagnose barriers to climate change adaptation. *Proc. Natl. Acad. Sci. U.S.A*. 107, 22026–22031. doi: 10.1073/pnas.1007887107

Muis, S., Apecechea, M. I., Dullaart, J., de Lima Rego, J., Madsen, K. S., Su, J., et al. (2020). A high-resolution global dataset of extreme sea levels, tides, and storm surges, including future projections. *Front. Mar. Sci*. 7:263. doi: 10.3389/fmars.2020.00263

Muis, S., Verlaan, M., Winsemius, H. C., Aerts, J. C., and Ward, P. J. (2016). A global reanalysis of storm surges and extreme sea levels. *Nat. Commun*. 7:11969. doi: 10.1038/ncomms12913

Nerem, R. S., Beckley, B. D., Fasullo, J. T., Hamlington, B. D., Masters, D., and Mitchum, G. T. (2018). Climate-change-driven accelerated sea-level rise detected in the altimeter era. *Proc. Natl. Acad. Sci. U.S.A*. 115, 2022–2025. doi: 10.1073/pnas.1717312115

Olesen, M., Madsen, K. S., Ludwigsen, C. A., Boberg, F., Christensen, T., Cappelen, J., et al. (2014). *Fremtidige Klimaforandringer i Danmark*. Technical Report 14-06, Danish Meteorological Institute.

Oppenheimer, M., Glavovic, B., Hinkel, J., van de Wal, R., Magnan, A. K., Abd-Elgawad, A., et al. (2019). "Sea level rise and implications for low-lying islands, coasts and communities," in *IPCC Special Report on the Ocean and Cryosphere in a Changing Climate*, eds H.-O. PRörtner, D. C. Roberts, V. Masson-Delmotte, P. Zhai, M. Tignor, E. Poloczanska, K. Mintenbeck, A. Alegría, M. Nicolai, A. Okem, J. Petzold, B. Rama, N. M. Weyer.

Permanent Service for Mean Sea Level (PSMSL) (2020). *Tide Gauge Data*. Available online at: http://www.psmsl.org/data/obtaining/ (Retrieved 13 April, 2020).

Prahl, B. F., Boettle, M., Costa, L., Kropp, J. P., and Rybski, D. (2018). Damage and protection cost curves for coastal floods within the 600 largest European cities. *Sci. Data* 5:180034. doi: 10.1038/sdata.2018.34

Rahmstorf, S. (2010). A new view on sea level rise. *Nat. Clim. Change* 1, 44–45. doi: 10.1038/climate.2010.29

Sella, G. F., Stein, S., Dixon, T. H., Craymer, M., James, T. S., Mazzotti, S., et al. (2007). Observation of glacial isostatic adjustment in stable? North America with GPS. *Geophys. Res. Lett*. 34. doi: 10.1029/2006GL027081

Shepherd, A., Ivins, E., Rignot, E., Smith, B., van den Broeke, M., Velicogna, I., et al. (2018). Mass balance of the Antarctic ice sheet from 1992 to 2017. *Nature* 558, 219–222. doi: 10.1038/s41586-018-0179-y

Slangen, A. B., Meyssignac, B., Agosta, C., Champollion, N., Church, J. A., Fettweis, X., et al. (2017). Evaluating model simulations of twentieth-century sea level rise. Part I: global mean sea level change. *J. Clim*. 30, 8539–8563. doi: 10.1175/JCLI-D-17-0110.1

Sørensen, C., Broge, N. H., Molgaard, M. R., Schow, C. S., Thomsen, P., Vognsen, K., et al. (2016). Assessing future flood hazards for adaptation planning in a Northern European coastal community. *Front. Mar. Sci*. 3:69. doi: 10.3389/fmars.2016.00069

Sørensen, C. S. (2016). "Water NOT wanted-coastal floods and flooding protection in Denmark," in *Sicherung von Dämmen, Deichen und Stauanlagen: Handbuch für Theorie und Praxis*, eds. R. A. Herrmann and J. Jensen (Siegen: Universität Siegen), 3–21.

Spada, G. (2017). Glacial isostatic adjustment and contemporary sea level rise: an overview. *Surv. Geophys*. 38, 153–185. doi: 10.1007/s10712-016-9379-x

Swart, R., [de Bruin], K., Dhenain, S., Dubois, G., Groot, A., and [von der Forst], E. (2017). Developing climate information portals with users: promises and pitfalls. *Clim. Serv*. 6, 12–22. doi: 10.1016/j.cliser.2017.06.008

Vestøl, O., Ågren, J., Steffen, H., Kierulf, H., and Tarasov, L. (2019). NKG2016LU: a new land uplift model for Fennoscandia and the Baltic Region. *J. Geodesy* 93, 1759–1779. doi: 10.1007/s00190-019-01280-8

Vousdoukas, M. I., Mentaschi, L., Voukouvalas, E., Bianchi, A., Dottori, F., and Feyen, L. (2018a). Climatic and socioeconomic controls of future coastal flood risk in Europe. *Nat. Clim. Change* 8, 776–780. doi: 10.1038/s41558-018-0260-4

Vousdoukas, M. I., Mentaschi, L., Voukouvalas, E., Verlaan, M., Jevrejeva, S., Jackson, L. P., et al. (2018b). Global probabilistic projections of extreme sea levels show intensification of coastal flood hazard. *Nat. Commun*. 9:2360. doi: 10.1038/s41467-018-04692-w

Wahl, T., Haigh, I. D., Nicholls, R. J., Arns, A., Dangendorf, S., Hinkel, J., et al. (2017). Understanding extreme sea levels for broad-scale coastal impact and adaptation analysis. *Nat. Commun*. 8:16075. doi: 10.1038/ncomms16075

Wahl, T., Haigh, I. D., Woodworth, P. L., Albrecht, F., Dillingh, D., Jensen, J., et al. (2013). Observed mean sea level changes around the North Sea coastline from 1800 to present. *Earth-Sci. Rev*. 124, 51–67. doi: 10.1016/j.earscirev.2013.05.003

Watson, C. S., White, N. J., Church, J. A., King, M. A., Burgette, R. J., and Legresy, B. (2015). Unabated global mean sea-level rise over the satellite altimeter era. *Nat. Clim. Change* 5, 565–568. doi: 10.1038/nclimate2635

Woodworth, P. L. (2006). Some important issues to do with long-term sea level change. *Philos. Trans. R. Soc. A* 364, 787–803. doi: 10.1098/rsta.2006.1737

Woodworth, P. L., Hunter, J., Marcos, M., Caldwell, P., Menéndez, M., and Haigh, I. (2016). Towards a global higher-frequency sea level dataset. *Geosci. Data J*. 3, 50–59. doi: 10.1002/gdj3.42

Woodworth, P. L., Melet, A., Marcos, M., Ray, R. D., Wöppelmann, G., Sasaki, Y. N., et al. (2019). Forcing factors affecting sea level changes at the coast. *Surv. Geophys*. 40, 1351–1397. doi: 10.1007/s10712-019-09531-1

Yu, H., Rignot, E., Seroussi, H., and Morlighem, M. (2018). Retreat of Thwaites Glacier, West Antarctica, over the next 100 years using various ice flow models, ice shelf melt scenarios and basal friction laws. *Cryosphere* 12, 3861–3876. doi: 10.5194/tc-12-3861-2018

Conflict of Interest: The authors declare that the research was conducted in the absence of any commercial or financial relationships that could be construed as a potential conflict of interest.

Copyright © 2021 Su, Andrée, Nielsen, Olsen and Madsen. This is an open-access article distributed under the terms of the Creative Commons Attribution License (CC BY). The use, distribution or reproduction in other forums is permitted, provided the original author(s) and the copyright owner(s) are credited and that the original publication in this journal is cited, in accordance with accepted academic practice. No use, distribution or reproduction is permitted which does not comply with these terms.

frontiers in Marine Science

ORIGINAL RESEARCH
published: 21 June 2021
doi: 10.3389/fmars.2021.665672

Coastal Flooding in the Maldives Induced by Mean Sea-Level Rise and Wind-Waves: From Global to Local Coastal Modelling

Angel Amores[1], Marta Marcos[1,2], Rodrigo Pedreros[3], Gonéri Le Cozannet[3], Sophie Lecacheux[3], Jérémy Rohmer[3], Jochen Hinkel[4], Geronimo Gussmann[4], Thomas van der Pol[4], Ali Shareef[5] and Zammath Khaleel[5]*

[1] Instituto Mediterráneo de Estudios Avanzados (UIB-CSIC), Esporles, Spain, [2] Departament de Física, Universitat de les Illes Balears, Palma, Spain, [3] French Geological Survey (BRGM), Orléans, France, [4] Global Climate Forum, Berlin, Germany, [5] Ministry of Environment, Malé, Maldives

The Maldives, with one of the lowest average land elevations above present-day mean sea level, is among the world regions that will be the most impacted by mean sea-level rise and marine extreme events induced by climate change. Yet, the lack of regional and local information on marine drivers is a major drawback that coastal decision-makers face to anticipate the impacts of climate change along the Maldivian coastlines. In this study we focus on wind-waves, the main driver of extremes causing coastal flooding in the region. We dynamically downscale large-scale fields from global wave models, providing a valuable source of climate information along the coastlines with spatial resolution down to 500 m. This dataset serves to characterise the wave climate around the Maldives, with applications in regional development and land reclamation, and is also an essential input for local flood hazard modelling. We illustrate this with a case study of HA Hoarafushi, an atoll island where local topo-bathymetry is available. This island is exposed to the highest incoming waves in the archipelago and recently saw development of an airport island on its reef via land reclamation. Regional waves are propagated toward the shoreline using a phase-resolving model and coastal inundation is simulated under different mean sea-level rise conditions of up to 1 m above present-day mean sea level. The results are represented as risk maps with different hazard levels gathering inundation depth and speed, providing a clear evidence of the impacts of the sea level rise combined with extreme wave events.

Keywords: coastal flooding, wind-waves, sea-level rise, global-to-local modelling, climate services

OPEN ACCESS

Edited by:
Juan Jose Munoz-Perez, University of Cádiz, Spain

Reviewed by:
Dean Bryan Gesch, United States Geological Survey (USGS), United States
Philip Thompson, University of Hawaii, United States

****Correspondence:***
Angel Amores
angel.amores@uib.es

Specialty section:
This article was submitted to Coastal Ocean Processes, a section of the journal Frontiers in Marine Science

Received: *08 February 2021*
Accepted: *19 May 2021*
Published: *21 June 2021*

Citation:
Amores A, Marcos M, Pedreros R, Le Cozannet G, Lecacheux S, Rohmer J, Hinkel J, Gussmann G, van der Pol T, Shareef A and Khaleel Z (2021) Coastal Flooding in the Maldives Induced by Mean Sea-Level Rise and Wind-Waves: From Global to Local Coastal Modelling. Front. Mar. Sci. 8:665672. doi: 10.3389/fmars.2021.665672

1. INTRODUCTION

Increased coastal flooding damages are among the potentially most hazardous and costliest aspects of global warming (Hinkel et al., 2014), impacting populations, ecosystems and assets. Coastal flood exposure is currently increasing at rates higher than inland due to population growth, urbanisation and the coastward migration of people (Merkens et al., 2018), and also due to coastal extreme water levels being raised by mean sea-level rise (Marcos and Woodworth, 2017). The Special Report on the Ocean and Cryosphere in a Changing Climate (SROCC) of the Intergovernmental Panel

on Climate Change (IPCC) projects that if greenhouse gas (GHG) emissions continue to rise unmitigated (i.e., RCP8.5) global-mean sea levels are likely to rise by 0.6–1.1 m by 2100, and 2.3–5.4 m by 2300 (Oppenheimer et al., 2019). Projected mean sea-level rise during the twenty-first century and beyond (Kopp et al., 2014) will inevitably increase the intensity of flood events and will thus exacerbate the exposure and vulnerability of coastal areas in the decades to come, with highest impacts expected in low-lying regions. Hinkel et al. (2014) estimated that, without adaptation, by 2100 almost 5% of the global population will be potentially flooded annually, with losses of up to 10% of the global GDP, under a 1.20 m mean sea-level rise. This will require the implementation of extensive and ubiquitous coastal adaptation solutions to avoid such large impacts (Hinkel et al., 2019). But also if emissions are reduced to meet the goal of the Paris Agreement to limit global warming "well bellow 2°C" (i.e., RCP2.6), global mean sea-level is likely to rise by 0.3–0.6 m in 2100 and 0.6–1.1 m by 2300, which will still be a tremendous challenge, in particular for very low lying regions such as atoll states.

The threats of flooding events are particularly worrisome in low-lying coastal zones, including large deltas and sinking coastal mega-cities; but the regions with the largest expected relative impacts are small island states (Nurse et al., 2014). The Maldivian archipelago is an iconic case of vulnerability to mean sea-level rise. Located in the equatorial region of the Tropical Indian Ocean, the Maldives consist of 1192 islands, dispersed across 860 km from 8° north to 1° south in latitude, of which 188 are inhabited (NBS, 2017; Wadey et al., 2017) (see **Figure 1**). The resident population in 2014 was 437,000 people and is estimated to reach 557,000 in 2020, with 40% of the population living in the capital, Malé, and its surrounding islands Villimalé and Hulhumalé (NBS, 2019). Average land elevations range from 0.5 m to 2.3 m above present-day mean sea level (Woodworth, 2005), with 80% falling below 1 m. Since the 1950s several land reclamation projects have been carried out to address land scarcity, for example in the southern lagoon of Malé in 1954 (Maniku, 1990). With the rapid economic development of the Maldives, land reclamation projects have also increased. The Maldivian government estimates that over 1300 hectares of reef or lagoon area have been reclaimed up until 2016 (MEE, 2017). This new land is required to be elevated between 1.5 and 1.75 m above mean sea-level. However, this static approach to island elevation ignores the differing wave exposure across the archipelago.

A lot of land reclamation is taking place in the Maldives and a new long-term regional development strategy is currently being prepared that prioritises islands for development (Gussmann and Hinkel, 2021). While it is known that wave exposure differs across islands, this has so far not been taken into account in land reclamation and regional development. The development of adaptation plans in the framework of coastline management aimed to address flood hazards requires accurate information and a deep understanding of the driving processes. Coastal flood events are caused by extreme coastal water levels that in turn result from the combination of relative mean sea-level, tides, storm surges, wind-waves, precipitation and/or river run-off

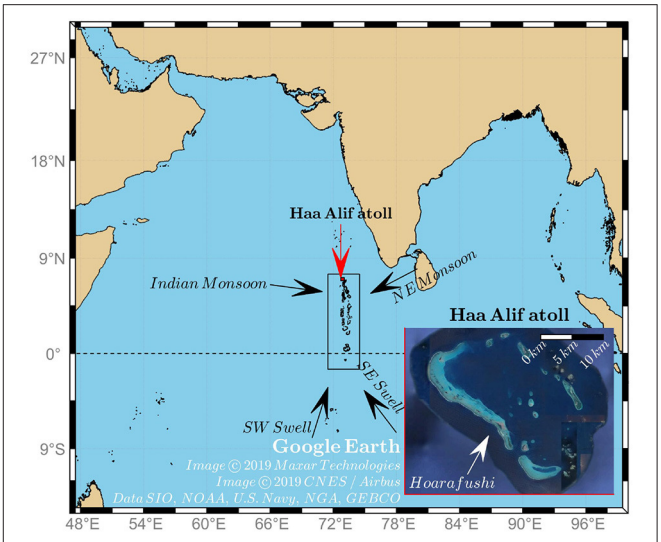

FIGURE 1 | Map of the Indian Ocean with the Maldivian archipelago inside the black box. The four black arrows indicate the main wave direction identified. The red arrow indicates the location of the Haa Alif atoll in which is located Hoarafushi island (satellite image in the bottom-right corner extracted from Google Earth. Image © 2019 Maxar Technologies; Image © 2019 CNES/Airbus; Data SIO, NOAA, U.S. Navy, NGA, GEBCO).

(Woodworth et al., 2019). The design of adaptation strategies therefore involves the knowledge of every individual driver and their future projections at the local scale, as well as their possible interactions (Nicholls et al., 2014). In the case of the Maldives, the tidal range is relatively small (<1 m of maximum high waters) and the storm surge contribution is negligible, as corresponds to an equatorial region (Wadey et al., 2017). Earlier studies have pointed at wind-waves as the primary mechanism causing flooding events in the Maldives, similarly to other Indian and Pacific islands (Hoeke et al., 2013). One of the first works was presented by Harangozo (2013), who investigated an event that occurred in April 1987 that flooded Mal?é, including reclaimed land below 1 m above mean sea-level and during which the hard structures designed to protect this land were destroyed. Based on altimetric wave measurements and *in-situ* sea-level observations, this event was attributed to prolonged swell waves originated in the Southern Indian Ocean and reaching the island during high tides. Similarly, in 2007, the Fares island, located in the southernmost atoll of the Maldives was flooded due to a series of remotely-generated swell events reaching the island (Wadey et al., 2017; Beetham and Kench, 2018) which also affected other areas of the eastern Indian Ocean (e.g., Lecacheux et al., 2012 in La Réunion Island). This event was particularly hazardous as it flooded almost the entire island and affected more than 1500 people as well as the limited water resources of the island. An extensive study was carried out in response to this event and a protective offshore breakwater was built to avoid future damages. For a comprehensive list of flooding events in the Maldives, the reader is referred to Wadey et al. (2017), where the available information of several flooding events has been collected from a number of sources.

Despite the recurrent flooding episodes associated with swells, overall, in the Maldivian archipelago a complete and accurate assessment on the wind-wave climate, including extreme waves, is hindered by the lack of observations and regionalisation of model runs. Numerical wind-wave simulations are available with a global coverage, including both re-analyses (i.e., Saha et al., 2010) and projections (i.e., Hemer and Trenham, 2016; Morim et al., 2019), although with a coarse resolution that prevents their use for many practical purposes, such as accurate local assessments. This work intends to fill this gap by providing the necessary information on waves to perform coastal studies along the Maldivian shorelines. The objectives of the present study are three-fold: first, we fully characterise the wave climate around the Maldives on the basis of global, coarse resolution numerical wave dynamical simulations for present-day, and we further evaluate the projected changes under climate change scenarios (section 3). Secondly, we downscale the extreme wave climate through propagation of the main extreme waves from the dominant directions toward the coastlines with a much higher resolution (section 4). And finally, we illustrate how this information can be translated into a flood hazard assessment in a selected location that is exposed to the largest incoming swell waves in the archipelago. To do so, we propagate wave conditions from the nearshore to the coastline under different mean sea-level rise scenarios and quantify the flooding extent with and without land reclamation (section 5). Data, methods and numerical models are described in section 2, while all the results are discussed together in section 6.

2. DATA AND METHODS

This section describes the global wave data that is used to characterise and downscale wave information to the nearshore in the Maldives, together with the numerical models and their implementation. Local wave modelling is used as the basis of flood hazard assessment for a case study. To do so, waves are combined with a set of mean sea-level changes using a scenario-independent approach. That is, waves are propagated toward the shoreline under prescribed mean sea-level increments of 0.25, 0.5, 0.75, and 1 m with respect to present-day averaged value. Note that these values are not necessarily interpreted as climate-induced mean sea-level rise; they can also be associated to tidal oscillations or to a combination of tides and mean sea-level rise.

2.1. Global Wind-Wave Datasets

We have used the CAWCR Global wind-wave data set that is freely distributed through the CSIRO data server (Hemer et al., 2015). This set, generated with the WaveWatch III wave model (version 3.14, Tolman, 2009) in a common $1^\circ \times 1^\circ$ resolution global grid, consists of a hindcast, historical runs (late twentieth century), and projections for the twenty-first century. The hindcast has been forced with surface wind fields from the NCEP CFSR (Saha et al., 2010) and covers the period from 1979 to 2009 with a temporal resolution of 1 h (this simulation is referred to as CFSR hereinafter). The historical runs and projections were generated using the output fields of 8 different CMIP5 models (ACCESS1.0, BCC-CSM1.1, CNRM-CM5, GFDL-ESM2M, HadGEM2-ES, INMCM4, MIROC5, and MRI-CGCM3), covering three different time periods with a temporal resolution of 6 h: historical runs for 1980-2005; and projected waves for mid-(2026–2045) and late-(2081–2100) twenty-first century. The projections for mid- and late-twenty-first century were run under two different emission scenarios, RCP4.5 and RCP8.5, although we will use only the latter. A detailed description of the wave climate dataset can be found in Hemer et al. (2013).

Global wave models are used to characterise the present-day and future projected changes of wave climate around the Maldivian archipelago, with emphasis on the extreme wave climate. Return levels of Hs for a set of prescribed return periods are calculated by fitting the top 1% waves to a Generalised Pareto Distribution. Given the coarse spatial resolution of the model configuration, we do not expect the small islands as the Maldives to be accurately represented by these global simulations. Given that the wave fields are modified by the presence of the islands (see for example Supplementary Video 1 from Amores and Marcos, 2019), the global fields must be downscaled in order to be usable for practical purposes. This process is described in the following.

2.2. Regional Wave Modelling

Global waves have been dynamically downscaled in the Maldives using the WaveWatchIII wave model (version 4.18, Tolman, 2014). The model was implemented on an unstructured mesh with 33160 nodes and 64456 elements over a domain ranging from 71.5 to $75.5^\circ E$ in longitude and from $-1.5^\circ N$ to $8.5^\circ N$ in latitude (black rectangle surrounding the Maldives in **Figure 1**). The spatial resolution of the unstructured mesh varied from 50 km along the boundaries of the domain down to 500 m in the channels between the atolls. Only the external coasts of the atoll islands were considered due to the lack of bathymetric information inside the atolls. The regional bathymetry used to build the model grid was the GEBCO bathymetry 2014 in a global 30 arc-second interval grid (https://www.gebco.net/). The wave spectrum was defined by a directional resolution of 10° and 24 frequency bands ranging non-linearly from 0.0373 to 1.1 Hz. Dynamical downscaling was preferred instead of statistical approaches because there is no local information on waves that can be used to calibrate the model.

2.3. Local Wave Modelling

Nearshore downscaled waves have been propagated toward the coastline for a case study site. The selected location corresponds to Haa Alif atoll (HA) at Hoarafushi island, located at the north of the archipelago (**Figure 1**). Hoarafushi has a maximum length of 2,500 m and a maximum width of 500 m (**Figure 1**). This site has been chosen for two main reasons: firstly, at the start of this study a land reclamation project to build a new airport next to the island was foreseen. The development of the regional airport on the newly reclaimed island on the reef of HA Hoarafushi is part of the government's regional development and decentralisation plans, which puts extra focus on the northernmost atoll Ihavandhippolhu. We therefore aimed

at evaluating the exposure of this new reclaimed land to incoming waves and how its presence can alter the wave propagation over the reef and the exposure of the current island. The process of land reclamation was started on April 16th, 2019 (https://edition.mv/news/10159) and finished almost 5 months later, on September 5th, 2019 (https://edition.mv/news/12266; see **Supplementary Figure 1**, to see the construction process on June 15th, 2019). Secondly, information on the local bathymetry and land elevation is available and allows to simulate the wave propagation. A bathymetry around the island was generated by combining measurements on the reef flat performed by the Maldives Transport and Contracting Company, who was in charge of the design of the land reclamation project. We completed these data with reef slope measurements taken during a field trip on February 2018 (using a single beam echosounder). Our measurements included a total of 10 profiles across-slope separated around 200–500 m between them as well as several along-slope transects. The minimum depth measured in the across-slope profiles was around 3 m, that was the closest the boat could get to the reef crest, and the maximum depth recorded, that was fixed by the maximum range of the echosounder, was around 50 m. Unfortunately, there is no detailed information on the topography of the island. Instead, a constant land height of 1.5 m above present-day mean sea level has been used, according to visual inspections and in accordance with existing regulations. The coastline of the island has been represented with a constant slope, given that there are not hard structures in the oceanward side. Two topo-bathymetries have been implemented, with and without the presence of the airport. Finally, it is worth mentioning that HA Hoarafushi island is exposed to the highest incoming waves around the archipelago, as will be shown below.

The local wave propagation has used the SWASH model (Zijlema et al., 2011, code available at http://swash.sourceforge.net/) in a 2D regular grid of 6,220 m in the W-E direction and 7,320 m in the S-N direction with 10 m of spatial resolution (see the domain in **Figure 8**). This model is suitable for our purposes as it is capable of simulating wave setup and runup and predicting infragravity waves in the nearshore (Rijnsdorp et al., 2012), a relevant process that contributes to the amount of flooding by raising temporary the sea level near the coast. The West and South boundaries were considered active introducing the wave forcing in the domain with Jonswap spectra with a wave dispersion of 20° and a peak enhancement parameter γ of 3.3. A different combination of wave dispersion and γ was tested (5° and 10°, respectively), resulting in essentially the same results in terms of flooding. A 150 m sponge layer was placed in the eastern boundary and 1,000 m sponge layer in the northern boundary, to avoid unrealistic wave forcing from the interior of the atoll given by spurious wave reflection from the those boundaries. The lack of *in-situ* measurements of wave propagation and transformation along the domain made it impossible to calibrate the Manning's friction coefficient. The values for coral reefs found in the literature vary from 0.01 to 0.2. For example, Zijlema (2012) used 0.01, Prager (1991) used 0.05, Kraines et al. (1998) used 0.1, and Cialone and Smith (2007) used spatially-varying Manning's coefficient values of 0.02, 0.19, and 0.2 depending on the region of their domain. The Manning's coefficient value was finally fixed to 0.019 following Suzuki et al. (2018), who investigated the most suitable value for SWASH model applied to overtopping computation along a beach profile with defined defenses. In our case, there is not a complete beach profile, but the overtopping, which is the process of interest here, is occurring at the shoreline of a sandy beach.

With this configuration, the total simulated time for each combination of parameters was 70 min, with an initial integration time of 0.05 s and having outputs every 5 s. This is computationally intensive but still feasible for the range of experiments and for the two topographies (with and without the airport).

3. CHARACTERISATION OF WAVE CLIMATE AROUND THE MALDIVES

3.1. Present-Day Wave Climate

The outputs of the CFSR wave hindcast at 24 grid points around the Maldives are used to describe the large-scale present-day wave climate in the archipelago (**Figure 2**). Wave roses in **Figure 2** identify, for each grid point, the direction of the dominant wave regimes with their corresponding significant wave heights (H_s) and peak periods (T_p). One prominent feature is that the largest significant wave heights are usually accompanied by peak periods longer than 10–12 s (and reaching up to 24 s), which suggests that these are remotely generated waves, i.e, swell waves. This is in agreement with the location of the Maldives in the Equatorial region, where winds are weak, and in a region exposed to swell waves from the Southern Ocean (Wadey et al., 2017; Amores and Marcos, 2019) and is further examined below.

Waves from the south-west ($\sim$ 205°) are the most common with H_s reaching values larger than 4 m (note that the angles follow the maritime convention, as indicated by the labels in the wave rose of point #1). This finding is in line with Amores and Marcos (2019) that demonstrated that between 80 and 90% of the swell events impacting along the Maldivian coastlines are from SW and originated in a region located between south of Africa and east of South America. The second most frequent direction is the south-east ($\sim$ 145°). These waves reach maximum values of H_s around 3 m, thus smaller than $\sim$ 205° waves, and with peak periods between 10 and 12 s. In addition to these two dominant swell wave directions, two other cases much less frequent but with non-negligible H_s are detected. In the north of the archipelago the largest waves with H_s of up to 5 m are from the west direction ($\sim$ 275°, see wave-rose #17 in **Figure 2**). And finally, waves from 60° are also found in the points of the northeastern side of the archipelago (see, for example, wave-rose #10 in **Figure 2**) with peak periods smaller than 10 s and H_s smaller than around 2.5 m.

The characteristics of the incoming large-scale waves are further analysed in greater detail for three grid points capturing the entire range of directions: point #17 (northwest), point #3 (south), and point #10 (northeast). **Figure 3** examines the annual and seasonal distribution of incoming waves for every direction and their classification in terms of wind-seas and swells, according to the spectral partitioning provided by the global wave models. These histograms, representing the number of

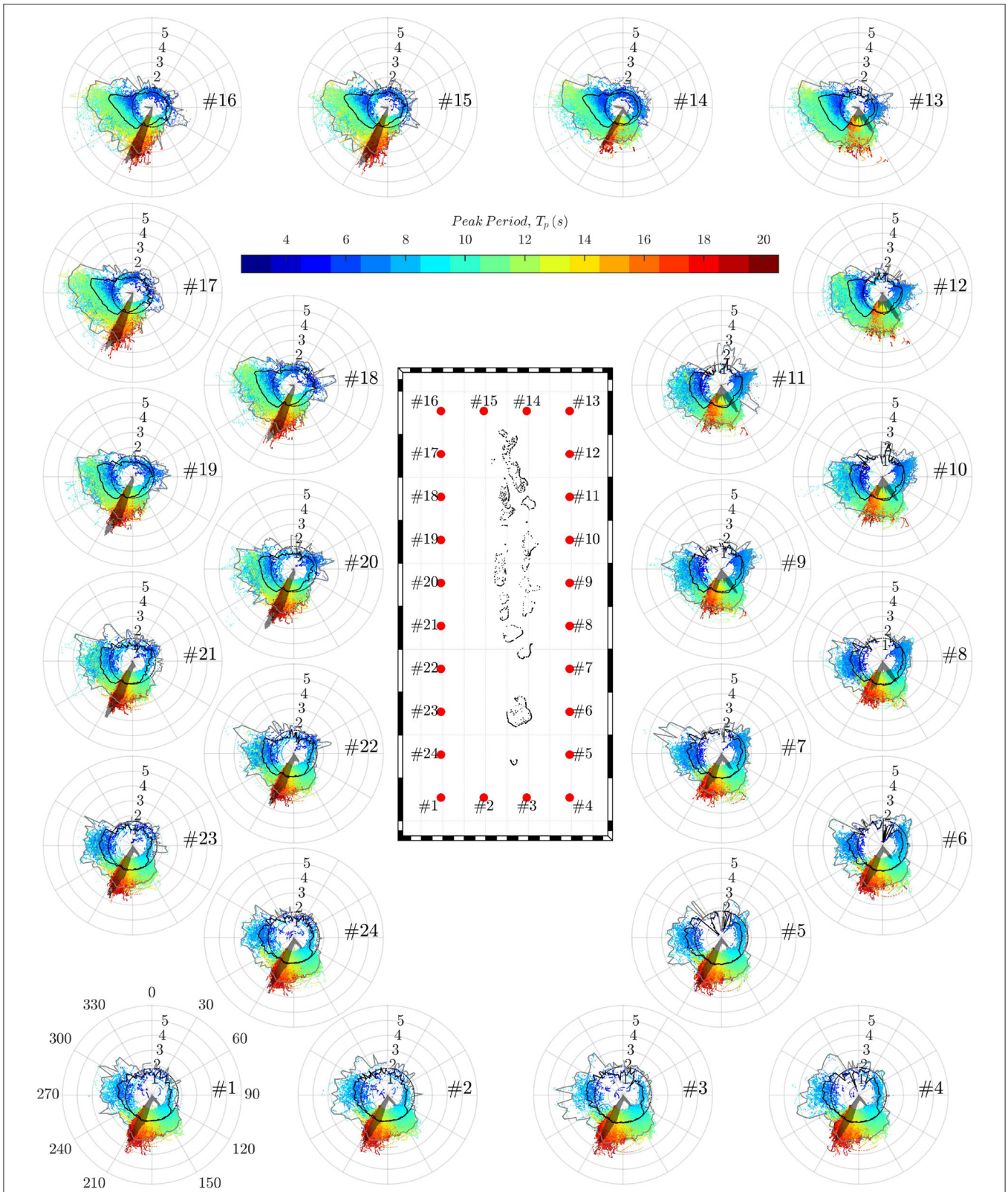

FIGURE 2 | Distribution of the ocean wave climate around the Maldives from the CFSR Hindcast. Each wind-rose-plot corresponds to one point of the central map. The radial distance of each single point in each wind-rose indicates the wave height (m) while the azimutal value indicates the direction that the waves are coming from in nautical convention. The colour of each point shows the peak period. The continuous black (grey) line indicates the quantile 50 (99) for each direction while the dashed black like shows the quantile 50 averaging all the directions. Shadowed areas in the wave roses indicate the most frequent incoming wave directions in a 1° bins (% referred to the radial axis).

events per year, have been constructed with wave events separated at least 3 days to avoid over-representation of the dominant directions and with a minimum peak prominence H_s of 0.2 m to remove noise from smaller waves. The three points are representative of the four incoming wave directions identified above and all register a similar number of waves during the hindcasted period (between 45 and 50 per year, as listed in the title of the panels in **Figure 3**). Their distribution in directions is, however, different, and depends on their position. The most frequent wave direction, around 205°, is evident in points #17 and #3 and is equally likely throughout the entire year (see panels d, e, g, h for comparison among seasons). A composite of the wave and wind fields corresponding to these events is mapped in **Supplementary Figure 2**, demonstrating that these waves indeed correspond to remotely generated southwestern swells, in line with the findings in Amores and Marcos (2019). Waves from the west direction, around 275°, are the second most frequent in point #17 with a marked seasonal character, being only detected between May and October (panel d) and classified as a mixed sea+swell. These waves are generated by the Indian monsoon and only affect the northernmost area of the archipelago. The corresponding composites are shown in **Supplementary Figure 3**. The presence of waves generated by the Indian monsoon likely has an impact on the wave type distribution of the southwestern swell at point #17, since its percentage of sea+swell is larger between May and October; also, the wind fields of the composites corresponding to both types of waves are identical (see last rows in **Supplementary Figures 2, 3**).

The second peak in point #3, seven times less frequent that the southwestern swell and also observed in point #10, corresponds to the direction around 145°, with waves detected throughout the entire year. According to the wave and wind fields composites (**Supplementary Figure 4**) these are waves generated in the Southern Ocean, in a region off the southeastern coast of Australia (Amores and Marcos, 2019). Finally, the fourth incoming direction, around 55°, is clearly detected in point #10, with a strong seasonal character. These waves correspond to the northeast monsoon (Wadey et al., 2017) and are only relevant between November and April, contrasting with the Indian monsoon (panel f and i).

Return levels of H_s for every direction and for the three grid points are shown in **Figure 4** and listed in **Supplementary Table 1**. Noteworthy are the flat tails for the southeastern swells evident in points #10 and #3. Independence among wave events is ensured with the 3-day declustering. A Generalised Pareto Distribution (GPD) has been fitted to the top 1% of the largest H_s; in the case that this subset is too small as to reliably fit the distribution, the 30 largest values (1 event per year on average) were used. The largest return levels correspond to waves generated by the Indian monsoon in point #17 (**Figure 4D**). This direction has a H_s of 4.75 m for a 10 year return period that is larger than all the return levels for the 500 year return periods for all cases (with the exception of the southeastern swell affecting point #3 that has 4.99 m as H_s associated with 500 year return period). On the other side, the lowest return levels correspond to the northeast monsoon affecting point #10 with a H_s equal to 2.74 m for a return period of 500 years, around 1 m lower from the closest return level (3.61 m for 500 year return period for the swell coming from southeast in point #3).

3.2. Wave Projections During the Twenty-First Century

The same three grid points analysed above are used as proxies to evaluate the projected changes in waves around the Maldives, using the output of historical simulations and projections during the twenty-first century. **Figure 5** represents changes in the frequency of arrival of waves for each direction of propagation by the end of the twenty-first century under RCP8.5 with respect to present-day values for each point. The median of the 8 climate model projections is shown in red (blue) when the projected changes indicate an increase (decrease) in the number of wave events and the grey area represents the model spread. Global models project an increase ($\sim$ 3%) of the southwestern swells, consistent with the findings in Amores and Marcos (2019), who showed a greater activity in swell generation in the region of formation of these waves later in this century. For the waves generated by the Indian monsoon, models show a smaller decrease in the number of waves. Other directions do not show robust projected changes, as the model spread is larger than the median change. The same applies to projected variations in median and extreme H_s in all directions of propagation (**Supplementary Figure 8**).

Overall, projected changes in H_s are smaller than the multi-model spread even under RCP8.5 climate scenario. Variations are expected to be even smaller under RCP4.5. In consequence, present-day significant wave height is considered to be largely representative of future wave climate for the purposes of this work and only CFSR wave fields will be downscaled and propagated toward the shorelines. It is worth noting that changes in the frequency of each wave direction (**Figure 5**) can be relevant to the transport of sediments and could modify current erosion patterns.

4. REGIONAL WAVE DOWNSCALING

Global wave information needs to be downscaled to become representative and usable in the nearshore; however, downscaling the full hourly 30-year CFSR hindcast is computationally too intensive. On the other hand, in terms of coastal impacts assessments and, in particular when coastal flooding is concerned, it is extreme values that are the most relevant metric. Therefore, our approach consists of dynamically downscaling the return levels for H_s calculated for 6 different return periods (namely, 10, 20, 50, 100, 500, and 1000 years) and the four main wave directions that were previously identified. To do so, we have used the Wave-WatchIII model configuration described in section 2.2. The H_s return level associated with a given wave direction is defined at a reference grid point and propagated along the corresponding boundary. In order to insert consistently the H_s at the rest of the grid points in the same boundary, the linear relationships between simultaneous events ($\pm 24\,h$), arriving from the same direction and reaching the reference point

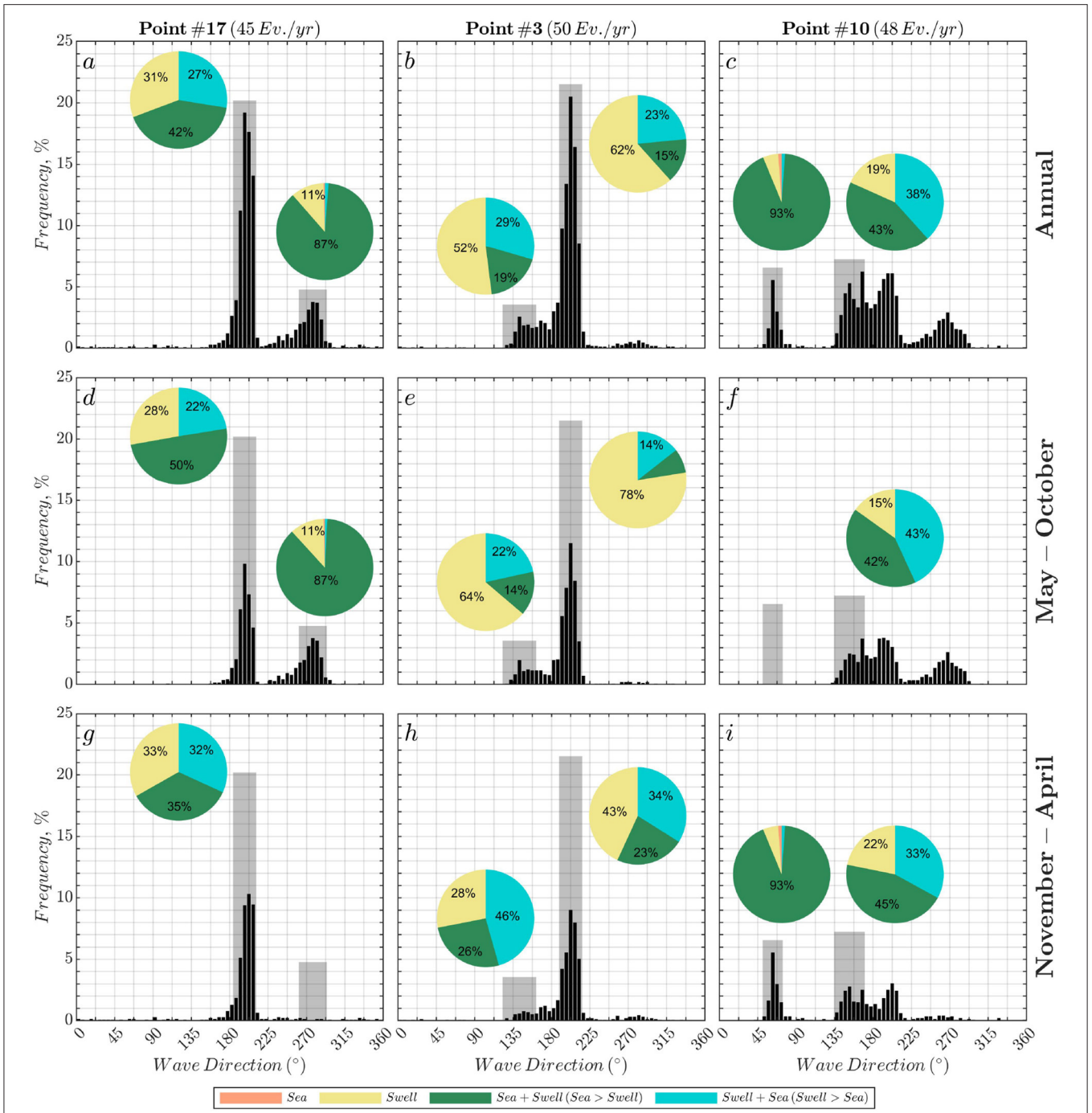

FIGURE 3 | Histograms of wave direction (in nautical convention) registered at the three points selected as being representative (point #17 in the first column (**a,d,g**), #3 in the second (**b,e,h**), and #10 in the third) (**c,f,i**). The first row shows the annual histograms (**a,b,c**), May-October histograms are shown in the second row (**d,e,f**) and November-April histograms are in the last row (**g,h,i**). Each pie chart indicates the spectral separation by type of wave produced by WaveWatch III model [pure sea (H_s of swell = 0), pure swell (H_s of sea = 0), sea + swell dominated by sea (H_s of sea > H_s of swell) and swell + sea dominated by swell (H_s of swell > H_s of sea)] corresponding to each wave component identified (grey shadows).

and the other boundary points were computed. This procedure is illustrated in **Supplementary Figures 9–12**, where also the reference grid points at each boundary are marked. The linear relationships between the reference grid point and the others are used to scale H_s at each active boundary point. The boundary points where no simultaneous events with the reference point were found or, alternatively, for which there is no correlation (we set the limit value of R^2 of the linear adjustment to 0.2),

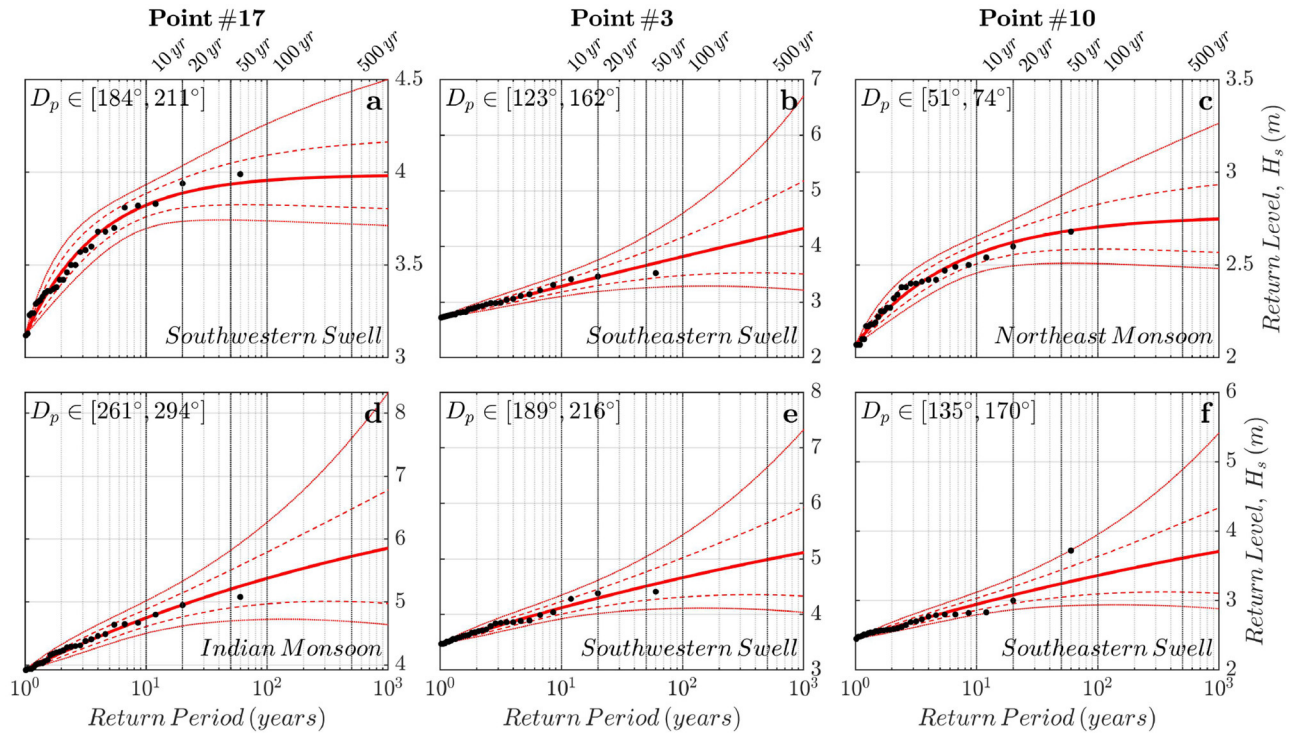

FIGURE 4 | Return levels associated with each return period (thick continuous lines) for the three representative points (point #17 in the first column **(a,d)**, #3 in the second **(b,e)**, and #10 in the third) **(c,f)** for the wave directions identified at each point (for example, panel a corresponds to the first grey shadow in **Figure 3a**). The uncertainty bands correspond to $\pm\sigma$ (dashed lines) and the 5–95 % intervals (dotted lines) and have been computed using the delta method. The return period indicated in the top of the panels (10, 20, 50, 100, and 500 years) are the ones selected to perform the regional downscaling with WaveWatch III. Note that the *y*-axis are different for each panel and do not allow a direct comparison.

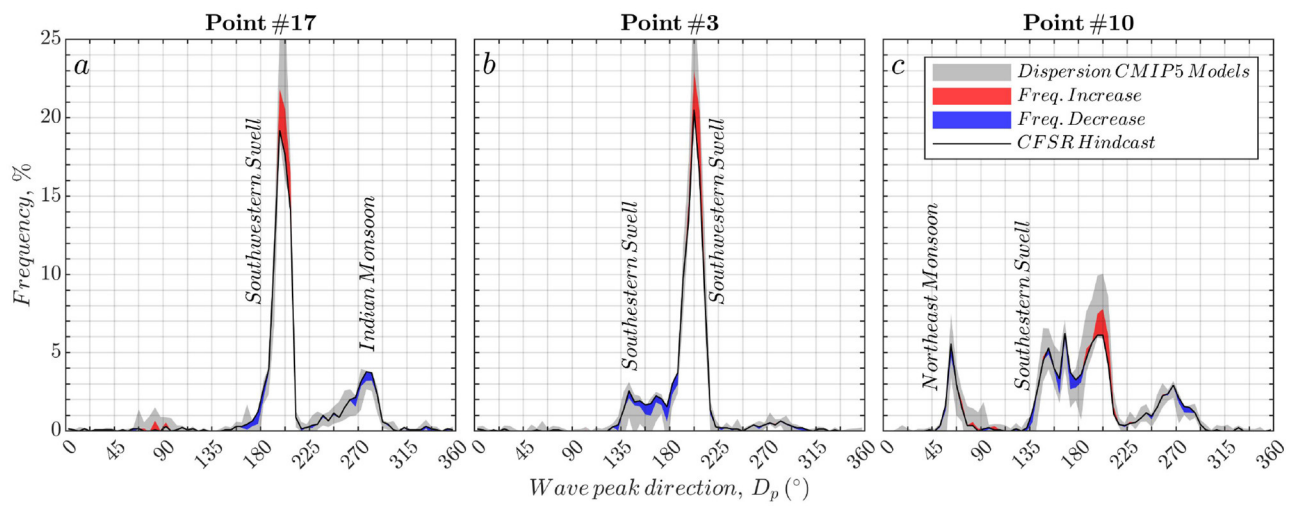

FIGURE 5 | Projected changes in wave direction by the CMIP5 models described in section 2.1 for each one of the representative points selected (**a** point #17, **b** point #3, and **c** point #10). Black line represents the CFSR hindcast histogram (same as the first row in **Figure 3**); grey shadow indicates the spread of the CMIP5 models (RCP8.5 - Historical); red (blue) shadows show where the models agree to project a frequency increase (decrease) of a given direction.

were assigned a linear slope of 0.01 in order to avoid introducing spurious waves. The peak period (T_p) of the incoming waves associated with each return level for H_s, have been determined using a linear relationship between all the (H_s,T_p) events extracted at each reference point for each of the four directions of the incoming waves (**Supplementary Figure 13**).

The resulting downscaled wave fields consist of a set of four return level curves at every coastal grid point with a spatial resolution of ∼500 m. This resolution permits to model wave propagation at the scale of the archipelago. Although it is not accurate enough to perform local assessments inside an atoll, it provides, instead, the necessary boundary condition for the forcing. The full data set is provided at the Zenodo repository under this doi: 10.5281/zenodo.3886273. **Figure 6** shows the results for the 100-year return level of the four directions over the entire domain, sorted by decreasing H_s. Note that the spatial patterns of different return levels will be the same for each wave direction and only the magnitude changes. Due to the limited resolution of the GEBCO topobathymetry ($\sim 1\ km$), an accurate representation of the islands and the inner part of the atolls is not feasible. Thus, the atolls have been considered as whole entities. This assumption implies that the side of the islands that faces toward the atoll's interior is not solved by our regional downscaling. Nevertheless, it is not relevant at this scale because this side of the islands is not directly impacted by waves. We consider that, given the limited depth on the atoll rims (roughly 1 m), this assumption is reasonable, especially because a more accurate assessment would require tide-current local modelling to capture lagoon/ocean interactions.

Figure 6 shows that the largest waves in the Maldives ($H_s > 5\,m$) are generated by the Indian monsoon (panel a) in the northwestern part of the archipelago, with values of H_s exceeding 2 m in the area northwards from 3°N (note that the same colour scale is used for the four maps). One remarkable feature is that these waves, although attenuated, reach the western side of the Kaafu atoll, the most populated atoll in the Maldives and where the capital city Malé is located. Because of the absence of shadow effects, the western coast of the Kaafu atoll, is the inner region of the Maldives exposed to waves with larger H_s, reaching values between 2.5 and 3.0 m. The southwestern swell (panel b), the second direction with largest H_s after the Indian monsoon, is the component that spreads larger H_s to a broader scale. More precisely, it generates ocean waves with H_s >3 m (even than 3.5 m) to all the western sides of the atolls comprising the Maldives. The third ocean wave direction in terms of H_s is the southeastern swell (panel c), that affects all the eastern side of the Maldives with H_s ranging from 2 to 3.5 m. Finally, the northeastern monsoon (panel d) is the ocean wave component with smaller H_s ($< 2\,m$). Its effects are concentrated in the central region of the eastern side of the archipelago, from 2 to 6.5°N. It does not strongly affect the northernmost part of the Maldives because this region is located under the shadow of the Indian continent to the monsoon winds (**Supplementary Figure 6**).

Combining the results of the four wave directions shown in **Figure 6**, we can identify the wave component with greater H_s at each grid point along the coastlines (**Figure 7a**), the value of this greater H_s (**Figure 7b**), as well as how many different directions each coastal point is exposed to **Figure 7c**; $H_s \geq 1.5\ m$. In relative numbers, 33% of the coastlines are exposed to the large waves from the Indian monsoon, in 25% of them the highest waves arrive from the southwestern swell, in 28% from southeastern swell, and only 14% from the northeastern monsoon. As in the case of the Kaafu atoll mentioned above, a similar effect is found in the eastern part of the Faafu and Dhaalu atolls, also located in the interior of the Maldives. Here the dominant wave component reaching the eastern coast of these atolls is the southeastern swell that penetrates in the middle of the Maldives between Thaa Atoll and Meemu Atoll.

In terms of maximum H_s (**Figure 7b**), around 15% of the coastal points, most of them located in the interior of the archipelago, are affected by waves with 100-year return periods smaller than 1 m. The most common values are between 1 and 2 m, affecting 35% of the coastal locations. In 22% of the coasts, the 100-year return levels of H_s vary between 2 and 3 m and in 17% H_s between 3 and 4 m. The largest values, over 4 m, affect around 11% of the coastal points which are found, as expected, in regions where the Indian Monsoon dominates (**Figure 7b**).

Another metric for the exposure of the coasts to incoming waves is the number of swell directions reaching every coastal point. This is illustrated in **Figure 7c**, where we have quantified how many wave directions, from the 4 represented in **Figure 6**, reach each coastal point with $H_s \geq 1.5\,m$ for the 100 year return period. The choice of the H_s threshold and the return period selected is arbitrary and used only for illustration purposes; it is not determinant for the resulting map. We conclude that, in 32% of the coastal points, the 100-year return level of H_s is always smaller than 1.5 m (grey points in **Figure 7c**), with these areas located mainly in the interior of the archipelago. In 29% of the coastal points waves arrive from a single direction (blue points) and in 38% from two directions (yellow points), with the latter case mainly affecting the eastern and western side of the Maldives. In only 1% of the coastal grid points waves arrive from 3 directions (red points), but these are concentrated in the easternmost side of the Vaavu atoll.

5. LOCAL WAVE MODELLING AND FLOOD HAZARD IN HOARAFUSHI ISLAND

The outputs of the regional wave downscaling developed in the previous section are used here in a local flood hazard assessment, illustrating its direct applicability. To do so, downscaled nearshore wave information in a coastal grid point next to Hoarafushi island is propagated toward the shoreline and used to assess coastal flooding under different mean sea-level rise scenarios. The are two reasons that make this location particularly interesting for local wave modelling: first, it is affected by the two largest wave components in the archipelago, i.e., the Indian Monsoon and the southwestern swell; and second, a new island was reclaimed to host a regional airport, which raises questions of present and future climate hazards (see section 2.3). The projected airport, that will have a length of around 1.5 km and a width of 300 m in its wider section, will be located in the reef of the island that faces toward the outer side of the atoll. This means that the shoreline of the airport will be substantially closer to the reef edge than the original island (150–200 m instead of 600 m), reducing the amount of wave energy that can be absorbed by the reef. This local-case study does not pretend to give any recommendation to stakeholders on the airport island height for this specific site. To do so, detailed

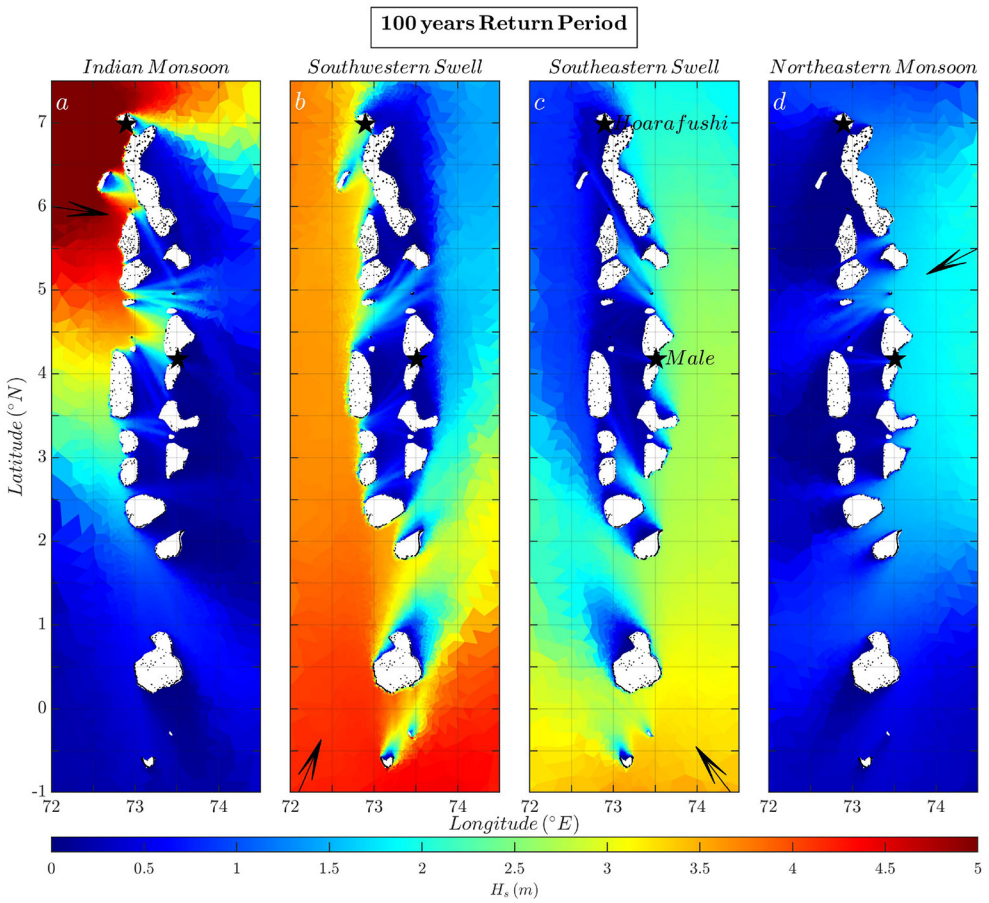

FIGURE 6 | Regional downscaling of the 100 year return period wave event performed with WaveWatch III model (see section 2.2 for the details) for each one of the wave components identified [**(a)** Indian Monsoon, **(b)** Southwestern Swell, **(c)** Southeastern swell, and **(d)** Northeastern Mosoon]. Black arrow in each panel indicated the wave direction. Black stars indicate the position of Malé, the main city of the Maldives, and Hoarafushi, the island where the local modelling was done.

local information, such as a high-resolution topo-bathymetry or ocean waves *in-situ* data to validate the model outputs would be required. This example illustrates the applicability of the regional wave downscaling developed here to a local study if precise local information was available.

Wave propagation with SWASH was carried out in the domains in **Figure 8**. In total, 60 different runs were completed by combining 3 different return periods of H_s (10, 50 and 100 years), two wave directions (Indian Monsoon and the southwestern swell), and 5 different mean sea levels (0, +0.25, +0.50, +0.75, and +1 *m*) for the island configuration with and without airport. We have followed a scenario-independent approach for mean sea-level rise, with 0 *m* corresponding to present-day mean sea level. Mean sea-level changes with respect to the current situation may be interpreted in terms of projected mean sea-level rise (e.g., +0.50 *m* is the median projected mean sea-level rise in 2068 under RCP8.5 and 2088 under RCP2.6, according to Kopp et al., 2014) or as a combination of mean sea-level rise and high tides (e.g., +0.50 *m* is the mean rise in 2041 under RCP8.5 plus +0.25 *m* of tidal amplitude). The mean sea-level changes tested may also include, besides projected mean sea-level rise and tides, other physical processes that can cause mean sea-level variations from seasonal to decadal time scales. We recall here that tides in the Maldives reach a maximum range of around 1 *m* (0.7 *m* median range, Wadey et al., 2017). Note that precise geodetic references relating altitudes and tidal levels are lacking in the Maldives, so these values should be considered as an order of magnitude only. Four examples of selected simulations can be found in **Supplementary Videos 1, 2**.

It has not been possible to validate the model outputs for the present-day situation due to the lack of observations. We are providing, nevertheless, a qualitative validation by comparing the velocity field obtained with the configuration that includes the airport to a satellite photography in which the airport is under construction (**Supplementary Figure 1**). There is a consistency between higher current velocities in the model and the imprint of sediment transport from the new-built airport that are likely driven away by the currents.

The outputs of the first set of 30 model runs, that correspond to the spatial configuration without the airport (**Figure 8a**), are used to evaluate the exposure of the island in terms of the amount of flooding under different forcing conditions. The outputs along

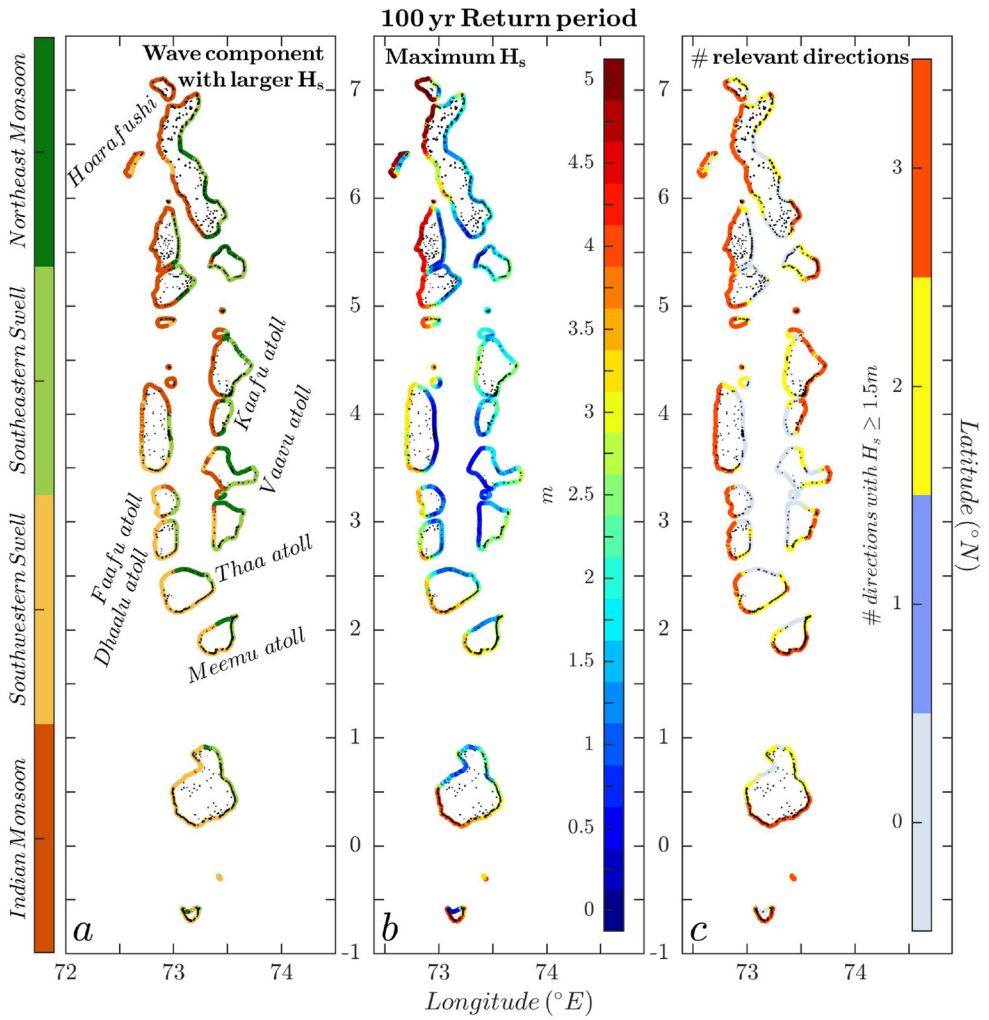

FIGURE 7 | Products derived by combining the regional downscaling for the 100 year return period of the 4 wave components in **Figure 6** along the Maldivian coastlines. **(a)** shows the wave component causing the largest H_s at each coastal point; **(b)** the maximum H_s at the coast; and **(c)**, the number of wave directions with H_s larger than 1.5 m that hit each coastal location for the 100 year return period.

a 100-m wide coastal strip covering the western coast of the island (plotted as grey area in **Figure 8a**) have been gathered together. To do so, the strip is divided in 25-m long sections resulting in 25 × 100 m boxes. Simulated water level time series were extracted for each box and used to compute median and maxima water levels for each model run in each of them. **Figure 9** represents the boxplots along the entire coastal strip of these median (left panel) and maxima (right panel) values under all mean sea levels and return levels considered. The horizontal black thick line in both panels marks the height of the island and the two incoming directions are separated by vertical shadowed areas for comparison. Median values of total water level, that correspond to the superposition of the mean sea level and wave setup, do not reach the threshold of land elevation, indicating that there is no overflow at any point along the coastline under all the forcing conditions considered. The results also point at the southwestern swells as the potentially most hazardous waves, as these systematically induce higher water levels than the Indian monsoon waves (shadowed areas against blanked areas). The reason lies in the longer T_p associated with the southwestern waves ($\sim$ 20 s) in front of the monsoon waves ($\sim$ 12 s). As expected, the larger wave setup for a given return period is obtained for the lowest mean sea level of 0 m: wave setup reaches almost 0.4 m under present-day mean sea level conditions and reduces to 0.3 m with an increase of 1 m. This is because in shallower waters the effects of wave shoaling and breaking leading to wave setup are larger. It is worth noting here that while an increased water level leads to a decreased setup, deeper water allows for larger H_s on the reef flat and an increased run-up potential which could be relevant in terms of impact to infrastructures and erosion. On the other hand, maximum values along the coastal strip have been used to measure whether there has been overtopping generated by the incoming waves. Overtopping occurs whenever these values exceed the island

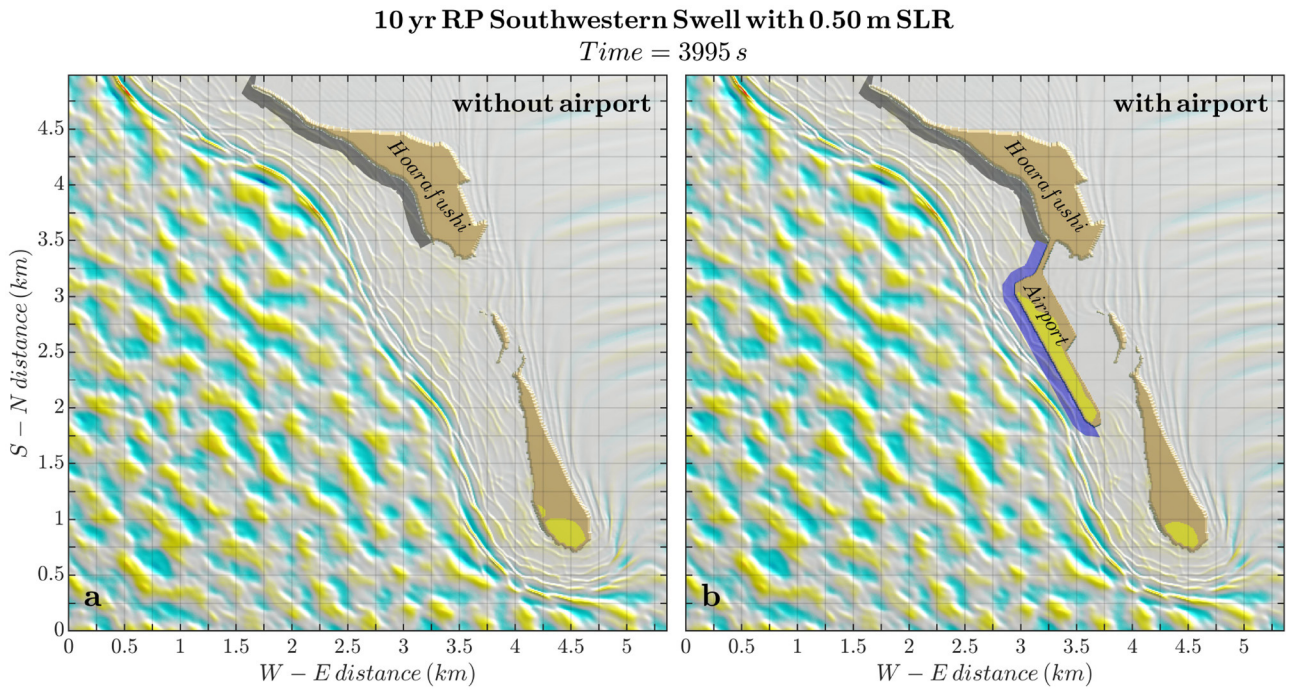

FIGURE 8 | Example of local downscaling simulations with SWASH model (see section 2.3 for details) for the 10 year return period southwestern swell event with 0.5 m of sea level rise (this increase in sea level could mean permanent sea level or high tide with present sea level) for the case without the airport **(a)** and with the new airport **(b)**. Grey (purple) stripe indicates the coastal region where the box plots from **Figure 9** (**Supplementary Figure 15**) are computed.

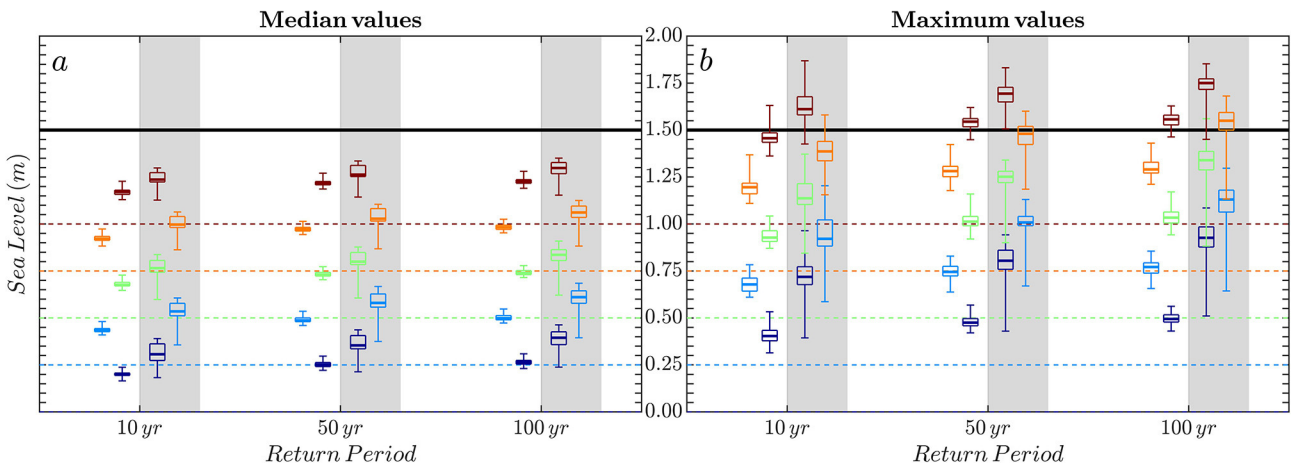

FIGURE 9 | Box plots along Hoarafushi coast without airport computed with time series of simulated water levels: **(a)** median values; **(b)** Maximum values. Box plot colours indicate the sea level of the simulation (dark blue 0 m; light blue 0.25 m; green 0.5 m; orange 0.75 m; dark red 1 m) and are referenced from the dashed line with the same colour. Box plots on grey (white) background are for the simulations for the southwestern swell (Indian Monsoon). The thicker line of the box plots shows the median values; the lower (upper) limit of the boxes indicates the 25th (75th) quantile; and the lower and upper whiskers indicate the minimum and maximum values. The horizontal thick black line indicates the island height.

elevation, with their magnitude indicating the severity of the flooding. The boxplots for the maximum values (right panel in **Figure 9**) point to the occurrence of overtopping under several forcing configurations. For example, 100-year return level waves from southwestern swell and $+0.5\,m$ mean sea level increase. Note that this may correspond to a 1 in 100-year events reaching the coast during the spring tides and under present-day mean sea level conditions. It also occurs for moderate extreme waves with a return period of 10-years in combination with $+1\,m$ of mean sea level (this case is also provided in the **Supplementary Video 1**)

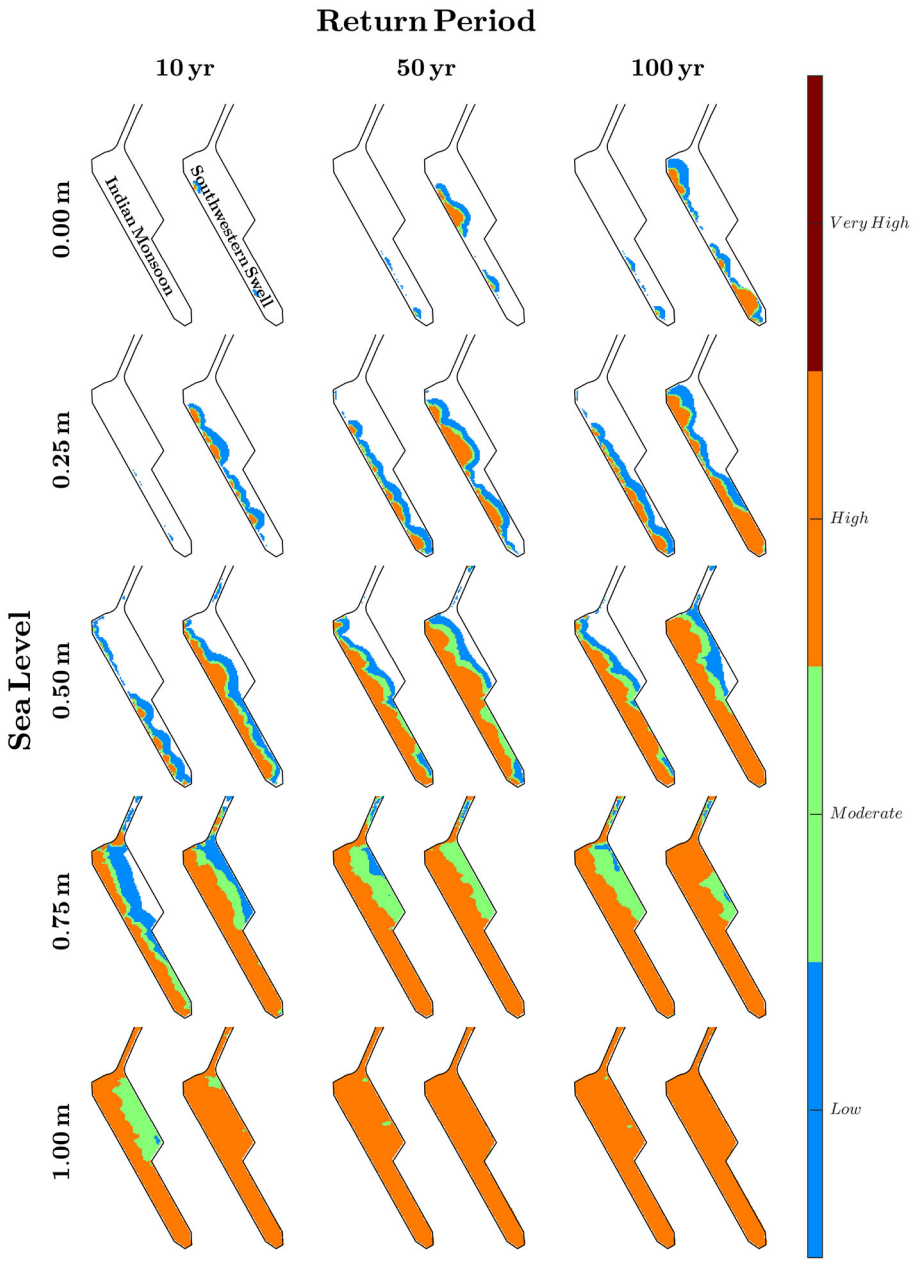

FIGURE 10 | Level of hazard on the new airport for all the SWASH simulations. The colourscale indicates the level of hazard defined by a combination of water height on the airport and water velocity (see **Supplementary Figure 16**). Different sea levels are represented at each row while the columns indicate return periods of H_s (10, 50, and 100 years) as defined in the text for the regional wave climate. For each combination of sea level and return period, the result for the Indian Monsoon and Southwestern swell are shown at left and right, respectively.

and for all the return periods for the southwestern swell with $+0.75\,m$ of mean sea level rise.

With the construction of the airport connected to Hoarafushi (**Figure 8b**), the median and maximum water level values computed along the coast (grey area in **Figure 8b**) slightly increased for all combinations of mean sea level, extreme waves and wave directions (see the equivalent figure to **Figure 9** in **Supplementary Figure 14**). On average, the median values of water level along the coast increase around 0.05 m solely due to the presence of the airport, that partially blocks the channel between Hoarafushi and the island located southwards, leading to higher wave setup. The new reclaimed land is also exposed to incoming waves, and this exposure has been measured in a similar manner as for Hoarafushi, i.e., along a coastal strip on its western coast (blue area in **Figure 8b**). We remark that the airport has been built 150-200 m away from the reef edge,

reducing to a large extent the protection of the wave damping induced by the reef flat. Consequently, both median and maxima water level values are significantly higher than in Hoarafushi island (**Supplementary Figure 15**). For example, with $+1\,m$ of increase in mean sea level, even moderate extreme waves would cause overtopping (e.g., 10-year return levels or less under high tide), and under current conditions a 50-year return level southwestern swell would partially flood the airport.

The flood hazard of the new reclaimed land is summarised in **Figure 10**, using the set of 30 simulation runs with the airport. The flood hazard has been defined following the French standards, that define four different flooding hazard levels (low, moderate, high, and very high) that arise as combinations of inundation level and the water speed over land (see **Supplementary Figure 16**). The artificial island built for the airport is completely flooded with a high level of hazard for most part of the island for both wave directions and all return periods with an increase in mean sea level of $\geq 0.75\,m$ (with the only exception of the Indian monsoon 10-year return period). It is foreseen that the reclaimed land suffers from partial flooding under a southwestern swell extreme of 50-year return period with current conditions of mean sea level. It is worth mentioning that, given the lack of topographic data for the new airport island, flooding hazard is possibly biased high. We simulated the island as being completely flat and without any coastal defenses. This is unlikely to be the case for a critical infrastructure. However, the actual defense height remains unknown, which is why we assume compliance to land reclamation regulations i.e., 1.5 m land elevation. Coastal defenses would only delay the impact of coastal flooding, but would not avoid it.

6. SUMMARY AND DISCUSSION

6.1. Global to Local Coastal Modelling

Mean sea-level rise, despite having a global origin, has severe local coastal impacts, as it raises the baseline level on top of which extreme events reach the coastlines. Yet, projections of changes in mean sea-level as well as assessments of marine extremes are often provided on a large-scale basis (e.g., Vousdoukas et al., 2017), while understanding the causes of coastal flooding and anticipating the impacts require quantitative information at the local scale. This can be feasible to implement in regions where monitoring networks, forecasting and operational systems and development programs for sustainable coastlines are well established and mature (for example, the Flood and Coastal Erosion Risk Management Programme in the UK, or the Delta Programme in the Netherlands). In many cases, however, even local assessments rely on coarse resolution, large-scale global climate information.

In this work we have focused on the Maldivian archipelago, a region where recurrent flooding episodes occur driven by remotely generated waves. These events are, furthermore, projected to become more frequent as mean sea level rises due to the low elevation of the islands. Despite their exposure to waves, to our knowledge, the only source of wave climate information in the region so far are the outputs of global wave reanalysis with a spatial resolution of the order of a degree. Our work illustrates how these global wave fields from coarse resolution climate models can be translated into usable information for regional and local studies and how it can be combined with regionalised projections of mean sea-level rise and local topo-bathymetries.

The first step consisted of a detailed analysis and characterisation of the global wave climate around the Maldives using the closest grid points from the CFSR wave reanalysis (section 2.1). This is a prior mandatory step before the design of the regionalisation. We identified four dominant incoming wave directions from remotely generated waves: the two most common, that originate in the Southern Ocean (Amores and Marcos, 2019), and swells generated by the Indian and Northwestern monsoons. In a second step, for each direction, extreme waves have been characterised in terms of H_s and T_p and a set of five return levels have been dynamically-downscaled using the spectral model WWIII (section 2.2). We have focused on extreme waves only because these are the most relevant for risk analyses; furthermore, the alternative of dynamically-downscaling a 35-year long reanalysis is unfeasible due to computational constraints (this worsens if historical runs and projections are considered). The regionalisation has resulted in a major product of the present work: a valuable data set of extreme waves along the Maldivian coasts with spatial resolutions down to 500 m in the points nearest to the coast. The data set is published at doi: 10.5281/zenodo.3886273. The output of our regionalisation provides quantitative information on extreme waves, in the form of return level curves, at the regional scale in the Maldives and for the first time. This dataset is useful for coastal engineering studies, for feeding local coastal models of flooding hazards and for planning land reclamation and other regional developments. It also serves to compute the inundation potential at every location and for every incoming swell direction, that depends on wave energy, $H_s^2 \cdot T_p$, in line with the "response approach" discussed in Sanuy et al. (2020). Overall, it is expected to become a compelling source of scientific information that can be embedded in coastal climate services (Le Cozannet et al., 2017; Kopp et al., 2019). The users should, nevertheless, ensure that the inherent uncertainties in the method and data are considered. This means that regional waves are representative of ocean swells in the vicinity of the atolls and that, for practical purposes, a detailed topobathymetry is needed is these regional outputs are to be used as boundary forcings. Also, the four main swell directions arriving to the archipelago are considered separately, since the generation mechanisms are independent; thus, every coastal location may be exposed to a different number of incoming wave directions, and all of them should be explored in a local case study, as illustrated in section 5 above.

There is a number of limitations in our regionalised wave fields. The bathymetry used in the regional wave model (GEBCO, see section 2.2) has a spatial resolution of $\sim$ 1 km, which is not enough to resolve the features inside the atolls. We have therefore included every atoll as a single entity in the model domain, neglecting the wave propagation in the inner region and the exchanges between the lagoon of the atoll and the ocean. We consider, nevertheless, that this assumption is reasonable because our results provide evidence that shadow effects of the atolls to

incoming waves are realistically simulated from all directions. That implies that we account for the waves that reach the external coast of the atolls everywhere in the Maldives. This limitation can be overcome in areas where mesoscale (∼ 100 m resolution) bathymetric data sets exist, in which case the interactions with the inner lagoon can also be accounted for. Another caveat of the regional product is that only selected return periods of H_s are provided, instead of an entire high-frequency time series at every coastal grid point. While the quantification of return levels is central to risk assessments, no information on averaged wave fields (useful for erosion studies, for example) is provided. Finally, it is worth pointing out that the regional product has not been validated against observations due to the lack of data.

6.2. Application for Coastal Flood Hazard

We have conducted a local flood hazard modelling experiment that demonstrates the applicability of the regionalised wave fields. Our case study is in the North of the archipelago, exposed to the largest incoming waves, and includes a land reclamation project. We have used the regionalised wave information to feed the wave propagation model SWASH around Hoarafushi island, where local bathymetry has been measured. We have estimated the flooding hazard under present-day conditions and also under projected future scenarios. Our analysis of the global wave climate revealed that projected changes in the large-scale wave characteristics during the twenty-first century are small in comparison to the multi-model spread even under the RCP8.5 scenario. Therefore, we rely on the downscaled regional wave reanalysis and assume that future changes in marine hazards will be driven only by mean sea-level rise. The local model does take into account the modification of the wave propagation due to higher mean sea levels, though. The set of the model experiments included the island configuration with and without the airport in order to determine how the presence of the new reclaimed land alters the flood hazard, the wave propagation and the associated currents.

Our results identified the southwestern swells as the potentially most hazardous waves in Hoarafushi, with 100-year return levels of H_s up to 4 m and associated T_p of ∼20 s. This is, in addition, the most common wave direction that reaches this part of the archipelago, although not the one with largest H_s (that are associated with the Indian monsoon). Our findings indicate that a moderate incoming southwestern swell corresponding to a return period of only 10 years will cause overtopping in Hoarafushi island if it reaches the shoreline under a mean sea level 0.75 m higher than its present-day value (**Figure 9**). The presence of the reclaimed land slightly increases these impacts (**Supplementary Figure 14**). The flood hazard is much stronger in the reclaimed land, that will experience overtopping episodes with sea levels only 0.25 m above present-day mean value (**Supplementary Figure 15**). The reason is its location close to the reef that reduces the wave damping over the reef flat. We recall here that we have adopted a scenario-independent approach for mean sea level increases; this may be justified given that the range of mean sea level changes that we are considering (below 1 m) will be reached even under strong mitigation, as the maximum value lies within the committed global mean sea-level rise of past GHGs emissions (Nauels et al., 2019). Thus, it is not about whether these higher mean sea levels will be reached, but when it will occur. Impact studies based on scenario-independent approaches in combination with ongoing monitoring of regional mean sea-level rise can facilitate the design of adaptive solutions to climate-induced hazards.

In addition, this approach also allows to evaluate the wave-induced flood hazard under particular tidal conditions. In the example above, mean sea level 0.75 m higher than present-day values can be interpreted as a combination of climate-induced mean sea-level rise and tidal oscillations. For instance, 0.75 m can be reached with 0.5 m of climate-induced mean sea level that, according to Kopp et al. (2014), corresponds to the median projected value in 2068 under the RCP8.5 scenario, plus 0.25 m of tidal amplitude. In consequence, according to our estimates, the recently developed (in 2019) regional airport will be flooded under present-day mean sea-level conditions and 0.25 m of tidal amplitude if a moderate extreme swell event (10-year return period) reaches the area, that is, within the present decade. Note that we are not computing the likelihood of co-occurrence of extreme swells and high tides. The reasons for that are, firstly, that these two processes are uncorrelated (astronomical tides and remotely-generated swell events have independent driving mechanisms) which means that their joint probability could be computed as the product of their marginal probability distributions (Pugh and Woodworth, 2014). However, this would require a complete set of time series of the two processes at every grid point. Although there are methods to generate a set of full synthetic time series from their statistical characterisation (e.g., Solari and Losada, 2011), this is a different type of product that is beyond the scope of the present work. Secondly, our approach is more flexible since it does not constrain the interpretation of the increments in mean sea level (either climate-induced sea level rise or tides or both), hence, allowing final users to tailor our approach to their needs, based on their respective risk-taking propensity.

The modification of the island configuration with the presence of the reclaimed land significantly modifies the patterns of the currents (**Supplementary Figure 1**). Such changes are determinant for coastal erosion, as they control the sediment transport along the coastlines. Coastal erosion is considered a central problem in the Maldives, especially in densely populated islands (Zahir et al., 2016; Duvat and Magnan, 2019). Erosion can be prevented or enhanced by many factors, including land reclamation, dredging and building coastal defenses. Here we demonstrate that our regional wave fields are a valuable tool also for anticipating possible erosion and changing spatial patterns in particular case studies.

The major limitation of our local coastal modelling exercise is the lack of a detailed topography of Hoarafushi and its nearby reclaimed airport. While we have measured bathymetric profiles during a field trip, the information on the topography is limited to the averaged elevation of the island. Likewise, the elevation of the reclaimed land (which was not yet built when the field trip took place) has been defined according to the national regulations. In consequence, we have not included coastal defenses and we have instead considered that both the island and the new reclaimed land are flat. This implies that our estimates of overtopping and flooding could be biased high;

however, the presence of coastal defenses would not completely avoid the flood hazard, they would simple delay the impacts of mean sea-level rise.

Another point worthy of discussion is the assumption of static bathymetry and null reef response to changing climatic conditions. It is clear that reefs can change over time. For example, they can accrete following sea level rise (Woodroffe and Murray-Wallace, 2012), they can degrade due to human activities (the construction of the airport is a good example) or they can die as a consequence of warmer temperatures (Bruno and Selig, 2007) (indeed, warm reefs are projected to significantly decline even with global warming only 1.5°C above pre-industrial levels (Bindoff et al., 2019) and to be virtually extinct with 2°C of warming (Hoegh-Guldberg et al., 2018). In any of these cases, changes in the reef would imply changes in the wave propagation and level of protection of the island (Sheppard et al., 2005). We disregard these potential changes in our local flood hazard modelling experiment because we analyse an artificially reclaimed island. Here, human activities generally have severe negative effects on the reef (Duvat, 2020) and the island is protected with hard measures. This is also to urban atoll islands, as Hoarafushi, that are continuously adapting to increased hazard potential by building coastal infrastructures or artificially raising the land (Duvat and Magnan, 2019; Esteban et al., 2019; Hinkel et al., 2019; Brown et al., 2020). This reduces the ability of the island to naturally increase its elevation by sediment deposition during overtopping events (Kench and Beetham, 2019). Hence, we argue that in this case human interventions are probably more important for wave propagation than changes in the reef (Duvat and Magnan, 2019). Contrastingly, in a natural island, assuming a static bathymetry and null reef response, would bias the results of model overtopping (Beetham et al., 2017; Beetham and Kench, 2018). Nevertheless, the regional downscaling that we provide serves as a boundary condition for subsequent studies of wave-induced flooding under future conditions, which then have to account for these uncertainties of future reef responses.

7. CONCLUDING REMARKS

Our study provides the framework to fill the gap between global information of marine climate drivers, including mean sea level and extremes, and local coastal flood hazard modelling. In particular, we demonstrate the feasibility of using large-scale data sets (regionalised sea-level projections and global wind-waves simulations) to inform regional planning and local decision-making. Our work focused in the Maldives, but our technique can be applied to any coastal region, being most relevant where regional and local climate information is not available. Together with the outputs, we have discussed a number of uncertainties in regional as well as local coastal modelling that are inherent to the methodology. Some of the limitations, though, stem, to a large extent, from the lack of coastal observations (i.e., local topo-bathymetries). Our study thus advocates for improved monitoring systems and data collection to reduce uncertainties and better inform final users.

We have generated a valuable regional wave data set that fulfils the purposes of characterisation of the wave climate in a sparsely observed area. This dataset, in combination with detailed local information (e.g., high-resolution topo-bathymetries), serves as a milestone for informing adaptation policy and Maldivian decision-makers facing the challenge of adapting to rising sea-levels.

DATA AVAILABILITY STATEMENT

The datasets presented in this study can be found in online repositories. The names of the repository/repositories and accession number(s) can be found below: https://zenodo.org/record/3886273#.YCFTAOhKhPY.

AUTHOR CONTRIBUTIONS

AA, MM, GL, and JH conceived the work. AA, MM, RP, and SL designed the numerical experiments. AA, MM, and JR analysed the return periods. AS and ZK retrieved the topobathimetric data. All authors contributed to the outline and writing of the manuscript.

FUNDING

This study was supported by the FEDER/Ministerio de Ciencia, Innovación y Universidades Agencia Estatal de Investigación through the MOCCA project (grant no. RTI2018-093941-B-C31) and by the INSeaPTION Project that is part of ERA4CS, an ERA-NET initiated by JPI Climate, and funded by Ministerio de Economía, Industria y Competitividad Agencia Estatal de Investigación (ES) (grant no. PCIN-2017-038), BMBF (DE), NOW (NL), and ANR (FR) with co-funding by the European Union (Grant 690462). This research has been also supported by the ANR project Storisk supported by the French Research Agency. AA was funded by the Conselleria d'Educació, Universitat i Recerca del Govern Balear through the Direcció General de Política Universitària i Recerca and by the Fondo Social Europeo for the period 2014–2020 (grant no. PD/011/2019). MM was supported by the Ministerio de Ciencia e Innovación and la Agencia Estatal de Investigación through grant no. IED2019-000985-I.

ACKNOWLEDGMENTS

We are grateful to Dr. Aurélie Maspataud for her support with bathymetric data and Dr. Fernando Méndez for advice on numerical wave modelling. We thank the Ministry of Environment, the Environmental Protection Agency, the Maldives Transport and Contracting Company and Water Solutions for their support during the field trip and data collection. AA is grateful to M. A. Blázquez for his support and comments during the preparation of the manuscript.

SUPPLEMENTARY MATERIAL

The Supplementary Material for this article can be found online at: https://www.frontiersin.org/articles/10.3389/fmars.2021.665672/full#supplementary-material

REFERENCES

Amores, A., and Marcos, M. (2019). Ocean swells along the global coastlines and their climate projections for the 21st century. *J. Clim.* 33, 185–199. doi: 10.1175/JCLI-D-19-0216.1

Beetham, E., and Kench, P. S. (2018). Predicting wave overtopping thresholds on coral reef-island shorelines with future sea-level rise. *Nat. Commun.* 9:3997. doi: 10.1038/s41467-018-06550-1

Beetham, E., Kench, P. S., and Popinet, S. (2017). Future reef growth can mitigate physical impacts of sea-level rise on atoll islands. *Earths Fut.* 5, 1002–1014. doi: 10.1002/2017EF000589

Bindoff, N. L., Cheung, W. W., Kairo, J. G., Arístegui, J., Guinder, V. A., Hallberg, R., et al. (2019). "Changing ocean, marine ecosystems, and dependent communities," in *IPCC Special Report on the Ocean and Cryosphere in a Changing Climate*, eds H. -O. Pörtner, D. C. Roberts, V. Masson-Delmotte, P. Zhai, M. Tignor, E. Poloczanska, K. Mintenbeck, A. Alegría, M. Nicolai, A. Okem, J. Petzold, B. Rama, N. M. Weyer, 477–587, in press.

Brown, S., Wadey, M. P., Nicholls, R. J., Shareef, A., Khaleel, Z., Hinkel, J., et al. (2020). Land raising as a solution to sea-level rise: an analysis of coastal flooding on an artificial island in the maldives. *J. Flood Risk Manag.* 13:e12567. doi: 10.1111/jfr3.12567

Bruno, J. F., and Selig, E. R. (2007). Regional decline of coral cover in the indo-pacific: timing, extent, and subregional comparisons. *PLOS ONE* 2:e711. doi: 10.1371/journal.pone.0000711

Cialone, M. A., and Smith, J. M. (2007). "Wave transformation modeling with bottom friction applied to southeast oahu reefs," in *10th International Workshop on Wave Hindcasting and Forecasting & Coastal Hazard Assessment*, (Citeseer), 1–12.

Duvat, V. K. (2020). Human-driven atoll island expansion in the maldives. *Anthropocene* 32:100265. doi: 10.1016/j.ancene.2020.100265

Duvat, V. K. E., and Magnan, A. K. (2019). Rapid human-driven undermining of atoll island capacity to adjust to ocean climate-related pressures. *Sci. Rep.* 9:15129. doi: 10.1038/s41598-019-54659-0

Esteban, M., Jamero, M. L., Nurse, L., Yamamoto, L., Takagi, H., Thao, N. D., et al. (2019). Adaptation to sea level rise on low coral islands: lessons from recent events. *Ocean Coas. Manag.* 168, 35–40. doi: 10.1016/j.ocecoaman.2018.10.031

Gussmann, G., and Hinkel, J. (2021). A framework for assessing the potential effectiveness of adaptation policies: coastal risks and sea-level rise in the maldives. *Environ. Sci. Policy* 115, 35–42. doi: 10.1016/j.envsci.2020.09.028

Harangozo, S. A. (2013). *Flooding in the Maldives and Its Implications for The Global Sea Level Rise Debate (First Published: 01 January 1992)*, (American Geophysical Union (AGU)), 95–99.

Hemer, M., Trenham, C., Durrant, T., and Greenslade, D. (2015). Cawcr global wind-wave 21st century climate projections (v2). *CSIRO Service Collect.* doi: 10.4225/08/55C991CC3F0E8

Hemer, M. A., Katzfey, J., and Trenham, C. E. (2013). Global dynamical projections of surface ocean wave climate for a future high greenhouse gas emission scenario. *Ocean Model.* 70, 221–245. doi: 10.1016/j.ocemod.2012.09.008

Hemer, M. A., and Trenham, C. E. (2016). Evaluation of a cmip5 derived dynamical global wind wave climate model ensemble. *Ocean Model.* 103, 190–203. doi: 10.1016/j.ocemod.2015.10.009

Hinkel, J., Church, J. A., Gregory, J. M., Lambert, E., Le Cozannet, G., Lowe, J., et al. (2019). Meeting user needs for sea level rise information: a decision analysis perspective. *Earths Fut.* 7, 320–337. doi: 10.1029/2018EF001071

Hinkel, J., Lincke, D., Vafeidis, A. T., Perrette, M., Nicholls, R. J., Tol, R. S. J., et al. (2014). Coastal flood damage and adaptation costs under 21st century sea-level rise. *Proc. Natl. Acad. Sci. U.S.A.* 111, 3292–3297. doi: 10.1073/pnas.1222469111

Hoegh-Guldberg, O., Jacob, D., Bindi, M., Brown, S., Camilloni, I., Diedhiou, A., et al. (2018). *Impacts of 1.5°c Global Warming on Natural and Human Systems*. Global warming of 1.5°C. An IPCC Special Report.

Hoeke, R. K., McInnes, K. L., Kruger, J. C., McNaught, R. J., Hunter, J. R., and Smithers, S. G. (2013). Widespread inundation of pacific islands triggered by distant-source wind-waves. *Glob. Planet. Change* 108, 128–138. doi: 10.1016/j.gloplacha.2013.06.006

Kench, P., and Beetham, E. P. (2019). Evidence of vertical building of reef islands through overwash and implications for island futures. *Coastal Sediments* 916–929. doi: 10.1142/9789811204487_0080

Kopp, R. E., Gilmore, E. A., Little, C. M., Lorenzo-Trueba, J., Ramenzoni, V. C., and Sweet, W. V. (2019). Usable science for managing the risks of sea-level rise. *Earths Fut.* 7, 1235–1269. doi: 10.1029/2018EF001145

Kopp, R. E., Horton, R. M., Little, C. M., Mitrovica, J. X., Oppenheimer, M., Rasmussen, D. J., et al. (2014). Probabilistic 21st and 22nd century sea-level projections at a global network of tide-gauge sites. *Earths Fut.* 2, 383–406. doi: 10.1002/2014EF000239

Kraines, S., Yanagi, T., Isobe, M., and Komiyama, H. (1998). Wind-wave driven circulation on the coral reef at bora bay, miyako island. *Coral Reefs* 17, 133–143. doi: 10.1007/s003380050107

Le Cozannet, G., Nicholls, R., Hinkel, J., Sweet, W., McInnes, K., Van de Wal, R., et al. (2017). Sea level change and coastal climate services: The way forward. *J. Mar. Sci. Eng.* 5, 49. doi: 10.3390/jmse5040049

Lecacheux, S., Pedreros, R., Le Cozannet, G., Thiébot, J., De La Torre, Y., and Bulteau, T. (2012). A method to characterize the different extreme waves for islands exposed to various wave regimes: a case study devoted to reunion island. *Natural Hazards Earth Syst. Sci.* 12, 2425–2437. doi: 10.5194/nhess-12-2425-2012

Maniku, H. A. (1990). *Changes in the Topography of the Maldives*. Forum of Writers on Environment (Maldives).

Marcos, M., and Woodworth, P. L. (2017). Spatiotemporal changes in extreme sea levels along the coasts of the north atlantic and the gulf of mexico. *J. Geophys. Res.* 122, 7031–7048. doi: 10.1002/2017JC013065

MEE. (2017). *State of the Environment 2016*. Ministry of Environment and Energy. Available online at: https://www.environment.gov.mv/v2/wp-content/files/publications/20170202-pub-soe-2016.pdf

Merkens, J.-L., Lincke, D., Hinkel, J., Brown, S., and Vafeidis, A. T. (2018). Regionalisation of population growth projections in coastal exposure analysis. *Clim. Change* 151, 413–426. doi: 10.1007/s10584-018-2334-8

Morim, J. L. M., Wang, H. X., Cartwright, N., Trenham, C., Semedo, A., Young, I., et al. (2019). Robustness and uncertainties in global multivariate wind-wave climate projections. *Nat. Clim. Change* 9, 711–718. doi: 10.1038/s41558-019-0542-5

Nauels, A., Gütschow, J., Mengel, M., Meinshausen, M., Clark, P. U., and Schleussner, C.-F. (2019). Attributing long-term sea-level rise to paris agreement emission pledges. *Proc. Natl. Acad. Sci. U.S.A.* 116, 23487–23492. doi: 10.1073/pnas.1907461116

NBS (2017). "Statistical yearbook of maldives 2016," in *National Bureau of Statistics Ministry of Finance and Treasury, Republic of Maldives* (Malé).

NBS (2019). "Maldives population projections 2014-2054, assumption and results analysis," in *National Bureau of Statistics Ministry of Finance and Treasury, Republic of Maldives* (Malé)

Nicholls, R. J., Hanson, S. E., Lowe, J. A., Warrick, R. A., Lu, X., and Long, A. J. (2014). Sea-level scenarios for evaluating coastal impacts. *WIRES Clim. Change* 5, 129–150. doi: 10.1002/wcc.253

Nurse, L., McLean, R., Agard, J., Bibruglio, L., Duvat, V., Pelesikoti, N., et al. (2014). "Small islands (chapter 29)," in *Climate Change 2014 : Impacts, Adaptation, and Vulnerability. Part B : Regional Aspects. Contribution of Working Group II to the Fifth Assessment Report of the Intergovernmental Panel on Climate Change*, eds V. R. Barros, C. B. Field, D. J. Dokken, M. D. Mastrandrea, K. J. Mach, T. E. Bilir, M. Chatterjee, K. L. Ebi, Y. O. Estrada, R. C. Genova, B. Girma, E. S. Kissel, A. N. Levy, S. MacCracken, P. R. Mastrandrea, and L. L.White (Cambridge, UK; New York, NY: Cambridge University Press), 1613–1654. Available online at: https://www.ipcc.ch/site/assets/uploads/2018/02/WGIIAR5-Chap29_FINAL.pdf

Oppenheimer, M., Glavovic, B., Hinkel, J., van de Wal, R., Magnan, A., Abd-Elgawad, A., et al. (2019). "Sea level rise and implications for low-lying islands, coasts and communities," in *IPCC Special Report on the Ocean and Cryosphere in a Changing Climate*, eds H.-O. Pörtner, D. C. Roberts, V. Masson-Delmotte, P. Zhai, M. Tignor, E. Poloczanska, K. Mintenbeck, A. Alegría, M. Nicolai, A. Okem, J. Petzold, B. Rama, N. M. Weyer. Available online at: https://www.ipcc.ch/srocc/chapter/chapter-4-sea-level-rise-and-implications-for-low-lying-islands-coasts-and-communities/

Prager, E. J. (1991). Numerical simulation of circulation in a caribbean-type backreef lagoon. *Coral Reefs* 10, 177–182. doi: 10.1007/BF00336771

Pugh, D., and Woodworth, P. (2014). *Sea-Level Science: Understanding Tides, Surges, Tsunamis and Mean Sea-Level Changes*. Cambridge: Cambridge University Press. doi: 10.1017/CBO9781139235778. Available

online at: https://www.cambridge.org/core/books/sealevel-science/C5E551D95DA4E8AF116FED9F0DEB289B

Rijnsdorp, D. P., Smit, P. B., and Zijlema, M. (2012). Non-hydrostatic modelling of infragravity waves using swash. *Coast. Eng. Proc.* 1:currents.27. doi: 10.9753/icce.v33.currents.27

Saha, S., Moorthi, S., Pan, H.-L., Wu, X., Wang, J., Nadiga, S., et al. (2010). The ncep climate forecast system reanalysis. *Bull. Am. Meteorol. Soc.* 91, 1015–1058. doi: 10.1175/2010BAMS3001.1

Sanuy, M., Jiménez, J. A., Ortego, M. I., and Toimil, A. (2020). Differences in assigning probabilities to coastal inundation hazard estimators: Event versus response approaches. *J. Flood Risk Manag.* 13:e12557. doi: 10.1111/jfr3.12557

Sheppard, C., Dixon, D. J., Gourlay, M., Sheppard, A., and Payet, R. (2005). Coral mortality increases wave energy reaching shores protected by reef flats: examples from the seychelles. *Estuarine Coast. Shelf Sci.* 64, 223–234. doi: 10.1016/j.ecss.2005.02.016

Solari, S., and Losada, M. A. (2011). Non-stationary wave height climate modeling and simulation. *J. Geophys. Res.* 116:C09032. doi: 10.1029/2011JC007101

Suzuki, T., Altomare, C., De Roo, S., Vanneste, D., and Mostaert, F. (2018). *Manning's Roughness Coefficient in Swash: Application to Overtopping Calculation*. FHR Reports. Available online at: https://publicaties.vlaanderen.be/view-file/32905.

Tolman, H. (2009). User manual and system documentation of wavewatch iii version 3.14. *NOAA/NWS/NCEP/MMAB Technical Note 276*, (Appendices), 194.

Tolman, H. (2014). User manual and system documentation of wavewatch iii version 4.18. *NOAA/NWS/NCEP/MMAB Technical Note 316*.

Vousdoukas, M. I., Mentaschi, L., Voukouvalas, E., Verlaan, M., and Feyen, L. (2017). Extreme sea levels on the rise along europe's coasts. *Earths Fut.* 5, 304–323. doi: 10.1002/2016EF000505

Wadey, M., Brown, S., Nicholls, R. J., and Haigh, I. (2017). Coastal flooding in the maldives: an assessment of historic events and their implications. *Natural Hazards* 89, 131–159. doi: 10.1007/s11069-017-2957-5

Woodroffe, C. D., and Murray-Wallace, C. V. (2012). Sea-level rise and coastal change: the past as a guide to the future. *Quatern. Sci. Rev.* 54, 4–11. doi: 10.1016/j.quascirev.2012.05.009

Woodworth, P. L. (2005). Have there been large recent sea level changes in the maldive islands? *Glob. Planetary Change* 49, 1–18. doi: 10.1016/j.gloplacha.2005.04.001

Woodworth, P. L., Melet, A., Marcos, M., Ray, R. D., Wöppelmann, G., Sasaki, Y. N., et al. (2019). Forcing factors affecting sea level changes at the coast. *Surveys Geophys.* 40, 1351–1397. doi: 10.1007/s10712-019-09531-1

Zahir, H., Asis, M., Rasheed, A., Musthafa, Z. M., Latheef, A. T., and Mohamed, I. (2016). "Second national communication of maldives to the united nations framework convention on climate change," in *Ministry of Environment and Energy. Republic of Maldives: Malé*.

Zijlema, M. (2012). "Modelling wave transformation across a fringing reef using swash," in *ICCE 2012: Proceedings of the 33rd International Conference on Coastal Engineering, Santander, Spain, 1-6 July 2012*. Coastal Engineering Research Council. doi: 10.9753/icce.v33.currents.26. Available online at: https://journals.tdl.org/icce/index.php/icce/article/view/6479

Zijlema, M., Stelling, G., and Smit, P. (2011). Swash: an operational public domain code for simulating wave fields and rapidly varied flows in coastal waters. *Coast. Eng.* 58, 992–1012. doi: 10.1016/j.coastaleng.2011.05.015

Conflict of Interest: The authors declare that the research was conducted in the absence of any commercial or financial relationships that could be construed as a potential conflict of interest.

Copyright © 2021 Amores, Marcos, Pedreros, Le Cozannet, Lecacheux, Rohmer, Hinkel, Gussmann, van der Pol, Shareef and Khaleel. This is an open-access article distributed under the terms of the Creative Commons Attribution License (CC BY). The use, distribution or reproduction in other forums is permitted, provided the original author(s) and the copyright owner(s) are credited and that the original publication in this journal is cited, in accordance with accepted academic practice. No use, distribution or reproduction is permitted which does not comply with these terms.

frontiers in Marine Science

ORIGINAL RESEARCH
published: 24 June 2021
doi: 10.3389/fmars.2021.683535

Visualising the Uncertainty Cascade in Multi-Ensemble Probabilistic Coastal Erosion Projections

Alexandra Toimil[1], Paula Camus[2], Iñigo J. Losada[1] and Moises Alvarez-Cuesta[1]*

[1] IHCantabria – Instituto de Hidráulica Ambiental de la Universidad de Cantabria, Santander, Spain, [2] Ocean and Earth Science, National Oceanography Centre, University of Southampton, Southampton, United Kingdom

Future projections of coastal erosion, which are one of the most demanded climate services in coastal areas, are mainly developed using top-down approaches. These approaches consist of undertaking a sequence of steps that include selecting emission or concentration scenarios and climate models, correcting models bias, applying downscaling methods, and implementing coastal erosion models. The information involved in this modelling chain cascades across steps, and so does related uncertainty, which accumulates in the results. Here, we develop long-term multi-ensemble probabilistic coastal erosion projections following the steps of the top-down approach, factorise, decompose and visualise the uncertainty cascade using real data and analyse the contribution of the uncertainty sources (knowledge-based and intrinsic) to the total uncertainty. We find a multi-modal response in long-term erosion estimates and demonstrate that not sampling internal climate variability's uncertainty sufficiently could lead to a truncated outcomes range, affecting decision-making. Additionally, the noise arising from internal variability (rare outcomes) appears to be an important part of the full range of results, as it turns out that the most extreme shoreline retreat events occur for the simulated chronologies of climate forcing conditions. We conclude that, to capture the full uncertainty, all sources need to be properly sampled considering the climate-related forcing variables involved, the degree of anthropogenic impact and time horizon targeted.

Keywords: multi-ensemble, probabilistic, coastal erosion projections, uncertainty cascade, climate change

OPEN ACCESS

Edited by:
Michael Dylan Sparrow, World Meteorological Organization, Switzerland

Reviewed by:
Alessandro Stocchino, Hong Kong Polytechnic University, Hong Kong, SAR China
Alejandro Orfila, Consejo Superior de Investigaciones Científicas (CSIC), Spain

****Correspondence:***
Alexandra Toimil
toimila@unican.es

Specialty section:
This article was submitted to Coastal Ocean Processes, a section of the journal Frontiers in Marine Science

Received: *21 March 2021*
Accepted: *14 May 2021*
Published: *24 June 2021*

Citation:
Toimil A, Camus P, Losada IJ and Alvarez-Cuesta M (2021) Visualising the Uncertainty Cascade in Multi-Ensemble Probabilistic Coastal Erosion Projections. Front. Mar. Sci. 8:683535. doi: 10.3389/fmars.2021.683535

INTRODUCTION

Mean sea level, wave conditions, storm surges and tides are shaping coasts worldwide (Wong et al., 2014). These coastal drivers are altered by global and regional climate change, bringing additional uncertainty to present conditions that grows toward the end of the century and beyond (Kopp et al., 2017). The way this uncertainty propagates from different levels of radiative forcing in the form of emission and concentration scenarios (RCPs) through global and regional climate models (GCMs and RCMs, respectively), and coastal regional forcing and erosion models is primarily assessed using top-down approaches (Ranasinghe, 2016; Toimil et al., 2020a), which require bias correction and downscaling procedures (Zscheischler et al., 2018). Top-down approaches involve undertaking a sequence of steps through which information and uncertainty cascade from one step to the next, leading to an expansion of the envelope of uncertainty, widely referred to as the cascade of uncertainty (Mitchell and Hulme, 1999; Wilby and Dessai, 2010) in the literature.

When it comes to develop coastal erosion projections, the uncertainty that arises from top-down approaches can be classified as intrinsic or knowledge-related (Toimil et al., 2020a). Intrinsic uncertainty is inherent to the climate change problem and irreducible (Giorgi, 2010) and includes uncertainty in emission scenarios and in the internal variability of the climate system. Conversely, knowledge uncertainty, which is said not to exist in the "real world" (Mankin et al., 2020), is rooted in our imperfect knowledge of atmospheric, biogeochemical, physical, dynamic and coastal processes and could be decreased by advancing science understanding and increasing computational resources. Knowledge uncertainty comprises concentration scenario uncertainty, GCM–RCM uncertainty, bias uncertainty, downscaling uncertainty, and (epistemic) coastal erosion model (CEM) uncertainty. Such uncertainty sources can dominate one another (Giorgi, 2010) and their importance depends on many factors that encompass the climate-related variable, the time horizon of the projection, the region, and the geographic scale (Hawkins and Sutton, 2009; Fernández et al., 2019).

It will never be possible to quantify very accurately the likelihood that future climate change will reach a particular magnitude, although some quantitative bounds can be assessed and potentially narrowed (Sutton, 2019). And even when uncertainty is large and irreducible and hampers communication, its characterisation remains the means to effective risk-informed decision-making (Mankin et al., 2020). To date, there have been many attempts to address uncertainty in climate projections, but little attention has been really paid to impacts and risks (IPCC, 2013, 2018), which require considering at least two important aspects that could bring additional challenges. Risk assessment seeks to account for the full range of potential unwanted or "bad" outcomes even when they are very uncertain (and very unlikely) (Sutton, 2019). The second aspect is associated with practical and conceptual barriers in how to approach uncertainty sampling across the entire top-down approach. Existing studies limit exploration to knowledge uncertainty and single dimensions, involving one or two steps in the top-down approach, for example, by considering different representative concentration pathways or RCPs, GCM, or GCM–RCM ensembles with a single realisation, a variation range of mean sea-level rise (SLR), or CEM ensembles (Toimil et al., 2020a). Accounting for these uncertainty sources in an aggregated manner, however, would help to identify what is the step in the top-down process contributing the most and where to focus efforts to reduce uncertainty. Internal variability uncertainty, which is due to the natural variations in the climate system, by contrast cannot be reduced and has been demonstrated to be large and persistent, having the potential to impoverish decision-making if disregarded (e.g., Mankin et al., 2020). In the same manner different GCMs and RCMs give different responses about future climate, so does different realisations of the same GCMs or RCMs (under the same assumptions) due to their stochastic nature. This noise arisen from internal variability can be a very valuable source of information for the assessment of coastal erosion, where the chronology of the climate-related forcing conditions could be determinant, especially on short-term timescales (Toimil et al., 2017).

Just as important as it is considering the cascade of uncertainty is to visualise it, and this is crucial because visualisation is usually the prelude to understanding. However, to our knowledge, very few studies to date have tried to visualise this cascade using real data, all of which focused on climate variables. For instance, Hawkins (2014) pioneered the visualisation of the uncertainty cascade in global mean surface temperature projections considering three pyramid levels (RCPs–GCMs-realisations). Following the same visualisation, Swart et al. (2015) analysed of the influence of internal variability on Arctic sea-ice extent (RCPs–GCMs-realisation) and, more recently, Fernández et al. (2019) presented a research work on seasonal precipitation and temperature changes and their dependence on GCMs and RCMs, realisations, emission scenarios or RCPs, and resolution. While studies on projections of coastal impacts and, in particular, of coastal erosion, have shown progress in the quantification of the relative contribution of uncertainty dimensions to the total uncertainty (e.g., Le Cozannet et al., 2019; Athanasiou et al., 2020), they mainly focus on the application of variance-based decomposition methods and mostly limit the top-down approach-related sources of uncertainty considered to RCPs, SLR, and CEMs, and do not provide neither a conception nor a visualisation of the full cascade.

In this paper, we develop coastal erosion projections following each of the steps of the top-down procedure and sampling the associated knowledge and intrinsic uncertainty. We decompose and factorise the cascade of uncertainty going from RCPs down to future coastal erosion estimates. Our approach combines the fully implementation of probabilistic SLR projections and dynamic projections of waves and storm surges in an ensemble of two CEMs for different RCPs and GCMs, including bias correction and the hybrid downscaling of waves to nearshore. In addition, we sample uncertainty in climate variability by generating thousands of synthetic multivariate time series of projected nearshore waves and storm surges, leading to chronologies different from the dynamic projections' original realisation. Using a real beach as an illustration and looking at long-term shoreline recession and non-stationary extreme retreat events, we analyse the dependence of far-future coastal erosion projections on RCPs and GCMs, climate variability, SLR percentiles, and CEMs.

The paper is structured as follows. Section "Study Area" provides a brief description of the study area where the analysis is performed. Section "Development of Coastal Erosion Projections" describes the approach proposed for the development of coastal erosion projections. Section "Visualisation and Communication of Uncertainty in Coastal Erosion Projections" analyses uncertainty in coastal erosion projections and discusses ways of visualisation. Finally, section "Conclusion" provides some concluding remarks.

STUDY AREA

The analysis is performed in San Lorenzo Beach, a pocket urban beach located in Gijon (Asturias), northern Spain. It has a macrotidal semidiurnal regime (2–5 m of spring tidal range) and fine (0.2–0.3 mm) quartz sand. The most energetic waves come

from the Northwest to the North-Northwest sectors. During extreme weather events, these waves can reach up significant wave heights of 10 m and peak periods of 20 s. San Lorenzo response to coastal climate forcing is cross-shore dominated as has negligible alongshore gradients in longshore sediment transport and does not experience significant rotation. It has homogenous grain size and composition along its whole cross section and has a constant berm height along its length. Toimil et al. (2017) derived these parameters from field surveys.

DEVELOPMENT OF COASTAL EROSION PROJECTIONS

We develop long-term multi-ensemble probabilistic coastal erosion projections for the period 2081–2100 in San Lorenzo Beach following the steps of the top-down approach to sufficiently quantify the associated uncertainty. Such steps are shown in **Figure 1**. We first compile dynamic projections of waves and storm surges developed for 2 RCPs (RCP4.5 and RCP8.5, box A) and 6 GCMs each (box b1). In a second step, we correct their bias (box b2) and downscale wave projections to the coast using a hybrid approach that combines statistical and numerical modelling and incorporates the effects of projected mean sea level on nearshore waves (box b3). We generate 1,000 synthetic multivariate time series of GCM-driven projected wave conditions and storm surges (box b4). Additionally, we obtain 3 SLR trajectories corresponding to three percentiles from probabilistic local SLR projections for the radiative forcings RCP4.5 and RCP8.5, and reconstruct the astronomical tide (boxes c2, D, respectively). Finally, we apply 2 CEMs that provide the beach response to cross-shore forcing (box e1). As a result (2 RCPs × 6 GCMs × 1,000 realisations × 3 SLR percentiles × 2 CEMs), we obtain 72,000 hourly time series of projected shoreline evolution (box e2). As can be seen, boxes a (RCP ensemble), b2 (GCM ensemble), b5 (climate variability uncertainty sampling, denoted as CLIM VAR), c2 (SLR percentiles), and e1 (CEM ensemble) correspond to the different levels of the cascade of uncertainty. Note that actions displayed in grey are the projections of waves, storm surge and SLR, which have not been developed in this study but used as input for the following steps.

Projections of Mean Sea-Level Rise

Projections of global mean SLR provide insufficient information to support climate change adaptation, as local decisions require local projections that accommodate different risk tolerances (Kopp et al., 2014). In this study, we use complete probability distributions of regional mean SLR considering Antarctic ice-sheet (AIS) simulations (DeConto and Pollard, 2016), including ice-shelf hydrofracturing and ice-cliff collapse (DP16, Kopp et al., 2017). The use of explicit physics has led to a significant upward shift in central projections for the RCP4.5 and RCP8.5 scenarios with respect to its predecessor Kopp et al. (2014), which relies on expert assessment and elicitation. While DP16 projections are only based on a single AIS model and need further development to increase confidence (Hinkel et al., 2019), they allow expanding the space of the physically coherent and can be a useful tool to explore the uncertainty in future extreme outcomes.

We obtain probabilistic SLR projections at Gijon tide-gauge, using the code provided by Kopp et al. (2017), for the RCP4.5 and RCP8.5 scenarios. For both RCPs, we account for SLR uncertainty by considering the 5, 50, and 95th percentiles of the simulated frequency distributions. As can be observed in **Figure 2**, the projected 50th percentile increases from 0.59 to 0.90 m, and from 0.87 to 1.46 m from 2081 to 2100 under the RCP4.5 and the

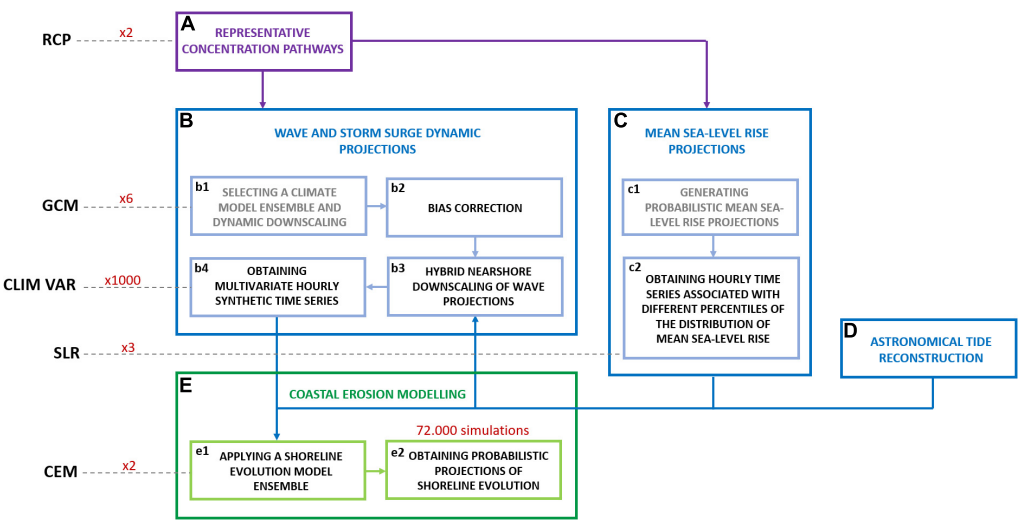

FIGURE 1 | Flowchart describing the methodology proposed for the development of coastal erosion projections. Boxes **A–E** represent different components of the top-down approach and, in particular, boxes **A** (RCP ensemble), b2 (GCM ensemble), b5 (internal climate variability sampling denoted as CLIM VAR), c2 (SLR percentiles), and e1 (CEM ensemble) relate to the different levels of the cascade of uncertainty. Actions displayed in grey colour involve actions not undertaken in this study although used as input for other steps.

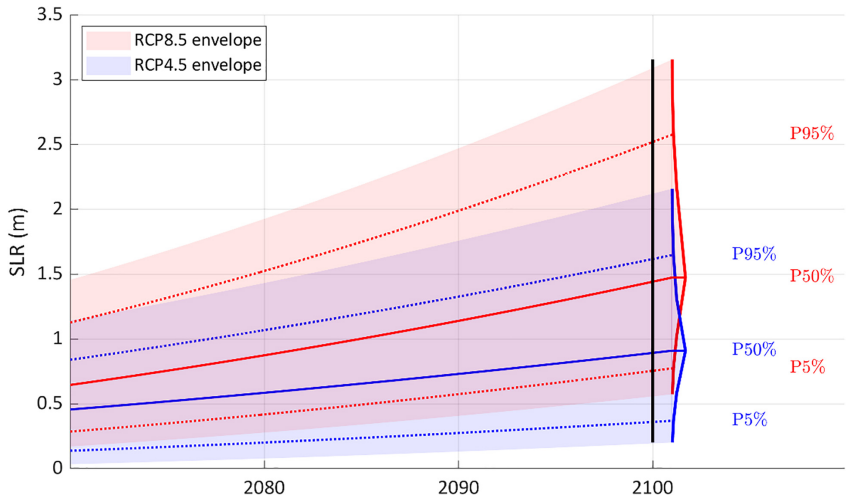

FIGURE 2 | Probabilistic projections of local-mean sea-level rise at Gijon tide-gauge for RCP4.5 and RCP8.5 from 2070 to 2100 using Kopp et al. (2017) framework. Solid lines indicate 50th percentile; dashed lines indicate 5 and 95th percentiles; shaded areas represent the 0.5 and 99.5th percentiles of the SLR distribution for 2100.

RCP8.5, respectively. While assuming constant acceleration of ice loss leads to an increase in forcing sensitivity, the central 90% of simulations by 2100 for the RCP4.5 (0.36–1.63 m) and the RCP8.5 (0.76–2.55 m), respectively, overlap near the mid-low RCP8.5 percentiles. The highest RCP8.5 percentiles spread significantly from the mean values.

Projections of Waves and Storm Surges

IHCantabria (2020) has recently generated dynamic multi-model projections of wave conditions and storm surge. Wave projections were developed for the Northeast Atlantic Ocean using the WaveWatch III third generation wave model (Tolman and The WaveWatch III® Development Group, 2014). In the model, three regional grids (Artic, Atlantic and Spain-Atlantic with resolutions of 1° × 1°, 0.5° × 0.5°, and 0.1°×0.1°, respectively) were nested to a global grid with a resolution of 1°×1°. The global grid was forced with winds and ice coverage from 6 GCMs.

Storm surge projections were produced for the Atlantic and Mediterranean coast of Spain using the ROMS ocean circulation model (Shchepetkin and McWilliams, 2005) with a 0.08° × 0.06° resolution grid. The grid was forced with winds and sea level pressure from 6 GCMs.

Ensemble of Climate Models and Dynamic Downscaling

The wave and ocean models were forced with the outputs of the GCMs described in **Supplementary Table 1**. The selection of the GCMs (with spatial resolution between 0.75° and 2.5°) was based on the provision of the variables of interest at the required temporal resolution (3-hourly), time periods (1985–2005, 2026–2045, and 2081–2100) and concentration scenarios (RCP4.5 and RCP8.5), and on if these variables were derived from the same GCM realisation and initialisation. For this study, we consider the model simulations for both RCPs, 6 GCMs (ACCESS1.0, CMCC-CC, CNRM-CM5, HadGEM2-ES, IPSL-CM5A-MR, and MIROC5) from the Coupled Model Intercomparison Project 5 (CMIP5), and two time periods, the long-term future (2081–2100) and the historical reference (1985–2005).

The wave model was run following a multigrid configuration as for the development of the global ocean wave database GOW2 (Pérez et al., 2017). Earth2014 (Hirt and Rexer, 2015) and GSHHG (Global Self-consistent Hierarchical High-resolution Geography) databases were used to define the bathymetry and the coastlines, respectively. The bathymetric information for ROMS came from the EMODnet database. The GCM variables used to force the wave and ocean models were wind fields at 10 m over the sea surface level and concentrations of ice coverage (from 0 to 1), and surface wind fields and sea level pressure, respectively. GCM-derived variables were in both cases interpolated at each node of the computational grid at an hourly scale for the complete simulated periods.

Bias Correction

GCM outputs contain important biases when compared to observations, which need to be corrected before using them for impact studies. As these outputs are not synchronised with reanalysis or hindcast data, bias correction cannot be applied on an hourly basis but on the distributions or statistics of the variables to be corrected (Maraun, 2016). In recent years, different methods for bias correction have been developed. These range from simple techniques based on the delta method (Hay et al., 2000) that are convenient for monthly or annual data, to more sophisticated approaches based on quantile–quantile mapping that are more suitable when working at daily scales (Gutiérrez et al., 2018).

In this study, we apply the empirical quantile mapping (EQM) method. The EQM consists of analysing the distribution of observed values and adjusting some characteristics of the empirical probability distribution function with projected values

by means of identifying quantiles. This adjustment applies to the wave and storm surge projections in the historical period (1986–2005) and in the future period (2081–2100) to correct the simulations (Dequé, 2007). The EQM is given by the following equation:

$$z = \mathrm{CDF}_{\mathrm{obs}}^{-1}\left(\mathrm{CDF}_{\mathrm{mod}}\left(y\right)\right) \quad (1)$$

where z and y are the corrected and original values of the model, respectively; and $\mathrm{CDF}_{\mathrm{obs}}$ and $\mathrm{CDF}_{\mathrm{mod}}$ are the empirical cumulative distribution functions of the observations and the model, respectively.

We define the quantiles following linear spacing $\left(q_i = 1,\ 5,\ 10, \ldots,\ 90\right)$ and Gumbel distribution fitting (for quantiles over the 90th percentile). For each quantile, we obtain the correction term and interpolate linearly between them. Then, we extrapolate the data outside the predefined quantile range using the same correction term found for the first and last quantiles (Lemos et al., 2020). Additionally, we define bias as a time-invariant component of a model error. For the historical period (reference), we use the GOW2 database to correct the wave climate simulations (significant wave height, Hs, and peak period, Tp) and the GOS dataset (Cid et al., 2014) to correct the storm surge.

In order to validate the EQM-based bias correction, we compare the GOW2 and GOS distribution functions with the climatic data from the GCMs using the $\mathrm{PDF}_{\mathrm{score}}$ (probability density function score), as proposed by Perkins et al. (2007). The $\mathrm{PDF}_{\mathrm{score}}$ measures the degree of similarity of two probability density functions, allowing the comparison of entire time series without the limitation of having non-simultaneous climatic data over time (it takes value 1 when the functions are similar, and 0 when there is no overlap between them). Further details on the validation are provided in the **Supplementary Material**.

Figure 3 shows the comparison of the distribution function of Hs for each GCM in the historical period (1985–2005) with the GOW2 historical distribution. The CMCC model, which is the GCM with the highest spatial resolution, is the ensemble member that better reproduces the hindcast simulations. The other members of the GCM ensemble underestimate Hs. **Figure 3A** illustrates the distribution function of Hs at deep water from the GOW2 hindcast and the climatic data from the ensemble members (ACCESS1.0, CMCC-CC, CNRM-CM5, HadGEM2-ES, IPSL-CM5A-MR, and MIROC5) with the corresponding $\mathrm{PDF}_{\mathrm{score}}$. **Figure 3B** shows the Q–Q plot of the original (uncorrected) Hs per ensemble member against GOW2 Hs. Five ensemble members show a consistent underestimation, especially at the upper quantiles (i.e., extreme values, over the 99th percentile). **Figures 3C,D** display the distribution function and the Q–Q plot for the corrected Hs, showing how bias correction leads to a better agreement between each ensemble member

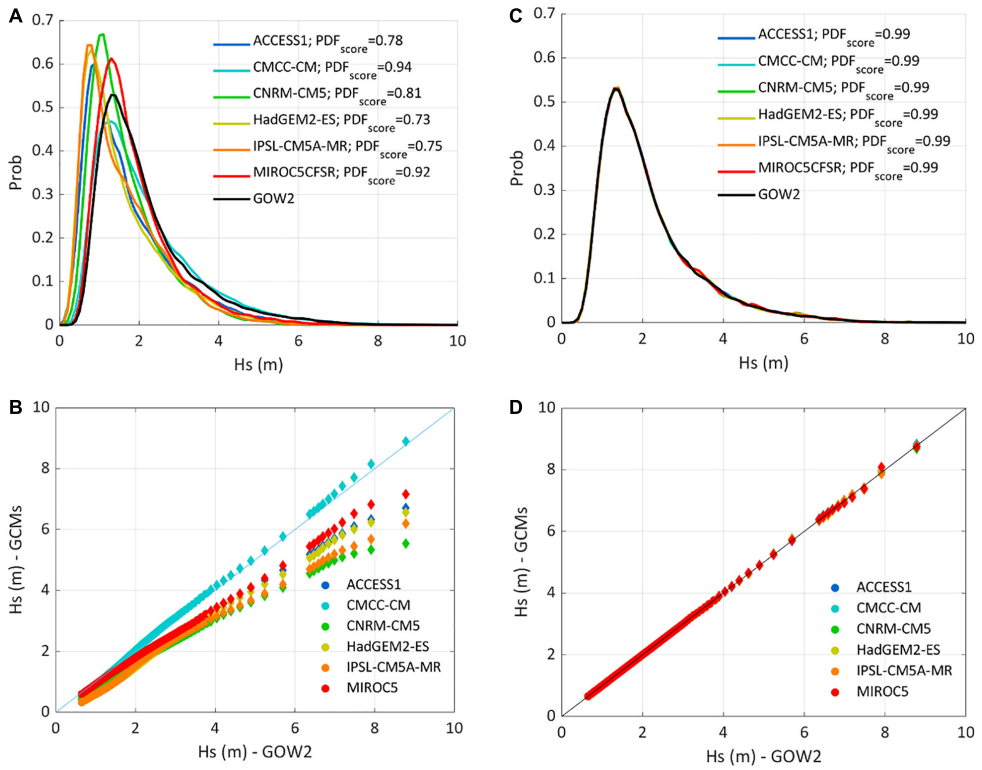

FIGURE 3 | (A) Probability distribution function of Hs at deep waters from the hindcast GOW2 database and the uncorrected climatic data from each ensemble member (i.e., ACCESS1.0, CMCC-CC, CNRM-CM5, HadGEM2-ES, IPSL-CM5A-MR, and MIROC5) with the corresponding PDFscore. **(B)** Q–Q plot of the original uncorrected Hs, per ensemble member. **(C)** Probability distribution functions of GOW2 Hs and corrected Hs associated with each ensemble member. **(D)** Q–Q plot of the original uncorrected Hs, per ensemble member.

and GOW2. The improvement in representing the most extreme events is due to the Gumbel distribution fitting for quantiles over the 90th percentile. **Supplementary Figure 1** presents the equivalent analysis for the storm surge.

Hybrid Downscaling of Waves Projections

Despite the dynamic projections present very high resolution along the Spanish coast, we nest a coastal wave propagation model to capture wave transformations that result from interactions with the bathymetry and future sea level (SLR, projected storm surge and astronomical tides). Since downscaling hourly wave conditions for 2 RCPs and 6 GCMs considering 3 SLR trajectories requires a huge computational effort, hybrid downscaling techniques can offer advantage. We apply the hybrid downscaling technique developed by Camus et al. (2011), which combines mathematical tools (i.e., a selection algorithm and a multidimensional interpolation method) with numerical simulations to obtain the future wave forcings of the CEMs. The steps of the hybrid downscaling approach are: (1) selection of the closest node to the study beach from dynamical wave projections at 0.1° resolution along the Spanish coast and the closest wind node from the corresponding GCM, and collection of the time series of the state parameters Hs, Tp and mean direction, as well as the wind velocity and direction for the target time period (2081–2100) and from the 6 GCMs; (2) selection of a limited number of cases (500), which are the most representative of all possible future wave conditions at 0.1° resolution; (3) propagation of the selected cases using a wave transformation model for each scenario considered at four sea levels (0.0, 2.5, 5.0, and 8.0 m) that cover the whole casuistry of storm surge, tide, and SLR by the end of the century; and (4) reconstruction of the time series of sea state parameters near the beach (but outside the active sediment transport extent) for each RCP and SLR scenario, and for each GCM independently at the corresponding hourly sea level. These steps are illustrated in **Supplementary Figure 2**.

In order to select the subset of sea states that best represent wave conditions at 0.1° and wind, we apply the maximum dissimilarity algorithm (MDA). We use this subset of conditions as boundary conditions to the SWAN model (Booij et al., 1999) nesting three grids to achieve a spatial resolution of 20 m in the area of San Lorenzo Beach. During the simulations, wave amplification due to non-linear interactions between waves and projected sea level is accounted for as in Camus et al. (2019). For the reconstruction of the nearshore wave time series, we use a multidimensional interpolation method based on radial basis functions (RBF). RBFs allow to define a statistical relationship between the offshore wave parameters and nearshore conditions, which are the output of the SWAN model.

Generation of Multivariate Synthetic Time Series

In nature, wave conditions and storm surges are random. This means that while each GCM simulation is a precise rendering of the future climate, no GCM projection will happen (Mankin et al., 2020). Internal climate variability is an intrinsic uncertainty inherent to the climate problem (Giorgi, 2010), which could be addressed through using ensembles of transient and credible simulations starting at different times in the control period (Toimil et al., 2020a), also known as initial condition ensembles (Mankin et al., 2020). Here, we build upon already elaborated multi-model projections that may undersample internal climate variability uncertainty. For this uncertainty to be accounted for, we apply a vector autoregressive (VAR) model (Solari and van Gelder, 2012) that considers empirical functions to stochastically generate 1,000 multivariate hourly time series of waves and storm surges for each (RCP-)GCM over the time periods 1986–2005 and 2081–2100. Similar to an initial condition ensemble, this allows to produce a distribution of outcomes consistent with the same assumptions underlying the original GCM-driven runs.

Vector autoregressive models are extensions of autoregressive models for multivariate data. Autoregressive models provide the present value of an observation as a linear function of past observations. A similar VAR model based on GEV functions was applied in Toimil et al. (2017) to obtain multivariate hourly time series of waves and storm surges in San Lorenzo Beach using historical data.

The statistical analysis of the persistence regimes allows to verify that the VAR model is able to reproduce the temporal dependence structure of the original time series. **Supplementary Figure 3** shows the persistence regimes of Hs over different thresholds and the joint probability distribution of sea state parameters and storm surge. The persistence regimes can be especially relevant when it comes to apply equilibrium models to reproduce the shoreline response to cross-shore forcing since their nature is such that a larger portion of the potential erosion (or accretion) can be attained for conditions which remain over long periods (Miller and Dean, 2004).

Coastal Erosion Modelling

The last step in the top-down approach is the coastal erosion modelling. CEMs can be sensitive to multiple factors, highly dependent on empirical parameters and present limitations to simulate physical processes realistically (Montaño et al., 2020; Toimil et al., 2020b). For this reason, we consider epistemic uncertainty in erosion modelling by performing an ensemble of CEMs. We set-up and apply two equilibrium models that couple short-term coastal dynamics and long-term SLR. The two models have been calibrated in the study beach over the period 1979–2020 using nearshore waves downscaled from GOW2, updated storm surges from GOS, and the reconstruction of the astronomical tide as forcing conditions, as well as aerial photographs and survey data as described in Toimil et al. (2017).

We run each CEM with 36,000 combinations of the projected forcing variables for the period 2081–2100 that result from 2 RCPs, 6 GCMs, and 1,000 synthetic multivariate hourly time series of waves and storm surges for each GCM and 3 alternative hourly SLR trajectories related to three percentiles. Additionally, we perform 6,000 extra runs with the forcing variables driven by the 6 GCMs over the period 1985–2005.

Ensemble of Cross-Shore Erosion Models

The CEMs we implement rely on the classical equilibrium or linear relaxation in which the difference with respect to an

equilibrium term drives shoreline evolution (Eq. 2). This short-term shoreline response, which can be induced by time-varying water levels or breaking waves combines with a long-term response due to SLR in a coupled fashion.

$$\frac{dy(t)}{dt} = VG\Delta D(t) \quad (2)$$

where y(t) is the shoreline position at time t; V is a constant governing the rate at which the shoreline approaches the equilibrium; G is a modulating function; and $\Delta D(t)$ is the disequilibrium term that forces shoreline evolution.

The first CEM we implement (CEM1) is the shoreline evolution model proposed by Toimil et al. (2017), which is composed of the equilibrium shoreline evolution model of Miller and Dean (2004) and a SLR-induced shoreline recession model that seeks to reproduce the landward displacement of the coast due to SLR, also known as the Bruun effect (Bruun, 1962). In this case, the shoreline change rate can adopt two values, one for erosion $V = k^-$ and another one for accretion $V = k^+$. The modulating function G is equal to one and the disequilibrium term responds to $\Delta D(t) = y_{eq}(t) - y(t)$. The equilibrium shoreline position thus combines short- and long-term effects following:

$$y_{eq}(t) = \Delta y_0 - W_b^*(t)\left(\frac{0.106H_b(t) + SS(t) + AT(t)}{B + 2H_b(t)}\right) - W^*(t)\frac{SLR(t)}{B + h^*} \quad (3)$$

where Δy_0 is an empirical parameter; W_b^* is the active surf zone width determined from the break point by $W^* = \left(H_b/\gamma A\right)^{1.5}$, in which A is the profile scale parameter (Dean, 1991); H_b is the breaking Hs obtained using $\gamma = 0.55$ spectral breaking criteria; SS is the storm surge; AT is the astronomical tide; B is the berm height; W^* is the active beach profile width; and h^* is the depth of closure calculated using the empirical formula of Birkemeier (1985).

The second CEM we implement (CEM2) is an equilibrium energy-based model modified from Yates et al. (2009) to consider SLR effects. The shoreline change rate is approximated to be the same for erosion and accretion events $V = C$, the modulating function is $V = E^{1/2}$ (where E means the wave energy), and the disequilibrium term is $\Delta D(t) = E(t) - E_{eq}(t)$. The equilibrium energy term $E_{eq}(t)$ accounts for the Bruun effect, which is treated as a long-term trend following Jaramillo et al. (2020):

$$E_{eq}(t) = a\left(y(t) + W^*(t)\frac{SLR(t)}{B + h^*}\right) + b \quad (4)$$

CEM1 and CEM2 are forced with wave-breaking parameters, which we estimate from nearshore waves. Considering the large number of VAR-based realisations, we apply a simple propagation technique based on wave energy conservation, the Snell's law of refraction, and a constant depth-breaking criterion.

Multi-Ensemble Probabilistic Projections of Shoreline Evolution

As a result of the thousands of CEM simulations, we obtain three different simulation packages (SP). The first SP (SP1) corresponds to 72,000 projected hourly shoreline evolutions from 2081 to 2100. These time series of shoreline change account for the uncertainty sampled at the steps of the top-down approach by considering 2 RCPs, 6 GCMs, 1,000 synthetic multivariate chronologies of future waves and storm surges for each RCP–GCM, 3 RCP–SLR trajectories related to three percentiles, and 2 CEMs. The second SP (SP2) includes 12,000 reference shoreline evolutions on hourly basis for the historical period 1985–2005, based on 6 GCMs, 1,000 synthetic multivariate chronologies of future waves and storm surges for each GCM, and 2 CEMs. Finally, the third SP (SP3) contains 72 projected hourly shoreline evolutions from 2081 to 2100 that differ from those of SP1 in that they do not consider climate variability uncertainty. The time series of shoreline change of SP3 account for 2 RCPs, 6 GCMs, 3 RCP–SLR trajectories related to three percentiles, and 2 CEMs.

Figure 4 displays the 72,000 simulations of SP1: 36,000 for the RCP4.5 (**Figure 4A**) and 36,000 for the RCP8.5 (**Figure 4B**). In each panel, shaded bands represent the 99% confidence levels related to the 5, 50, and 95th percentiles of SLR (colour code), superimposed by the simulations of SP3 (grey solid lines). The grey dashed line indicates the physical boundary of the beach (beyond this limit it would have disappeared). The blue and red dashed lines define the mean plus/minus standard deviation space associated with CEM1 and CEM2, respectively. As can be observed, such space is overall wider (higher upper-bound and lower lower-bound) for CEM2, especially resulting in larger erosion over time for the RCP–SLR combinations considered. Another aspect worth mentioning is the influence of GCMs internal climate variability in shoreline change. There is a hint that SP3 time series virtually never reach the 99% confidence levels of SP1, so not considering chronologies alternative to each GCM simulation could translate into the exclusion of potential outcomes. Importantly, these outcomes are more likely to be associated with erosion than with accretion phases, and this is more apparent for the RCP8.5. This may be because the exploration of different chronologies, even though they maintain the same pdf as the original GCM-driven simulations, may allow detecting different extreme retreat events that could result from cumulative effects such as less storm spacing or calm conditions over shorter periods of time.

For both RCPs, results are strongly clustered by the SLR percentiles. In the case of the SLR 50th percentile, SP1 mean shoreline retreats increase from 52 to 64 m and from 75 to 103 m between 2081 and 2100 for the RCP4.5 and the RCP8.5, respectively. As expected, the greatest dispersion of the results occurs by 2100, where SP1 and SP3 shoreline retreats roughly range, respectively, between 9–138 and 25–115 m for the RCP4.5, and between 37–200 and 52–177 m for the RCP8.5. These ranges cover all possible outcomes from the lower bound of the 99% confidence level associated with the SLR 5th percentile to the upper bound of the 99% confidence level for the SLR 5th percentile.

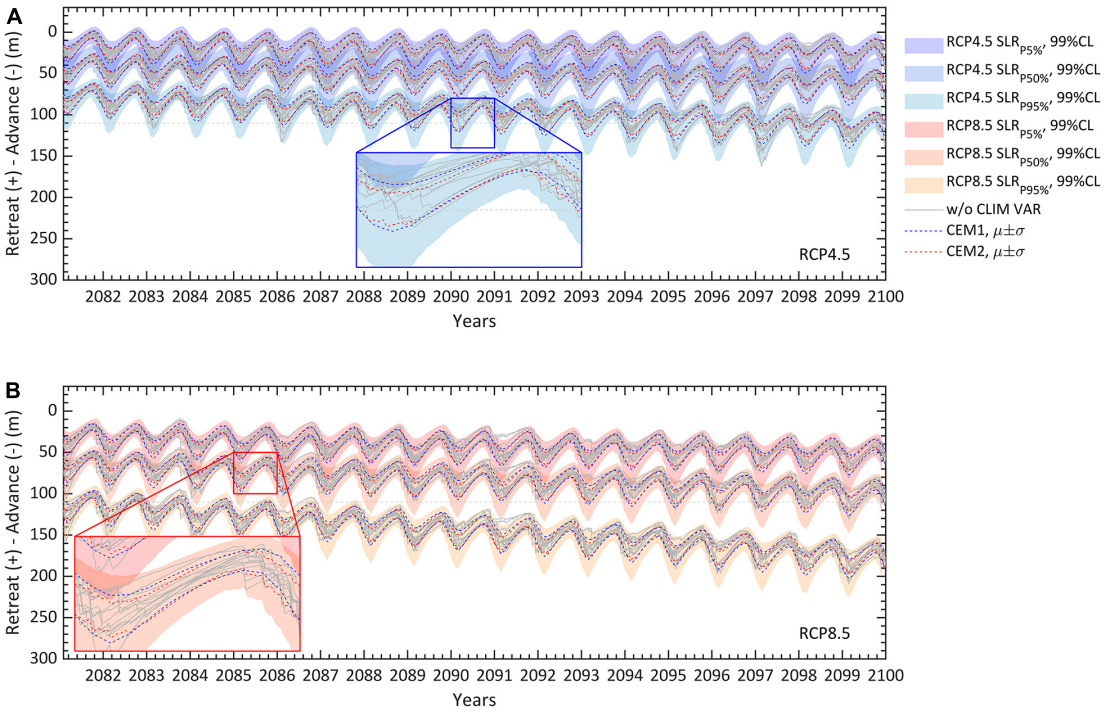

FIGURE 4 | Shoreline evolution projections for the period 2081–2100 in San Lorenzo Beach. Shoreline position retreat (positive values) and advance (negative values) with respect to the present position. Coloured shaded bands and dashed lines are related to the 72,000 simulations of SP1 generated for 2 RCPs (RCP4.5 and RCP8.5, **A,B**, respectively), 6 GCMs (ACCESS1.0, CMCC-CC, CNRM-CM5, HadGEM2-ES, IPSL-CM5A-MR and MIROC5), 3 SLR percentiles (5, 50, and 95th), climate variability (1,000 multivariate realisations per each RCP-GCM) and 2 CEMs. The 72 simulations of SP3 (without considering climate variability) are represented by the grey solid lines. The grey dashed line represents the threshold beyond which the beach would have disappeared.

Using the complete time series, we compute an indicator of the long-term or structural shoreline recession in 2081 and 2100 relative to 2005 (hereinafter R2081 and R2100, respectively) by subtracting the 2-year average initial position from the 2-year average final position of the shoreline from each model simulation. Additionally, we analyse changes in (episodic) extreme retreat events over the period 2081–2100 by fitting annual maxima shoreline retreats to non-stationary extreme value distributions. These outcomes are further described and analysed in section "Visualisation and Communication of Uncertainty in Coastal Erosion Projections".

VISUALISATION AND COMMUNICATION OF UNCERTAINTY IN COASTAL EROSION PROJECTIONS

Based on SP1, SP2, and SP3 shoreline evolution time series, we develop four analyses that provide different although complementary ways of visualising and communicating uncertainty in coastal erosion projections. We decompose the uncertainty cascade down to coastal erosion projections using real data, factorise long-term erosion estimates by the uncertainty dimensions deemed and determine their relative importance, and explore non-stationary extreme retreat events and the influence of climate variability on them.

The Cascade of Uncertainty

The paradigm of the cascade of uncertainty (Mitchell and Hulme, 1999; Wilby and Dessai, 2010) has been used in the literature to illustrate theoretically both the information and the uncertainty cascading across the modelling chain of the top-down approach, from the RCPs to coastal impact estimates, whether in the form of a triangle (e.g., Toimil et al., 2020a,b) or as a sequential diagram (e.g., Ranasinghe, 2016). However, more challenging is moving from theory to practice, particularly when the cascade extends down to impact models' response. **Figure 5** attempts to visualise the real cascade of uncertainty in coastal erosion projections in San Lorenzo Beach built upon actual data (SP1), expanding from the RCPs (upper tip where all lines converge; top layer) to the R2100 indicator (bottom layer). From top to bottom, the second layer shows an ensemble of 6 GCMs (ACCESS1.0, CMCC-CC, CNRM-CM5, HadGEM2-ES, IPSL-CM5A-MR, and MIROC5) forced by 2 future concentration pathways (RCP4.5 and RCP8.5). The following layer illustrates the role of uncertainty sampling in internal climate variability (denoted as CLIM VAR in the vertical axis). 1,000 multivariate realisations of potential chronologies of future wave conditions and surges for each RCP-GCM account for the stochastic nature of these dynamics. The fourth layer represents the combination of the multiple realisations of projected waves and storm surges with 3 different RCP-induced SLR trajectories (5, 50 and 95th percentiles) to force the CEMs. Next, each line splits into 2 CEMs,

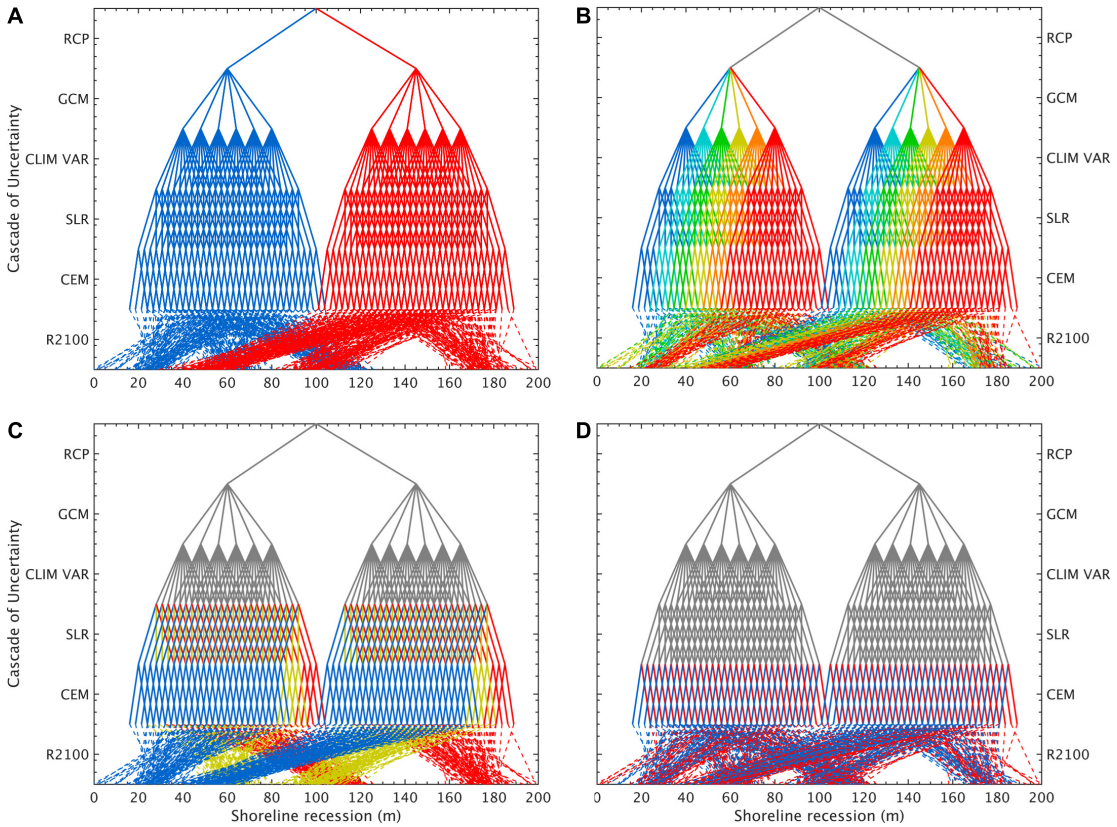

FIGURE 5 | Visualisation of the cascade of uncertainty in coastal erosion projections by 2100. The cascade is built upon SP1 simulations. From top to bottom: first layer shows the 2 RCPs, second layer shows the ensemble of 6 GCMs, third layer shows climate variability, fourth layer shows the 3 SLR percentiles, fifth layer shows the ensemble of 2 CEMs and the last layer shows the R2100 indicator (actual values displayed on the horizontal axis). **(A–D)** illustrate the cascade under four factorisations that highlight the uncertainty spread due to the choice of RCPs, GCMs (considering climate variability realisations), SLR percentiles, and CEMs. For the sake of visibility, we plot 720 SP1 simulations (out of 72,000) covering the full range of 2100 and distribute RCP, GCM, CLIM VAR, SLR, and CEM levels evenly in space.

each of which delivers its corresponding R2100 value. For the sake of visibility and to avoid overplotting, we only plot 720 simulations (out of 72,000), although covering the full R2100 range, and distribute RCP, GCM, CLIM VAR, SLR, and CEM levels evenly in space, with R2100 reaching real values along the horizontal axis. Likewise, we neither depict the threshold beyond which the beach would have disappeared and that would be placed in 110 m (horizontal axis).

Figures 5A–D illustrate the cascade of uncertainty in R2100 under four different factorisations. These factorisations seek to disentangle the uncertainty in R2100 estimates based on the choice of RCP (**Figure 5A**), GCM including the associated climate variability realisations (**Figure 5B**), SLR percentile (**Figure 5C**), and CEM (**Figure 5D**). As such, the range of R2100 values is the same in all panels, extending roughly from 0 to 200 m. In **Figure 5A**, each colour shows a different RCP-driven R2100 pathway (RCP4.5-blue and RCP8.5-red). Thus, the ensemble of GCM forced by the same RCP are coloured alike, and the same applies to the subsequent layers down to coastal erosion projections. In **Figure 5B**, we start decomposing by GCM and each colour represents a different GCM-driven R2100 pathway (ACCESS1.0-blue, CMCC-CC-cyan, CNRM-CM5-green, HadGEM2-ES-yellow, IPSL-CM5A-MR-orange, and MIROC5-red). Likewise, in **Figure 5C**, SLR percentiles are decomposed next and coloured according to the R2100 pathway they drive (P5%-blue, P50%-yellow, and P95%-red). Finally, **Figure 5D** shows R2100 factorised by the CEM dimension (CEM1-blue and CEM2-red).

Looking at the bottom layer, the dashed lines thus inherit their colour from the choices of RCP, GCM, SLR percentile, and CEM and allow to visualise the uncertainty range in R2100 that can be attributed to them at a glance. For instance, R2100 roughly range from 0 to 120 m for the RCP4.5 and from 30 to 200 m for the RCP8.5 (**Figure 5A**). As we focus on the long term (2100), GHG concentration differences are high and the different scenarios clearly represent two different R2100 populations that cannot be easily merged, which is further emphasised by the choice of SLR percentile (colour differentiated in **Figure 5C**). This results in a strong multi-modal response in R2100 induced by RCP–SLR with 4 different clusters: (1) P5% RCP4.5–SLR, (2) P50% RCP4.5–SLR and P5% RCP8.5–SLR, (3) P95% RCP4.5–SLR and P50% RCP8.5–SLR, and (4) P95%

RCP8.5–SLR. This could be explained by the facts that we concentrate in a far future and that DP16 projections provide SLR extreme outcomes (e.g., a rise of 2.55 m for the RCP8.5 by 2100 in Gijon). Such multi-modal response gets weaker as we move into close time horizons. **Supplementary Figure 4** shows the equivalent cascade of uncertainty for R2081 (also calculated using SP3 data). As it illustrates, not only are the clusters more diffuse by 2081, but the uncertainty spread in coastal erosion projections has narrowed and shifted toward smaller values on the horizontal axis.

Figure 5D reinforces the idea that, in general, CEM2 (wave energy-based including SLR trend) provides more extreme values, widening the range and thus, the uncertainty, in R2100. The GCM dimension (**Figure 5B**) does not appear to dominate the spread in the simulated projections. However, that does not mean that the additional simulations derived stochastically do not play an important role. **Figure 6** shows the same plots as in **Figure 5** but with the superimposition of SP3 R2100 (72 simulations) represented by solid black lines, which cover shoreline retreats roughly ranging from 15 to 185 m. R2100 uncertainty spread is thus increased by nearly 20% when considering a more complete sampling of climate variability compared to the more common approach of using a single realisation of GCM-driven wave and storm surge projections. This could be because, while it is known that the chronology can highly influence short-term shoreline changes (Toimil et al., 2017), certain chronologies may eventually affect long-term erosion (R2100), which if disregarded may lead to the misallocation of adaptation resources.

Factorisation of Uncertainty Sources

The R2100 cascade of uncertainty shows a clear multi-modal response dominated by the choice of the RCP and the SLR percentile. To isolate the effects of each uncertainty source over the coastal erosion projections, **Figure 7** illustrates R2100 values factorised by the dimensions considered in absolute terms (column on the right) and nondimensionalised by SLR (column on the left). These R2100 values are based on SP1 (72,000 simulations accounting for climate variability) and SP3 (72 simulations not considering climate variability) data, which are represented using coloured and black symbology, respectively. R2100 values are factorised by their driving RCPs (**Figures 7A,B**), GCMs (**Figures 7C,D**) and CEMs (**Figures 7E,F**), all of which are in turn disaggregated by the SLR percentiles (5, 50, and 95th).

One of the most apparent features of **Figure 7** is the role of climate variability in the R2100 spread range. While SP3

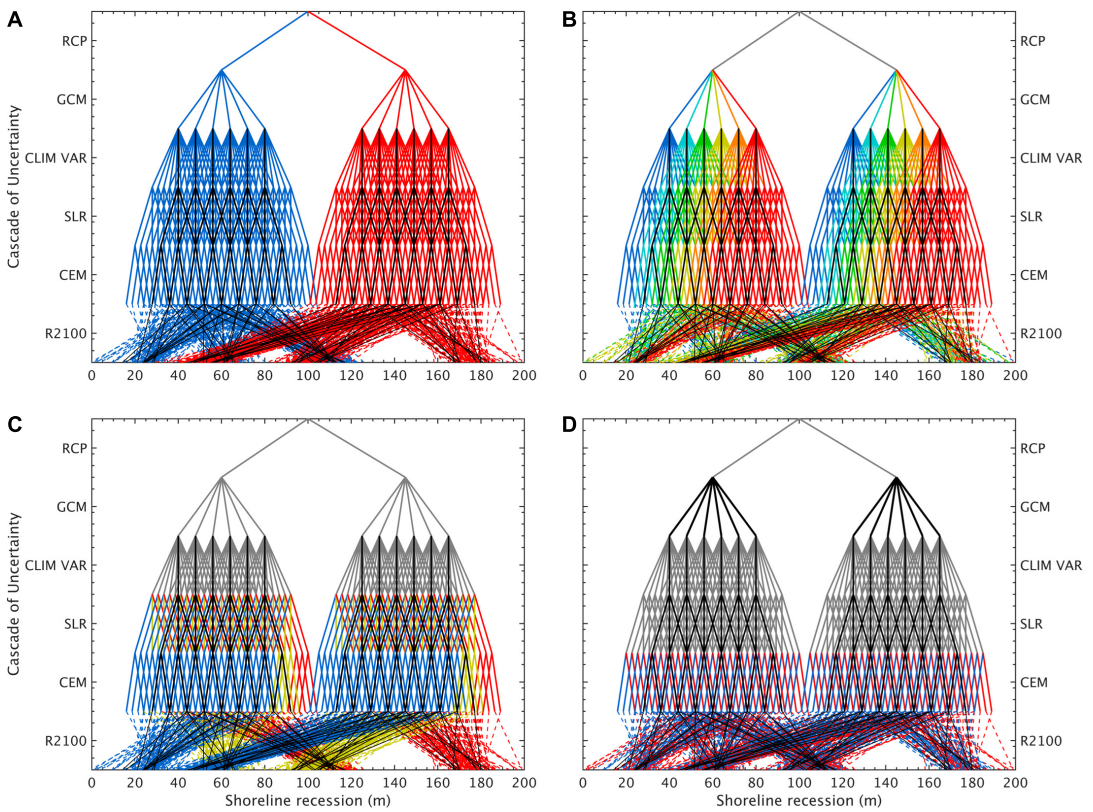

FIGURE 6 | Visualisation of the cascade of uncertainty in coastal erosion projections by 2100 using SP1 and SP3 simulations. SP1 data (720 simulations out of 72,000) is displayed as in **Figure 5** and SP3 data (72 simulations) are superimposed and represented by solid black lines. From top to bottom: first layer shows the 2 RCPs, second layer shows the ensemble of 6 GCMs, third layer shows climate variability, fourth layer shows the 3 SLR percentiles, fifth layer shows the ensemble of 2 CEMs and the last layer shows the R2100 indicator (actual values displayed on the horizontal axis). **(A–D)** illustrate the cascade under four factorisations that highlight the uncertainty spread due to the choice of RCPs, GCMs (considering climate variability realisations), SLR percentiles, and CEMs.

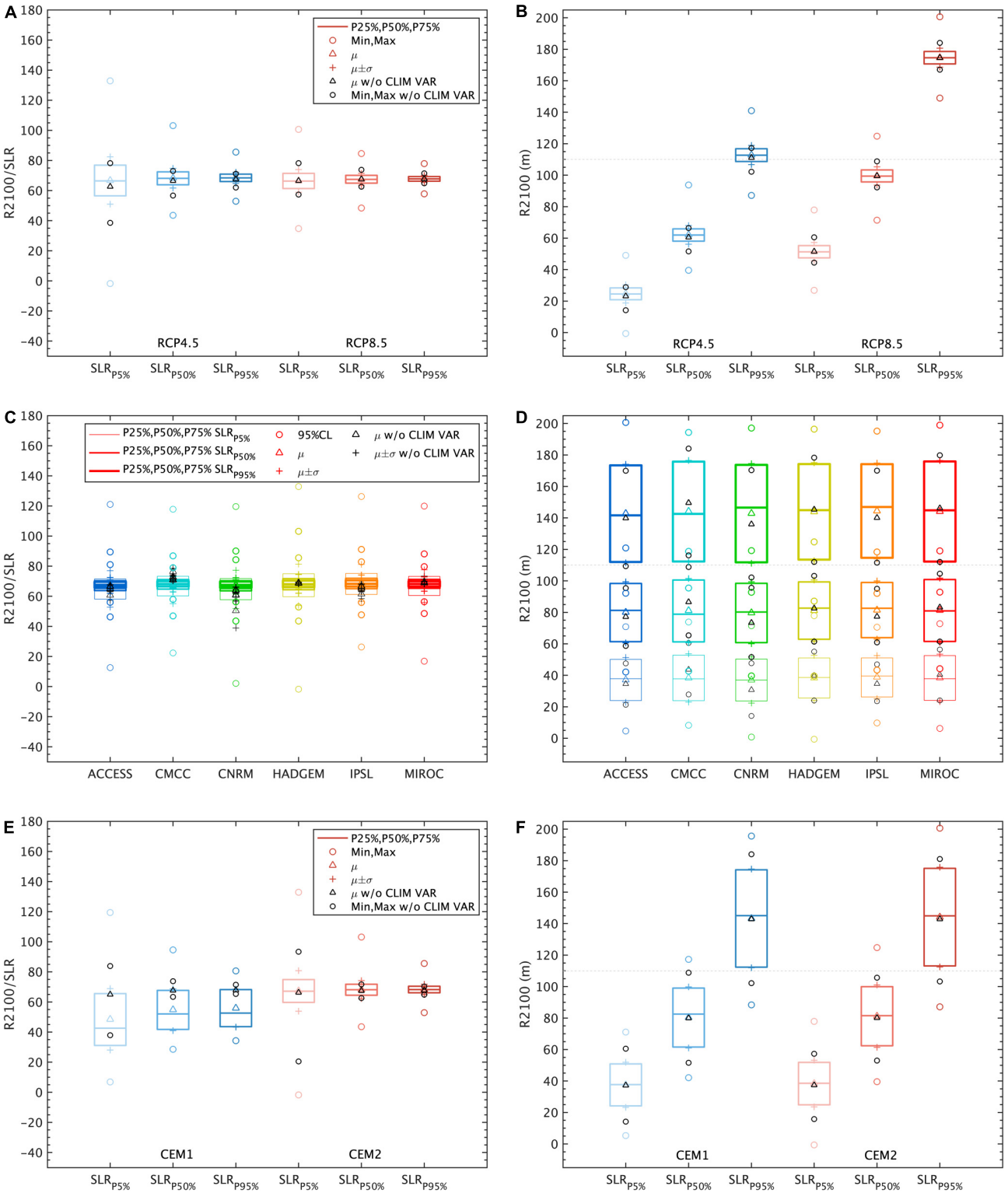

FIGURE 7 | R2100 values factorised by their driving RCPs **(A,B)**, GCMs **(C,D)** and CEMs **(E,F)**, all of them disaggregated in turn by the SLR percentiles (5, 50, and 95th). R2100 factorisation is provided in absolute terms (m) on the right column and nondimensionalised by SLR on the left column. SP1 (72,000 simulations considering climate variability) and SP3 (72 simulations without considering climate variability) are represented using coloured and black symbology, respectively. Note that in **B, D** and **F** the grey dashed line represents the threshold beyond which the beach would have disappeared.

mean values can be either above or below SP1 mean values, SP3 maximum and minimum values are far (or very far in nondimensionalised panels) from the same statistics of SP1, highlighting the fact that not quantifying internal variability's full extent sufficiently could be critical from a decision standpoint. As can be observed in **Figure 7D**, the variability inter-GCM for any SLR percentile is low for SP3 data, and very low for SP1. This could be expected because the multi-model projections of waves and storm surges show very little change in the signal and among GCMs, and due to the fact that we have corrected their bias (this can be deemed some sort of standardisation) and generated thousands of realisations with the VAR model under the same assumptions.

The highest the SLR percentile, the most the R2100 spread range is reduced when nondimensionalised, a reduction that is more significant for the RCP8.5 (**Figure 7A**) and longer-term horizons (**Supplementary Figure 5**). This could be explained because the higher the SLR, the more it dominates the central values of the R2100 distribution and, although the variability range is similar regarding the SLR percentile in absolute terms, when nondimensionalised by SLR, this variability is reduced the higher the SLR value. This decrease is sharper for the 25–75th percentiles of CEM2-driven R2100 than for CEM1-related outcomes (**Figure 7E**). However, CEM2 minimum and maximum values are shown to be more extreme than those from CEM1, whether or not nondimensionalised, as partly seen in **Figures 5**, **6**.

Fraction of the Total Uncertainty

To further quantify the dominant drivers of uncertainty in these projections of coastal erosion and their relative contribution to R2100 uncertainty, we apply a four-factor, ANOVA-based variance decomposition to three experiments where RCPs, GCMs, SLR percentiles and CEMs are the uncertainty sources. The first experiment (A) consists of comparing the variance partitioning between SP1 72,000 simulations and SP3 72 simulations (A1 and A2, respectively). The second experiment (B) compares this variance partitioning between SP1 and SP3, both excluding the SLR 95th percentile (48,000 and 48 simulations, and B1 and B2, respectively). Finally, the third experiment (C) concentrates on the RCP8.5 and the SLR 50th percentile of SP1 and SP3, which reduces the simulations involved to 12,000 and 12 (C1 and C2), respectively.

Figure 8 shows for the experiments A–C the contribution of the uncertainty sources and their interaction to R2100 total uncertainty. The findings are consistent with the results obtained from previous analyses. Overall, we find a strong dominating influence of the SLR and RCP dimensions, which could be attributable to the horizon considered (2100), where RCPs diverge significantly, and the extreme SLR projections used.

Experiment A highlights the virtually negligible influence of GCM uncertainty (∼0%) compared with RCP's (∼18%) and SLR's (>80%) when considering the full range of R2100 (SP1, A1). This could be explained by the fact that the 1,000 additional realisations per each RCP–GCM to sample intrinsic uncertainty

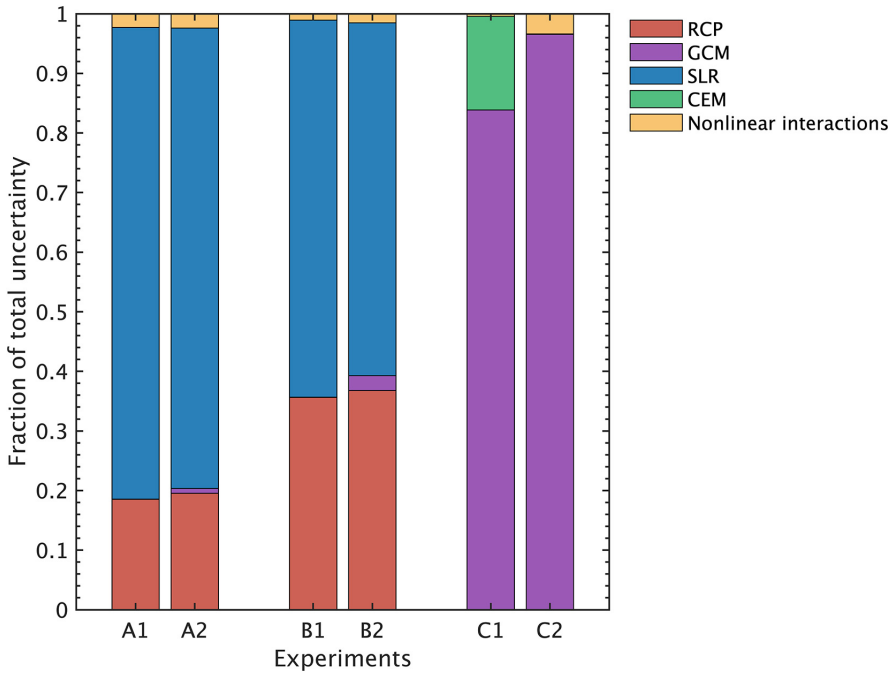

FIGURE 8 | Contribution of each uncertainty source (RCPs, GCMs, SLR percentiles, and CEMs) and their interactions to total R2100 uncertainty. The variance partitioning is based on a four-factor ANOVA-based decomposition method. Experiment A compares SP1 72,000 simulations, with SP3 72 simulations (A1 and A2, respectively); experiment B compares SP1 48,000 simulations and SP3 48 simulations, both excluding the SLR 95th percentile (B1 and B2, respectively); and experiment C compares SP1 12,000 simulations and SP3 12 simulations, both constrained to RCP8.5 and SLR 95th percentile (C1 and C2, respectively).

hide the variability of the GCMs themselves (**Figure 7D**), to which bias correction has also been applied. In A2, while SLR (∼75%) and RCP (∼20%) uncertainty continue to dominate, there is some (although little) room for GCM uncertainty contribution (∼1%).

As DP16 projections provide extreme SLR outcomes, experiment B seeks to analyse how the contributions would change if the SLR upper bound were the 50th percentile. Compared to experiment A, RCPs' uncertainty contribution increases (∼36 and ∼37% for B1 and B2, respectively), SLR's decreases (∼64 and ∼60% for B1 and B2, respectively) and, as could be expected, GCMs' increases its relative importance (up to 3%) as for B2.

Finally, experiment C leaves RCP and SLR out of the equation. As a result, GCM uncertainty dominates but its contribution is still weaker in C1 than in C2 (∼84 and ∼97%, respectively) because of the effect of climate variability uncertainty. In C1 there is new room for the contribution of CEM uncertainty (∼16%). In any case, the contribution of the pairwise (RCP–GCM, RCP–SLR, RCP–CEM, GCM–SLR, GCM–CEM, and SLR–CEM)

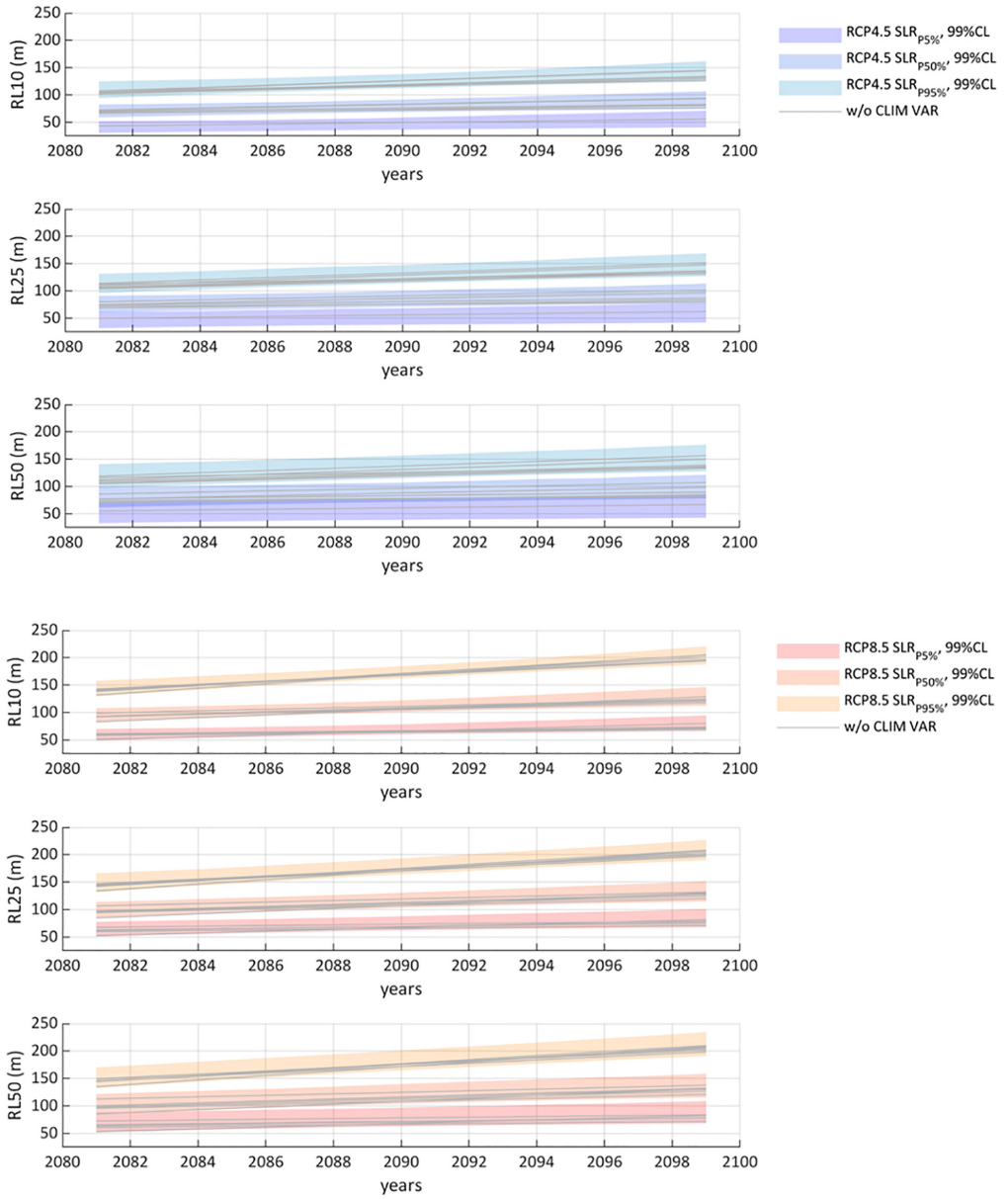

FIGURE 9 | Effective return levels corresponding to 10, 25, and 50 years under the non-stationary assumption for the period 2080–2100 and for the SLR trajectories (associated with the 5, 50, and 95th percentiles) under the RCP4.5 (blue panels) and the RCP8.5 (red panels). Grey solid lines represent the return periods calculated from the GCM-driven simulations of SP3 (without climate variability). Coloured shaded areas show the 99% confidence bands of the non-stationary GEV fit to the annual maxima shoreline retreats derived from SP1 simulations.

triple (RCP–GCM–SLR, RCP–GCM–CEM, RCP–SLR–CEM, and GCM-SLR-CEM) and quadruple (RCP–GCM–SLR–CEM) interactions to R2100 uncertainty is <3%.

Non-stationary Extreme Value Analysis and Influence of Climate Variability

Extreme shoreline positions are characterised by return levels of erosion, which can provide very valuable information for decision-making, as risk-reduction actions (e.g., beach nourishment design) often take place in response to unusually large shoreline recession. The analysis of the variability of extreme erosion events, however, is a complex issue as processes at two different time scales occur simultaneously: the interannual variability due to the combined effect of waves and storm surges, and the slow-onset SLR and its long-term effect, which leads to the gradual, persistent landward and upward displacement of the coastline. SLR, thus, introduces a positive and persistent erosive trend that can only be properly addressed by conducting non-stationary extreme-value analysis.

In this study, we use the Non-stationary Extreme Value Analysis (NEVA) package (Cheng et al., 2014) to estimate effective return levels, which indicate the return level that should be considered to have the same probability of occurrence over time. In NEVA, non-stationarity is based on the assumption that the location parameter of the Generalised Extreme Value (GEV) distribution is linearly time dependent according to the trend. We apply the non-stationary GEV distribution to annual maxima shoreline retreats. We obtain the effective return levels corresponding to 10, 25, and 50 years over the period 2081–2100 for the SP1 and SP3 time series of shoreline evolution. **Figure 9** illustrates the time evolution of mean effective return levels (SP3, grey solid lines) and 99% confidence levels (SP1, coloured shaded areas) disaggregated by SLR percentiles and RCPs, where only time series with significant SLR trend are shown. There is more overlap among the RCP4.5 results (upper panels), especially for the SLR 50 and 95th percentiles and longer return levels. For the RCP8.5 (red panels), the mean effective return level of a 10-year extreme erosion in 2080 is 58.9, 92.8, and 140.7 m, while in 2100 is 78.8, 127.1, and 202.6 m for the 3 SLR percentiles, respectively. As can be observed, the time evolution of the effective return levels for the 6 GCMs of SP3 simulations has significant variability, which increases considerably for SP1 outcomes (with VAR-based simulations). The 99% confidence bands become wider as the corresponding year of the return level gets higher. These bands are asymmetric, with the higher

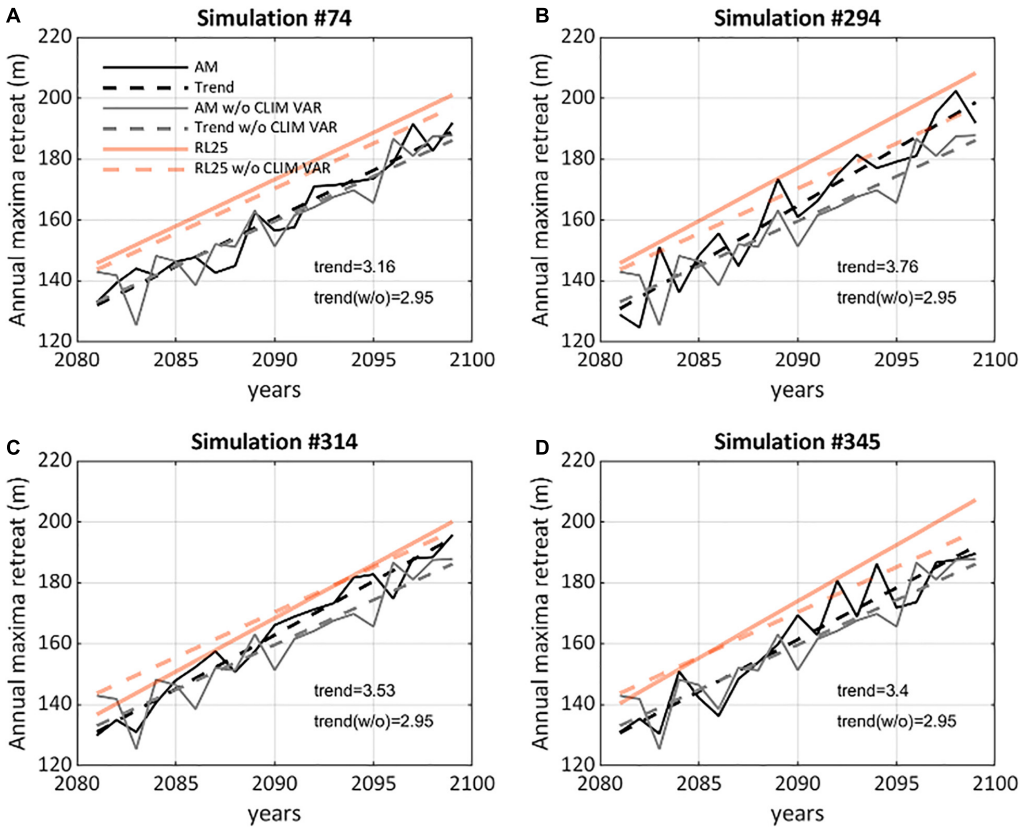

FIGURE 10 | Time series of annual maxima shoreline retreat corresponding to the IPSL-CM5A-MR model (solid grey line) and the simulations #74 **(A)**, #294 **(B)**, #314 **(C)**, and #345 **(D)** of SP1 associated with this GCM (solid black line). Dashed lines represent the annual maxima shoreline retreat trends. Effective 25-year return levels under the non-stationary assumption over 2080–2100 for the SLR 95th percentile and for the RCP8.5. The pink solid line shows the results of the SP1 simulation; and the pink dashed line represents the results associated with the original GCM simulation (SP3).

spread of the return levels with respect to the mean for the high percentiles rather than for the low ones. Overall, RCP4.5's exhibit higher variability and this could be explained by the lesser influence of SLR, which leads to chronology having greater impact on the results.

Figure 10 shows the time series of annual maxima shoreline retreat for the IPSL-CM5A-MR model (solid grey line), where we compare its original run (SP3) and four different VAR-based simulations (#74, #294, #314, and #345 of SP1, represented by solid black lines) for the RCP8.5. We calculate the shoreline

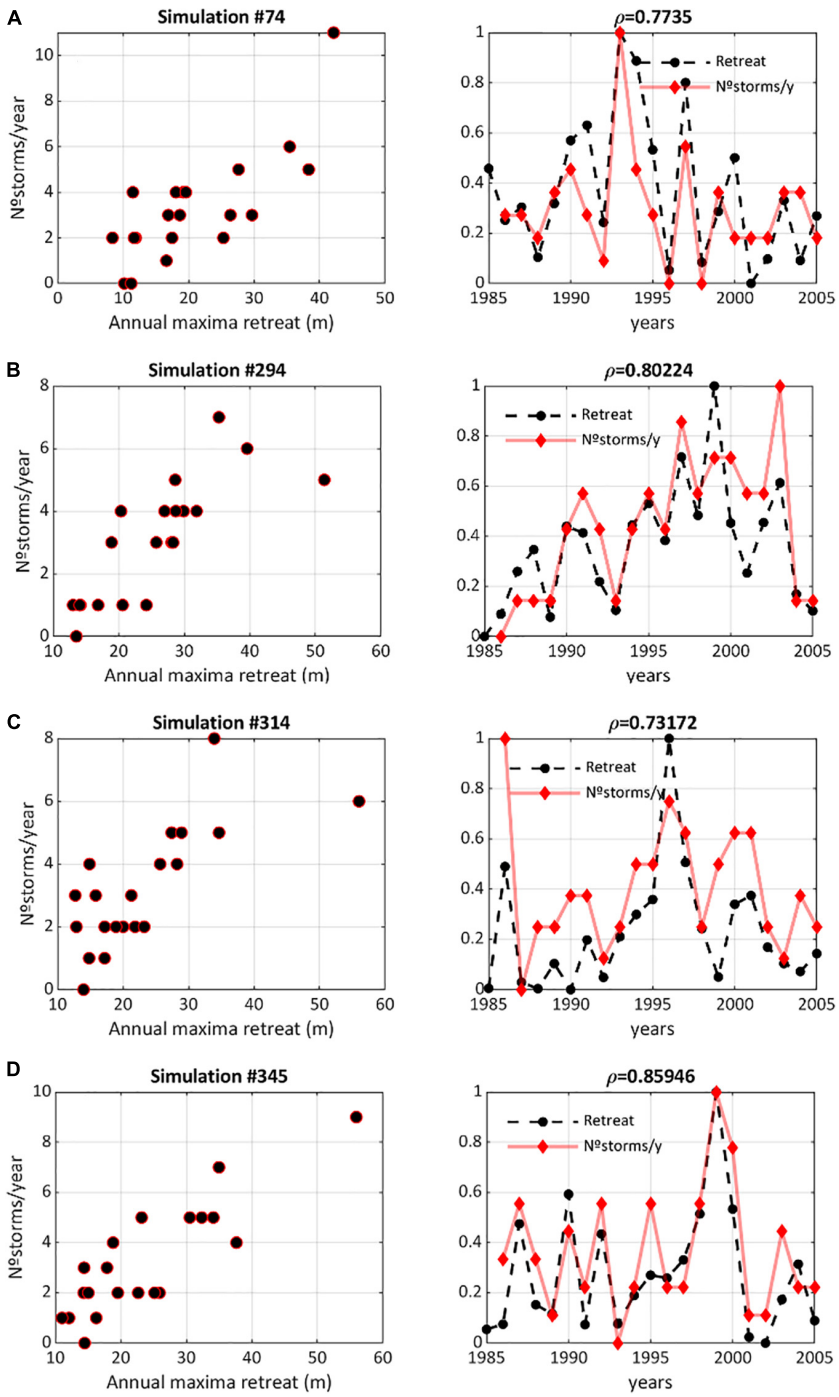

FIGURE 11 | Scatter plot of the annual maxima shoreline retreat compared to the annual number of storms (left column). Time series of the normalised annual maxima shoreline retreat and normalised annual number of storms for the simulations #74 **(A)**, #294 **(B)**, #314 **(C)**, and #345 **(D)** of SP2 associated with the IPSL-CM5A-MR model in the historical period (1985–2005) (right column).

retreat annual maxima trend for each simulation (dashed lines). The trends of the SP3 run and the simulation #74 are similar (**Figure 10A**). However, the trends of the other three VAR-based simulations (**Figures 10B–D**) are higher than the SP3 run due to more erosive shoreline retreat evolution over the period 2081–2100. These higher trends reflect a higher increase of effective return levels of 25 years by 2100 compared to those from the SP3 run (pink lines). In addition, we find that shoreline retreat in 2081 influences the effective return levels over the following years. Take the case of simulation #314 (**Figure 10C**), where shoreline retreat is significantly lower than for the SP3 run, constraining the return level reached in 2100, although with a higher trend. The return level of the simulation #294 (**Figure 10B**) reflects by 2100 a combination of large shoreline recession in 2081 and a high erosion trend. The interannual variability of this return levels thus explains the wide extension of the confidence bands of the effective return levels, especially as for the upper bound. This confirms the influence of sampling climate variability uncertainty using the VAR model in the R2100 indicator identified in the previous analysis.

It seems that the chronology of the sea state parameters and storm surge is the factor that most influences the interannual evolution of shoreline retreat, rather than the magnitude of these dynamics during storms. To further verify the effect of climate variability in short-term erosion, we analyse the relationship between the number of storms per year and the annual maxima shoreline retreat over the historical period of several IPSL-CM5A-MR simulations of SP2 (**Figure 11**). We define storm events as independent 3-day events over the threshold of Hs that guarantees an average of 3 storms per year. For instance, the largest shoreline retreat in simulation #74 (**Figure 11A**) exceeds 42 m and happens in 1993 due to the cumulative effect of more than 10 storms over that year. Another example is the maximum shoreline retreat in simulation #294 (**Figure 11B**, higher in magnitude than in #74), which roughly reaches 52 m in 1999 because of the combined effect of many storms and a positive erosive trend over the previous years. In simulations #314 and #345 (**Figures 11C,D**, respectively), the largest annual maxima shoreline retreat occurs due to the significant erosion over the two preceding years (the beach is not able to recover in summer) induced by the large number of storms per year. In the original IPS-CM5A-MR run, the maximum shoreline retreat does not exceed 37 m and occurs in 1994, when also the highest number of storms happened (**Supplementary Figure 6**). From this analysis, we can conclude that the most extreme shoreline retreats are generated by "extreme" synthetic chronologies of wave and storm surge conditions simulated by the VAR model.

CONCLUSION

Climate projections have brought into focus the imperative need to adapt coastal areas to a changing climate under conditions of deep uncertainty. Positioning decision-making in the best situation requires substantial efforts to better attribute uncertainty in impact assessments. This involves identifying and sampling sources of uncertainty and considering their nature, spreading and cumulative effect. The visualisation of this whole process can help understand the relative importance of the steps of the top-down approach to full uncertainty in impact estimates and where to concentrate energy and resources.

In this paper, we developed long-term multi-ensemble probabilistic coastal erosion projections following the steps of the top-down approach with the primary objectives of decomposing and visualising the cascade of uncertainty using real data and analysing the contribution of each step to the total uncertainty. For that purpose, we compiled dynamic projections of waves and storm surges (for 2 representative concentration pathways and 6 global climate models), corrected their bias and transferred projected offshore waves to nearshore by applying a hybrid downscaling technique that allows to consider sea-level effects on wave propagation. Next, we stochastically generated 1,000 additional multivariate realisations of projected waves and storm surges per each combination of representative concentration pathway and global climate model to account for different chronologies potentially driven by climate variability. We combined these 12,000 time series of future nearshore waves and storm surges with three mean sea-level rise trajectories corresponding to 3 percentiles of the simulated frequency distributions for the radiative forcing scenarios considered. Finally, we forced 2 coastal erosion models and derived 72,000 future time series of shoreline evolution. Based on these time series we calculated long-term and episodic (non-stationary) erosion, which could be useful tools to inform decision-makers on the shoreline future mean position and its variance.

It is noteworthy to mention that our choice to have applied bias correction before the hybrid downscaling in this study is based on the availability of reliable historical wave data in deep water. Besides, we consider that it is more realistic to propagate every hourly sea state at each corrected sea level, and this implies to correct the storm surge bias before downscaling waves. However, these two steps could be exchanged if robust historical nearshore data are available to apply the correction.

By means of this approach, we considered both knowledge uncertainty and intrinsic uncertainty. The first was characterised by using ensembles of representative concentration pathways, global climate models, and coastal erosion models, and a range of mean sea-level rise trajectories. Intrinsic uncertainty was accounted for by performing multiple multivariate realisations of projected waves and storm surges that were based on the same assumptions that the original projections but provided alternative chronologies that allowed to consider an overall larger range of variability and different extreme retreat events. Further developments of this approach could consider additional uncertainty sources such as coastal erosion model parameterisations (e.g., model coefficient adjustments would be needed as the 1979–2020 model structure will not necessarily remain unaltered in the future) or the application of different bias correction methods.

Two aspects that highly conditioned the results were our focus on the far future (2081–2100) and the use of projections of mean sea-level rise using Antarctic ice-sheet simulations. A justification for these choices is that risk assessments usually

consider far-future lead times (i.e., 2100) and always require the full range of potential damaging outcomes, including low-probability high-impact scenarios. In the visualisation of the cascade of uncertainty, this resulted in a multi-modal response that was stronger in 2100 than in 2081, and where we identified four different clusters combining representative concentration pathways and mean sea-level rise percentiles. Both the cascade and the subsequent factorisation of long-term coastal erosion values highlighted that not quantifying internal variability's full extent sufficiently could lead to a truncated range of outcomes, and adverse implications for decision-making. Another key feature relates to the influence of climate models uncertainty to the total uncertainty, which we found virtually negligible for the simulations that consider climate variability uncertainty sampling, partly due to the climate variables considered and bias correction (necessary for impact assessments), and because of the thousands of multivariate realisations we produced stochastically. Such realisations have the same underlying assumptions but provide alternative chronologies of wave conditions and storm surges. This noise itself has proven to be an important part of the full range of outcomes, as we found that the most extreme annual maxima shoreline retreats occurred for synthetic chronologies simulated by the stochastic model. These findings show that in order to capture the full uncertainty in coastal erosion projections, all uncertainty sources need to be adequately sampled considering case-specific aspects such as the climate variables, the degree of anthropogenic impact (e.g., radiative forcing or Antarctic ice-sheet contribution) and time horizon. In the near future (e.g., 2021–2050), the small differences in greenhouse gas concentration between radiative forcing scenarios could show greater inter-model variability, which would be similar to a random sample of realisations from the same climate model (e.g., as in Fernández et al., 2019). Further, projected changes in wave conditions and storm surge are relatively small in the study area. However, in other regions where future changes are more significant and the deviation in the ensemble projections is wider, climate model uncertainty could certainly account for a larger fraction of the total uncertainty.

Importantly, this study should be viewed as a way to expand scientific understanding of uncertainty treatment in coastal erosion projections when using the top-down approach, rather than providing the best projections of what coastal erosion in San Lorenzo Beach will be like. In particular, we tried to make progress on the incorporation, visualisation and analysis of the sources of uncertainty involved. For the sake of facilitating a better explanation of our final aim, namely visualising the uncertainty we used a pilot site for which data and models were at hand. The combination of better suited climate projections, improved downscaling methods and more detailed coastal erosion models (including more sophisticated wave-breaking propagation) would presumably result in a different range of shoreline recession values, and extreme retreat events of different magnitude and frequency. However, the approach and the uncertainty treatment herein proposed applies in any case.

DATA AVAILABILITY STATEMENT

The original contributions presented in the study are included in the article/**Supplementary Material**, further inquiries can be directed to the corresponding author/s.

AUTHOR CONTRIBUTIONS

AT developed the concept and wrote the original manuscript. AT and PC designed the analysis and designed the figures and their descriptions. AT, PC, and MA-C performed the analysis. IL verified the analysis. AT, PC, MA-C, and IL discussed and commented on the manuscript. All authors contributed to the article and approved the submitted version.

FUNDING

AT acknowledges the financial support from the FENIX Project by the Government of Cantabria. This research was also funded by the Spanish Government via the grant RISKCOADAPT (BIA2017-89401-R).

ACKNOWLEDGMENTS

The authors thank the Working Group on Coupled Modelling of the World Climate Research Programme, which is responsible for the CMIP, and the climate modelling groups for producing and making available their model output.

SUPPLEMENTARY MATERIAL

The Supplementary Material for this article can be found online at: https://www.frontiersin.org/articles/10.3389/fmars.2021.683535/full#supplementary-material

REFERENCES

Athanasiou, P., van Dongeren, A., Giardiono, A., Vousdoukas, M. I., Ranasinghe, R., and Kwadijk, J. (2020). Uncertainties in projections of sandy beach erosion due to sea level rise: an analysis at the European scale. *Sci. Rep.* 10:11895.

Birkemeier, W. A. (1985). Field data on seaward limit of profile change. *J. Waterw. Port. Coast Ocean. Eng.* 111, 598–602. doi: 10.1061/(asce)0733-950x(1985)111:3(598)

Booij, N., Ris, R. C., and Holthuijsen, L. H. (1999). A third-generation wave model for coastal regions 1. Model description and validation. *J. Geophys. Res. Oceans* 104, 7649–7666. doi: 10.1029/98JC02622

Bruun, P. (1962). Sea-level rise as a cause of shore erosion. *J. Waterways Harbors Division ASCE* 88, 117–130. doi: 10.1061/jwheau.0000252

Camus, P., Méndez, F. J., and Medina, R. (2011). A hybrid efficient method to downscale wave climate to Coastal areas. *Coast. Eng.* 58, 851–862. doi: 10.1016/j.coastaleng.2011.05.007

Camus, P., Tomás, A., Díaz- Hernández, G., Rodríguez, B., Izaguirre, C., and Losada, I. J. (2019). Probabilistic assessment of port operation downtimes under climate change. *Coast. Eng.* 147, 12–24. doi: 10.1016/j.coastaleng.2019.01.007

Cheng, L., AghaKouchak, A., Gilleland, E., and Katz, R. W. (2014). Non-stationary extreme value analysis in a changing climate. *Clim. Change* 127, 353–369. doi: 10.1007/s10584-014-1254-5

Cid, A., Castanedo, S., Abascal, A. J., Menéndez, M., and Medina, R. (2014). A high resolution hindcast of the meteorological sea level component for Southern Europe: the GOS dataset. *Clim. Dyn.* 43, 2167–2184. doi: 10.1007/s00382-013-2041-0

Dean, R. G. (1991). Equilibrium beach profiles: principles and applications. *J. Coast. Res.* 7, 53–84.

DeConto, R. M., and Pollard, D. (2016). Contribution of Antarctica to past and future sea-level rise. *Nature* 531, 591–597. doi: 10.1038/nature17145

Dequé, M. (2007). Frequency of precipitation and temperature extremes over France in an anthropogenic scenario: model results and statistical correction according to observed values. *Glob. Planet. Change* 57, 16–26. doi: 10.1016/j.gloplacha.2006.11.030

Fernández, J., Frías, M. D., Cabos, W. D., Cofiño, A. S., Domínguez, M., Fita, L., et al. (2019). Consistency of climate change projections from multiple global and regional model intercomparison projects. *Clim. Dyn.* 52, 1139–1156. doi: 10.1007/s00382-018-4181-8

Giorgi, F. (2010). "Uncertainties in climate change projections, from the global to the regional scale," in *Proceedings of the EPJ Web of conferences*, Vol. 9 (Les Ulis: EDP Sciences), 115–129. doi: 10.1051/epjconf/201009009

Gutiérrez, J. M., Maraun, D., Widmann, M., Huth, R., Hertig, E., Benestad, R., et al. (2018). An intercomparison of a large ensemble of statistical downscaling methods over Europe: results from the VALUE perfect predictor cross-validation experiment. *Int. J. Climatol.* 39, 3750–3785. doi: 10.1002/joc.5462

Hawkins, E. (2014). *The cascade of Uncertainty in Climate Projections.* In. Climate Lab Book (Open Climate Science). Available online at: http://www.climate-lab-book.ac.uk/2014/cascade-of-uncertainty doi: 10.1002/joc.5462 (accessed April, 2021)

Hawkins, E., and Sutton, R. (2009). The potential to narrow uncertainty in regional climate predictions. *Bull. Am. Meteorol. Soc.* 90, 1095–1108. doi: 10.1175/2009bams2607.1

Hay, L. E., Wilby, R. J. L., and Leavesley, G. H. (2000). A comparison of delta change and downscaled GCM scenarios for three mountainous basins in the United States. *J. Am. Water Resour. Assoc.* 36, 387–397. doi: 10.1111/j.1752-1688.2000.tb04276.x

Hinkel, J., Church, J. A., Gregory, J. M., Lambert, E., Le Cozannet, G., Lowe, J., et al. (2019). Meeting user needs for sea level rise information: a decision analysis perspective. *Earths Future* 7, 320–337. doi: 10.1029/2018EF001071

Hirt, C., and Rexer, M. (2015). Earth2014: 1 arc-min shape, topography, bedrock and ice-sheet models – available as gridded data and degree-10,800 spherical harmonics. *Int. J. Appl. Earth Obs. Geoinf.* 39, 103-112. doi: 10.1016/j.jag.2015.03.001

IHCantabria (2020). *High-Resolution Projections of Waves and Water Levels Along the Spanish Coast.* Spanish Ministry for the Ecological Transition and the Demographic Challenge, 60 pages (in Spanish). Avilable online at: www.miteco.gob.es/es/costas/temas/proteccion-costa/tarea_2_informe_pima_adapta_mapama_tcm30-498855 pdf (accessed April, 2021)

IPCC (2013). "Summary for Policymakers," in *Climate Change 2013: The Physical Science Basis. Contribution of Working Group I to the Fifth Assessment Report of the Intergovernmental Panel on Climate Change*, eds T. F. Stocker, D. Qin, G.-K. Plattner, M. Tignor, S. K. Allen, J. Boschung, et al. (Cambridge: Cambridge University Press).

IPCC (2018). "Summary for Policymakers," in *Global Warming of 1.5°C. An IPCC Special Report on the Impacts of Global Warming of 1.5°C above Pre-industrial Levels and related Global Greenhouse Gas Emission Pathways, in the Context of Strengthening the global Response to The Threat of climate Change, Sustainable Development, and Efforts to Eradicate Poverty*, eds V. Masson-Delmotte, P. Zhai, H.-O. Pörtner, D. Roberts, J. Skea, P. R. Shukla, et al. (Geneva: World Meteorological Organization), 32.

Jaramillo, C., Jara, M. S., González, M., and Medina, R. (2020). A shoreline evolution model considering the temporal variability of the beach profile sediment volume (sediment gain/loss). *Coast. Eng.* 156:103612. doi: 10.1016/j.coastaleng.2019.103612

Kopp, R. E., DeConto, R. M., Bader, D. A., Hay, C. C., Horton, R. M., Kulp, S., et al. (2017). Evolving understanding of Antartic ice-sheet physics and ambiguity in probabilistic sea-level projections. *Earths Future* 5, 1217–1233. doi: 10.1002/2017ef000663

Kopp, R. E., Horton, R. M., Little, C. M., Mitrovica, J. X., Oppenheimer, M., Rasmussen, D. J., et al. (2014). Probabilistic 21st and 22nd century sea-level projections at global network of tide-gauge sites. *Earths Future* 2, 383–406. doi: 10.1002/2014ef000239

Le Cozannet, G., Castelle, B., Ranasinghe, R., Wöppelmann, G., Rohmer, J., Bernon, N., et al. (2019). Quantifying uncertainties of sandy shoreline change projections as sea level rises. *Sci. Rep.* 9:42. doi: 10.1038/s41598-018-37017-4

Lemos, G., Menendez, M., Semedo, A., Camus, P., Hemer, M., Dobrynin, M., et al. (2020). On the need of bias correction methods for wave climate projections. *Glob. Planet. Change* 186:103109. doi: 10.1016/j.gloplacha.2019.103109

Mankin, J. S., Lehner, F., Coats, S., and McKinnon, K. A. (2020). The value of initial condition large ensembles to robust adaptation decision-making. *Earths Future* 8:e2012EF001610.

Maraun, D. (2016). Bias correcting climate change simulations – a critical review. *Curr. Clim. Change Rep.* 2, 211–220. doi: 10.1007/s40641-016-0050-x

Miller, J. K., and Dean, R. G. (2004). A simple new shoreline change model. *Coast. Eng.* 51, 531–556. doi: 10.1016/j.coastaleng.2004.05.006

Mitchell, T. D., and Hulme, M. (1999). Predicting regional climate change: living with uncertainty. *Prog. Phys. Geogr.* 23, 57–78. doi: 10.1191/030913399672023346

Montaño, J., Coco, G., Antolínez, J. A. A., Beuzen, T., Bryan, K. R., Cagigal, L., et al. (2020). Blind testing of shoreline evolution models. *Sci. Rep.* 10:2137.

Pérez, J., Menéndez, M., and Losada, I. J. (2017). GOW2: a global wave hindcast for coastal applications. *Coast. Eng.* 124, 1–11. doi: 10.1016/j.coastaleng.2017.03.005

Perkins, S. E., Pitman, A. J., Holbrook, N. J., and McAneney, J. (2007). Evaluation of the AR4 climate models' simulated daily maximum temperature, minimum temperature, and precipitation over Australia using probability density functions. *J. Clim.* 20, 4356–4376. doi: 10.1175/jcli4253.1

Ranasinghe, R. (2016). Assessing climate change impacts on open sandy coasts: a review. *Earth Sci. Rev.* 160, 320–332. doi: 10.1016/j.earscirev.2016.07.011

Shchepetkin, A. F., and McWilliams, J. C. (2005). The regional oceanic modeling system (ROMS): a split-explicit, free-surface, topography-following-coordinate oceanic model. *Ocean Modelling* 9, 347–404. doi: 10.1016/j.ocemod.2004.08.002

Solari, S., and van Gelder, P. H. (2012). "On the use of vector autoregressive VAR and regime switching VAR models for the simulation of sea and wind state parameters," in *Marine Technology and Engineering*, eds C. G. Soares, Y. Garbatov, N. Fonseca, and A. P. Texeira (London: Taylor&Francis Group), 217–230.

Sutton, R. T. (2019). Climate science needs to take risk assessment much more seriously. *Bull. Am. Meteorol. Soc.* 100, 1637–1642. doi: 10.1175/bams-d-18-0280.1

Swart, N. C., Fyfe, J. C., Hawkins, E., Kay, J. E., and Jahn, A. (2015). Influence of internal variability on Arctic sea-ice trends. *Nat. Clim. Change* 5, 86–89. doi: 10.1038/nclimate2483

Toimil, A., Camus, P., Losada, I. J., Le Cozannet, G., Nicholls, R. J., Idier, D., et al. (2020a). Climate change-driven coastal erosion modelling in temperate sandy beaches: methods and uncertainty treatment. *Earth Sci. Revi.* 202:103110. doi: 10.1016/j.earscirev.2020.103110

Toimil, A., Losada, I. J., Camus, P., and Diaz-Simal, P. (2017). Managing coastal erosion under climate change at the regional scale. *Coast. Eng.* 128, 106–122. doi: 10.1016/j.coastaleng.2017.08.004

Toimil, A., Losada, I. J., Nicholls, R. J., Dalrymple, R. A., and Stive, M. J. F. (2020b). Addressing the challenges of climate change risks and adaptation in coastal areas: a review. *Coast. Eng.* 156;103611. doi: 10.1016/j.coastaleng.2019.103611

Tolman, H., and The WaveWatch Iii® Development Group (2014). *User Manual and System Documentation of WAVEWATCH III® version 4.18. Tech. Note 316, NOAA/NWS/NCEP/MMAB*, Maryland: U.S. Department of Commerce, National Oceanic and Atmospheric Administration, National Weather Service,

National Centers for Environmental Prediction, University Research Court College Park, 282. doi: 10.1021/ic501637m Appendices

Wilby, R. L., and Dessai, S. (2010). Robust adaptation to climate change. *Weather* 65, 180–185.

Wong, P. P., Losada, I. J., Gattuso, J. P., Hinkel, J., Khattabi, A., McInnes, K. L., et al. (2014). "Coastal systems and low-lying areas," in *Climate Change 2014: Impacts, Adaptation, and Vulnerability; Part A: Global and Sectoral Aspects. Contribution of Working Group II to the Fifth Assessment Report of the Intergovernmental Panel on Climate Change*, eds C. B. Field, V. R. Barros, D. J. Dokken, K. J. Mach, M. D. Mastrandrea, T. E. Bilir, et al. (Cambridge: Cambridge University Press), 361–409.

Yates, M. L., Guza, R. T., and O'reilly, W. C. (2009). Equilibrium shoreline response: observations and modeling. *J. Geophys. Res. Oceans* 114, C09014.

Zscheischler, J., Westra, S., van den Hurk, B. J. J. M., Seneviratne, S. I., Ward, P. J., Pitman, A., et al. (2018). Future climate risk from compound events. *Nat. Clim. Change* 8, 469–477. doi: 10.1038/s41558-018-0156-3

Conflict of Interest: The authors declare that the research was conducted in the absence of any commercial or financial relationships that could be construed as a potential conflict of interest.

Copyright © 2021 Toimil, Camus, Losada and Alvarez-Cuesta. This is an open-access article distributed under the terms of the Creative Commons Attribution License (CC BY). The use, distribution or reproduction in other forums is permitted, provided the original author(s) and the copyright owner(s) are credited and that the original publication in this journal is cited, in accordance with accepted academic practice. No use, distribution or reproduction is permitted which does not comply with these terms.

frontiers in Marine Science

PERSPECTIVE
published: 22 July 2021
doi: 10.3389/fmars.2021.670089

A Roadmap for Policy-Relevant Sea-Level Rise Research in the United Arab Emirates

Hannah Melville-Rea[1,2], Clare Eayrs[1], Nasser Anwahi[2], John A. Burt[3], Denise Holland[1], Fatin Samara[4], Francesco Paparella[5], Ahmed Hassan Al Murshidi[6], Maryam Rashed Al-Shehhi[7] and David M. Holland[1,8]*

[1] Center for Global Sea Level Change, New York University Abu Dhabi, Abu Dhabi, United Arab Emirates, [2] Department of Political Science, New York University Abu Dhabi, Abu Dhabi, United Arab Emirates, [3] Water Research Center and Center of Genomics and Systems Biology, New York University Abu Dhabi, Abu Dhabi, United Arab Emirates, [4] Department of Biology, Chemistry and Environmental Sciences, College of Arts and Sciences, American University of Sharjah, Sharjah, United Arab Emirates, [5] Center for Stability, Instability, and Turbulence, Division of Science, New York University Abu Dhabi, Abu Dhabi, United Arab Emirates, [6] College of Humanities and Social Sciences, United Arab Emirates University, Al-Ain, United Arab Emirates, [7] Department of Civil, Infrastructural and Environmental Engineering, Khalifa University, Abu Dhabi, United Arab Emirates, [8] Courant Institute of Mathematical Sciences, New York University, New York City, NY, United States

OPEN ACCESS

Edited by:
Julie Billy,
Bureau de Recherches Gologiques et Minières, France

Reviewed by:
Helena Granja,
University of Minho, Portugal
Lei Ren,
Sun Yat-Sen University, China

***Correspondence:**
Hannah Melville-Rea
hannah.melvillerea@nyu.edu

Specialty section:
This article was submitted to Coastal Ocean Processes, a section of the journal Frontiers in Marine Science

Received: *20 February 2021*
Accepted: *21 June 2021*
Published: *22 July 2021*

Citation:
Melville-Rea H, Eayrs C, Anwahi N, Burt JA, Holland D, Samara F, Paparella F, Al Murshidi AH, Al-Shehhi MR and Holland DM (2021) A Roadmap for Policy-Relevant Sea-Level Rise Research in the United Arab Emirates. Front. Mar. Sci. 8:670089. doi: 10.3389/fmars.2021.670089

The United Arab Emirates (UAE) has a long-term policy horizon, the financial capital, and a vision for a sustainable knowledge-based economy. These characteristics uniquely situate it as a potential leader for sea-level rise research. Climate science is already growing, and at the center of the UAE's pivot toward climate research is a burgeoning concern for sea-level rise. Over 85% of the UAE's population and more than 90% of the nation's infrastructure is within a few meters of present-day sea-level. With its low-lying and shallow-sloping geography (about 35 cm per km), this high-value coastline, including the rapidly expanding cities of Dubai and Abu Dhabi, is particularly vulnerable to sea-level rise. Meanwhile, limited regional research and data scarcity create deep uncertainty for sea-level projections. We set out a potential roadmap for the UAE to capitalize on its strengths to create usable and relevant sea-level projections for the region. With a newly established Climate Change Research Network, the UAE government is beginning to draw together universities and research centers for "furthering effective data collection and management, and advancing policy-relevant research on climate impacts and adaptation[1]." By consolidating ideas from the science community within the UAE, we identify promoters and barriers to data gathering, information sharing, science-policy communication, and funding access. Our paper proposes pathways forward for the UAE to integrate sea-level science with coastal development and form best practices that can be scaled across climate science and throughout the region.

Keywords: sea-level rise, climate change, adaptation, United Arab Emirates, Arabian Gulf

[1]https://www.moccae.gov.ae/en/climate-change-research-network-about.aspx (accessed 2 Feb 2021).

1. INTRODUCTION

Obscured by the dominance of pandemic-related news, the world set new records for global temperatures, hurricanes, wildfires, and Arctic sea ice loss in 2020 (World Meteorological Organization, 2021). Meanwhile, incontrovertible evidence of the climate crisis can be observed in a shrinking Greenland Ice Sheet (IPCC, 2019), increased ocean heat content (Trewin et al., 2020), and poleward shifts of temperature-sensitive species (Hastings et al., 2020). Among such disasters, rising sea-levels already impact shorelines around the world and are projected to worsen for centuries to come (IPCC, 2013). How much and how fast will coastal communities be impacted? At present, our limited scientific understanding of the Antarctic Ice Sheet (IPCC, 2019), a tipping element within the climate system (Lenton et al., 2008), drives deep uncertainty for sea-level projections. Some studies predict as much as 7.5 m of sea level rise by 2200 in the case of instabilities (Bamber et al., 2019). Other work suggests that upper-end contributions from West Antarctica are unlikely (Ritz et al., 2015). The uncertainty in future contributions of the West Antarctic Ice Sheet to sea-level rise is highlighted by two, recent studies. Edwards et al. (2021) show a wide range of model responses, including some where increased snowfall could balance out a warming atmosphere and ocean. Whereas, DeConto et al. (2021) demonstrate a potential order of magnitude increase in global mean sea-level rise within the next 30 years. Untangling these uncertain dynamics, translating the impacts to local contexts, and taking rapid resilience measures are key to saving countless lives and dollars.

Amid this deep uncertainty, building the necessary tools to adapt to sea-level rise requires unprecedented levels of collaboration. Climate services are models and information that aid decision-making on climate change (Hewitt et al., 2012). Seamless climate services can give decision-makers reliable tools to analyze and manage climate risks, both under current hydro-meteorological conditions and in the face of climate variability and change (World Meteorological Organization, 2020). In response to observable climate impacts and advances in modeling capabilities, climate science has slowly expanded to include a major focus on usability and communication (Dilling and Lemos, 2011). Tight integration between scientists and the decision-making community is key to safeguarding populations from climate impacts for three major reasons.

First, scientific understanding of sea-level rise is advancing at a rapid pace. Projections of future sea-level rise have increased substantially (e.g., Siegert et al., 2020; Slater et al., 2021) and these projections will continue to change as scientific understanding rapidly advances. The planet as a physical system is more sensitive than previously thought (Lenton et al., 2019). The IPCC's projections for 2100 under strong warming involve the ice sheets providing less than 1% of their potential contribution (IPCC, 2019). Adapting to sea-level rise clearly needs to be flexible in the face of uncertain and changing projections, posing challenges for decision makers seeking to anticipate, identify, manage, and communicate risks (Ramm et al., 2018a,b). This requires close communication from scientists to policy makers.

Second, projecting regional sea-level faces unique knowledge gaps and requires local information gathering. Relative sea-level change, the local change in the time-average height of the sea-surface above the sea floor, displays complex patterns along coastlines due to land altitude, ocean dynamics, gravitational forces, subsidence, and susceptibility to extreme sea-level events—the combination of tides and storm surges that lead to flooding (Tebaldi et al., 2012; Wahl et al., 2017). For any given location, local sea-level rise may deviate significantly from the global mean. For example, sea-level rise in New York is more than three times the global average (Gornitz et al., 2019). Further, sea-level rise interacts with other changes and there is a need to couple sea-level projections with geomophological, ecological, economic, and population models to provide a more realistic representation of exposure and vulnerability (Kopp et al., 2019). Thus, adaptation planning needs comprehensive, localized information gathering and science which governments must often support and oversee.

Third, policy makers need to work with the science community to ensure the usability of sea-level projections. Governments and policy makers must employ two-way engagement with researchers to ensure that sea-level projections and hazard maps are provided in appropriate formats and contexts. Often, the most useful approaches to summarizing scientific knowledge are not the most useful approaches for public policy decision makers (Kopp et al., 2019).

While collaboration between sea-level researchers and decision-makers poses coordination challenges, the benefits of investing in science are clear. Damage and disruption from natural disasters annually cost at least $390 billion in low- and middle-income countries, but investing in more resilient infrastructure can provide a net benefit of $4.2 trillion (Hallegatte et al., 2019). Similarly, $1 spent on disaster prevention can save $15 in future damages (Healy and Malhotra, 2009). Therefore, developing scientific models to predict and prepare for sea-level rise has distinct economic benefits.

Given the need for greater science-policy interface, how can we achieve these collaborations? Previous scholarship has delved into how to create linkages between science and policy for climate adaptation. For instance, uncertainties in sea-level projections are most useful to decision makers when communicated as ranges (Hinkel et al., 2019). In addition, scientists may adopt a trans-disciplinary iterative approach to ensure that the results of scientific studies are "legitimate, relevant, and credible for coastal stakeholders" (Kopp et al., 2019). Ultimately, efforts must be context-specific, a need that we focus on here.

This paper is written from the perspective of climate scientists, to identify ways that the United Arab Emirates (UAE) can rapidly advance regional sea-level rise research. We aim to identify opportunities for scientists and governments to collaborate on sea-level research, thereby kick-starting discussions around science-policy integration in the newly launched UAE Climate Change Research Network. In doing so, we highlight best practices for regions with significant data gaps, centralized government systems, and newly established research structures. In particular,

insights from this paper can be scaled throughout the Arabian Gulf.

We begin by providing context on the scientific gaps and policy landscape of the UAE, in relation to the region. Next, we recommend steps that the UAE can take to build and leverage sea-level science for coastal adaptation. Finally, we discuss linkages between our recommendations and possible next steps.

2. CONTEXT

2.1. Knowledge Gaps in the Arabian Gulf

Sea-level rise is both a global and local issue. The overwhelmingly dominant driver of future flood risk is the melting of land-based ice (IPCC, 2019). The fate of the Antarctic Ice Sheet represents by far and wide the largest uncertainty in future global sea-level rise (Ritz et al., 2015; DeConto and Pollard, 2016; Edwards et al., 2019). In particular, Thwaites Glacier in West Antarctica may have already passed a threshold for a shift to a reduced state that will likely involve more than 3 m of sea-level rise (Alley et al., 2014). However, there is a lack of consensus on the future rate of this change, and unless fundamental observational research is carried out in West Antarctica to address the physical understanding of ice mass change, there is no possibility of ever producing a credible projection of sea-level rise over the coming century.

Global sea-level rise will determine the order of magnitude of sea-level rise, but regional and local sea-level changes can vary substantially from the global mean (Milne et al., 2009). Baseline studies to understand the status of the UAE coastline, to identify vulnerable regions,and to determine the key processes driving shoreline change are an essential first step. There is also much to learn about catastrophic events, such as the large-amplitude seiche that flooded the Iranian cities of Dayyer and Asaluyeh in 2017 (Salaree et al., 2018; Heidarzadeh et al., 2020). However, understanding and responding to local impacts requires suitable datasets. Deficiencies in the availability and quality of datasets for the region prevent rigorous assessment of current changes and further preclude the ability to develop models to understand future change. Alothman et al. (2014) estimated sea-level rise in the western Arabian Gulf during 1979–2007 at 0.22 ± 0.05 cm/year which is below the global estimate for 1993–2010 (IPCC, 2013, 0.32 cm/year). However, land subsidence caused by groundwater pumping and oil extraction can play a significant role (Alothman et al., 2014, up to 0.07 cm/year in the western Gulf). There is also a lack of information on how the shoreline will change as a result of erosion and accretion. Alothman et al. (2014) showed atmospheric pressure changes of the order of 10 mbar in the Arabian Gulf, which corresponds roughly to an annual variation of 10 cm in sea level (Mathers and Woodworth, 2004). Bold programs are critical to provide the scientific evidence needed to support policy needs across the region.

2.2. The UAE as a Case Study

Within the Arabian Gulf, the UAE is particularly vulnerable to sea-level rise and faces similar knowledge gaps. Much of the low-lying UAE coastline is shallow-sloping (about 35 cm per km) and therefore highly susceptible to potential flooding. With over 85% of the population and more then 90% of the UAE's infrastructure situated within several meters of present-day sea level (Al Ahbabi, 2017), the UAE is susceptible to flooding, erosion, saltwater intrusion, impeded drainage, and change/loss of coastal ecosystems. Two highly developed areas that will be particularly affected by future flooding include the cities of Abu Dhabi and Dubai (**Figure 1**).

Despite climate vulnerabilities and major data gaps, the UAE is particularly suited to science-policy collaborations. Firstly, the UAE is a high-income country with the means and commitment to invest in preventative measures against sea-level rise. Already the UAE has demonstrated its interest in sustainable infrastructure by investing US$16.8 billion in renewable energy ventures across 70 countries, and allocating US$400 million in aid and concessional loans for clean energy projects.[2] Meanwhile, the UAE is able to implement policies with long-term horizons, unconstrained by short political cycles. This is demonstrated by its readiness to take upon agendas that set the future trajectory of the nation, such as the Environment Vision of 2030 as well as the UAE's Centennial Vision of 2071, both of which pursue sustainable and, most of all, efficient systems. Finally, part of the UAE's vision is to transition from an oil-based to knowledge-based economy. In doing so, the nation positions itself to build up its scientific capacity in order to lead regional sea-level science, a trajectory that places the UAE at the forefront of scientific research while prioritizing the cultivation of human capital and scientific discourse. Thus, the UAE presents a unique landscape for the progression of climate research and development.

The UAE's approach to climate adaptation has been defined by several developments. In 2006, the UAE established the Ministry of Environment and Water. Among many responsibilities, the Ministry oversaw issues related to climate change, food and water security, and agriculture.[3] However, it should be acknowledged that much of the UAE's research into sea-level rise has been also conducted by private contractors and semi-private entities. A prominent example of such a case is Nakheel, a property developer responsible for the development of the famous Palm Islands. Upon construction, Nakheel was required to assess the longevity of the Palm Island project and dispute allegations of the possibility of a failed project due to sea-level rise.[4] Similarly, there are numerous cases where private firms have contributed, to an extent, toward climate change research to solve the various context-specific issues they respectively faced. A major reason for this is that the UAE has developed at exceptional speed, learning to adapt and reshape in response to a dynamic global context. As Feary et al. (2013) and Burt and Bartholomew (2019) observe, this rapid development sometimes meant that swiftness superseded diligence . As the nation built up its own technical capacity, much of this research was sub-contracted

[2]https://www.moccae.gov.ae/en/media-center/news/30/12/2020/uae-announces-ambitious-climate-commitments-as-part-of-second-nationally-determined-contribution.aspx#page=1 (accessed 23 Jan 2021).

[3]https://www.moccae.gov.ae/en/about-ministry/about-the-ministry.aspx (accessed 21 Jan 2021).

[4]https://www.thenationalnews.com/business/property/palm-is-not-sinking-says-nakheel-1.498047.aspx (accessed 23 Jan 2021).

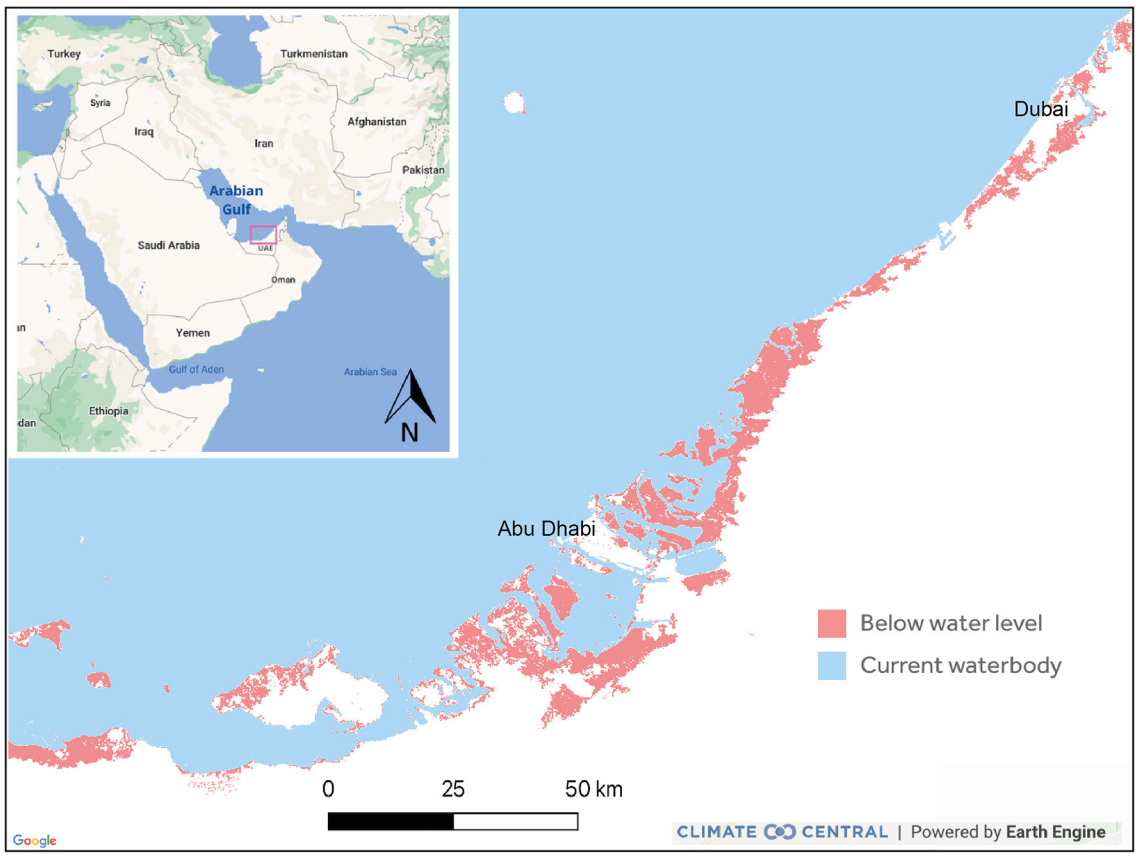

FIGURE 1 | Extent of projected Sea-Level Rise for two major cities in the UAE from Climate Central CoastalDEM (Kulp and Strauss, 2019). Red shading shows regions expected to experience flooding by 2100 under a moderate 2° Celsius warming scenario (RCP 4.5) and a Kopp et al. (2014) mid-range projection.

to consultants from outside of the region who may not have familiarity with the local environment, data sources or cultural context for decision-making.

However, the past 5 years triggered a paradigm shift in policy-making, in which a swift approach was no longer suitable. In 2016, in order to ensure a more specific policy-making approach that would do justice to the most pressing issues, the UAE announced the establishment of a dedicated Ministry of Climate Change and Environment. Shortly after, the country announced the appointment of the Minister of Food and Water Security, highlighting the country's intention to foster more stable food and water systems. This is reflected through the trajectory of government-led initiatives. For instance, the Ministry of Climate Change and Environment conducted four sector-specific climate risk assessment reports in 2019, and took stock of national climate science in a State of the Climate Report in 2020. These national bodies oversee sub-national agencies that have collected much of the country's environmental data and have conducted climate research.

Furthermore, the COVID-19 pandemic has crystallized such sentiments, as the UAE was exposed to vulnerabilities that have been echoed in its history yet overlooked by its dynamic present. The novel pandemic temporarily threatened the provision of goods in the UAE.[5] Being exposed to such vulnerability allowed the UAE to question and enhance existing systems. As such, the UAE is now prioritizing mending the gap between science and policy, a gap that becomes costlier as variability around the world increases. The UAE aims to leverage its current infrastructure, industries, academic networks, and policy acumen in order to propagate regenerative systems that can create a more circular economy.

If the UAE is successful at leveraging its potential to lead in collaborative sea-level science, the lessons it develops can transcend its borders. Firstly, neighboring countries along the Arabian Gulf face a similar major sea-level risk for which regional data sets and models developed in the UAE can provide crucial information. Meanwhile, lessons can be shared across the region. Coordination between the eight nations bordering the Arabian Gulf is paramount to understanding and addressing the environmental pressures facing this shared body of water (Sale et al., 2011; Van Lavieren et al., 2011). Abdulla and Naser (2021) found that developing a system of understanding between those governing and benefiting from the marine environment is

[5]https://www.khaleejtimes.com/coronavirus-pandemic/UAE-has-learnt-from-Covid-to-boost-food-security-Sheikh-Mohammed--.aspx (accessed 23 Jan 2021).

a key component in addressing growing marine environmental challenges in Bahrain. Similarly, McEvoy et al. (2021) highlight that sharing approaches and experiences across countries can help vulnerable nations plan for adaptation. The globe is simultaneously navigating the uncertainty of sea-level rise, which demonstrate the necessity for countries similar to the UAE to participate and be a part of the frontier. As the UAE continues to build and establish a knowledge-based economy and gathers researchers from its universities to develop sea-level projections and science-based adaptation policies, the Gulf can become a standard bearer for coastal cities around the world.

Moreover, tackling climate change is multifaceted. As demonstrated by Hummel et al. (2020), it is not enough to understand risk—interactions between adaptation measures and infrastructure networks can have surprising results on the overall impact on the system. In addition, policy plays an interconnected and integral role in determining the success of implementation and strategy. Instead of assuming the exclusivity of science in tackling sea-level rise challenges, it would be advantageous to take into account the development and implementation of policy within a country.

The UAE can position itself to be one of the first in the region to properly understand the nexus of academia, industry, and government, which transcends the country's contribution beyond coastal cities of similar topographies. Already, the Gulf is demonstrating new appetite for communication and collaboration between the science, regulatory and policy communities for the purposes of understanding and addressing environmental challenges. For example, ecosystem-based management approaches that require integration of perspectives across these stakeholders are increasingly being employed in the region (Fanning et al., 2021; Mateos-Molina et al., 2021). By pursuing scientifically informed coastal management, the UAE can spur a dialectical approach of research and development, which will help in tackling many other challenges that require the conjoint effort of science and policy.

3. PATHWAYS FORWARD

The following recommendations are synthesized from ideas collected from consultations with the climate science community within the UAE, on how to drive sea-level research forward. The suggestions are aimed at generating discussions to shape future support and interactions between science and policy stakeholders. While the recommendations emerged with a focus on the UAE and sea-level science, they are largely applicable to research throughout the Arabian Gulf on broader environment or climate issues.

3.1. Science and Policy Coordination

1. Build trust between government and the research community by pursuing the following initiatives:
   (a) Draw scientists and government together in conferences and forums to integrate impacts and adaptation options following best practice (e.g., Haasnoot et al., 2020), and to identify research priorities. For instance, the Gulf Environment Conference can continue to demonstrate the impact of research and the benefits of cooperating with the research community, including with industry and international partners.
   (b) Build a scientific collective voice to highlight cutting edge scientific concerns. For instance, the Mohammed Bin Rashid Academy of Scientists[6] can emulate the US National Academy of Scientists model, to provide a forum for leading experts to promote key scientific issues.
2. Invest in the next generation of scientists by providing research opportunities to youth and establishing graduate programs in environmental science. There are currently few graduate-level environmental science programs, which stymies the growth of technical capacity in the local citizenry (Sale et al., 2011). Capacity building is essential to achieve sustained observations that meet internationally-agreed standards; these observations can in turn be transformed into information that can support decision making (Miloslavich et al., 2018).

3.2. Data Collection and Sharing

1. Pursue Gulf-wide campaigns for data collection. To date, only five Gulf-wide campaigns have taken place in 1965, 1977 (Al-Yamani and Naqvi, 2019), 1992 (Reynolds, 1993), 1998 (Yoshida et al., 1998), 2000, 2001, and 2006 (Polikarpov et al., 2016), with no Gulf-wide observations after 2006. A 2018–2019 campaign collected data across the northern Arabian Gulf (Saleh et al., 2021). These datasets are not readily available to the research and management community—to date, researchers in the UAE have not been able to access data post-1998.
2. Streamline approval processes and requirements for scientific data collection by pursuing the following:
   (a) Facilitate the import and export of scientific equipment for environmental measurements.
   (b) Fast-track systems for approving fieldwork (including licensing information).
3. Create a national data archive of ocean, land, and atmospheric measurements. Such an archive could be extended to potentially host Gulf-wide datasets as part of the Regional Organization for the Protection of the Marine Environment (ROPME[7]). The archive should:
   (a) Evaluate existing data, and unless it poses serious security concerns, make it available to the public. In addition, encourage the sharing of new data collected, excluding any appropriate embargo.
   (b) Follow best practice principles of Findability, Accessibility, Interoperability, and Reusability (Wilkinson et al., 2016) to maximise reuse of data.

[6]https://mbras.ae/ (accessed 2 Feb 2021).
[7]http://ropme.org/home.clx (accessed 2 Feb 2021).

4. Require local research on climate impacts and preparedness to be published as open-access articles and provide funding support to do so.

3.3. Funding and Cost Savings

1. Build a public inventory to facilitate the sharing of instruments, equipment and computing resources between universities, research entities, and local agencies.
2. Link research labs with private sector partners, such as real-estate developers, to fund relevant research. In addition, recognize open-access research funded by companies as corporate social responsibility.
3. Launch a competitive national funding program for technical research on priority areas, and require public level communication of results by researchers. Use this program to prioritize continuous data sampling to build up time-series.
4. Expand upon ROPME to coordinate funding for regional climate measurements in the Arabian Gulf.
5. Collaborate on in-kind multinational projects to efficiently participate in regional and global data gathering. Some of the most challenging and important scientific questions require resources that no one country can provide and multinational projects can spread these costs. For instance, Antarctic expeditions share logistic and data collection costs. To ensure that the UAE has the boundary conditions needed to understand how future sea-level rise will impact coastal communities, consider collaborating on the following major initiatives:

   (a) Establish the first National Antarctic Research Program in the Middle East, to coordinate research with global leaders in the field (e.g., USA, UK, China, Russia, Australia, and South Korea).
   (b) Invest in a Polar Class 1 icebreaker to facilitate critical sea-level research in the waters surrounding Antarctica.
   (c) Set up a year-round research outpost in Antarctic to facilitate continuous observations of sea-level change.

4. DISCUSSION

While we aim to separate out themes in our recommendations, many of them are interconnected. For instance, a regional funding program could support capacity building at a shared cost throughout the region. In addition, data co-production and sharing are fundamental tools of capacity building. A national funding program could target priority research questions that are needed to drive sustainable policy decisions and require that data and publications are made publicly available to further future research.

These recommendations range from small and immediate (sharing scientific equipment between research entities) to long-term and global (entering the Antarctic science arena). Significant financial commitments are needed for research, observations, information products, literacy and science policy interactions at both national and regional levels. Sea-level science across the globe is lacking vital understanding of how fast ice sheets will melt and these questions call for international commitment. The United Nations Decade of Ocean Science for Sustainable Development 2021–2030 (Ryabinin et al., 2019), a global effort to create collaborations across disciplines, geographies and generations, provides an ideal opportunity to launch observation programs to fill the regional data gaps.

Climate services are being developed at an ever-increasing rate across the world (Hewitt et al., 2020). Comparatively, climate services for the Arabian Gulf are constrained by a short record of scientific measurements and limited protocols for data collection. Yet, the nascent nature of climate research in the region also provides a clean slate to build upon, with best practices. The Gulf can pursue a demand-driven, trans-disciplinary, data-informed approach to tackle sea-level rise and other climate-related risks (Lourenço et al., 2016).

The UAE is no stranger to investing in ambitious science questions, for example, the development of the Mohammed Bin Rashid Space Center and its Mars Mission, Hope Probe (Extance, 2014). By committing to regional and international collaborations, the UAE can leverage in-kind funding and obtain the data needed to base future sea-level projections. Subsequently, the UAE Climate Change Research Network can provide a strategic building block to bring together scientists and policy makers and develop climate services for coastal adaptation. Ensuring the involvement of the beneficiaries of climate services leads to better-informed decision-making (Hewitt et al., 2020). Sustained communication between researchers and decision makers will be key to delivering seamless integration of climate knowledge into policy decisions for the UAE.

DATA AVAILABILITY STATEMENT

The original contributions presented in the study are included in the article/supplementary material, further inquiries can be directed to the corresponding author/s.

AUTHOR CONTRIBUTIONS

HM-R coordinated the research project and is the primary author. CE supported the research process and is the primary contributor to section 2.1. NA is the primary contributor to section 2.2. All authors participated in rounds of discussions to shape section 3, and provided feedback on drafts of the manuscript and responses to reviewers' comments.

FUNDING

This work was supported by the Center for global Sea Level Change (CSLC) of NYU Abu Dhabi Research Institute (G1204) in the UAE. Funding to JB was provided by the NYU Abu Dhabi Water Research Center grant (project CG007).

ACKNOWLEDGMENTS

Special thanks is due to the UAE Ministry of Climate Change and Environment for launching the Climate Change Research Network, which inspired this collaboration. We thank Philip Rodenbough and the Scientific Writing Program at NYU Abu Dhabi for insightful feedback and proofreading.

REFERENCES

Abdulla, K. H., and Naser, H. A. (2021). Protection of marine environmental quality in the Kingdom of Bahrain. *Ocean Coastal Manag.* 203:105520. doi: 10.1016/j.ocecoaman.2021.105520

Al Ahbabi, F. (2017). Department of Urban Planning and Municipalities. Plan Maritime: Abu Dhabi coastal and marine framework plan. Abu Dhabi, p. 238.

Alley, R. B., Anandakrishnan, S., Christianson, K., Horgan, H. J., Muto, A., Parizek, B. R., et al. (2014). Oceanic forcing of ice-sheet retreat: west antarctica and more. *Ann. Rev. Earth Planet. Sci.* 43, 1–25. doi: 10.1146/annurev-earth-060614-105344

Alothman, A., Bos, M., Fernandes, R., and Ayhan, M. (2014). Sea level rise in the north-western part of the Arabian Gulf. *J. Geodynamics* 81, 105–110. doi: 10.1016/j.jog.2014.09.002

Al-Yamani, F., and Naqvi, S. W. (2019). Chemical oceanography of the Arabian Gulf. *Deep Sea Res. II Top. Stud. Oceanogr.* 161, 72–80. doi: 10.1016/j.dsr2.2018.10.003

Bamber, J. L., Oppenheimer, M., Kopp, R. E., Aspinall, W. P., and Cooke, R. M. (2019). Ice sheet contributions to future sea-level rise from structured expert judgment. *Proc. Natl. Acad. Sci. U.S.A.* 116, 11195–11200. doi: 10.1073/pnas.1817205116

Burt, J. A., and Bartholomew, A. (2019). Towards more sustainable coastal development in the Arabian Gulf: opportunities for ecological engineering in an urbanized seascape. *Marine Pollut. Bull.* 142, 93–102. doi: 10.1016/j.marpolbul.2019.03.024

DeConto, R. M., and Pollard, D. (2016). Contribution of Antarctica to past and future sea-level rise. *Nature* 531, 591–597. doi: 10.1038/nature17145

DeConto, R. M., Pollard, D., Alley, R. B., Velicogna, I., Gasson, E., Gomez, N., et al. (2021). The Paris Climate Agreement and future sea-level rise from Antarctica. *Nature* 593, 83–89. doi: 10.1038/s41586-021-03427-0

Dilling, L., and Lemos, M. C. (2011). Creating usable science: opportunities and constraints for climate knowledge use and their implications for science policy. *Glob. Environ. Change* 21, 680–689. doi: 10.1016/j.gloenvcha.2010.11.006

Edwards, T. L., Brandon, M. A., Durand, G., Edwards, N. R., Golledge, N. R., Holden, P. B., et al. (2019). Revisiting Antarctic ice loss due to marine ice-cliff instability. *Nature* 566, 58–64. doi: 10.1038/s41586-019-0901-4

Edwards, T. L., Nowicki, S., Marzeion, B., Hock, R., Goelzer, H., Seroussi, H., et al. (2021). Projected land ice contributions to twenty-first-century sea level rise. *Nature* 593, 74–82. doi: 10.1038/s41586-021-03302-y

Extance, A. (2014). UAE fires up space agency with Mars mission. *Phys. World* 27, 11–11. doi: 10.1088/2058-7058/27/11/19

Fanning, L. M., Al-Naimi, M. N., Range, P., Ali, A.-S. M., Bouwmeester, J., Al-Jamali, F., et al. (2021). Applying the ecosystem services-EBM framework to sustainably manage Qatar's coral reefs and seagrass beds. *Ocean Coastal Manag.* 205:105566. doi: 10.1016/j.ocecoaman.2021.105566

Feary, D. A., Burt, J. A., Bauman, A. G., Al Hazeem, S., Abdel-Moati, M. A., Al-Khalifa, K. A., et al. (2013). Critical research needs for identifying future changes in gulf coral reef ecosystems. *Mar. Pollut. Bull.* 72, 406–416. doi: 10.1016/j.marpolbul.2013.02.038

Gornitz, V., Oppenheimer, M., Kopp, R., Orton, P., Buchanan, M., Lin, N., et al. (2019). New York city panel on climate change 2019 report chapter 3: sea level Rise. *Ann. N.Y. Acad. Sci.* 1439, 71–94. doi: 10.1111/nyas.14006

Haasnoot, M., Biesbroek, R., Lawrence, J., Muccione, V., Lempert, R., and Glavovic, B. (2020). Defining the solution space to accelerate climate change adaptation. *Reg. Environ. Change* 20:37. doi: 10.1007/s10113-020-01623-8

Hallegatte, S., Rentschler, J., and Rozenberg, J. (2019). "Sustainable Infrastructure," in *Lifelines* : *The Resilient Infrastructure Opportunity*. Washington, DC: World Bank.

Hastings, R. A., Rutterford, L. A., Freer, J. J., Collins, R. A., Simpson, S. D., and Genner, M. J. (2020). Climate change drives poleward increases and equatorward declines in marine species. *Curr. Biol.* 30, 1572.e2–1577.e2. doi: 10.1016/j.cub.2020.02.043

Healy, A., and Malhotra, N. (2009). Myopic voters and natural disaster policy. *Am. Pol. Sci. Rev.* 103, 387–406. doi: 10.1017/S0003055409990104

Heidarzadeh, M., Šepić, J., Rabinovich, A., Allahyar, M., Soltanpour, A., and Tavakoli, F. (2020). Meteorological Tsunami of 19 March 2017 in the Persian Gulf: observations and analyses. *Pure Appl. Geophys.* 177, 1231–1259. doi: 10.1007/s00024-019-02263-8

Hewitt, C., Mason, S., and Walland, D. (2012). The global framework for climate services. *Nat. Clim. Change* 2, 831–832. doi: 10.1038/nclimate1745

Hewitt, C. D., Allis, E., Mason, S. J., Muth, M., Pulwarty, R., Shumake-Guillemot, J., et al. (2020). Making society climate resilient: international progress under the global framework for climate services. *Bull. Am. Meteorol. Soc.* 101, E237–E252. doi: 10.1175/BAMS-D-18-0211.A

Hinkel, J., Church, J. A., Gregory, J. M., Lambert, E., Le Cozannet, G., Lowe, J., et al. (2019). Meeting user needs for sea level rise information: a decision analysis perspective. *Earths Future* 7, 320–337. doi: 10.1029/2018EF001071

Hummel, M. A., Siwe, A. T., Chow, A., Stacey, M. T., and Madanat, S. M. (2020). Interacting infrastructure disruptions due to environmental events and long-term climate change. *Earths Future* 8:e2020EF001652. doi: 10.1029/2020EF001652

IPCC (2013). "Climate Change 2013: The Physical Science Basis," in *Contribution of Working Group I to the Fifth Assessment Report of the Intergovernmental Panel on Climate Change*. (Cambridge, UK; New York, NY: Cambridge University Press)

IPCC (2019). *Special Report on the Ocean and Cryosphere in a Changing Climate*. Available online at:https://www.ipcc.ch/site/assets/uploads/sites/3/2019/12/SROCC_FullReport_FINAL.pdf.

Kopp, R. E., Gilmore, E. A., Little, C. M., Lorenzo-Trueba, J., Ramenzoni, V. C., and Sweet, W. V. (2019). Usable science for managing the risks of sea-level rise. *Earths Future* 7, 1235–1269. doi: 10.1029/2018EF001145

Kopp, R. E., Horton, R. M., Little, C. M., Mitrovica, J. X., Oppenheimer, M., Rasmussen, D. J., et al. (2014). Probabilistic 21st and 22nd century sea-level projections at a global network of tide-gauge sites. *Earths Future* 2, 383–406. doi: 10.1002/2014EF000239

Kulp, S. A., and Strauss, B. H. (2019). New elevation data triple estimates of global vulnerability to sea-level rise and coastal flooding. *Nat. Commun.* 10:4844. doi: 10.1038/s41467-019-12808-z

Lenton, T. M., Held, H., Kriegler, E., Hall, J. W., Lucht, W., Rahmstorf, S., et al. (2008). Tipping elements in the earth's climate system. *Proc. Natl. Acad. Sci. U.S.A.* 105, 1786–1793. doi: 10.1073/pnas.0705414105

Lenton, T. M., Rockstrm, J., Gaffney, O., Rahmstorf, S., Richardson, K., Steffen, W., et al. (2019). Climate tipping points too risky to bet against. *Nature* 575, 592–595. doi: 10.1038/d41586-019-03595-0

Lourenço, T. C., Swart, R., Goosen, H., and Street, R. (2016). The rise of demand-driven climate services. *Nat. Clim Change* 6, 13–14. doi: 10.1038/nclimate2836

Mateos-Molina, D., Ben Lamine, E., Antonopoulou, M., Burt, J., Das, H., Javed, S., et al. (2021). Synthesis and evaluation of coastal and marine biodiversity spatial information in the United Arab Emirates for ecosystem-based management. *Mar. Pollut. Bull.* 167:112319. doi: 10.1016/j.marpolbul.2021.112319

Mathers, E. L., and Woodworth, P. L. (2004). A study of departures from the inverse-barometer response of sea level to air-pressure forcing at a period of 5 days. *Q. J. R. Meteorol. Soc.* 130, 725–738. doi: 10.1256/qj.03.46

McEvoy, S., Haasnoot, M., and Biesbroek, R. (2021). How are European countries planning for sea level rise? *Ocean Coastal Manag.* 203:105512. doi: 10.1016/j.ocecoaman.2020.105512

Milne, G. A., Gehrels, W. R., Hughes, C. W., and Tamisiea, M. E. (2009). Identifying the causes of sea-level change. *Nat. Geosci.* 2, 471–478. doi: 10.1038/ngeo544

Miloslavich, P., Seeyave, S., Muller-Karger, F., Bax, N., Ali, E., Delgado, C., et al. (2018). Challenges for global ocean observation: the need for increased human capacity. *J. Operat. Oceanogr.* 12(Suppl. 2):S137–S156. doi: 10.1080/1755876X.2018.1526463

Polikarpov, I., Saburova, M., and Al-Yamani, F. (2016). Diversity and distribution of winter phytoplankton in the Arabian Gulf and the Sea of Oman. *Continental Shelf Res.* 119, 85–99. doi: 10.1016/j.csr.2016.03.009

Ramm, T. D., Watson, C. S., and White, C. J. (2018a). Describing adaptation tipping points in coastal flood risk management. *Comput. Environ. Urban Syst.* 69, 74–86. doi: 10.1016/j.compenvurbsys.2018.01.002

Ramm, T. D., Watson, C. S., and White, C. J. (2018b). Strategic adaptation pathway planning to manage sea-level rise and changing coastal flood risk. *Environ. Science Policy* 87, 92–101. doi: 10.1016/j.envsci.2018.06.001

Reynolds, R. M. (1993). Physical oceanography of the Gulf, Strait of Hormuz, and the Gulf of Oman Results from the Mt Mitchell expedition. *Mar. Pollut. Bull.* 27, 35–59. doi: 10.1016/0025-326X(93)90007-7

Ritz, C., Edwards, T. L., Durand, G., Payne, A. J., Peyaud, V., and Hindmarsh, R. C. A. (2015). Potential sea-level rise from Antarctic ice-sheet instability constrained by observations. *Nature* 528, 115–118. doi: 10.1038/nature16147

Ryabinin, V., Barbire, J., Haugan, P., Kullenberg, G., Smith, N., McLean, C., et al. (2019). The UN decade of ocean science for sustainable development. *Front. Mar. Sci.* 6:470. doi: 10.3389/fmars.2019.00470

Salaree, A., Mansouri, R., and Okal, E. A. (2018). The intriguing tsunami of 19 march 2017 at bandar dayyer, iran: field survey and simulations. *Nat. Hazards* 90, 1277–1307. doi: 10.1007/s11069-017-3119-5

Sale, P. F., Feary, D. A., Burt, J. A., Bauman, A. G., Cavalcante, G. H., Drouillard, K. G., et al. (2011). The growing need for sustainable ecological management of marine communities of the persian Gulf. *AMBIO* 40, 4–17. doi: 10.1007/s13280-010-0092-6

Saleh, A., Abtahi, B., Mirzaei, N., Chen, C.-T. A., Ershadifar, H., Ghaemi, M., et al. (2021). Hypoxia in the persian Gulf and the strait of hormuz. *Mar. Pollut. Bull.* 167, 112354. doi: 10.1016/j.marpolbul.2021.112354

Siegert, M., Alley, R. B., Rignot, E., Englander, J., and Corell, R. (2020). Twenty-first century sea-level rise could exceed IPCC projections for strong-warming futures. *ONE Earth* 3, 691–703. doi: 10.1016/j.oneear.2020.11.002

Slater, T., Lawrence, I. R., Otosaka, I. N., Shepherd, A., Gourmelen, N., Jakob, L., et al. (2021). Review article: earth's ice imbalance. *Cryosphere* 15, 233–246. doi: 10.5194/tc-15-233-2021

Tebaldi, C., Strauss, B. H., and Zervas, C. E. (2012). Modelling sea level rise impacts on storm surges along US coasts. *Environ. Res. Lett.* 7:014032. doi: 10.1088/1748-9326/7/1/014032

Trewin, B., Cazenave, A., Howell, S., Huss, M., Isensee, K., Palmer, M. D., et al. (2020). Headline indicators for global climate monitoring. *Bull. Am. Meteorol. Soc.* 102, E20–E37. doi: 10.1175/BAMS-D-19-0196.1

Van Lavieren, H., Burt, J., Feary, D., Cavalcante, G., Marquis, E., Benedetti, L., et al. (2011). *Managing the Growing Impacts of Development on Fragile Coastal and Marine Ecosystems: Lessons From the Gulf.* Technical Report, United Nations University.

Wahl, T., Haigh, I. D., Nicholls, R. J., Arns, A., Dangendorf, S., Hinkel, J., et al. (2017). Understanding extreme sea levels for broad-scale coastal impact and adaptation analysis. *Nat. Commun.* 8:16075. doi: 10.1038/ncomms16075

Wilkinson, M. D., Dumontier, M., Aalbersberg, I. J., Appleton, G., Axton, M., Baak, A., et al. (2016). The FAIR guiding principles for scientific data management and stewardship. *Sci. Data* 3, 160018. doi: 10.1038/sdata.2016.18

World Meteorological Organization (2021). *State of the Global Climate 2020.* Technical report, World Meteorological Organization.

World Meteorological, O.rganization, (2020). *2020 State of Climate Services.* Technical report, World Meteorological Organization.

Yoshida, J., Matsuyama, M., Senjyu, T., Ishimaru, T., Morinaga, T., Arakawa, H., et al. (1998). "Hydrography in the RSA during the RT/V Umitaka-Maru cruises," in *Offshore Environment of ROPME Sea Area after the War-related Oil Spill*, Tokyo. 1–22.

Conflict of Interest: The authors declare that the research was conducted in the absence of any commercial or financial relationships that could be construed as a potential conflict of interest.

Copyright © 2021 Melville-Rea, Eayrs, Anwahi, Burt, Holland, Samara, Paparella, Al Murshidi, Al-Shehhi and Holland. This is an open-access article distributed under the terms of the Creative Commons Attribution License (CC BY). The use, distribution or reproduction in other forums is permitted, provided the original author(s) and the copyright owner(s) are credited and that the original publication in this journal is cited, in accordance with accepted academic practice. No use, distribution or reproduction is permitted which does not comply with these terms.

frontiers in Marine Science

POLICY AND PRACTICE REVIEWS
published: 03 August 2021
doi: 10.3389/fmars.2021.703902

Climate Services Transformed: Decision-Making Practice for the Coast in a Changing Climate

Judy Lawrence[1], Scott Stephens[2], Paula Blackett[2], Robert G. Bell[2] and Rebecca Priestley[3]*

[1] Climate Change Research Institute, Te Herenga Waka – Victoria University of Wellington, Wellington, New Zealand, [2] National Institute of Water and Atmospheric Research, Hamilton, New Zealand, [3] Centre for Science in Society, Te Herenga Waka – Victoria University of Wellington, Wellington, New Zealand

Climate services play an important role in informing decision makers about how to reduce the impact of climate-related hazards, by building capacity through access to relevant data and information globally and regionally. Different types of climate services include long-term warning systems, projections, monitoring/triggers and signals, risk evaluation tools, and behavior change tools. However, climate services are often promoted as "improving uptake" and "translating and communicating science" This framing, which assumes that climate services are developed by scientists and "provided" to users, has limitations for decision makers designing actions to address changing coastal hazard risk driven by sea-level rise. Acting upon the IPCC 1.5 Degree Special Report imperative for urgent actions to reduce exposure and vulnerability at the coast will require a transformation in the way climate services are developed and delivered, in tandem with an understanding of the decision-making and policy context. Tools and policies must explicitly address deepening uncertainty and changing risk over long timeframes. Their use also must be compatible with the jurisdiction's institutional frameworks and decision-making practice and relevant to user needs as changing risks unfold. Attention to both short- and long-term decisions are paramount to avoid lock-in and path dependency of decisions taken today, and to ensure relevance for the timeframes of investments in infrastructure and settlements. This requires actionable science and usable tools developed through multi-disciplinary efforts by scientists, co-producing them with decision agencies and communities. We give examples of different types of climate services developed with users and draw out some universal lessons learned in developing and applying them in New Zealand.

Keywords: climate services, sea-level rise, coastal hazards, adaptive planning, coastal flooding, policy

OPEN ACCESS

Edited by:
Goneri Le Cozannet, Bureau de Recherches Géologiques et Minières, France

Reviewed by:
Pushpa Dissanayake, University of Kiel, Germany
Dewi Le Bars, Royal Netherlands Meteorological Institute, Netherlands

****Correspondence:***
Judy Lawrence
judy.lawrence@vuw.ac.nz

Specialty section:
This article was submitted to Coastal Ocean Processes, a section of the journal Frontiers in Marine Science

Received: *01 May 2021*
Accepted: *16 July 2021*
Published: *03 August 2021*

Citation:
Lawrence J, Stephens S, Blackett P, Bell RG and Priestley R (2021) Climate Services Transformed: Decision-Making Practice for the Coast in a Changing Climate. Front. Mar. Sci. 8:703902. doi: 10.3389/fmars.2021.703902

INTRODUCTION

In 2011, the World Meteorological Organization issued a global framework for climate services focused on assisting decision makers. The framework envisaged that the development of climate services would involve engagement between users and providers and would lead to a reduction in the impact of climate-related hazards and an increase in the benefits from benign climate

conditions. Inherent in the framework was the building of capacity, and open access to relevant data and information globally and regionally, resulting in a shift in risk reduction (Hewitt et al., 2012).

However, the literature reports that in UK and USA the public does not feel well informed about, and has difficulty understanding sea-level rise (SLR) (Thomas et al., 2015; Covi and Kain, 2016), despite ample evidence of SLR causing coastal flooding now, the low uncertainty bounds around SLR to 2050, and the current and projected impacts of SLR on people and their assets (Kulp and Strauss, 2019; Paulik et al., 2020). A New Zealand study confirmed these findings (Priestley et al., 2021) and showed that the public mistakenly overestimates the scientifically plausible amount of SLR by 2100 and incorrectly identifies melting sea ice as its primary causal mechanism.

A review in 2016 of lessons learned and future prospects for climate services (Brasseur and Gallardo, 2016) highlighted that there was insufficient awareness by stakeholders of their vulnerability to climate change, a lack of relevant products and services, and inappropriate product formats and delivery mechanisms. In a paper focusing on SLR, Hinkel et al. (2019) highlighted the lack of systematic analyses of users' needs, in particular, in different decision contexts and the users' level of risk and uncertainty tolerances. The principal reason for these disconnections between climate services and users, was a "top down" framing of climate services by those providing them, on the assumption that users did not understand the contextual issues – creating a disjunct between science outputs and decision-making needs and outcomes. Furthermore, there was a lack of understanding by scientists that their users and requirements were diverse, and that a range of formats and products were needed. A tension was highlighted between the different timeframes of the scientists and users and whether the analytical tools available (predominantly statistical and projections) could provide the certainty that decision makers say they need, within the institutional decision and legal frameworks in which they operate. Users typically work within a context that demands certainty which is often reflected in short-term and reactive decision-making processes. Lastly, the delivery mechanisms were not tuned to user needs. The 2016 review identified the need for a more nuanced architecture for climate services with attention to tailoring climate services to different users and delivering climate services at difference scales – global, national, and subnational. Furthermore, it highlighted the need for more diverse teams producing climate services and distributing and communicating the products. The review highlighted the need to build the capability of users and scientists in designing policies to reduce the risks of climate change and develop the enabling conditions necessary for climate resilient decisions, such as legislation and funding mechanisms, that support the implementation of policies.

The current focus on "improving uptake" and "translating and communicating science," assumes a business model where climate services are developed by scientists and "provided" to users (Cavelier et al., 2017). This approach assumes that "client" needs have been assessed and that services provided will realize those needs. It can also follow a "deficit model" approach to science communication (Irwin, 2014), where knowledge holders (in this case scientists) assume that providing accurate and up to date information to users (correcting their "knowledge deficit") is enough to ensure rational decision making with regard to climate risk.

This approach has severe limitations for decision makers assessing climate risks and designing actions to address changing coastal risks from sea-level rise, for example. In their paper on managing the risks of SLR, Kopp et al. (2019) discuss the need for usable science to inform decision making that must address long lag-times, irreversible losses, and deep uncertainty. For intra and intergenerational decisions to be made at different spatial scales, they stress the importance of multidisciplinary understanding across natural and social sciences, engineering, decision science, and political economy.

In New Zealand we have found that the factors discussed by Kopp et al. (2019) are necessary for climate services to address uncertainty and ongoing changing risk and enable actions to be taken pre-emptively, to avoid and reduce the worsening impacts of SLR. For example, this understanding informed the move to provide SLR projections as increments of SLR (Stephens et al., 2017), rather than specific projection scenarios. It has enabled SLR to be directly linked to local adaptation thresholds (Kool et al., 2020). This approach enables coastal hazard and risk assessments to be scenario-neutral, rather than having to make decisions on what RCP to use. This facilitates a direct line of enquiry by stakeholders to what the adaptation thresholds might be in different parts of low-lying localities. Scenarios for SLR can then be used to bracket the timing of the adaptation threshold and enable stress-testing of the lifetime and efficacy of short-term actions and longer-term adaptation options (Stephens et al., 2017)[1].

If the institutional frameworks and decision-making practice are compatible with the problem space (change and deepening uncertainty), both short- and long-term decisions can help avoid lock-in and path dependency (Haasnoot et al., 2013). Integrating the timeframes of investments in infrastructure and settlements can also assist (Kool et al., 2020). Multi-disciplinary efforts by scientists working together closely and co-productively with decision agencies, their professional advisors, and communities enables knowledge acquisition for developing a range of approaches and understanding values and preferences. However, Hinkel et al. (2019) point out that the preferences of users may not always lead to good outcomes, due to biases, partial knowledge, and conventions.

Here, we present different types of climate services such as long-term warning systems, projections, monitoring/triggers and signals, risk evaluation tools, and behavior change tools, illustrating them with New Zealand examples, including a red-alert tide calendar to pre-warn of potential coastal flooding days in low-lying areas; sea-level rise exceedance nomographs; serious games to embed understanding of uncertainty and changing risk that can bridge to the application of dynamic adaptive pathways planning (DAPP) (see section "Dynamic Adaptive Pathways Planning"); national-scale application of a risk-evaluation tool to

[1]Refer Table 1 and Figure 5 of Stephens et al. (2017)

identify what is at risk and its cost; information defining asset exposure and flooding likelihood relevant to the banking and insurance industries as they enter the new transparent disclosure regimes; and lessons from the application of DAPP processes. From these examples grounded in real-world practice, we draw out universal lessons learned in developing and applying them.

WARNING OF COASTAL FLOODING

Coastal flooding is a major global hazard with records of historical events back to 1200 AD killing hundreds of thousands of people and causing billions of dollars of damage to property and infrastructure (Pugh, 1987; Lagmay et al., 2015; Needham et al., 2015; Haigh et al., 2016). Globally, it has been estimated that up to 310 million people are already exposed to a 1 in 100-year flood from the sea (Jongman et al., 2012; Hinkel et al., 2014; Muis et al., 2016). In New Zealand, this includes 72,000 people, or 1.5% of the population (Paulik et al., 2020). The number of people exposed to such flooding will markedly increase globally. It has been estimated that 0.2–4.6% of global population will be flooded annually under 25–123 cm (RCP2.6–RCP8.5) of global mean SLR without additional adaptations (Hinkel et al., 2014). Furthermore globally, 630 million exposed people currently live on land below projected annual flood levels for 2100 (Kulp and Strauss, 2019). Flooding can occur during very high tides (Ray and Foster, 2016), or during storm-surges and any associated wave overtopping, combined with higher tides when low atmospheric pressure and strong winds drive the sea onto land (Tebaldi et al., 2012). Sometimes these processes can combine to produce very high storm-tides. Improved understanding of extreme sea level and coastal flooding events and the role of higher spring tides (Stephens et al., 2020) and their consequences is therefore important.

To understand and manage this risk exposure, government agencies, environmental and emergency managers and the insurance and banking sectors, all require knowledge of the likely frequency and magnitude of extreme storm-tide and wave overtopping events, how they compound with multiple drivers, and their clustering in time and space. Forecasts of the timing and magnitude of coastal hazards allow coastal or emergency managers to design appropriate responses, so they can significantly reduce risk and warn the communities affected. Two simple decision-relevant examples used in New Zealand are the "red-alert" tide calendar and sea-level exceedance nomographs.

The "Red-Alert" Tide Calendar

Stephens et al. (2014) was developed to support coastal management decisions (see **Supplementary Material**). It is a simple and practical tool that clearly communicates dates of higher-than-normal high tides to indicate when low-lying land is particularly vulnerable to coastal flooding (**Figure 1**). The red-alert tide calendar works well in regions where the variability of extreme sea levels is influenced substantially by the height of high tide (as in important precursor of for coastal flooding), rather than just by storm surges and associated waves) – such as in regions that do not experience tropical cyclones (hurricanes). In this respect, tides dictate the occurrence of extreme coastal sea levels over much of the world (Merrifield et al., 2013; Rueda et al., 2017; Stephens et al., 2020) with storm surges being a secondary effect. On that basis, the annual or 3 monthly red-alert calendars highlight the highest tide days so users can watch for adverse weather forecasts (onshore winds, low barometric pressure, wind waves and swell) leading up to the red-alert tide days (Stephens et al., 2014). The calendar is based on the premise that most extreme storm-tides are driven by more common moderate storm-surges combined with high perigean-spring ("king") high tides, in tide-dominated locations, for example, within the United Kingdom and New Zealand (Haigh et al., 2016; Stephens et al., 2020). Extreme storm-tide elevations in New Zealand are highly correlated with and linearly related to mean spring high-tide elevation, noting spring-tide ranges (meso-tidal) at main coastal cities/towns vary from 1.4 to 3.8 m (Stephens et al., 2020). Climate-change impacts on extreme storm surge and waves are predicted to be modest in the New Zealand region (Cagigal et al., 2020).

Tides are routinely predictable using tidal harmonic analysis of sea-level gauge records or global ocean tide models (Ray, 1999; Matsumoto et al., 2000; Egbert and Erofeeva, 2002; Lyard et al., 2006). This means that red-alert tide calendars can be tailored and applied regionally and used as an early warning system for increased risk of coastal flooding in low-lying areas relative to local spring tide levels.

Red-alert tide calendars are highly visual and easily interpreted, and do not require technical expertise or interpretation of large amounts of data or text (**Figure 1**). Providing several alert thresholds allows users to use their experience to "tune in" to the calendar, by correlating the alert level with the severity of past local consequences. Thus, the high-water calendar can be used, for example, by local fishers making decisions on where to moor vessels, or by emergency managers, knowing that even a moderate swell event could cause significant flooding if it coincides with a red-alert date. The high-water calendar is easily updated and displayed on a web site or can be sent electronically for local distribution. There is demand now to upload these calendars months ahead of a new calendar year. The red-alert tide calendar has also spawned a citizen science programme in Auckland (New Zealand) through the King Tides Auckland Initiative (2020)[2] which is aligned to the global network of King Tide Projects (e.g., Australia, Hawaii, Oregon). This initiative focuses on public engagement and awareness around the highest red-alert days each year, encouraging citizens to "snap the coast" at the designated time of the high tide and upload the photograph to the public web site. This forward-thinking public engagement initiative allows both scientists and citizens to utilize these red-alert tide days and visualize the impacts rising sea level may have on their communities in the future (Román-Rivera and Ellis, 2018).

Sea-Level Exceedance Nomographs

Are another simple tool for visually demonstrating the effect of SLR on the frequency of present-day high-water thresholds

[2]Retrieved from: https://auckland.kingtides.org.nz/

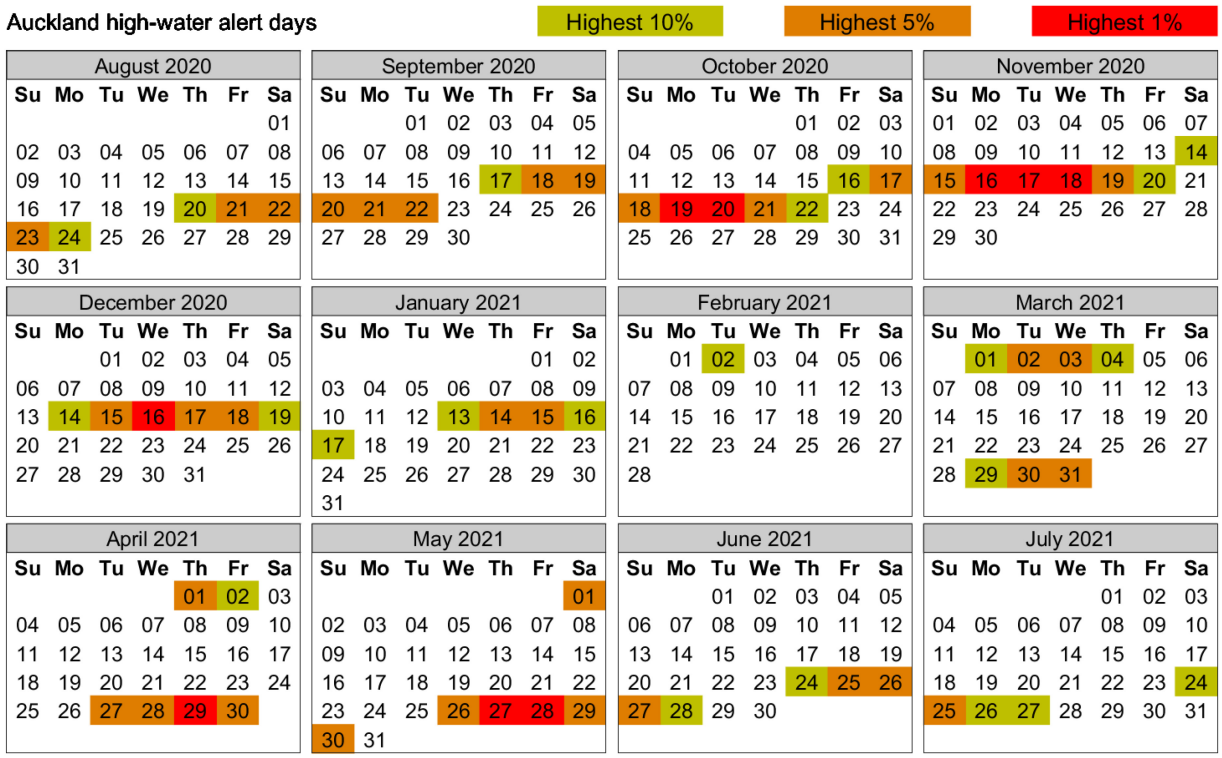

FIGURE 1 | Red-alert tide calendar at Auckland, New Zealand. Color bars above show the highest 10% (green), 5% (brown) and 1% (red) of predicted high tides for that year.

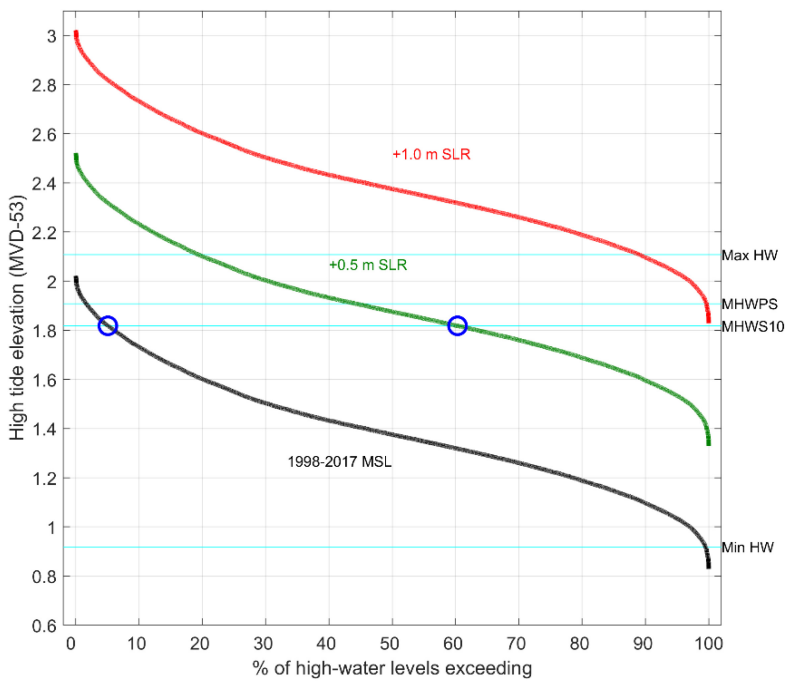

FIGURE 2 | Tidal high-water exceedance nomographs for Tararu (Thames, Coromandel, New Zealand), at present-day mean sea level (MSL) and also offset by + 0.5 and + 1.0 m sea-level rise. Max HW, maximum predicted astronomical tide, MHWPS, mean high-water perigean springs, MHWS10, high-tide height exceeded by the highest 10% of all predicted high tides, Min HW, minimum predicted astronomical tide. (MVD-53 is the regional vertical datum).

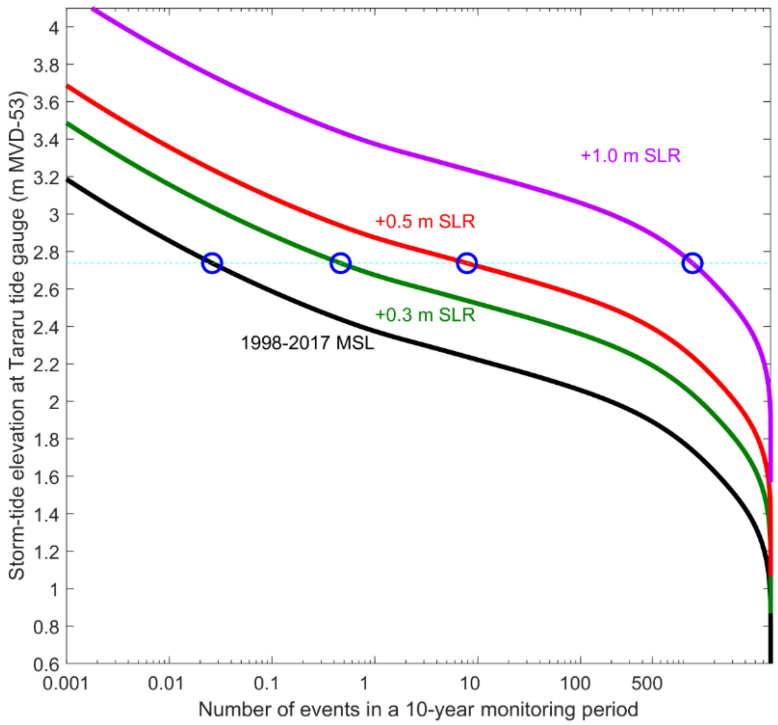

FIGURE 3 | Change in frequency of storm-tide flooding with SLR at Tararu, Thames, Coromandel, New Zealand. The nomographs are derived by transforming the high-water exceedance curve in **Figure 2** following methods in Stephens et al. (2018).

(**Figures 2**, **3**). High-water exceedance nomographs can be used to assess the increase in the frequency of high waters exceeding present-day thresholds for different rises in mean sea level, under the assumption that future modification to tidal characteristics is relatively small (Bell, 2007, 2010). This is reasonable for open coast locations as an approximation to convey the key message of changes and onset of semi-permanent high-tide inundation. However, the nomographs should be used with caveats, particularly in estuaries and shallow semi-enclosed bays, where tidal ranges may change significantly either way, depending on sedimentation rates and morphology, which require detailed modeling to ascertain the changes over time. In the case where tidal changes over time are modest, the entire present-day high-water exceedance curve can be raised vertically by different values of SLR. Rueda et al. (2017); Stephens et al. (2014), and Stephens et al. (2018) showed that tide-dominated coastal flooding regimes will be more sensitive to SLR influenced by increasing frequency of extreme storm-tide events, compared to storm surge-dominated regions exposed to hurricanes, typhoons or tropical cyclones. This is particularly the case in New Zealand, where the tide is the key determinant of extreme storm-tide levels or wave overtopping. Sea-level exceedance nomographs have been found to simplify communication for users where a 0.5 m SLR would result in 60% of all high tides exceeding the present-day spring-tide mark (MHWS-10) (**Figure 2** circles), which is exceeded currently by only 10% of high tides. This assumes that changes in tidal characteristics with rising sea level are not markedly different, as indicated by Devlin et al. (2017). Even higher percentages of high-tide exceedances will occur, relative to present-day spring tides, in areas with smaller tide ranges (micro-tidal regions), for a given increment of SLR (Bell, 2007, 2010).

Red alert tide days, rising high-tide exceedance and flood frequency nomographs present long-lead-time warning information in a way that is readily usable. In particular, the red-alert tide calendars were tested and revised with a range of users over a period of a few years, largely at local government levels of decision making, with users' input reflected in the alerts and thresholds finally adopted. The simplicity of the tools, which each convey a single idea on potential and increasing frequency of coastal flooding, is shown in **Figures 1**–**3**. This has engendered increased confidence by users in the application of the science underpinning the calendars and nomographs, based on feedback from users, particularly in understanding the increasing frequency of coastal flooding as the first tangible impact of SLR.

BUILDING AN INTEGRATED UNDERSTANDING OF COASTAL FLOODING AND DECISION MAKING

Climate services are often provided as discrete pieces of information for an area at risk or particular type of hazard. However, adaptation to climate change and increasing capacity to manage climate and other risks, reinforces the need for sets of information relevant to different stages of the decision-making

process. This would support a broader array of risk management planning and implementation activities, beyond traditional climate services (Lawrence et al., 2019a; Jacobs and Street, 2020) for example, where changing risks have significant consequences and where they are foreseeable. It would also address the problems when information on climate change hazards, their impacts and risks into the future become intertwined in ways that create barriers for developing alternative options/pathways for adaptive management. For example, when the hazard is merged with the risk. The latter is an expression of what is exposed, its vulnerability, and agents and communities' preferences. The former is a technical analysis, while the latter is deliberative and political. Furthermore, the sheer volume of information (quantitative or quantitative) that individuals or groups are asked to assimilate in many assessments can generate default qualitative decisions that lead to mal-adaptive actions that can lock in current risk and make it harder and costlier to address as the climate changes intensify. Three examples of climate services have been developed and/or applied in New Zealand that can help address these outcomes – serious games, DAPP and bespoke services for the finance sector.

Serious Games

Are designed to educate, train, and inform (Michael and Chen, 2005) and can be computer or board based. They have been developed and used globally across many domains of interest including military strategy, health planning, public policy and public awareness raising. Their use in climate change decision-making processes has helped to build understanding of risk and develop capacity to act that is robust across many different potential outcomes (Lawrence and Haasnoot, 2017). Serious games enable complex strands of information from different sources (e.g., technical values, objectives, changing risk over time) to be considered systematically, by testing how different outcomes can be achieved in the face of the uncertainty presented by a changing climate and associated hazards (Flood et al., 2018). While serious games are abstractions from reality and as such enable place-based interests to be suspended, they retain the central decision-making tensions present in the real world, by creating a simplified decision-making experience that can embed learning for real-world decision making.

Four different types of serious games have been developed in New Zealand as climate change services (**Table 1**; see **Supplementary Material**).

(a) Simple serious games where the player makes the decision in the absence of other groups or players – the player acts toward their own desired outcomes with feedbacks on the choices made, from the game.
(b) Games where there are other non-player characters or groups (of players) representing other interests which seek to influence the choices – at different levels of complexity not tied to a specific place.
(c) Bespoke games designed for specific locations, people and sets of decisions.
(d) Computer simulated games with climate model data driving the feedback on choices made by single or many players.

All games, however, are designed using the same set of steps (**Figure 4**). What varies is the level of detail provided through the game to the participants, the complexity of the storyline and whether they are computer simulated. Tier 1 games are short games (5–10 min) designed to convey a set of simple messages using a simple storyline and a generic location. They are co-designed with technical partners and key stakeholder groups. They do not need detailed numerical data and rely on abstracted scientific knowledge. An example is the NIWA flood adaptation and SLR game[3]. Tier 2 games use more complex decision questions and have nuanced storylines that are supported by more detailed data and information. Such games can be placed-based and constructed from quantitative data, but the presentation of the information remains simplified to be more accessible. In the Coastal Adaptive Futures tier 2 game (Blackett et al., 2019) community representatives contributed real-world issues relevant to decision- making context. While tier 1 and 2 games provide learning and dialogue opportunities, tier 3 games are bespoke, for supporting real-life decision making in place. The Marae-Opoly Game is a tier 3 game designed for a particular place, with real alternatives, finances and used to support the development of DAPP (Colliar and Blackett, 2018) (see **Supplementary Material**).

These games build on the Te Ara River Game and Tainui Coastal Game developed in 2015 based on the Dutch Delta Game (Haasnoot et al., 2013)[4], the evaluation of their uptake (Lawrence and Haasnoot, 2017) and its application in the Hutt River flood risk management plan (Lawrence et al., 2019a). The games and their use with DAPP applications have motivated

[3]https://niwa.co.nz/natural-hazards/our-services/serious-games-as-a-tool-to-engage-people

[4]https://www.deltares.nl/en/software/sustainable-delta-game/

TABLE 1 | Game complexity typologies.

Game	Type	Complexity	Characteristics
"Climate adaptation challenge"	Board game	Low	Simple narrative Generic location Simple range of options Individual player choices
"Adaptive futures"	Online game	Medium	Simplified narrative Generic location Individual player choices but influenced by non-player characters
"Marae-Opoly"	Board game	High	Complex place-based narrative Collective decisions Real place-based options Complex choices and feedback
"Tainui coastal game"	Computer-based game	High	Complex narrative Collective decisions Complex choices and feedback Plausible options

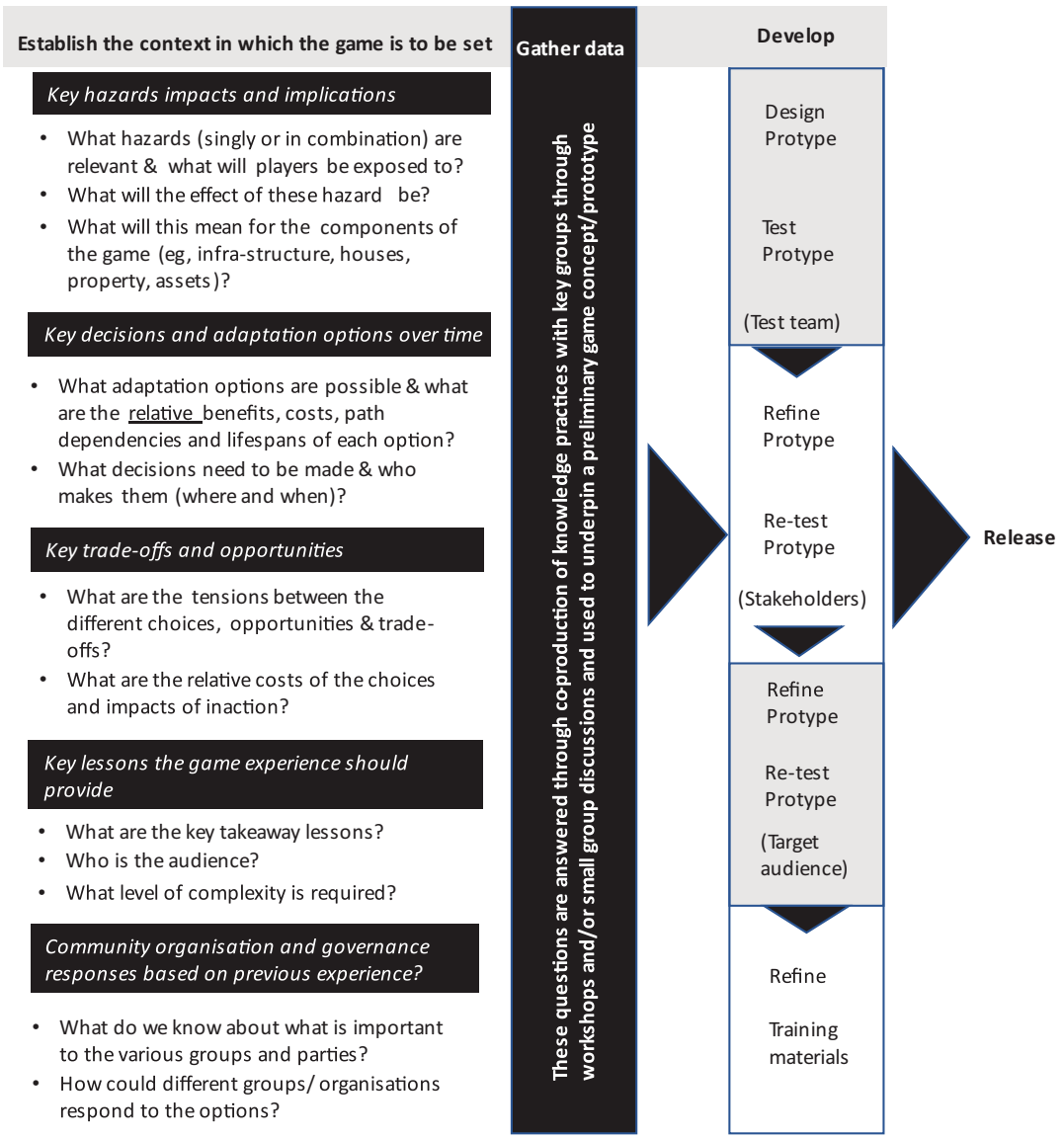

FIGURE 4 | Process for developing and testing serious games.

the development of signals and triggers for monitoring DAPP pathways by decision makers (Stephens et al., 2018).

For games to be effective in priming long-term thinking and adaptive action in a climate change setting, they require multi-disciplinary perspectives, and an ability to reduce and reframe complexity in a way that makes it possible to navigate choices over time (Simpson et al., 2021). Clarity of outcomes, values, objectives of different interests, options effectiveness, and costs and trade-offs are essential elements of any decision context. Since the information and expertise required will seldom be held in one knowledge basket, different disciplinary, value and cultural perspectives are necessary to inform the assessment of climate change risk (Blackett et al., 2019). This changes the face of what we know as climate services, from discrete to integrated information and learning processes to support assessments.

For games to be effective as learning devices, understanding decision tensions relevant to the intended audience, is needed to capture enough of their life experiences and scenarios of the future, to generate a meaningful experience that can be robust over time as risks change. Our experience in developing and using games has been iterative as we test and refine their effectiveness in different settings (see tier 1–3 examples above). **Figure 4** shows the process employed to develop and test serious games with users.

Several examples (see **Supplementary Material** and **Supplementary Figure 1**) illustrate how serious games played in decision contexts can prime decision makers and communities to enable them to plan and adapt to changing climate risks. They generate learning about what climate change impacts could be, the changing nature of the risk to those affected, the limits

of different adaptation options and the values and preferences of other people and organizations. They do this by enabling thinking beyond the normal range of preferences in a setting where failure is hypothetical and leads to testing previously unconsidered or rejected strategies. By considering all aspects of the system at risk, serious games provide a simple way of looking at the whole system in an integrated way, by looking at the wider societal consequences of taking different courses of action over different timeframes and what it takes to implement an end objective that is highly challenging for current generations, such as managed retreat. Bespoke games, can be used to develop adaptation pathways, building from the options chosen in the game, or lead to the application of the DAPP planning process to build up pathway's options with signals and triggers of change between different pathways (Colliar and Blackett, 2018) as conditions change (see **Supplementary Material**).

By using games to experiment with different audiences and in different decision settings, those providing the climate services can learn how their information can be more relevant to different decision processes. For example, the long-term planning for a marae[5] threatened by SLR became a catalyst for a wider conversation about climate services, their funding, and responsibility for them and opened up the space to discuss how the wider community might benefit from short-term and long-term actions to adapt to sea-level rise.

The games applications highlighted the value of developing climate services with the affected agents and communities and challenged assumptions made about the ability of the users to apply the services received and source data and other climate information (quantitative and qualitative) in a usable form. They also enabled other tools to be used effectively, by increasing understanding of changing climate risk and enabling discussion of adaptation options when using DAPP in a way that embeds values and preferences into the decision outcomes.

Dynamic Adaptive Pathways Planning

Climate services took a turn toward adaptive risk management tools for decision making under changing climate conditions following Kwadijk et al. (2010), who demonstrated the value of shifting from a pressures/state/impact model for addressing sea-level rise, to an anticipatory tipping point model. Usability of climate services (Kopp et al., 2019) is at the center of the climate services in this paper. Usability, is a critical criteria for the design of any climate service. This implies that the information is robust across a range of futures and is relevant to the decision space of the users. But how can this information inform the decision process in a way that reduces the uncertainty and changing risk at the coast and facilitates engagement with stakeholders?

This is where DAPP can provide a decision process to integrate the climate information when assessing adaptation options and alternative pathways in the face of the accelerating, compounding and cascading climate change hazards and risk.

Dynamic adaptive pathways planning mirrors choices made on a metro map (**Figure 5**), testing each option for travel to a destination against different operating conditions over time (scenarios). By making choices for short-term options where there is greater certainty of outcome, the DAPP can identify signals (warnings) and triggers (decision points) with enough lead-time to implement alternative options on the pathway chosen or to switch to another pathway to reach the objective. The process is based on the principle that there is uncertainty about the future in some respects and that locking in a particular pathway will result in path dependency from which it becomes more difficult over time to shift, due to the advancing hazard risk. Leaving options open in the future by taking short-term decisions that enable option/pathway change later, gives flexibility to reassess the options and chart a different course depending on how the future turns out. This iterative and adaptive process addresses both uncertainty of outcome and the rate of change. Its application in coastal and river flooding contexts is now well-tested in many locations globally (Haasnoot et al., 2013, 2018; Ranger et al., 2013; Kingsborough et al., 2016; Bloemen et al., 2019; Lawrence et al., 2019a).

The recent shift in approach for undertaking coastal mapping and risk assessments, toward providing SLR projections in terms of increments of SLR (Stephens et al., 2018), rather than specific projection scenarios referred to in the introduction, has enabled SLR to be aligned with local adaptation thresholds (Kool et al., 2020), thus allowing signals (to warn of changes in conditions) and triggers (for deciding on alternative options and pathways) (Haasnoot et al., 2013) to be integrated into coastal hazard and risk assessments by bracketing the timing of the adaptation thresholds and for stress-testing the shelf-life and efficacy of short-term actions and longer-term adaptation options using DAPP.

In New Zealand, the application of serious games with local government officials has led to experimentation with DAPP in real-life decision making (Lawrence and Haasnoot, 2017; Lawrence et al., 2019a) and the inclusion of DAPP as a primary adaptive decision-making process in the national coastal hazards and climate change guidance (MFE, 2017; Lawrence et al., 2018). Furthermore, this has spawned the tailored development of the DAPP, again in real-life decision settings at the coast (OECD, 2019), through development of signals and triggers for decisions based on the robust science that underpins the red tide alert and coastal flood frequency climate services and the development and application of real options analysis to pathways planning in fluvial and coastal flooding contexts (Lawrence et al., 2019a). A multi-disciplinary team within New Zealand and with international colleagues has enabled climate services to be integrated for application by decision makers.

Bespoke Climate Services for the Finance Sector

The New Zealand Government has introduced legislation for mandatory disclosures of climate-related risks by companies and financial institutions which comes into effect in 2023. It requires all banks, asset managers and insurance companies with more than NZ$1 billion in assets to disclose their climate risks, in line with the emerging global standard from the Task

[5] A Maori community meeting house

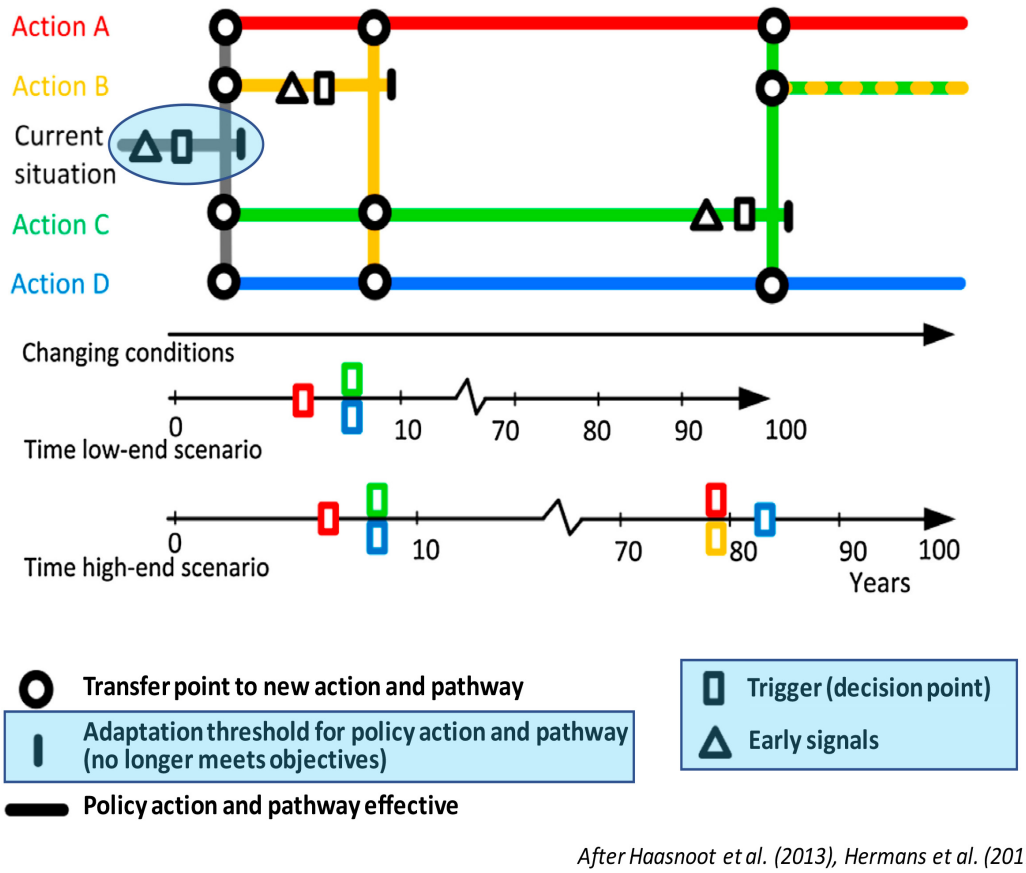

FIGURE 5 | Adaptive pathways showing signals, triggers, and pathways.

Force on Climate-related Financial Disclosures (TCFD). This will require banks to consider the transition, physical and liability risk when lending and offering insurance to households and small and medium size enterprises. This matters most to domestic real estate, which is the largest item on the balance sheet of New Zealand banks, and agricultural and small businesses. Figuring out what climate risks banks are exposed to is not a simple task. Banks and insurance companies will need to scale up their ability to estimate flooding risk from extreme rain, storms and SLR on residential housing[6].

The RiskScape tool (Schmidt et al., 2011) developed in New Zealand can help address TCFD requirements (**Figure 6**). RiskScape combines datasets of hazard, exposure (i.e., elements-at-risk), and vulnerability, in a state-of-the-art software engine that quantifies risk of exposure or impact at national- to local-scales (**Figure 6**). RiskScape has been used in New Zealand at a national scale to enumerate the built-environment land and assets, and their geometric quantities directly exposed to coastal flooding (Paulik et al., 2020). Paulik et al. (2020) evaluated a 1% annual exceedance probability (AEP) storm-tide levels and sea-level rise. A present-day 1% AEP storm-tide event is quite large and rare, by definition, but will be exceeded with rapidly increasing frequency as sea-level rises (Hunter, 2012; Sweet and Park, 2014; Stephens et al., 2018). A 1% AEP event, when added to SLR estimates, provides suitable scenarios to meet New Zealand Coastal Policy Statement objectives that require coastal-flood hazards to be identified to avoid increasing risk over "at least the next 100 years" (DoC., 2010; MFE, 2017).

However, meeting TCFD requirements requires scenarios tailored to shorter-term decision making, typically $\leq$ 30 years which is the typical domestic real estate mortgage lifetime. Discussions with the banking industry indicate that a 10% AEP storm-tide flooding event is a more relevant event to model for TCFD requirements than a 1% AEP event – a 10% AEP event is likely to occur 3 times over a 30-year mortgage (although could occur more or less frequently depending on climate variability).

A key element of climate change planning is understanding the potential timing of impacts. Stephens et al. (2017) provided a table of the approximate years, from possible earliest to latest, when specific SLR increments (meters above the IPCC AR5 1986–2005 baseline epoch) could be reached for various scenarios of SLR for the wider New Zealand region – the table is included in national guidance for coastal climate change adaptation (MFE, 2017; Lawrence et al., 2018). **Table 2** provides SLR projections designed to meet TCFD requirements out to 0.3 m SLR. For

[6]https://theconversation.com/new-zealand-will-make-big-banks-insurers-and-firms-disclose-their-climate-risk-its-time-other-countries-did-too-146392

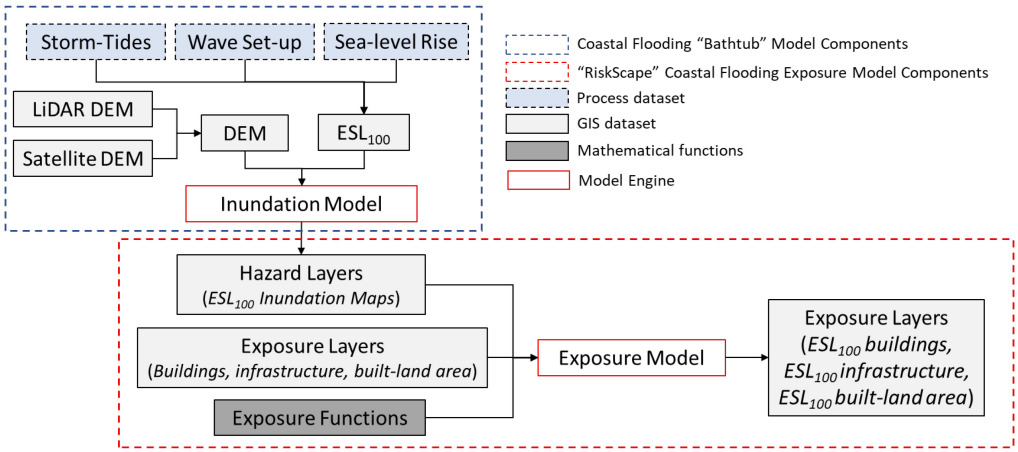

FIGURE 6 | RiskScape model framework applied by Paulik et al. (2020). ESL100 = 100-year average recurrence interval extreme sea-level. DEM = digital elevation model. Adapted from Paulik et al. (2020).

TABLE 2 | Expected year to reach 0, 0.1, 0.2, and 0.3 m SLR relative to 2020 base year, for fast and slow SLR scenarios Slow SLR scenario is RCP 2.6 median.

Scenario	Present-day MSL	Present-day MSL + 0.1 m SLR	Present-day MSL + 0.2 m SLR	Present-day MSL + 0.3 m SLR
SLR(m)	0	0.1	0.2	0.3
Year SLR reached slow SLR	2020	2040	2062	2082
Year SLR reached fast SLR	2020	2033	2044	2054

Fast SLR scenario is RCP 8.5 upper 83rd percentile (H+) (MFE, 2017). MSL, mean sea level. Source: Stephens et al. (2017).

a fast SLR rate [RCP8.5 H^+, MFE (2017)] 0.3 m is projected to be reached by 2054, which is slightly more than a 30-year mortgage lifetime from now – this will take longer under a slow SLR scenario.

DISCUSSION

Climate services are not an end in themselves. They are for motivating and supporting decisions which fit within the prevailing governance and institutional frameworks in each jurisdiction. The applications demonstrated in this paper have been applied to decisions for reducing climate change risks. Typically, hazard and risk reduction has been set in static institutional contexts. For example, a hazard is identified in one place at one time or as an event that happens and creates a disaster from which recovery and rebuild is the usual track to follow. Climate change challenges that approach. While extreme events will continue to occur, and some with greater frequency and intensity, hazards at the coast will exacerbate the risk by being ongoing (sea-level rise) for centuries even if emissions are reduced to achieve 1.5 degrees (Paris Agreement). SLR is already exacerbating the high tidal effects discussed above. Where there is a tidal footprint in groundwater, water tables are rising and creating coastal flooding; this will continue and create an existential threat in many low-lying parts of the world.

These characteristics of climate change impacts reveal that for effective adaptive planning, new institutional arrangements and planning practice are required. To date planning and legal mechanisms to reduce climate change risks have proven inadequate (Lawrence, 2015), for example: warnings of flood risk on property titles; mixed jurisdictional authority between the two levels of local government has hindered regional planning which could have enabled territorial local government to prohibit further exposure in risk prone areas; and special legislation to increase housing development has allowed risk reduction provisions where they exist, to be sidestepped. This is despite national coastal hazards and climate change guidance that embeds DAPP and the New Zealand Coastal Policy Statement which requires councils to take a precautionary approach, including the place of managed retreat as an adaptation option. The New Zealand government is currently (June 2021) developing a Strategic Planning Act and a Climate Change Adaptation Act to provide the enablers for adaptation, such as, new funding and legal instruments to address existing land uses and managed retreat and the integration of DAPP and strategic risk management into the new statutory regime. Both climate services and the institutional arrangements must be in sync with the dynamics of change at the coast.

The on-the-ground experience presented here, demonstrates the type of climate services that are useful and effective for addressing the risks of climate change in coastal areas, in particular, for addressing the ongoing changing risks and the long-term uncertainties related to sea-level rise. These risks are changing rapidly, and physical and social thresholds are approaching. Decisions are being taken now that continue investment in at-risk coastal areas and expose more people and assets to harm. Developing climate services in isolation from users, and "selling" them as "services" confuses supply

with demand. It risks development of unusable services that can divert effort on adaptation to purely tweaking business-as-usual approaches. This has potentially significant maladaptive outcomes that will make adaptation in the future hard to implement and very costly.

Our experience is that it is extremely effective for applied researchers to work closely and on a regular basis with end-users who can spot gaps in the climate service knowledge or systems. This enables decision problems to be researched quickly, tested with the users and useful tools delivered for adaptation decision making. The benefits of the climate service, though, can take time for uptake. For example, the red-alert tide calendar was initially slow to be taken up, but then pressure built up from a range of users, wanting next year's calendar to use for coastal emergency management planning. The catalysts for uptake of DAPP approaches were: (i) a series of changes to New Zealand's resource-management legislation in 2004, 2010, and 2017 (requiring councils, when developing land-use plans, to have particular regard to the effects of climate change, develop 100-year strategies for adapting existing development and manage significant risks from natural hazards); (ii) by the publication of academic papers (Haasnoot et al., 2018; Stephens et al., 2018; Lawrence et al., 2019a,b) and policy reports and reviews which primed understanding through training and development of DAPP (Lawrence and Haasnoot, 2017); (iii) development of council climate change strategies (e.g., Greater Wellington Regional Council 2015)[7]; (iv) integration of DAPP in national coastal hazards guidance (MFE, 2017); and (v) a sequence of damaging coastal storms and floods in 2018. The role of the media in informing the public about climate change and SLR has also motivated political attention to the adaptation solutions space (Haasnoot et al., 2020). The process can be categorized as creating interest, increasing awareness, and experimenting in real-life decision contexts, through a reinforcing set of parallel activities to enable uptake of the climate services set out in this paper.

User relevance has evolved as an effectiveness criterion for the funding of national research. New Zealand has two research models that bring researchers and users closer together on climate service production. First, a consultation and involvement model funded for researchers and users to interact closely on decision-relevant research to fill knowledge gaps or develop decision tools that meet user needs Lawrence and Manning (2012) with a focus on smaller resource-poor councils or for research of general relevance across many councils. The development of the DAPP approach and the use of Real Options Analysis developed from this model. Second, a co-production model, through which researchers and users jointly produce climate services. The Tauranga City Council sea-level rise flood tool (see **Supplementary Figure 2**) was developed in this way. Researchers advised on appropriate storm-tide and SLR scenarios then used a dynamic model to predict flooding for several scenarios, which were mapped. Tauranga City Council then ground-truthed the maps and constructed an interactive web-based tool.

The games applications have created a key learning environment for decision makers when addressing coastal hazards, and the risks they bring for communities, sectors and government – greater understanding of the formal and informal rules that constrain or facilitate different types of adaptation; the role that values and aspirations play in decision making and how contested worldviews and competition for resources can be resolved in acceptable ways; how feedback from decision choices influence how paths can change as conditions change; how actions can be staged over time and funding prioritized; that risk cannot be totally removed and residual risk managed. The freedom to experiment and test different strategies within the rules and constraints of the game is perhaps one of the key strengths of the gaming approach. Players can fail and learn from that failure with no real consequences. However, if the rules are constructed to reflect a simplified version of reality, those lessons can be applied in the real world where choices do have implications.

[7]Available at http://www.gw.govt.nz/assets/council-reports/Report_PDFs/2017.194a1.pdf

TABLE 3 | Type of climate service with examples, purpose and lessons learned.

Type of climate service	Example	Purpose	Lesson learned
Long-term warning	Red-alert tide calendar	Annual to 3-monthly warning information of potential coastal flooding	Simple to grasp and use, visual aid, spawned citizen programme raising awareness
Long-term warning and raising awareness	Sea-level rise nomographs for frequency of high-tide exceedances	Long lead time warning information to create awareness of increasing coastal flooding	Increased confidence in the underpinning science, especially of the first tangible impact of SLR
Interactive spatial visual aids and maps ("sliders")	Coastal inundation for increasing SLR	Quick, visual, assessment of spatial risk exposure	Easy to use and appraise, informs spatial risk exposure. Applicable at many levels of public interest
Behavior change	Serious games	A decision learning tool that confronts participants with the implications of SLR and deepening uncertainty	Freedom to experiment and receive consequence feedback in a safe space. Raises need for adaptive decision making
Risk assessment and evaluation	RiskScape – a quantitative modular loss/damage system	Data on assets and people at risk and spatial analysis of consequences with SLR	Increased confidence by decision-makers in the quantum of risk in 0.1 m increments of SLR, informs adaptation priorities
Uncertainty and change assessment	Dynamic Adaptive Pathways Planning	An assessment and planning tool to address uncertainty and changing risk	Shifts thinking and planning from short-term protection strategies to longer-term on ongoing and changing risks

CONCLUSION

Making decisions in a dynamically changing environment poses significant challenges to coastal managers and decision makers. Assessment, planning, design of adaptations in coastal settings have been historically driven by impact/response models of decision making which have proven inadequate for a changing coastal setting where SLR is becoming the dominant driver of change (Le Cozannet et al., 2015).

The use of multiple reinforcing climate services that warn, monitor, review, and update, anticipate, build understanding and a capacity to act, operating within a fit for purpose institutional framework, can enable risks to be anticipated and deliver more robust decisions that are grounded in real-world practice. Synergies between these applications is giving a more nuanced understanding of what climate services are and how they can best be delivered. This has built trust in science where tools are clear, simple and address the users' problems (Schneider et al., 2020). The lessons learned in the application of the climate services discussed here have the prospect of shifting the perspectives about ongoing SLR (**Table 3**) and thus contributing further to the climate services field.

However, climate services by them selves are insufficient for addressing SLR. Increasingly, the role of the institutional context, multi-disciplinary practice and engagement with users and communities affected, are being recognized as essential for leveraging changed practice toward the use of adaptive processes supported by more relevant decision tools. For example, we have identified that the following institutional enablers have universal relevance.

- The critical importance of transparent and enabling governance arrangements (including Memoranda of Understanding with the parties) prior to starting strategy development.
- The value of a regional/local government partnership for coastal strategy development.
- The value of engaging collaboratively with communities by providing a "safe space" for deliberation, resulting in social learning about the practical issues around resilience efforts.
- The need for wider community engagement to encapsulate views on managing the risk and side-effects of options.
- The importance of considering a 100-year timeframe for vulnerability and risk assessments (using narratives and scenarios) and distilling the emergence of adaptation thresholds (i.e., when agreed objectives around levels of service and risk would no longer be met).
- Understanding how coastal hazard and risk/vulnerability assessments and the options/pathways assessment process using DAPP can be integrated and scaled, depending on the level of uncertainty and the planning situation.
- The value of an adaptive pathways approach for shifting thinking from short-term protection strategies to a longer-term focus on ongoing and changing risks.
- The risk of underestimating the time needed for developing the implementation plan, which includes regulatory planning, governance, funding, design and costings, triggers for monitoring and review.
- The importance of building capacity to employ the services, especially where resources are slim and there are few experts to work alongside decision makers.

Embedding new practice into "the way we do things around here," however, is often hampered by the slowness of policy decision making, which can swing wildly depending on political philosophy at national and local levels. This is a problem for consistency and alignment of values and outcomes which require bipartisan "agreement," adequate capacity building and the use of policy commitment devices (Boston and Lawrence, 2018). Climate services alone will not serve decisionmakers in the dynamic coastal space without the alignment of institutional frameworks across relevant domains of interest to increase the ability to implement adaptation options.

AUTHOR CONTRIBUTIONS

JL conceived the manuscript as a contribution to the Workshop on WCRP Grand Challenge and Climate Services BRGM Orleans France 12–13 November 2019. JL and SS developed the outline of the manuscript and wrote the first draft with input from RB, PB, and RP. All authors are accountable for the content of the manuscript.

FUNDING

JL, RB, SS, and PB were supported through the Resilience to Nature's Challenges National Science Challenge "Enabling Adaptation" programme funded by the New Zealand Ministry of Business, Innovation and Employment (GNDGNS-RNC040) through the University of Auckland. JL, RB, and RP also received funding from the NZ SeaRise Endeavour Project through Victoria University of Wellington (RTUV1705). PB was partly funded from the Deep South National Science Challenge (Contract CO1X1445), the Natural Hazards Research Platform (CO5X0907). PB and RB were partly funded from the NIWA Strategic Science Investment Funding (SSIF) (CAVA 1904).

ACKNOWLEDGMENTS

We acknowledge the many stakeholders involved in applying and refining the climate services presented in this paper. We also acknowledge the input to the research over many years by Derek Goring (retired, formerly of NIWA) and Doug Ramsay (NIWA) on development of red-alert tide calendars for New Zealand and Kosrae, Federated States of

Micronesia. We thank Marjolijn Haasnoot, Deltares, Delft, Netherlands and University of Utrecht, Utrecht, Netherlands for reviewing an earlier draft of this manuscript and making useful suggestions. We thank the two reviewers for their feedback which improved the final manuscript.

SUPPLEMENTARY MATERIAL

The Supplementary Material for this article can be found online at: https://www.frontiersin.org/articles/10.3389/fmars.2021.703902/full#supplementary-material

REFERENCES

Bell, R. G. (2007). "Use of exceedance curves for defining MHWS and future sea-level rise," in *Proceedings of the 18th Australasian Coastal & Ocean Engineering Conference 2007 and the 11th Australasian Port and Harbour Conference 2007 (Coasts & Ports 2007)*, Australia.

Bell, R. G. (2010). "Tidal exceedances, storm tides and the effect of sea-level rise," in *Proceedings of 17th Congress of the Asia and Pacific Division of the IAHR*, Auckland.

Blackett, P., Davies, K., Davies, B., Holland, P., and Cradock-Henry, N. (2019). *Adaptive Futures: an Interactive Serious Game for Decision-Making and Coastal Hazards. Prepared for Natural Hazards Research Platform*. NIWA Client Report No. 2019328HN. New Zealand: NIWA

Bloemen, P., van der Steen, M., and van der Wal, Z. (2019). Designing a century ahead: climate change adaptation in the Dutch Delta. *Policy Soc.* 38, 58–76. doi: 10.1080/14494035.2018.1513731

Boston, J., and Lawrence, J. (2018). Funding climate change adaptation: the case for a new policy framework. *Policy Q.* 14, 40–49. doi: 10.4324/9780203073384-10

Brasseur, G. P., and Gallardo, L. (2016). Climate services: lessons learned and future prospects. *Earth Future* 4, 79–89. doi: 10.1002/2015ef000338

Cagigal, L., Rueda, A., Castanedo, S., Cid, A., Perez, J., Stephens, S. A., et al. (2020). Historical and future storm surge around New Zealand: from the 19th century to the end of the 21st century. *Int. J. Climatol.* 40, 1512–1525. doi: 10.1002/joc.6283

Cavelier, R., Borel, C., Charreyron, V., Chaussade, M., and Le Cozannet, G. (2017). Conditions for a market uptake of climate services for adaptation in France. *Clim. Serv.* 6, 34–40. doi: 10.1016/j.cliser.2017.06.010

Colliar, J., and Blackett, P. (2018). *Tangoio Climate Change Adaptation Decision Model: a Process for Exploring Adaptation Pathways for Tangoio Marae. Prepared for Maungaharuru-Tangitû Trust and Deep South National Science Challenge*. NIWA Client Report 2018242HN. New Zealand: NIWA

Covi, M. P., and Kain, D. J. (2016). Sea-level rise risk communication: public understanding, risk perception, and attitudes about information. *Environ. Commun.* 10, 612–633. doi: 10.1080/17524032.2015.1056541

Devlin, A. T., Jay, D. A., Talke, S. A., Zaron, E. D., Pan, J., and Lin, H. (2017). Coupling of sea level and tidal range changes, with implications for future water levels. *Sci. Rep.* 7:17021.

DoC. (2010). *New Zealand Coastal Policy Statement 2010*. New Zealand: Department of Conservation.

Egbert, G. D., and Erofeeva, S. Y. (2002). Efficient inverse modeling of barotropic ocean tides. *J. Atmos. Ocean. Technol.* 19, 183–204. doi: 10.1175/1520-0426(2002)019<0183:eimobo>2.0.co;2

Flood, S., Cardock-Henry, N. A., Blackett, P., and Edwards, P. (2018). Adaptive and interactive climate futures: systematic review of 'serious games' for enagement and decision-making. *Environ. Res. Lett.* 13:063005. doi: 10.1088/1748-9326/aac1c6

Haasnoot, M., Biesbroek, R., Lawrence, J., Muccione, V., Lempert, R., and Glavovic, B. (2020). Defining the solution space to accelerate climate change adaptation. *Reg. Environ. Change* 20:37.

Haasnoot, M., Kwakkel, J., Walker, W., and ter Maat, J. (2013). Dynamic adaptive policy pathways: a method for crafting robust decisions for a deeply uncertain world. *Global Environ. Change* 23, 485–498. doi: 10.1016/j.gloenvcha.2012.12.006

Haasnoot, M., van t' Klooster, S., and van Alphen, J. (2018). Designing a monitoring system to detect signals to adapt to uncertain climate change. *Glob. Environ. Change* 52, 273–285. doi: 10.1016/j.gloenvcha.2018.08.003

Haigh, I. D., Wadey, M. P., Wahl, T., Ozsoy, O., Nicholls, R. J., and Brown, J. M. (2016). Spatial and temporal analysis of extreme sea level and storm surge events around the coastline of the UK. *Sci. Data* 3:160107.

Hermans, L. M., Haasnoot, M., ter Maat, J., and Kwakkel, J. H. (2017). Designing monitoring arrangements for collaborative learning about adaptation pathways. *Environ. Sci. Policy* 69, 29–38. doi: 10.1016/j.envsci.2016.12.005

Hewitt, C., Mason, S., and Walland, D. (2012). The global framework for climate services. *Nat. Clim. Change* 2, 831–832. doi: 10.1038/nclimate1745

Hinkel, J., Church, J. A., Gregory, J. M., Lambert, E., Le Cozannet, G., Lowe, J., et al. (2019). Meeting user needs for SLR information: a decision analysis perspective. *Earth's Future* 7, 320–337. doi: 10.1029/2018ef001071

Hinkel, J., Lincke, D., Vafeidis, A. T., Perrette, M., Nicholls, R. J., and Tol, R. S. (2014). Coastal flood damage and adaptation costs under 21st century sea-level rise. *Proc. Natl. Acad. Sci. U.S.A.* 111, 3292–3297. doi: 10.1073/pnas.1222469111

Hunter, J. (2012). A simple technique for estimating an allowance for uncertain sea-level rise. *Clim. Change* 113, 239–252. doi: 10.1007/s10584-011-0332-1

Irwin, A. (2014). From deficit to democracy (re-visited). *Public Underst Sci.* 23, 71–76. doi: 10.1177/0963662513510646

Jacobs, K. L., and Street, R. B. (2020). The next generation of climate services. *Clim. Serv.* 20:100199. doi: 10.1016/j.cliser.2020.100199

Jongman, B., Ward, P. J., and Aerts, J. C. J. H. (2012). Global exposure to river and coastal flooding: long term trends and changes. *Glob. Environ. Change* 22, 823–835. doi: 10.1016/j.gloenvcha.2012.07.004

Kingsborough, A., Borgomeo, E., and Hall, J. W. (2016). Adaptation Pathways in practice: Mapping options and reade-offs for London's water resources. *Sustain. Cities Soc.* 27, 386–397. doi: 10.1016/j.scs.2016.08.013

Kool, R., Lawrence, J., Bell, R. G., and Drews, M. (2020). Preparing for sea-level rise through adaptive managed retreat. *Infrastructures* 5:90.

Kopp, R. E., Gilmore, E. A., Little, C. M., Lorenzo-Trueba, J., Ramenzoni, V. C., and Sweet, W. V. (2019). Usable science for managing the risks of sea-level rise. *Earth's Future* 7, 1235–1269. doi: 10.1029/2018ef001145

Kulp, S. A., and Strauss, B. H. (2019). New elevation data triple estimates of global vulnerability to sea-level rise and coastal flooding. *Nat. Commun.* 10:4844.

Kwadijk, J., Haasnoot, M., Mulder, J., Hoogvliet, M., Jeuken, A., Van der Krogt, R., et al. (2010). Using adaptation tipping points to prepare for climate change and sea level rise: a case study in the Netherlands. *Wiley Interdiscip. Rev. Clim. Change* 1, 729–740. doi: 10.1002/wcc.64

Lagmay, A. M. F., Agaton, R. P., Bahala, M. A. C., Briones, J. B. L. T., Cabacaba, K. M. C., Caro, C. V. C., et al. (2015). Devastating storm surges of Typhoon Haiyan. *Int. J. Disaster Risk Reduct.* 11, 1–12. doi: 10.1016/j.ijdrr.2014.10.006

Lawrence, J. (2015). *The Adequacy of Institutional Frameworks and Practice for Climate Change Adaptation Decision Making*. PhD thesis. New Zealand: Victoria University of Wellington.

Lawrence, J., and Haasnoot, M. (2017). What it took to catalyse a transition towards adaptive pathways planning to address climate change uncertainty. *Environ. Sci. Policy* 68, 47–57. doi: 10.1016/j.envsci.2016.12.003

Lawrence, J., and Manning, M. (2012). *Developing Adaptive Risk Management for Our Changing Climate. A Report of Workshop Outcomes Under an Envirolink Grant*. NZCCRI 2012 report 2012-1 June 2012. New Zealand: Victoria University of Wellington. .

Lawrence, J., Bell, R., and Stroombergen, A. (2019a). A hybrid process to address uncertainty and changing climate risk in coastal areas using dynamic adaptive pathways planning, multi-criteria decision analysis & real options analysis: a New Zealand application. *Sustain. Special Issue* 11, 1–18.

Lawrence, J., Bell, R., Blackett, P., Stephens, S., and Allan, S. (2018). National guidance for adapting to coastal hazards and sea-level rise: Anticipating change, when and how to change pathway. *Environ. Sci. Policy* 82, 100–107. doi: 10.1016/j.envsci.2018.01.012

Lawrence, J., Haasnoot, M., McKim, L., Atapattu, D., Campbell, G., and Stroombergen, A. (2019b). "From theory to practice: a timeline of interventions by a change agent with the developers and users of Dynamic Adaptive Policy

Pathways (DAPP)," in *Decisionmaking Under Deep Uncertainty: From Theory to Practice*, eds V. Marchau, W. Walker, and P. Bloeman (Berlin: Springer).

Le Cozannet, G., Rohmer, J., Cazenave, A., Idier, D., and van De Wal, R. (2015). Evaluating uncertainties of future marine flooding occurrence as sea-level rises. *Environ. Model. Softw.* 73, 44–56. doi: 10.1016/j.envsoft.2015.07.021

Lyard, F., Lefevre, F., Letellier, T., and Francis, O. (2006). Modelling the global ocean tides: modern insights from FES2004. *Ocean Dyn.* 56, 394–415. doi: 10.1007/s10236-006-0086-x

Matsumoto, K., Takanezawa, T., and Ooe, M. (2000). Ocean tide models developed by assimilating TOPEX/POSEIDON altimeter data into hydrodynamical model: a global model and a regional model around Japan. *J. Oceanogr.* 56, 567–581.

Merrifield, M. A., Genz, A. S., Kontoes, C. P., and Marra, J. J. (2013). Annual maximum water levels from tide gauges: contributing factors and geographic patterns. *J. Geophys. Rese. Oceans* 118, 2535–2546. doi: 10.1002/jgrc.20173

MFE (2017). *Coastal Hazards and Climate Change: Guidance for Local Government*. Wellington: Ministry for the Environment Publication ME1341.

Michael, D., and Chen, S. (2005). *Serious Games: Games That Educate, Train, and Inform*, 1st Edn. USA: Course Technology PTR.

Muis, S., Verlaan, M., Winsemius, H. C., Aerts, J. C. J. H., and Ward, P. J. (2016). A global reanalysis of storm surges and extreme sea levels. *Nat. Commun.* 7:11969.

Needham, H. F., Keim, B. D., and Sathiaraj, D. (2015). A review of tropical cyclone-generated storm surges: global data sources, observations, and impacts. *Rev. Geophys.* 53, 545–591. doi: 10.1002/2014rg000477

OECD (2019). *Responding to Rising Seas: OECD Country Approaches to Tackling Coastal Risks*. France: OECD Publishing.

Paulik, R., Stephens, S. A., Bell, R. G., Wadhwa, S., and Popovich, B. (2020). National-scale built-environment exposure to 100-year extreme sea levels and sea-level rise. *Sustainability* 12:1513. doi: 10.3390/su12041513

Priestley, R. K., Milfont, T. L., and Heine, Z. (2021). Public understanding of climate change-related sea-level rise. *PLoS One* 16:e0254348. doi: 10.1371/journal.pone.0254348

Pugh, D. T. (1987). *Tides, Surges and Mean Sea-Level*. Chichester: John Wiley & Sons.

Ranger, N., Reeder, T., and Lowe, J. (2013). Addressing 'deep' uncertainty over long-term climate in major infrastructure projects: four innovations of the thames estuary 2100 Project. *EURO J. Decis. Process.* 1, 233–262. doi: 10.1007/s40070-013-0014-5

Ray, R. D. (1999). *A Global Ocean Tide Model From TOPEX/POSEIDON Altimetry: GOT99.2. NASA Technical Memorandum TM-1999-209478* (Greenbelt, MD: Goddard Space Flight Center), 58.

Ray, R. D., and Foster, G. (2016). Future nuisance flooding at Boston caused by astronomical tides alone. *Earths Future* 4, 578–587. doi: 10.1002/2016ef000423

Román-Rivera, M. A., and Ellis, J. T. (2018). The king tide conundrum. *J. Coast. Res.* 34, 769–771. doi: 10.2112/jcoastres-d-18a-00001.1

Rueda, A., Vitousek, S., Camus, P., Tomás, A., and Espejo, A. (2017). A global classification of coastal flood hazard climates associated with large-scale oceanographic forcing. *Sci. Rep.* 7:5038.

Schmidt, J., Matcham, I., Reese, S., King, A., Bell, E., and Henderson, R. (2011). Quantitative multi-risk analysis for natural hazards: a framework for multi-risk modelling. *Nat. Hazards* 58, 1169–1192. doi: 10.1007/s11069-011-9721-z

Schneider, P., Lawrence, J., Glavovic, B., Ryan, E., and Blackett, P. (2020). The rising tide of adaptation action: comparing two coastal regions of Aotearoa-New Zealand. *Climate Risk Manag.* 30:100244. doi: 10.1016/j.crm.2020.100244

Simpson, N., Mach, K. J., Constable, A., Hess, J., Hogarth, R., and Howden, M. (2021). A framework for complex climate change risk assessment. *One Earth* 4, 489–501.

Stephens, S. A., Bell, R. G., and Haigh, I. D. (2020). Spatial and temporal analysis of extreme storm-tide and skew-surge events around the coastline of New Zealand. *Nat. Hazards Earth Syst. Sci.* 20, 783–796. doi: 10.5194/nhess-20-783-2020

Stephens, S. A., Bell, R. G., Ramsay, D., and Goodhue, N. (2014). High-water alerts from coinciding high astronomical tide and high mean sea level anomaly in the Pacific Islands region. *J. Atmos. Ocean. Technol.* 31, 2829–2843. doi: 10.1175/jtech-d-14-00027.1

Stephens, S. A., Bell, R., and Lawrence, J. (2017). Applying principles of uncertainty within coastal hazard assessments to better support coastal adaptation. *J. Mar. Sci. Eng.* 5:40. doi: 10.3390/jmse5030040

Stephens, S., Bell, R., and Lawrence, J. (2018). Developing signals to trigger adaptation to sea-level rise. *Environ. Res. Lett.* 13:104004. doi: 10.1088/1748-9326/aadf96

Sweet, W. V., and Park, J. (2014). From the extreme to the mean: Acceleration and tipping points of coastal inundation from SLR. *Earths Future* 2, 579–600. doi: 10.1002/2014ef000272

Tebaldi, C., Strauss, B. H., and Zervas, C. E. (2012). Modelling SLR impacts on storm surges along US coasts. *Environ. Res. Lett.* 7:014032.

Thomas, M., Pidgeon, N., Whitmarsh, L., and Ballinger, R. (2015). Mental models of sea-level change: a mixed methods analysis on the Severn Estuary, UK. *Glob. Environ. Change* 33, 71–82. doi: 10.1016/j.gloenvcha.2015.04.009

Conflict of Interest: The authors declare that the research was conducted in the absence of any commercial or financial relationships that could be construed as a potential conflict of interest.

Publisher's Note: All claims expressed in this article are solely those of the authors and do not necessarily represent those of their affiliated organizations, or those of the publisher, the editors and the reviewers. Any product that may be evaluated in this article, or claim that may be made by its manufacturer, is not guaranteed or endorsed by the publisher.

Copyright © 2021 Lawrence, Stephens, Blackett, Bell and Priestley. This is an open-access article distributed under the terms of the Creative Commons Attribution License (CC BY). The use, distribution or reproduction in other forums is permitted, provided the original author(s) and the copyright owner(s) are credited and that the original publication in this journal is cited, in accordance with accepted academic practice. No use, distribution or reproduction is permitted which does not comply with these terms.

frontiers in Marine Science

ORIGINAL RESEARCH
published: 09 August 2021
doi: 10.3389/fmars.2021.676452

Coastal Flooding in the Balearic Islands During the Twenty-First Century Caused by Sea-Level Rise and Extreme Events

Pau Luque[1,2]*, *Lluís Gómez-Pujol*[3], *Marta Marcos*[2,4] *and Alejandro Orfila*[2]

[1] Balearic Islands Coastal Observing and Forecasting System (SOCIB), Palma, Spain, [2] Mediterranean Institute for Advanced Studies (IMEDEA), Spanish National Research Council-University of Balearic Islands (CSIC-UIB), Esporles, Spain, [3] Earth Sciences Research Group, Department of Biology, University of Balearic Islands (UIB), Palma, Spain, [4] Department of Physics, University of Balearic Islands (UIB), Palma, Spain

Sea-level rise induces a permanent loss of land with widespread ecological and economic impacts, most evident in urban and densely populated areas. Potential coastline retreat combined with waves and storm surges will result in more severe damages for coastal zones, especially over insular systems. In this paper, we quantify the effects of sea-level rise in terms of potential coastal flooding and potential beach erosion, along the coasts of the Balearic Islands (Western Mediterranean Sea), during the twenty-first century. We map projected flooded areas under two climate-change-driven mean sea-level rise scenarios (RCP4.5 and RCP8.5), together with the impact of an extreme event defined by the 100-year return level of joint storm surges and waves. We quantify shoreline retreat of sandy beaches forced by the sea-level rise (scenarios RCP4.5 and RCP8.5) and the continuous action of storm surges and waves (modeled by synthetic time series). We estimate touristic recreational services decrease of sandy beaches caused by the obtained shoreline retreat, in monetary terms. According to our calculations, permanent flooding by the end of our century will extend 7.8–27.7 km^2 under the RCP4.5 scenario (mean sea-level rise between 32 and 80 cm by 2100), and up to 10.9–36.5 km^2 under RCP8.5 (mean sea-level rise between 46 and 103 cm by 2100). Some beaches will lose more than 50% of their surface by the end of the century: 20–50% of them under RCP4.5 scenario and 25–60% under RCP8.5 one. Loss of touristic recreational services could represent a gross domestic product (GDP) loss up to 7.2% with respect to the 2019 GDP.

Keywords: coastal flooding, beach erosion, sea-level rise, Western mediterranean, Balearic islands

OPEN ACCESS

Edited by:
Goneri Le Cozannet, Bureau de Recherches Géologiques et Minières, France

Reviewed by:
Claudia Wolff, University of Kiel, Germany
Deborah Idier, Bureau de Recherches Géologiques et Minières, France

***Correspondence:**
Pau Luque
pluque@socib.es

Specialty section:
This article was submitted to Coastal Ocean Processes, a section of the journal Frontiers in Marine Science

Received: *05 March 2021*
Accepted: *12 July 2021*
Published: *09 August 2021*

Citation:
Luque P, Gómez-Pujol L, Marcos M and Orfila A (2021) Coastal Flooding in the Balearic Islands During the Twenty-First Century Caused by Sea-Level Rise and Extreme Events. Front. Mar. Sci. 8:676452. doi: 10.3389/fmars.2021.676452

1. INTRODUCTION

Mean sea-level rise (MSLR) is one of the most certain consequences of human-driven climate change (Nicholls and Lowe, 2004). MSLR is quite relevant because of its potential impact over highly densely populated coastal zones, which also concentrate important natural and socioeconomic assets (Nicholls and Cazenave, 2010). It is expected that MSLR will partly submerge

low-lying areas and increase coastal exposure to extreme events. According to projections, these changes will differ substantially among different regions due to the spatially varying mechanisms contributing to MSLR (such as ocean circulation and steric modifications, variations in the wind patterns, and water mass redistribution resulting from gravitational changes due to mass load variations) (Slangen et al., 2014).

The impacts of MSLR in the Mediterranean region are particularly worrisome since the population fraction living up to 10 m above mean sea level (MSL) reaches 34%, in contrast to 10% worldwide (Lionello et al., 2012). Moreover, the touristic boom experienced during the 1960s promoted an enormous population and urbanization boost on Mediterranean coastal areas, which continues nowadays. The phenomenon is more intense in sandy coastal environments, which provide the natural resource that attracts tourists to the region (Roig-Munar et al., 2019).

Beaches are among the most vulnerable ecosystems to MSLR (Vitousek et al., 2017; Vousdoukas et al., 2020), facing shoreline erosion and coastal flooding. Under natural conditions, beaches can adapt to MSLR by retreating, provided enough landward space and sediment supply are available (Cooper et al., 2020). Instead, most Mediterranean beaches lose width (i.e., backshore surface narrowing) due to the lack of accommodation space caused by heavy urbanization.

Beaches play an important role as natural coastal defenses, so their retreat and eventual disappearance increase the hazard vulnerability of the coastal region. Moreover, beach narrowing implies a loss in beach environmental services, which are critical to the economy of tourist destinations, since recreational services are dependent on the beach backshore functional surface for recreational activities (e.g., Valdemoro and Jiménez, 2006; Jiménez et al., 2007).

In this work, we assess the physical impacts of MSLR along the sandy coast of the Balearic Islands archipelago (Western Mediterranean sea), adopting a regional approach. Projections of MSLR, outputs of basin-scale wind waves and storm surge hindcasts, as well as local high-resolution topographic information, are combined to assess the long-term (up to 2100) flooding and erosion along 160 km of sandy beaches. Coastal flooding results are classified and quantified in terms of land use to aid the development of future adaptation mechanisms. The Balearic Islands are a well-known tourist destination dependent on sun-and-beach recreation activities. Furthermore, an economic assessment of the loss in recreational services is provided, based on shoreline retreat results. This assessment translates into monetary terms the effects of climate change over those beaches, which may lead to future exploration on how the Balearic Islands economy and society will be affected by climate change.

The paper is structured as follows. Section 2 presents the geographical context of the Balearic Islands, their coastal areas, and beaches. Section 3 describes the methodology used to obtain the necessary data and perform the flooding, erosion, and monetary analyzes. Sections 4, 5 present the obtained results. Finally, section 6 reviews the effects of coastal flooding over the different land uses, and section 7 quantifies the economic impact of beach erosion.

2. STUDY SITE

The Balearic Islands (Western Mediterranean sea) form an archipelago composed of four major islands: Mallorca, Menorca, Eivissa, and Formentera; and some small unpopulated islets. They constitute a prolongation of the Baetic mountain range, more than 100 km away from the east coast of the Iberian Peninsula and oriented in a SW-NE distribution. Eivissa and Formentera constitute a differentiated subarchipelago known as the Pitiüses (**Figure 1**).

The archipelago has about 1,700 km of coastline, where 867 beaches make up 10% of that length. The typical Balearic beach appears sparsely along the coast, accommodated in the space allowed by a physiographic control. It is short and narrow; presents features such as rocks, cliffs, and islets; and tends to be at the bottom of a wall-sided embayment. However, 2.4% of the Balearic beaches are longer than 1 km (Gómez-Pujol et al., 2019). According to Gómez-Pujol et al. (2019), who assessed regional shoreline change at the Balearic Islands from 2002 to 2012, 80% of beaches are stable, meaning they do not erode nor accrete more than 50 cm per year.

According to Wright and Short 1984 classification, approximately 20% of the Balearic Islands' beaches are enclosed and present reflective conditions; 42% of them are semi-enclosed, exhibiting intermediate but reflective-skewed conditions; 27% are exposed, non-protected beaches (Gómez-Pujol et al., 2007). The remaining 11% corresponds to anthropic or artificial beaches (generated by the presence of a groin or a dike).

Regarding beach sediment, most beaches are composed of sand, although more than 20% of them are mixed or bigger-sediment beaches. There is no substantial sediment fraction of fluvial origin since water streams in the Balearic Islands are ephemeral. Moreover, the connection to the mainland undergoes depths greater than 800 m, so sediment has a local origin. About 50–75% of sediment is bioclastic, although up to 10–30% of it can be of lithoclastic origin depending on the availability of cliff-detached material (Gómez-Pujol et al., 2007). The leading producer of biogenic material is the endemic seagrass *Posidonia oceanica* (Fornos and Ahr, 1997). It colonizes nearshore zones all around the Balearic Islands and provides housing to a variety of marine species. It also stabilizes submerged beach sediment and attenuates wave energy (Infantes et al., 2009).

Concerning marine forcings, the Balearic Islands' beaches are microtidal: the spring tidal range is smaller than 25 cm (Orfila et al., 2005). Regional winds are moderate and have a short fetch. As a result, they produce moderately short period waves: the typical significant wave height (H_s) range is 0.1–1 m and the associated periods are between 3 and 6 s (Alvarez-Ellacuria et al., 2011). The mean incoming wave direction is from the north and the north-west, caused by the Pyrenees and the Ebro valley (see **Figure 1**). The most energetic conditions occur between December and January, and the least ones during June and August (Cañellas et al., 2007). However, frontogenetic activity is very relevant in the basin (i.e., many atmospheric fronts are generated in the region), producing a large variability in wave regime (Morales-Márquez et al., 2020).

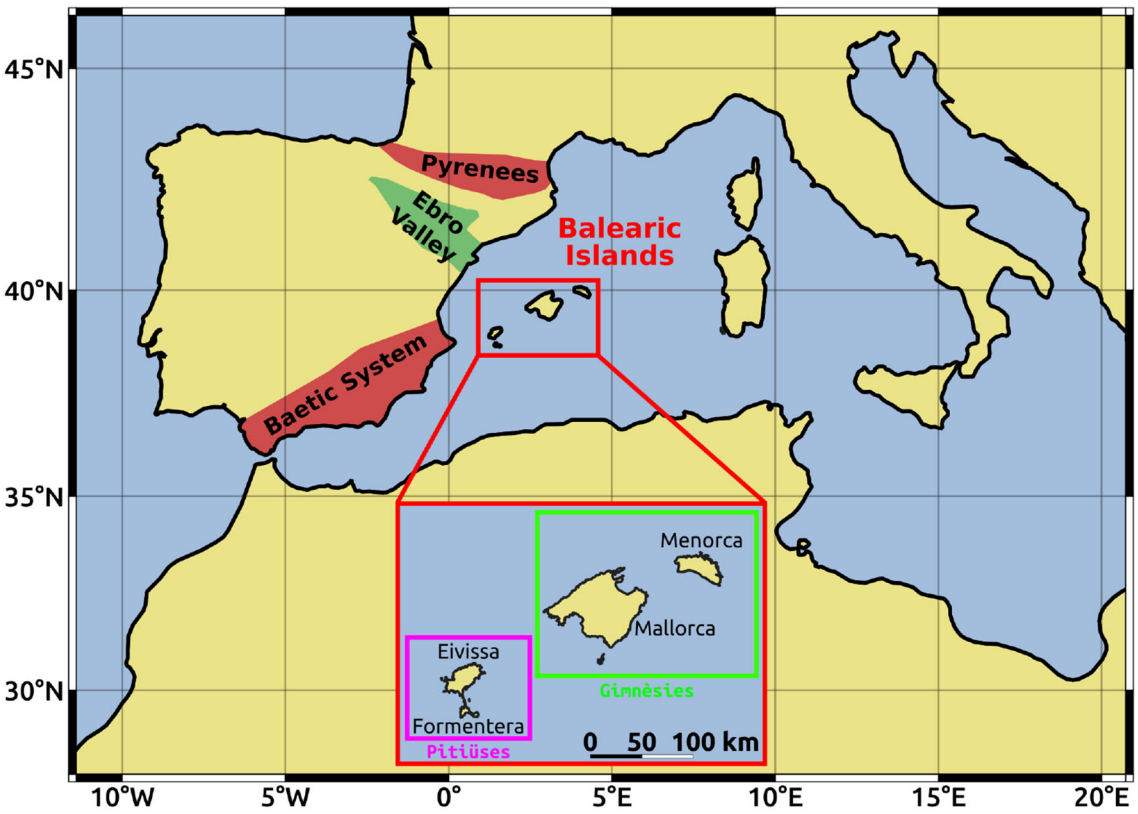

FIGURE 1 | Map of the Western Mediterranean with some geographical features are highlighted. Inset showing the structure of the Balearic Islands. Made with Natural Earth and Open Street Map, © OpenStreetMap contributors.

Beach morphodynamics is mainly controlled by wave climate: the cross-shore coordinate is controlled by wave height and wave period, while the alongshore also depends on wave energy flux. For the few cases with available data, beach planform is stable (meaning no significant changes occur in the wave energy flux direction) and presents a seasonal cross-shore variation, which consists of an aerial beach loss during severe storms and a gradual recovery during mild wave conditions (Enríquez et al., 2017; Morales-Márquez et al., 2018).

Beach tourism has a large impact on the economy of the Balearic Islands, accounting for a 35% of the total Gross Domestic Product (GDP) (Llompart et al., 2020). In 2019 the Balearic Islands received 16.4 million visitors, mostly seeking beach and recreation during summer. This quantity represents more than 10 times the amount of archipelago inhabitants and makes the Balearic Islands one of the most popular destinations in Europe (Llompart et al., 2020).

Regional coastal management has focused on providing leisure services and keeping the backshore functional for recreational uses, with activities such as terrain smoothing, mechanical cleaning, *Posidonia oceanica* beach wrack (Balestri et al., 2006) withdrawal, and sand nourishments (Roig-Munar et al., 2019).

In the following, we analyze beach erosion and coastal flooding associated with climate change over 192 beaches in Mallorca (ranging 56.9 km of coastline), 132 beaches in Menorca (ranging 21.5 km of coastline), and 140 beaches in the Pitiüuses (ranging 46.1 km of coastline). A complete list of beach names and locations is provided as **Supplementary Material**, as well as an image showing the distribution of the analyzed beaches (indicated as red dots in "beaches_and_reference_points_and_flooding_zones.png").

3. DATA AND METHODS

3.1. Regional Mean Sea Level, Storm Surges and Wind-Waves

The marine forcing around the Balearic Islands has been characterized under different scenarios at the regional scale. For flooding analysis, the magnitude of interest is the total water level, defined here as:

$$\mathrm{TWL} = \mathrm{MSL} + \mathrm{WS} + \mathrm{SS} \quad (1)$$

where MSL is the mean sea level projected for the different scenarios considered, WS the component associated with the wave setup, and SS the storm surge. The latter two consist of 3-h time series, which add higher-frequency variability. Astronomic tides were omitted in this study. The portion of wave run-up not associated with wave setup was not considered because we focus

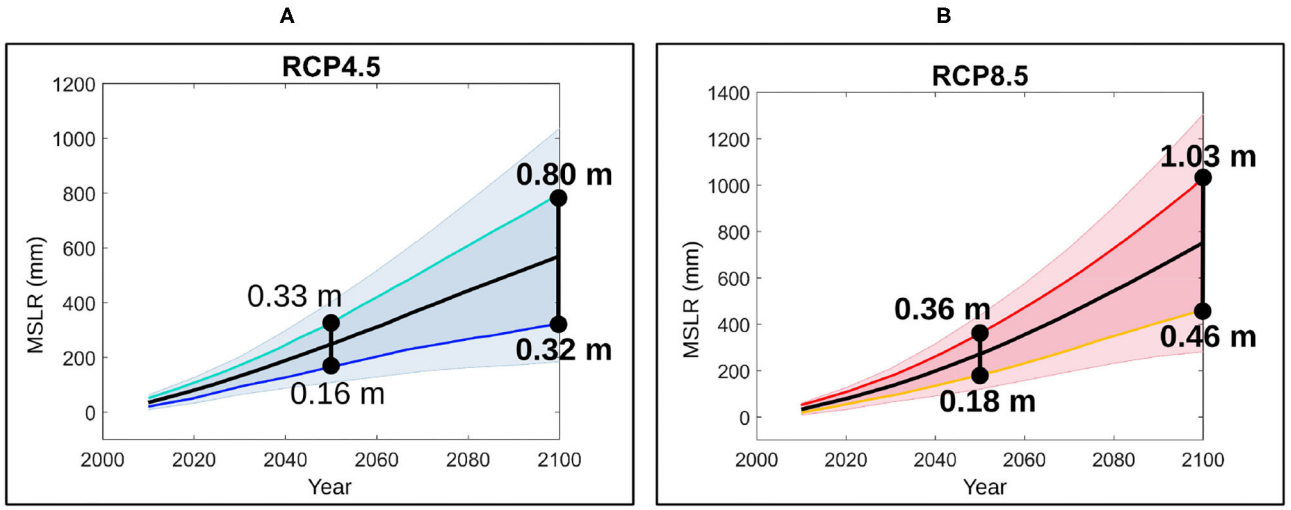

FIGURE 2 | MSLR projections under RCP4.5 **(A)** and RCP8.5 **(B)** climate scenarios, calculated according to Kopp et al. (2014). Black lines indicate the multi-model ensemble median and shadowed regions indicate the 17–83% and the 5–95% probability intervals. The four colored lines indicate the MSLR evolutions considered for the analysis of beach erosion, while the six values labeled in bold indicate the MSLR cases considered for the analysis of coastal flooding.

on coastal extreme water levels that cause temporary flooding at time scales of hours to days. On the contrary, wave run-up acts on shorter time scales around a mean value of sea level.

MSL projections were obtained following Kopp et al. (2014). **Figure 2** represents local MSLR projections for RCP4.5 and RCP8.5 climate scenarios. We considered the multi-model ensemble 17 and 83% probabilities, defining a central 67% probability interval ("likely" range in the IPCC report of Stocker et al., 2014).

For WS and SS, we used data from Mentaschi et al. (2017) to Vousdoukas et al. (2017), who computed waves with the wind-wave spectral model WaveWatch III (Tolman, 2002), and storm surges with the hydrodynamic model Delft3d-FLOW (Deltares, 2006), consistently forced by atmospheric pressure and surface wind fields from ERA-Interim reanalysis (hindcast spanning the period 1979–2014) and from 6 CMIP5 GCMs for the historical period (1970–1999) and future projections (2070–2099). The temporal sampling of the hindcast is 3 h for H_s and 6 h for SS.

Figure 3 shows the dynamic models' grid points around the Balearic Islands, depicting the differences in the 50-year return period of H_s and SS between the projections and the historical records. Multi-model mean differences for H_s are shown in panels **Figure 3A** (RCP4.5) and **Figure 3C** (RCP8.5), while multi-model standard deviations of the differences are shown in panels **Figure 3B** (RCP4.5) and **Figure 3D** (RCP8.5). The same information is provided for SS in panels **Figures 3E–H**. Results indicate that the dispersion of extreme values among the models is larger than the expected changes in most locations. Moreover, it is unlikely to extract a realistic uncertainty from such a limited number of models (the datasets we use for H_s and SS, from Vousdoukas et al. (2017), are obtained from 6 climate models: ACCESS1.0, ACCESS1.3, CSIRO-Mk3.6.0, EC-EARTH, GFDL-ESM2G, GFDL-ESM2M).

Consequently, given the unclear tendency and magnitude of the potential change plus the lack of precision in the uncertainty characterization, we decided not to account for any projected change in sea-level extremes. In other words, we assume that wave climate and storm surges will remain unaltered in the future. Therefore, we only used the hindcast outputs for both waves and storm surges, even to compute extremes. This way, we focus on the largest uncertainty (that from mean sea-level projections) and do not consider the others, such as those from storm surges and waves, which is in agreement with a fraction of the existing studies (e.g., Toimil et al., 2017b; Sanuy et al., 2018).

3.2. Wave Propagation

We selected 11 points (virtual buoys) that face all islands' orientations from the wave hindcast described above (see **Figure 4**). Deepwater conditions of those virtual buoys were propagated up to a set of reference points located about 30 m in depth, considered as representative of nearshore conditions. A map with the reference points locations (indicated as purple stars) is provided as **Supplementary Material**.

Due to the high computational cost of the 3-h 36-year-long wave hindcast numerical propagation, linear wave theory was applied to build time series of nearshore waves, as described in detail in the following.

Considering a wave propagating over a slowly varying bathymetry, before breaking and in the absence of wind and diffraction, its wave height H_r at depth h_r (before breaking) is related to its deepwater wave height H_0 as Dean and Dalrymple (1991):

$$H_r = H_0 \, K_s(T, h_r) \, K_r(\theta_0) \quad (2)$$

where K_s is the shoaling coefficient (which depends on local depth and wave period), and K_r is the refraction coefficient

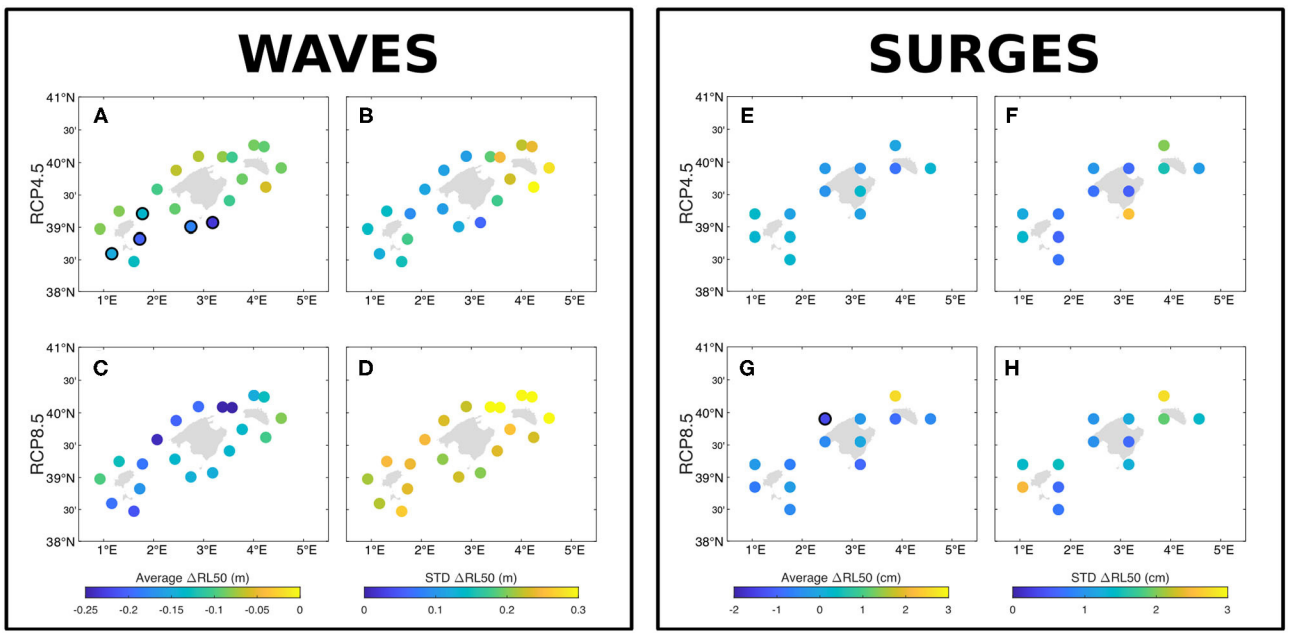

FIGURE 3 | Multi-model mean differences in 50-year return levels between projections (2070–2099) and historical (1970–1999) runs of Hs are shown in panels **(A)** (RCP4.5) and **(C)** (RCP8.5), while multi-model standard deviations of the differences are shown in panels **(B)** (RCP4.5) and **(D)** (RCP8.5). The same information is provided for SS in panels **(E)**, **(F)**, **(G)**, and **(H)**. Grid points circled black indicate that projected changes are greater than the standard deviation between models.

(which depends on the bathymetry and the direction of the wave at deep waters, θ_0). The shoaling coefficient relating the variation in wave height from deep to intermediate waters is given by:

$$K_s = \frac{T}{2\pi}\sqrt{\frac{g}{h_r}}\sqrt{\frac{k_r h_r}{1+\xi_r}} \tag{3}$$

where g is the acceleration of gravity, T is the wave period (which is not modified during propagation), h_r is the water depth at the propagation destination point, k_r is the wave wavelength, and $\xi_r = 2k_r h_r / \sinh 2k_r h_r$. In order to solve Equation (2), it is necessary to infer $K_r(\theta_0)$ and, since this equation relates the change in wave height between two specific (though arbitrary) locations, we need to do so for each pair of virtual buoy and reference point. The process to obtain K_r is explained in the following paragraphs. Hereafter, we consider all wave heights as significant wave heights (H_s), all periods as peak periods, and all directions as peak directions.

We classified all hindcast sea states of each deepwater virtual buoy (red dots in **Figure 4**) in eight octants (waves coming from the N, NE, E, SE, S, SW, W, and NW). Each octant's monthly maximum wave height was propagated (with their corresponding period and direction) over 500 m resolution meshes (shown in Equation 4) using the action balance model SWAN (Booij et al., 1999), by forcing the described sea states along all the mesh side of that virtual buoy and neglecting the effects of wind. Propagations were conducted independently for Mallorca, Menorca, and the Pitiüses, defining a total of 42,528 propagations (3 domains × 4 deepwater points × 8 octants × 443 months). An example of the SWAN configuration file, the code used to generate SWAN forcing files, and the code used to order all SWAN runs are included as **Supplementary Material**.

For each reference point and deep water virtual buoy, we computed the ratio $K_r = H_r/H_0 \cdot 1/K_s$ relating the wave height at the virtual buoy and the reference point. $K_r(\theta_0)$ was estimated by polynomial fitting, using the computed ratios for wave height of all octants at the same time. After a trial and error process, we found a fitting of the form:

$$K_r^{fit}(\theta_0) \equiv p_1\left(1-\left(\text{abs}\left(\frac{\theta_0 - p_2}{180}\right)\right)^{p_3}\right)^{p_4} \tag{4}$$

with p_1, p_2, p_3, and p_4 parameters to be adjusted, abs the absolute value and θ_0 (the virtual buoy peak direction) between −180° and +180°. **Figure 5** shows an example of fitting, which is representative of the majority of wave propagations. Four time series of wave height for each reference point were obtained applying Equation (2) and the fitted $K_r(\theta_0)$. The final 3-h H_s time series, representative of beach wave conditions, was built as the timewise maximum of its four reference points H_s time series. The corresponding T series was defined as the peak period associated with the selected H_s at each time. In line with the regional approach, wave trains were assumed to reach the coast perpendicularly. For this reason, nearshore wave direction time series were not computed. Also, to facilitate the understanding of this explanation, a graphical summary of the wave propagation process is presented as **Supplementary Material**.

Many studied beaches receive wave trains from multiple deep-water points (especially those oriented toward the computational

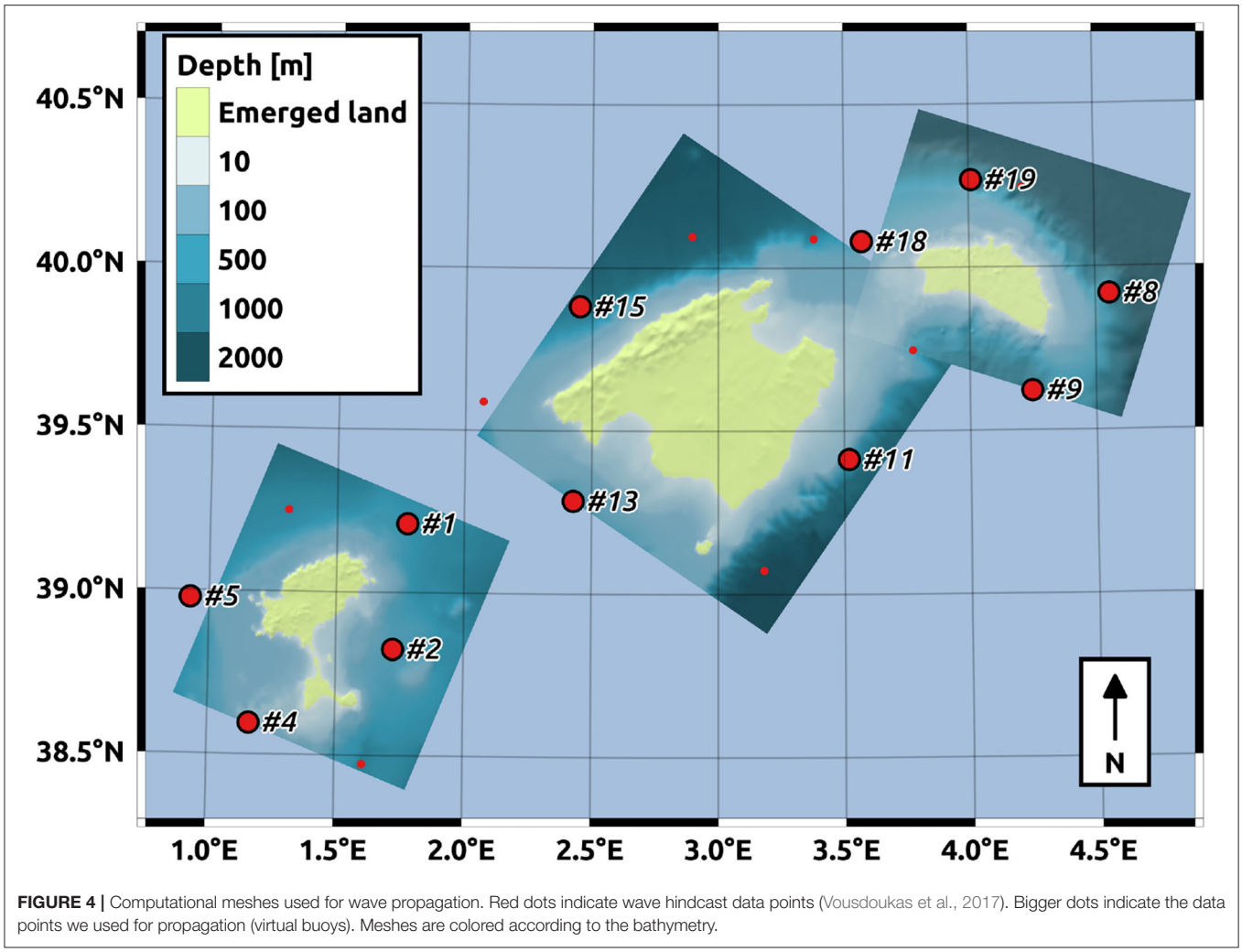

FIGURE 4 | Computational meshes used for wave propagation. Red dots indicate wave hindcast data points (Vousdoukas et al., 2017). Bigger dots indicate the data points we used for propagation (virtual buoys). Meshes are colored according to the bathymetry.

domain vertices). However, wave trains that impact an island on one side should not affect the opposite side. We could manually decide which deep-water points should be considered for each beach, but this procedure is subjective and arbitrary. Instead, we assumed that wave trains with any direction coming from any deep-water point could reach (potentially) all beaches and thus we computed all the associated K_r fittings. For the cases where the bulk of and island blocks wave train propagation, the obtained K_r fitting presents small values (near to zero), and the resulting nearshore wave heights associated with those wave trains (computed with Equation 2) are negligible. Since the final nearshore wave height is the maximum among the four propagated waves from deep-water points, our model accounts for shadowing intrinsically.

Regarding diffraction, SWAN does not solve diffraction directly but uses a phase-decoupled approach. This method provides the qualitative behavior of diffraction processes for a restricted set of conditions listed in the technical manual of SWAN (the SWAN team, 2019a). In principle, features large enough to be represented in the 500 m computational meshes induce diffraction in the SWAN model (which can be captured by Equation (2), since K_r is adjusted considering SWAN outputs). However, SWAN needs a grid size five to ten times smaller than the wavelength of a wave train to compute its diffraction adequately (Kim et al., 2017; the SWAN team, 2019b). On the contrary, smaller features are not represented in the computational meshes, and thus their diffraction can not be estimated. Unfortunately, high resolution bathymetries are only available for specific locations. Considering all these reasons, we did not use the diffraction option of SWAN (DIFFRAC). Handling of diffractive obstacles is out of the scope of our regional approximation and is left to future, local studies.

In order to validate the reference points' H_s, we compared our time series with the available *in situ* data at three coastal locations. The root mean square error at these locations ranges 0.20–0.28 m for H_s and 1.04–1.54 s for T, while the bias (generated time series with respect to measures) takes values between –0.16 and –0.05 m for H_s and between –0.29 and 0.01 s for T. The results and details of the comparison process, as well as the definition of the metrics used, are contained in **Appendix A**.

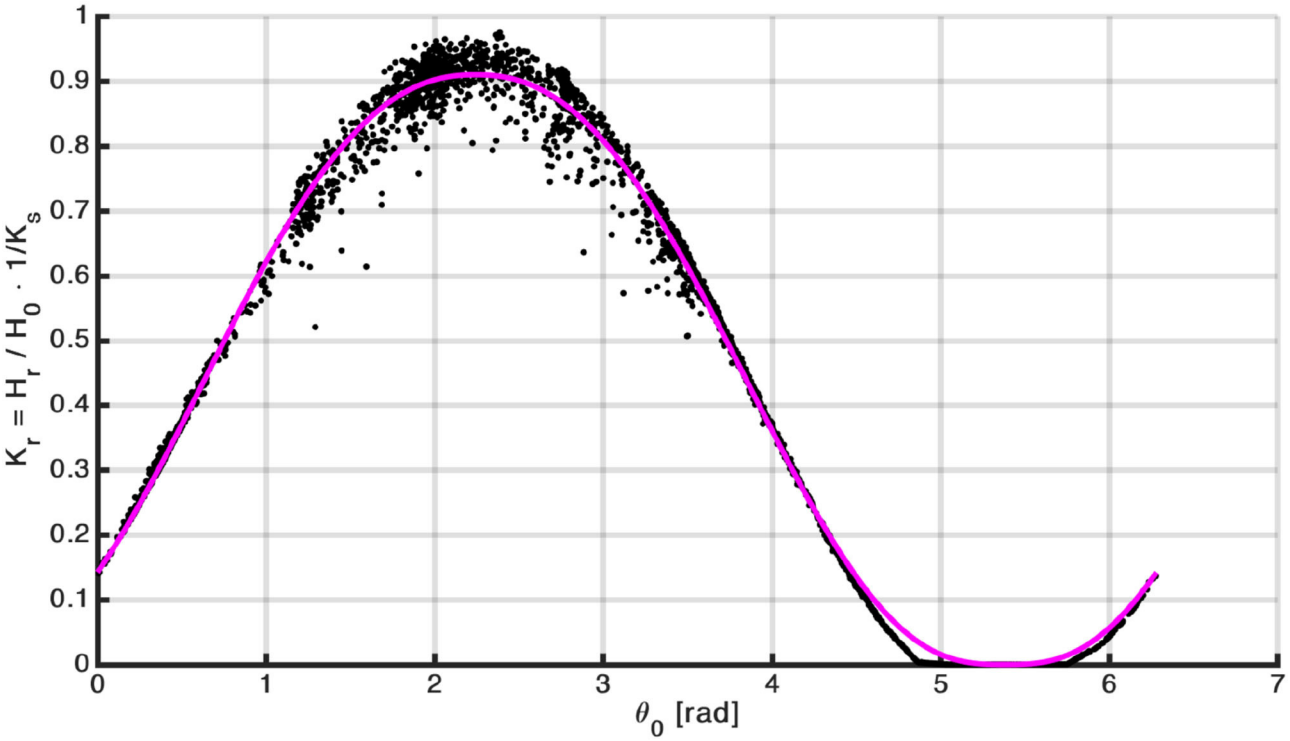

FIGURE 5 | Black dots represent refraction coefficients $K_r = H_r/H_0 \cdot 1/K_s$ computed for one pair of deep water point (virtual buoy) and one reference point *vs.* virtual buoy peak wave direction (θ_0) for each case. Magenta line indicates the polynomial fitting [Equation (4)] performed over those points.

3.3. Computation of the Coastal Flooding Extent

Flooding is conducted over multiple zones, selected by considering the beaches under study and the topography, using terrain with high elevation as boundaries. A map with the location of all the flooding zones is provided as **Supplementary Material**. We employed the topography of "Servei d'Informació Territorial de les Illes Balears" (SITIBSA), as given by its 2 m resolution Digital Surface Model (DSM). The DSM is derived from LiDAR data of 0.5 points/m^2 point density and whose vertical RMSE is at most 20 cm. It can be consulted at (https://www.caib.es/sites/sitibsa/es/n/mdt-70457/).

3.3.1. Permanent Flooding Induced by MSLR

The values of MSLR used to quantify the permanently flooded coastal areas in 2050 and 2100 were the 17th and 83rd percentiles of both RCP4.5 and RCP8.5 multi-model ensemble spreads (**Figure 2**).

Permanent flooding was modeled using a bathtub method. Classical bathtub models consider all areas with an elevation below a given MSL as flooded (Yunus et al., 2016; Teng et al., 2017), being computationally cheap and thus suitable for regional assessments. However, they usually neglect physical processes, hence reporting greater flooding extents (Seenath et al., 2016). Aiming to diminish those undesired effects, we performed a multi-step correction over the bathtub results.

The application of our bathtub approach is as follows. First, we use the DSM to create a binary mask under each MSL value, where each DSM pixel is classified as flooded or not flooded depending on whether its elevation is lower or higher than the MSL considered, respectively. This binary map is then manually corrected to ensure surface hydrological connectivity, characterizing those elements misrepresented in the DSM (irrigation channels, thin walls, etc.). Afterward, we identify which binary flooding mask pixels are connected to the sea through a flood-filling algorithm. Flood-filling algorithms take an input point and find all pixels presenting the same value of a certain variable (what is called the region of that pixel), surrounded exclusively by pixels that present a different value on that variable (Rogers, 1998). Here, the initial point is an arbitrary pixel over the open sea, while the region comprises those flooded pixels connected to the initial one by a path made entirely of flooded pixels. After flood-filling, all pixels outside the region are marked as not flooded. Finally, small isolated groups of non-flooded pixels were also classified as flooded since they usually indicate undesired effects over the elevation map. Specifically, we reclassified groups of $\leq$50 pixels ($\leq$200 m^2) if their elevation was lower than 20 cm above the MSL considered, and groups o of $\leq$100 pixels ($\leq$400 m^2) otherwise. For each MSL case, we defined a new coastline as all non-flooded pixels connected with flooded pixels. This coastline was the one considered during the temporary flooding simulations. The whole modified bathtub process is summarized in the **Supplementary Material**.

3.3.2. Temporary Flooding Induced by Coastal Extreme Sea Levels and MSLR

Coastal extreme sea levels arise from the combination of storm surges (SS) and wave setup (WS), i.e., WS + SS, over the corresponding MSL. The spatial extent of coastal flooding induced by coastal extreme sea levels was simulated, at each flooding zone, with the LISFLOOD-FP model (version 7.0.6, http://www.bristol.ac.uk/geography/research/hydrology/models/lisflood/), which is based on the shallow-water equations (Vreugdenhil, 1994). We performed 1-day simulations over the DSM described above, using the acceleration mode (i.e., neglecting convective acceleration but keeping the local acceleration term in the shallow-water equations), a constant Manning parameter of 0.06, and the default diffusion controlling weighting factor of 0.9 (which modifies the discharge time derivative to incorporate information about the discharge in surrounding cells in such a way that diffusive effects appear, thus reducing numerical instabilities) (de Almeida et al., 2012). An instantaneous sea-level time series was used to force the model along the coastline defined for every MSL value (the ones resulting from our permanent flooding estimation). To apply LISFLOOD-FP over the totality of each flooding zone (this is, including the regions between the beaches of the flooding zone), a single WS + SS time series was forced within each flooding zone, defined as the weighted mean of WS + SS from all the beaches inside this flooding zone, where the weights are the alongshore sizes of each beach. Following Stockdon et al. (2006), the WS of each beach can be estimated as:

$$\mathrm{WS} = 0.35\beta_f\sqrt{\mathrm{H_0 L_0}} = 0.35\beta_f \mathrm{T}\sqrt{\frac{g}{2\pi}\mathrm{H_0}} \quad (5)$$

with β_f being the foreshore slope of the beach, and L_0 the peak wavelength at deep waters. The value 0.35 is a constant calibrated using experimental data. We remark that for the second equality of Equation (5) we have assumed deep water conditions. Here, we propose a modification of this equation as:

$$\mathrm{WS} = \alpha\beta_f \mathrm{T}\sqrt{\frac{g}{2\pi}\mathrm{H_r}} \quad (6)$$

i.e., incorporating reference point's significant wave height (H_r), where α is a factor to be calibrated. H_r is used instead of H_0 to remove those deepwater conditions that do not reach the coast due to their propagation direction. Factor α is obtained by dividing Equation (5) by Equation (6) and using a characteristic value for the ratio H_r/H_0 according to the results of the numerical wave propagation (the value corresponding to the average angle of the H_r/H_0 slopes bigger than 0.05). Foreshore slope β_f is estimated using the distance between the coastline and the −10 m isobath, obtained from the nautical charts of the "Instituto Hidrográfico de la Marina" (this isobath is the shallowest one reported for the set of studied beaches in those nautical charts). We used a different β_f value for each beach, and within each beach we used the same value for all the studied cases (i.e., we assumed that β_f does not change with time or with MSLR).

Extreme values from the weighted WS + SS time series were characterized by fitting a Generalized Pareto Distribution to its exceedances over the 99th percentile. Independence among events was ensured by declustering with a time window of 72 h. The magnitude of the extreme water level event was defined as the fitted Generalized Pareto Distribution 100-year return level and its duration as the median duration of the exceedances (events exceeding the 99th percentile).

Finally, the time series forced over the flooding zone coastline was constructed as a triangular pulse over the corresponding MSL with an intensity and a duration as defined above (we keep sea level at the corresponding MSL after the end of the triangular pulse, until the simulation ends). The decision to use a triangular shape for the forcing is justified in **Appendix B**. An example of the LISFLOOD configuration for one of the flooding zones is provided as **Supplementary Material**.

Note that our LISFLOOD setup was not validated in the flooding zones studied due to the lack of measurements. Instead, we performed a sensitivity analysis in one flooding zone (the one presented in of the **Supplementary Material**). In our case, the only free parameter is the Manning coefficient (since all the other inputs are study design decisions that have been already discussed: mean sea level; extreme event shape, duration, and intensity). The Manning coefficient was varied from 0.006 to 0.6 with a change in the flooding extent lower than 0.04% for MSLR=0; 0.1% for MSLR=18 cm; 5.9% for MSLR=32 cm; 6.9% for MSLR=36 cm; 23.6% for MSLR=46 cm; 4.6% for MSLR=80 cm; and 0.36% for MSLR=103 cm (all of them with respect to the original simulations with Manning coefficient of 0.06). Changes are small except for the case of MSLR=46 cm, coinciding with a big area presenting an elevation near to this value and thus being more sensitive to the Manning coefficient.

3.3.3. Filtering of Water Bodies

Flooding masks were combined with the 2018 Corine Land Cover database, available through Copernicus services (https://land.copernicus.eu/pan-european/corine-land-cover/clc2018). The categories considered were "artificial surfaces" (LU-ART, which include urban areas), "agricultural areas" (LU-AGR), "seminatural areas and forests" (LU-SAF), and "wetlands" (LU-W). We omitted the areas categorized as "water bodies" (LU-WB).

Total flooded areas reported in this manuscript are the sum of the flooding extents categorized as one of the four land-uses we considered. Inner water bodies are not well characterized in the DSM because they are not identified as such. Moreover, interpolation errors occur over them. By removing the areas marked as LU-WB in the Corine database those effects are reduced, since those areas currently flooded (permanently or periodically) are not included in the results.

3.4. Computation of Beach Erosion

Balearic Islands beach sediment has a biogenic origin, without river income. Thus, all the sediment involved in beach erosion and accretion is already within the system. Under these conditions, morphodynamic variability can be split in the cross-shore and alongshore directions. Beaches accommodate

maximizing wave energy dissipation, rotating until its alongshore direction is normal to the mean wave energy flux at the breaking point. Cross-shore variability (i. e., beach profiles) is the response to waves (shorter time scales) and to MSL (longer time scales).

That being said, the most accurate way to evaluate a specific beach is to perform a whole 3D simulation taking into account all changes inherent to the different scenarios. However, that is not affordable, neither for a specific beach (up to the 2100 horizon) nor for the regional approach we adopted. Therefore, we were forced to assume some simplifications to the problem.

In the first place, as stated in section 2, only 27% of the Balearic Islands' beaches are open (and thus can freely exchange sediment with its surroundings). Accordingly, we neglected the alongshore transport between the beach and its surroundings. In the second place, generalized information about wave energy flux does not exist, so beach planform changes can not be assessed; moreover, beach planform is stable for the few cases where this information is available. Therefore, alongshore averaged cross-shore beach width was used. In the third place, the number of recreational activities occurring at beaches depends directly on the aerial beach surface, equivalent through the alongshore beach size to the average cross-shore beach width. Since we focused on an alongshore-averaged magnitude, internal alongshore transport (i.e., occurring between the beach and itself).

Because of these reasons, we quantified beach erosion as the average cross-shore beach width recession. Classically, the Bruun Rule (Bruun, 1962) has been used for this purpose. It indicates that the beach tends to an equilibrium state whose changes in shoreline can be described (in the form presented by Dean, 1991) as:

$$\Delta y = -W_* \cdot \frac{S}{B + h_*} \tag{7}$$

where Δy is the (seawards) change in equilibrium beach shoreline position with respect to a reference sea level, S indicates the elevation of sea level with respect to that reference, B is the berm height, h_* is the breaking depth, and W^* is the active profile width, computed as $W^* = (h_*/A)^{3/2}$ (Dean, 1991), where $A = 0.067\,\omega_s^{0.44}$, with ω_s being the settling velocity of mean sand diameter (D50) (van Rijn, 1984). According to similarity theory, the following relation holds at the breaking point: $H_b/h_* = \kappa$, where H_b the wave height over breaking depth, and κ is the breaker index (which we assumed to be 0.71).

As stated in section 2, most of the Balearic Islands' beaches lack accommodation space, either because of heavy urbanization or because of natural physiographic controls (pocket beaches in front of cliff walls). In line with our regional approximation, we assumed the backshore of all beaches would remain fixed, so shoreline position changes equal to cross-shore beach width changes ($\Delta y = \Delta w$). Taking this into consideration, using the current mean sea level (MSL_0) as the sea-level reference, and neglecting changes in sea level other than MSLR, Equation (7) can be rewritten as:

$$\Delta w = w - w_0 = -\left(\frac{H_b}{\kappa A}\right)^{3/2} \cdot \frac{MSL - MSL_0}{B + H_b/\kappa} \tag{8}$$

w_0 is the equilibrium beach width for the case $MSL = MSL_0$ and w the equilibium beach width for a MSLR equal to $MSL - MSL_0$.

Bruun's Rule has some limitations since it assumes a constant wave climate, a constant sediment budget, and the existence of a depth of closure, and also neglects the effect of longshore sediment transport gradients. However, given the nature, dynamics and physiography of the analyzed beaches, as well as the regional context of the study, Bruun's Rule provides an acceptable first approach to the expected beach width changes.

Regarding to the rest of variables needed, according to Gómez-Pujol et al. (2019) beaches in the Balearic Islands are in equilibrium, and so we assumed w_0 as the one measured by the most recent orthographic aerial photographs. For each beach, we estimated a single B value considering the LiDAR point cloud used to generate SITIBSA's DSM. Wave height was computed at different depths by propagating the wave height time series of the beach reference point (H_r), first to deep waters and then to the desired depth. We accomplished that using Equation (2) and assuming K_r equal to one.

Following Toimil et al. (2017a), we applied Equation (8) to a set of multiple synthetic time series of H_b, thus producing multiple potential realizations of beach width evolution. Our synthetic H_b time series are statistically consistent with the corresponding reference point time series at every site (*i. e.*, they have the same statistics but with a different chronology). Since the set of synthetic time series generated is representative of the potential future conditions, the resulting realizations of beach width time series can be used to estimate the statistics of the future beach width evolution. The details of the synthetic time series generation process and its validation are described in **Appendix C**.

For each beach, we generated 500 synthetic H_b time series and inputted them into Equation (8), in combination with the projected evolutions of MSLR corresponding to the 17 and 83% of RCP4.5 and RCP8.5, obtaining 500 time series of w for each MSLR evolution, from which mean beach width evolution and standard deviation were computed. Since both metrics presented a strong seasonality, resulting time series were filtered with a 5-year running average.

3.5. Beach Recreational Services Monetary Valuation

Beach narrowing due to erosion resulting from our analyzes was used to estimate the decrease or loss of beach recreational services in monetary terms. We adopted the results presented in Enríquez and Bujosa Bestard (2020), who measured the economic impact of beach loss on beach tourism through choice experiments focused on the Balearic Islands. Other works also assessed the recreational services provided by beaches at the Balearic Islands (Pérez-López and Roig-Munar, 2007; Riera et al., 2007), but their surveys were not focused on climate change impacts or on the tourists that comprise the largest portion of yearly beach users in the entire archipelago. Enríquez and Bujosa Bestard (2020) specifically assessed tourists' willingness to pay for the introduction of policies aimed at reducing climate change impacts.

Choice experiment methodology is a stated preference non-market valuation methodology based on experimental surveys. In these surveys respondents are presented with different scenarios describing specific changes in the levels of the good under valuation (in this case the surface of aerial beach) and are asked to choose the scenario providing the highest level of well-being. This is a standard method to assess economic impacts of climate change (Shoyama et al., 2013; Andreopoulos et al., 2015; Remoundou et al., 2015; Rodrigues et al., 2016; Chaikaew et al., 2017; Torres et al., 2017; Faccioli et al., 2019).

In their assessment, they estimated that tourists are willing to pay 1.23 €/day of stay (on average) to recover one meter of beach shoreline to compensate beach retreat due to MSLR. Using this value we estimated the loss of beach recreational value in monetary terms. In this regard, we combined the data obtained in section 3.4 with the Enríquez and Bujosa Bestard (2020) results, as well as with different attributes of each beach (beach location, type, accessibility, *etc.*) to determine the beach recreational economic value loss (BREV) as follows:

$$\mathrm{BREV_n}\left(\frac{€}{\mathrm{yr}}\right) = \frac{\mathrm{WEBS_n}\left(\mathrm{m^2}\right)}{\sum_n \mathrm{WEBS_n}\left(\mathrm{m^2}\right)} \cdot \mathrm{TOUR_n\ (tourists)} \cdot \mathrm{WTPV}\left(\frac{€}{\mathrm{m \cdot yr}}\right) \cdot \mathrm{ER_n\ (m)} \quad (9)$$

where $\mathrm{BREV_n}$ is the loss of beach recreational economic value for a specific beach, $\mathrm{WEBS_n}$ is the weighted effective beach surface for a specific beach, $\mathrm{TOUR_n}$ is the number of tourists (corresponding to the 2019 official estimate of the Balearic Islands Institute of Statistics, IBESTAT), WTPV is the amount of money each tourist is willing to pay in constant monetary units for an individual day of stay considering the average stay length of 6 days (Llompart et al., 2020), and $\mathrm{ER_n}$ is the averaged shoreline retreat for each beach obtained in section 3.4.

Beaches in the Balearic Islands tend to be high-frequented (Mas Parera and Blázquez-Salom, 2005; Roig-Munar et al., 2020). In a small island (as each one of the Balearics, with travel times from one side to another lower than 1 h) tourists move from one beach to another. For this reason, the number of users is mainly related to the available dry beach surface. The articles cited above also indicate that the most frequented beaches are those that are in front of tourist stations and also those iconic virgin beaches publicized in touristic guides and brochures. Therefore, according to this descriptive data, we obtain the weighted effective beach surface for a specific beach by means of:

$$\mathrm{WEBS_n}\left(\mathrm{m^2}\right) = \mathrm{S_n}\left(\mathrm{m^2}\right) \cdot \mathrm{F_{type}} \cdot \mathrm{F_{access}} \quad (10)$$

where S_n is the beach surface for a specific beach; F_{type} is a correction factor that introduces the typology of beach that, ranging from 0.5 for isolated beaches to 1 for urban beaches and isolated iconic beaches (**Table 1**), as the two latter ones comprise most of the demand (Roig-Munar et al., 2020); F_{access} is a correction factor related with the beach accessibility (access, public transport, parking facilities) and beach recreation services (beach cleaning, sun huts, lifeguards...), creating a variation from 0.05 to 1 according to **Table 1**.

4. RESULTS FOR COASTAL FLOODING

The results of areas permanently and temporarily flooded due to MSLR combined with storm surges and extreme waves are summarized in **Table 2**, separately for each region, and classified by its land use. Note that temporary flooding due to extreme events is indicated as increases with respect to permanent flooding induced by MSLR only. Total extent of flooding in the case of extreme events is the addition of the two. Also, note that results are listed in terms of increases in MSL rather than in time horizons. All values reported in the table correspond

TABLE 1 | Location-based beach correction factor typologies and correction factors derived from beach accessibility and quality services.

Factor	Category	Value	Description
F_{type}	Urban beaches	1	Natural or artificial beaches fronting urban settlements, backed by promenades or boulevards. Lack of foredunes or coastal dunes in the backshore.
	Semi-urban beaches	0.8	Beaches close to urban settlements that can maintain or not their pristine features. They can front cliff walls, stream mouths, weakly developed dunes, or promenades.
	Isolated iconic beaches	1	Pristine beaches far away from urban settlements recognized and publicized in tourist brochures, guides, journals, webs, etc.
	Isolated beaches	0.5	Pristine beaches far away from urban settlements.
F_{access}	Category 1	1	Safe and easy access. Parking facilities. Lifeguard and cleaning services. Amenities and complementary offer. High-quality sand, environment, and water.
	Category 2	0.8	Safe and easy access. Parking facilities. Lifeguard and cleaning services. Amenities and complementary offer. High-quality sand, environment, and water.
	Category 3	0.5	Easy access. Quality services absent.
	Category 4	0.5	Usual access. Parking facilities. Lifeguard and cleaning services. Medium-quality sand, environment, and water.
	Category 5	0.3	Usual access. Parking facilities. Cleaning services. Medium-quality sand, environment, and water.
	Category 6	0.05	Difficult access. Quality services absent.

to either mid or late twenty-first century (see **Figure 2** for the equivalence between timing and value of MSLR). The complete set of flooding extent masks can be consulted online at https://ideib.caib.es/impactes_costa_canvi_climatic/. Finally, note that those are estimates for the case that no action is taken. **Figure 6** shows the permanent flooding extent for a MSLR of 103 cm over the entire archipelago, classified by municipalities.

The area permanently flooded increases linearly with MSLR. Namely, in Mallorca flooding extent changes 24 ha/cm of MSLR (R^2 of 0.977), in Menorca 2 ha/cm of MSLR (R^2 of 0.975) and at

TABLE 2 | Coastal flooding extent (in hectares) resulting from the permanent and temporary flooding analysis.

			MEAN SEA-LEVEL RISE (cm)						
Island	**Flooding type**	**Land Use**	**0**	**18**	**32**	**36**	**46**	**80**	**103**
Mallorca	Permanent (ha)	Artificial surfaces	0	16	31	42	59	209	329
		Agricultural areas	0	3	16	20	56	171	347
		Seminatural areas, forest	0	8	14	17	20	76	131
		Wetlands	0	391	598	638	773	1533	1883
		ALL	**0**	**418**	**659**	**717**	**909**	**1989**	**2690**
	Extreme (ha)	Artificial surfaces	46	62	89	90	112	150	166
		Agricultural areas	4	3	4	4	7	19	30
		Seminatural areas, forest	25	26	30	29	36	46	52
		Wetlands	10	0	5	8	11	12	66
		ALL	**85**	**92**	**128**	**131**	**165**	**226**	**314**
Menorca	Permanent (ha)	Artificial surfaces	0	2	4	4	6	14	25
		Agricultural areas	0	0	3	4	8	15	36
		Seminatural areas, forest	0	15	31	34	43	97	130
		Wetlands	0	1	17	18	23	27	28
		ALL	**0**	**18**	**54**	**61**	**80**	**153**	**219**
	Extreme (ha)	Artificial surfaces	11	13	16	16	17	20	22
		Agricultural areas	2	6	9	9	18	24	27
		Seminatural areas, forest	38	45	43	43	43	46	43
		Wetlands	1	11	2	2	2	1	4
		ALL	**52**	**74**	**70**	**70**	**81**	**91**	**95**
Pitiüses	Permanent (ha)	Artificial surfaces	0	5	8	11	12	36	62
		Agricultural areas	0	1	1	3	3	44	83
		Seminatural areas, forest	0	13	20	24	28	61	96
		Wetlands	0	31	40	49	60	487	498
		ALL	**0**	**50**	**69**	**87**	**104**	**628**	**740**
	Extreme (ha)	Artificial surfaces	19	23	27	26	30	36	49
		Agricultural areas	3	4	6	6	10	31	38
		Seminatural areas, forest	85	88	97	97	103	118	121
		Wetlands	14	18	42	65	138	3	3
		ALL	**120**	**133**	**173**	**194**	**282**	**188**	**210**
TOTAL	Permanent (ha)	Artificial surfaces	0	22	42	57	78	258	417
		Agricultural areas	0	4	20	26	67	230	466
		Seminatural areas, forest	0	36	64	76	92	234	357
		Wetlands	0	423	656	705	857	2047	2409
		ALL	**0**	**485**	**781**	**864**	**1094**	**2770**	**3649**
	Extreme (ha)	Artificial surfaces	76	98	132	132	159	206	237
		Agricultural areas	8	13	18	19	35	74	94
		Seminatural areas, forest	147	160	170	169	183	209	216
		Wetlands	25	29	50	74	151	16	73
		ALL	**257**	**299**	**371**	**394**	**528**	**505**	**620**

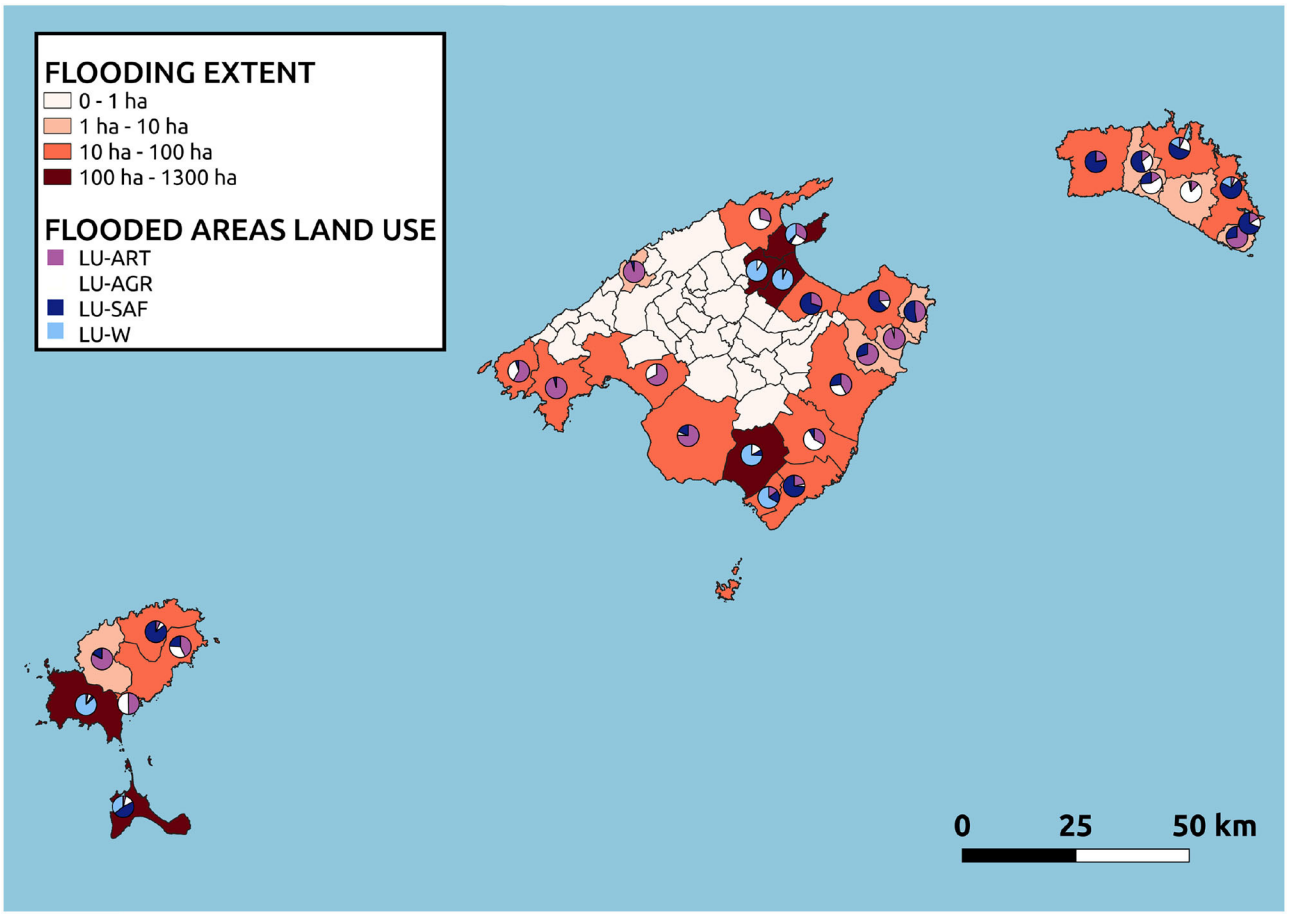

FIGURE 6 | Permanent flooding extent (classified by municipality) for the case of 103 cm of MSLR, with information on land use of flooded areas. Each municipality polygon is colored according to its flooding extent, and has a circular symbol containing the fractions of land use composing that extent (LU-ART, LU-AGR, LU-SAF, LU-W; see Section 3.3.3 for the land use classification).

the Pitiüses the rate reaches 33 ha/cm of MSLR (R^2 of 0.956). Due to the different coastal lengths, absolute values of flooded extents are clearly dissimilar, ranging between areas up to thousands of hectares in Mallorca to a few hundreds of hectares in Menorca and Pitiüses, for MSLR above 0.5 m. Temporary flooding caused by coastal extreme sea levels increases mostly in Mallorca and Pitiüses (100–300 ha) and is smaller in Menorca, due to the more elevated coastal land.

In terms of relative impacts of flooding, by mid-century and under RCP8.5 (MSL between 18 and 36 cm), permanent flooding reaches between 4.9 and 8.6 km^2 (0.10–0.17% of the archipelago surface), while extreme flooding adds an extra loss of 0.06 –0.07% to the archipelago land surface. This represents an increase of 16–53% with respect to the flooding extent of an extreme event occurring today. We expect these quantities to be very similar to those of RCP4.5 for the same time horizon.

Likewise, by the end of the century, under the RCP4.5 scenario (MSLR between 32 cm and 80 cm), the permanent flooding extent would fall between 7.8 and 27.7 km^2 (0.16–0.56% of the archipelago surface). Extreme flooding represents an extra 0.07–0.10% of archipelago surface, which is 44–96% bigger than the extreme flooding extent of the present. Under RCP8.5 scenario (46 cm and 103 cm limits) permanent flooding can extend up to 10.9–36.5 km^2 (0.20–0.70% of the archipelago surface) and extreme flooding adds 0.11–0.12%, an increase of 105–141% with respect to the extreme flooding that may occur nowadays.

5. RESULTS FOR BEACH EROSION

A compilation of the results for all the beaches is represented in **Figure 7** as the CDF of the relative widths with respect to their present state for mid and late twenty-first century. Note that those are estimates for the case that no action is taken.

Around 2050, beach width distributions obtained for the lower and upper limits of RCP4.5 and RCP8.5 are similar. In Mallorca and Menorca around 3–15% of beaches are projected to lose half of their current surface, 0% in the Pitiüses. Between 25 and 55% of the beaches are projected to reduce their present area by less than 10%. Changes are significantly larger by the end of the century. Under the RCP4.5 scenario up to 10% of the Balearic Islands' beaches will lose 90% of the current area.

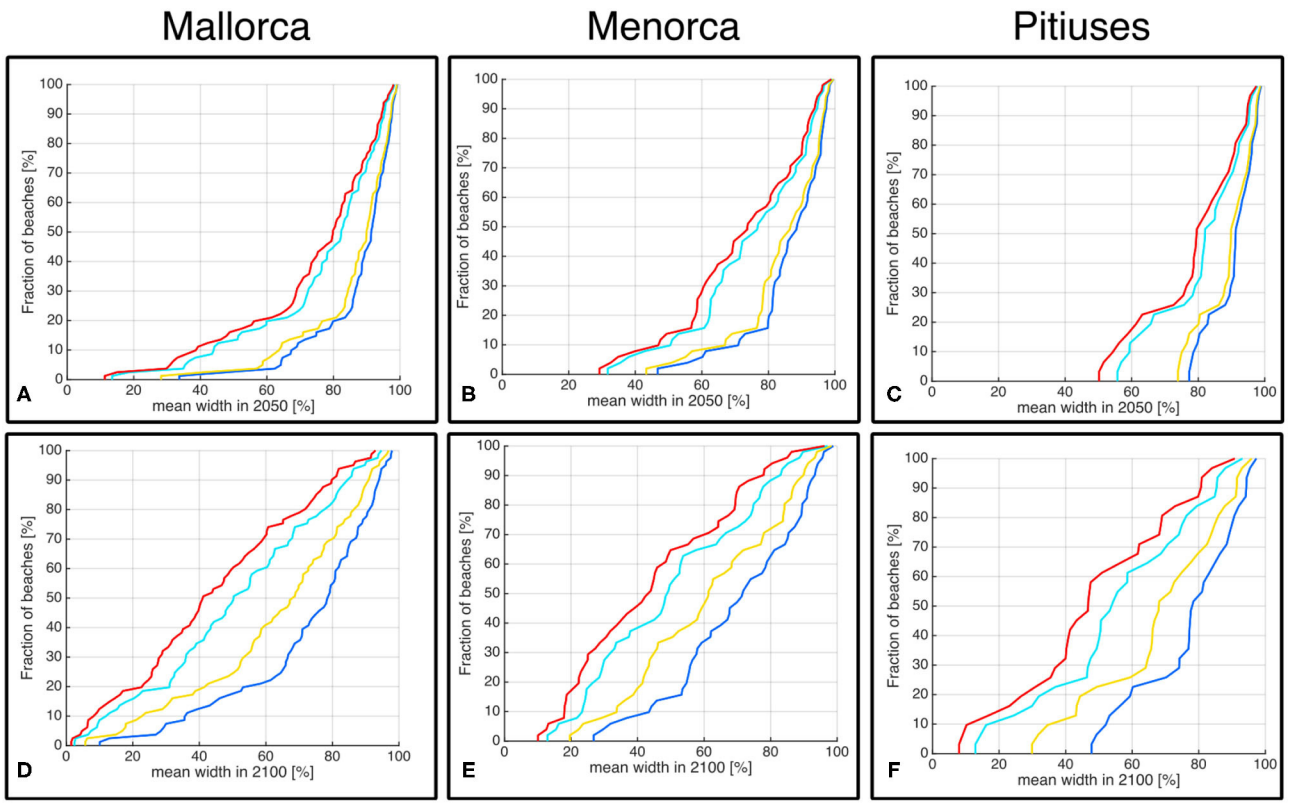

FIGURE 7 | Cumulative density functions (CDF) of beach relative mean width (referred to nowadays width), computed from the time averaged mean evolutions of each beach according to the MSL forcing of the RCP4.5 and RCP8.5 scenarios (lower and upper bounds). Each panel line corresponds to a MSL evolution, using the color code presented in **Figure 2**. **(A–C)** Use data extracted from year 2050, and **(D–F)** Use data from 2100. CDFs are computed for beaches of Mallorca **(A,D)**, Menorca **(B,E)** and the Pitiüses **(C,F)**.

20–50% of the beaches in Mallorca, 15–50% in Menorca and 5–40% in the Pitiüses are projected to reduce their current size by half. In the worst-case scenario, under RCP8.5 by 2100, up to 15% of the archipelago beaches are expected to lose more than 90% of their surface, while 25–60% of beaches in Mallorca, 35–65% of beaches in Menorca and 23 –60% of beaches in the Pitiüses will lose more than 50% of their current surface. In order to illustrate the spatial distribution of beach erosion, **Figure 8** shows the beach surface loss between the present and the 2100 RCP8.5 upper limit of MSLR projection classified by municipality.

6. COASTAL FLOODING IMPACTS ON LAND USE

The classification of the extent of flooded areas by their land use, according to Corine 2018, is listed in **Table 2**. Note that those are estimates for the case that no action is taken. Our analyzes demonstrate that wetlands are disproportionally affected by coastal flooding in the Balearic Islands, being clearly dominant in Mallorca and Pitiüses. Overall, these areas represent 65–85% of the total permanently flooded surface. In Menorca, semi-natural areas and forests are the most impacted. Flooding of coastal wetlands increases fast as MSL rises up to 0.5 m, due to their typical low elevation gradient. Above this value these impacts stabilize, indicating that the totality of coastal wetlands is lost. It must be mentioned that we have neglected the dynamic response of coastal wetlands, which may accrete in response to mean sea-level changes, depending on the rising rate and the space availability for sediment accumulation (Schuerch et al., 2018). The latter is rather limited in our case studies, though, but still our estimates should be considered as an upper bound for the given MSLR values.

The areas most affected by coastal flooding, coinciding with the low-lying regions, are formed essentially by lagoons and salt evaporation ponds. There are five flooding zones that account for 85% of the extent of total permanent flooding in the worst-case scenario (MSLR of 103 cm). These are concentrated in the North of Mallorca Island (Alcúdia, Pollença), the South of Mallorca (es Trenc), and parts of Eivissa and Formentera. Therefore, coastal flooding impacts are unevenly distributed around the archipelago. These results are relevant for public policies regarding the prioritization of most vulnerable coastal areas to MSLR.

Frequently, large areas are projected to be flooded because of the presence of a narrow connection to the sea, such as channels, torrents, or salt work entrances. This is illustrated in

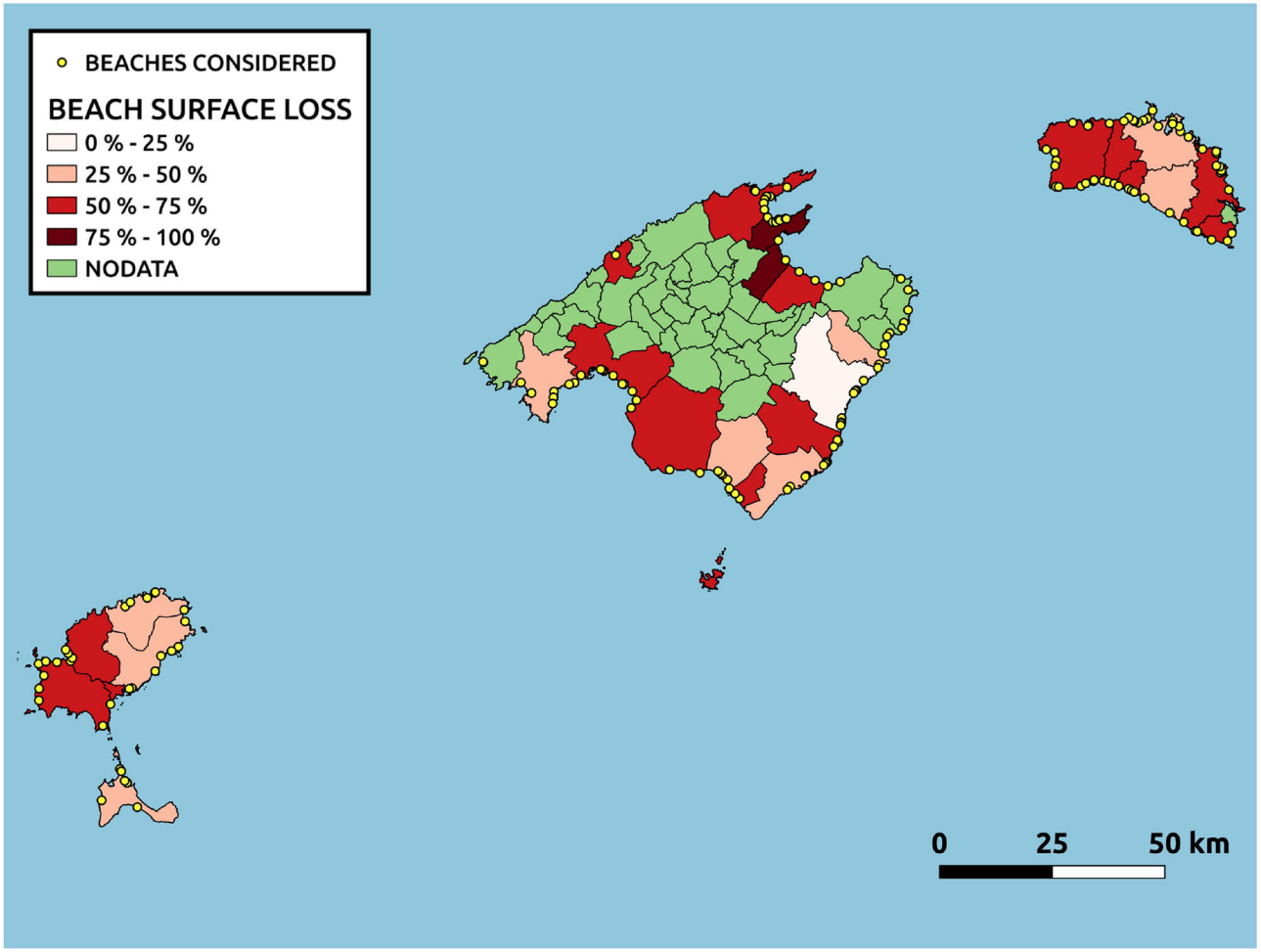

FIGURE 8 | Aerial beach surface loss by 2100 under the RCP8.5 upper limit of MSLR, relative to that of today, classified by municipality. Beaches considered are also shown.

Figures 9A,B, where Port of Alcúdia flooding zone is the most paradigmatic example: the vast majority of its streets and multiple channels allow flooding of the urban nucleus and the wetland area due to MSLR. The city of Eivissa (**Figures 9C,D**) includes a good example of an artificially guided torrent.

In these maps, public facilities such as schools, sanitary buildings as well as energy infrastructure are marked to illustrate the utility of the assessment to identify critical infrastructures at risk. Major impacts on infrastructures and equipment affect streets, secondary roads, and tracking pathways. This is quite evident in **Figures 9A,B**, where urban streets at tourist stations and rural secondary roads communications become flooded, especially for MSLR larger than 40 cm. Municipalities are the administration in charge of the most affected communication and transport infrastructure. The power plant at the Alcúdia Bay (**Figure 9A**) or the Eivissa airport are not affected by MSLR, neither by the associated extreme events, but they will be resting closer to the shoreline. Permanent and eventual floods do not affect any sanitary equipment (**Figure 9**), while some educational equipment may be damaged at Alcúdia bay (1 school and 1 institute, **Figures 9A,B**) and Eivissa (1 school, **Figures 9C,D**) if MSLR surpasses 46 cm.

Figure 6 shows the fraction of permanent flooding extent associated to each land use considered, by municipalities, for the case of 103 cm of MSLR, for the entire archipelago.

7. LOSS OF RECREATIONAL VALUE DUE TO BEACH EROSION

The estimated losses of recreational value in the beaches of the Balearic Islands are shown in **Table 3** for each island separately and for the entire archipelago. Note that those are estimates for the case that no action is taken. The loss ranges from 415 to 827 million euros under RCP4.5 for 2050, from 481 to 932 million euros under RCP8.5 for 2050, from 1,000 to 2,067 million euros under RCP4.5 for 2100, and from 1,421 to 2,428 million euros under RCP8.5 for 2100.

Under the RCP8.5 scenario, beach recreational services loss by 2050 could represent between 1.4 and 2.8% of the 2019 Balearic

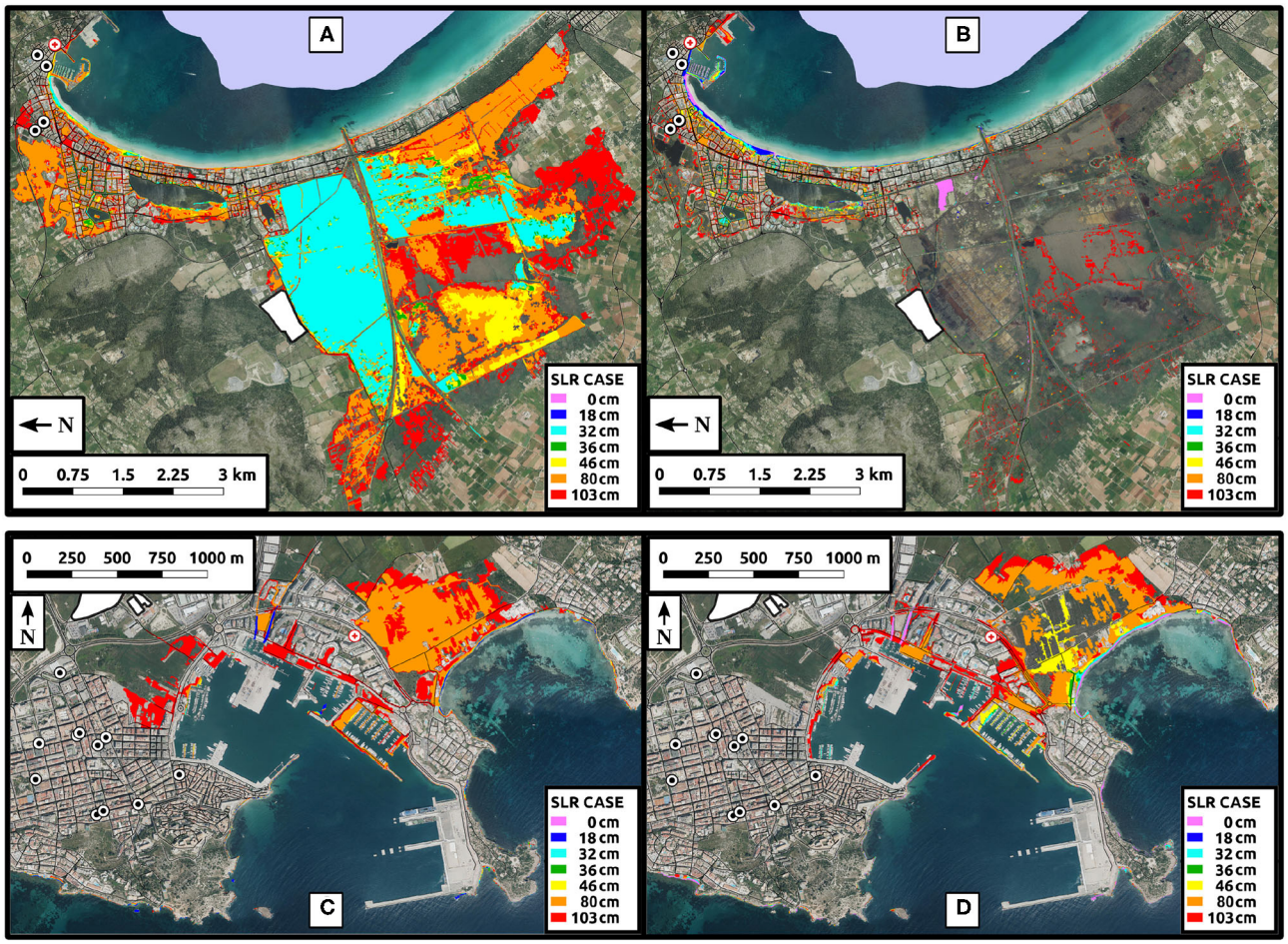

FIGURE 9 | Permanent and extreme flooding extent over the Alcúdia wetland **(A,B)** and city of Eivissa **(C,D)**. Roads and streets are marked using black lines. Education facilities are indicated as black dots, sanitary buildings as red crosses, and energy production plants as white polygons.

TABLE 3 | Loss of beach recreational services in monetary value (millions of euros) under RCP4.5 and RCP8.5 climate change scenarios for 2050 and 2100.

	2050				2100			
	RCP4.5		RCP8.5		RCP4.5		RCP8.5	
Balearic Islands	415.07	826.59	481.18	932.49	999.58	066.95	1420.64	2428.31
Mallorca	322.65	643.02	374.10	726.21	779.35	1620.79	1111.59	1901.65
Menorca	32.48	61.53	37.50	68.03	72.87	129.89	96.40	148.89
Pitiüses	59.95	122.04	69.58	138.24	147.36	316.28	212.65	377.76

Islands GDP, while by 2100 it represents between 4 and 7% of the 2019 Balearic Islands GDP. The Balearic Islands GDP is estimated at 33,800 million euros for 2019.

It should be noticed that this economic value refers to services provided for tourism recreation, not including the local population. Otherwise, beaches provide other additional environmental services, such as coastal protection. In monetary terms, the most damaged beaches of the archipelago under the RCP8.5 scenario in 2100 correspond with the largest beaches located in the major coastal basins of the island: Alcúdia beach in the northern coast of Mallorca and "s'Arenal" in the southern coast of Mallorca, with 574 and 169 million euros of recreational services loss, respectively. In Eivissa, "Platja d'en Bossa" is the most affected beach, with a loss of recreational services equivalent to 147 million euros, whereas the rest of the beaches of the island remain one order of magnitude below this value. The impact on Menorca beaches, in terms of recreational economic value, is lower than in the rest of the islands. The largest impact belongs to Son Bou beach (southern Menorca) with a recreational service loss equivalent to 38 million euros for 2100 under the RCP8.5 scenario.

8. CONCLUDING REMARKS

In this work, we estimated the extent of coastal flooding and beach erosion along sandy coastlines in the Balearic Islands as a result of projected MSLR during the twenty-first century. These coastal impacts were quantified for two climate change scenarios, namely RCP4.5 and RCP8.5, combining regional projected MSLR and marine extreme events caused by waves and storm surges. Our analysis constitutes the first study of mean sea-level rise impacts in the Balearic Islands at the regional scale, comprising all sandy coasts. Due to the size of the study site, the analysis was conducted as a regional approach, meaning that we considered a series of methodological approximations. Most of these approximations are related to beach erosion. We assumed that shoreline retreat was equivalent to beach width loss, while those beaches without an urbanized backshore will just displace landwards, as stated by Cooper et al. (2020). Also, we used Bruun's Rule for the computation of beach shoreline evolution which, although provides an acceptable first approach to the expected beach width changes, possess many limitations. For this reason, we believe future studies using more advanced models, such as that of McCarroll et al. (2021), should be conducted.

The approach permitted to identify the potentially most affected areas in the region: the wetlands of Alcúdia, Pollença and es Trenc in Mallorca, and the saltworks of Eivissa (accounting for 85% of the 103 cm of MSLR permanent flooding); as well as the number of beaches undergoing a critical state of erosion: up to 60% of beaches in the region may erode more than a 50% of its current width for a MSLR of 103 cm. Thus, our results can be used to inform the regional and national administrators about the most critical zones in order to prioritize their actuation.

The estimated loss of recreational value for the considered beaches is estimated between 1.4 and 2.8% of 2019 Balearic Islands GDP by 2050 and between 4.2 and 7.2% by 2100, under the worst-case scenario. Importantly, these values do not include the value provided by other beach services such as its role in coastal protection.

DATA AVAILABILITY STATEMENT

The raw data supporting the conclusions of this article will be made available by the authors, without undue reservation.

AUTHOR CONTRIBUTIONS

LG-P, MM, and AO conceived the idea of the study with the support of PL. PL, LG-P, MM, and AO developed the methodology. PL produced the results with the support of LG-P, MM, and AO. All authors analyzed the results and equally contributed to writing the manuscript.

FUNDING

This study was supported by PIMA ADAPTA-Balears Project funded by Conselleria de Transició Energética, Sectors Productius i Memòria Democràtica, Govern Balear, and by the FEDER/Ministerio de Ciencia, Innovación y Universidades - Agencia Estatal de Investigación through the MOCCA project (RTI2018-093941-B-C31 MINECO-AEI-UE-FEDER). LG-P is also funded by the CGL2016-79246-P MINECO-AEI-UE-FEDER project. PL was supported by the FPU19/03081 grant from Ministerio de Ciencia, Innovación y Universidades of Spain.

ACKNOWLEDGMENTS

We want to thank the Balearic Islands Coastal Observing and Forecasting System (SOCIB), who shared their data and collaborated collectively during the development of this project. We are grateful to Jeffrey Neal from the University of Bristol for sharing the latest version of LISFLOOD-FP. Comments from our three referees are greatly appreciated.

SUPPLEMENTARY MATERIAL

The Supplementary Material for this article can be found online at: https://www.frontiersin.org/articles/10.3389/fmars.2021.676452/full#supplementary-material

REFERENCES

Alvarez-Ellacuria, A., Orfila, A., Gómez-Pujol, L., Simarro, G., and Obregon, N. (2011). Decoupling spatial and temporal patterns in short-term beach shoreline response to wave climate. *Geomorphology* 128, 199–208. doi: 10.1016/j.geomorph.2011.01.008

Andreopoulos, D., Damigos, D., Comiti, F., and Fischer, C. (2015). Estimating the non-market benefits of climate change adaptation of river ecosystem services: a choice experiment application in the aoos basin, greece. *Environ. Sci. Policy* 45, 92–103. doi: 10.1016/j.envsci.2014.10.003

Balestri, E., Vallerini, F., and Lardicci, C. (2006). A qualitative and quantitative assessment of the reproductive litter from posidonia oceanica accumulated on a sand beach following a storm. *Estuarine Coastal Shelf Sci.* 66, 30–34. doi: 10.1016/j.ecss.2005.07.017

Booij, N., Ris, R. C., and Holthuijsen, L. H. (1999). A third-generation wave model for coastal regions: 1. Model description and validation. *J. Geophys. Res.* 104, 7649–7666. doi: 10.1029/98JC02622

Bruun, P. (1962). Sea-level rise as a cause of shore erosion. *J. Waterways Harbors Div.* 88, 117–130. doi: 10.1061/JWHEAU.0000252

Cañnellas, B., Orfila, A., Méndez, F. J., Menéndez, M., Gómez-Pujol, L., and Tintoré, J. (2007). Application of a POT model to estimate the extreme significant wave height levels around the Balearic Sea (Western Mediterranean). *J. Coastal Res.* 50, 329–333.

Chaikaew, P., Hodges, A. W., and Grunwald, S. (2017). Estimating the value of ecosystem services in a mixed-use watershed: a choice experiment approach. *Ecosyst. Serv.* 23, 228–237. doi: 10.1016/j.ecoser.2016.12.015

Cooper, J. A. G., Masselink, G., Coco, G., Short, A. D., Castelle, B., Rogers, K., et al. (2020). Sandy beaches can survive sea-level rise. *Nat. Clim. Chang* 10, 993–995. doi: 10.1038/s41558-020-00934-2

de Almeida, G. A. M., Bates, P., Freer, J. E., and Souvignet, M. (2012). Improving the stability of a simple formulation of the shallow water equations for 2-D flood modeling. *Water Resour Res.* 48:W05528. doi: 10.1029/2011WR011570

Dean, R. G. (1991). Equilibrium beach profiles: characteristics and applications. *J. Coastal Res.* 7, 53–84.

Dean, R. G., and Dalrymple, R. A. (1991). *Water Wave Mechanics for Engineers and Scientists, Vol. 2 of Advanced Series on Ocean Engineering*. World Scientific.

Deltares (2006). *Simulation of Multi-Dimensional Hydrodynamic Flows and Transport Phenomena, Including Sediments*. Delft: Deltares.

Enríquez, A. R., and Bujosa Bestard, A. (2020). Measuring the economic impact of climate-induced environmental changes on sun-and-beach tourism. *Clim Change* 160, 203–217. doi: 10.1007/s10584-020-02682-w

Enríquez, A. R., Marcos, M., Álvarez-Ellacuría, A., Orfila, A., and Gomis, D. (2017). Changes in beach shoreline due to sea level rise and waves under climate change scenarios: application to the Balearic Islands (Western Mediterranean). *Natural Hazards Earth Syst. Sci*. 17, 1075–1089. doi: 10.5194/nhess-17-1075-2017

Faccioli, M., Kuhfuss, L., and Czajkowski, M. (2019). Stated preferences for conservation policies under uncertainty: insights on the effect of individuals' risk attitudes in the environmental domain. *Environ. Resour. Econ*. 73, 627–659. doi: 10.1007/s10640-018-0276-2

Fornos, J. J., and Ahr, W. M. (1997). Temperate carbonates on a modern, low-energy, isolated ramp: the Balearic Platform, Spain. *SEPM J. Sediment. Res. Vol*. 67. doi: 10.1306/D4268572-2B26-11D7-8648000102C1865D

Gómez-Pujol, L., Orfila, A., Ca nellas, B., Alvarez-Ellacuria, A., Méndez, F. J., Medina, R., et al. (2007). Morphodynamic classification of sandy beaches in low energetic marine environment. *Mar. Geol*. 242, 235–246. doi: 10.1016/j.margeo.2007.03.008

Gómez-Pujol, L., Orfila, A., Morales-Márquez, V., Compa, M., Pereda, L., Fornós, J. J., et al. (2019). "Beach systems of Balearic Islands: nature, distribution and processes," in *The Spanish Coastal Systems: Dynamic Processes, Sediments and Management*, ed J. A. Morales (Cham: Springer International Publishing), 269–287.

Infantes, E., Terrados, J., Orfila, A., Canellas, B., and Alvarez-Ellacuria, A. (2009). Wave energy and the upper depth limit distribution of *Posidonia oceanica*. *Bot. Mar*. 52, 419–427. doi: 10.1515/BOT.2009.050

Jiménez, J., Osorio, A., Marino-Tapia, I., Davidson, M., Medina, R., Kroon, A., et al. (2007). Beach recreation planning using video-derived coastal state indicators. *Coastal Eng*. 54, 507–521. doi: 10.1016/j.coastaleng.2007.01.012

Kay, S. M. (1993). *Fundamentals of Statistical Signal Processing*. Prentice Hall Signal Processing Series. Prentice-Hall PTR.

Kim, G. H., Jho, M. H., and Yoon, S. B. (2017). Improving the performance of swan modelling to simulate diffraction of waves behind structures. *J. Coastal Res*. 79, 349–353. doi: 10.2112/SI79-071.1

Kopp, R. E., Horton, R. M., Little, C. M., Mitrovica, J. X., Oppenheimer, M., Rasmussen, D. J., et al. (2014). Probabilistic 21st and 22nd century sea level projections at a global network of tide-gauge sites. *Earths Future* 2, 383–406. doi: 10.1002/2014EF000239

Lionello, P., Abrantes, F., Congedi, L., Dulac, F., Gacic, M., Gomis, D., et al. (2012). *Introduction: Mediterranean Climate—Background Information*. Oxford: Elsevier, XXXV–XC.

Llompart, M., Sergio, B., Díaz, J. G., Lora, S., Montejano, S., and Navinés, F. (2020). *Memòria del Consell Econòmic i Social de les Illes Balears sobre l'economia, el treball i la societat de les Illes Balears 2019*. Technical Report 2019, Consell Econòmic i Social de les Illes Balears, Palma, Spain.

Mas Parera, L., and Blázquez-Salom, M. (2005). Anàlisi de la freqüentació d'ús a les platges i estudi de paràmetres de sostenibilitat associats. *Doc. Anàl. Geogr*. 45, 15–40.

McCarroll, R. J., Masselink, G., Valiente, N. G., Scott, T., Wiggins, M., Kirby, J.-A., et al. (2021). A rules-based shoreface translation and sediment budgeting tool for estimating coastal change: shoretrans. *Ma.r Geol*. 435:106466. doi: 10.1016/j.margeo.2021.106466

Mentaschi, L., Vousdoukas, M. I., Voukouvalas, E., Dosio, A., and Feyen, L. (2017). Global changes of extreme coastal wave energy fluxes triggered by intensified teleconnection patterns. *Geophys. Res. Lett*. 44, 2416–2426. doi: 10.1002/2016GL072488

Morales-Márquez, V., Orfila, A., Simarro, G., Gómez-Pujol, L., Álvarez-Ellacuría, A., Conti, D., et al. (2018). Numerical and remote techniques for operational beach management under storm group forcing. *Natural Hazards Earth Syst. Sci*. 18, 3211–3223. doi: 10.5194/nhess-18-3211-2018

Morales-Márquez, V., Orfila, A., Simarro, G., and Marcos, M. (2020). Extreme waves and climatic patterns of variability in the eastern north atlantic and mediterranean basins. *Ocean Sci*. 16, 1385–1398. doi: 10.5194/os-16-1385-2020

Nicholls, R. J., and Cazenave, A. (2010). Sea-level rise and its impact on coastal zones. *Science* 328, 1517–1520. doi: 10.1126/science.1185782

Nicholls, R. J., and Lowe, J. A. (2004). Benefits of mitigation of climate change for coastal areas. *Glob. Environ. Change* 14, 229–244. doi: 10.1016/j.gloenvcha.2004.04.005

Orfila, A., Jordi, A., Basterretxea, G., Vizoso, G., Marbà, N., Duarte, C., et al. (2005). Residence time and *Posidonia oceanica* in Cabrera Archipelago National Park, Spain. *Cont. Shelf Res*. 25, 1339–1352. doi: 10.1016/j.csr.2005.01.004

Pérez-López, M., and Roig-Munar, F. (2007). "ValoraciÓn económica de los sistemas arenosos de Menorca: una contribución a la revalorización de la geomorfología litoral," in *Investigaciones Recientes (2005-2007) en Geomorfología Litoral*, eds L. Gómez-Pujol and J. Fornós (Palma: UIB, IMEDEA, SHNB, SEG), 123–127.

Purvis, M. J., Bates, P. D., and Hayes, C. M. (2008). A probabilistic methodology to estimate future coastal flood risk due to sea level rise. *Coastal Eng*. 55, 1062–1073. doi: 10.1016/j.coastaleng.2008.04.008

Remoundou, K., Diaz-Simal, P., Koundouri, P., and Rulleau, B. (2015). Valuing climate change mitigation: a choice experiment on a coastal and marine ecosystem. *Ecosyst. Serv*. 11, 87–94. doi: 10.1016/j.ecoser.2014.11.003

Riera, A., Álvarez Díaz, M., Crespía, R., and Gómez-Pujol, L. (2007). El valor d'ús recreatiu de la badia de Santa Ponça (Calvià). *Cojuntura* 20, 66–71.

Rodrigues, L. C., van den Bergh, J. C. J. M., Loureiro, M. L., Nunes, P. A. L. D., and Rossi, S. (2016). The cost of mediterranean sea warming and acidification: a choice experiment among scuba divers at medes islands, Spain. *Environ. Resour. Econ*. 63, 289–311. doi: 10.1007/s10640-015-9935-8

Rogers, D. (1998). *Procedural Elements for Computer Graphics*. Boston, MA: WCB/McGraw-Hill.

Roig-Munar, F. X., Pintó, J., Garcia-Lozano, C., Martín-Prieto, J. A., and Rodríguez-Perea, A. (2020). Análisis de los patrones de uso y frecuentación (2000-2017) en las playas de la isla de Menorca (Islas Baleares). *Cuad. Geogr*. 59, 171–195. doi: 10.30827/cuadgeo.v59i1.8761

Roig-Munar, F. X., Prieto, J., Á. M., Pintó, J., Rodríguez-Perea, A., and Gelabert, B. (2019). "Coastal management in the Balearic islands," in *The Spanish Coastal Systems: Dynamic Processes, Sediments and Management*, ed J. A. Morales (Cham: Springer International Publishing), 765–787.

Sanuy, M., Duo, E., Jäger, W. S., Ciavola, P., and Jiménez, J. A. (2018). Linking source with consequences of coastal storm impacts for climate change and risk reduction scenarios for mediterranean sandy beaches. *Natural Hazards Earth Syst. Sci*. 18, 1825–1847. doi: 10.5194/nhess-18-1825-2018

Schuerch, M., Spencer, T., Temmerman, S., Kirwan, M. L., Wolff, C., Lincke, D., et al. (2018). Future response of global coastal wetlands to sea-level rise. *Nature* 561, 231–234. doi: 10.1038/s41586-018-0476-5

Seenath, A., Wilson, M., and Miller, K. (2016). Hydrodynamic versus GIS modelling for coastal flood vulnerability assessment: which is better for guiding coastal management? *Ocean Coastal Manag*. 120, 99–109. doi: 10.1016/j.ocecoaman.2015.11.019

Shoyama, K., Managi, S., and Yamagata, Y. (2013). Public preferences for biodiversity conservation and climate-change mitigation: a choice experiment using ecosystem services indicators. *Land Use Policy* 34, 282–293. doi: 10.1016/j.landusepol.2013.04.003

Slangen, A. B. A., Carson, M., Katsman, C. A., van de Wal, R. S. W., Köhl, A., Vermeersen, L. L. A., et al. (2014). Projecting twenty-first century regional sea-level changes. *Clim. Change* 124, 327–332. doi: 10.1007/s10584-014-1080-9

Soares, C. G., Ferreira, A. M., and Cunha, C. (1996). Linear models of the time series of significant wave height on the Southwest coast of Portugal. *Coastal Eng*. 29, 149–167. doi: 10.1016/S0378-3839(96)00022-1

Stockdon, H. F., Holman, R. A., Howd, P. A., and Sallenger, A. H. (2006). Empirical parameterization of setup, swash, and runup. *Coastal Eng*. 53, 573–588. doi: 10.1016/j.coastaleng.2005.12.005

Stocker, T. F., Qin, D., Plattner, G.-K., Tignor, M. M., Allen, S. K., Boschung, J., et al. (eds.). (2014). *Climate Change 2013-The Physical Science Basis: Working Group I Contribution to the Fifth Assessment Report of the Intergovernmental Panel on Climate Change*. Cambridge: Cambridge University Press.

Teng, J., Jakeman, A., Vaze, J., Croke, B., Dutta, D., and Kim, S. (2017). Flood inundation modelling: a review of methods, recent advances and uncertainty analysis. *Environ. Model. Softw*. 90, 201–216. doi: 10.1016/j.envsoft.2017.01.006

The SWAN Team (2019a). Swan scientific and technical documentation, swan cycle iii version 41.20ab. Technical University of Delft. Available online at: http://swanmodel.sourceforge.net/ (accessed July 20, 2021).

The SWAN Team (2019b). Swan user manual, swan cycle iii version 41.20ab. Technical University of Delft. Available online at: http://swanmodel.sourceforge.net/ (accessed July 20, 2021).

Toimil, A., Losada, I. J., Camus, P., and Díaz-Simal, P. (2017a). Managing coastal erosion under climate change at the regional scale. *Coastal Eng.* 128, 106–122. doi: 10.1016/j.coastaleng.2017.08.004

Toimil, A., Losada, I. J., Díaz-Simal, P., Izaguirre, C., and Camus, P. (2017b). Multi-sectoral, high-resolution assessment of climate change consequences of coastal flooding. *Clim. Change* 145, 431–444. doi: 10.1007/s10584-017-2104-z

Tolman, H. L. (2002). *User Manual and System Documentation of Wavewatch-III Version 2.22*. Technical report, Technical Note, US Department of Commerce, NOAA, NWS, NCEP, Washington, DC.

Torres, C., Faccioli, M., and Riera Font, A. (2017). Waiting or acting now? the effect on willingness-to-pay of delivering inherent uncertainty information in choice experiments. *Ecol. Econ.* 131, 231–240. doi: 10.1016/j.ecolecon.2016.09.001

Valdemoro, H. I., and Jiménez, J. A. (2006). The influence of shoreline dynamics on the use and exploitation of Mediterranean tourist beaches. *Coastal Manag.* 34, 405–423. doi: 10.1080/08920750600860324

van Rijn, L. C. (1984). Sediment transport, part II: suspended load transport. *J. Hydraulic Eng.* 110, 1613–1641. doi: 10.1061/(ASCE)0733-9429(1984)110:11(1613)

Vitousek, S., Barnard, P. L., and Limber, P. (2017). Can beaches survive climate change? *J. Geophys. Res. Earth Surf.* 122, 1060–1067. doi: 10.1002/2017JF004308

Vousdoukas, M. I., Mentaschi, L., Voukouvalas, E., Verlaan, M., and Feyen, L. (2017). Extreme sea levels on the rise along Europe's coasts. *Earths Future* 5, 304–323. doi: 10.1002/2016EF000505

Vousdoukas, M. I., Ranasinghe, R., Mentaschi, L., Plomaritis, T. A., Athanasiou, P., Luijendijk, A., et al. (2020). Sandy coastlines under threat of erosion. *Nat. Clim. Chang* 10, 260–263. doi: 10.1038/s41558-020-0697-0

Vreugdenhil, C. B. (1994). *Numerical Methods for Shallow-Water Flow. Water Science and Technology Library*. Dordrecht: Kluwer Academic Publishers.

Yunus, A., Avtar, R., Kraines, S., Yamamuro, M., Lindberg, F., and Grimmond, C. (2016). Uncertainties in tidally adjusted estimates of sea level rise flooding (bathtub model) for the Greater London. *Remote Sens.* 8, 366. doi: 10.3390/rs8050366

Conflict of Interest: The authors declare that the research was conducted in the absence of any commercial or financial relationships that could be construed as a potential conflict of interest.

The reviewer DI declared a past co-authorship with one of the authors, MM, to the handling editor.

Publisher's Note: All claims expressed in this article are solely those of the authors and do not necessarily represent those of their affiliated organizations, or those of the publisher, the editors and the reviewers. Any product that may be evaluated in this article, or claim that may be made by its manufacturer, is not guaranteed or endorsed by the publisher.

Copyright © 2021 Luque, Gómez-Pujol, Marcos and Orfila. This is an open-access article distributed under the terms of the Creative Commons Attribution License (CC BY). The use, distribution or reproduction in other forums is permitted, provided the original author(s) and the copyright owner(s) are credited and that the original publication in this journal is cited, in accordance with accepted academic practice. No use, distribution or reproduction is permitted which does not comply with these terms.

APPENDIX

A. Wave Propagation Validation

This appendix describes the instrumental data and the method used to validate the wave time series. The instrumental data consists of the available nearshore wave time series, which comprises data from three study sites: Cala Millor in the East of Mallorca, Platja de Palma in the Southwest of Mallorca, and Son Bou in the South of Menorca. Data was acquired using *in situ* Acoustic Wave and Current meters (AWACs) deployed at coordinates listed in **Table A1** and 18 m depth, managed by SOCIB. The AWAC configurations can be consulted on the SOCIB webpage.

Pairs of simultaneous measured and synthetic H_s and T as well as the quantiles (q_n) associated with the percentiles (0,1,2,...,99,100) of each time series are considered to compute the following metrics:

$$\text{Bias} = \overline{x^m} - \overline{x^s} \tag{A1}$$

$$\text{RMSE} = \sqrt{\frac{1}{N}\sum_{i=1}^{N}\left(x_i^m - x_i^s\right)^2} \tag{A2}$$

$$\text{Correlation} = \frac{\sum_{i=1}^{N}\left(x_i^s - \overline{x^s}\right)\left(x_i^m - \overline{x^m}\right)}{\sigma_{x^s}\sigma_{x^m}} \tag{A3}$$

$$\text{Slope} = \frac{\sum_{i=1}^{N} x_i^s x_i^m}{\sum_{i=1}^{N} x_i^s x_i^s} \tag{A4}$$

$$\text{R}_2 = 1 - \frac{\sum_{i=1}^{N}\left(x_i^m - x_i^s\right)^2}{\sum_{i=1}^{N}\left(x_i^m - \overline{x^m}\right)^2} \tag{A5}$$

$$\text{Slope}^Q = \frac{\sum_{n=1}^{101} q_n^s q_n^m}{\sum_{n=1}^{101} q_n^s q_n^s} \tag{A6}$$

$$\text{R}_2^Q = 1 - \frac{\sum_{n=1}^{101}\left(q_n^m - q_n^s\right)^2}{\sum_{n=1}^{101}\left(q_n^m - \overline{q^m}\right)^2} \tag{A7}$$

where x symbolizes H_s or T; N is the number of time series samples considered for the analysis; x_i^m, $\overline{x^m}$ and σ_{x^m} refer to the ith sample, the mean and the standard deviation of the instrumental time series, respectively; while x_i^s, $\overline{x^s}$ and σ_{x^s} refer to the ith sample, the mean and the standard deviation of the synthetic time series, respectively. Also, q_n^s and q_n^m are the quantiles of the percentile n, for synthetic and measured time series, respectively (both for H_s and T); while $\overline{q^s}$ and $\overline{q^m}$ stand for the mean of the quantiles of the synthetic and measured time series, respectively. The results of the seven metrics described are listed in **Table A1**. **Figure A1** shows scatter plots and QQ-plots for these data pairs.

B. Justification of the Triangular Flooding Forcing

In order to define the form for the forcing of the temporary flooding, the WS + SS exceedances of all the flooding zones were considered. A prior visual inspection indicated that the shape of the exceedances tends to be triangular-like, at least at the sampling rate used.

TABLE A1 | Coordinates of the AWACs used for the validation of wave propagations and metrics resulting from the comparison between the instrumental and the propagated time series.

		Cala millor	Son Bou	Platja de Palma
AWAC position	Latitude	39° 35' 55" N	39° 53' 47" N	39° 30' 22" N
	Longitude	3° 23' 59" E	4° 3' 49" E	2° 43' 13" E
Significant Wave Height (H_s)	Bias (m)	−0.05	−0.15	−0.16
	RMSE (m)	0.20	0.28	0.28
	Correlation	0.86	0.85	0.79
	Slope	1.03	1.14	1.17
	R2	0.72	0.59	0.41
	Slope^Q	1.09	1.18	1.20
	R_2^Q	0.96	0.87	0.80
Peak Period (T)	Bias (s)	−0.15	0.01	−0.29
	RMSE (s)	1.54	1.04	1.12
	Correlation	0.68	0.79	0.72
	Slope	1.02	0.99	1.04
	R2	0.46	0.61	0.46
	Slope^Q	1.04	1.01	1.05
	R_2^Q	0.89	0.96	0.94

A more quantitative analysis of the exceedances shape was conducted, consisting of the following. First, the time series were upsampled by a factor of 100 using linear interpolation, in order to capture the complete shape of each exceedance. Then, the exceedances were split in the rising and the falling parts (i.e., the part of the exceedances between the threshold up-crossing and the exceedance peak, and between the exceedance peak and the threshold down-crossing, respectively). The exceedance rises and falls were normalized to give values between zero and one, both in time and intensity. Later, the exceedance rises and falls were interpolated to a common grid, in order to compare the shape between all the exceedance rises and falls. Also, the ratios between the exceedance rise durations and the complete exceedance durations were computed.

The distribution of the exceedance rise and exceedance fall shapes, as well as the distribution of the ratio between the exceedance rise duration and the complete exceedance duration, are provided as **Supplementary Material** ("exceedance_shape_statistics.png"). The results shown in that image allow us to conclude that the most plausible shape for the temporary flooding (that indicated by the 50th percentile) is somewhat more concave than a triangular pulse. Also, the histogram of the ratio between the exceedance rise duration and the complete exceedance duration indicates that the rise duration should be equal to the fall duration. Since the most plausible shape is close to a triangular shape, which is easier to generate and which has used before in the Literature (e.g., Purvis et al., 2008), we decided to use a triangular shape, with the same duration for the rise and the fall.

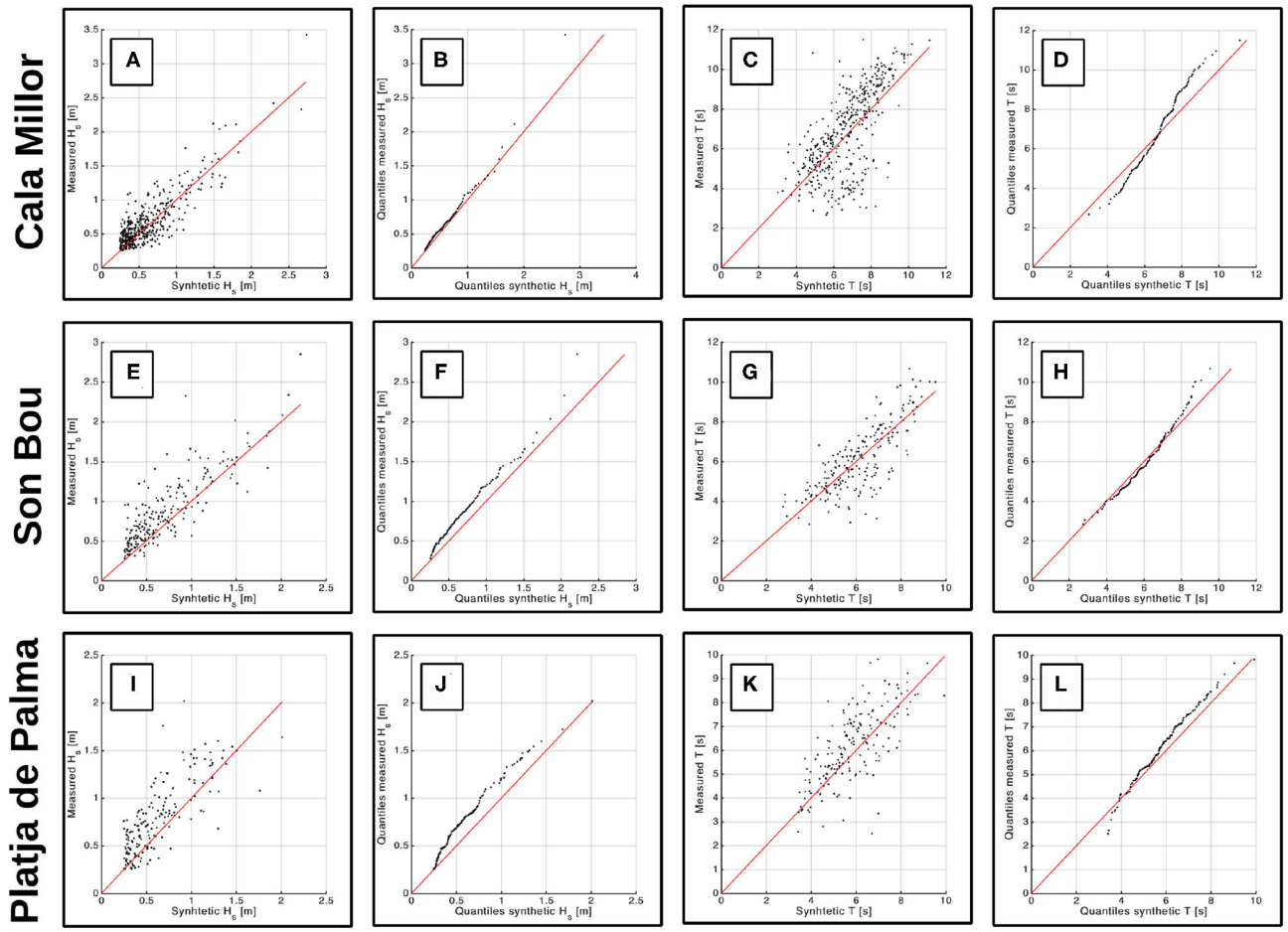

FIGURE A1 | Comparison of *in situ* and synthetic time series (unitary slope lines indicated in red). **(A,E,I)** Show H_s scatter plots. **(B,F,J)** Show H_s QQ-plots. **(C,G,K)** Show *T* scatter plots. **(D,H,L)** Show *T* QQ-plots. **(A–D)** Correspond to Cala Millor data; **(E–H)** to Son Bou data; **(I–L)** to Platja de Palma data.

C. Synthetic Storm Surge and Significant Breaking Wave Height Time Series Generation

To characterize the statistics of H_b time series, it is necessary to consider the intensity of their samples, as well as the time distribution and persistence of storms, which in this case are defined as the events where the intensity of the forcing exceeds some threshold during a certain time, called persistence of the event (Toimil et al., 2017a). Once the statistics of the forcings are known, it is possible to generate synthetic time series that are statistically consistent with the original one, but with a different chronology, in this case based on Soares et al. (1996). These can be used to generate an estimation of the beach width time evolutions probability distribution, by means of a Monte Carlo method (by using Equation (7). We characterize the logarithm of H_b (clipped below -2) instead of H_b itself.

The forcing time series present annual stationarity. Thus, instead of characterizing the statistics of the whole time series, we classified their samples depending on their position inside the seasonal period and used the fragments of time series corresponding to each season (December, January, and February; March, April, and May; June, July, and August; September, October, and November).

For each group, we estimated its cumulative density function (CDF). For the logarithm of H_b we used a piecewise function with two intervals, where the range below the 99.9th quantile was computed by linear interpolation, and the interval above that threshold was computed as $1 - (1 - 0.999) \cdot (1 - CDF_{GPD})$, where CDF_{GPD} is a Generalized Pareto distribution CDF, fitted by least squares.

Once the CDF of each group was estimated, we applied the inverse transformation method (Soares et al., 1996) to made each group's data follow a Gaussian distribution. Then, we computed and solved the Yule-Walker equations associated with each group's gaussianized data, obtaining an autoregressive filter for each group (Kay, 1993).

To obtain synthetic time series we generated Gaussian white noise and filtered it using the previously calibrated autoregressive

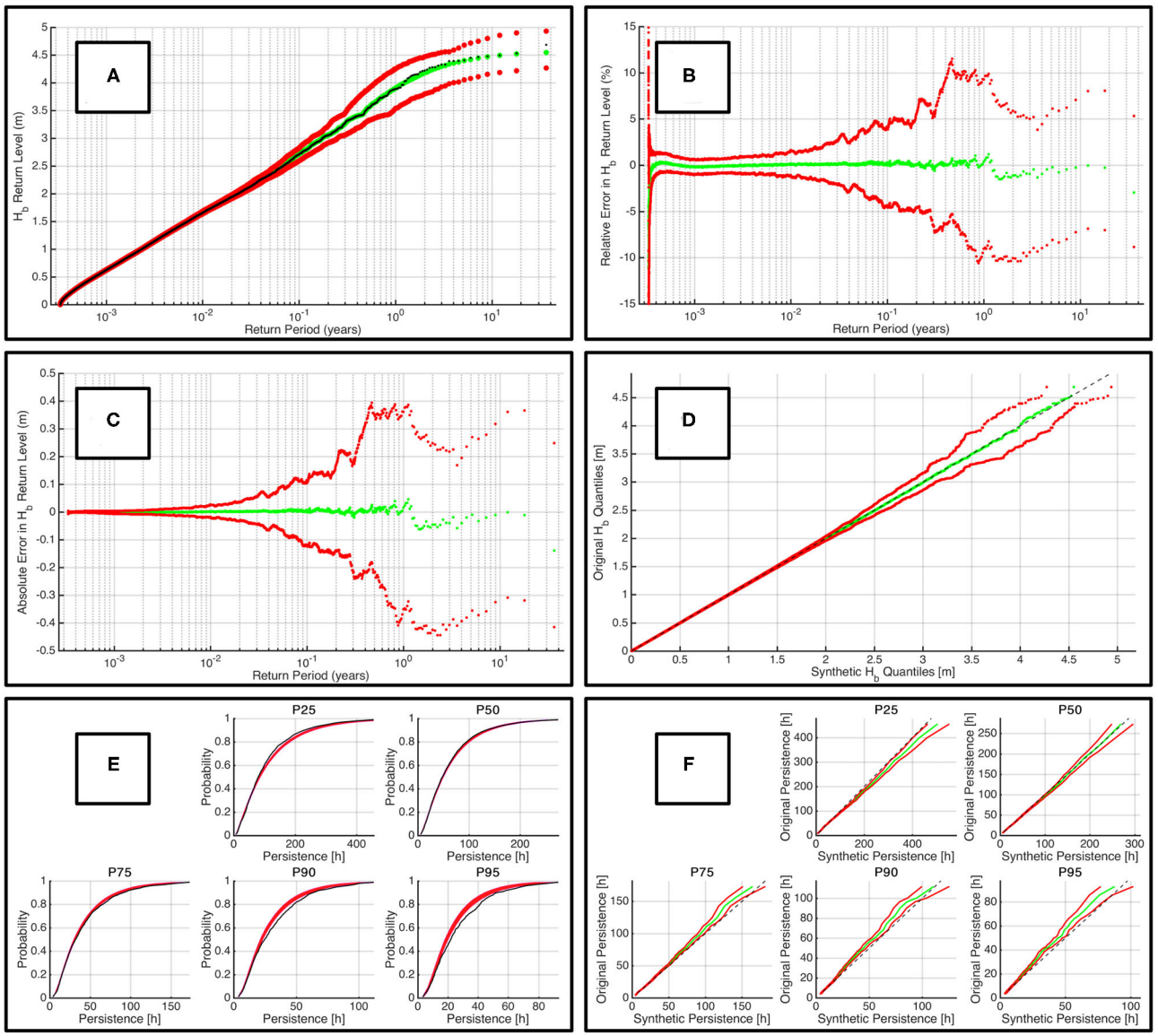

FIGURE A2 | Comparison between the statistics of the original and 1000 synthetic time series of H_b for one beach. In all panels, black dots (or lines) indicate the values computed using the original time series; while the lower red dots, central green dots, and upper red dots (or lines) indicate the 5, 50, and 95th percentiles of the values computed from the synthetic time series. **(A)** Shows the return plots. **(B)** Shows the error of the synthetic time series return plots with respect to the original time series return plot, while **(C)** depicts the same but in terms of relative error. **(D)** Shows the QQ-plots between the original and the synthetic time series. **(E)** Shows the cumulative density functions of the persistence over different thresholds (defined as the original time series percentiles, marked above each subpanel), both for the original time series (black dots) and the range between the 5 and 95th percentiles of the synthetic time series (red shaded areas). **(F)** Shows the QQ-plots of the persistence over different thresholds (defined as the original time series percentiles) between the original and the synthetic time series.

filter (the output of the filter presents the same time correlation as the data used to calibrate the filter, though it follows a gaussian distribution). Afterward, the inverse transformation method was applied to obtain a time series presenting both the same time correlation and marginal distribution as the original data. Finally, in order to mimic the seasonality of the forcings, the filter and CDF of each season were switched periodically between the ones of the different groups. A comparison between the original and multiple synthesized time series for one beach is summarized in **Figure A2** in the form of different statistics.

frontiers in Marine Science

PERSPECTIVE
published: 25 August 2021
doi: 10.3389/fmars.2021.706048

Effective Coastal Climate Services—An End-User Perspective for Resilient Infrastructure

Jonathan Simm, Ben Gouldby, Darren Lumbroso and Tom Matthewson*

HR Wallingford, Wallingford, United Kingdom

This paper focusses on identifying the responses to coastal climate change that are of interest for decision-making by end users and the delivery and the necessary communication process for this information. The focus is on representation of climate (response) information in a form that provides sufficient clarity in the midst of uncertainty for end-users who are seeking to develop or maintain resilient infrastructure. The paper recommends that the use of the term climate services in situations unrelated to supporting adaptation to and mitigation of climate change should be avoided. Better investment decisions could be made if Bayesian frameworks were used to assign probabilities to RCP scenarios. Associated predictions need to cover all types of climate change influences not just sea level rise and ideally provide concurrent time series to allow evaluation of dependencies. Guidance on climate information published by official bodies needs to adopt a consistent approach, with a clear narrative that describes the transition from science to guidance. The form in which climate services information is needed for the required end user decisions needs careful thought, including appropriate communication of the associated uncertainties using good practices and experiences from related sectors.

Keywords: climate services, infrastructure, resilient, uncertainty, communication

OPEN ACCESS

Edited by:
Robert James Nicholls, University of East Anglia, United Kingdom

Reviewed by:
Goneri Le Cozannet, Bureau de Recherches Géologiques et Minières, France
Dimitris Stagonas, University of Cyprus, Cyprus

****Correspondence:***
Jonathan Simm
j.simm@hrwallingford.com

Specialty section:
This article was submitted to Coastal Ocean Processes, a section of the journal Frontiers in Marine Science

Received: *06 May 2021*
Accepted: *26 July 2021*
Published: *25 August 2021*

Citation:
Simm J, Gouldby B, Lumbroso D and Matthewson T (2021) Effective Coastal Climate Services—An End-User Perspective for Resilient Infrastructure. Front. Mar. Sci. 8:706048. doi: 10.3389/fmars.2021.706048

INTRODUCTION—THE SITUATION OF END-USERS SEEKING RESILIENT INFRASTRUCTURE

This paper uses the definition of coastal climate services by Le Cozannet et al. (2017) as "any type of service using (coastal area) climate information and supporting adaptation to and mitigation of climate change." Most of the discussion in the literature of climate services has been on their development, implementation in policy and expected benefits (see e.g., Hewitt et al., 2012; Brasseur and Gallardo, 2016). This paper focusses instead more on their operationality. Furthermore whilst climate services information is essential for infrastructure creators and managers, climate change is only one of a number of considerations that practitioners need to address in developing and investing in sustainable and resilient infrastructure From the literature and interaction with end users, we infer that the creation and management of such infrastructure has a spectrum of requirements including:

- "**Everydayness**." Coastal infrastructure assets need to function to deliver their everyday requirements, such as access, transportation, power supply, recreation, agriculture, environmental and ecological improvement (see e.g., CIRIA, 2013, p. 60–70), irrespective of socio-economic and climate changes (including sea level rise). Investment decisions will inevitably reflect this need, recognizing that some public assets will have importance for the wider community surrounding the asset and should work for them as well. Ideally green solutions should be considered whenever possible as part of the investment mix which enable natural processes to continue as far as possible, including sustaining the coastal sediment balance and encouraging habitats.
- **Survivability**. Infrastructure assets need to survive extreme events, with risk of failure and/or downtime appropriately managed, taking into account the non-stationarity (in many cases increases in severity) of severe events. Deterministic approaches that focus on single design events have well-known limitations in the coastal context. Annual exceedance probability cannot be unambiguously defined when there are multiple variables that require consideration (Serinaldi, 2015; Gouldby et al., 2017) and hence probabilistic methods that require analysis of large numbers of different events are increasingly being applied to assess failure in terms of the structural response (e.g., Gouldby et al., 2017). Given the uncertainty of future events, the idea of "designing for exceedance," first articulated for urban drainage (see e.g., Digman et al., 2006), becomes important. In particular, understanding the performance of the structure in more extreme scenarios (than used within the design basis) and gaining insights into "cliff-edge effects becomes essential. This is identified as a specific requirement in some sectors, nuclear for example (Office for Nuclear Regulation [ONR], 2018). Such a resilience based approach requires a clear understanding of how the structural, hydraulic and geotechnical performance of infrastructure assets will be affected and an approach to manage any performance reductions (see e.g., Chester et al., 2021). For example, it is likely that any green solutions will need to be backed up by substantial conventional engineering measures.
- **Recoverability**. If damage or disruption does occur as a result of extreme events, then minimizing downtime and ensuring rapid recovery becomes essential. However, damaged infrastructure should be replaced with solutions that anticipate long-term changes in climate (as well as business and socio economic drivers), avoiding the presumption of replacing like for like and embracing opportunities for transformation in approach (see e.g., Royal Society, 2014).

In assessing the nature and form of climate services required to deliver such requirements, two main areas will be discussed: the required basic climate information likely to be relevant and the nature and format of processed information required about responses in order to support decision making. Two "use cases" of coastal nuclear power plants and coastal ports are used to illustrate some of the points made.

END-USER ISSUES WITH BASIC COASTAL CLIMATE INFORMATION

The three requirements for managing infrastructure in the face of climate change suggests that climate services need reliable probabilistic information across the range of parameters affected by climate change and across the spectrum of climate manifestations (from everyday to extreme), provided in a form where uncertainties are quantified. It also suggests that official guidance for assessing such matters should be unambiguous and without contradiction. This section addresses some issues related to these needs.

Probabilities for Climate Change Scenarios

Current guidance and data relating to coastal flooding and climate change, quantifies uncertainty in some aspects but not in others. For example, the UKCP18 information relating to sea level rise provides probabilistic estimates of sea level rise for given R. The general UK government guidance for flood risk assessments is based on the use of the RCP8.5 scenario and specifies the consideration of the upper 70th percentile for design and risk assessment with a suggestions to use the 95th percentile for sensitivity analysis. The guidance, in line with the approach described by Nicholls et al. (2014), also advises consideration of the H++ scenario. These probabilistic estimates are conditional on the specific RCPs being realized. There is, however, no likelihood associated with the RCPs themselves. Risk-based decision making requires the quantification of uncertainty and therefore requires a likelihood to be associated with the RCPs. Whilst to many climate scientists this may seem an elusive goal, and beyond their remit, the lack of this information significantly hampers risk-based decision making for infrastructure investments of typical design life 100 years.

Quantifying the likelihood of a future RCPs (and the related Shared Socio-economic Pathways that are emerging (Riahi et al., 2017). Occurring would not be viable under a traditional frequentist framework; however, the well-known Bayesian Framework can be used for this purpose. The Bayesian framework supports quantification of uncertainty through the use of expert judgment (see e.g., Morriss, 1977), and also permits the reconciliation of conflicting multi-model forecasts through Bayesian consolidation of parameters. Further evidence to support likelihood assessment of RCPs is continuously emerging (see Hausfather and Peters, 2020, for example). This framework also provides a natural updating process that evolves when new evidence emerges.

Whilst there is extensive literature relating to climate change in this regard (Allen et al., 2001; Tebaldi et al., 2005; Smith et al., 2009; Qian et al., 2016, Oppenheimer et al., 2016), the approach has not yet filtered through to mainstream data sets and guidance that are applied in practice. It should, however, only be a matter of time for these approaches to be adopted within

mainstream guidance, in which hopefully quantified estimates of the uncertainty of different scenarios will be provided.

Understanding All Climate Change Influences—Not Just Sea Level Rise

Other Key Influences

Recognition that sea level rise is only one of many change drivers which need to be considered. Other changes affecting coasts may include average and extreme winds and waves, tide range and tidal streams, pressure on water supplies and risks to health from hotter summers (see for example, Wong et al., 2014; Vousdoukas et al., 2020).

Scenarios of Concurrent Time Series for Coastal Forcings

The need for concurrent time series data across a range of different forcings. This concurrent date is needed to facilitate analysis of dependencies and permit understanding of multiple source or compound flooding. Note that whilst concurrent forcing data series are available for typical marine parameters (e.g., water levels and waves), time series data to allow evaluation of dependencies between coastal forcing and other forcings such as rainfall and river flows is limited.

Inconsistent Climate Information Guidance Published by Official Bodies

Guidance on climate change allowances to apply in practice is underpinned by climate science. There is, however, often a need to distill complex processes with the many uncertainties discussed in the scientific literature into simplified allowances that are applied in practice. To date, in the UK at least, two problems appear to arise in this process: (1) thinking becomes disjointed and hence inconsistent data sets or scenarios are referenced in official guidance; (2) the narrative that describes the transition from the science to the guidance is not routinely published and this lack of transparency can potentially undermine the authority of the guidance and cause confusion for practitioners.

Examples of this in UK guidance include:

- **H++ scenario**. The very high scenario used for sea level change (H++) is rarely updated at the same time as general climate projections.
- **Storm surge:** Both UKCP09 and UKCP18 (Palmer et al., 2018) could find no significant evidence for increase in storm surge. Pre UKCP18, the government guidance for allowance for storm surge under the H++ scenario was 0.7 m to 2080. The latest guidance for the H + + scenario, post UKCP18, is 2mm per year, equating to 0.13 m to 2080. This is a decrease in allowance of around 80%. There is no accompanying discussion relating to this significant reduction.
- **Storminess (storm surge sensitivity)**: Changes in storminess can potentially influence wind speeds, wave conditions and storm surges. All are directly related to mid-latitude storms. Neither UKCP09 or UKCP18 found significant evidence relating to changes in storminess. Pre-UKCP18, there was a recommendation for sensitivity testing of increase to winds and waves of 10% for epochs of 2055 and onward, but no requirement for storm surge sensitivity (other than the allowance under the H++ scenario). No explanation was given for why it was not necessary to test the sensitivity relating to increases in storm surge.
- **Storminess (sensitivity to allowance)**: Even though no evidence was found of increases in storminess with either UKCP09 or UKCP18, the sensitivity tests advised pre UKCP18 were changed to required allowances in the latest guidance.

There is no doubt that climate science evolved and attitudes to risk change. Nevertheless, the updates to the published guidance can give the impression that these are somewhat arbitrary, and hence portray a lack of credibility. Publication of the narrative that justifies updates, or changes, to the guidance would alleviate the situation and provide more transparency.

SUPPORTING END-USER DECISION MAKING BY CLIMATE SERVICES

Meaning of "Climate Services"

Careful use of language when describing climate services. This includes the need to be clear where the service being offered is full coastal engineering/management and not just climate services, involving (full) evaluation of present day conditions/requirements and then variation/sensitivity analysis to understand the implications, e.g., of sea level rise. This lack of focus prevents users from perceiving easily the real added value of climate services for adaptation to sea-level rise. This challenge would be addressed by a more consistent restriction of the use of "climate services" as being related to mitigation of or adaptation to the effects of climate change, as in the definition of Le Cozannet et al. (2017) cited in section ""Introduction—The Situation of End-Users Seeking Resilient Infrastructure" above.

Clear and Appropriate Communication

Clear and appropriate communication leading to appropriate services delivery. Climate services is as much about process as product, engaging end-users and scientists in a two-way conversation which understands the outputs/outcomes in which the end-user is interested. For example, does the end user want the "answers" about responses to climate drivers (e.g., increased wave overtopping rates at sea walls) or would they prefer to be provided with a tool that they can use to explore alternative scenarios involving multiple hazards and impacts and from this to identify and prioritize adaptation strategies. The case of climate services for ports will be discussed below, where end users will want to take account of the likely life of the port infrastructure being evaluated, the operability of the port, resilience under extreme conditions, and the need to build future adaptability into present day port investments.

If end-users are using climate services information for public communication, the existing challenges of communicating

natural hazard risks (see e.g., Arvai and Rivers, 2013) is compounded when the issue of climate change is added. It is therefore recommended that communication about climate services builds upon knowledge and lessons learned in communication practices (e.g., define clear role of each actor for communicating, etc.) in relevant related areas, e.g., risk management.

Clarity About Acceptable Uncertainties for Both Basic and "Processed" Information

Clarity about the limits/uncertainties on available information about climate change drivers and recognition of the fact that better quantified drivers may not resolve uncertainty in response predictions, if the physical process understanding of responses (e.g., wave overtopping) has greater uncertainties. As part of this, it is necessary to identify (if they are known) any "cliff edge" effects which may cause dramatic changes in responses. Communicating these uncertainties is a significant challenge and good communication needs to recognize (a) a realistic assessment of the available accuracy of the data (avoiding unwarranted implications of regional/local accuracy) and (b) the purpose for which the information will be used which may vary between different decisions.

For example, effective decisions of different types related to sea level rise could be made with input information ranging from (a) simple Red Amber Green classifications (based on ranges of expected sea level rise) through to (b) multiple possible future sea level rise growth curves, each with their uncertainty ranges.

USE CASE 1—NUCLEAR POWER PLANTS ON THE COAST

Decisions relating to climate change, and sea level rise scenarios, are particularly important in the design of new nuclear facilities, given the potential hazard, the long operational lifespan and decommissioning period (typically of the order of 100–200 years). Within the UK, the Office for Nuclear Regulation (ONR) and the Environment Agency (EA) published a joint position following the UKCP18 update (Office for Nuclear Regulation and Environment Agency [ONR and EA], 2017, 2020). (Note that the operator (rather than ONR or EA) is responsible for the safety of nuclear plants.) The paper (Office for Nuclear Regulation and Environment Agency [ONR and EA], 2020) sets out the position each organization adopts with regard to climate change allowances and flooding:

- ONR indicate a starting point for climate change allowances could be based on a Medium High emission; this equates to RCP 4.5 from a UKCP18 Marine perspective and the percentile could be interpreted as the 84th percentile (see **Figure 1**), as this is what is suggested is used as a starting point for uncertainties relating to other external hazards.

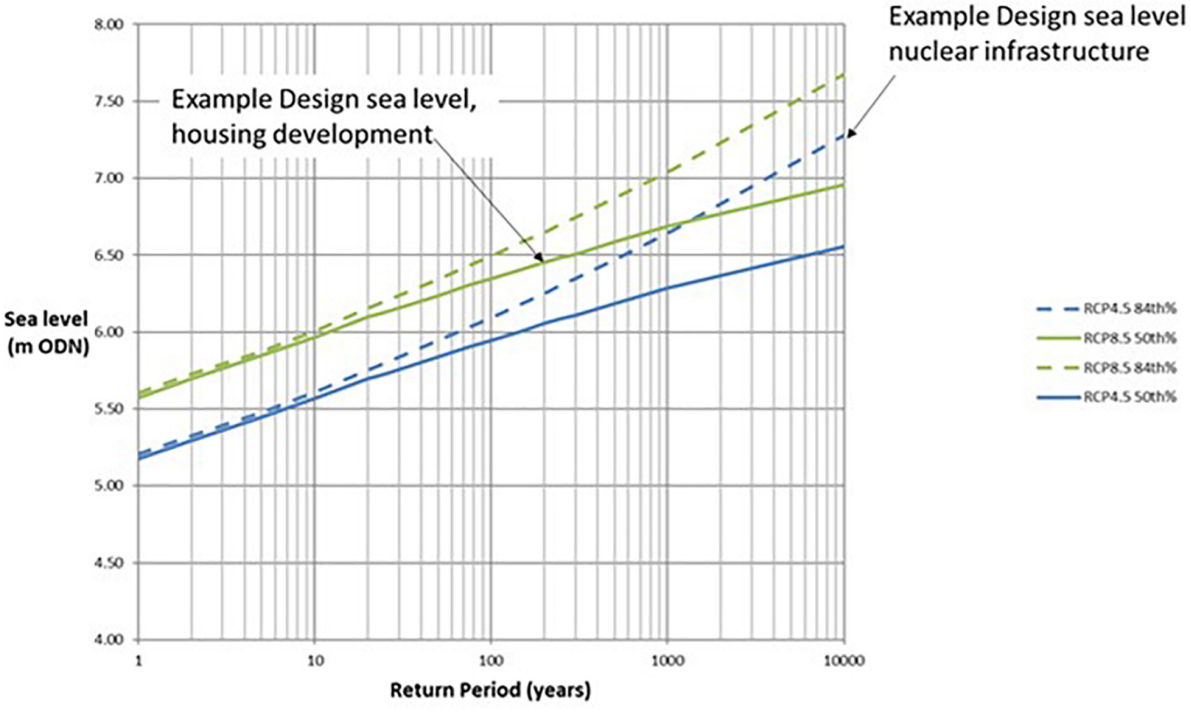

FIGURE 1 | Illustrative exemplar estimates of extreme sea levels for the year 2100 for different end applications for a hypothetical site. The figure utilizes the 9th percentile SLR estimate of the RCP8.5 and 4.5 scenarios, respectively. The percentile annotated in the legend relates to the uncertainty associated with the extrapolation of historical data to extreme values.

They also recommend further sensitivity testing related to the H + + scenario.
- EA guidance (Environment Agency [EA], 2020) prescribes RCP 8.5 and a 95th percentile for the sea level rise scenario (this was subsequently updated to the 70th percentile (for design) and 95th percentile (sensitivity), but implies use of the a 50th percentile when estimating the design return period events (see **Figure 1**). The EA guidance also requires consideration of the H++ scenario.

It may appear to members of the public that the Environment Agency's design requirements are more stringent (conservative) than ONR's. In practice, however, higher return periods (i.e., nominal 10,000 years return period v 200 years return period) and related safety factors to account for uncertainty (84th percentile vs. 50th percentile) are used for nuclear facilities (see **Figure 1**). As would be expected, these return periods and safety factors provide more conservative design criteria, but there is a curious difference relating to the climate change scenarios discussed within the position statement.

The consideration of an ostensibly less stringent climate change scenario within the nuclear sector can cause challenges when communicating with a wider audience. The complexities around communicating uncertainties are further exacerbated by the two sets of percentiles being considered (for extrapolation and for sea level rise uncertainty). Furthermore, the motivation for different organizations adopting different climate change scenarios is not currently provided within the position statement. In the future, statements that provided some background relating to the statement could aid communication.

With regard to the development of new infrastructure, and also protecting existing infrastructure, there is significant current emphasis on a managed adaptive approach and incorporating flexibility (Office for Nuclear Regulation and Environment Agency [ONR and EA], 2017) into designs. This offers an attractive strategy for handling the uncertainty associated with climate change. The approach guards against the unnecessary initial over-design of infrastructure. An initial over-design can impose prohibitive upfront costs and unnecessary environmental implications in terms of the construction footprint and longer-term visual impairment.

Nevertheless, particularly in the case of construction of new infrastructure, there can be an unavoidable requirement to make non-reversible decisions. These could relate to the specification of the level of the footings (platform level) of a nuclear power station development, for example. In these situations, the emphasis can then shift to trading off climate change risks between the platform level for the construction of the new development and a flexible ability introduced within the flood defense component to manage the residual risk associated with climate change uncertainty. Significant research has been conducted into the benefits of adaptive flood defenses and how the economics of these can be used to manage climate change uncertainties (e.g., Woodward et al., 2012; Woodward et al., 2014; Guthrie, 2021).

USE CASE 2—COASTAL PORTS

Ports are not just subject to sea level rise. A number of other climate drivers (National Committee on Coastal and Ocean Engineering [NCCOE], 2004; Stenek et al., 2011; Lumbroso and Woodhouse, 2014) are important including changes to:

- Extreme waves/storm surge, which may damage breakwaters, berthing infrastructure and floating assets and create delays and disruption to port operations.
- Long term wave and current climates, which may increase sedimentation and scour.
- Extremes of rainfall resulting in both river floods and low flows, which may increase sediment loads and damage assets or limit navigation.
- Extreme rainfall resulting in surface water flooding and disruption to port landside operations.
- High winds, damaging vessels and tall assets such as cranes and creating operational delays.

As indicated in **Table 1**, climate services are required for ports both for decision making for routine operations in the short to medium term, but also in the long term for decision making for port planning and infrastructure investment.

When considering infrastructure investment, the anticipated life of the various types of port assets has a big impact on the extent to which climate change needs to be considered. Port investments often fall into two broad categories: those such as crane systems which will probably only have a life of the order of a generation (i.e., around 30 years or less) and those such as breakwaters and quay structures which are anticipated to last (in some form) for a number of generations (at least 100 years).

For investment in single generation assets, it is likely that investment decisions will primarily be influenced by factors other than climate change, such as ship capacity/dwt, required speed of turnaround, storage and transshipment.

TABLE 1 | Types of climate services and decision-making processes potentially supported (after Lumbroso and Woodhouse, 2014).

	Short term (<10 days) weather forecasting	**Medium term (10 days to 1 year) seasonal weather forecasting**	**Long term (>10 years) climate change projections, and baseline climate**
Climate services	Short term forecasts of key variables such as wave agitation (heights, periods, directions) wind speed, storm surge	Medium term forecasts of storminess, extreme tide levels	Historical climate data Assessments of the impacts of observed hazards Projections of change in key variables such as sea level, wave heights, wind speed, storm surge
Decision making processes	Managing risks to operational activities such as berthing and cargo handling	Planning and scheduling operational activities, e.g., maintenance	Strategic port planning Feasibility and design of infrastructure

For investment in multi-generational assets, their capacity to be adapted for climate change should become a much bigger consideration, as this affects the delivery of 24/7 operations, survival of extreme events and post extreme event adaptation.

Future adaptation options for the above may include:

- Ensuring appropriate levels of robustness for a range of future conditions, including building in allowances for increases at the time of construction/installation.
- Investments in tangible assets such as provisions to facilitate future raising of the crest of breakwaters, the operating level of quay walls and berthing/mooring facilities at quay walls.
- Advance planning for replacement structures in the event of damage/failure. The philosophy of the Sendai Build Back Better disaster recovery framework (United Nations Office for Disaster Risk Reduction [UNISDR], 2015) applies here and requires advance planning to avoid a knee-jerk reaction to replace structures on a like-for-like basis.

A mix of measures is therefore needed to adapt to climate change in ports, according to the nature of port operations, assets and their risk exposure. PIANC provides international guidance (PIANC – World Association for Waterborne Transport Infrastructure., 2020) on such a portfolio of measures, which lists a wide range of options (structural, operational and institutional) for adapting or strengthening the resilience of navigation infrastructure assets, operations and systems. Methodologies are also described in PIANC – World Association for Waterborne Transport Infrastructure. (2020) for conducting climate change risk assessment in existing ports. These use quantitative evaluation of multiple hazards and impacts to provide port managers with essential information to identify and prioritize adaptation strategies.

CONCLUSION

This paper has set out a number of considerations to encourage the provision of more appropriate climate services information for end users. Use of the term climate services in situations unrelated to supporting adaptation to and mitigation of climate change should be avoided.

Better investment decisions could be made if Bayesian frameworks were used to assign probabilities to RCP scenarios. Associated predictions need to cover all types of climate change influences not just sea level rise and ideally provide concurrent time series to allow evaluation of dependencies. Guidance on climate information published by official bodies needs to adopt a consistent approach, with a clear narrative that describes the transition from science to guidance. The form in which climate services information is needed for the required end user decisions needs careful thought, including appropriate communication of the associated uncertainties using good practices and experiences from related sectors.

DATA AVAILABILITY STATEMENT

The original contributions presented in the study are included in the article/supplementary material, further inquiries can be directed to the corresponding author/s.

AUTHOR CONTRIBUTIONS

JS drafted overall manuscript and acted as editor. BG provided important material on climate services challenges and the nuclear power use case. DL and TM provided the information for the ports use case. All authors contributed to the article and approved the submitted version.

FUNDING

This work was funded by our employer, HR Wallingford.

REFERENCES

Allen, M., Raper, S., and Mitchell, J. (2001). Uncertainty in the IPCC's Third Assessment Report. *Science* 293, 430–433.

Arvai, J., and Rivers, III. (2013). *Effective risk communication*. New York, NY: Routledge.

Brasseur, G. P., and Gallardo, L. (2016). Climate services: Lessons learned and future prospects. *Earth's Future* 4, 79–89. doi: 10.1002/2015ef000338

Chester, M., Underwood, B. S., Allenby, B., Garcia, M., Samaras, C., Markolf, S., et al. (2021). Infrastructure resilience to navigate increasingly uncertain and complex conditions in the Anthropocene. NPJ *Urb. Sustainab.* 1:4. doi: 10.1038/s42949-021-00016-y

CIRIA (2013). *The International Levee Handbook*. Report C731. London: CIRIA.

Digman, C., Balmforth, D., Kellagher, R., and Butler, D. (2006). *Designing for exceedance in urban drainage - good practice*. Report C635, London: CIRIA.

Environment Agency [EA] (2020). *Flood risk assessments: climate change allowances*. Bristol: Environment Agency.

Gouldby, B., Wyncoll, D., Panzeri, M., Franklin, M., Hunt, T., Hames, D., et al. (2017). Multivariate extreme value modelling of waves, winds and sea levels around the coast of England. *Proc. Inst. Civ. Eng..Mar. Eng.* 1, 3–20. doi: 10.1680/jmaen.2016.16

Guthrie, G. (2021). Adapting to rising sea levels: how short-term responses complement long-term investment. *Env. Resour. Econ.* 78, 635–668. doi: 10.1007/s10640-021-00547-z

Hausfather, Z., and Peters, G. P. (2020). Emissions–the 'business as usual' story is misleading. *Nature* 577, 618–620. doi: 10.1038/d41586-020-00177-3

Hewitt, C., Mason, S., and Walland, D. (2012). The global framework for climate services. *Nat. Clim. Change* 2, 831–832. doi: 10.1038/nclimate1745

Le Cozannet, G., Nicholls, R. J., Hinkel, J., Sweet, W. V., McInnes, K. L., Van de Wal, R. S. W., et al. (2017). Sea level change and coastal climate services: the way forward. *J. Mar. Sci. Eng.* 5:49. doi: 10.3390/jmse5040049

Lumbroso, D., and Woodhouse, G. (2014). *Future Climate Change for Africa - The use of climate services for decision making in the port sector*. Report MAR5322-RT003-R02-00, HR Wallingford: Wallingford.

Morriss, P. (1977). Combining Expert Judgments: A Bayesian Approach. *Manag. Sci.* 23, 679–693. doi: 10.1287/mnsc.23.7.679

National Committee on Coastal and Ocean Engineering [NCCOE] (2004). *Guidelines for Responding to the Effects of Climate Change in Coastal and Ocean Engineering, 2004 Update*. Engineers Australia: The National Committee on Coastal and Ocean Engineering.

Nicholls, R. J., Hanson, S. E., Lowe, J. A., Warrick, R. A., Lu, X., and Long, A. J. (2014). Sea-level scenarios for evaluating coastal impacts. Wiley Interdisciplinary Reviews: Climate Change, 5, 129–150. doi: 10.1002/wcc.253

Office for Nuclear Regulation and Environment Agency [ONR and EA]. (2017). *Principles for Flood and Coastal Erosion Risk Management, Joint Advice Note, Version 1*. Redgrave Court: Office for Nuclear Regulation.

Office for Nuclear Regulation and Environment Agency [ONR and EA]. (2020). *Use of UK Climate Projections 2018 (UKCP18) Position Statement – November 2020 Revision*. Redgrave Court: Office for Nuclear Regulation.

Office for Nuclear Regulation [ONR]x. (2018). *External Hazards*. Report NS-TAST-GD-013 Revision. Redgrave Court: Office for Nuclear Regulation, 7.

Oppenheimer, M., Little, C., and Cooke, R. (2016). Expert judgement and uncertainty quantification for climate change. *Nat. Clim. Change* 6, 445–451. doi: 10.1038/nclimate2959

Palmer, M., Howard, T., Tinker, J., Lowe, J., Bricheno, L., Calvert, D., et al. (2018). *UKCP18 Marine report - November 2018*. Exeter, The Met Office. Bristol: Environment Agency.

PIANC – World Association for Waterborne Transport Infrastructure. (2020). *Climate change adaptation planning for ports and inland waterways*. Report 178. Brussels: PIANC.

Qian, Y., Jackson, C. S., Giorgi, F., Booth, B., Duan, Q., Forest, C., et al. (2016). Uncertainty quantification in climate modeling and projection. *Bull. Am. Meteorol. Soc.* 97, 821–824. doi: 10.1175/BAMS-D-15-00297.1

Riahi, K., Van Vuuren, D. P., Kriegler, E., Edmonds, J., O'neill, B. C., Fujimori, S., et al. (2017). The shared socioeconomic pathways and their energy, land use, and greenhouse gas emissions implications: an overview. *Glob. Environ. Change* 42, 153–168.

Royal Society. (2014). *Resilience to extreme weather*. Science Policy Centre report 02/14, London: The Royal Society.

Serinaldi, F. (2015). Dismissing return periods! *Stoch Environ. Res. Risk Assess* 29, 1179–1189. doi: 10.1007/s00477-014-0916-1

Smith, R., Tebaldi, C., Nychka, D., and Omearns, L. (2009). Bayesian Modeling of Uncertainty in Ensembles of Climate Models. *J. Am. Stat. Assoc.* 2009, 97–116. doi: 10.1198/jasa.2009.0007

Stenek, V., Amado, J. C., Connell, R., Palin, O., Wright, S., Pope, B., et al. (2011). *Climate risk and business: ports*. Washington, D.C: International Finance Corporation.

Tebaldi, C., Smith, R., Nychka, D., and Omearns, L. (2005). Quantifying Uncertainty in Projections of Regional Climate Change: A Bayesian Approach to the Analysis of Multimodel Ensembles. *Journal of Climate* g1524–g1540. doi: 10.1175/JCLI3363.1

United Nations Office for Disaster Risk Reduction [UNISDR] (2015). *Sendai Framework for Disaster Risk Reduction 2015-2030*. Geneva: UNISDR.

Vousdoukas, M. I, Mentaschi, L., and Hinkel, J. (2020). Economic motivation for raising coastal flood defenses in Europe. *Nat. Commun.* 11:2119. doi: 10.1038/s41467-020-15665-3

Wong, P. P., Losada, J. P., Gattuso, J., Hinkel, A., Khattabi, K. L., McInnes, Y., et al. (2014). *Coastal systems and low-lying areas*. Cambridge, MA: Cambridge University Press, 361–409.

Woodward, M., Gouldby, B., Kapelan, Z., Khu, S. T., and Townend, I. (2012). Real options in flood risk management decision making. *J. Flood Risk Man* 4, 339–349. doi: 10.1111/j.1753-318x.2011.01119.x

Woodward, M., Kapelan, Z., and Gouldby, B. (2014). Adaptive Flood Risk Management Under Climate Change Uncertainty Using Real Options and Optimization. *Risk Analysis* 34, 75–92. doi: 10.1111/risa.12088

Conflict of Interest: The authors declare that the research was conducted in the absence of any commercial or financial relationships that could be construed as a potential conflict of interest.

Publisher's Note: All claims expressed in this article are solely those of the authors and do not necessarily represent those of their affiliated organizations, or those of the publisher, the editors and the reviewers. Any product that may be evaluated in this article, or claim that may be made by its manufacturer, is not guaranteed or endorsed by the publisher.

Copyright © 2021 Simm, Gouldby, Lumbroso and Matthewson. This is an open-access article distributed under the terms of the Creative Commons Attribution License (CC BY). The use, distribution or reproduction in other forums is permitted, provided the original author(s) and the copyright owner(s) are credited and that the original publication in this journal is cited, in accordance with accepted academic practice. No use, distribution or reproduction is permitted which does not comply with these terms.

frontiers in Marine Science

REVIEW
published: 03 September 2021
doi: 10.3389/fmars.2021.703425

European Copernicus Services to Inform on Sea-Level Rise Adaptation: Current Status and Perspectives

Angélique Melet[1], Carlo Buontempo[2], Matteo Mattiuzzi[3], Peter Salamon[4], Pierre Bahurel[1], George Breyiannis[4], Samantha Burgess[2], Laurence Crosnier[1], Pierre-Yves Le Traon[1], Lorenzo Mentaschi[4], Julien Nicolas[2], Lorenzo Solari[3,5], Freja Vamborg[2] and Evangelos Voukouvalas[6]*

[1] Mercator Ocean International, Ramonville-Saint-Agne, France, [2] European Centre for Medium Range Weather Forecasts, Reading, United Kingdom, [3] European Environment Agency, Copenhagen, Denmark, [4] European Commission, Joint Research Center, Ispra, Italy, [5] Centre Tecnològic de Telecomunicacions de Catalunya (CTTC/CERCA), Castelldefels, Spain, [6] Unisystems Luxembourg Sàrl, Luxembourg, Luxembourg

OPEN ACCESS

Edited by:
Robert James Nicholls, University of East Anglia, United Kingdom

Reviewed by:
Maria Gabriella Gaeta, University of Bologna, Italy
Milena Menna, Istituto Nazionale di Oceanografia e di Geofisica Sperimentale, Italy

***Correspondence:**
Angélique Melet
amelet@mercator-ocean.fr

Specialty section:
This article was submitted to Coastal Ocean Processes, a section of the journal Frontiers in Marine Science

Received: 30 April 2021
Accepted: 26 July 2021
Published: 03 September 2021

Citation:
Melet A, Buontempo C, Mattiuzzi M, Salamon P, Bahurel P, Breyiannis G, Burgess S, Crosnier L, Le Traon P-Y, Mentaschi L, Nicolas J, Solari L, Vamborg F and Voukouvalas E (2021) European Copernicus Services to Inform on Sea-Level Rise Adaptation: Current Status and Perspectives. Front. Mar. Sci. 8:703425. doi: 10.3389/fmars.2021.703425

Sea-level rise is a direct consequence of climate change. Primarily due to ocean thermal expansion and transfer from land ice (glaciers, ice sheets) to the ocean, sea-level rise is therefore an integrated indicator of climate change. Coastal zones and communities are expected to be increasingly threatened by sea level changes, with various adverse and widespread impacts. The European Union's Earth Observation Programmed, Copernicus, monitors our planet and its environment, for the ultimate benefit of society. This includes the monitoring of sea level changes and the provision of ancillary fields needed to assess sea-level rise coastal risks, to guide adaptation and to support related policies and directives. Copernicus is organized with a space component, including dedicated Earth Observation satellites (Sentinel missions), and services, which transform the wealth of satellite, in situ and integrated numerical model information into added-value datasets and information usable by scientists, managers and decision-makers, and the wider public. Here, an overview of the Copernicus products and services to inform on sea level rise adaptation is provided. Perspectives from Copernicus services on future evolutions to better inform on coastal sea level rise, associated risks, and support adaptation are also discussed.

Keywords: sea level rise, Copernicus, climate services, coastal zone, flooding, satellite observations, numerical models

INTRODUCTION

Sea-level (SL) changes are a major threat for coastal zones (Cazenave and Le Cozannet, 2014; Hinkel et al., 2015; Oppenheimer et al., 2019), causing flooding, salinization of soils, aquifers and surface water, degrading coastal ecosystems. At the same time, population and economic assets are increasingly exposed to sea-level rise (SLR) adverse effects due to current and projected growth in coastal population and urbanization (e.g., Neumann et al., 2015; Wolff et al., 2020). In Europe alone, more than 50 million people live in the low-elevation coastal zone and 30 million in the 100-year event flood coastal plain (Neumann et al., 2015). Risks (including these associated with sea-level rise) are due to a combination of sea-level hazards, exposure, and vulnerability

(Cardona et al., 2012). Mitigation and adaptation measures can reduce SLR related risks (e.g., Hinkel et al., 2014; Oppenheimer et al., 2019), and should be supported by useful and authoritative information.

In terms of hazards, sea level has risen by ∼20 cm since 1900 (Dangendorf et al., 2017; Oppenheimer et al., 2019). In 2100, compared to the 1986-2005 baseline, sea level is projected to rise by 43 ± 15 cm (likely range, probability higher than 66% that SLR falls within this range) in a low-emission/high-mitigation scenario (RCP2.6), or 84 ± 30 cm in a high-emission/low-mitigation scenario (RCP8.5) (Oppenheimer et al., 2019). Historical extreme water levels, such as these experienced during storms, will be reached more often during the 21st century due to the gradual mean sea level rise, transforming historical centennial events into yearly events in many parts of the world before 2100 (Vousdoukas et al., 2018a; Oppenheimer et al., 2019). Locally, this trend can be exacerbated or reduced by the projected changes in magnitude and frequency of meteorological extremes such as storm surges (Vousdoukas et al., 2018a; Mori et al., 2019), waves (Mentaschi et al., 2017; Morim et al., 2019; Meucci et al., 2020), and their interaction with precipitations (Wahl et al., 2015; Bevacqua et al., 2019, 2020) and other extremes. As a consequence, the 100-year extreme water levels (with a chance of occurence of 1% every year) will increase, on a global average, from 34 to 76 cm under a moderate-emission/moderate-policy scenario (RCP4.5) to 58-172 cm in a high-emission/low-mitigation scenario (RCP8.5) in 2100, compared to 2000 (Vousdoukas et al., 2018a). An increase of sea levels also poses a threat as a driver of coastal erosion (Mentaschi et al., 2018), and could lead to an obliteration of significant portions of coasts and beaches, especially in low-lying areas (Vousdoukas et al., 2020a).

Coastal zones are increasingly more densely populated and host megacities, critical assets, and are fostering economic growth, a trend accompanied by land conversion and urbanization (e.g., Neumann et al., 2015). The exposure of people and assets to SLR hazards is therefore widespread and increasing. Changes in the coastal environment can also enhance the vulnerability of coastal zones. For instance, coastal ecosystems such as dunes, reefs, mangroves are playing a regulating role and protect the shoreline (Temmerman et al., 2013; Ferrario et al., 2014; Fernandez-Montblanc et al., 2020). The degradation of such ecosystems can increase the exposure of coastal zones, population and assets to extreme sea levels.

In Europe, several regions are particularly exposed to SLR and its adverse effects, which include flooding and submergence of coastal areas, erosion, saltwater intrusion in surface and ground waters, degradation of coastal ecosystems and habitats, and impeded drainage. Deltas, such as the Rhine-Meuse-Escault (NL), Rhone (FR), Pô (IT), and Ebro (SP), are regions particularly vulnerable to SLR. Rotterdam and Amsterdam especially are amongst the world's most exposed cities in terms of population living in the 100-year event flood plain (Hallegatte et al., 2013). In addition to human fatalities, economic losses due to coastal flood risks are huge. The Mediterranean coast concentrates cities where the annual average losses due to coastal flooding will increase the most by 2050, if adaptation only maintains present defense standards or flood probability (Hallegatte et al., 2013). This is due to the fact that many of these cities were built close to the shore, in a region where historical sea level variability has been low (e.g., small tidal range, interannual variability). Presently, the expected annual damage of coastal flood in Europe is of €1.25 billion euros, but could increase by 2-3 orders of magnitudes if coastal adaptation is only maintained to its current level (Vousdoukas et al., 2018b). The increased hazards posed by sea-level rise in response to climate change has been identified as the main driver of future rise in coastal flood losses, with the relative importance of exposure (coastward migration, urbanization and rising asset values) diminishing over time (Vousdoukas et al., 2018b).

To decrease SLR induced risks and increase the resilience of our coastal zones and societies, different adaptation measures can be implemented. Main SLR adaptation responses include hard protection (e.g., dykes), accommodation (e.g., flood-resistant buildings, lifted housing), ecosystem-based protection (e.g., dunes, mangroves, reefs), and inland retreat (planned relocation) (Oppenheimer et al., 2019). A cost-benefit analysis of adaptation to SLR through additional protection with dykes showed that at least 83% of flood damages in Europe could be avoided by elevating dykes along a quarter to a third of Europe's coastline (Vousdoukas et al., 2020b). Although the focus is here on adaptation, mitigation of climate change through reduction of emissions of greenhouse gasses and / or carbon dioxide removal (Rogelj et al., 2018) should be pursued as well to reduce hazards themselves as SLR and extreme sea levels are projected to be approximately halved in a low-emission/high-mitigation scenario (RCP2.6) compared to a high-emission/low-mitigation climate change scenario (RCP8.5) (Oppenheimer et al., 2019).

Faced with sea-level rise potential adverse effects, countries and state organizations have issued various policies to monitor, mitigate and adapt to SLR risks. Among the different existing policies, the Integrated Coastal Zone Management, EU Flood Risk Directive, EU Water Framework Directive, the EU Green Deal and the new EU Strategy on Adaptation to Climate Change[1] are of particular importance (e.g., Nixon, 2015; Bisaro et al., 2020). To guide adaptation, information is a prerequisite. Different kinds of SLR information are needed for different kinds of contexts to support coastal adaptation decision making (Hinkel et al., 2019).

Europe's Earth Observation (EO) Program, Copernicus, monitors our planet and its environment, for the ultimate benefit of society. The Program is funded, coordinated and managed by the European Commission and is driven by policies, to support them, and by requirements from users, including coastal managers. The space component of Copernicus, with the Sentinel satellite family, is currently the largest world producer of freely and openly available EO data (Benveniste et al., 2020). Sentinel-1, 2, 3, and 6 deliver information on sea level and on other required fields to monitor drivers of sea level hazards (e.g., surface wind and waves) and on risk itself (Melet et al., 2020a). Copernicus Services then transform the wealth of satellite data and combine them with in-situ and integrated numerical models to produce added-value, relevant, quality-assessed datasets and information (sections "Sea-Level Change Hazard" to "Vulnerability"). On top of this integrated-system, added-value products layer, additional

[1]https://eur-lex.europa.eu/legal-content/EN/TXT/?uri=COM:2021:82:FIN

layers have been developed in Copernicus Services to analyze and process the data into information usable by the scientific community, managers and policy makers, other downstream sectors and to provide services associated to information delivery (sections "Managing and Monitoring of Coastal Floods and Risks" to "A Service Layer").

Copernicus value-adding activities and products are streamlined through six services. Of particular importance for SLR adaptation are:

The Copernicus Marine Environment Monitoring Service (CMEMS[2]), also known as the Copernicus Marine Service, implemented by Mercator Ocean International. CMEMS provides regular and systematic reference information on the physical and biogeochemical state, variability and dynamics of the ocean, including sea level, for the European regional seas and the global ocean, over the past decades, for the current state and for the coming days (forecasts).

The Copernicus Land Monitoring Service (CLMS[3]), implemented by the European Environment Agency (EEA) and the European Commission Directorate General Joint Research Centre (JRC). CLMS provides geospatial information on land cover and its changes, land use, vegetation state, water cycle, cryosphere and earth surface energy to a broad range of users in Europe and across the world in the field of environmental applications.

The Copernicus Climate Change Service (C3S[4]), implemented by the European Centre for Medium-Range Weather Forecasts (ECMWF). C3S supports the adaptation and mitigation policies of the European Union by providing consistent and authoritative information about the past, present and future climate change in Europe and the rest of the world.

The Copernicus Emergency Management Service (CEMS[5]), implemented by the JRC. CEMS supports all actors involved in the management of natural or manmade disasters by providing geospatial data and images for informed decision making. CEMS constantly monitors Europe and the globe for signals of an impending disaster, such as flooding, or evidence of one happening in real time and provides maps, time-series or other relevant information to better manage disaster risk.

The Copernicus Program is long-term oriented, and Copernicus Services will start a new phase for the 2021-2027 period.

This paper provides a review of the current status of Copernicus Services with respect to sea level rise adaptation, describing products, information and services provided to users (section "Current Status of Copernicus Services Information for Sea-Level Rise Adaptation"). Perspectives from Copernicus services on future evolutions during the 2021-2027 period to better inform on coastal sea-level changes and associated risks are discussed in section "Perspectives on Copernicus Services for SLR Adaptation".

[2]https://marine.copernicus.eu/

[3]https://land.copernicus.eu/

[4]https://climate.copernicus.eu/

[5]https://emergency.copernicus.eu/

CURRENT STATUS OF COPERNICUS SERVICES INFORMATION FOR SEA-LEVEL RISE ADAPTATION

An overview of the current information provided by Copernicus Services for SLR adaptation is provided in this section. Generally speaking, risk is the combination of hazard, exposure, and vulnerability (Cardona et al., 2012). This section starts by addressing these three components (**Figure 1**).

Sea-Level Change Hazard

Sea-level changes and their different components are being monitored in Copernicus across a wide range of time-scales based on observations (in situ and satellite) and numerical models (climate models, reanalyses, forecasts). Monitoring over the last decades can provide a historical baseline of sea level changes, which is instrumental in characterizing e.g., sea level extremes, return periods, contributions of different drivers. Forecasts with a few days lead time can feed early warning systems. Projections over the 21st century can inform mid to long-term adaptation strategies.

A multitude of processes are driving relative (i.e., relative to land elevation) sea level changes at global, regional and coastal scales (e.g., Woodworth et al., 2019). Global mean sea level (GMSL) rise is due both to thermal expansion of the warming ocean and to the transfer of land ice and water mass to the ocean (from ice sheets, glaciers and land water storage changes) (e.g., WCRP Global Sea Level Budget Group, 2018). The glacial isostatic adjustment (GIA) also induces GMSL changes due to modifications in ocean basin geometry (e.g., Spada and Melini, 2019). At regional scales, sea level changes are mostly driven by the redistribution of heat, salt and mass within the ocean forced by ocean circulations (e.g., Meyssignac and Cazenave, 2012; Forget and Ponte, 2015). Transfers of mass from land to the ocean (GIA, contemporary land ice mass loss) induce changes in Earth's gravity, rotation as well as solid Earth viscoelastic deformations, which in turn induce regional relative sea level changes (Farrell and Clark, 1976; Riva et al., 2010). In terms of SLR related hazards, the sea level that matters is the relative coastal sea level change. At the coast, sea level changes are due to the superimposition of the offshore regional mean sea level and of changes driven by additional processes which express themselves or are amplified in the coastal zone such as tides, wave set up and swash, storm surges, river discharges (e.g., Woodworth et al., 2019) and their interactions (Idier et al., 2019). Tides, storm surges and waves are especially important for extreme events, which pose the greatest hazards. Monitoring the different processes causing relative coastal sea level changes is important in assessing the local coastal zone risk as they can impact the coast differently.

Sea Level Observations

In situ and satellite observations of sea level deliver time-series of past and near-real-time sea-level changes. The accuracy of high-frequency tide gauge sea level measurements is of 1-cm (Intergovermental Oceanographic Commission (IOC), 2006)

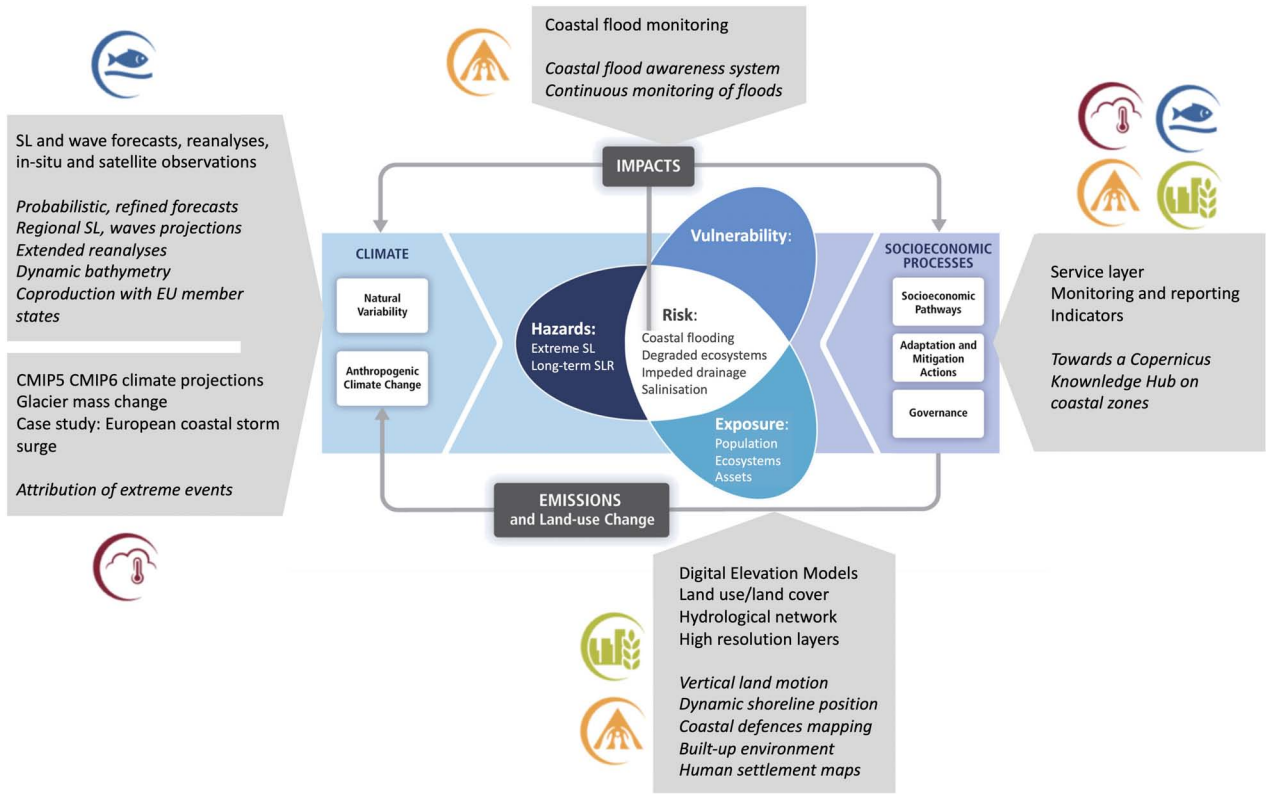

FIGURE 1 | Illustrative Copernicus services products and activities relevant to sea-level rise adaptation (in gray boxes). Activities listed in italics correspond to potential new services in Copernicus 2 (2021-2027). Symbols indicate the different corresponding Copernicus Services: CMEMS in blue, C3S in red, CEMS in orange, CLMS in green. In the figure center, the components of SLR related risks, e.g., hazard, exposure and vulnerability, are listed. Adaptation aims at reducing SLR risks. Based on figure 1.1. from the IPCC SREX report (Lavell et al., 2012). SL stands for sea level.

while uncertainties for sea level rise observed by spatial altimetry are of 0.4 mm year^{-1} for global mean sea level rise (Ablain et al., 2019) and are lower than 1.5 mm year^{-1} for trends at regional scale at the 90% confidence level (Prandi et al., 2021). They provide the ground truth for assessment of numerical models used to produce forecasts (and are constraining them through data assimilation), climate hindcasts and projections. They also form the historical baseline to monitor the evolution of sea level, including extremes, or the reference level used for national height systems (Wöppelmann et al., 2014). Observations are also key for understanding the factors causing sea level changes.

Tide gauges provide local observations of relative sea level changes at a high frequency, which is needed to capture sea level extremes (Woodworth et al., 2016, see also an example in **Figures 2C,D** for Venice in November 2019). Some tide gauge records date back to the 18th century and the network has extended over time (Marcos et al., 2019). Tide gauge records are provided in CMEMS with a focus on Europe and on near-real time and high-frequency data. Real time quality control procedures are applied following GLOSS standards and a collaboration with the EuroGOOS Tide Gauge Task Team has been set up to improve the quality control of tide gauge records in CMEMS. Wave buoys data are also distributed. In addition to their own value, these datasets are used for the quality assessment of modeled sea level forecasts and reanalyses in CMEMS.

Satellite radar altimetry, including data from the reference Jason-3 mission optimized for climate monitoring (to be replaced in 2021/2022 by Sentinel 6 M. Freilich) and from the complementary Sentinel-3A&B missions, provides information on the mean, offshore regional absolute sea level. Altimetric products have been a reference source of information for global mean and regional sea level rise since 1993 (**Figure 3**). A review of altimetric products for sea-level monitoring in Copernicus can be found in Legeais et al. (under review in this issue). Copernicus Marine Service provides along-track (level 3) and gridded (level 4) regional (all European seas) and global altimetric products based on level 2P and level 3 datasets provided by space agencies (especially EUMETSAT for Jason-3 and Sentinel 3A&B). C3S provides specific global and regional gridded (level 4) products optimized for climate change monitoring.

Both CMEMS and C3S provide a global, reprocessed, delayed-time gridded (1/4°) daily altimetric product covering the altimetric era (starting in 1993, **Figure 3**). The underpinning system is the Data Unification and Altimeter Combination System reprocessed delayed-time altimeter sea level product release, DUACS DT2018 (Taburet et al., 2019). This version does not correct for the known drift of the TOPEX-A instrument

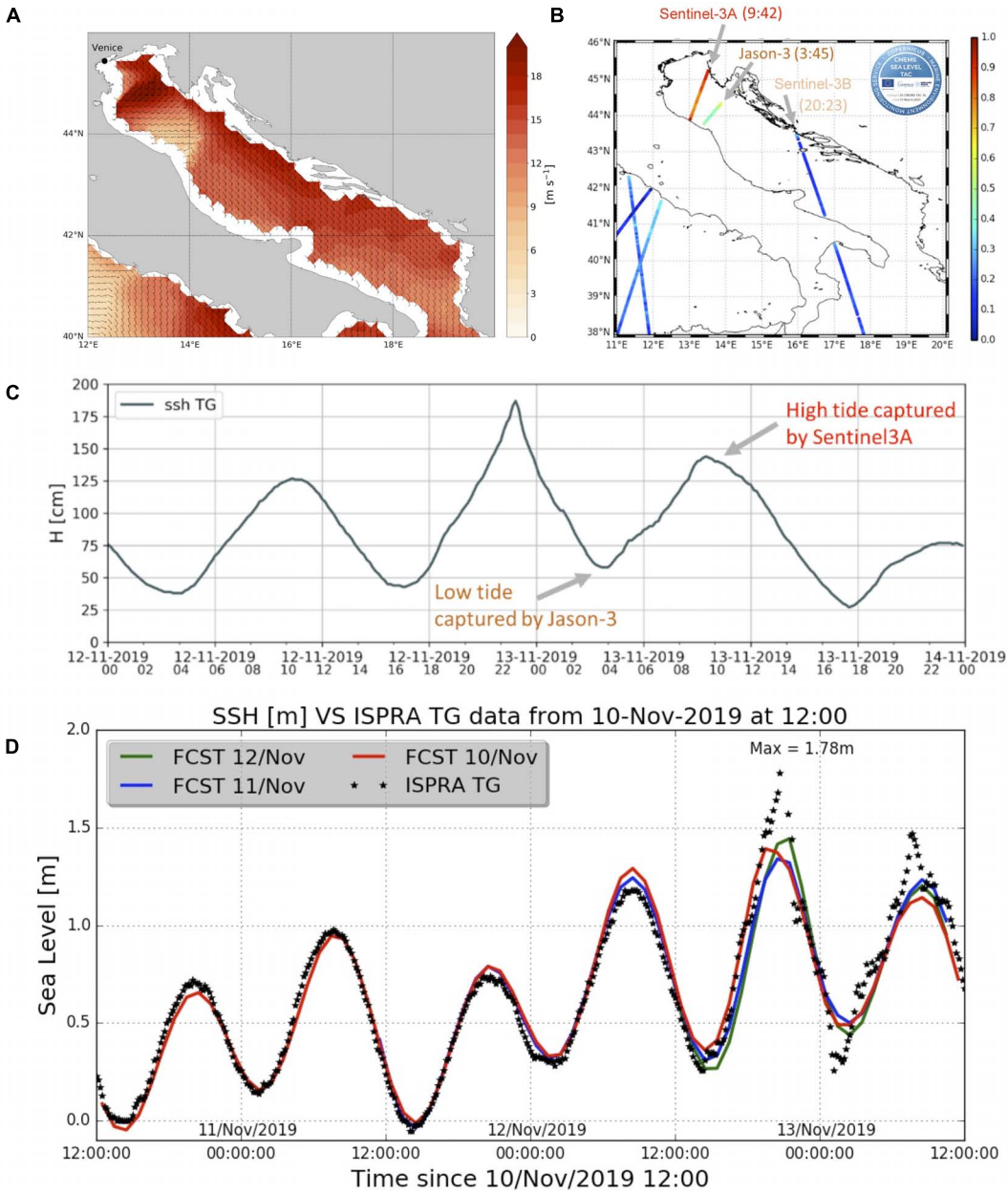

FIGURE 2 | Copernicus Marine Service satellite and forecasting information for Storm Detlef, causing flooding in Venice in November 2019. **(A)** Sea surface winds in the Adriatic Sea about 2 h before the record flood event of 12/11/2019, as measured by ASCAT satellite scatterometers and highlighting southeastern, Sirocco winds. Source: CMEMS Wind TAC (Thematic Assembly Center). **(B)** Sea level anomalies measured by the altimetry constellation over the Adriatic seas on 13/11/2019. The Sea Level represented is the total elevation (not suppressing tides or atmospheric effect). Unit: Elevation in m, Time in GMT. S3A (Sentinel-3A). Source: CMEMS Sea level TAC. **(C)** Sea level variations measured by the Punta Della Salute tide gauge (in cm, Time in GMT). The times of the Sentinel-3A and Jason overpasses (panel **B**) are added to the graph. Source: CMEMS In Situ TAC. **(D)** Forecasted sea levels in Venice region during the mid-November, 2019 acqua alta events. CMEMS MedFS forecasts with a lead time of 3 days are shown: forecast produced on 10/11/2019 (red line), recomputed on 11/11/2019 (blue line) and on 12/11/2019 (green line). Forecasts are compared to observations (black dots) at the ISPRA Tide Gauge. Source: CMEMS Mediterranean Sea Monitoring and Forecasting Center.

during 1993-1998 (Legeais et al., 2020) nor for glacial isostatic adjustment at regional scales. The C3S sea level Climate Data Record (CDR) is optimized for long-term homogeneity and stability and follows the recommendations of the ESA Sea Level CCI project (Legeais et al., 2018). The C3S CDR covers the period from January 1993 onward and relies on 1 Hz altimeter measurements from a two-satellite constellation throughout the period. In this configuration, one satellite is used as reference and ensures the long-term stability of the data record while the other (complementary) satellite is used to improve accuracy,

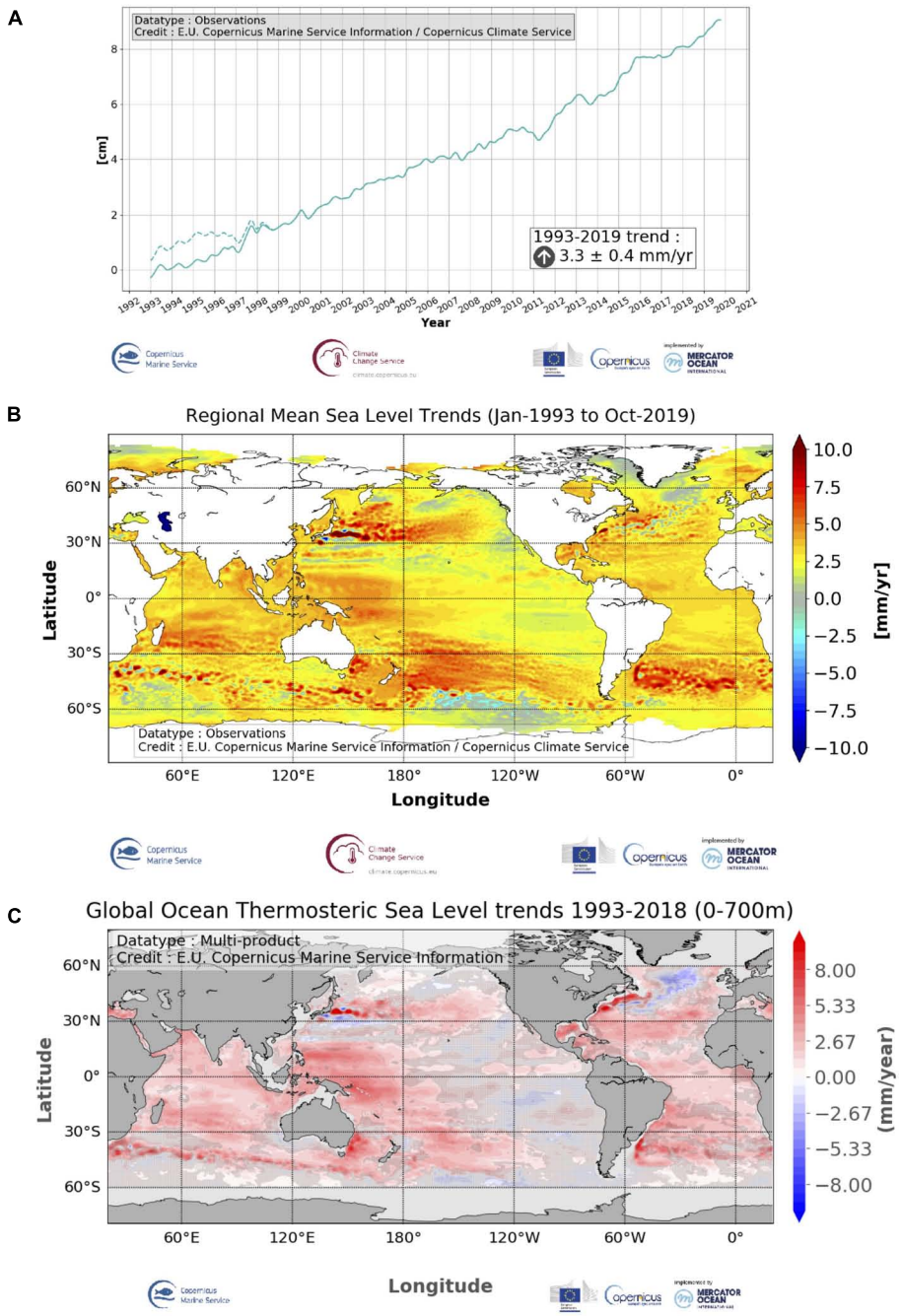

FIGURE 3 | Ocean Monitoring Indicators for sea level rise since 1993. **(A)** Global mean sea level evolution over January 1993-October 2019 (in cm) from the satellite altimetry using the DUACS delayed-time (reprocessed version DT-2018) altimeter sea level gridded products distributed by the C3S and CMEMS. The timeseries is low-pass filtered, the annual and semi-annual periodic signals are adjusted, and the curve is corrected for the GIA using the ICE5G-VM2 GIA model (Peltier, 2004). During 1993-1998, the dashed line shows an estimate of the global mean sea level corrected for the TOPEX-A instrumental drift, based on comparisons between altimeter and tide gauges measurements (Ablain et al., 2020). **(B)** Spatial distribution of the trends of the satellite altimeter sea level observations (in mm/yr) over January 1993-October 2019 using the DT-2018 altimeter sea level gridded products distributed by C3S and by CMEMS. No Glacial Isostatic Adjustment correction is applied on the altimeter data. **(C)** Regional trends over the period 1993-2018 of ocean heat content (0-700 m) anomalies relative to the 1993-2014 reference period based on the ensemble mean of the multi-product approach (2 global reanalyses: GLORYS, ORAS5; 2 in situ based reprocessed products: CORA, ARMOR).

sample mesoscale processes and enhance coverage poleward of 66° latitude. The reference missions include TOPEX/Poséidon, Jason-1 and Jason-2 and Jason-3. The complementary missions consist of ERS-1, ERS-2, Envisat, SARAL/AltiKa and Sentinel-3A. The CMEMS gridded reprocessed altimetric product uses the same reference missions but includes all available complementary

altimeter missions. It is more focused on providing the best estimate of sea level at a given time (in particular to best capture ocean mesoscale activity) than on long-term homogeneity of the time-series. As a result, this product is based on multi-satellite missions with a varying coverage over the period (from 1 to 6 missions depending on the satellite constellation, including TOPEX/Poséidon, ERS, Envisat, GFO, Jason-1, Jason-2, Jason-3, Cryosat, Altika, HY2BA, Sentinel 3-A and B). Different reference mean sea surface fields are also used in CMEMS and C3S (Legeais et al., under review in this issue).

The two-satellite constraint in the C3S CDR leads to lower spatial sampling of the ocean surface than in the CMEMS sea level product and thus greater uncertainty over coastal areas, but to a stronger stability of the time-series for climate applications. Fully reprocessed CDR, produced in collaboration between C3S and CMEMS, are scheduled for release in 2021 and will benefit from reprocessed L2P input data for some missions, new L2 geophysical corrections (including atmospheric corrections forced by ERA5) and optimized L3/L4 mapping procedures.

Future evolution of the C3S and CMEMS gridded reprocessed products will include the replacement of the current reference mission (Jason-3) with the Sentinel-6 Michael Freilich after the completion of a cross-calibration phase (section "New Satellite Missions").

In addition to the global gridded products, regional reprocessed gridded products are also distributed by CMEMS and C3S for the Mediterranean and Black Seas, at a higher resolution (1/8°) for refined regional sea level rise estimates.

Near-real time along-track sea level products tailored for data assimilation in ocean models (used to produce sea level reanalyses and forecasts, see section "Sea Level Observations") are also available at global and regional scales (see an example in **Figure 2B**). The reference products are at 1 Hz resolution (7 km resolution along the satellite tracks). Such products have limitations in coastal zones, due to land contamination of the radar signal, less accurate geophysical corrections, editing of the data etc. (e.g., Birol et al., 2017; Cipollini et al., 2017; Benveniste et al., 2019; Melet et al., 2020a).

Recently, a higher-resolution along-track satellite product has been added to the CMEMS portfolio. This high-resolution altimetric product is at 5 Hz (1.3 km along the track), covers the North Atlantic and European Seas, and is provided together with the so-called geophysical corrections applied to the altimetric signal (e.g., tides, dynamic atmospheric correction which includes storm surge signals, long-wave errors, etc.) so that the physical content of the sea level from the data can be adapted to user needs. This higher-resolution product better captures the sea level signal in tide gauge records compared to the conventional along-track product. This product is currently only available over May 2016 to Dec 2018, but will be operationally produced in the coming years.

In addition to the mean, offshore sea level provided by altimetry, ancillary fields are needed to get the total water level at the coast (e.g., Melet et al., 2018; Marcos et al., 2019). These include tides, waves, surface atmospheric pressure and winds. Near real time information on significant wave height from spatial missions (Jason-3, Sentinel-3A, Sentinel-3B, Cryosat-2, SARAL/AltiKa, CFOSAT and HY-2B) are provided in CMEMS over the global ocean both as a gridded and along-track products. Swell systems integral parameters including partition significant wave height, partition peak period and partition peak or principal direction, inferred from Sentinel-1 missions, are given along swell propagation paths for individual storms in near-real time. Finally, satellite-based wind products are delivered, using in particular scatterometer observations (**Figure 2A**). Satellite observed wind fields can be used to correct atmospheric forcing, which are of prime importance to forecasting extreme events and their timing.

Forecasts and Hindcasts of Sea Level

Numerical modeling systems are the backbone of ocean and wave hindcasts (modeling past evolutions over the last decades), reanalyses (hindcasts constrained by observations through routine assimilation of in situ and space observations) and forecasts (over a few days to weeks). Such models are solving the equations governing ocean and wave dynamics and are often constrained by observations through assimilation of in situ and satellite observations. They provide a synoptic spatial and temporal monitoring of the ocean. This is especially important given the existing limitations of satellite altimetry in coastal zones and the sampling issue related to along-track satellite data and in situ measurements such as tide gauges (**Figure 2**). The coastal zone is indeed a dynamic area with strong spatial and temporal variability making it unlikely for satellite missions with revisit times of several days to capture localized events (Benveniste et al., 2019).

Relative SLR is the main driver of past and projected rise in extreme sea levels (e.g., Menendez and Woodworth, 2010; Vousdoukas et al., 2017). As extreme events pose the greatest hazards in terms of coastal flooding, sea level forecasts are also relevant to SLR adaptation. In particular, regional forecasts of sea level and waves can be instrumental in forcing more local forecasting systems (section "Downscaling Copernicus Forecasts") and coastal flood early warning systems (EWS). EWS improve coastal flood risk preparedness by delivering timely, authoritative and targeted information for decision making and for guiding actions aiming at reducing subsequent potential damages and impacts on the society (e.g., Alfieri et al., 2012; Harley et al., 2016; Idier et al., 2020).

The Copernicus Marine Environment Monitoring Service is providing sea level analyses, forecasts and reanalyses over the global ocean and European regional seas. Characteristics of the regional forecasting systems are provided in **Figure 4**. They provide hourly sea levels with a forecast lead time of at least 5 days, refreshed daily or twice-daily, at a spatial resolution ranging between 1.5 and 4.5 km, depending on the region. Most systems are currently using the GEBCO2008 or GEBCO2014 bathymetry (more information on the models can be found in the online Product User Manual associated to CMEMS each product). Atmospheric surface pressure forcing is included, as well as tides (for most of these ocean forecasting systems). Most systems assimilate satellite altimetry data and in situ profiles of temperature and salinity. The major contribution of assimilation of satellite altimetry in constraining such forecasting systems to increase their skills has been shown in Le Traon et al. (2019);

3D ocean	ARCTIC	BALTIC	BLACK SEA	IBI	MED SEA	NWS
Resolution	3 km	2 km	3 km	2-3 km	4.5 km	1.5 km
Tides	✓	✓	In 2021	✓	In 2021	✓
Atm. Pressure	✓	✓	✓	✓	✓	✓
Data assim.	● ● ● ●		● ● ●	● ● ●	● ● ●	● ● ●
Wave coupling	No	✓ Stokes drift	No	✓ (Stokes, wind stress, energy flux)	✓ wind stress	No
FRCST	7d (d)	6d (twice-d)	5d (d)	5d (d)	10d (d)	6d (d)

Waves	ARCTIC	BALTIC	BLACK SEA	IBI	MED SEA	NWS
Resolution	3 km	2 km	3 km	5 km	4.5 km	1.5 km
Ocean-wave coupling	Surface currents	Surface currents	Surface currents	Surface currents	Surface currents	Surface currents
Data assim.					●	
FRCST	7d (twice-d)	6d (twice-d)	10d (d)	5d (twice-d)	10d (d)	6d (d)

FIGURE 4 | Characteristics of CMEMS ocean and wave monitoring and forecasting center (MFC) systems as of December 2020. Colored circles in the data assimilation (data assim.) row indicate the assimilation of satellite sea surface temperature (black), altimetry sea level anomaly (red), temperature and salinity vertical profiles (gray), sea ice concentration (orange) and significant wave height from altimetry (blue). FRCST stands for forecast lead time. In the FRCST row, the first number indicates the forecast lead time (in days) of the system with high-frequency outputs and the frequency of the update of the forecasts (daily, d, or twice daily, twice-d). The row labeled with "Tides" and "Atm. Pressure," respectively, indicate the explicit representation of tides in the baroclinic models and of surface atmospheric pressure forcing.

Hamon et al. (2019). An illustration of the regionally averaged quality of sea level forecasts in CMEMS is provided in **Figure 5**.

An example of CMEMS sea level forecasts (Mediterranean regional system, **Figure 5**) and satellite information is provided in **Figure 2** for an Acqua Alta event in Venice in November 2019. The tidal peak on November 12th 2019 reached 189 cm in Venice (**Figure 2D**; Cavaleri et al., 2020), which corresponds to the second highest sea level ever recorded in Venice, second only to the devastating event of 1966, and flooded the city. The timely combination of wind setup from strong south easterly Sirocco winds (**Figure 2A**), an inverted barometer effect due to the storm's low atmospheric pressure, high tides, and anomalously high mean sea levels in the Adriatic Sea (**Figure 2B**) resulted in this exceptional high-water level in Venice (**Figure 2C**). Several Adriatic Sea or more local forecasting systems are operated for the Venice region (e.g., Umgiesser et al., 2020), some of them using CMEMS forcing conditions. The CMEMS MedFS system forecasted high water levels, although with an underestimate of the peak of the event on November 12th (**Figure 2D**) (a feature common to all operational forecasting systems for Venice for this event, due to errors in atmospheric conditions forecasts). Copernicus Marine Service satellite and *in situ* observation (sea level, wind) and model-based (ocean forecasts) data provide key information for downstream storm surge forecast models, supporting emergency and safety response missions with great accuracy. This data is also essential to better understand the main

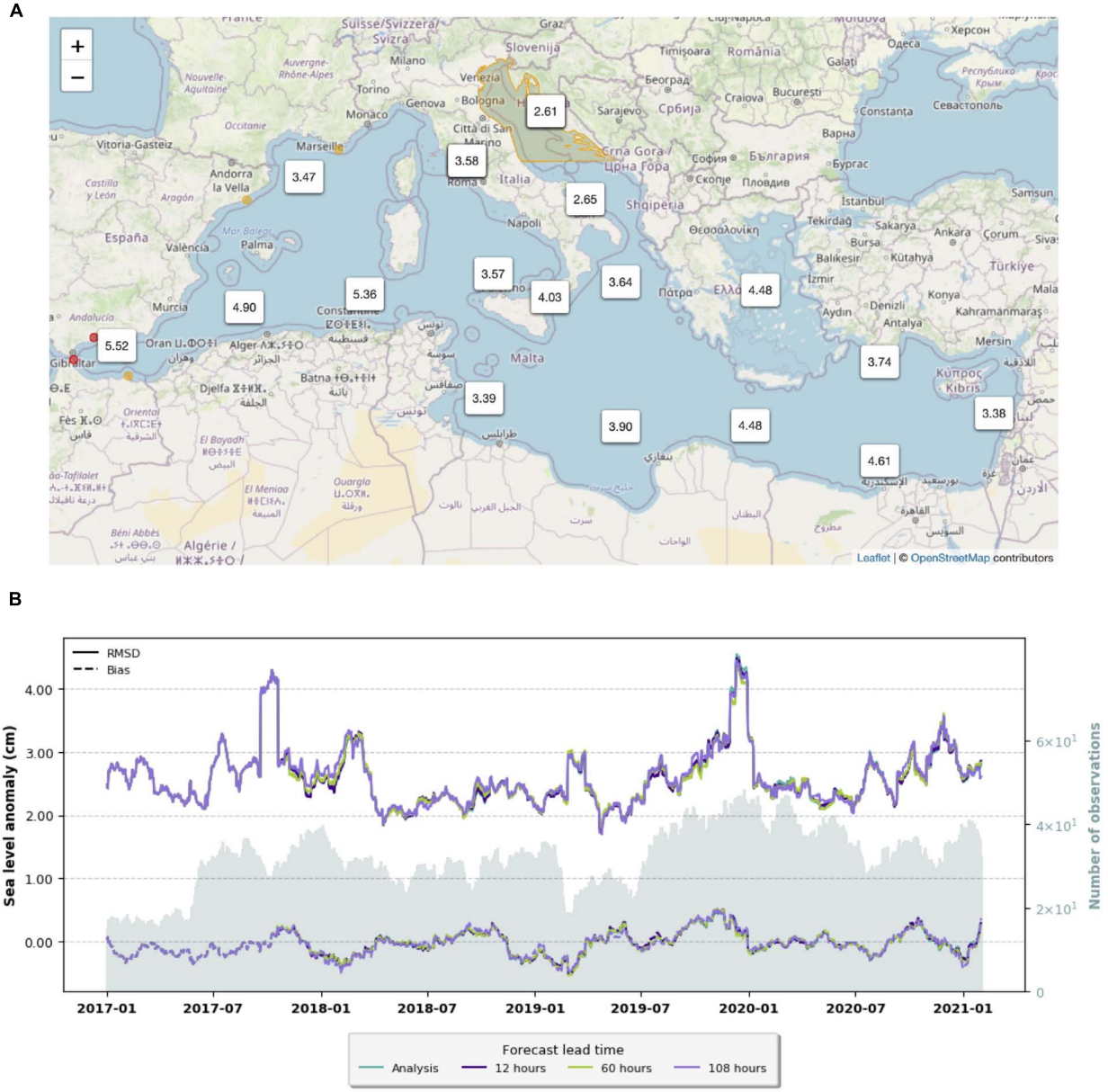

FIGURE 5 | Assessment of sea level forecast quality in the Mediterranean Sea CMEMS forecasting system. **(A)** Estimated accuracy numbers (corresponding to typical RMS differences in cm between the CMEMS forecasts and along-track altimetry SLA) over different Mediterranean Sea regions. **(B)** Zoom over the northern Adriatic Sea (see yellow contour in panel A) with RMS errors (plain lines) and biases (dashed lines) between the CMEMS Mediterranean Sea forecast and CMEMS along-track altimetry SLA for different forecast lead times (ranging from 12 h to 204 h) and analysis. Extracted from CMEMS' product quality dashboard.

mechanisms involved in such extreme events and improve the operational storm surge forecast models.

Forecasting sea level at the coast at spatio-temporal scales relevant for decision-making remains, however, challenging due to the short scales of coastal zone dynamics and due to the multitude of processes driving coastal sea level changes (Ponte et al., 2019) (see also sections "Downscaling Copernicus Forecasts" and "At Global Scale").

Monitoring of sea level change over past decades provides the historical baseline for quantifying SLR, extremes, their return periods and synoptic sea level variability in a broader sense. Ocean (wave) reanalyses combine ocean (wave) model dynamics with in situ and satellite observations through data assimilation. As such, reanalyses provide a consistent view of the ocean in space, time, and across variables, accounting for observation information and dynamics. The reliability of ocean reanalyses has increased over the last decade, as shown for the steric sea level inter-annual variability in CMEMS reanalyses in Storto et al. (2019a). In terms of past regional sea level variability, the skill of ocean

reanalyses is currently similar to that of objective analyses of observations or to sea level reconstructions (e.g., Storto et al., 2017).

The comprehensive and consistent view of the ocean provided by reanalyses allows for process-oriented studies, for instance to better partition sea level variability due to different mechanisms and over different time-scales (e.g., Forget and Ponte, 2015), or to separate the steric and mass components of regional sea level trends. The increasing reliability of ocean reanalyses make them useful for the monitoring of the ocean state (e.g., von Schuckmann et al., 2018; **Figure 3**) and for climate applications (Stammer et al., 2016).

CMEMS provides ocean reanalyses at global and regional scales (see **Figure 4** for regional domains) covering at least the altimetric era (starting in 1993) and using the ERA5 atmospheric reanalysis (Hersbach et al., 2020) produced and distributed by C3S. Along-track reprocessed altimetric sea level data are assimilated together with other observations. The new generation of CMEMS global reanalysis is at a 1/12°, ocean eddy permitting resolution (Storto et al., 2019b; Lellouche et al., 2021). At global scale, a multi-system approach is also taken in CMEMS to improve uncertainty estimates through the ensemble spread of global ocean reanalyses. The spread information was found to significantly contribute to the crucial requirement of uncertainty estimates for climatic datasets, assessed for ocean heat content and steric sea level in Storto et al. (2019a).

Regional ocean reanalyses covering the EU seas have higher resolutions, ranging from 3 km to 12 km, benefit from ocean models adapted to the regional dynamics and from the representation of additional processes. Global and regional reanalyses capture the spatial variability of altimetry derived sea level trends (e.g., Storto et al., 2019c). They were used to compute trends in ocean heat content (e.g., **Figure 3C**; von Schuckmann et al., 2018), which is related to ocean warming and thermal expansion, a prime contributor to SLR.

Using wave and ocean reanalyses with tides and surface atmospheric pressure forcing to represent storm surges, extreme (annual mean 99th percentile) wave and sea level conditions were compared with in situ observations (wave buoys and tide gauges) in Alvarez Fanjul et al. (2019), highlighting the reanalyses' skill in reproducing such extremes in most places and allowing to characterize them in coastal areas lacking in situ observations (**Figure 6**).

Climate Projections

On longer past and future time scales, i.e., from the pre-industrial mid 19th century to 2100 and beyond, climate models are the

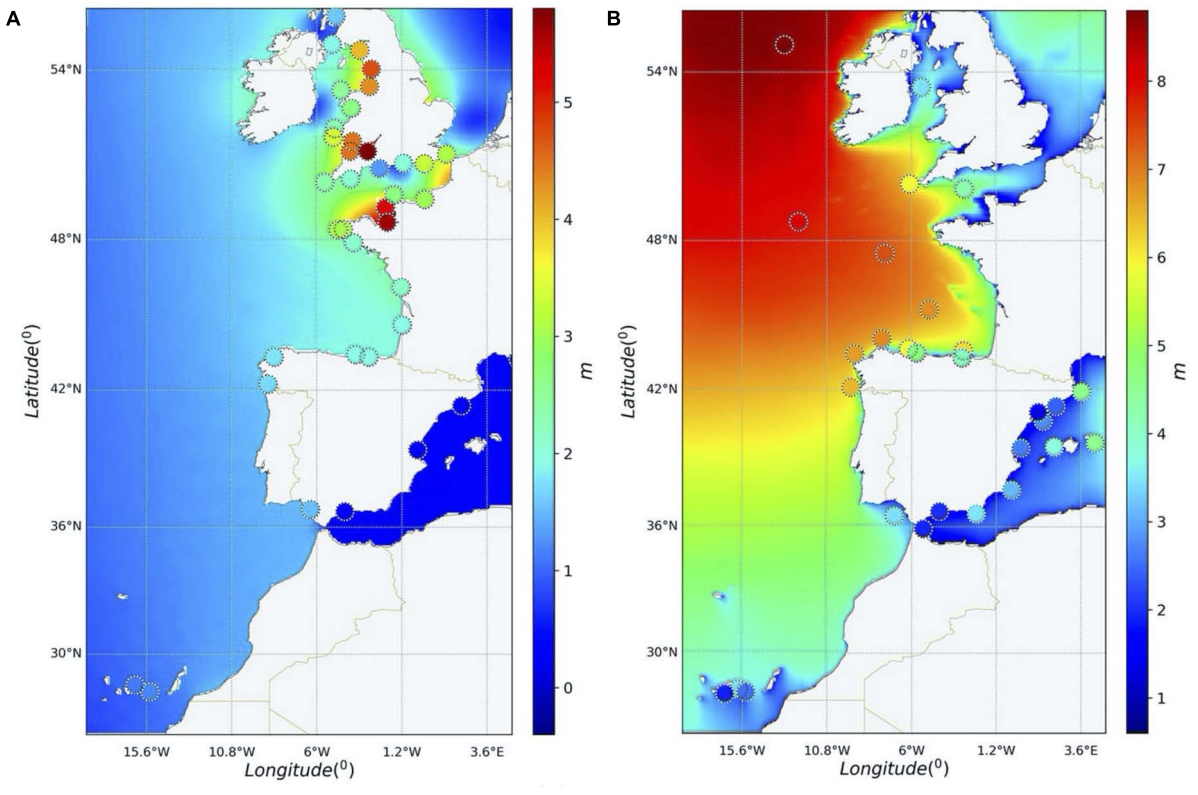

FIGURE 6 | (A) The annual mean 99th percentile of sea level. **(B)** The annual mean 99th percentile of significant wave height (in m, considering the 2000-2016 period) over in the IBI CMEMS regional ocean and wave reanalysis (shading) and from tide gauges and wave mooring CMEMS reprocessed data sets (inset circles). After Alvarez Fanjul et al. (2019).

primary tools for constructing regional sea level change time-series (e.g., Oppenheimer et al., 2019). Climate models directly simulate the ocean-related sea level rise, i.e., the dynamic regional sea level changes induced by ocean circulations, and changes in ocean temperature and salinity, from which the global mean thermal expansion can be calculated. Outputs from climate models are used to estimate glaciers and ice sheets' mass loss contributing to SLR with offline, dedicated models (e.g., Slangen et al., 2014a). The ability of climate models-based estimates of SLR to reproduce observed SLR at regional and global scales over the 20th century has been assessed in Meyssignac et al. (2017); Slangen et al. (2017).

As part of the C3S commitment to climate projections, the program redistributes a selection of variables, including monthly mean values of dynamic sea level (i.e., the zos variable) and sea level pressure (for the inverted barometer component of storm surges) from CMIP5 and CMIP6 models. The selection of variables was established when the dataset interface of the Climate Data Store catalog was first set up. Alongside the ocean components of the models, C3S also provides access to several other (mostly atmospheric) variables which could be used to estimate the surface mass balance of both ice sheets and mountain glaciers. More information on the variables available can be found in the Climate Data Store[6].

Exposure to Sea-Level Rise

Translating a given sea level (corresponding to the long-term mean SLR or to the sea level reached during extreme events, section "Sea-Level Change Hazard") into exposure of land area, population and assets to coastal flood is essential to inform adaptation decisions. Coastal flood exposure can be estimated based on different methodologies and underlying datasets, to which Copernicus contributes.

Global and broadscale exposure assessments largely relied on the passive "bathtub" mapping approach, whereby land areas with an elevation lower than the reported sea level and which are hydrologically connected to the sea are considered flooded (e.g., Hinkel et al., 2014). In that regard, digital elevation models (DEM) are critical to coastal flood exposure assessment. Census data (population, assets) and more recently, spatio-temporal dynamic population distribution models, are then analyzed jointly with the DEM to determine coastal flood exposure. Kulp and Strauss (2019) highlighted the importance of DEM accuracy for estimates of population exposure to extreme sea levels, as the vertical error in DEM is sizable compared to the estimated SLR by the end of the century. A review of assessments of population exposure to sea level rise is provided in McMichael et al. (2020).

Since 2019, the Copernicus Land Monitoring Service has delivered the Copernicus DEM (Copernicus Dem Product Handbook, 2020[7]). Copernicus DEM is derived from an edited digital surface model named WorldDEM^{TM}, based on TanDEM-X missions. Editions of data in the Copernicus DEM include the flattening of water bodies and consistent flow of rivers, shoreline and coastlines, as well as special features such as airports and implausible terrain structures.

The Copernicus DEM is provided in three different instances (**Figure 7**):

1. EEA-10: With a 10 m × 10 m ground sampling size, it is the spatially most detailed instance. The EEA-10 covers the land area of the EEA member states and the 6 cooperating countries (EEA39, also known as EIONET-39). The license conditions[8] are restricted to a limited number of user categories.
2. GLO-30: A global 30 m × 30 m ground sampling size DEM, with partial licensing restrictions.
3. GLO-90: A global 90 m × 90 m ground sampling size DEM, freely available to registered users.

The absolute vertical accuracy of WorldDEM^{TM}, underlying the Copernicus DEM, has been assessed using a linear error at a 90% confidence level at ICESat GLAS reference points. The absolute vertical accuracy is estimated to 1.92 m for the global mean (excluding Greenland and Antarctica) and to 1.66 m for the EEA39 European region covered by the EEA-10 DEM (Copernicus Dem Product Handbook, 2020). The vertical accuracy therefore remains a limitation to estimate with high confidence exposure to SLR during the coming decades and, as such, for sub-secular planning horizons (e.g., Gesch, 2018).

Exposure can be reduced in places protected by coastal defenses. Features such as dikes, groynes, seawalls are not resolved in the Copernicus DEM. Their mapping could be performed in the future in Copernicus (section "Coastal Defense Structures").

At more regional to local scales, hydrodynamic models can be used to refine assessments of coastal flood exposure (e.g., Vousdoukas et al., 2016) by accounting for hydrodynamic processes that can modify the ability of the flood to progress landward. Such hydrodynamic processes include e.g., land surface roughness for flood water-level attenuation and routing of flood waters. Accounting for water-level attenuation by land surface roughness during a flood indeed decreases estimated coastal flood exposure and expected damages by decreasing the inundation extent and depth (Orton et al., 2015; Vafeidis et al., 2019).

The Copernicus Land Monitoring Service provides land-cover/land-use products to monitor over time biophysical characteristics of the Earth's surface (updated every 6 years). In contrast to pure Land Cover data derived from classification, all vector LC/LU products provided by CLMS are mostly based on photo interpretation. This labor-intensive approach allows to map contextual information, such as mapping ecosystem types or the mapping of Land Use aspects. CLMS LC/LU products provide relevant information on different LC/LU classes that can then be used to specify water-level attenuation coefficients used in coastal flood models. CLMS offers two LC/LU datasets which cover coastal areas in Europe. The first one is the CORINE Land Cover

[6]https://cds.climate.copernicus.eu/cdsapp#!/dataset/projections-cmip5-monthly-single-levels?tab=overview

[7]https://spacedata.copernicus.eu/documents/20126/0/GEO1988-CopernicusDEM-SPE-002_ProductHandbook_I1.00.pdf

[8]https://spacedata.copernicus.eu/documents/20126/0/DAP+Release+phase2+V2_8.pdf/cb6b98a9-5d3b-dbc5-956d-e7f633cd6489?t=1615826769517

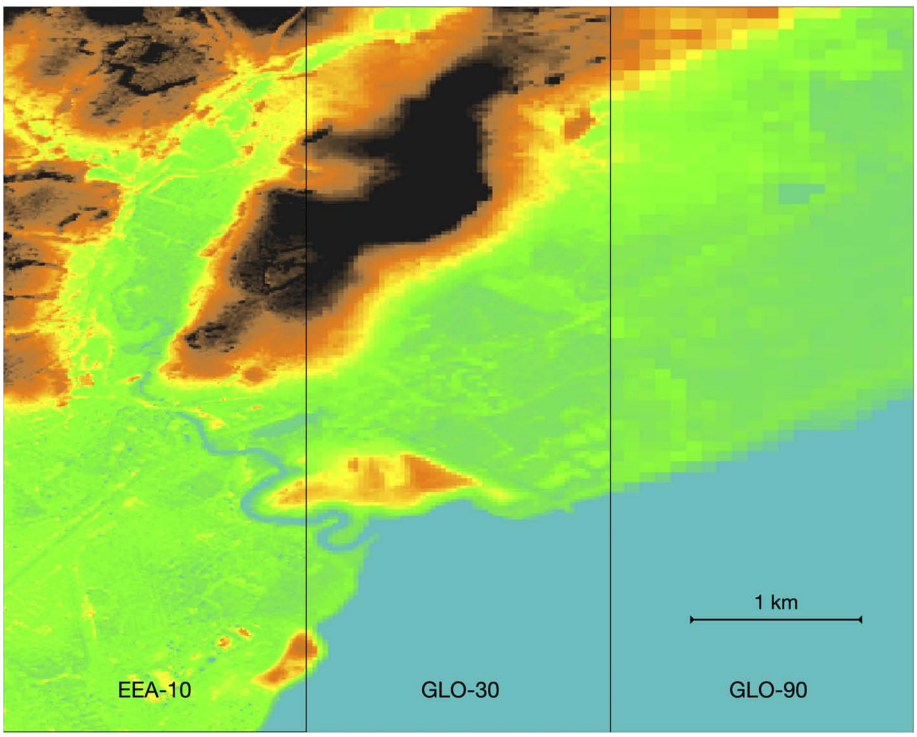

FIGURE 7 | Illustration of the EEA-10 (left), GLO-30 (middle) and GLO-90 (right) Copernicus DEMs showing the Rhymney River and an area north-east of Cardiff, UK.

(CLC) inventory[9], a vector dataset with a minimum mapping unit of 25 ha for status and 5 ha for change covering Europe (not only coastal zones). The CLC nomenclature includes 44 land cover classes which are grouped within a three-level hierarchy[10]. The five main (level-one) categories are artificial surfaces, agricultural areas, forests and semi-natural areas, wetlands, water bodies. CLC reaches back to 1990, and has been updated every 6 years since 2000. Besides offering a homogeneous wall-to-wall coverage across Europe, the long time series is probably the most valuable aspect of CLC. A major shortcoming, though, is its coarse spatial resolution. The minimum mapping units were defined in the 1980s and represent a trade-off between cost and detail of land cover information at the time. To overcome the limitations of the low spatial resolution of CLC, CLMS has delivered since February 2021 a Coastal Zones LC/LU (CZ LC/LU). The CZ LC/LU nomenclature includes 71 classes[11], providing more details on coastal aspects, such as port areas, or shoretypes (**Figure 8**). Shoretype information can be used to assess whether wave setup or runup can be estimated from empirical formulations, mostly dedicated to sandy or shingle beaches (e.g., Stockdon et al., 2006; Dodet et al., 2019) and incorporated in total water level estimates (e.g., Melet et al., 2018, 2020b).

The CZ LC/LU product covers an area of 10 km landwards from the shoreline, with a minimum mapping unit of 0.5 ha and a minimum mapping width of 10 m. The CZ LC/LU product is shown for two contrasted coastal areas in **Figure 9**. Land cover products usually do not provide accurate information on the type and location of economic assets, as the latter are often connected to land use aspects. The CZ LC/LU product from CLMS distinguishes between infrastructure types, such as nuclear power plants, different densities of urban fabrics, commercial or military areas, road networks, etc. (**Figures 8**, **9**).

In addition to surface roughness, the hydrological network and its topological relationship which are mapped in the CLMS EU-Hydro[12] dataset (channel density and connectivity) can exert a control on the duration and routing of floodwaters. The Thematic Hotspot Mapping on riparian zones delivered by CLMS provides three complementary product groups with detailed information on the state and characteristics of riparian zones across the EEA member and cooperating countries[13]. Other local hotspot monitoring components include Natura2000 zones and the Urban Atlas.

The Copernicus Land Monitoring Service offers Pan European wall-to-wall High-Resolution Layers (HRL) of interest to derive land surface parameters for coastal flood modeling and coastal flood exposure assessment, complementing the CZ LC/LU product. HRL are split into 5 different layers which are regularly updated every 3 years, each of them addressing a specific land cover at a 10 m × 10 m ground sampling size. These HRL

[9]https://land.copernicus.eu/pan-european/corine-land-cover
[10]https://land.copernicus.eu/user-corner/technical-library/clc2018technicalguidelines_final.pdf
[11]https://land.copernicus.eu/local/coastal-zones/resolveuid/58beba1d87d24b2aa9e2b5a9f6b5541b
[12]https://land.copernicus.eu/imagery-in-situ/eu-hydro
[13]https://land.copernicus.eu/local/riparian-zones

FIGURE 8 | Extract of the Copernicus Land Monitoring Service coastal zone land cover/land use (CZ LC/LU) product classes with particular relevance for coastal flooding.

provide information on (i) land imperviousness, capturing the spatial distribution of artificially sealed areas, the degree of imperviousness and the part of sealed areas corresponding to built-up areas (above-ground building constructions); (ii) forests, with the forest type, tree cover density, and dominant leaf type; (iii) grassland areas (surface roughness is much lower over grassland than over urban areas); and (iv) water and wetness, distinguishing permanent water, temporary water, permanent wetness and temporary wetness.

Regarding population exposure, the European Settlement Map (ESM) distributed by CLMS represents the percentage of built-up area coverage per spatial unit, at a resolution up to 2.5 m, using SPOT 5 and 6 missions and machine learning techniques in order to understand systematic relations between morphological and textural features.

For several of the above products, change layers are also provided (e.g., 2012-2018 changes). The combination of the different datasets described in this section can refine population and asset exposure to coastal flood.

Since coastal zones are typically subjected to multiple, strong, and often diametrically opposing societal interests in a very limited space, coastal landscape and ecosystems are experiencing high levels of pressure. Coastal habitats and ecosystems (e.g., dunes, aquatic vegetation, etc.), besides the intrinsic value they represent for biodiversity, for wellbeing and tourism, do fulfill the fundamental role of natural protection against SLR and coastal erosion. A degradation of these habitats results in an increased vulnerability and exposure of coastal areas (e.g., Hanley et al., 2020).

Specific instruments such as the Integrated Coastal Zone Management (ICZM), Marine Strategy Framework Directive (MSFD) but also the recently published EU Strategy on Adaptation to Climate Change[14], were put in place as a result of recognizing the need to coordinate a situation of high pressure on coastal areas on one side and the importance of preserving the functioning of natural habitats on the other side. Together with socio-economic data, geographically explicit and quantitative information are key for knowledge-based decision making, such as ICZM and MSFD. To provide such validated geographic data is a key role of the Copernicus Programme.

[14]https://eur-lex.europa.eu/legal-content/EN/TXT/?uri=COM:2021:82:FIN

Vulnerability

In the risk conceptual framework, vulnerability can be defined as a function of sensitivity and the nature of the hazard to which a system/population is exposed (Brooks, 2003; Abram et al., 2019). It includes social vulnerability, which depends on economic well-being, health and education status, preparedness and coping ability to sea-level rise induced hazards. It also includes biophysical vulnerability, which relates to ultimate impacts of a hazard event, and is often viewed in terms of the amount of damage experienced by a system as a result of an encounter with a hazard.

Data needed to assess vulnerability of population or assets (for instance, technical characteristics of building and the built environment) are not provided in Copernicus Services. Economic damages directly induced by floods are usually estimated through depth-damage curves which relate flood damage for a specific flood water-depth per asset (e.g., residential buildings, industry, transport, agriculture, etc.) or land-use class (Huizinga et al., 2017). In that regard, a better assessment of flood water-depth and of land-cover/land-use classes as provided by CLMS (section "Exposure to sea level rise") can contribute to refine vulnerability assessments.

Managing and Monitoring of Coastal Floods and Risks

The on-demand mapping component of CEMS, which can be triggered by authorized users (mostly national civil protection authorities), can be used to monitor coastal floods or to provide coastal flood risk maps for areas in Europe or globally. In the rapid mode, once a user has activated it, the service provides flood delineation or damage grading maps of a coastal flood event within hours or a few days based on the acquisition, processing, and analysis of satellite imagery and other geospatial raster and vector data sources. An example of such rapid mapping that supported the emergency response to the coastal flooding caused by tropical cyclone Idai is illustrated in **Figure 10**. Tropical Cyclone Idai made landfall during the night of March 14, 2019 at 23.30 UTC close to Beira City in central Mozambique. On 15 March 2019 at 0.00 UTC, its center was located approximately 25 km north-west of the center of Beira, with maximum sustained winds up to 167 km/h. Heavy rainfall, strong winds

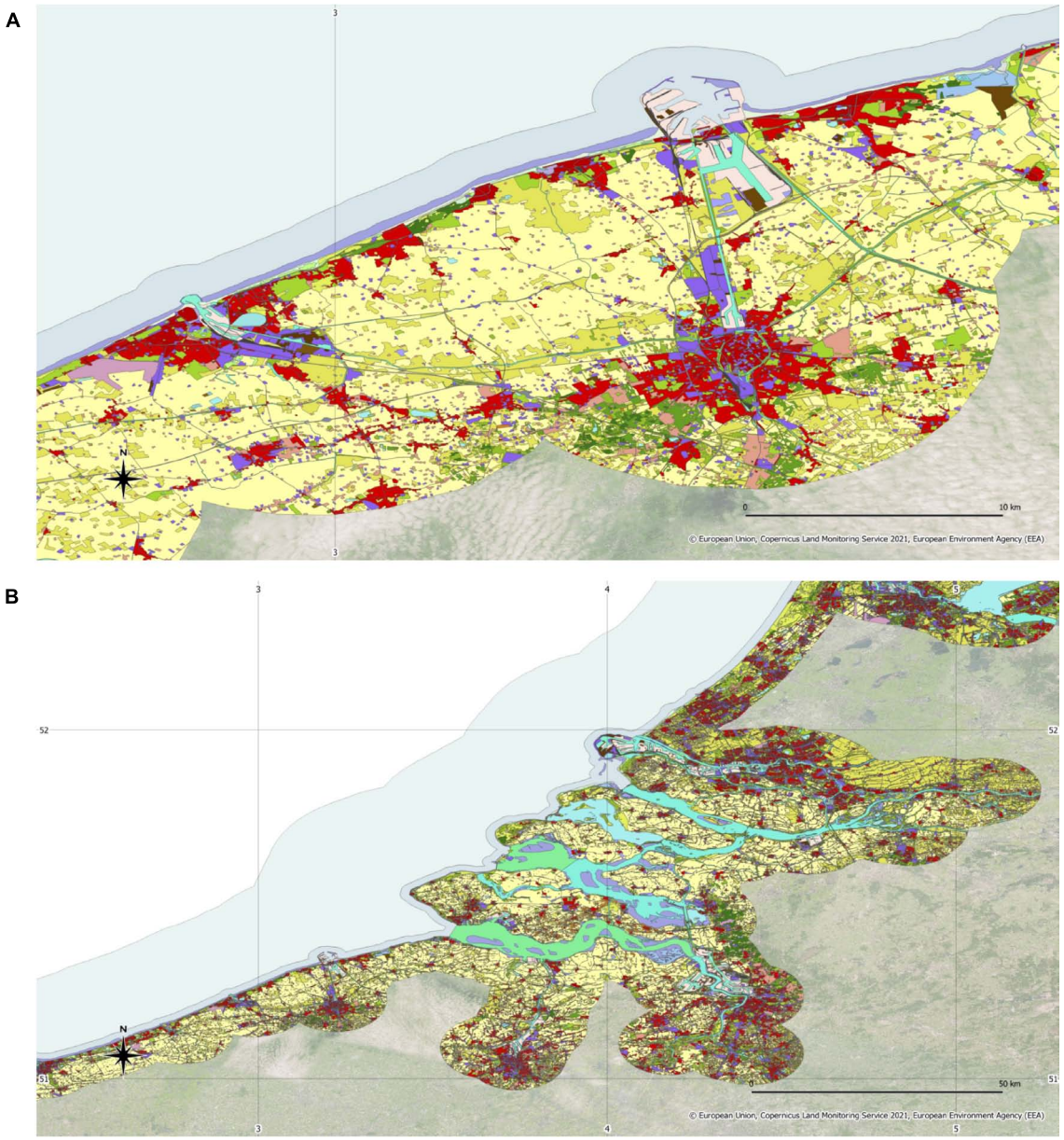

FIGURE 9 | Visualization of the coastal zone land cover/land use (CZ LC/LU) product of CLMS **(A)** for a coastal area nearby Bruges (BE) and **(B)** for the Rhein-Maas-Schelde-Delta (BE, NL). Colors refer to different LC/LU classes. Some of them, particularly relevant for SLR impact assessment, are described in **Figure 8**. The description of all LC/LU classes can be found on the CLMS website [11], https://land.copernicus.eu/local/coastal-zones/coastal-zones-2018.

and storm surge affected the coastal area of the Sofala region, in particular Beira.

To support risk prevention and planning for coastal floods the on-demand mapping component of CEMS can also provide detailed coastal flood risk maps. The flood risk maps are derived by using a wide variety of reference data such as hydrography, bathymetry, physiography, land cover/land use, building footprints, transportation network, populated places and administrative boundaries in combination with flood probability scenarios from flood hazard models. An example of a detailed coastal flood risk map from CEMS is illustrated in **Figure 11** where the hazard was calculated using total water level during a storm and extrapolating the water level on the digital terrain model following a bathtub approach.

Sea Level Monitoring and Reporting Activities

An Ocean State Report (OSR) is published on an annual basis (von Schuckmann et al., 2016, 2018, 2019, 2020) by CMEMS for the scientific community, with a summary which is more tailored for policy and decision-makers. Ocean State Reports

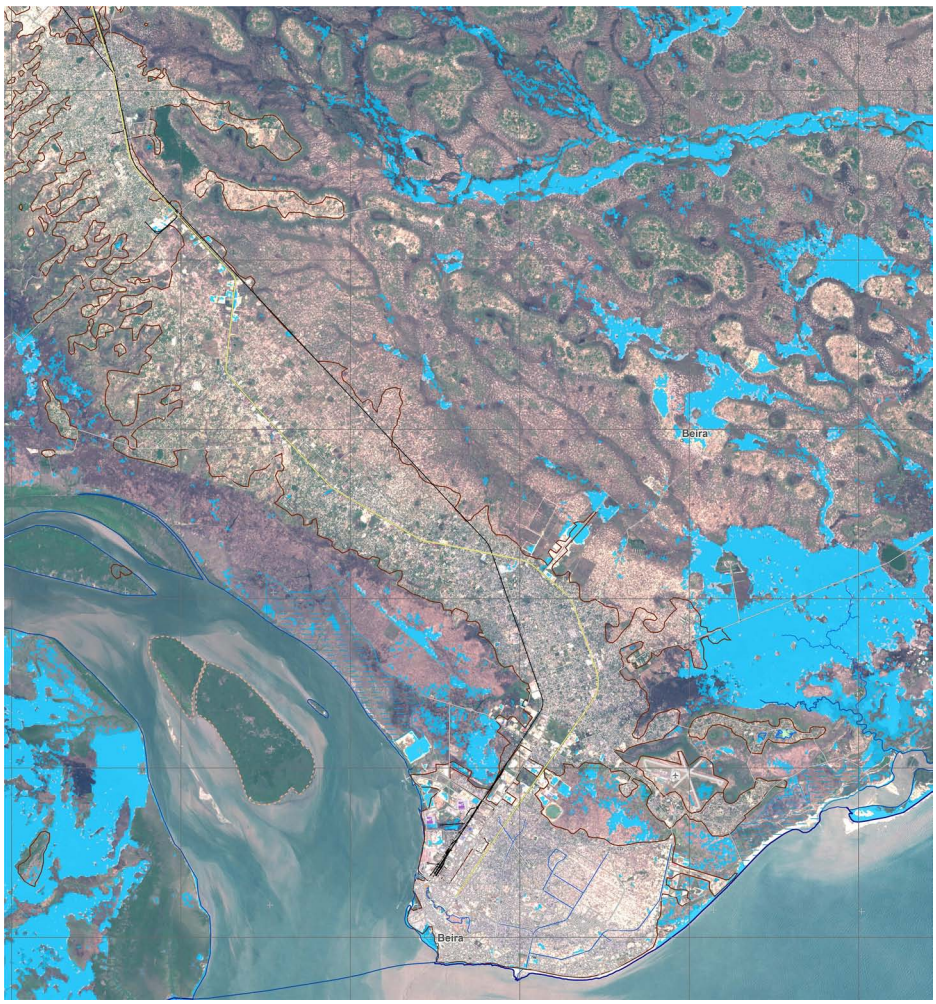

FIGURE 10 | Flood delineation map based on a Sentinel-1 image acquired on 20 March 2019 03:08UTC for the city of Beira and surroundings, Mozambique. Flooded areas are indicated in bright blue. Source: Copernicus Emergency Management Service, map available online https://emergency.copernicus.eu/mapping/ems-product-component/EMSN034_01COSTADACAPARICA_M1-COASTALFLOODHAZARD_OVERVIEWA1/1.

provide information on the state, variability and change of the European regional seas and the global ocean. They rely on the unique capability and expertise that CMEMS gathers in Europe to monitor, assess and report on past and present marine environmental conditions and to analyze and interpret changes and trends in the marine environment.

In particular, in the summary of the last OSR issue, regional sea level trends were provided (**Figure 12**) and contributed to the Word Meteorological Organization (WMO) (2020, 2021). OSR also includes case studies. With regard to sea level rise, a study was dedicated to the TOPEX-A altimeter instrumental anomaly and acceleration of the global mean sea level over the altimetric era (Legeais et al., 2020; **Figure 3A**). OSR also reports on specific events (see section "Downscaling Copernicus Forecasts" for an illustration).

Based on OSR results, CMEMS produces Ocean Monitoring Indicators (OMIs) that are used to monitor the main changes and trends in the marine environment over the past 25 years. OMIs on sea level rise are provided at global and EU seas regional scales based on data provided by C3S/ CMEMS and are regularly updated (**Figures 3**, **12**).

As change in mean sea level is an essential indicator of our evolving climate, GMSLR is one climate indicator covered in the C3S Service's European State of the Climate (ESOTC) report, which is published annually. GMSLR is due to two main factors: land ice mass loss and thermal expansion of the ocean (section "Sea-Level Change Hazard"). Therefore, it is not possible to determine the attribution of changes to sea level without also understanding the climate system and its associated impacts. Land ice includes the polar ice sheets in Greenland and Antarctica, and all glaciers worldwide. To estimate the contribution from each source to GMSLR requires consistent data records that cover corresponding time periods. During the 2006-2015 period, ocean thermal expansion explains more than 40% of the GMSLR (Oppenheimer et al., 2019). The remaining contribution comes mostly from land ice

FIGURE 11 | Coastal flood risk map for the coast of Caparica in Setubal, Portugal. Colors from dark blue (return period 5 years) to light blue (100 years return period) indicate the flood hazard for different return periods. Source: Copernicus Emergency Management Service.

mass loss, but also from land water storage, such as ground reservoirs and the Glacial Isostatic Adjustment (GIA, Peltier, 2004).

Ice sheets and glaciers gain mass through snowfall and lose mass through ablation, melting or calving. For ice sheets, ice flows from its center towards the ocean through glaciers and ice streams, ultimately forming floating ice shelves and calving icebergs from the edge of glaciers. The mass change of ice sheets and glaciers is converted to an equivalent sea level contribution by assuming that around 360 Gt of ice mass loss is equivalent to 1 mm of GMSLR. Within European territories, glaciers that have the largest contributions to GMSLR are located in Greenland, Svalbard and Iceland (**Figure 13**). During the 2019 summer, the Greenland ice sheet experienced record melting, with close to 96% of the surface experiencing melting at least once (Sasgen et al., 2020). Below average snowfall and an early start to the melting season resulted in early exposure of bare ice, which further enhanced melting, as bare ice reflects less solar energy than fresh snow, in what is termed melt-albedo feedback (e.g., Ryan et al., 2019).

A Service Layer

In addition to producing scientific information, Copernicus Services deliver open and free services including manned service desks, tailored user access to data and user notifications, training, tutorials, outreach actions and expert support. Each service has a unique and standardized entry point to its catalog of products and information. Visualization interfaces, processing tools and digital services have been developed for users to explore the data, to extract parts of the data and to process them.

Cloud infrastructures have also been developed and used for Copernicus Services. For C3S, it is now represented mostly by the Climate Data Store but expected to be expanded and enriched by the DIAS platforms, adding a way for the users to interrogate the data and convert it into something directly usable. As key organizations in the Copernicus Programme, EUMETSAT, ECMWF Mercator Ocean and recently EEA, have combined their experience to jointly develop the WEkEO Copernicus DIAS service. WEkEO is the EU's Copernicus DIAS reference service for environmental data, virtual environments for data processing and skilled user support.

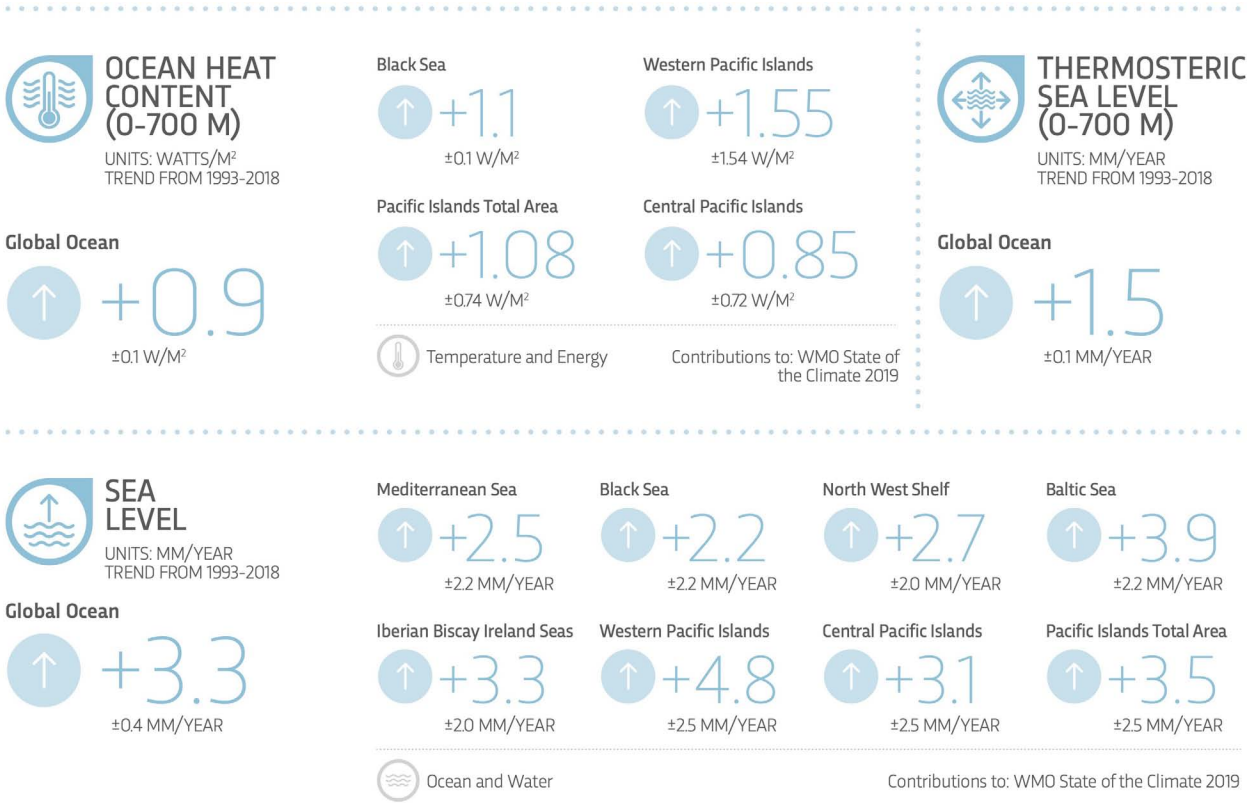

FIGURE 12 | Information on sea level rise averaged over the global ocean, EU regional seas and Pacific Islands regions. Source: Ocean State Report issue 4 Summary, von Schuckmann et al. (2020).

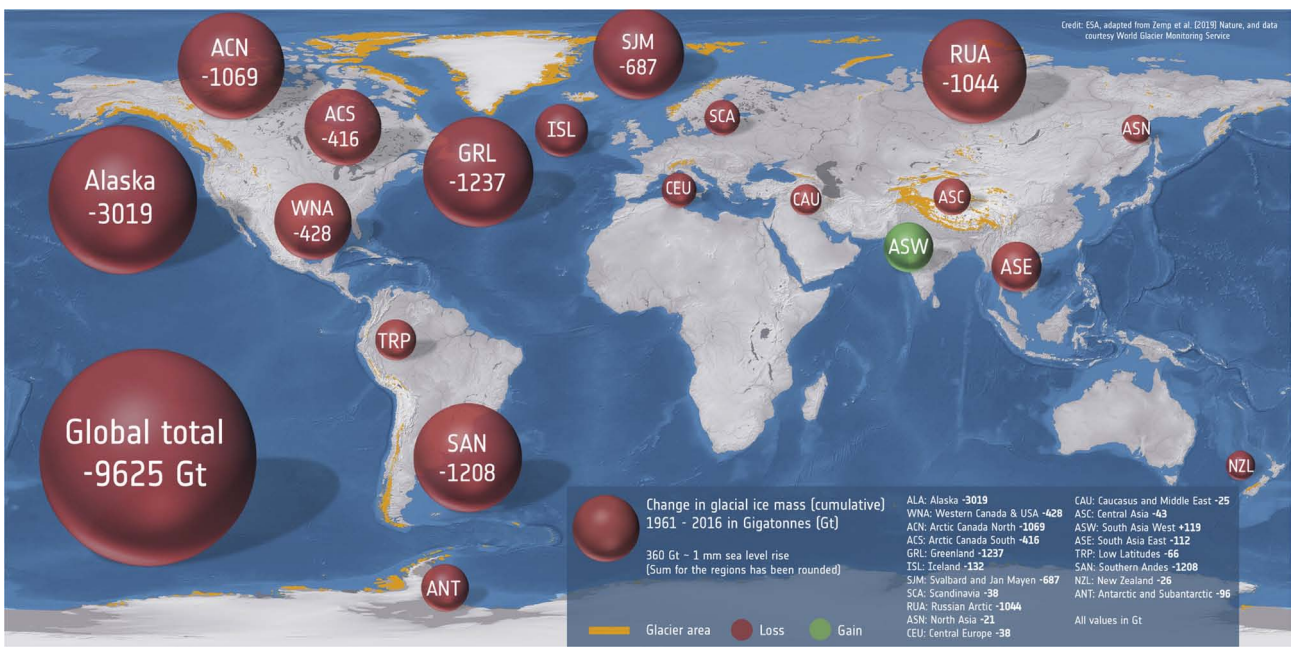

FIGURE 13 | Glacier mass change from 1961 to 2016 estimated for different regions, from the European State of the Climate (ESOTC) (2019). The cumulative global and regional mass changes (in Gt, represented by the size of the bubble) are illustrated. 360 Gt of land ice mass loss rises the global mean sea level by 1 mm. Data from Zemp et al. (2019).

Case Studies for Sea-Level Rise Adaptation

This section provides some illustrations of the use of Copernicus data for SLR adaptation.

European Coastal Storm Surge

The Copernicus Climate Change Water level change indicators for the European coast dataset presents extreme-value, return period, and percentile indicators for coastal sea levels in a European-wide domain. These indicators are computed from tidal dynamics, storm surge and SLR data based upon past observational data and future climate projections, covering 1977-2100.

The C3S water level indicators are underpinned by the Deltares Global Tide and Surge Model (GTSM) version 3.0 (Muis et al., 2020) together with regional climate forcing and SLR initial conditions. In addition to the climate change scenarios, a reanalysis dataset is computed by forcing GTSM with the ERA5 reanalysis. This provides recent historical water-levels that can be used to look at specific (extreme) events in the past.

To demonstrate the value of the C3S water level indicators, the contractor undertook case studies, including improving local hydrological and coastal flooding models for Clontarf (Dublin) and Salthill (Galway)[15], on the Irish East and West coast, respectively. These two locations were chosen in conjunction with participating stakeholders who are facing an increased risk of coastal flooding due to climate change. This dataset allowed end users to gain a full understanding of the expected impact of climate change along the Irish coast at customized time scale for current, near and far future scenarios.

Downscaling Copernicus Forecasts

Copernicus Services provide generic 'core' information supporting expert value-adding services, thereby complying with the Copernicus Programme delineation process of core versus public and commercial downstream activities.

Downscaling of Copernicus products might be needed to provide more accurate local information, especially on the hazard side. CMEMS operational ocean systems are routinely used as forcing for more local, downscaled ocean operational systems. An overview of the current European capacity in terms of operational modeling of marine and coastal systems was recently presented in Capet et al. (2020) and indicated that about half of the reported regional / local ocean modeling systems rely on CMEMS models for open boundary conditions. A review of storm surge modeling for Europe is provided in Umgiesser et al. (2020), with several systems also part of CMEMS or using CMEMS as boundary conditions. Recently, the OPENCoastS service has been developed to generate on-demand coastal ocean forecasts (Oliveira et al., 2020). CMEMS data are available in OPENCoastS as ocean forcing at the local model boundaries for daily coastal predictions.

An example of downscaling CMEMS's forecasts is provided below for harbor operations in Spain. CMEMS forecasts are routinely downscaled into higher resolution models able to forecast the ocean state inside around ten harbors. The ability of the CMEMS and downstream systems to forecast extreme events was showcased during Storm Emma in the Gulf of Cadiz, which experiences a heavy maritime traffic. The systems were found to have properly forecasted Storm Emma extreme sea levels and significant wave heights (>7 m) in March 2018, as reported in the CMEMS Ocean State Report #4 (De Alfonso et al., 2020). The combination of CMEMS wave buoy observations and reanalysis information indicated that Emma was the most severe wave storm for that region in the past 20 years. Thanks to CMEMS downstream services for those harbors (Sotillo et al., 2020), alert systems were activated before the storm arrived and users were warned early. Safety could be ensured in port facilities and no personal damages were reported.

[15]https://cds.climate.copernicus.eu/cdsapp#!/dataset/sis-water-level-change-indicators?tab=overview

PERSPECTIVES ON COPERNICUS SERVICES FOR SLR ADAPTATION

The Copernicus Programme has been renewed and funded over the 2021-2027 period, leading to the so-called Copernicus 2. This section discusses evolutions that could be implemented in the core Copernicus Services of relevance for SLR adaptation.

New Satellite Missions

During 2021-2027, the Sentinel missions family will continue to expand. New units (C and D) will be launched for Sentinels 1, 2, and 3 and will guarantee sustained observations of sea level, surface wind waves, nearshore bathymetry and shoreline position, land cover and land use etc. The first unit of Sentinel 6, called Sentinel 6-Michael Freilich, was launched in November 2020 and a second unit will be launched during Copernicus 2. Sentinel 6 will improve the monitoring of sea level, with enhanced accuracy and long-term stability. It will become the new reference mission for altimetry in CMEMS and C3S (Legeais et al., under review in this issue) and will be used to calibrate other missions. An important advance from Sentinel 6 will be its capacity to monitor sea level at higher resolution, and closer to the coasts where altimetry data are less reliable (Birol et al., 2017; Cipollini et al., 2017). In addition to the Sentinels, other satellite missions will contribute to the monitoring of relevant environmental fields for sea level. This includes for instance the SWOT mission (Morrow et al., 2019) for a high-resolution monitoring of sea level along 2D swaths. The corresponding data will be processed and add value to products delivered by Copernicus Services.

Altimetric data processing and mapping procedure updates are also to be expected in the coming years, contributing to further improvements in altimetric products in coastal zones.

On a longer term, six High Priority Candidate Missions (HPCM) could expand the capabilities of the current Sentinel family to fill gaps in Copernicus user needs and to better support policies. Of particular importance for SLR induced risks are the CRISTAL mission (Sentinel 9), for monitoring ice sheets and glaciers height changes; ROSE-L (Sentinel 12) for monitoring ice-sheets and land subsidence; CHIME (Sentinel 10) for monitoring

land cover. The HPCM missions will feed into Copernicus Services as well.

Upgraded and New Products and Service Lines

In addition to ensuring the continuity of the existing Copernicus Programme achievements and to incremental improvements in their existing products and services in Copernicus 1, Copernicus services will keep evolving in Copernicus 2 (2021-2027) to better answer user needs and support policies. A series of major product improvements, new products and service lines could be implemented in Copernicus 2 depending on funding, on precursor projects (e.g., H2020, Horizon Europe projects for Copernicus Evolution), and on evolving user and policy needs. This section lists a series of potential evolutions envisioned by the Copernicus services that are relevant to SLR adaptation, with no guarantee, so far, that these evolutions will actually be implemented by 2027.

Monitoring of the Coastal Zone

Dynamic Nearshore Bathymetry

A new core, pan-European satellite-derived nearshore bathymetry dynamic product could be produced in the framework of CMEMS, based on Sentinel and other contributing missions. As the bathymetry is dynamic in coastal zones (e.g., Bergsma et al., 2019), the product would be regularly updated to capture the evolution of bathymetry, and developed in synergy with EMODnet who provides a static pan-EU bathymetry product. An improved coastal zone bathymetry characterization would be beneficial notably for estimates of total water level at the coast.

Dynamic Shoreline Position and Tidal Ranges

The evolution of the shoreline position represents the dynamic response of the coastal system to the changing geophysical climatic and anthropogenic forces on the coastal zone. Products implemented by the CLMS are typically addressing land phenomena with lower dynamicity as compared to the shoreline. Thanks to recent algorithm developments, instantaneous (at time of observation) shoreline positions can be extracted from satellite imagery (Pardo-Pascual et al., 2018; Vos et al., 2019). Repeating the mapping of the shoreline using a high number of available Sentinel 1 and 2 data, by intersecting this spatial information with validated in situ data, moon calendar, and an accurate DEM, the dynamicity of the shoreline can be derived in a spatially explicit manner. Analyses of time-series of satellite-derived shoreline positions inform on the stability, erosion or accretion of the shoreline (e.g., Luijendijk et al., 2018; Mentaschi et al., 2018; Castelle et al., 2021) as well as on tides, and flood events. In consequence it also means to monitor the extent of intertidal flats and its evolution over time.

Vertical Land Motion

Land subsidence causes relative sea level rise that should be accounted for in SLR related risk assessments (Wöppelmann and Marcos, 2016). Subsidence is classically measured with topographic surveys or continuous GNSS networks but, in the last decade, the interferometric analysis of Synthetic Aperture Radar (SAR) images became one of the most exploited tools for subsidence estimation along coastal areas (Melet et al., 2020a). Thanks to the technological advancements of SAR satellites, to the readiness of algorithms, to the available computational capabilities and to the launch of the Sentinel-1 constellation, it is nowadays possible to measure subsidence, and other ground motions, over the entire Europe. The European Ground Motion Service (EGMS) of the CLMS will be the first worldwide service offering to a wide range of users certified ground motion information derived from the analysis of Sentinel-1 images. The first end-to-end implementation and operation of the Service will cover the Copernicus Participating States and will provide consistent, standardized, interoperable, and harmonized across national borders products in three different formats:

1. Level 2a (*Basic*): displacement data in ascending and descending orbits measured along the line-of-sight of the sensor and referred to a local reference point.
2. Level 2b (*Calibrated*): as Level 2a but calibrated with a GNSS reference network. The measurements are referred to an absolute geodetic reference frame.
3. Level 3 (*Ortho*): horizontal and vertical components of motion calculated from multi-orbit level 2b. As for level 2b, level 3 is anchored to the geodetic reference frame.

The baseline portfolio (levels 2a, 2b and 3), using Sentinel-1 data from February 2015 to December 2020, will be delivered at the beginning of 2022 and will be followed by three annual updates. External validation will be performed at the end of every production cycle. EGMS data will be distributed through a dedicated dissemination platform. Additional information can be found in Crosetto et al. (2020) and in the dedicated page of the CLMS website[16].

The EGMS will certainly provide accurate and reliable information for the estimation of the relative sea level rise in many low-lying areas along the coasts of the Copernicus Participating States. Moreover, it will give access to an unprecedented density of measurement points, especially in urban areas, with an accuracy level similar to the one obtainable with topographic measurements. Quantifying subsidence will allow for the refinement of relative sea level rise and flood impact models. The availability of time series of deformation will permit the reconstruction of subsidence in the recent past and the detection of accelerations in the subsidence rates.

Monitoring and Forecasting of Coastal Floods

In addition to the gradual rise in sea level, relevant for submersion, SLR is also leading to ever more frequent extreme events (Oppenheimer et al., 2019). This makes the monitoring and forecasting of coastal flood events and the subsequent assessment of their impact of primary importance for CEMS.

Evolutions of Total Water Forecasts

Accurate total water level forecasts are crucial for early warning systems and for operating mobile coastal defenses that can close to protect coastal cities from forecasted extreme events (e.g., MOSE barrier for Venice, Umgiesser et al., 2020).

[16] https://land.copernicus.eu/pan-european/european-ground-motion-service

To improve total water level forecasts, several evolutions could be foreseen within CMEMS. First, regional forecasting systems could be run at higher resolution, reaching a kilometric resolution. This would allow a better characterization of the regional to coastal circulation patterns and features. More integrated systems in terms of coupling between the ocean, wave and atmospheric model components of the forecasting system would also be beneficial to extreme sea level forecasts. Indeed, extreme water levels are often due to the combination of atmospheric conditions (strong winds, low atmospheric pressure), of high waves, and of high tides. It should be noted, however, that lower frequency sea level variability, such as that due to oceanic general circulations (including mesoscale activity, seasonal to interannual and decadal variability) can also contribute to extreme water levels (e.g., Melet et al., 2016; Fernandez-Montblanc et al., 2020; Lowe et al., 2021). Non-linear effects and retroactions between wave, ocean and atmosphere can alter the simulation of extreme events. For instance, higher sea levels can alter wave dissipation through depth-limited breaking, mean sea level rise can alter barotropic tides and surges through changes in bottom friction, surface currents can lead to wave refraction, sea surface roughness due to the presence of waves can alter the wind stress and momentum flux to the ocean, etc. (Idier et al., 2019). Another coupling effect comes from the land, with river discharges and runoff. A better characterization of the land boundary and of the land to sea forcing, in particular for river discharges, is needed. The co-occurrence of high sea levels and of large runoff and river discharges induced by precipitation during storms can result in compound flooding events (e.g., Bevacqua et al., 2019).

In Copernicus 1, ocean and wave forecasts produced by CMEMS (section "Sea Level Observations") were deterministic. New probabilistic forecasts based on model ensembles could be proposed to provide a better characterization of forecast uncertainties. As extreme sea levels are also often due to the timing of different drivers (e.g., tides and storm surge), ensemble forecasting would better sample different possible phasing of the contributions to total water levels. Probabilistic forecasts could better characterize the confidence level associated with the provided forecasts and the probability of exceeding sea level thresholds for coastal defenses operations for instance. As such, probabilistic forecasts will be instrumental for early warning systems and to support decision-making based on operational products. Indeed, forecasts leading to a false alarm and closure of mobile surge barriers can disrupt economic activities and cause unnecessary evacuation of inhabitants.

Finally, as coastal downscaling can be needed to resolve fine coastal features, a European Union leverage could be proposed by implementing a co-production of model-derived information between Member States services and Copernicus Services for core users (i.e., those that must implement European Union policies at national and regional level). A series of coastal models operated by EU Member States could be coupled with Copernicus Marine Service models and could be integrated in the Copernicus Marine Service portfolio. This will allow an improved monitoring and forecasting of coastal zones, and will support and advance knowledge of the coastal environment and associated economies (including coastal management and storm surge forecasts). A co-designed cloud environment and tools could be setup with Member States for the co-production of these coastal models.

EU Coastal Flood Awareness System

Preparedness towards natural hazards through the development and implementation of early warning systems is a key factor in the reduction of their societal impact. Specifically, continental scale forecasting systems, such as the European Flood Awareness System of CEMS (Smith et al., 2016) for rivers, can complement national systems through the provision of harmonized, trans-boundary, probabilistic and medium-range forecast information.

Efforts are currently ongoing to develop a European coastal flood awareness system capitalizing on the product portfolio of CEMS, CMEMS and CLMS and making use of recent developments in hydrodynamic models. For instance, the recently launched H2020 Copernicus Evolution project ECFAS (European Coastal Flood Awareness System) aims at providing a "Proof of Concept" to demonstrate the practical feasibility of implementing such a pan-European system. ECFAS will also develop innovative solutions for providing rapid mapping of forecasted flooding and will benefit from the integration of space research with other non-space domains, like oceanographic modeling and coastal risk assessment. In addition, efforts are on-going to prove the feasibility for providing high-resolution forecasting of the near-shore storm surge based on CEMS, CMEMS and CLMS products and large-scale hydrodynamic simulations using different models and configurations. The final product should deliver an open source, portable, reproducible and expandable framework that can be utilized from local to global scale in a consistent way. Furthermore, it can be expanded to include inundation analysis, thus providing a complete impact analysis in support of adaptation policies. It is envisioned that coupling this system to hydrological models (Ye et al., 2020) could lead to a holistic overview of the flood risk in a dynamic and compound mode, complimenting and supporting systems based on monitoring.

Continuous Monitoring of Coastal Floods

The monitoring of coastal flooding based on a user activation and for a specific area is already possible as part of the service portfolio of CEMS (section "Managing and Monitoring of Coastal Floods and Risks"). However, state-of-the-art, scientific methods for automatically detecting and identifying flood events, based on a global, continuous supply of all-weather, day-and-night satellite images, such as those provided by the Sentinel-1 satellites are now mature and ready for operational implementation (Matgen et al., 2020). This would allow a continuous, fully automatic monitoring of coastal flooding without the activation by a user or limited to a specific area of interest, hence improving timeliness and coverage of the product.

Within CEMS the set-up of such a systematic global flood monitoring product that will immediately process and analyze all incoming Sentinel-1 Interferometric Wide Swath data, is currently ongoing (Salamon et al., 2021). While in traditional flood mapping efforts focused on deriving information from a limited number of available images and potentially an image

where no flooding is visible for comparison or thresholding purposes, the flood mapping algorithms used for the new global flood monitoring product will make use of the data cube approach which offers a number of key benefits. A data cube provides fast access to S-1 time series, which supports the implementation of algorithms that require data-driven model training. Furthermore, by providing access to the historic data record, which for S-1 reaches back to 2014, it allows for placing the flood situation in its historical and geographical context. Based on the features of S-1 and the algorithm set up, it is foreseen that the global flood monitoring product will have a timeliness of < 8 h between image acquisition and product availability and a revisit frequency of approx. 1-3 days for Europe and 3-14 days for the rest of the world.

Long-Term Sea-Level Changes: Reanalyses and Climate Projections

At Global Scale

C3S has distributed CMIP5 and CMIP6 outputs, including dynamic sea level and atmospheric variables. Other sea level variables, for example the sterodynamic sea level which adds the global mean thermal expansion to the dynamic sea level change (i.e., zos + zostoga, Gregory et al., 2019, directly simulated by climate models), could be included in the future if there are clear and strong user community requests. Prioritizing these additional sea level variables will be defined during future climate projection workshops organized by C3S.

During the first phase of the program (2015-2021) C3S developed a demonstration project on coastal inundation in the North Sea as part of its Sectoral Information System (SIS). For the next phase of Copernicus (2021-2027) C3S is investigating the possibility of defining a traceable Toolbox application able to calculate projections of total regional sea-level by combining the fields available on from all relevant Copernicus services.

At Regional Scale

Ocean reanalyses (global ocean and European regional seas, see also section "Sea Level Observations") could be extended further back in time in the 20th century to better assess and monitor the long-term evolution of the ocean state, including sea-level changes, notably in response to climate change. Historical in situ observations would be assimilated (e.g., sea surface temperature and tide gauges mainly for the first half of the century and temperature and salinity profiles from 1950 onwards).

Future climate change information is increasingly needed for mitigation and adaptation to climate change, including SLR adverse effects. Current climate change oceanic projections, as provided by C3S, are global and rely on the information derived from global climate models. However, relevant core information is needed at regional to local scales to support decision-making for SLR adaptation.

CMEMS envisions to develop a new line of regionally downscaled, refined projections of the ocean state from global projections (C3S) (e.g., Adloff et al., 2018; Hermans et al., 2020; Meier et al., 2021) to translate and refine global projections at scales fitting more decision making. Regional downscaling will be developed by leveraging on regional ocean and wave modeling systems operated in the Copernicus Marine Service to overcome limitations of global climate models (e.g., coarse resolution, missing representation of important physical processes, e.g., tides, waves etc.).

Attribution of Extreme Events

Changes in SL at any scale are driven by a range of natural and anthropogenic forcings. While GMSLR and its major components (global mean thermal expansion and glaciers mass loss) over the last decades have been attributed to climate change (e.g., Marzeion et al., 2014; Slangen et al., 2014b, Slangen et al., 2016; Nerem and Fasullo, 2019), the climate signal in regional SLR and associated extremes is often not distinguishable from the climate variability noise (e.g., Richter et al., 2020). Depending on the location, the anthropogenic forced signal is expected to be discernible from natural variability induced signals at different times throughout the 21st century (Lyu et al., 2014; Richter et al., 2017).

Changes in extreme SL (increase in their amplitude or decrease of their return period) are mostly driven by changes in mean SL rather than by changes in storminess (e.g., Menendez and Woodworth, 2010; Vousdoukas et al., 2017, 2018b). Projected changes in SL extremes and their amplification have been the focus of several studies, highlighting that due to mean SLR, extreme sea level events that have historically been rare, such as historical 100-year extreme sea levels, will become common at the end of the century posing more and more threats to coastal communities (e.g., Vousdoukas et al., 2018a; Oppenheimer et al., 2019).

The attribution of specific events to anthropogenic climate change is still in its infancy and in 2016, the National Academy of Sciences published a review on the capabilities of event-attribution, listing extreme cold and extreme heat events as those being more mature. There is an ever-growing body of literature (e.g., see the annual BAMS special issue since 2011 on 'Explaining Extreme Events from a Climate Perspective'[17], e.g., Herring et al., 2021), focusing mainly on weather-related events. Sweet et al. (2013) discussed the implications of SLR on the extreme water levels reached during hurricane Sandy in 2012. During the first phase of the Copernicus Programme (2015-2021) C3S funded a climate attribution activity. This focused primarily on the development of a protocol to initiate an attribution study after an extreme weather event and then put the event in the context of climate change to characterize how much of a role climate change could have played in altering the probability of occurrence of the event.

C3S intends to continue and if possible, extend the current activities on climate attribution. The focus will be at first on maintaining up-to-date a catalog focusing on a variety of meteo-climatic extreme events for which the science of attribution is the most mature. The future ambition would be to have an on-demand activation of a full attribution study for some of the most impactful of these events, with the types of events covered increasing as the science matures.

[17] https://www.ametsoc.org/index.cfm/ams/publications/bulletin-of-the-american-meteorological-society-bams/explaining-extreme-events-from-a-climate-perspective/

Exposure Mapping

Coastal Defense Structures

Coastal defense structures can be absolutely essential for protecting human infrastructure and activities. For instance, without such structures large parts of the Netherlands would be permanently submerged or threatened by flood events as about a third of the Netherlands is located below sea level. Recently, Lowe et al. (2021) found that considering a sea level rise ranging from 0.3 to 2.0 m by 2100, it is economically efficient to protect 13% of the global coastline (which encompasses 90% of the global flood plain population). In Europe, elevating dykes in an economically efficient way along the 24-32% of the coastline would allow to avoid at least 83% of flood damages, with a benefit to cost ratio of such an investment ranging from 7 to 15 depending on climate change and socio-economic scenarios (Vousdoukas et al., 2020b).

The exact knowledge about the type and location of coastal defenses structures is an essential input for flood modeling. Due to their mostly narrow (less than 10 m) shape coastal defense structures are not sufficiently addressed by the CZ LC/LU product due to its minimum mapping unit of 10 m. For this reason, CLMS plans among the upcoming activities to add a dedicated product for mapping of coastal defense structures across Europe's coasts.

Human Population Maps

Mapping the distribution of the human population is fundamental to measure the degree of urbanization at the coast, the population that is exposed to future SLR or to better manage the risk of coastal storm surges (see also section "long-term sea level changes"). The availability of Sentinel-1 and 2 data with high frequency of revisit and systematic global coverage provides the opportunity to produce human settlement maps at an unprecedented level (e.g., Corbane et al., 2017).

As part of the evolution of CEMS and in coordination especially with CLMS but also with other relevant Copernicus services, the provision of highly accurate geospatial information about the status of human settlements and their dynamics is foreseen, both in terms of built-up areas and population at the global level. The methodology to derive these products is based on the Global Human Settlement Layer (Pesaresi et al., 2016) and will maximize the use of Copernicus missions (Sentinel-1 and Sentinel-2) in conjunction with in-situ population data (census data).

DISCUSSION

The European Union's Earth Observation Programme, Copernicus, monitors various aspects of SLR-induced risk. Four of the six Copernicus Services, distributed across the land, marine environment, climate change and emergency management, provide core information on various components of SLR risk that could guide adaptation. A review of the current status of the Copernicus services regarding SLR adaptation has been presented. The comprehensive, operational, timely, quality-assessed, authoritative, reliable, free and open information delivered by Copernicus Services can also be used by other, more downstream climate services to better inform decision-making and adaptation measures.

In the coming years, as the Copernicus Programme unfolds its second phase (2021-2027), several evolutions could be implemented by the services, pending on funding. Such evolutions would provide relevant information for risk assessment. This could include an improved characterization of coastal zone's environmental states, including of dynamic phenomena, and exposure to SLR, upgraded sea level forecasts and better characterized uncertainties, implementation of an EU early warning system for coastal flooding. Precursor activities, such as on-going and planned European projects, could also contribute to the long-term evolution of Copernicus services with regard to SLR adaptation. Examples of such projects are the H2020 ECFAS (European Coastal Flood Awareness System) and CoCliCo (Core Climate Coastal Services, a project to start in 09/2021 and addressing coastal zones and infrastructures at risk from SLR during the 21st century) projects.

Users and policy needs are also driving Copernicus Services evolutions. While this review mostly focused on products, information and services provided to users with regard to SLR adaptation, activities to strengthen interactions between the services and their users are foreseen in the coming years. For instance, interactions between CMEMS and EU Member States will be deepened. A National Marine Stakeholders Group is to be setup to allow specific and direct discussions between Member States and the Entrusted Entity for the Marine Service. This will contribute to a better integration of the CMEMS with Member States expectations and assets, which is of particular importance in the context of the co-design of products and services and for implementing actions with Member States in the coastal marine areas.

A strong cooperation between Copernicus Services is essential to address the broad and diverse range of requirements to inform and support SLR and related adaptation in coastal zones. During Copernicus 1 (2014-2021), workshops and consultation meetings were organized to analyze priorities for the evolution of the Copernicus Services (CMEMS and CLMS) to better address coastal user needs. A corresponding roadmap for the evolution of CMEMS and CLMS was delivered to the EC (Copernicus Coastal Roadmap, 2018). Furthermore, discussions were engaged with C3S and CEMS for coordinated developments addressing the coastal zone.

In the coming years, a strengthening of interfaces, cooperation and co-production between the services is foreseen and will allow to maximize the added-value of the Copernicus Programme. This could be exemplified by the development (pending on the EC authorization) of a Copernicus Thematic Hub (CTH) on coastal zone during Copernicus 2 (2021-2027). Such a coastal CTH would provide an integrated catalog of products for coastal zones, an easier user journey with a simplified access to key information on coastal zones under a single-entry point, and with a central service desk to provide guidance and support to users. The coastal CTH would gather and maintain the products and information generated on coastal zones by several Copernicus Services, also including access to Sentinel data with different levels of processing (L2 to L4) and to other relevant information

providers (e.g., EMODnet). New products will also be discussed, proposed and produced either within a given Copernicus service, or through collaborations between services. By essence, coastal zones represent a thematic area where the synergy from multiple Copernicus core services has the potential to contribute to the converging interests of various stakeholders and of a diversity of users and policy makers. If implemented, a coastal CTH will allow Copernicus to address a range of policy aspects, which can hardly be addressed by a single Copernicus service.

AUTHOR CONTRIBUTIONS

AM initiated and coordinated the review and wrote the first draft of the manuscript. CB, MM, PS, GB, SB, JN, LS, and FV contributed to the writing of sections of the manuscript. All authors contributed to manuscript revision, read, and approved the submitted version.

FUNDING

The ECFAS project has received funding from the European Union's Horizon 2020 program under Grant Agreement No 101004211. The CoCliCo project will receive funding from the European Union's Horizon 2020 program under Grant Agreement No 101003598.

ACKNOWLEDGMENTS

The authors thank the organizers of the WCRP workshop on Regional sea level rise and coastal risks (Orléans, November 2019) which led to this Special Issue and to this contribution. The authors also thank all Copernicus Services producers, contractors, and management teams. A special thank goes to Karina von Schuckmann for comments on the manuscript.

REFERENCES

Ablain, M., Jugier, R., Zawadki, L., and Taburet, N. (2020). *The TOPEX-A Drift and Impacts on GMSL Time Series (poster), Ocean Surface Topography Science Team Meeting, 2017*. Available online at: https://meetings.aviso.altimetry.fr/fileadmin/user_upload/tx_ausyclsseminar/files/Poster_OSTST17_GMSL_Drift_TOPEX-A.pdf (accessed January 16, 2020)

Ablain, M., Meyssignac, B., Zawadzki, L., Jugier, R., Ribes, A., Spada, G., et al. (2019). Uncertainty in satellite estimates of global mean sea-level changes, trend and acceleration. *Earth Syst. Sci. Data* 11, 1189–1202. doi: 10.5194/essd-11-1189-2019

Abram, N., Gattuso, J. P., Prakash, A., Cheng, L., Chidichimo, M. P., Crate, S., et al. (2019). "Framing and context of the report," in *IPCC Special Report on the Ocean and Cryosphere in a Changing Climate*, ed. H.-O. Pörtner (Cambridge: Cambridge University Press).

Adloff, F., Jorda, G., Somot, S., Sevault, F., Arsouze, T., Meyssignac, B., et al. (2018). Improving sea level simulation in Mediterranean regional climate models. *Clim. Dyn.* 51, 1167–1178. doi: 10.1007/s00382-017-3842-3

Alfieri, L., Salamon, P., Pappenberger, F., Wetterhall, F., and Thielen, J. (2012). Operational early warning systems for water-related hazards in Europe. *Environ. Mental Sci. Policy* 21, 35–49. doi: 10.1016/j.envsci.2012.01008

Benveniste, J., Cazenave, A., Vignudelli, S., Fenoglio-Marc, L., Shah, R., Almar, R., et al. (2019). Requirements for a coastal hazards observing system. *Front. Mar. Sci.* 6:348. doi: 10.3389/fmars.2019.00348

Benveniste, J., Mandea, M., Melet, A., and Ferrier, P. (2020). Earth observations for coastal hazards monitoring and international services: a european perspective. *Surv. Geophys.* 41, 1185–1208. doi: 10.1007/s10712-020-09612-6

Bergsma, E., Conley, D., Davidson, M., O'Hare, T., and Almar, R. (2019). Storm event to seasonal evolution of nearshore bathymetry derived from shore-based video imagery. *Remote Sens.* 11:519. doi: 10.3390/rs11050519

Bevacqua, E., Maraun, D., Vousdoukas, M. I., Voukouvalas, E., Vrac, M., Mentaschi, L., et al. (2019). Higher probability of compound flooding from precipitation and storm surge in Europe under anthropogenic climate change. *Sci. Adv.* 5, eaaw5531. doi: 10.1126/sciadv.aaw5531

Bevacqua, E., Vousdoukas, M. I, Zappa, G., Hodges, K., Shepherd, T. G., Maraun, D., et al. (2020). More meteorological events that drive compound coastal flooding are projected under climate change. *Commun. Earth Environ.* 1:47. doi: 10.1038/s43247-020-00044-z

Birol, F., Fuller, N., Lyard, F., Cancet, M., Niño, F., Delebecque, C., et al. (2017). Coastal applications from nadir altimetry: example of the X-TRACK regional products. *Adv. Space Res.* 59, 936–953. doi: 10.1016/j.asr.2016.11.005

Bisaro, A., de Bel, M., Hinkel, J., Kok, S., Stojanovic, T., and Ware, D. (2020). Multilevel governance of coastal flood risk reduction: a public finance perspective. *Environ. Sci. Policy* 112, 203–212. doi: 10.1016/j.envsci.2020.05.018

Brooks, N. (2003). *Vulnerability, Risk and Adaptation: A Conceptual Frame- work. Tyndall Centre for Climate Change Research*. Norwich: University of East Anglia.

Capet, A., Fernandez, V., She, J., Dabrowski, T., Umgiesser, G., Staneva, J., et al. (2020). Operational modeling capacity in european seas—an eurogoos perspective and recommendations for improvement. *Front. Mar. Sci.* 7:129. doi: 10.3389/fmars.2020.00129

Cardona, O. D., van Aalst, M. K., Birkmann, J., Fordham, M., McGregor, G., Perez, R., et al. (2012). *Managing the Risks of Extreme Events and Disasters to Advance Climate Change Adaptation. A Special Report of Working Groups I and II of the Intergovernmental Panel on Climate Change (IPCC)*. Cambridge: Cambridge University Press, 65–108.

Castelle, B., Masselink, G., Scott, T., Stokes, C., Konstantinou, A., Marieu, V., et al. (2021). Satellite-derived shoreline detection at a high- energy meso-macrotidal beach. *Geomorphology* 383:107707. doi: 10.1016/j.geomorph.2021.107707

Cavaleri, M., Bajo, F., Barbariol, M., Bastianini, Benetazzo, A., Bertotti, L., et al. (2020). The 2019 flooding of venice and its implications for future predictions. *Oceanography* 33, 42–49. doi: 10.5670/oceanog.2020.105

Cazenave, A., and Le Cozannet, G. (2014). Sea level rise and its coastal impacts. *Earths Future* 2, 15–34.

Cipollini, P., Calafat, F. M., Jevrejeva, S., Melet, A., and Prandi, P. (2017). Monitoring sea level in the coastal zone with satellite altimetry and tide gauges. *Surv. Geophys.* 38, 33–57. doi: 10.1007/s10712-016-9392-0

Copernicus Coastal Roadmap (2018). *Mercator Ocean International and European Environmental Agency, 2018, Roadmap for the Evolution of Copernicus Marine and Land Services to Better Serve Coastal Users.*

Copernicus Dem Product Handbook (2020). *Copernicus Digital Elevation Model Product Handbook, v2.1; Airbus Defence and Space GmbH, 2020.* Available online at: https://spacedata.copernicus.eu/documents/20126/0/GEO1988-CopernicusDEM-SPE-002_ProductHandbook_I1.00.pdf/082dd479-f908-bf42-51bf-4c0053129f7c?t=1586526993604

Corbane, C., Pesaresi, M., Politis, P., Syrris, V., Florczyk, A. J., Soille, P., et al. (2017). Big earth data analytics on Sentinel-1 and Landsat imagery in support to global human settlements mapping. *Big Earth Data* 1, 118–144. doi: 10.1080/20964471.2017.1397899

Crosetto, M., Solari, L., Mroz, M., Balasis-Levinsen, J., Casagli, N., Frei, M., et al. (2020). The evolution of wide-area DInSAR: from regional and national services to the european ground motion service. *Remote Sens.* 12:2043. doi: 10.3390/rs12122043

Dangendorf, S., Marcos, M., Wöppelmann, G., Conrad, C. P., Frederikse, T., and Riva, R. (2017). Reassessment of 20th century global mean sea level rise. *Proc. Natl. Acad. Sci.U.S.A.* 114, 5946–5951. doi: 10.1073/pnas.1616007114

De Alfonso, M., Garcia-Valdecasas, J. M., Aznar, R., Perez-Gomez, B., Rodriguez, P., de los Santos, F. J., et al. (2020). Record wave storm in the Gulf of Cadiz

over the past 20 years and its impact on harbours. In: copernicus marine service ocean state report, issue 4. *J. Operat. Oceanogr.* 13, S137–S144.

Dodet, G., Melet, A., Ardhuin, F., Bertin, X., Idier, D., and Almar, R. (2019). The contribution of wind-generated waves to coastal sea-level changes. *Surv. Geophys.* 40, 1563–1601. doi: 10.1007/s10712-019-09557-5

Alvarez Fanjul, E., Pascual Collar, A., P ìerez G ìomez, B., De Alfonso, M., Garcia Sotillo, M., Staneva, J., et al. (2019). *Copernicus Marine Service Ocean State Report, Issue 3. Journal Of Operational Oceanography*, Vol. 12. Washington, D.C: NOAA, S1–S123.

European State of the Climate (ESOTC) (2019). *Copernicus Climate Change Service, Full Report.* Available online at: https://climate.copernicus.eu/ESOTC/2019/about-european-state-climate-2019

Farrell, W. E., and Clark, J. A. (1976). On Postglacial Sea Level. *Geo phys. J. R. Astron. Soc.* 46, 647–667. doi: 10.1111/j.1365-246X.1976.tb01252.x

Fernandez-Montblanc, T., Gomez-Enri, J., and Ciavola, P. (2020). The role of mean sea level annual cycle on extreme water levels along european coastline. *Remote Sens.* 12:3419. doi: 10.3390/rs12203419

Ferrario, F., Beck, M. W., Storlazzi, C. D., Micheli, F., Shepard, C. C., and Airoldi, L. (2014). The effectiveness of coral reefs for coastal hazard risk reduction and adaptation. *Nat. Commun.* 5:3794. doi: 10.1038/ncomms4794

Forget, G., and Ponte, R. M. (2015). The partition of regional sea level variability. *Progr. Oceanogr.* 137, 173–195. doi: 10.1016/j.pocean.2015.06.002

Gesch, D. B. (2018). Best practices for elevation-based assessments of sea- level rise and coastal flooding exposure. *Front. Earth Sci.* 6:230. doi: 10.3389/feart.2018.00230

Gregory, J. M., Griffies, S. M., Hughes, C. W., Lowe, J. A., Church, J. A., Fukimori, I., et al. (2019). Concepts and terminology for sea level: mean, variability and change, both local and global. *Surv. Geophys.* 40, 1251–1289. doi: 10.1007/s10712-019-09525-z

Hallegatte, S., Green, C., Nicholls, R. J., and Corfee-Morlot, J. (2013). Future flood losses in major coastal cities. *Nat. Clim. Chang.* 3, 802–806.

Hamon, M., Greiner, E., Le Traon, P. Y., and Remy, E. (2019). Impact of multiple altimeter data and mean dynamic topography in a global analysis and forecasting system. *J. Atmosp. Oceanic Technol.* 36, 1255–1266. doi: 10.1175/JTECH-D-18-0236.1

Hanley, M. E., Bouma, T. J., and Mossman, H. L. (2020). The gathering storm: optimizing management of coastal ecosystems in the face of a climate-driven threat. *Ann. Bot.* 125, 197–212. doi: 10.1093/aob/mcz204

Harley, M. D., Valentini, A., Armaroli, C., Perini, L., Calabrese, L., and Ciavola, P. (2016). Can an early-warning system help minimize the impacts of coastal storms? A case study of the 2012 Halloween storm, north- ern Italy. *Nat. Hazards Earth Syst. Sci.*16, 209–222.

Hermans, T. H. J., Tinker, J., Palmer, M. D., Katsman, C. A., Vermeersen, B. L. A., and Slangen, A. B. A. (2020). Improving sea-level projections on the North-western European shelf using dynamical downscaling. *Clim. Dyn.* 54, 1987–2011. doi: 10.1007/s00382-019-05104-5

Herring, S. C., Christidis, N., Hoell, A., Hoerling, M. P., and Stott, P. A. (2021). Explaining extreme events of 2019 from a climate perspective. *Bull. Am. Meteorol. Soc.* 102, S1–S116. doi: 10.1175/BAMS-ExplainingExtremeEvents2019.1

Hersbach, H., Bell, B., Berrisford, P., Hirahara, S., Hor ìanyi, A., Mun þoz-Sabater, J., et al. (2020). The ERA5 global reanalysis. *Q. J. R. Meteorol. Soc.* 146, 1999–2049. doi: 10.1002/qj.3803

Hinkel, J., Church, J. A., Gregory, J. M., Lambert, E., Le Cozannet, G., Lowe, J., et al. (2019). Meeting user needs for sea level rise information: a decision analysis perspective. *Earth's Future* 7, 320–337. doi: 10.1029/2018EF001071

Hinkel, J., Jaeger, C., Nicholls, R. J., Lowe, J., Renn, O., and Peijun, S. (2015). Sea-level rise scenarios and coastal risk management. *Nat. Clim. Chang.* 5, 188–190. doi: 10.1038/nclimate2505

Hinkel, J., Lincke, D., Vafeidis, A. T., Perrette, M., Nicholls, R. J., Tol, R. S. J., et al. (2014). Coastal flood damage and adaptation costs under 21st century sea-level rise. *Proc. Natl. Acad. Sci.U.S.A.* 111, 3292–3297. doi: 10.1073/pnas.1222469111

Huizinga, H. J., Moel, H., and Szewczyk, W. (2017). *Global Flood Depth-Damage Functions: Methodology and the Database with Guidelines. EUR 28552 Technical Report of the European Commission, Joint Research Centre*. Ispra: Joint Research Centre.

Idier, D., Aurouet, A., Bachoc, F., Baills, A., Betancourt, J., Durand, J., et al. (2020). Toward a user-based, robust and fast running method for coastal flooding forecast, early warning, and risk prevention. *J. Coastal Res.* 95:1111. doi: 10.2112/SI95-216.1

Idier, D., Bertin, X., Thompson, P., and Pickering, M. D. (2019). Interactions between mean sea level, tide, surge, waves and flooding: mechanisms and contributions to sea level variations at the coast. *Surv. Geophys.* 40, 1603–1630. doi: 10.1007/s10712-019-09549-5

Intergovermental Oceanographic Commission (IOC). (2006). *Manual on sea level measurement and interpretation - Volume IV-an update to 2006. Manual and Guides 14*. Lausanne: IOC, 88.

Kulp, S. A., and Strauss, B. H. (2019). New elevation data triple estimates of global vulnerability to sea-level rise and coastal flooding. *Nat. Commun.* 10:4844. doi: 10.1038/s41467-019-12808-z

Lavell, A., Oppenheimer, M., Diop, C., Hess, J., Lempert, R., Li, J., et al. (2012). "Climate change: newdimensions in disaster risk, exposure, vulnerability, and resilience," in *Managing the Risks of Extreme Events and Disasters to Advance Climate Change Adaptation. A Special Report of Working Groups I and II of the Intergovernmental Panel on Climate Change (IPCC)*, eds C. B. Field, V. Barros, T. F. Stocker, D. Qin, D. J. Dokken, K. L. Ebi, et al. (New York, NY: Cambridge University Press), 25–64.

Le Traon, P. Y., Reppucci, A., Alvarez Fanjul, E., Aouf, L., Behrens, A., Belmonte, M., et al. (2019). From observation to information and users: the copernicus marine service perspective. *Front. Mar. Sci.* 6:234. doi: 10.3389/fmars.2019.00234

Legeais, J. F., Ablain, M., Zawadzki, L., Zuo, H., Johannessen, J. A., Scharffenberg, M. G., et al. (2018). An improved and homogeneous altimeter sea level record from the ESA climate change initiative. *Earth Syst. Sci. Data* 10, 281–301. doi: 10.5194/essd-10-281-2018

Legeais, J. F., Llovel, W., Melet, A., and Meyssignac, B. (2020). Evidence of the TOPEX-A altimeter instrumental anomaly and acceleration of the global mean sea level. in: copernicus marine service ocean state report, issue 4. *J. Operat. Oceanogr.* 13, S77–S82.

Legeais, J.-F., Meyssignac, B., Faugíre, Y., Guerou, A., Ablain, M., Pujol, M.-I., et al. (under review). Copernicus sea level space observations: a basis for developing adaptation strategies to sea level rise. *Front. Mar. Sci.* (section Coastal Ocean Processes).

Lellouche, J. M., Greiner, E., Bourdallé-Badie, R., Garric, G., Melet, A., Drevillon, M., et al. (2021). The Copernicus global 1/12° oceanic and sea ice GLORYS12 reanalysis. *Front. Earth Sci.* 9:698876. doi: 10.3389/feart.2021.698876

Lincke, D., and Hinkel, J. (2018). Economically robust protection against 21st century sea-level rise. *Glob. Environ. Chang.* 51, 67–73.

Lowe, R. J., Cuttler, M. V. W., and Hansen, J. E. (2021). Climatic drivers of extreme sea level events along the coastline of Western Australia. *Earth's Future* 9:e2020EF001620.

Luijendijk, A., Hagenaars, G., Ranasinghe, R., Baart, F., Donchyts, G., and Aarninkhof, S. (2018). The state of the World's beaches. *Sci. Rep.* 8:6641. doi: 10.1038/s41598-018-24630-6

Lyu, K., Zhang, X., Church, J. A., Slangen, A. B. A., and Hu, J. (2014). Time of emergence for regional sea-level change. *Nat. Clim. Chang.* 4, 1006–1010.

Marcos, M., Wöppelmann, G., Matthews, A., Ponte, R. M., Birol, F., Ardhuin, F., et al. (2019). Coastal sea level and related fields from existing observing systems. *Surv. Geophys.* 40, 1293–1317. doi: 10.1007/s10712-019-09513-3

Marzeion, B., Cogley, J. G., Richter, K., and Parkes, D. (2014). Attribution of global glacier mass loss to anthropogenic and natural causes. *Science* 345, 919–921.

Matgen, P., Martinis, S., Wagner, W., Freeman, V., Zeil, P., and McCormick, N. (2020). *Feasibility Assessment Of An Automated, Global, Satellite-Based Flood Monitoring Product for the Copernicus Emergency Management Service. European commission. Joint Research centre*. Brussels: European commission.

McMichael, C., Dasgupta, S., Ayeb-Karlsson, S., and Kelman, I. (2020). A review of estimating population exposure to sea-level rise and the relevance for migration. *Environ. Res. Lett.* 15:123005. doi: 10.1088/1748-9326/abb398

Meier, M. H. E., Dieterich, C., and Gröger, M. (2021). Natural variability is a large source of uncertainty in future projections of hypoxia in the Baltic Sea. *Commun. Earth Environ.* 2:50. doi: 10.1038/s43247-021-00115-9

Melet, A., Almar, R., Hemer, M., Le Cozannet, G., Meyssignac, B., and Ruggiero, P. (2020b). Contribution of wave setup to projected coastal sea level changes. *J. Geophys. Res. Oceans* 125:e2020JC016078. doi: 10.1029/2020JC016078

Melet, A., Almar, R., and Meyssignac, B. (2016). What dominates sea level at the coast: a case study for the Gulf of Guinea. *Ocean Dyn.* 66, 623–636. doi: 10.1007/s10236-016-0942-2

Melet, A., Meyssignac, B., Almar, R., and Le Cozannet, G. (2018). Under- estimated wave contribution to coastal sea-level rise. *Nat. Clim. Chang.* 8, 234–239. doi: 10.1038/s41558-018-0088-y

Melet, A., Teatini, P., Le Cozannet, G., Jamet, C., Conversi, A., Benveniste, J., et al. (2020a). Earth observations for monitoring marine coastal hazards and their drivers. *Surv. Geophys.* 41, 1489–1534. doi: 10.1007/s10712-020-09594-5

Menendez, M., and Woodworth, P. L. (2010). Changes in extreme high-water levels based on a quasi-global tide-gauge data set. *J. Geophys. Res.* 115:C10011.

Mentaschi, L., Vousdoukas, M. I., Pekel, J. F., Voukouvalas, E., and Feyen, L. (2018). Global long-term observations of coastal erosion and accretion. *Sci. Rep.* 8:12876. doi: 10.1038/s41598-018-30904-w

Mentaschi, L., Vousdoukas, M. I., Voukouvalas, E., Dosio, A., and Feyen, L. (2017). Global changes of extreme coastal wave energy fluxes triggered by intensified teleconnection patterns. *Geophys. Res. Lett.* 44, 2416–2426. doi: 10.1002/2016GL072488

Meucci, A., Young, I. R., Hemer, M., Kirezci, E., and Ranasinghe, R. (2020). Projected 21st century changes in extreme wind-wave events. *Sci. Adv.* 6:eaaz7295. doi: 10.1126/sciadv.aaz7295

Meyssignac, B., and Cazenave, A. (2012). Sea level: a review of present-day and recent-past changes and variability. *J. Geodyn.* 58, 96–109.

Meyssignac, B., Slangen, A. B. A., Melet, A., Church, J. A., Fettweis, X., Marzeion, B., et al. (2017). Evaluating model simulations of twentieth-century sea-level rise Part II: Regional sea-level changes. *J. Clim.* 30, 8565–8593. doi: 10.1175/JCLI-D-17-0112.1

Mori, N., Shimura, T., Yoshida, K., Mizuta, R., Okada, Y., Fujita, M., et al. (2019). Future changes in extreme storm surges based on mega-ensemble projection using 60-km resolution atmospheric global circulation model. *Coastal Eng. J.* 61, 295–307. doi: 10.1080/21664250.2019.1586290

Morim, J., Hemer, M., Wang, X. L., Cartwright, N., Trenham, C., Semedo, A., et al. (2019). Robustness and uncertainties in global multivariate wind-wave climate projections. *Nat. Clim. Chang.* 9, 711–718. doi: 10.1038/s41558-019-0542-5

Morrow, R., Fu, L. L., Ardhuin, F., Benkiran, M., Chapron, B., Cosme, E., et al. (2019). Global observations of fine-scale ocean surface topography with the Surface Water and Ocean Topography (SWOT) mission. *Front. Mar. Sci.* 6:232. doi: 10.3389/fmars.2019.00232

Muis, S., Apecechea, M. I., Dullaart, J., de Lima Rego, J., Madsen, K. S., Su, J., et al. (2020). A high-resolution global dataset of extreme sea levels, tides, and storm surges, including future projections. *Front. Mar. Sci.* 7:263. doi: 10.3389/fmars.2020.00263

Nerem, R. S., and Fasullo, J. (2019). "Observations of the rate and acceleration of global mean sea level change," in *Explaining extreme events of 2017 from a climate perspective of Special Supplement to the Bulletin of the American Meteorological Society*, Vol. 100, eds S. C. Herring, N. Christidis, A. Hoell, M. P. Hoerling, and P. A. Stott (Washington, D.C: NOAA).

Neumann, B., Vafeidis, A. T., Zimmermann, J., and Nicholls, R. J. (2015). Future coastal population growth and exposure to sea-level rise and coastal flooding – a global assessment. *PLoS One* 10:e0118571. doi: 10.1371/journal.pone.0118571

Nixon, S. (2015). *EU overview of methodologies used in preparation of Flood Hazard and Flood Risk Maps*. Brussels: European Commission.

Oliveira, A., Fortunato, A., Rogeiro, J., Teixeira, J., Azevedo, A., Lavaud, L., et al. (2020). OPENCoastS: an open-access service for the automatic generation of coastal forecast systems. *Environ. Model. Softw.* 124:104585. doi: 10.1016/j.envsoft.2019.104585

Oppenheimer, M., Glavovic, B., Hinkel, J., van de Wal, R. S. W., Magnan, A., Abd-Elgawad, A., et al. (2019). "Sea level rise and implications for low lying islands, coasts and communities," in *IPCC Special Report on the Ocean and Cryosphere in a Changing Climate*, eds H.-O. Pörtner, et al. (Cambridge: Cambridge University Press).

Word Meteorological Organization (WMO) (2020). *State of the Global Climate 2019 (WMO- No. 1248)*. Geneva: WMO.

Word Meteorological Organization (WMO) (2021). *State of the Global Climate 2020 (WMO- No. 1624)*. Geneva: WMO.

Orton, P., Vinogradov, S. V., Georgas, S., Blumberg, N., Lin, N., Gornitz, V., et al. (2015). "Dynamic coastal flood modeling," in *Building the Knowledge Base for Climate Resiliency: New York City Panel on Climate Change 2015 Report*, eds C. Rosenzweig and W. Solecki (New York: Annals of the New York academy of sciences), 56–66.

Pardo-Pascual, J., Sanchez-Garcia, E., Almonacid-Caballer, J., Palomar-Vazquez, J., Priego de los Santos, E., Fernandez-Sarria, A., et al. (2018). Assessing the accuracy of automatically extracted shorelines on microtidal beaches from landsat 7, landsat 8 and sentinel-2 imagery. *Remote Sens.* 10:326. doi: 10.3390/rs10020326

Peltier, W. (2004). Global glacial isostasy and the sur- face of the ice-age earth: the Ice-5G (VM2) model and grace. *Ann. Rev. Earth Planet. Sci.* 32, 111–149. doi: 10.1146/annurev.earth.32.082503.144359

Pesaresi, M., Ehrlich, D., Ferri, S., Florczyk, A. J., Carneiro Freire, S., Halkia, S., et al. (2016). *Operating Procedure For The Production Of The Global Human Settlement Layer From Landsat data of the epochs 1975, 1990, 2000, and 2014. European Commission. Joint Research Centre*. Brussels: European Commission.

Ponte, R. M., Carson, M., Cirano, M., Domingues, C. M., Jevrejeva, S., Mar-cos, M., et al. (2019). Towards comprehensive observing and modeling systems for monitoring and predicting regional to coastal sea level. *Front. Mar. Sci.* 6:437. doi: 10.3389/fmars.2019.00437

Prandi, P., Meyssignac, B., Ablain, M., Spada, G., Ribes, A., and Benveniste, J. (2021). Local sea level trends, accelerations and uncertainties over 1993–2019. *Sci. Data* 8:1. doi: 10.1038/s41597-020-00786-7

Richter, K., Marzeion, B., and Riva, R. (2017). The effect of spatial averaging and glacier melt on detecting a forced signal in regional sea level. *Environ. Res. Lett.* 12:034004.

Richter, K., Meyssignac, B., Slangen, A. B., Melet, A., Church, J. A., Fettweis, X., et al. (2020). Detecting a forced signal in satellite- era sea-level change. *Environ. Res. Lett.* 15:094079. doi: 10.1088/1748-9326/ab986e

Riva, R. E. M., Bamber, J. L., Lavallée, D. A., and Wouters, B. (2010). Sea-level fin- gerprint of continental water and ice mass change from GRACE: grace SEA-LEVEL FINGERPRINT. *Environ. Res. Lett.* 37:L044770. doi: 10.1029/2010GL044770

Rogelj, J., Shindell, D., Jiang, K., Fifita, S., Forster, P., Ginzburg, V., et al. (2018). "Mitigation pathways compatible with 1.5°c in the context of sustainable development," in *Global Warming of 1.5°C. An IPCC Special Report On The Impacts Of Global Warming Of 1.5°C Above Pre-Industrial Levels And Related Global Greenhouse Gas Emission Pathways, In The Context Of Strengthening The Global Response To The Threat Of Climate Change, Sustainable Development, And Efforts To Eradicate Poverty*, eds V. Masson-Delmotte, P. Zhai, H. O. Pörtner, D. Roberts, J. Skea, R. Pidcock, et al. (Cambridge: Cambridge University Press).

Ryan, J. C., Smith, L. C., van As, D., Cooley, S. W., Cooper, M. G., Pitcher, L. H., et al. (2019). Greenland Ice Sheet surface melt amplified by snowline migration and bare ice exposure. *Sci. Adv.* 5:eaav3738. doi: 10.1126/sciadv.aav3738

Salamon, P., McCormick, N., Reimer, C., Clarke, T., Bauer-Marschallinger, B., Wagner, W. et al. (2021). "The new, systematic global flood monitoring product of the copernicus emergency management service," in *International Geoscience and Remote Sensing Symposium*.

Sasgen, I., Wouters, B., Gardner, A. S., King, M. D., Tedesco, M., Landerer, F. W., et al. (2020). Return to rapid ice loss in greenland and record loss in 2019 detected by the GRACE-FO satellites. *Commun. Earth Environ* 1:8. doi: 10.1038/s43247-020-0010-1

von Schuckmann, K., Le Traon, P. Y., Alvarez-Fanjul, E., Axell, L., Balmaseda, M., Breivik, L. A., et al. (2016). The copernicus marine environment monitoring service ocean state report. *J. Operat. Oceanogr.* 9, S235–S320. doi: 10.1080/1755876X.2016.1273446

von Schuckmann, K., Le Traon, P. Y., Smith, N., Pascual, A., Brasseur, P., Fennel, K., et al. (2018). Copernicus marine service ocean state report, issue 2. *J. Operat. Oceanogr.* 11, S1–S142. doi: 10.1080/1755876X.2018.1489208

von Schuckmann, K., Le Traon, P. Y., Smith, N., Pascual, A., Djavidnia, S., Gattuso, J. P., et al. (2019). Copernicus marine service ocean state report, issue 3. *J. Operat. Oceanogr.* 12, S1–S123. doi: 10.1080/1755876X.2019.1633075

von Schuckmann, K., Le Traon, P. Y., Smith, N., Pascual, A., Djavidnia, S., Gattuso, J. P., et al. (2020). Copernicus marine service ocean state report, issue 4. *J. Operat. Oceanogr.* 13, S1–S172. doi: 10.1080/1755876X.2020.1785097

Slangen, A. B. A., Carson, M., Katsman, C. A., van de Wal, R. S. W., Kohl, A., Vermeersen, L. L. A., et al. (2014a). Projecting twenty-first century regional sea-level changes. *Clim. Chang.* 124, 317–332.

Slangen, A. B. A., Church, J. A., Zhang, X., and Monselesan, D. (2014b). Detection and attribution of global mean thermosteric sea level change. *Geo phys. Res. Lett.* 41, 5951–5959. doi: 10.1002/2014GL061356

Slangen, A. B. A., Church, J. A., Agosta, C., Fettweis, X., Marzeion, B., and Richter, K. (2016). Anthropogenic forcing dominates global mean sea-level rise since 1970. *Nat. Clim. Chang.* 6, 701–705. doi: 10.1038/nclimate2991

Slangen, A. B. A., Meyssignac, B., Agosta, C., Champollion, N., Church, J. A., Fettweis, X., et al. (2017). Evaluating model simulations of twentieth-century sea level rise Part I: Global mean sea level change. *J. Clim.* 30, 8539–8563. doi: 10.1175/JCLI-D-17-0110.1

Smith, P., Pappenberger, F., Wetterhall, F., Thielen, del Pozo, J., Krzeminski, B., et al. (2016). "Chapter 11 – on the operational implementation of the European Flood Awareness System (EFAS)," in *Flood Forecasting*, eds T. E. Adams and T. C. Pagano (Boston: Academic Press), 313–348. doi: 10.1016/B978-0-12-801884-2.00011-6

Sotillo, M. G., Cerralbo, P., Lorente, P., Grifoll, M., Espino, M., Sanchez-Arcilla, A., et al. (2020). Coastal ocean forecasting in Spanish ports: the SAMOA operational service. *J. Operat. Oceanogr.* 13, 37–54. doi: 10.1080/1755876X.2019.1606765

Spada, G., and Melini, D. (2019). On some properties of the glacial isostatic adjustment fingerprints. *Water* 11:1844. doi: 10.3390/w11091844

Stammer, D., Balmaseda, M., Heimbach, P., Kohl, A., and Weaver, A. (2016). Ocean data assimilation in support of climate applications: status and perspectives. *Ann. Rev. Mar. Sci.* 8, 491–518. doi: 10.1146/annurev-marine-122414-034113

Stockdon, H. F., Holman, R. A., Howd, P. A., and Sallenger, A. H. (2006). Empirical parameterization of setup, swash, and runup. *Coastal Eng.* 53, 573–588.

Storto, A., Alvera-Azcarate, A., Balmaseda, M. A., Barth, A., Chevallier, M., Counillon, F., et al. (2019a). Ocean reanalyses: recent advances and unsolved challenges. *Front. Mar. Sci.* 6:418. doi: 10.3389/fmars.2019.00418

Storto, A., Bonaduce, A., Feng, X., and Yang, C. (2019b). Steric sea level changes from ocean reanalyses at global and regional scales. *Water* 11:1987. doi: 10.3390/w11101987

Storto, A., Masina, S., Simoncelli, S., Iovino, D., Cipollone, A., Drevillon, M., et al. (2019c). The added value of the multi-system spread information for ocean heat content and steric sea level investigations in the CMEMS GREP ensemble reanalysis product. *Clim. Dyn.* 53, 287–312. doi: 10.1007/s00382-018-4585-5

Storto, A., Masina, S., Balmaseda, M., Guinehut, S., Xue, Y., Szekely, T., et al. (2017). Steric sea level variability (1993–2010) in an ensemble of ocean reanalyses and objective analyses. *Clim. Dyn.* 49, 709–729. doi: 10.1007/s00382-015-2554-9

Sweet, W., Zervas, C., Gill, S., and Park, J. (2013). "Hurricane Sandy inundation probabilities today and tomorrow. *Bull. Am. Meteorol. Soc.* 94, S17–S2.

Taburet, G., Sanchez-Roman, A., Ballarotta, M., Pujol, M. I., Legeais, J. F., Fournier, F., et al. (2019). DUACS DT2018: 25 years of reprocessed sea level altimetry products. *Ocean Sci.* 15, 1207–1224. doi: 10.5194/os-15-1207-2019

Temmerman, S., Meire, P., Bouma, T. J., Herman, P. M. J., Ysebaert, T., and De Vriend, H. J. (2013). Ecosystem-based coastal defence in the face of global change. *Nature* 504, 79–83. doi: 10.1038/nature12859

Umgiesser, G., Bajo, M., Ferrarin, C., Cucco, A., Lionello, P., Zanchettin, D., et al. (2020). The prediction of floods in Venice: methods, models and uncer- tainty. *Natural Hazards Earth Syst. Sci. Discuss.* 2020, 1–47. doi: 10.5194/nhess-2020-361

Vafeidis, A. T., Schuerch, M., Wolff, C., Spencer, T., Merkens, J. L., Hinkel, J., et al. (2019). Water-level attenuation in global-scale assessments of exposure to coastal flooding: a sensitivity analysis. *Natural Hazards Earth Syst. Sci. Discuss.* 19, 973–984. doi: 10.5194/nhess-19-973-2019

Vos, K., Splinter, K. D., Harley, M. D., Simmons, J. A., and Turner, I. L. (2019). Coast-sat: a google earth engine-enabled python toolkit to extract shorelines from publicly available satellite imagery. *Environ. Model. Softw.* 122:104528. doi: 10.1016/j.envsoft.2019.104528

Vousdoukas, M. I., Mentaschi, L., Voukouvalas, E., Verlaan, M., Jevrejeva, S., Jackson, L. P., et al. (2018a). Global probabilistic projections of extreme sea levels show intensification of coastal flood hazard. *Nat. Commun.* 9:2360. doi: 10.1038/s41467-018-04692-w

Vousdoukas, M. I., Ranasinghe, R., Mentaschi, L., Plomaritis, T. A., Athanasiou, P., Luijendijk, A., et al. (2020a). Sandy coastlines under threat of erosion. *Nat. Clim. Chang.* 10, 260–263. doi: 10.1038/s41558-020-0697-0

Vousdoukas, M. I., Mentaschi, L., Hinkel, J., Ward, P. J., Mongelli, I., Ciscar, J. C., et al. (2020b). Economic motivation for raising coastal flood defenses in Europe. *Nat. Commun.* 11:2119. doi: 10.1038/s41467-020-15665-3

Vousdoukas, M. I., Mentaschi, L., Voukouvalas, E., Bianchi, A., Dottori, F., and Feyen, L. (2018b). Climatic and socioeconomic controls of future coastal flood risk in Europe. *Nat. Clim. Chang.* 8, 776–780. doi: 10.1038/s41558-018-0260-4

Vousdoukas, M. I., Mentaschi, L., Voukouvalas, E., Verlaan, M., and Feyen, L. (2017). Extreme sea levels on the rise along Europe's coasts. *Earth's Future* 5, 304–323. doi: 10.1002/2016EF000505

Vousdoukas, M. I., Voukouvalas, E., Mentaschi, L., Dottori, F., Giardino, A., Bouziotas, D., et al. (2016). Developments in large-scale coastal flood hazard mapping. *Natural Hazards Earth Syst. Sci. Discuss.* 16, 1841–1853. doi: 10.5194/nhess-16-1841-2016

Wahl, T., Jain, S., Bender, J., Meyers, S. D., and Luther, M. E. (2015). Increas- ing risk of compound flooding from storm surge and rainfall for major US cities. *Nat. Clim. Chang.* 5, 1093–1097. doi: 10.1038/nclimate2736

WCRP Global Sea Level Budget Group. (2018). Global sea-level bud- get 1993–present. *Earth Syst. Sci. Data* 10, 1551–1590. doi: 10.5194/essd-10-1551-2018

Wolff, C., Nikoletopoulos, T., Hinkel, J., and Vafeidis, A. T. (2020). Future urban development exacerbates coastal exposure in the Mediterranean. *Sci. Rep.* 10:14420. doi: 10.1038/s41598-020-70928-9

Woodworth, P. L., Hunter, J. R., Marcos, M., Caldwell, P., Menéndez, M., and Haigh, I. (2016). Towards a global higher-frequency sea level dataset. *Geoscience Data Journal* 3, 50–59. doi: 10.1002/gdj3.42

Woodworth, P. L., Melet, A., Marcos, M., Ray, R. D., Wöppelmann, G., Sasaki, Y. N., et al. (2019). Forcing factors affecting sea level changes at the coast. *Surv. Geophys.* 40, 1351–1397. doi: 10.1007/s10712-019-09531-1

Wöppelmann, G., and Marcos, M. (2016). Vertical land motion as a key to understanding sea level change and variability: vertical land motion and sea level change. *Rev. Geophys.* 54, 64–92. doi: 10.1002/2015RG000502

Wöppelmann, G., Marcos, M., Coulomb, A., Martín Míguez, B., Bonnetain, P., Boucher, C., et al. (2014). Rescue of the historical sea level record of Marseille (France) from 1885 to 1988 and its extension back to 1849Ű1851. *J. Geod.* 88, 869–885. doi: 10.1007/s00190-014-0728-6

Ye, F., Zhang, Y. J., Yu, H., Sun, W., Moghimi, S., Myers, E., et al. (2020). Simulating storm surge and compound flooding events with a creek-to-ocean model: importance of baroclinic effects. *Ocean Model.* 145, 101526. doi: 10.1016/j.ocemod.2019.101526

Zemp, M., Huss, M., Thibert, E., Eckert, N., McNabb, R., Huber, J., et al. (2019). Global glacier mass changes and their contributions to sea-level rise from 1961 to 2016. *Nature* 568, 382–386. doi: 10.1038/s41586-019-1071-0

Conflict of Interest: The authors declare that the research was conducted in the absence of any commercial or financial relationships that could be construed as a potential conflict of interest.

Publisher's Note: All claims expressed in this article are solely those of the authors and do not necessarily represent those of their affiliated organizations, or those of the publisher, the editors and the reviewers. Any product that may be evaluated in this article, or claim that may be made by its manufacturer, is not guaranteed or endorsed by the publisher.

Copyright © 2021 Melet, Buontempo, Mattiuzzi, Salamon, Bahurel, Breyiannis, Burgess, Crosnier, Le Traon, Mentaschi, Nicolas, Solari, Vamborg and Voukouvalas. This is an open-access article distributed under the terms of the Creative Commons Attribution License (CC BY). The use, distribution or reproduction in other forums is permitted, provided the original author(s) and the copyright owner(s) are credited and that the original publication in this journal is cited, in accordance with accepted academic practice. No use, distribution or reproduction is permitted which does not comply with these terms.

frontiers in Marine Science

POLICY AND PRACTICE REVIEWS
published: 30 September 2021
doi: 10.3389/fmars.2021.710342

Check for updates

OPEN ACCESS

Edited by:
Ivica Vilibic,
Ruđer Bošković Institute, Croatia

Reviewed by:
Patrick Barnard,
United States Geological Survey (USGS), United States
Joy Jacqueline Pereira,
National University of Malaysia, Malaysia

***Correspondence:**
Robert J. Nicholls
robert.nicholls@uea.ac.uk

†ORCID:
Robert J. Nicholls
orcid.org/0000-0002-9715-1109
Richard P. Beaven
orcid.org/0000-0002-1387-8299
Daniel Monfort
orcid.org/0000-0003-2038-4139
Thomas Wahl
orcid.org/0000-0003-3643-5463
Julia Gebert
orcid.org/0000-0002-7805-5373
Arne Arns
orcid.org/0000-0002-3709-2514
Kate L. Spencer
orcid.org/0000-0001-6621-6945
Victor M. Santos
orcid.org/0000-0002-4458-0890
Alejandra R. Enríquez
orcid.org/0000-0001-7836-6748

Specialty section:
This article was submitted to Coastal Ocean Processes, a section of the journal Frontiers in Marine Science

Received: *16 May 2021*
Accepted: *30 August 2021*
Published: *30 September 2021*

Citation:
Nicholls RJ, Beaven RP, Stringfellow A, Monfort D, Le Cozannet G, Wahl T, Gebert J, Wadey M, Arns A, Spencer KL, Reinhart D, Heimovaara T, Santos VM, Enríquez AR and Cope S (2021) Coastal Landfills and Rising Sea Levels: A Challenge for the 21st Century. Front. Mar. Sci. 8:710342. doi: 10.3389/fmars.2021.710342

Coastal Landfills and Rising Sea Levels: A Challenge for the 21st Century

Robert J. Nicholls[1*†], Richard P. Beaven[2†], Anne Stringfellow[2], Daniel Monfort[3†], Gonéri Le Cozannet[3], Thomas Wahl[4†], Julia Gebert[5†], Matthew Wadey[6], Arne Arns[7†], Kate L. Spencer[8†], Debra Reinhart[4], Timo Heimovaara[5], Víctor M. Santos[9,10†], Alejandra R. Enríquez[4†] and Samantha Cope[11]

[1] Tyndall Centre for Climate Change Research, University of East Anglia, Norwich, United Kingdom, [2] School of Engineering, University of Southampton, Southampton, United Kingdom, [3] Bureau de Recherches Géologiques et Minières, Orléans, France, [4] Department of Civil, Environmental and Construction Engineering, University of Central Florida, Orlando, FL, United States, [5] CITG, Delft, Netherlands, [6] Bournemouth, Christchurch and Poole Council, Bournemouth, United Kingdom, [7] Department of Agriculture and Environmental Sciences, University of Rostock, Rostock, Germany, [8] School of Geography, Faculty of Humanities and Social Sciences, Queen Mary University of London, London, United Kingdom, [9] Department of Civil, Environmental and Construction Engineering and National Center for Integrated Coastal Research, University of Central Florida, Orlando, FL, United States, [10] Department of Estuarine and Delta Systems, NIOZ Royal Netherlands Institute for Sea Research, Yerseke, Netherlands, [11] Coastal Partners, Havant Borough Council, Havant, United Kingdom

Populated coastal areas worldwide have a legacy of numerous solid waste disposal sites. At the same time, mean sea level is rising and likely to accelerate, increasing flooding and/or erosion. There is therefore concern that landfill sites located at and near the coast pose a growing risk to the environment from the potential release of liquid and solid waste materials. This paper aims to assess our present understanding of this issue as well as research and practice needs by synthesizing the available evidence across a set of developed country cases, comprising England, France, Germany, the Netherlands, and the United States (Florida). Common insights gained here include: (1) a lack of data and limited appreciation of waste release from coastal landfill as a potential problem; (2) recognition of the scale and diversity of coastal landfill waste within a range of generic settings (or situations); and (3) a lack of robust protocols that allow the impact of different categories of waste release to the coast to be assessed in a consistent and evidence-based manner, most particularly for solid waste. Hence, a need for greater understanding of the following issues is identified: (1) the amount, character and impact of waste that could be released from landfill sites; (2) the acceptability and regulation of waste eroding from coastal landfills; (3) present and future erosion rates at landfill sites suggesting the need for more monitoring and relevant predictive tools; (4) the full range of possible management methods for dealing with waste release from landfills and the science to support them; and (5) relevant long-term funding mechanisms to address this issue. The main focus and experience of current management practice has been protection/retention, or removal of landfills, with limited consideration of other feasible solutions and how they might be facilitated. Approaches to assess and address solid waste release to the marine/coastal environment represent a particular gap. Lastly, as

solid waste will persist indefinitely and sea levels will rise for many centuries, the long timescale of this issue needs wider appreciation and should be included in coastal and waste policy.

Keywords: landfill, waste, erosion, flood, sea-level rise

INTRODUCTION

Our historic use of the coastal zone for the disposal of solid wastes has left a significant legacy, with a large (but unknown) number of landfills worldwide. In Europe alone, it is estimated that there are 350,000–500,000 landfills in total containing wide-ranging wastes – industrial, commercial, domestic, hazardous, and liquid sludge (Hogland et al., 2011). Around 90% of these pre-date modern European legislation pertaining to waste control and landfill (EURELCO, 2019) and significant numbers are located in coastal and alluvial areas prone to flooding and/or erosion (Wille, 2018). In 2019, the US Government Accountability Office reported that nationally at least 945 US "Superfund" waste sites, many of which are municipal solid waste landfills, face increasing risks from climate change effects including rising seas (Grandoni and Dennis, 2019). There is also increasing evidence that extreme flood and erosion events result in the release of large volumes of toxic material to adjacent waters. For example, 13 toxic waste sites in Texas were flooded by Hurricane Harvey in 2017 (USEPA, 2017), while storm-induced failure of the Fox River historic landfill in New Zealand polluted hundreds of kilometers of coastline (JonoB, 2019). In the developed world, improved regulations for landfills combined with waste minimization hopefully mean that new coastal landfill sites are limited or absent, but in the developing world it is almost certain that the volume and legacy of waste in vulnerable coastal areas continues to grow (e.g., Zalasiewicz et al., 2016).

At the same time, we are experiencing a significant global rise in mean sea levels due to human-induced climate change: stringent climate mitigation as proposed in the Paris Agreement will slow but not stop this rise which will continue for centuries (Oppenheimer et al., 2019). Sea-level rise (SLR) will cause a significant increase in a range of coastal hazards, including more flooding and erosion of landfills unless there is appropriate adaptation. There is therefore growing concern that such waste could be released at an increasing rate and pose a significant risk to the coastal and marine environment over the coming decades.

Importantly, while all potential consequences of the release of soluble and solid wastes to the marine environment are unknown, they are of significant concern (Chen et al., 2020). Where legacy or eroded wastes have been examined, organic and inorganic contaminants [e.g., lead, mercury and poly-aromatic hydrocarbons (PAHs)] are present at levels that could cause significant harm to the marine environment (e.g., Pope et al., 2011; Brand and Spencer, 2020), and whilst soluble contaminants released may be much lower (O'Shea et al., 2018; Brand and Spencer, 2020) elevated concentrations of emerging contaminants of concern have been identified in historical landfill leachate decades after disposal (Propp et al., 2021). In addition, a range of other solid waste materials could be released including asbestos, plastics and composite waste materials (e.g., batteries) that would cause physical damage to marine biota through ingestion, abrasion, and entanglement, as well as a reduction in amenity value for people using the coast for recreation. Even without considering SLR, Chen et al. (2020) have estimated that the cumulative plastic waste inputs to the ocean will continue growing due to mismanaged plastic waste (e.g., in open dumps and some landfills) in coastal areas.

Approaches to assessing and managing historical landfills have been considered in a number of countries but appear to vary widely. For example, in the United States, coastal landfills in some states have been ranked with respect to their vulnerability to climate change including SLR, tidal flooding, erosion and increased precipitation to assist the prioritization of remediation efforts (e.g., ADEC, 2015; Asher, 2019). Belgium is considering the possibility of eliminating landfills (through waste relocation and/or landfill mining) in areas prone to flooding (Wille, 2018). However, such national analyses are unusual. A series of recent papers have analyzed this issue for England (Brand et al., 2018; Wadey et al., 2019; Beaven et al., 2020; Nicholls et al., 2020). Given that coastal waste and landfill and the effects of SLR and climate change are a universal problem, and best management practices are lacking, more international exchange of these experiences could be beneficial.

Uncontrolled release of solid wastes to the coast by erosion would seem to be unacceptable, as evidenced by widespread scientific consensus that release of plastics into the marine environment is damaging to marine and human life (Eriksen et al., 2014; Bergmann et al., 2017). There is also widespread public/emotional concern over the issue (Dunn et al., 2020). In addition, waste has a long timescale – many solid wastes are persistent, potentially over geological timescales (Zalasiewicz et al., 2016). While solid wastes may be modified by leaching and degradation within a landfill, the risks associated with the release of solid waste are a long-term problem which will persist and become more widespread because of SLR.

Hence, coastal landfills and the threats of waste release will pose ongoing coastal management questions over the coming decades and longer. This raises fundamental questions such as should waste release be avoided at all costs, or is there an acceptable rate of release, depending on the nature of the waste material? If release is unacceptable how can this be prevented in terms of remediation and/or protection in perpetuity (e.g., Bardos et al., 2020) or relocation of the waste material outside areas subject to flooding and/or erosion? Funding for these issues will generally fall on public funds requiring a budget item that was not appreciated when the landfills were active and is still not fully appreciated today. While there is some guidance on coastal landfill management (Cooper et al., 2013;

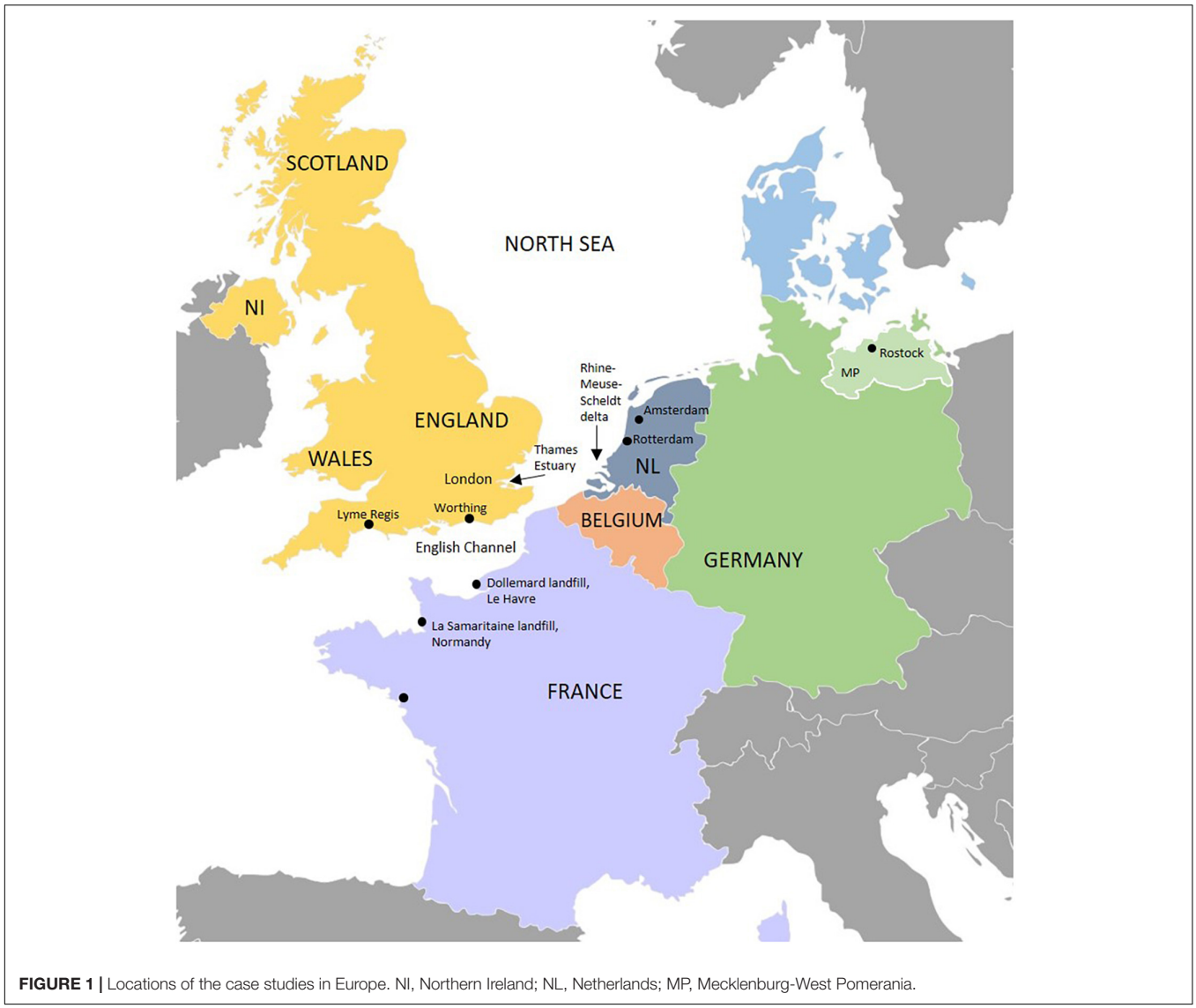

FIGURE 1 | Locations of the case studies in Europe. NI, Northern Ireland; NL, Netherlands; MP, Mecklenburg-West Pomerania.

Nicholls et al., 2018b), there is an absence of protocols that allow the impact of different categories of waste release to the sea to be assessed in a consistent and evidence-based manner, especially for solid wastes. This hinders strategic action and planning on this important issue.

The aim of this paper is to assess the implications of the release of waste materials from landfills into the marine environment, including erosion of solid waste and migration of leachates, and set our current understanding into a wider context, including research and development needs. We use the available evidence and experience in developed country settings, based on case studies in Europe (England, Germany, Netherlands, and France) (**Figure 1**) and the United States (Florida). First, it presents a generic typology of coastal landfills and waste release that is applicable across all the sites considered. It then reviews the evolution of landfills in the EU, setting the scene for the European case studies that follow. Then the status of landfills with respect to present and future flooding and erosion in each jurisdiction, including linking the analysis to the landfill and release typology. These case studies are heterogeneous by nature, reflecting different levels of awareness, analysis to date and policy responses in each country. This is followed by a cross-nation synthesis and an assessment of the status of coastal landfill management approaches for erosion and flooding. Finally the generic lessons are summarized, including research and development needs.

A GENERIC TYPOLOGY OF COASTAL LANDFILLS AND WASTE RELEASE

CIRIA guide C718 (Cooper et al., 2013) provides generic guidance on the identification and management of landfill sites and areas of land contamination located on eroding or low-lying coastlines drawing on United Kingdom experience.

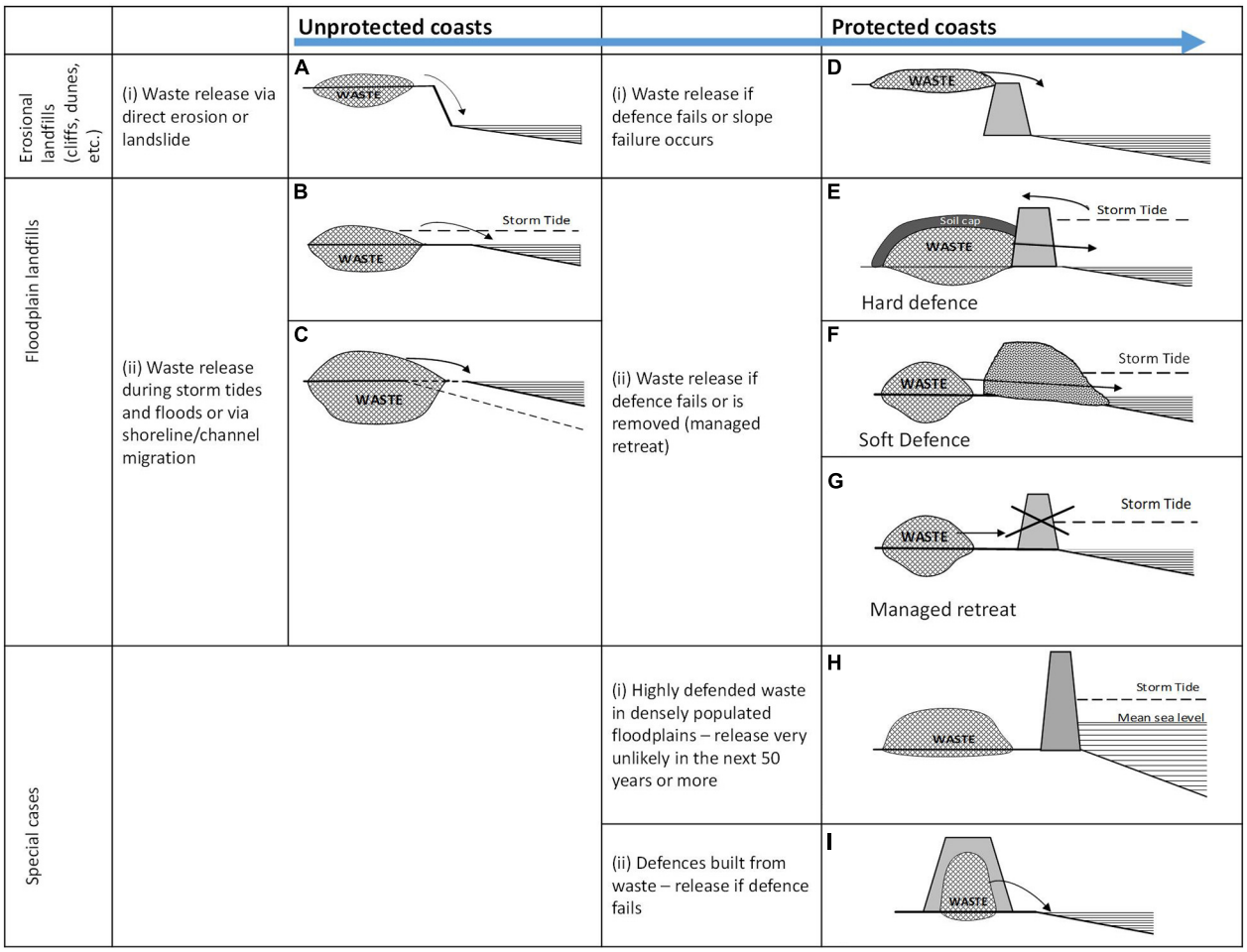

FIGURE 2 | The potential situations recognized in this paper where landfill materials can be released to the sea. The situations labelled **(A)** to **(I)** are described in the text.

The guide identified four main situations where wastes or materials could be released from a landfill by erosion or sea flooding (Beaven et al., 2020). Here we expand these to nine situations (A to I) that are broadly applicable across all the case studies considered in the paper. These include the geomorphological setting where the landfill is located and resulting hazards of concern – erosion and/or flooding – and also the presence or absence of coastal protection – undefended versus defended landfill sites (**Figure 2**). It also recognizes two special cases (H and I) that are relevant to the overall discussion of coastal landfills and waste release. The typology emphasizes the importance of coastal protection on future outcomes, whether the defense is built specifically to protect the waste or not.

Explaining **Figure 2** in detail, situations A and D occur on erosional coasts where flooding is not a consideration and landfills are situated, for example, on cliffs or in sand dunes. Here, waste can be released by episodic (e.g., individual storms) or chronic erosion. In general, SLR will exacerbate erosion although this is a complex process (e.g., for dunes, de Winter and Ruessink, 2017; for beaches Ranasinghe, 2016; Toimil et al., 2020; for cliffs, Walkden and Dickson, 2008). Landfill is also found widely in coastal floodplains. On undefended coasts (situation B and C), waste can be eroded during episodic events linked to extreme flood events and high tides. Waste release will be more of an issue under ongoing erosion as the shoreline and/or associated channels progressively migrate landward, a process which will be increased by SLR. On coasts with hard defenses, landfill releases depend on the nature and integrity of the defenses. Wastes defended by engineered structures (situation E) can be released by extreme events exceeding (or over-topping) the defenses, defense deterioration, or event-induced structure failure (ranging from minor exposure of waste to complete failure of large sea wall sections). Soft defenses, whether natural or artificial (e.g., beach nourishment), can stop or retard waste release (situation F) although they may still be subject to event-induced failure. The duration of release in these cases will depend on the management response. Deliberate defense abandonment (managed retreat) or removal of structures (situation G) is being actively debated and considered in many locations (Nicholls et al., 2013; CCC, 2018;

Siders et al., 2019), although the presence of waste sites often constrains decisions about how best to manage the coast given SLR and in some situations, new defenses are planned to defend waste at sites where otherwise retreat might be preferred (Wadey et al., 2019; Beaven et al., 2020). Two special cases are identified. Many coastal landfills around major urban areas (e.g., London, Netherlands, German North Sea Coast) are protected to such a high standard that landfill erosion is unlikely in the next few decades (situation H). The legacy of this waste will persist into the future as sea levels continue rising and, to avoid release, protection will be needed forever. There are also cases where coastal defenses themselves contain waste, so defense failure will release waste material (situation I) as is the case on the Thames estuary (Brand and Spencer, 2020).

This typology is used to compare the different sites across our case studies, including considering risks, long-term management options and their implications.

LANDFILLING WITHIN THE EUROPEAN UNION

Landfills in member states of the EU (which included England and the United Kingdom prior to January 2020) have been subject to the same European Directives that harmonize the regulation, financing, and certain design and operating requirements of landfill. Important Directives include the Waste Framework Directive, which originated in 1975 (EEC, 1975; latest amendment in 2006), and the Landfill Directive of 1999 [as amended in 2018 (EU, 2018)]. The Waste Framework Directive required the consistent regulation of waste disposal across member states, and the use of permits to ensure that waste disposal does not endanger health or harm the environment. Important provisions of the Landfill Directive control the type of wastes suitable for different classes of landfill, stipulate some minimum landfill engineering and technical requirements, and introduced the concept of landfill aftercare during which the operator of the landfill remains responsible for the contents of the site for however, long the site could pose a hazard. The reliance on landfill as a disposal route for wastes in Europe has decreased since the implementation of the Waste Framework Directive and, especially since the 1990s, a major emphasis on waste prevention, recycling, and processing of waste using alternative waste treatment technologies. Many countries have used landfill tax to reduce landfill use (e.g., Scharff, 2014). The landfill tax charge varies considerably across member states, but often now represents the largest component of cost for the disposal of waste in landfill. These policies, together with the change in the nature of wastes produced by society, mean that the composition of waste in landfills has changed over time.

European Directives are implemented through national legislation, which has obviously differed between member states. However, in broad terms landfills across Europe fall into two distinct categories:

(1) Landfills that closed prior to 1996, especially those prior to 1975, which will generally no longer have a permit and are usually referred to as legacy landfills. These are likely to make up the vast majority of the estimated 350,000+ landfills (Hogland et al., 2011). Most of these historical or legacy landfills have no leachate or gas management, or impermeable liners and there is evidence that during historical waste decomposition leachate has been released to the surrounding sub-surface environment where natural attenuation has resulted in localized 'hot spots' of sediment contamination (Njue et al., 2012; O'Shea et al., 2018).

(2) Post-Landfill Directive sites that have been constructed to high engineering standards, and will have permits to allow for ongoing long-term regulation. Landfill Directive sites are generally larger than legacy sites.

AN ENGLISH PERSPECTIVE ON COASTAL LANDFILLS

There are approximately 20,000 legacy or historical landfills in England. Around 1,200 historical landfills in England are located in coastal settings within the tidal flood zone (0.5% annual probability of coastal flooding) with many clustered around estuaries, large cities and industrial centers (Brand et al., 2018). They have a strong association with designated and environmentally sensitive areas because these areas were once considered low value land and hence suitable for waste disposal. Approximately 3,400 ha of landfill is at risk of flooding (0.1% probability or greater) (CCC, 2018). Many of these historical landfill sites are defended and in south east England there are a number of waste-filled coastal defenses such as along parts of the Thames estuary (Situation I, **Figure 2**).

Wadey et al. (2019) analyzed in detail the Central English Channel Coast (Lyme Regis to Worthing, **Figure 1**), a region where there is a concentration of coastal landfill sites which contain a mixture of waste types. By intersecting flood and erosion hazard data with historical landfill locations, they identified 144 historical coastal landfills covering 22 km^2 and occupying 86 km of shoreline length. About 89 sites are considered at risk of coastal erosion today (i.e., the landfill intersects with the present shoreline), while 136 landfills are in the coastal floodplain. As sea levels rise and the shoreline retreats, these sites are increasingly at risk of leakage, along with new sites further inland. Most landfills are in relatively low energy sites, mainly estuaries, with less than a quarter of landfills at sites exposed to larger waves. The predominant land use for these low energy sites is recreation and open space, with some commercial and/or industrial activity. However, about 6,500 residential properties are located on areas of historical landfill, with 4,400 of these in Portsmouth where substantial new defenses are being built over the next 10 years. The majority of the landfills are located on publicly owned land (local authority) and through Shoreline Management Plans (SMP) have a 'Hold the Line' (HTL) policy (Beaven et al., 2020). This is aspirational, however, as central government funding is not guaranteed unless there are additional benefits, particularly protection of other properties. As a regional illustration of the scale of potential costs involved, removal of all 144 threatened landfills to 'safe' locations is estimated to cost at least £4.3 billion (€4.9 billion; 2019 prices) based on landfill tax, with additional and substantial costs for

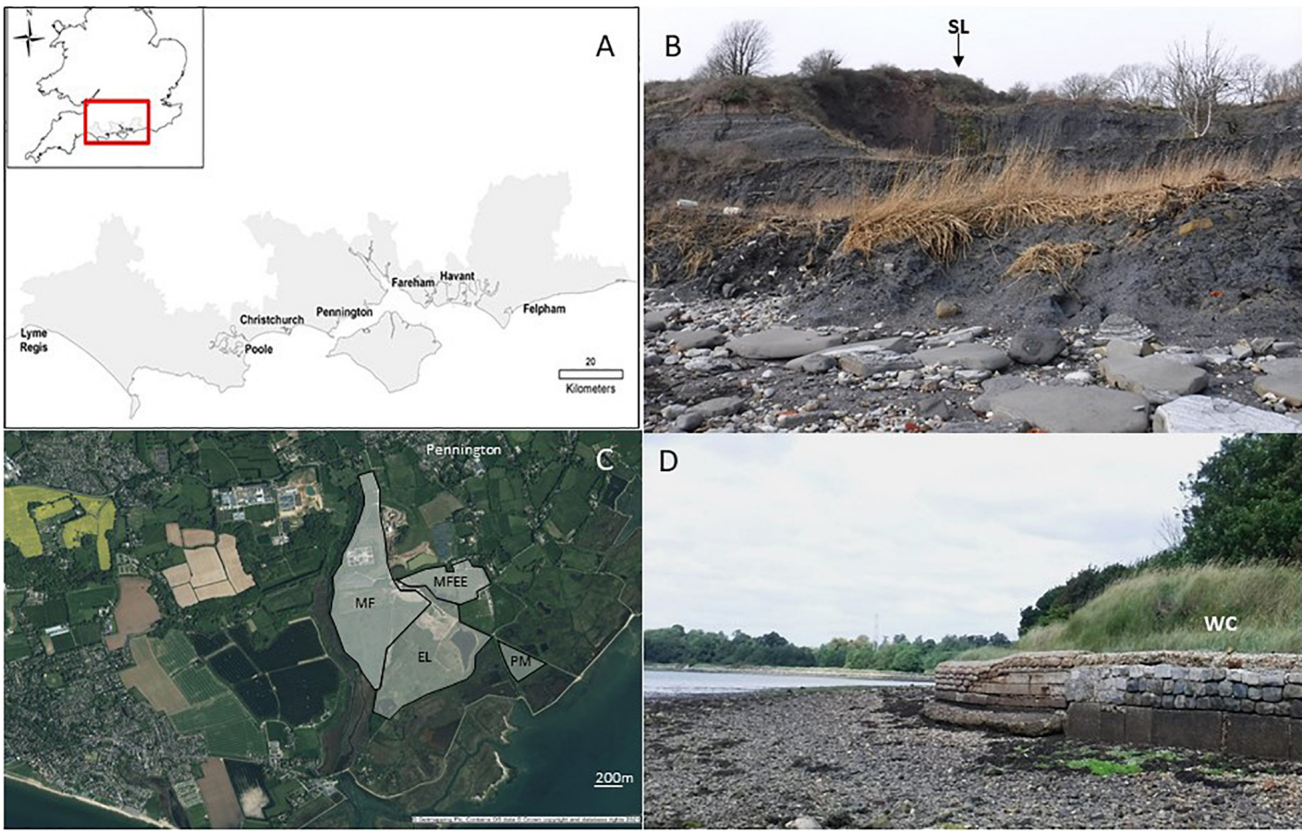

FIGURE 3 | (A) Location of study sites in England, highlighted is the region assessed by Wadey et al. (2019) and the locations of the case study areas referred to in Column 1 of **Table 1**. **(B)** View from the beach below Spittles Lane landfill site (SL), Lyme Regis. **(C)** Aerial photograph showing the location of Pennington Marshes landfill (PM), and the larger more landward landfill complex at Pennington comprising three landfills –EL, Efford Landfill; MF, Manor Farm Landfill; and MFEE, Manor Farm Eastern Extension. © Getmapping Plc. Contains OS data. © Crown copyright and database rights 2021. **(D)** View showing the informal coastal defenses of Wicor Cams landfill (WC) and foreshore, Fareham. Photographs B and D courtesy of Anne Stringfellow.

excavation and transport. Alternatively, to defend the 80 'higher priority' sites which are at risk of flood and coastal erosion over the next 100 years, would cost roughly £150 million (€170 million; 2019 prices), an order of magnitude less than the £1.3 billion (€1.5 billion; 2019 prices) estimate to remove this same waste.

Wadey et al. (2019) also assessed seven locations containing 13 distinct landfill areas in more detail (**Figure 3A** and **Table 1**). The survey underlined the complexity for future management with most landfills being situated behind natural and/or artificial defenses with a desire to continue to protect them, but no certainty of funding being available. Detailed analysis for three of these sites, also drawing on Beaven et al. (2020), illustrate the challenges (**Figure 3**).

The Spittles Lane landfill site at Lyme Regis (**Figure 3B**) is located on a 50 m high eroding cliff top where the cliff is prone to large-scale landslides, weathering, and surface and toe erosion (situation A, **Figure 2**). Average retreat rates are uncertain and in the range 0.3–3 m/year at present (Beaven et al., 2020). In 2008, a 400 m long stretch of cliff collapsed, releasing waste from the landfill to the cliff face and ultimately the beach below. The release of waste raised concerns of potential contamination and pollution. While an assessment found no significant contamination of controlled waters, lead and PAHs were found in the sediments together with fragments of asbestos or asbestos-containing materials which were attributed to the waste. Frequent beach inspections were established due to the risk assessment, and waste materials removed as necessary to prevent harm to beach users. No protection is planned at the site, so it is almost certain that the whole landfill (estimated to be 50,000 tonnes; Nicholls et al., 2018b) will erode into the sea over decades or longer (timescales are highly uncertain). Management options are limited due to the active erosion. Removal of the *in situ* waste and geotechnical stabilization of the site is one approach that could be considered, but these works could destabilize the cliff and increase the risk of further landslides limiting full consideration of the approach. Hence, monitoring and removal of these items at beach level appear to be the only practical steps available to limit harm to beach users. Given the long-term outlook of complete release of the landfill to the marine environment over many decades or longer, this approach will need to be sustained. The potential for adverse public reaction after a major waste release should also be considered.

There are four historical and authorized (permitted) landfills at Pennington to the southwest of Lymington, Hampshire

TABLE 1 | Selected case studies of coastal landfill sites on the central south coast of England [adapted from Wadey et al. (2019) with additional information for Spittles Lane, Pennington and Wicor Cams from Nicholls et al. (2018b) and Beaven et al. (2020)].

Case study area (see Figure 3)	Site name, location (and Situation defined in Figure 2)	Period active	Waste type	Size[1] (Ha)	Current land use	Shoreline length (km)	Coastal Type	Defended (Yes or No)	Current SMP Policy (over 100 years)	Releasing solid waste (Yes or No)
Lyme Regis	Refuse Tip East of Spittles Lane (A)	1910s–1978	Inert, Ind, Com, House	1.6*	Amenity	0.1	Open Coast; Cliff	N	NAI	Y
	Former Gas Holder Site (D)	1993–1994	Inert, Ind, Com, House	0.3	Residential	0.1		Y	HTL	N
Poole	Foreland Road, Turlin Moor, Eastern Lytchett Bay (C, E)	1984–1990	Inert, Ind	17.8	School, recreational	0.8	Sheltered Estuary; Floodplain	N	MR, then HTL	N
	Holes Bay North (E)	1977–1985	Inert, Com, House	45.4	Industrial/ Commercial, transport (road, cycleway)	2.1		Y	HTL	N
	Holes Bay South (E)	1982–1984	Inert							
	Whitecliff-Baiter (E)	1984–1990	Building rubble, House	24.3	Recreational, cycleway	1.8		Y/N	HTL	N
Christchurch	Stanpit Marsh (F)	1938–1981	Inert, Ind, Com, House	19.0	Amenity	1.4	Sheltered Estuary; Floodplain	N (protective marsh)	HTL, then MR, then HTL	N
Pennington	HCC Pennington Marshes Site A (E)	1962–1969	Inert, Ind, Com, House	7.5	Designated grazing marsh/habitat, adjacent to a regulated landfill	8.1	Exposed Estuary; Floodplain	Y	HTL (Currently under review)	N
	Efford (E)	1962–1969		147.2						
	Manor Farm (E)	1989-?								
	Manor Farm Eastern Extension (E)	–								
Fareham	Wicor-Cams I: Cams Bay Tip – Birdwood Grove (B, E)	1942–1993 -	Com, House	22	Recreation	2.5	Sheltered Estuary; Floodplain	Y/N (failing or absent)	HTL	Y (presently limited)
	Wicor-Cams II: Birdwood Grove Tip (B, E)		Inert, Ind							
	Wicor-Cams III: near Wicor Hard Cranleigh Road (B, E)		House							
	Portchester Quay, Land South of Hamilton Road (E)	–	Not known	11.7	Amenity, Industry		Sheltered Estuary; Floodplain	Y (Upgrade under consideration)	HTL	N

(Continued)

TABLE 1 | (Continued)

Case study area (see Figure 3)	Site name, location (and Situation defined in Figure 2)	Period active	Waste type	Size[1] (Ha)	Current land use	Shoreline length (km)	Coastal Type	Defended (Yes or No)	Current SMP Policy (over 100 years)	Releasing solid waste (Yes or No)
Havant	Harts Farm Way 'Broadmarsh'(E)	–	House	36.2	Amenity	1.1	Sheltered Estuary; Floodplain	Y	HTL	N
	Brockhampton (B, E)	–	House	12.2		0.7		N	HTL	? (waste visible)
Felpham	Longbrook (E, F)	1982–1983	Inert	2.5	Private Leisure	0.2	Open Coast; Floodplain	Y	HTL	N

*Ind, Waste Types – Industrial; Com, Commercial; House, Household and Domestic; SMP Policy, Current Shoreline Management Policy; HTL, Hold the Line; NAI, No Active Intervention; MR, Managed Realignment. *, at Spittles lane, 0.2 ha of landfill has been lost due to erosion. [1]A common feature of the analysis for all landfills was the difficulty in obtaining accurate waste depth and volume estimates from historical records.*

(situation E, **Figure 2**). These sites lie on low-lying land (collectively covering some 500 ha) adjacent to important designated habitat and landward of substantial coastal defenses exposed to high energy wave action. The most seaward historical landfill – Pennington Marshes landfill – occupies a triangle of land to the south-east of the main landfill complex (**Figure 3C**). SLR is reducing the level of protection offered by the seawall, while the protective saltmarsh fronting the seawall is also rapidly eroding and has completely disappeared on much of the frontage. The SMP policy is HTL for the next 100 years. To prevent flooding, the seawall will need to be raised and widened. Capital costs were estimated to range from £42 to £97.5 million (€48 to €111 million) under low to extreme high SLR scenarios (up to 1.5 m rise by 2100) (Nicholls et al., 2018b), with additional maintenance costs. Alternative management options include 'Managed Realignment' and the removal of the Pennington Marshes landfill. The former option would allow the sea to access the currently protected zone expanding the intertidal area, although habitat compensation would still be required showing the complexity within these choices. A new seawall could be relocated inland on higher ground, but the main, much larger Pennington landfill complex (**Figure 3C**) would still need to be defended to prevent erosion of waste. The capital cost of this option is reduced by 20–50%. If a 'No Active Intervention' policy was adopted the seawall would eventually breach. Pollution could be mitigated by removing the Pennington Marshes landfill, costing £10 to £21 million (€11 to €24 million), depending on the rate of landfill tax incurred (Nicholls et al., 2018b).

The Wicor Cams landfill complex, Fareham (situation E, **Figures 2**, **3D**) is situated on a low wave energy, estuarine environment adjacent to designated habitat. There are three landfills (**Table 1**); the last closed in 1993, and the site has been restored to recreational open space. The landfills are partly protected by informal coastal defense structures such as concrete sandbags or rock, while some landfill waste is unprotected and visible. The preferred SMP policy is HTL. With SLR, erosion is likely to release landfill without upgrading defenses. Defense costs were estimated to be up to £3 million (€3.4 million), although there are no clear funding avenues to implement the preferred SMP policy. An alternative approach would be to remove the landfill. Cost estimates range from £70 to £140 million (€80 to €160 million) depending on the rate of landfill tax paid, meaning that the removal of waste is not financially viable (Nicholls et al., 2018b).

These national, regional and local assessments of the historical coastal landfill in England indicate that it is, and will continue to be, a major issue which requires significant investment. Currently, there is insufficient funding to either manage these issues using conventional approaches or develop and test innovative management approaches.

A FRENCH PERSPECTIVE ON COASTAL LANDFILLS

About 1,000 French municipalities are located close to the coast, and each of them owns at least one landfill. A first inventory of

old landfills was financed by the French Environment Agency (ADEME) in the 2000s in order to assess the potential risks for ground and surface water, for the environment (e.g., impacts on landscape) and for human security (e.g., potential for landslides, etc.), as well as to assess the need for rehabilitation works. All these sites are in the BASIAS database (Basias-Georisques, 2021), the inventory of old industrial activities in France. Rehabilitation typically consists of preventing infiltration of rainwater by adding impermeable layers, conducting geotechnical works where needed, and landscaping. Hence, the wastes remain *in situ*. However, as in other countries, this national inventory remains incomplete. For example, the exact landfill location is often unknown, which prevents assessment of those located in erosion or flood prone areas. Furthermore, the surface area and/or volume of wastes, and their nature (household, inert, industrial, asbestos, etc.) are often poorly documented.

Coastal erosion and major storm surge events such as Xynthia (2010) (e.g., Lumbroso and Vinet, 2011) have exposed a few historical landfills on the French coast (Ouest France, 2014; La Presse de la Manche, 2020). These extreme events led public authorities to conduct emergency works such as reinforcement and waste containment, and then assess and ultimately rehabilitate the situation. Yet there is no specific consideration of the effects of SLR on coastal landfills over the 21st century and beyond. Adaptation in France is currently limited to informing coastal risk prevention plans with the impacts of a 60 cm SLR scenario by 2100 in order to prevent further urbanization of hazard-prone areas (Le Cozannet et al., 2017). A specific guide for coastal landfill is being prepared by BRGM and the Environment Ministry.

While coastal landfill erosion and flooding is expected to occur at multiple locations in the future, it is also already happening at a few sites. Two case examples are outlined here: (a) La Samaritaine landfill, Lingreville, and (b) Dollemard landfill, Le Havre, both in the Normandy region (**Figure 1**) and reflecting situation A (**Figure 2**). Waste release by chronic erosion, the willingness of the authorities to restore the coastal landscape, and societal pressure for restoration meant that removal of the landfill was the preferred solution in both cases.

La Samaritaine landfill (EPF Normandie, 2018) was located close to the shoreline in sand dunes (**Figure 4**) near the natural harbor of La Venlée in Lingreville municipality on the west coast of the Cherbourg Peninsula. It was a municipal landfill from the 1960s to the 1980s, then decommissioned and buried with sand in the 1990s. The landfill was then forgotten, not even recorded in the national database of landfills, until waste was uncovered due to chronic erosion of about 2 m/year of the sandy shoreline in the 2010s (**Figure 4A**). In November 2016, a storm accelerated the erosion of the waste and a temporary riprap and waste containment were installed in an attempt to prevent further release (**Figure 4B**) (La Presse de la Manche, 2020). To find a permanent solution, the owner of the site, the French Coastal Conservation agency, supervised the removal of 14,000 m^3 of waste mixed with sand from November 2017 to February 2018 (**Figure 4C**) (Ouest France, 2018). In this case, the ultimate aim was to restore the recreational and landscape value of the site, which is classified as Natura-2000. The main rehabilitation work involved sifting the sand for reuse *in situ* (4,000 tonnes; Les Champs Jouault, 2019), conducting a post-excavation diagnosis, sending the wastes to an inland landfill (12,652 tonnes; Les Champs Jouault, 2019) and restoring the site by filling with clean sand. The main difficulties encountered during the rehabilitation were adverse weather conditions, as a winter storm accelerated the erosion and rainfall slowed the sifting of the sand. Furthermore, asbestos was discovered in the waste requiring additional processing. The cost of this rehabilitation work was about €1.6 million, which was funded by public agencies and the administration (EPF Normandie, 2018). This includes the French landfill tax at €35/tonne in 2020.

The Dollemard landfill is part of a set of landfills which have been receiving construction and demolition waste since the 1960s. It is located north of Le Harve on top of 90 m high eroding cliffs composed of chalk and other materials (**Figure 5**). As at Spittles Lane (England), retreat of the cliff top allowed waste to be progressively released to an unstable vegetated slope at the toe of the cliff, which is difficult to access. This unstable slope is eroding at approximately 1–2 m/year, so the waste ultimately reaches the beach/sea. The total amount of waste is estimated to be 200,000 m^3 (SCE, 2012), predominantly comprising inert waste (concrete, stone, brick), mixed with other wastes such as metals (steel bars), plastic and rubber. The volume of plastic and metals migrating from the unstable slope to the beach is estimated at about 30 m^3/year, and this causes visual pollution on the coast, plastic pollution in the sea, as well as risks of injury for walkers (SCE, 2012). These issues were identified in the 1980s, but landfilling of waste continued until 2000 (SCE, 2012). Since 2009, the Le Havre municipality has funded an association to conduct cleaning operations at beach level (1–2 tons/year, €22,000/year). The scenarios available to manage this landfill in the long term include: (1) removal of the landfill, including excavation on the top of the cliff, transportation and treatment of all wastes (as at La Samaritaine), (2) confinement of the wastes with riprap or other coastal defenses, and (3) continue regular manual cleaning along the shoreline over the next 40 years. The costs of the removal action were estimated at €20 million (including landfill tax) over a 10–15 years work span, against €5 million for waste confinement, and €2 million for sustained cleaning. Despite its higher costs, the waste removal option has been chosen (Le Parisien, 2020) funded by the French Environment Agency ADEME (70% of the budget), City Council (20%) and the Water Agency (10%). A demonstration of the feasibility of waste removal and treatment was conducted in 2020 (**Figure 6**). Equipment and personnel reached the site by barge, wastes were removed from the cliff in big-bags by helicopter, transported by truck to a waste treatment center, separated into recyclable waste (mostly metals and inerts) and the residual waste landfilled. This demonstration also provided an improved assessment of waste characteristics.

In both these cases, the total amount and the nature of waste was not precisely known until the landfill began to rapidly erode (around 2 m/year). Funding of the remediation was difficult, especially at La Samaritaine, as no organization was willing to fund the entire costs. There, the 2016 storm and the potential for greater release of waste to the sea

FIGURE 4 | La Samaritaine landfill **(A)** prior to waste removal in 2016, **(B)** during waste excavation (November 2017) with erosion being stopped by riprap and a geotextile, **(C)** the restored site (May 2018). Photography **(A)** courtesy of Ouest-France archives, **(B,C)** courtesy of Geraldine Lebourgeois/La Presse de la Manche.

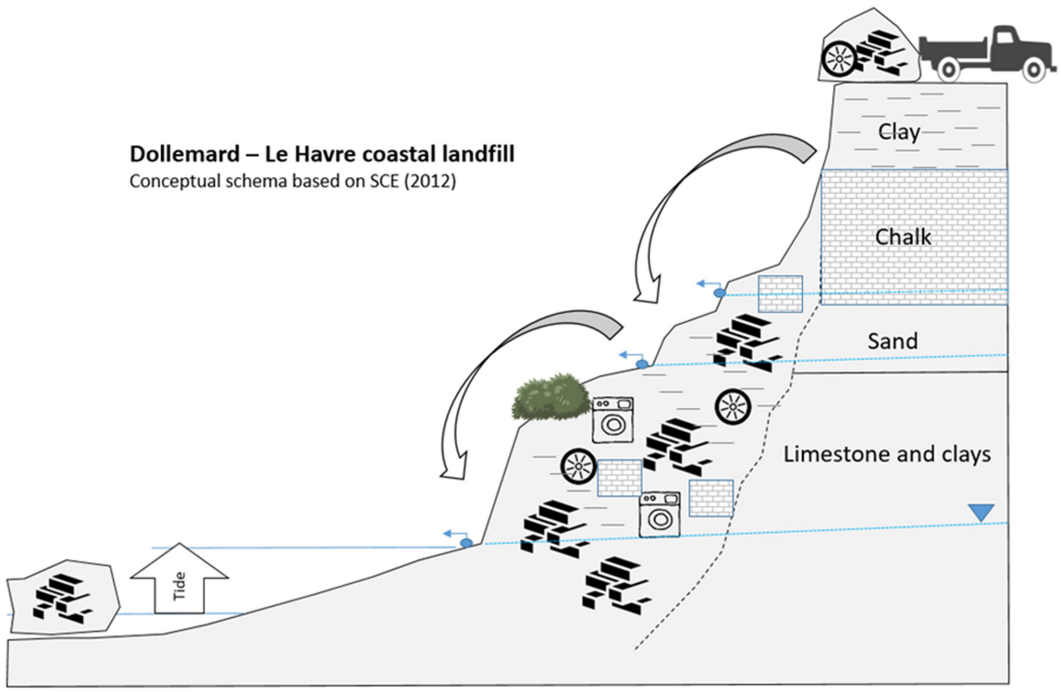

FIGURE 5 | Conceptual cross-section of the Dollemard landfill in Le Havre (France). Adapted from SCE (2012).

was key to stimulating a decision, and the operations were ultimately funded by a partnership of state agencies (Water Agency), the region, the department and the municipalities. Although removal was the selected option for both case studies, removal is not a national policy in France and other options were considered for the Dollemard case. These case studies highlight the need to anticipate better where and when other French coastal landfills might be flooded or eroded as sea level rises, so that more proactive management approaches can be followed.

FIGURE 6 | Trial waste removal at the Dollemard landfill (summer 2020). Photograph courtesy of Le Havre council.

A GERMAN PERSPECTIVE ON COASTAL LANDFILLS

Currently, 1,027 landfills are in active operation in Germany, of which 849 are landfills for excavated soil or inert waste and 213 sites receive hazardous wastes (DESTATIS, 2021). These numbers contrast with the vast legacy of nearly 67,000 inactive (i.e., former) waste disposal sites (LABO, 2018). Germany comprises a federal republic of 16 states, each being responsible for its own waste management. Five federal states (Hamburg, Bremen, Lower-Saxony, Schleswig-Holstein, Mecklenburg-West Pomerania) are potentially affected by coastal flooding, erosion and SLR. There is no systematic assessment on the number or size of active or inactive landfills directly on Germany's coastline and few active landfills are situated near the coast. Further, unlike in England and France, there are no reports of landfill waste being released to the marine environment. The extensive and continuous flood defense systems along the North Sea coast suggest that waste release is unlikely (Sterr, 2008), while on the Baltic coast there is more variability in terms of both geomorphology and presence of coastal defenses (van der Pol et al., 2021). For legacy sites, targeted information on the number close to the coast is also not available; although more information could be harvested from GIS data on location and local topography, which is available for some states. Readily available data, published on the websites of the respective five federal states, report the overall number of landfill sites as:

- Hamburg: No specific data on old waste deposits, but 1,099 confirmed contaminated sites (Hamburg, 2021)
- Bremen: 141 old waste deposits (Bauumwelt Bremen, 2021)
- Lower Saxony: 10,508 old waste deposits (LBEG Niedersachsen, 2021)
- Schleswig-Holstein: 3,023 old waste deposits (Schleswig-Holstein, 2021)
- Mecklenburg-West Pomerania: 2,400 old waste deposits (Regierung MV, 2021).

Note that in Germany the risk of flooding and the effects of erosion on landfills may also arise along rivers where climate change may increase peak flows. In Austria for example, Laner et al. (2009) showed that around 30% of the old waste deposits are located in areas prone to river flooding once every 200 years, indicating the potential scale of the problem.

As an exemplar, we consider the Hanseatic City of Rostock (**Figure 1**), which is one of 294 counties in Germany. With around 200,000 inhabitants and a land area of around 181 km^2, Rostock is the largest city in Mecklenburg-West Pomerania (MV) and is located where the Warnow (the largest river in MV) drains into the Baltic Sea. There are no active landfill sites. However, the inventory of potentially harmful soil changes, contaminated sites, and suspected contaminated sites for Rostock contains more than 3,550 historical sites, including 350 locations where waste and harmful substances have been deposited (e.g., landfills, including illegal sites). The majority of these sites have been assessed and 57 landfills are defined as contaminated, or sites that are still suspected of being contaminated.

We investigated the flood risk for these historical landfills. Landfills potentially flooded in a 200-year event (2.3 m water level; StALU MM, 2012) today are identified considering local topography assuming a simple first-order bathtub method and assuming that the existing coastal defenses are removed. As all the relevant landfills are inside the flood protected areas, they are all presently protected to design level or even higher with heights between 2.8 and 3.0 m. Mean SLR projections by 2100 associated with two Representative Concentration Pathways, RCP4.5 and RCP8.5 emission scenarios (Church et al., 2013), are added linearly to estimate the 200-year return levels by 2100 (2.78 and

3.07 m, respectively) and again potentially flooded landfills are identified using the same assumptions. Today, nine individual sites (16% of the contaminated locations) in Rostock are below the 200-year return water level. Under the RCP4.5 and RCP8.5 scenarios, current design levels are exceeded and the number of potentially affected landfills increases to 26 and 27 sites (64 and 47%), respectively. Assuming defenses continue to be upgraded for SLR, the risks to 2100 still appear low.

More generally, around 70% of the German Baltic Sea coast is affected by erosion, with recession rates of 34 m in 100 years, on average (Gurwell, 2008). All the landfills investigated here are situated at least 300 m inland of the open coast, so erosion is not expected to affect them appreciably over the coming decades. Nonetheless, given the long timescales of landfill waste degradation, more detailed assessments are worthwhile considering sites where release is most likely, as well as exploring the long-term implications for coastal management and defense.

A PERSPECTIVE ON COASTAL WASTE AND LANDFILLS FROM THE NETHERLANDS

The Netherlands is located in the low-lying delta of the Rhine, Meuse and Scheldt rivers which flow into the North Sea (**Figure 1**). The elevation of around half of the Netherlands' surface area does not exceed 1 m above mean sea level and around one third of the country lies below sea level. This region is also the most densely populated area in north-western Europe, home to the megalopolis formed by the county's main cities including Amsterdam and Rotterdam (Dutch: Randstad), and protected from flooding by a system of dike rings (Priemus, 2018). For centuries, land reclamation, continued pumping of water, and heightening of strategic areas have enabled human settlement and economic activities (Van Koningsveld et al., 2008; de Moel et al., 2011).

Next to the rise in mean sea level, threats of flooding induced by climate change include increased storm surges and increased river discharge (Katsman et al., 2011). Effects are aggravated by land subsidence rates of up to 5–8 mm/year (Hoogland et al., 2012). However, intrusion of saltwater, resulting from SLR in combination with lower river discharge during summer, is currently projected to threaten freshwater supplies from ground and surface waters more than direct flooding (Kwadijk et al., 2010). Coastal defenses in the Netherlands include the six key storm surge barriers such as the Eastern Scheldt and the Maeslant Barrier, dikes, flood protection walls, but also the coastal dune belt. Protection against coastal erosion is based on the principle of dynamic preservation of the sediment balance (Van Koningsveld and Mulder, 2004) by adding sand nourishment of the order of 12M m^3 annually. Options for adaptation to SLR in the Netherlands include additional/upgraded storm surge barriers, strengthening of dikes and dams, enhanced sand nourishment, increased pumping, construction of flood-proof buildings, land reclamation, and planned (or managed) retreat (Haasnoot et al., 2020).

A direct result of the dense settlement and the intensive economic activity in the Dutch delta is the multitude of former or legacy landfills, which are defined as landfills that ceased operation before September 1996. The base of most of these sites is located below current sea level and approximately 25% are in direct contact with the groundwater as backfills, for example, of sand or gravel pits. Post-medieval coastal defense structures in the Netherlands usually do not contain waste materials, although the filling of waste into concrete blocks for coastal defense structures has been considered in the recent past (Land+Water en Milieumarkt, 1994). The location of Dutch waste disposal sites therefore mostly corresponds to the situation depicted by **Figure 2**, situation H. A specific legal framework for legacy landfills is missing and competent authorities act on the basis of the Soil Protection Act and provincial environmental regulations. Information on type and volume of landfilled material is not available at a national level as records reside with the provincial or municipal authorities (Lieten, 2018) and, for around 10% of these legacy sites, information on their specific location is missing. In the 1990s, the Dutch government commissioned the NAVOS project (Dutch: Advies Nazorg Voormalige Stortplaatsen, "Advice on aftercare of former landfills"), which carried out a comprehensive inventory of the estimated 4,000–6,000 Dutch legacy sites (Tauw B V, 2016; Lieten, 2018). These sites, of which half are smaller than 0.6 ha, comprise an estimated surface area of 8,000 ha and possess neither bottom nor surface sealing systems. The absence of sealing components effectively means that the waste body has been leached for decades. The objective of the study was to assess the related environmental impacts, regulatory deficiencies and societal problems in order to estimate the scope, organization and financial implications of necessary aftercare or remediation measures. The assessment was based on historical data of waste composition, visual inspection of the cover soil, quality of the groundwater in the sites' vicinity and size of the affected plume based on a limited number of monitoring wells positioned on an assumed principal groundwater flow direction.

With respect to the condition of the landfill cover, it was found that in about 90% of cases the cover did not fulfill the regulatory thickness requirements of the Soil Protection Act. With respect to groundwater, the study concluded that for 75% of the sites the downstream groundwater quality was degraded, restricting its use, for example, for agricultural purposes. However, it was also seen that in some provinces, metal contamination in groundwater was more related to the elevated background geological conditions than to the landfill site. Furthermore, investigations into the natural attenuation potential concluded that in 70% of the cases the contamination was not spreading. Hence, it was judged that those landfills did not pose a significant environmental risk. In the remaining 30% of cases, further monitoring and possibly remediation measures were deemed necessary.

There are approximately 70 modern engineered landfills, with 19 of these sites still in operation (Lieten, 2018). All these landfills are constructed on elevated areas, meeting the distance between the bottom liner and the location-specific highest free groundwater table as required in the European Landfill Directive.

Not all, or not all individual landfill cells, however, are equipped with a combination base liner [high-density polyethylene (HDPE) membrane underlain by a mineral sealing layer].

The Dutch sustainable landfill project (iDS), enabled by a Green Deal between the Dutch competent authorities and Dutch landfill operators, comprises full-scale pilot stabilization projects by aeration and leachate recirculation at three closed landfills (Lammen et al., 2019; Dutch Foundation for Sustainable Landfilling, 2021). This project is at the forefront of international efforts to solve the long-term legacy issues relating to leachate and landfill gas emissions but does not consider the excavation and relocation of solid waste.

Experience with landfill mining in the Netherlands is limited. The projects carried out were motivated by property redevelopment, by gain in landfill capacity and by the need for remediation including installation of a bottom lining system, rather than risks posed by flooding or coastal erosion. However, the main hurdles to economically successful mining projects were found to be contamination with asbestos, availability of effective mining and separation techniques and the need to pay landfill tax for re-disposal of the excavated non-reusable or recyclable wastes (Lieten, 2018).

In view of the large uncertainties related to prediction of SLR, the Netherlands follow the adaptive Delta program 2021 (National Delta Programme, 2020), initiated in 2010 and updated annually, which strives to keep the Netherlands as the 'best protected river delta in the world'. Every 6 years, short- and long-term strategies for coastal and flood defense are reviewed and adapted based on predefined tipping points. The Delta program aims at: (1) protecting the country against flooding, now and in the future; (2) ensuring sufficient freshwater supplies; and (3) climate-proofing the country's spatial planning using the full range of adaptation options. Continued waste and landfill management in compliance with European, national and provincial regulations, are inevitably included in these aims and the corresponding actions, although not explicitly addressed in the Delta program. Therefore, it is not foreseen that SLR will motivate excavation, treatment or re-disposal of wastes in order to minimize environmental impact. This would only be needed if a planned retreat strategy is ultimately implemented triggered by large and rapid rises in sea level (cf. Olsthoorn et al., 2008; Haasnoot et al., 2020). To prepare for such an eventuality, the most obvious step would be to re-visit the assessment of the risk to the groundwater quality emanating from legacy landfills and from modern landfills lacking a bottom liner in light of increased saltwater intrusion. Possibly, the outcome might suggest future investment in surface sealing systems. The country's engineered landfills that are protected by dual-component bottom liners pose no concern in this respect. The clay component in the mineral layer may suffer from dispersion effects due to exchange of polyvalent cations with sodium; the functionality of the second component, the HDPE liner, should however, not be affected by increased groundwater salinity. In the unlikely event of a severe flooding disaster occurring because of failing flood defenses, the contribution of the former landfills in the region to environmental damages will be relatively small compared to those caused by all other anthropogenic contaminant sources.

A FLORIDA PERSPECTIVE ON COASTAL WASTE

Similar to the European examples discussed in the previous sections, thousands of active and inactive landfills are located in coastal counties around the United States, which is where nearly 40% of the population reside (NOAA, 2013). Amongst all 50 states, Florida is often considered most vulnerable to the effects of SLR with several population hotspots like Miami and Tampa/St. Petersburg listed globally in the top 10 among large coastal cities in terms of present and future flood risk (Hallegatte et al., 2013). Therefore, we focus here on Florida, but the general conclusions apply in similar ways to other U.S. coastal regions (as shown for Texas; Kiaghadi et al., 2020).

In addition to a high population density along its coastline, Florida's low-lying topography and geology, comprising porous limestone on top of bedrock, make the state susceptible to flood impacts. High-tide (or nuisance) flooding events already occur regularly in coastal cities like Miami and the number of events and places affected are projected to increase substantially even under moderate SLR scenarios (Sweet et al., 2018). Florida also lies in the paths of tropical cyclones, which can produce dangerous storm surges and waves and associated flooding and beach erosion, as experienced, for example, during Hurricanes Irma (in 2017) and Michael (in 2018).

Design and construction of municipal solid waste and hazardous waste landfills in the U.S. is regulated by Subtitle D and C, respectively, of the Resource Conservation and Recovery Act (RCRA) initially passed in 1989. Subtitle D requires composite liners with a minimum of 61 cm of 10^{-7} cm/s clay underlying a 1.5 mm HDPE membrane. The U.S. Environmental Protection Agency (USEPA) states that "landfills in 100-year floodplains must demonstrate that the unit will not restrict the flow of the 100-year flood, reduce the temporary water storage capacity of the floodplain, or result in washout of solid waste so as to pose a hazard to human health and the environment." However, prior to the RCRA, few if any regulations on landfill location existed. The legacy landfills in coastal areas are therefore of particular concern in terms of being affected by SLR, coastal flooding and erosion.

The Florida Department of Environmental Protection (FDEP) has been delegated by the USEPA to regulate landfills in the state following RCRA Subtitle D. Because of the geological conditions outlined above, the excavation depths for landfills are relatively shallow and they are elevated, instead of below ground. Hence, landfills in Florida are often landmarks and high points in the landscape. The FDEP Solid Waste Facility Locator shows over 10,000 sites in the state, including closed (the vast majority) and active municipal solid waste and construction and demolition debris landfills (95 at present), transfer stations, tire dumps, etc. This also includes disaster debris management sites used as intermediate staging areas in the wake of natural or man-made disasters. Hurricane Irma in 2017, for example, created up to 22M m^3 of debris across the state of Florida, as estimated by the U.S. Army Corps of Engineers (Florida Counties Foundation, 2021). Hurricane Maria in the same year produced 4.7M m^3 of debris (Kennedy and Migaki, 2017) overloading Puerto Rico's existing landfills, so that soccer fields and grounds of closed public schools

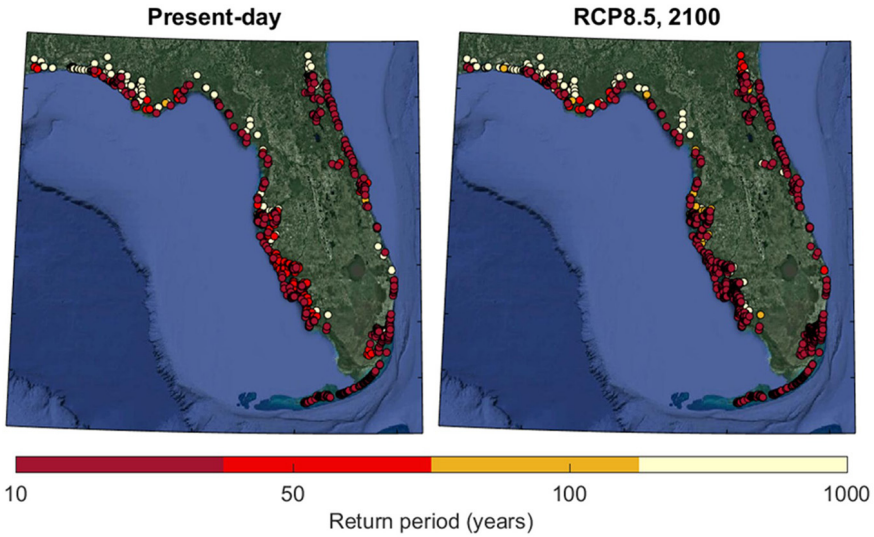

FIGURE 7 | Landfills across Florida located in the floodplain associated with different return periods (see color bar) under present sea level conditions (left) and with future SLR, considering the RCP8.5 scenario (right).

had to be used as interim storage sites; the heavy rain also left many landfills uncovered. These examples highlight that dealing with natural disaster debris is a recurring issue (as outlined in USEPA, 2019) that will escalate as the frequency and magnitude of these events is likely to increase due to SLR and global warming in the case of tropical storms.

In the FDEP database, we identified 8,082 individual locations in terms of latitude and longitude information (sometimes multiple facilities or components are at the same location). Of these, 3,026 are located within the Federal Emergency Management Agency's (FEMA) 100-year flood hazard zone, where the chance of experiencing flooding is at least 1% in any given year; 97 are in the V zone and 2,929 in the A zone. Sites located in the A zone may be affected by inland flooding or coastal flooding (or both), while the V zone is a particular case within the A zone, designating higher risk areas from storm surge flooding and wave impacts, potentially leading to erosion. Focusing only on the 473 sites categorized as Class I, II, or III municipal landfills [classified based on the amount of solid waste received daily, following Florida Administrative Code Rule 62-701.340(3)], 143 are within FEMA's 100-year flood hazard zone (3 in the V zone, 140 in the A zone).

While FEMA's flood zones are derived from extensive hydrodynamic numerical modeling and provide useful information on contemporary flood risk for given exceedance probabilities, the information is often insufficient to identify facilities threatened by flooding (Kiaghadi et al., 2020). Importantly, the effects of SLR are not included and it is also unclear which locations in the A zone are at risk from coastal versus inland flooding. Hence, we used a simple first-order bathtub approach with hydrologic connectivity to identify landfills that are at risk from coastal flooding resulting from extreme storm tides under present conditions and with different SLR scenarios. Note that this approach excludes velocity reduction due to bottom friction and therefore the flood extent could be overestimated. On the other hand, the extreme water level on the coast could be underestimated because wave action is not considered. A digital elevation model (NOAA, 2001) and extreme sea-level information derived with the latest version of the Global Tide and Surge Model (Muis et al., 2020) for the period 1979 to 2017 was used. The extreme sea-level data was bias corrected using tide gauge information and inverse distance weighting as described in Arns et al. (2015). Return periods (RPs) and associated water levels are derived with annual maxima and a Generalized Extreme Value distribution as well as peaks-over-threshold (using the 99th percentile) with a Generalized Pareto Distribution; the root mean squared error between empirical and theoretical distributions is used to select the best approach for a given grid point along the coast. For SLR scenarios, we consider a uniform rise of 0.5 m as a low-end scenario, 0.62 and 0.81 m as the average of the 50th percentile SLR by 2100, derived by Kopp et al. (2014) for the Florida coastline under RCP4.5 and RCP8.5 emissions respectively, and 1.5 m as a high-end scenario.

We estimate that 1,099 landfills are located within the present 100-year coastal flood zone (see **Figure 7**, left); this number increases to 1,642 by 2100 under the RCP8.5 scenario (see **Figure 7**, right) and reaches 2,454 when considering the 1,000 year return level and high-end SLR scenario. The results for a range of different return levels (10-, 50-, 100-, and 1000-years) and the four SLR scenarios are summarized in **Table 2**.

As an indicator for erosion potential, we use the coastal vulnerability index (CVI) (Thieler and Hammar-Klose, 2000). This is preferred over shoreline change rates derived from satellites and/or beach surveys (e.g., Kratzmann et al., 2017; Luijendijk et al., 2018) as it excludes the influence of the regular beach nourishment of Florida beaches (Elko et al., 2021); our goal is to combine information on flood potential with information on erosion potential and compare it with landfill locations. For

TABLE 2 | Number of landfills located in the coastal floodplain associated with different return periods and SLR projections.

SLR scenario (m)	Return period (years)			
	10	50	100	1000
0 (present)	616	1088	1099	1677
0.5 (low-end)	1051	1278	1357	1990
0.62 (RCP4.5)	1217	1440	1536	1997
0.81 (RCP8.5)	1404	1497	1642	2039
1.5 (high-end)	1611	1672	1869	2545

TABLE 3 | Number of landfills located near a coastline with low, moderate, or high coastal vulnerability index (CVI) under water levels associated with different return periods.

RP (years)	Coastal vulnerability index (CVI)		
	Low	Moderate	High
10	24	208	384
50	85	589	414
100	87	592	420
1000	188	875	614

example, of the 1,099 landfills located in the present 100-year coastal flood zone, 87 are located near a coastline with a low CVI, 592 with a moderate CVI, and 420 with a high CVI (**Figure 8**). Results for other return periods and under present-day sea level conditions are summarized in **Table 3**.

These results highlight that landfills along the entire Florida coast are exposed to SLR, especially on the east coast, from Cape Canaveral to the Keys, where a high CVI amplifies the threat of flooding and erosion. **Figures 9A,B** show two examples from South Florida, the South Dade landfill in Miami and Long Key landfill in Monroe County, both located at the water's edge. Another example is Virginia Key off the coast of Miami, where one of the city's biggest parks is being built on an old landfill (**Figure 9C**). The landfill opened in 1960, was closed in 1977 and capped in 1980. The cap has not been maintained and has been eroded by rainfall events to as little as several centimeters thick in places. Now, 60 cm of lime-rock fill, in combination with two pumps and a deep injection well to remove contaminated groundwater, will be installed (Viglucci, 2017). Being built up to 9 m high, the risk for overtopping is relatively low but being located on a barrier island the base of the site is highly exposed to future impacts from SLR, surges and wave impacts. In Key West, the Stock Island landfill (**Figure 9D**) collected waste from 1930 until its closure in 1990 (released from long-term care in 2016), growing to 27 m above sea level and occupying a 7.3 ha parcel (for comparison, the highest natural elevation across the entire Florida Keys is about 6 m). The landfill has passed testing for compliance with federal regulations, but does not have a liner, raising concerns about contamination of the surrounding soil. However, removing the landfill to road level and transporting the waste to other facilities has an estimated cost of $70 to $190 million (€60 to €160 million) and this has not been pursued (Blinckmann, 2018). All examples shown in **Figure 9** can be classified as situations B and C in **Figure 2**.

The results highlight the existing risk of flooding and erosion from storm surges and waves for coastal landfills across Florida, and by implication nationally. This risk will increase as sea level continues to rise and exacerbates beach erosion, which is constantly battled in Florida by recurring beach nourishment in support of the thriving tourism industry which is one of the largest contributors of the state's GDP (Elko et al., 2021). In the long-term, nourishment costs will increase as frequency is increased and sand availability is expected to decline. Ultimately, and without additional adaptation measures being implemented (e.g., building dunes, using sand fences or vegetation as sand traps, providing accommodation space for beach/dune

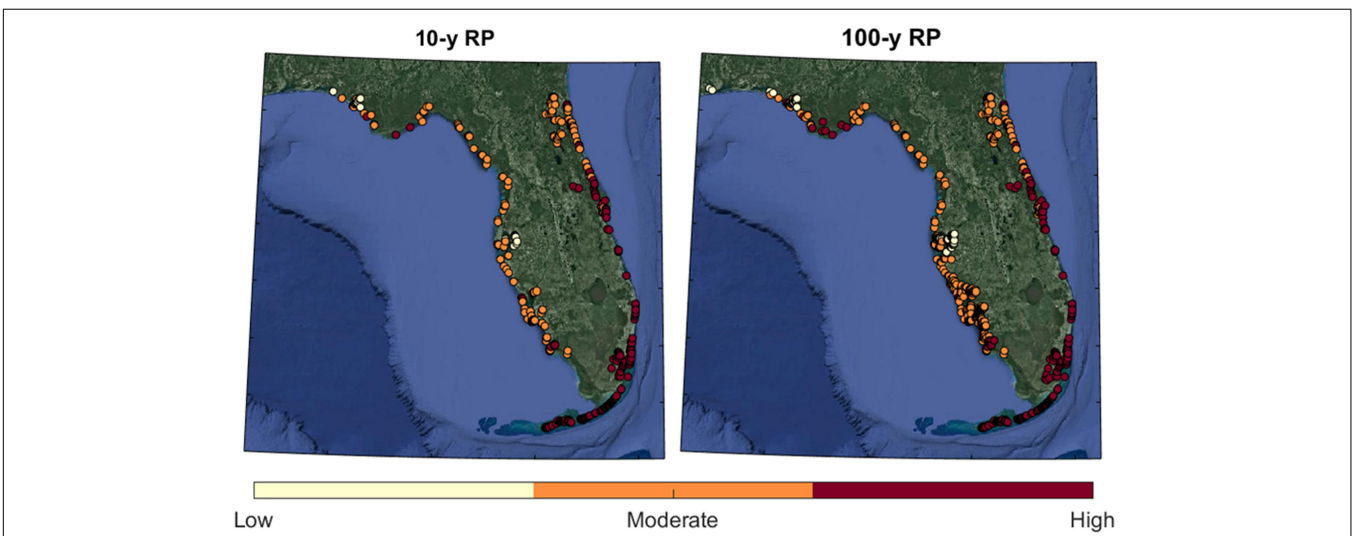

FIGURE 8 | Coastal vulnerability index (CVI) for coastline stretches with landfills located in the 10-year coastal flood plain (left) and 100-year coastal floodplain (right).

FIGURE 9 | Aerial photos of **(A)** the Long Key landfill in Monroe County, FL, next to the Gulf of Mexico, **(B)** the South Dade landfill in Miami, FL, next to Biscayne Bay, **(C)** the Virginia Key landfill in Miami Dade County, FL, between Biscayne Bay and the Atlantic Ocean, and **(D)** the Stock Island landfill in Key West, Monroe County, FL, next to the Gulf of Mexico (source: Google Earth).

migration), this may lead to shoreline retreat exposing some landfills to erosion. As experience of landfill reclamation grows globally (Jones et al., 2013), in the United States (USEPA, 1997) and in Florida (e.g., Jain et al., 2013), new options may arise (see section "Synthesis of the National Case Studies and Management Options for Historical Coastal Landfill"). Overall, the awareness of climate impacts on coastal landfills is increasing in the United States. Citizen concerns have been raised regarding the Key West landfill as discussed, but even in Alaska a report has identified solid waste management sites as vulnerable to flooding and proposed action plans for those of most concern (ADEC, 2015).

SYNTHESIS OF THE NATIONAL CASE STUDIES AND MANAGEMENT OPTIONS FOR HISTORICAL COASTAL LANDFILL

Table 4 summarizes the preceding case studies. This emphasizes the scale of the problem that exists today; there are thousands of coastal landfills that are of concern under present conditions and waste release events are already documented in England, France, and the United States. SLR (and maybe wider climate change) will increase this number, but are certainly not creating them alone. The wide range of situations where landfill releases can occur is apparent, and coastal adaptation choices are critical in future outcomes. For example, the expected abandonment of large lengths of defenses in England over the next century (CCC, 2018) has profound implications for landfill release beyond the magnitude of SLR. Without recognition of the problem, substantial release of waste into the sea would appear inevitable. The long timescale inherent in the management of landfill sites is also apparent, with potential consequences growing over time.

The management responses to these actual and potential landfill problems are wide-ranging and, in many instances untested. Building on earlier experience of Cooper et al. (2013); Nicholls et al. (2018b), Wadey et al. (2019); Beaven et al. (2020), and the results of this paper (see above sections), **Table 5** summarizes available options and current experience. These approaches draw on the source-pathway-receptor model used for controlling pollution risks (Watts, 1998). Beyond '*do nothing*' and simple '*inspection and surveillance,*' several distinct options can be selected over time to manage a coastal landfill, e.g., starting with '*reactively removing released waste*' after a storm, proactively '*remove the source*' of waste, '*break the pathway*' between the source and the receptor, and finally '*remove the receptor.*' While there is much experience of protection (break the pathway), and experience is growing for other options, such as waste relocation in France, or landfill mining in Belgium

TABLE 4 | Synthesis of the case study results.

Location	Number of landfills (to nearest 10^3)		Landfill Situations found (as defined in Figure 2)	Present and future coastal erosion and flood threats to coastal landfill (long-term > 50 years)
	At location	In coastal flood plain today		
England	20,000	1,200 occupying about 3,400 ha	All Situations found, except G, although expected to arise	Some active erosion and immediate threats, with many landfills threatened in the longer term – the long-term growth in these threats links as much to coastal management policy change as the magnitude of SLR – at least before 2100
Lyme Regis to Worthing (England)	Not known	144 threatened by flooding and/or erosion (covering 2,200 ha and 86 km of coast)	Situations A to F found, with Situation E being most common	
France	>14,000 nationally; 1,000 in coastal departments	Not known	Not known, but wide range of Situations possible	Some immediate threats, but poorly characterized nationally, longer term threats are uncertain
Germany (coastal states)	> 14,000 in all five coastal states	Not known	North Sea – mainly Situation H; Baltic – not known, but more variable	Long-term threat on North Sea, on the Baltic potentially more immediate in some areas, but no detailed assessment
Rostock (Germany)	57	9 rising to 27 with SLR of 0.8 m	Situation F and H	Long-term threat
Netherlands	4,000–6,000, occupying 8,000 ha (most are in flood plains)		Mainly Situation H	Long-term threat if current management policies change
Florida	<8,100	1,100 (rising to 1,900 with high end SLR of 1.5 m)	Mainly Situations B, C and F – landfills often form a high point in the landscape.	Some immediate threats, especially during hurricane landfall events, which will increase significantly and rapidly with SLR

TABLE 5 | Summary of potential historical coastal landfill management options from this analysis, using the source-pathway-receptor terminology for pollution risk (see also Cooper et al., 2013; Wadey et al., 2019).

Option	Description	Status	Implications	
Do nothing		Current situation for most historical landfills, mostly reflecting the default situation (rather than a deliberate policy decision) that exists through lack of funding and/or awareness of landfill erosion and flooding risks. Since many sites are situated on relatively stable (i.e., exposed to low energy wave conditions, estuaries, etc.), unmonitored shorelines, any erosion is unnoticed.	Emerging problems not appreciated. Change to another option triggered by unexpected waste release [e.g., Spittles Lane, England (Section "An English Perspective on Coastal Landfills") or La Samaritaine, France, Section "A French Perspective on Coastal Landfills"]. Hence, as a minimum a low level "Inspection and surveillance regime" is recommended – see below.	
Inspection and surveillance (monitoring)	Characterize risk/hazard by sampling and monitoring shoreline change	*Ad hoc* and unsystematic and a risk is that data is not being archived or shared – those responsible for these sites are often cautious about intrusive investigations due to potential legal implications and uncertainty over responsibility.	No standard method so significant uncertainty and inconsistency in how to use the monitoring data. Where waste release occurs in some cases there is an aspiration to follow the precautionary principle i.e., release should be stopped, but in other cases erosion is accepted with no mitigation.	
Reactively remove released waste from foreshore	Regular collection and disposal of waste materials identified as posing a risk	Has been practiced occasionally where eroding landfill is on a dynamic wave-exposed coast [e.g., Spittles Lane (section "An English Perspective on Coastal Landfills"), and as an emergency measure]. Liability issues and motivation often unclear (i.e., whether to avoid pollution to sea or risk to health).	Does not fully prevent waste posing a hazard especially on wave-exposed foreshores where fines and low-density wastes are rapidly dispersed. The landscape value is negatively affected (one of the reasons this option was rejected at Dollemard landfill, France, section "A French Perspective on Coastal Landfills"). Needs sustained funding. Absence of appropriate science hinders evidence-based analysis.	
Remove the source of the risk	Treat the waste	No experience in coastal landfills yet. The concept is to remove the more toxic waste components and leave a residual inert material which is acceptable to release to the environment.	Develops previous landfill mining and recovery experience for this application. A potential research and/demonstration activity to be explored; may be more viable/lower cost than total excavation (below).	
	Excavate/remove	A few examples: La Samaritaine and Dollemard landfills, France (section "A French Perspective on Coastal Landfills"), and Trow Quarry northeast England where partial removal occurred to regrade and stabilize the slope.	High costs due to landfill tax can be a major barrier to this option, especially where high tax rates are charged (e.g., United Kingdom), representing an unintended consequence of landfill tax policy. Finding disposal sites can be problematic, including transport of more hazardous substances increasing uncertainty about costs.	
Break the pathway between the source and the receptor	Erosion defenses (for cliffs, dunes, etc.)	The most commonly observed solution due to well-practiced coast protection methods; although, for example in England (and perhaps elsewhere), this is rarely implemented to protect landfill itself: funding depends on non-landfill benefits. It is unclear if the pathway is completely broken when defenses focus on non-landfill objectives (i.e., consider leachate gas, groundwater migration beneath the defenses, etc.).	Defend and prevent erosion – extensive and widespread experience, but can it be funded and for how long? Restricts sustainable shoreline evolution which may be preferable.	Waste remains *in situ* with uncertain long-term implications
	Flood defenses (for flood plains around estuaries or the open coast)		Defend and prevent flooding and erosion – extensive and widespread experience – only likely to be implemented in more developed areas. Can be expensive, especially when defenses are integrated with drainage solutions.	
	Beach nourishment (soft defenses)		Increasingly applied in all countries considered (e.g., Florida, the Netherlands). However, sediment supply is finite and SLR increases costs of this strategy.	
	Nature-based solutions	Natural defenses protect many landfills today but are widely declining. Artificial saltmarsh restoration via beneficial dredge re-use being investigated (e.g., in Poole Harbour, **Table 1**).	Limited experience and understanding of artificial enhancement – but rapidly developing area of research and practice.	
Remove the receptor to the risk	Move away from the landfill	It is usually not possible to move the coastal/marine environment (receptor) away from a landfill. In the other direction, people have been relocated from inland chemical dumps, but no experience/examples to date with coastal landfill.	With people as receptors this only occurs when health implications become obvious and critical.	

(Winterstetter et al., 2018), many gaps in knowledge are apparent which hinder the full range of these options being applied in an evidence-based manner. The large differences in cost between break the pathway (protect) and waste removal identified in the English case studies are noteworthy and suggest protection would be preferred. However, as the waste needs to be protected in perpetuity, the time dimension also needs to be considered and developing affordable, acceptable and more permanent solutions is essential. The lack of a method to assess the harm from waste release is a major limitation as it hinders the definition of (1) acceptable (if any) flux of release of different types of solid wastes into the marine environment, and (2) potential standards for landfill mining to remove the more hazardous materials. It is also noteworthy that landfill taxes can hinder relocation of waste, which was not part of its original intention: waiving or greatly reducing the tax could facilitate more use of this approach.

DISCUSSION

Based on the case studies discussed here, and the wider assessment of the status of coastal historical landfills, five main issues emerge which resonate with earlier assessments in England (Nicholls et al., 2018b; Wadey et al., 2019). First, the potential scale and implications of waste release to the coastal and marine environment is not sufficiently understood or appreciated. Hence, it remains important to develop a better understanding of the amount, character (biological, physical, and chemical) and potential impact on human health and the environment of waste release from coastal landfill sites for the countries considered and by implication, globally. While some national or regional situations have been assessed, as reviewed here, these are incomplete and have significant gaps. The case studies also highlight the large uncertainties at individual sites and that basic information such as the depth and volume of waste in historical landfills is often missing. A fundamental gap is the lack of methodology and suitable protocols to characterize waste in modern and historical landfills which captures waste heterogeneity and assesses the potential impact of solid wastes release into the marine environment. There is also a need to develop appropriate sampling protocols linked to the outcomes of any new waste characterization review. Landfills are currently being managed without this important information.

Second, there is a need to better address the regulation of solid wastes eroding from coastal landfills. To date, there has been only limited investigation of the hazards associated with the release of these waste materials to the marine environment. Current projections of waste release into the ocean are not compliant with the Sustainable Development Goals (Chen et al., 2020). This raises the following questions: are all such releases unacceptable, or is there an acceptable rate of discharge of certain solid wastes under specific circumstances? How can the limited funding available be used most effectively to manage/address the risk of waste release to the ocean from landfill erosion and flooding?

Third, while flooding and groundwater flushing of coastal landfills can generally be assessed to some degree, there are significant gaps in information and understanding on present and future release of waste due to erosion, including the impact of SLR. To understand this a wide range of factors beyond climate change need to be considered for each landfill site, including: (1) the dominant coastal hazard; (2) the coastal geomorphology/setting; (3) present and future coastal adaptation; (4) adjacent land use, including habitat designations; and (5) the waste and landfill properties (cf. Beaven et al., 2020). While systematic coastal monitoring data are becoming more widely available from national and regional monitoring activities like the Channel Coastal Observatory[1] and satellite-based observations in more data-sparse areas (e.g., Luijendijk et al., 2018), this problem requires more focus on local changes around coastal landfill sites. Small erosional changes can release significant amounts of waste materials as shown in the two French case studies. In addition, there is a need for more analysis of future geomorphic change in the diverse range of settings where coastal waste is found, especially estuarine settings where landfill sites are concentrated. It should be noted that changes in designated coastal habitats are often linked to, and significant for, coastal landfills. This suggests the need for an integrated climate service that takes information on SLR and climate change and other coastal data to translate these changes into threats to all human activities at the coast. In this regard coastal landfills could be seen as part of coastal infrastructure from this climate service perspective. Climate services have mainly focused on either the land, the sea, or climate change, without much focus at the coastal interface. A new core climate service for coastal adaptation to SLR is being developed as part of the European research project CoCliCo. There is a strong focus on flooding and erosion, but downstream services assessing cascading impacts of SLR, such as risks associated with landfills, could be developed as well.

Fourth, there is a need to develop more pragmatic and cost-effective remediation options that facilitate action rather than encouraging 'kicking the can down the road', which would seem to characterize many historical responses. In the case studies, identified problems are generally being ignored, but in the cases where it cannot be ignored, the main solution is to protect or relocate the landfills which are both expensive options. What other options are available (**Table 5**) such as landfill mining to remove the most toxic and unsightly materials and allow the residual more inert materials to erode? The role of landfill taxes in shaping these solutions should also be noted as the high costs attached to moving landfill are having effects that the original proposers did not have in mind. In general, the menu of proactive measures needs to be enhanced and developed.

Lastly, the widespread lack of funding hinders progress across these issues as these costs are not appreciated or considered in national budgets for coastal and environmental management. In highly developed flood-prone areas like the Netherlands, the German North Sea coast and the Thames Estuary in England, high and extensive defenses already protect most landfills so this is less of a consideration today. Elsewhere

[1] https://www.channelcoast.org/

funding is a real concern. In England, whilst HTL is the stated policy around most landfill sites, funding is limited and unless protection of other properties from flood and coastal erosion risk is also a benefit, the proposed policy often cannot be delivered (CCC, 2018; Wadey et al., 2019). This is increasingly recognized in policy circles (Stratton, 2019) and a national steering group has been established to champion these challenges to government in England. In France and the United States, funding is also raised as a challenge. Landfill mining experience in Belgium (Winterstetter et al., 2018) shows that the main benefit is the enhanced land value. However, mining has yet to be explored for coastal landfills (**Table 5**). To ensure long-term safety, dedicated funding is required to assess and proactively manage landfills rather than reacting to crises such as sudden waste release in a stormy year, as illustrated by La Samaritaine landfill, France. The appropriate scale of funding is open to debate.

This paper has focused on the current management challenges. The timescale of leachate release from modern landfills is already well-known as a concern that may last for centuries (Belevi and Baccini, 1989; Laner et al., 2012), and the concept of landfills acting as "final sinks" for wastes on a geological scale has also been recognized (e.g., Brunner, 2013). However, as far as we are aware, this paper is the first to acknowledge the geological scale of the problems that may arise from the release of solid waste to the environment through long-term erosion processes. As SLR will also continue for many centuries even if the Paris Agreement is fully implemented (Nicholls et al., 2018a; Oppenheimer et al., 2019), these problems will persist and worsen far into the future, reinforcing the need for research to improve scientific understanding and policy in this area.

The management measures for coastal landfills (**Table 5**) also need to be set in the wider context of coastal adaptation planning where a variety of strategies are available, including advance, protect, accommodate and planned retreat and growing interest in nature-based approaches (Oppenheimer et al., 2019; Hinkel and Nicholls, 2020). There are strong advocates for large-scale retreat (Siders et al., 2019) and the extent to which this occurs has significant implications for coastal landfill release and management (**Figure 2**). Using a benefit-cost analysis approach, Lincke and Hinkel (2018) conclude that 13% of the world's coast by length is worth protecting against SLR over the 21st century irrespective of the scenario and discount rate uncertainties, while 65% of the world's coast by length is never worth protecting and some form of retreat is likely. In terms of assets, the 13% of coast contains 96% of assets and any protection will therefore benefit many coastal landfill sites (situation H in **Figure 2**). If coastal defenses are deliberately abandoned or fail, large amounts of waste would be released, but as argued from the Netherlands perspective, in this situation other sources of anthropogenic material may dwarf the contribution of the historical landfill sources considered here. Nonetheless, further analysis of the implications of coastal landfill within strategic coastal adaptation planning would be prudent, especially when managed retreat is being considered.

CONCLUSION

Based on this analysis, the potential release of liquid and solid wastes from coastal landfill is an important threat which will worsen with SLR. Improved guidance is required to support risk assessment in relation to the long (geological) timescales of landfill sites, supported where necessary by new research and development activities to provide the required scientific understanding and evidence. This includes improved methods to characterize waste in landfills in terms of the potential impact of different categories of solid waste if released into the coastal and marine environment. The magnitude, transport, and impact of solid wastes need more consideration to develop appropriate assessment methods, including ranking sites for action. There is also a need to understand better the behavior of waste-associated contaminants in historical landfill materials and the likely response to leaching across the range of salinities from fresh to fully ocean conditions. Furthermore, there is a need to better identify both the site characteristics of coastal landfills and the potential costs (over different time frames) of the range of adaptation measures available to avoid adverse impacts.

Where protect (HTL) is the preferred adaptation policy for coastal landfills, the costs and benefits beyond avoided erosion and flood damage need to be considered. This is not arguing for universal defense, but rather asking what are the appropriate resources to plan and implement a response. Funding mechanisms need to be reviewed and coastal societies need to ask what level of current and future funding is appropriate for this issue. It should be noted that where landfill tax has been implemented, this may be a major cost impediment to removing historical landfill material to less vulnerable locations. This was not its original intention. A number of other remediation approaches are possible, but they are at various stages of development and providing a comprehensive menu requires science-based evidence that is not yet available. The cases considered in this paper are drawn from European and U.S. situations, but they are transferable more widely: while the context will vary, the fundamental issues appear generic. In conclusion, managing the legacy of coastal landfills over the next century (and beyond) poses a significant challenge to coastal societies, and our scientific tools to analyze these problems and the policies that are applied require significant enhancement.

AUTHOR CONTRIBUTIONS

RN, RB, and AS conceived the manuscript, produced the overall manuscript framework, discussion and conclusions and together with KS. MW, and SC wrote the England section. DM and GL wrote the French section. TW, DR, VS, and AE wrote the Florida section. JG and TH wrote the Netherlands section. AA wrote the German section. All the authors completed and reviewed the final manuscript.

FUNDING

RN, RB, and AS were supported by the UK's Natural Environment Research Council's (NE/N012909/1). DM was supported by the support policy-makers project from the French Environment Ministry and he also thanks the support of C. Cousin (BRGM). TW acknowledges support by the National Science Foundation (Grant Number 1854896). KS acknowledges support from the Environment Agency and from the UK's Natural Environment Research Council (NE/I018212/1). This publication was supported by PROTECT. RN and GL received funding from the European Union's Horizon 2020 Research and Innovation Program under grant agreement No. 869304, PROTECT contribution number 22.

ACKNOWLEDGMENTS

Susan Hanson is thanked for reviewing an earlier draft of this manuscript.

REFERENCES

ADEC (2015). *Waste Erosion Assessment and Review (WEAR)*. Available online at: https://dec.alaska.gov/eh/solid-waste/wear-project/ (accessed May 12, 2021).

Arns, A., Wahl, T., Haigh, I. D., and Jensen, J. (2015). Determining return water levels at ungauged coastal sites: a case study for northern Germany. *Ocean Dyn.* 65, 539–554. doi: 10.1007/s10236-015-0814-1

Asher, C. (2019). "Climate change and cleanup: a vulnerability assessment and adaptation strategy for Washington State's contaminated sites," in *Proceedings of Coastal Sediments 2019*, (Singapore: World Scientific), 2247–2259.

Bardos, P., Spencer, K. L., Ward, R. D., Maco, B. H., and Cundy, A. B. (2020). Integrated and sustainable management of post-industrial coasts. *Front. Environ. Sci.* 8:86. doi: 10.3389/fenvs.2020.00086

Basias-Georisques (2021). *Inventaire Historique Des Anciens Sites Industriels et Activités de Service*. Available online at: https://www.georisques.gouv.fr/risques/basias/donnees#/ (accessed April 13, 2021).

Bauumwelt Bremen (2021). *Contaminated Sites and Harmful Soil Changes*. Available online at: https://www.bauumwelt.bremen.de/umwelt/boden_und_altlasten/altlasten_und_schaedliche_bodenveraenderungen-24962#abs_804786 (accessed August 8, 2021).

Beaven, R. P., Stringfellow, A. M., Nicholls, R. J., Haigh, I. D., Kebede, A. S., and Watts, J. (2020). Future challenges of coastal landfills exacerbated by sea level rise. *Waste Manag.* 105, 92–101. doi: 10.1016/j.wasman.2020.01.027

Belevi, H., and Baccini, P. (1989). Long-term behavior of municipal solid waste landfills. *Waste Manag. Res.* 7, 43–56. doi: 10.1016/0734-242X(89)90007-4

Bergmann, M., Tekman, M. B., and Gutow, L. (2017). Sea change for plastic pollution. *Nature* 544, 297–297. doi: 10.1038/544297a

Blinckmann, H. (2018). *Key West City Commission Debates Landfill*. Available online at: https://keysweekly.com/42/key-west-city-commission-debates-landfill/ (accessed January 26, 2021).

Brand, J. H., and Spencer, K. L. (2020). Will flooding or erosion of historic landfills result in a significant release of soluble contaminants to the coastal zone? *Sci. Tot. Environ.* 724, 138150. doi: 10.1016/j.scitotenv.2020.138150

Brand, J. H., Spencer, K. L., O'Shea, F. T., and Lindsay, J. E. (2018). Potential pollution risks of historic landfills on low-lying coasts and estuaries. *WIREs Water* 5:e1264. doi: 10.1002/wat2.1264

Brunner, P. H. (2013). Cycles, spirals and linear flows. *Waste Manag. Res.* 31, 1–2. doi: 10.1177/0734242X13501152

CCC (2018). *Managing The Coast in a Changing Climate*. Available online at: https://www.theccc.org.uk/publication/managing-the-coast-in-a-changing-climate/ (accessed May 12, 2021).

Chen, D. M.-C., Bodirsky, B. L., Krueger, T., Mishra, A., and Popp, A. (2020). The world's growing municipal solid waste: trends and impacts. *Environ. Res. Lett.* 15:074021. doi: 10.1088/1748-9326/ab8659

Church, J. A., Clark, P. U., Cazenave, A., Gregory, J. M., Jevrejeva, S., Levermann, A., et al. (2013). "Sea level change," in *Climate Change 2013: The Physical Science Basis. Contribution of Working Group I to the Fifth Assessment Report of the Intergovernmental Panel on Climate Change*, eds T. F. Stocker, D. Qin, G.-K. Plattner, M. Tignor, S. K. Allen, J. Boschung, et al. (Cambridge, MA: Cambridge University Press).

Cooper, N. J., Bower, G., Tyson, R., Flikweert, J. J., Rayner, S., and Hallas, A. (2013). *Guidance on the Management of Landfill Sites and Land Contamination or Eroding or Low-Lying Coastlines*. London: CIRIA.

de Moel, H., Aerts, J. C. J. H., and Koomen, E. (2011). Development of flood exposure in the Netherlands during the 20th and 21st century. *Glob. Environ. Change* 21, 620–627. doi: 10.1016/j.gloenvcha.2010.12.005

de Winter, R. C., and Ruessink, B. G. (2017). Sensitivity analysis of climate change impacts on dune erosion: case study for the Dutch Holland coast. *Clim. Change* 141, 685–701. doi: 10.1007/s10584-017-1922-3

DESTATIS (2021). *Waste Disposal - Number of Landfills and Input*. Wiesbaden: Statistisches Bundesamt.

Dunn, M. E., Mills, M., and Veríssimo, D. (2020). Evaluating the impact of the documentary series Blue Planet II on viewers' plastic consumption behaviors. *Conserv. Sci. Pract.* 2:e280. doi: 10.1111/csp2.280

Dutch Foundation for Sustainable Landfilling (2021). *Introducing Sustainable Landfill programme (iDS)*. Available online at: https://duurzaamstorten.nl/en/#stortbeheer (accessed April 12, 2021).

EEC (1975). *Council directive 75/442/EEC of 15 July 1975 on waste (OJ L 194, 25.7.1975, p.39-41), 75/442/EEC*. Available online at: https://www.eea.europa.eu/policy-documents/council-directive-75-442-eec (accessed May 14, 2021).

Elko, N., Briggs, T. R., Benedet, L., Robertson, Q., Thomson, G., Webb, B. M., et al. (2021). A century of U.S. beach nourishment. *Ocean Coast. Manag.* 199:105406. doi: 10.1016/j.ocecoaman.2020.105406

EPF Normandie (2018). *Fin Des Travaux De Renaturation De L' Ancienne Décharge De "La Samaritaine*. Available online at: https://www.robindesbois.org/wp-content/uploads/decharge-Lingreville-conservatoire-du-Littoral-communique-mai2018.pdf (accessed April 10, 2021).

Eriksen, M., Lebreton, L. C. M., Carson, H. S., Thiel, M., Moore, C. J., Borerro, J. C., et al. (2014). Plastic pollution in the world's oceans: more than 5 trillion plastic pieces weighing over 250,000 Tons Afloat at Sea. *PLoS One* 9:e111913. doi: 10.1371/journal.pone.0111913

EU (2018). *Directive (EU) 2018/850 of the European Parliament and of the Council of 30 May 2018 Amending Directive 1999/31/EC on the Landfill of Waste*. Available online at: https://www.eea.europa.eu/policy-documents/directive-eu-2018-850-amending (accessed May 14, 2021).

EURELCO (2019). *Data Launched on the Landfill Situation in the EU-28*. Available online at: https://eurelco.org/infographic/ (accessed March 23, 2019).

Florida Counties Foundation (2021). *Hurricane Irma - Debris*. Available online at: http://factor.fl-counties.com/hurricane-irma-debris (accessed January 26, 2021).

Grandoni, D., and Dennis, B. (2019). *60% of Superfund Sites Could Be Hit by Climate Change, New Government Report Finds*. Available online at: https://www.washingtonpost.com/climate-environment/2019/11/18/about-percent-superfund-sites-could-be-hit-by-climate-change-new-government-report-finds/ (accessed May 13, 2021).

Gurwell, B. (2008). *Coastal protection along the Baltic Sea coast - MecklenburgVorpommern*. Available online at: https://izw.baw.de/die-kueste/0/k074114.pdf (accessed May 12, 2021).

Haasnoot, M., Kwadijk, J., van Alphen, J., Le Bars, D., van den Hurk, B., Diermanse, F., et al. (2020). Adaptation to uncertain sea-level rise; how uncertainty in Antarctic mass-loss impacts the coastal adaptation strategy of the Netherlands. *Environ. Res. Lett.* 15:034007. doi: 10.1088/1748-9326/ab666c

Hallegatte, S., Green, C., Nicholls, R. J., and Corfee-Morlot, J. (2013). Future flood losses in major coastal cities. *Nat. Clim. Change* 3, 802–806. doi: 10.1038/nclimate1979

Hamburg (2021). *Processing of Contaminated Sites and Surface Recycling: Decades of Industrial Use Have Left Traces in the Soil and Groundwater*. Available online at: https://www.hamburg.de/altlasten/135322/altlasten-allgemein (accessed August 8, 2021).

Hinkel, J., and Nicholls, R. J. (2020). *Responding to Sea Level Rise*. Available online at: https://www.nae.edu/228938/Responding-to-Sea-Level-Rise (accessed May 14, 2021).

Hogland, W., Hogland, M., and Marques, M. (2011). "Enhanced landfill mining: material recovery, energy utilization and economics in the EU (Directive) perspective," in *Proceedings International Academic Symposium on Enhanced Landfill Mining*, Houthalen-Helchteren, 233–247.

Hoogland, T., van den Akker, J. J. H., and Brus, D. J. (2012). Modeling the subsidence of peat soils in the Dutch coastal area. *Geoderma* 171-172, 92–97. doi: 10.1016/j.geoderma.2011.02.013

Jain, P., Townsend, T. G., and Johnson, P. (2013). Case study of landfill reclamation at a Florida landfill site. *Waste Manag.* 33, 109–116. doi: 10.1016/j.wasman.2012.09.011

Jones, P. T., Geysen, D., Tielemans, Y., Van Passel, S., Pontikes, Y., Blanpain, B., et al. (2013). Enhanced landfill mining in view of multiple resource recovery: a critical review. *J. Clean. Product.* 55, 45–55. doi: 10.1016/j.jclepro.2012.05.021

JonoB (2019). *Compromised Landfills at Risk During Extreme Weather. Office of the Prime Minister's Chief Science Advisor*. Available online at: https://www.pmcsa.ac.nz/2019/11/05/compromised-landfills-at-risk-during-extreme-weather/ (accessed May 14, 2021).

Katsman, C. A., Sterl, A., Beersma, J. J., van den Brink, H. W., Church, J. A., Hazeleger, W., et al. (2011). Exploring high-end scenarios for local sea level rise to develop flood protection strategies for a low-lying delta—the Netherlands as an example. *Clim. Change* 109, 617–645. doi: 10.1007/s10584-011-0037-5

Kennedy, M., and Migaki, L. (2017). *After Maria, Puerto Rico Struggles Under the Weight of Its Own Garbage*. Available online at: https://www.npr.org/sections/thetwo-way/2017/12/14/570927809/after-maria-puerto-rico-struggles-under-the-weight-of-its-own-garbage (accessed February 11, 2021).

Kiaghadi, A., Govindarajan, A., Sobel, R. S., and Rifai, H. S. (2020). Environmental damage associated with severe hydrologic events: a LiDAR-based geospatial modeling approach. *Nat. Hazards* 103, 2711–2729. doi: 10.1007/s11069-020-04099-1

Kopp, R. E., Horton, R. M., Little, C. M., Mitrovica, J. X., Oppenheimer, M., Rasmussen, D. J., et al. (2014). Probabilistic 21st and 22nd century sea-level projections at a global network of tide-gauge sites. *Earth's Future* 2, 383–406. doi: 10.1002/2014EF000239

Kratzmann, M. G., Himmelstoss, E. A., and Thieler, E. R. (2017). *National Assessment of Shoreline Change – A GIS Compilation of Updated Vector Shorelines and Associated Shoreline Change Data for the Southeast Atlantic Coast: Data Release*. New York, NY: U.S. Geological Survey.

Kwadijk, J. C. J., Haasnoot, M., Mulder, J. P. M., Hoogvliet, M. M. C., Jeuken, A. B. M., van der Krogt, R. A. A., et al. (2010). Using adaptation tipping points to prepare for climate change and sea level rise: a case study in the Netherlands. *WIREs Clim. Change* 1, 729–740. doi: 10.1002/wcc.64

La Presse de la Manche (2020). *La mer met au Jour Une Ancienne Décharge : Des Travaux Lancés En Urgence Sur Une Plage Du Cotentin*. Available online at: https://actu.fr/normandie/vicq-sur-mer_50142/la-mer-met-jour-une-ancienne-decharge-travaux-lances-urgence-sur-une-plage-cotentin_33303189.html (accessed May 12, 2021).

LABO (2018). *Daten / Informationssysteme. Bund/Länder-Arbeitsgemeinschaft Bodenschutz (LABO)*. Available online at: https://www.labo-deutschland.de/Veroeffentlichungen-Daten-Informationssysteme.html (accessed January 14, 2021).

Lammen, H., Van Zomeren, A., Dijkstra, J. J., and Comans, R. N. J. (2019). "Sustainable landfill management: solid waste sampling and geochemical characterization prior to (an)aerobic stabilization of three old landfills," in *Proceedings of the Seventeenth International Waste Management and Landfill Symposium*, (London: International Waste Working Group).

Land+Water en Milieumarkt (1994). *Storten Over De Eeuwgrens*. London: VNU Business Publications.

Laner, D., Crest, M., Scharff, H., Morris, J. W. F., and Barlaz, M. A. (2012). A review of approaches for the long-term management of municipal solid waste landfills. *Waste Manag.* 32, 498–512. doi: 10.1016/j.wasman.2011.11.010

Laner, D., Fellner, J., and Brunner, P. H. (2009). Flooding of municipal solid waste landfills–an environmental hazard? *Sci. Tot. Environ.* 407, 3674–3680. doi: 10.1016/j.scitotenv.2009.03.006

LBEG Niedersachsen (2021). *Old deposits. Landesamt fur Bergbau, Energie und Geologie, Niedersachsen, Germany*. Available online at: https://www.lbeg.niedersachsen.de/boden_grundwasser/altlasten/altablagerungen/altablagerungen-927.html (accessed August 8, 2021).

Le Cozannet, G., Nicholls, R. J., Hinkel, J., Sweet, W. V., McInnes, K. L., Van de Wal, R. S. W., et al. (2017). Sea level change and coastal climate services: the way forward. *J. Mar. Sci. Eng.* 5:49. doi: 10.3390/jmse5040049

Le Parisien (2020). *Au Havre, Premiers Tests Pour Nettoyer la Décharge de Dollemard*. Available online at: https://www.leparisien.fr/environnement/au-havre-premiers-tests-pour-nettoyer-la-decharge-de-dollemard-26-08-2020-8373354.php (accessed May 12, 2021).

Les Champs Jouault (2019). *Installation de Stockage de Déchets Ultimes Non Dangereux en mode Bioréacteur CUVES (50)*. Rapport annuel d'exploitation 2018. Available online at: https://www.manche.gouv.fr/content/download/48163/336961/file/Rapport%202020_ISDUND%20Bioreacteur%20-%20SAS%20Les%20Champs%20Jouault.pdf (accessed May 12, 2021).

Lieten, S. H. (2018). *Landfill management in the Netherlands. Witteveen+Bos Raadgevende ingenieurs B.V*. Available online at: https://www.interregeurope.eu/fileadmin/user_upload/tx_tevprojects/library/file_1534506068.pdf (accessed May 12, 2021).

Lincke, D., and Hinkel, J. (2018). Economically robust protection against 21st century sea-level rise. *Glob. Environ. Change* 51, 67–73. doi: 10.1016/j.gloenvcha.2018.05.003

Luijendijk, A., Hagenaars, G., Ranasinghe, R., Baart, F., Donchyts, G., and Aarninkhof, S. (2018). The state of the world's beaches. *Sci. Rep.* 8:6641. doi: 10.1038/s41598-018-24630-6

Lumbroso, D. M., and Vinet, F. (2011). A comparison of the causes, effects and aftermaths of the coastal flooding of England in 1953 and France in 2010. *Nat. Hazards Earth Syst. Sci.* 11, 2321–2333. doi: 10.5194/nhess-11-2321-2011

Muis, S., Apecechea, M. I., Dullaart, J., de Lima Rego, J., Madsen, K. S., Su, J., et al. (2020). A high-resolution global dataset of extreme sea levels, tides, and storm surges, including future projections. *Front. Mar. Sci.* 7:263. doi: 10.3389/fmars.2020.00263

National Delta Programme (2020). *Delta Programme 2021*. Available online at: https://english.deltaprogramma.nl/ (accessed May 14, 2021).

Nicholls, R. J., Beaven, R., Stringfellow, A., Spencer, K. L., Tarrant, O., and Cope, S. (2020). "Coastal landfills, rising sea levels and shoreline management: a challenge for the 21st century," in *Coastal Management 2019*, eds N. Hardiman and T. Ice (London: Insitution of Civil Engineers), 391–404.

Nicholls, R. J., Brown, S., Goodwin, P., Wahl, T., Lowe, J., Solan, M., et al. (2018a). Stabilization of global temperature at 1.5°C and 2.0°C: implications for coastal areas. *Philos. Trans. R. Soc. A Math. Phys. Eng. Sci.* 376:20160448. doi: 10.1098/rsta.2016.0448

Nicholls, R. J., Stringfellow, A., and Beaven, R. P. (2018b). *Guidance on the Management of Landfill Sites and Land Contamination Or Eroding or Low-Lying Coastlines - Supplementary Guide*. London: CIRIA.

Nicholls, R. J., Townend, I. H., Bradbury, A. P., Ramsbottom, D., and Day, S. A. (2013). Planning for long-term coastal change: experiences from England and Wales. *Ocean Eng.* 71, 3–16. doi: 10.1016/j.oceaneng.2013.01.025

Njue, C. N., Cundy, A. B., Smith, M., Green, I. D., and Tomlinson, N. (2012). Assessing the impact of historical coastal landfill sites on sensitive ecosystems: a case study from Dorset, Southern England. *Estuar. Coast. Shelf Sci.* 114, 166–174. doi: 10.1016/j.ecss.2012.08.022

NOAA (2001). *U.S. Coastal Relief Model Vol.3 - Florida and East Gulf of Mexico*. National Geophysical Data Center.

NOAA (2013). *Population trends from 1970 to 2020, National Coastal Population Report*. Available online at: https://coast.noaa.gov/digitalcoast/training/population-report.html (accessed January 26, 2021).

Olsthoorn, X., van der Werff, P., Bouwer, L. M., and Huitema, D. (2008). Neo-Atlantis: the Netherlands under a 5-m sea level rise. *Clim. Change* 91, 103–122. doi: 10.1007/s10584-008-9423-z

Oppenheimer, M., Glavovic, B., Hinkel, J., van der Wal, R., Magnan, A. K., Abd-Elgawad, A., et al. (2019). *Sea Level Rise and Implications for Low Lying Islands, Coasts and Communities*. Available online at: https://www.ipcc.ch/srocc/home/ (accessed May 12, 2021).

O'Shea, F. T., Cundy, A. B., and Spencer, K. L. (2018). The contaminant legacy from historic coastal landfills and their potential as sources of diffuse pollution. *Mar. Pollut. Bull.* 128, 446–455. doi: 10.1016/j.marpolbul.2017.12.047

Ouest France (2014). *Après la Tempête, à La Torche on Trouve De Tout*. Available online at: https://www.ouest-france.fr/bretagne/apres-la-tempete-la-torche-trouve-de-tout-1844585 (accessed May 12, 2021).

Ouest France (2018). *Lingreville. La Décharge Sauvage de la Samaritaine, C'est Du Passé*. Available online at: https://www.ouest-france.fr/normandie/manche/lingreville-la-decharge-sauvage-de-la-samaritaine-c-est-du-passe-5762681 (accessed May 12, 2021).

Pope, N. D., O'Hara, S. C. M., Imamura, M., Hutchinson, T. H., and Langston, W. J. (2011). Influence of a collapsed coastal landfill on metal levels in sediments and biota—a portent for the future? *J. Environ. Monit.* 13, 1961–1974. doi: 10.1039/C0EM00741B

Priemus, H. (2018). How housing, infrastructure and water determined the spatial structure of the Randstad. *Eur. Plan. Stud.* 26, 546–570. doi: 10.1080/09654313.2017.1402867

Propp, V. R., De Silva, A. O., Spencer, C., Brown, S. J., Catingan, S. D., Smith, J. E., et al. (2021). Organic contaminants of emerging concern in leachate of historic municipal landfills. *Environ. Pollut.* 276:116474. doi: 10.1016/j.envpol.2021.116474

Ranasinghe, R. (2016). Assessing climate change impacts on open sandy coasts: a review. *Earth Sci. Rev.* 160, 320–332. doi: 10.1016/j.earscirev.2016.07.011

Regierung MV (2021). *Contaminated Sites Situation in MV. Mecklenberg-Vorpommern Ministerium fur Landwirtschaft und Umwelt*. Available online at: https://www.regierung-mv.de/Landesregierung/lm/Umwelt/Boden/Altlastenbearbeitung/Altlastensituation-in-MV (accessed August 8, 2021).

SCE (2012). *Diagnostic Environnemental et Propositions de Solutions de Gestion des Décharges de Dollemard*. Available online at: https://www.lehavre.fr/sites/default/files/atoms/files/diagnostic_environnemental_et_propositions_de_solutions_de_gestion_des_decharges_de_dollemard_-_tranche_conditionnelle_definition_de_solutions_doptimisation_de_gestion.pdf (accessed April 12, 2021).

Scharff, H. (2014). Landfill reduction experience in The Netherlands. *Waste Manag.* 34, 2218–2224. doi: 10.1016/j.wasman.2014.05.019

Schleswig-Holstein (2021). *Legacy: Contaminated Sites. Schleswig-Holstein*. Available online at: https://www.schleswig-holstein.de/DE/Fachinhalte/G/grundwasser/gefaehrdungspotenzialeAltlasten.html (accessed August 8, 2021).

Siders, A. R., Hino, M., and Mach, K. J. (2019). The case for strategic and managed climate retreat. *Science* 365:761. doi: 10.1126/science.aax8346

StALU MM (2012). *Coastal Protection Regulations Mecklenburg-Western Pomerania. Staatliches Amt für Landwirtschaft und Umwelt Mittleres Mecklenburg*. Available online at: http://www.stalu-mv.de/mm/Themen/K%C3%BCstenschutz/Regelwerk-K%C3%BCstenschutz-Mecklenburg%E2%80%93Vorpommern/ (accessed August 8, 2021).

Sterr, H. (2008). Assessment of vulnerability and adaptation to sea-level rise for the coastal zone of Germany. *J. Coast. Res.* 24, 380–393.

Stratton, M. (2019). *Historic Coastal Landfill - Time to Clean Up Our Act*. Berlin: Springer.

Sweet, W. V., Dusek, G., Obeysekera, J. T. B., and Marra, J. J. (2018). *Patterns and Projections of High Tide Flooding Along the US Coastline Using A Common Impact Threshold. NOAA Center for Operational Oceanographic Products and Services*. Available online at: https://tidesandcurrents.noaa.gov/publications/techrpt86_PaP_of_HTFlooding.pdf (accessed May 12, 2021).

Tauw B V. (2016). *Advies Nazorg Voormalige Stortplaatsen (NAVOS)*. Netherlands: Rijkswaterstaat.

Thieler, E. R., and Hammar-Klose, E. S. (2000). *National Assessment of Coastal Vulnerability To Sea-Level Rise; Preliminary Results for the US Pacific Coast (Report No. 2000-178)*. Available online at: https://www.usgs.gov/centers/whcmsc/science/national-assessment-coastal-vulnerability-sea-level-rise?qt-science_center_objects=0#qt-science_center_objects (accessed May 12, 2021).

Toimil, A., Camus, P., Losada, I. J., Le Cozannet, G., Nicholls, R. J., Idier, D., et al. (2020). Climate change-driven coastal erosion modelling in temperate sandy beaches: methods and uncertainty treatment. *Earth Sci. Rev.* 202:103110. doi: 10.1016/j.earscirev.2020.103110

USEPA (1997). *Landfill Reclamation*. Washington, DC: US Environmental Protection Agency.

USEPA (2017). *Hurricane Harvey*. Available online at: https://response.epa.gov/site/site_profile.aspx?site_id=12353. (accessed June 12, 2019).

USEPA (2019). *Planning for Natural Disaster Debris*. Available online at: https://www.epa.gov/sites/production/files/2019-04/documents/final_pndd_guidance_0.pdf (accessed May 12, 2021).

van der Pol, T., Hinkel, J., Merkens, J., MacPherson, L., Vafeidis, A. T., Arns, A., et al. (2021). Regional economic analysis of flood defence heights at the German Baltic Sea coast: a multi-method cost-benefit approach for flood prevention. *Clim. Risk Manag.* 32:100289. doi: 10.1016/j.crm.2021.100289

Van Koningsveld, M., and Mulder, J. P. M. (2004). Sustainable coastal policy developments in the Netherlands. A systematic approach revealed. *J. Coast. Res.* 20, 375–385.

Van Koningsveld, M., Mulder, J. P. M., Stive, M. J. F., Van Der Valk, L., and Van Der Weck, A. W. (2008). Living with sea-level rise and climate change: A case study of the Netherlands. *J. Coast. Res.* 24, 367–445.

Viglucci, A. (2017). *Say bye to Virginia Key's toxic old landfill, and hi to Miami's biggest park*. Available online at: https://www.miamiherald.com/news/local/community/miami-dade/article156328394.html (accessed January 26, 2021).

Wadey, M. P., Kermode, T., Cope, S., and Neill, S. (2019). *Landfill Sites at Risk of Flooding and Erosion within the SCOPAC Area. Southern Coastal Group and SCOPAC*. Available online at: https://scopac.org.uk/research/scopac-landfills-study/ (accessed May 12, 2021).

Walkden, M., and Dickson, M. (2008). Equilibrium erosion of soft rock shores with a shallow or absent beach under increased sea level rise. *Mar. Geol.* 251, 75–84. doi: 10.1016/j.margeo.2008.02.003

Watts, R. J. (1998). *Hazardous Wastes : Sources, Pathways, Receptors*. New York, NY: J. Wiley.

Wille, E. (2018). "Flooding risks at old landfill sites: linear economy meets climate change," in *Proceedings of the 4th International Symposium on Enhanced Landfill Mining*, New York, NY, 361–365.

Winterstetter, A., Wille, E., Nagels, P., and Fellner, J. (2018). Decision making guidelines for mining historic landfill sites in Flanders. *Waste Manag.* 77, 225–237. doi: 10.1016/j.wasman.2018.03.049

Zalasiewicz, J., Waters, C. N., Ivar, do Sul, J. A., Corcoran, P. L., Barnosky, A. D., et al. (2016). The geological cycle of plastics and their use as a stratigraphic indicator of the Anthropocene. *Anthropocene* 13, 4–17. doi: 10.1016/j.ancene.2016.01.002

Conflict of Interest: The authors declare that the research was conducted in the absence of any commercial or financial relationships that could be construed as a potential conflict of interest.

Publisher's Note: All claims expressed in this article are solely those of the authors and do not necessarily represent those of their affiliated organizations, or those of the publisher, the editors and the reviewers. Any product that may be evaluated in this article, or claim that may be made by its manufacturer, is not guaranteed or endorsed by the publisher.

Copyright © 2021 Nicholls, Beaven, Stringfellow, Monfort, Le Cozannet, Wahl, Gebert, Wadey, Arns, Spencer, Reinhart, Heimovaara, Santos, Enríquez and Cope. This is an open-access article distributed under the terms of the Creative Commons Attribution License (CC BY). The use, distribution or reproduction in other forums is permitted, provided the original author(s) and the copyright owner(s) are credited and that the original publication in this journal is cited, in accordance with accepted academic practice. No use, distribution or reproduction is permitted which does not comply with these terms.

frontiers in Marine Science

ORIGINAL RESEARCH
published: 18 November 2021
doi: 10.3389/fmars.2021.704721

Copernicus Sea Level Space Observations: A Basis for Assessing Mitigation and Developing Adaptation Strategies to Sea Level Rise

Jean-François Legeais[1], Benoît Meyssignac[2], Yannice Faugère[1], Adrien Guerou[1], Michaël Ablain[3], Marie-Isabelle Pujol[1], Claire Dufau[1] and Gérald Dibarboure[4]*

[1] Collecte Localisation Satellites, Ramonville Saint-Agne, France, [2] LEGOS, CNES, CNRS, UPS, IRD, Université de Toulouse, Toulouse, France, [3] Magellium, Ramonville Saint-Agne, France, [4] CNES, Toulouse, France

It is essential to monitor accurately current sea level changes to better understand and project future sea level rise (SLR). This is the basis to support the design of adaptation strategies to climate change. Altimeter sea level products are operationally produced and distributed by the E.U. Copernicus services dedicated to the marine environment (CMEMS) and climate change (C3S). The present article is a review paper that intends to explain why and to which extent the sea level monitoring indicators derived from these products are appropriate to develop adaptation strategies to SLR. We first present the main key scientific questions and challenges related to SLR monitoring. The different processing steps of the altimeter production system are presented including those ensuring the quality and the stability of the sea level record (starting in 1993). Due to the numerous altimeter algorithms required for the production, it is complex to ensure both the retrieval of high-resolution mesoscale signals and the stability of the large-scale wavelengths. This has led to the operational production of two different sea level datasets whose specificities are characterized. We present the corresponding indicators: the global mean sea level (GMSL) evolution and the regional map of sea level trends, with their respective uncertainties. We discuss how these products and associated indicators support adaptation to SLR, and we illustrate with an example of downstream application. The remaining gaps are analyzed and recommendations for the future are provided.

Keywords: Copernicus, sea level rise (SLR), satellite altimetry, adaptation strategies to climate change, ocean monitoring indicators

OPEN ACCESS

Edited by:
Michael Dylan Sparrow, World Meteorological Organization, Switzerland

Reviewed by:
Giovanni Besio, University of Genoa, Italy
Robert James Nicholls, University of East Anglia, United Kingdom

****Correspondence:***
Jean-François Legeais
jlegeais@groupcls.com

Specialty section:
This article was submitted to Coastal Ocean Processes, a section of the journal Frontiers in Marine Science

Received: *03 May 2021*
Accepted: *19 October 2021*
Published: *18 November 2021*

Citation:
Legeais J-F, Meyssignac B, Faugère Y, Guerou A, Ablain M, Pujol M-I, Dufau C and Dibarboure G (2021) Copernicus Sea Level Space Observations: A Basis for Assessing Mitigation and Developing Adaptation Strategies to Sea Level Rise. Front. Mar. Sci. 8:704721. doi: 10.3389/fmars.2021.704721

INTRODUCTION

Since the mid-nineteenth century, the increasing amount of greenhouse gases stored in the atmosphere has led to an imbalance at the top of the atmosphere between the incoming solar radiation and the outgoing infrared emission of the Earth (with a higher proportion of the former). The Earth system is forced to adapt to this excess of energy that is entering the system, with

various consequences such as decreasing land ice, snow cover and glaciers and increasing ocean temperature, surface temperature and mean sea level rise (SLR), as well as coastal flooding and erosion, with also more extreme events in heat waves, precipitation and sea level. The Global Mean Sea Level (GMSL) rise is a precise indicator of this climate change since most of the energy in excess on the Earth is stored into the ocean and the cryosphere (von Schuckmann et al., 2020) and contributes directly to the SLR through thermal expansion and land ice melt (ice sheets and glaciers). Observing precisely current GMSL rise and understanding the different contributions to this rise (WCRP Global Sea Level Budget Group, 2018) allows to estimate the excess of energy in the climate system (Meyssignac et al., 2019) and the regions where this excess of energy is stored, leading to a better validation of climate models and their simulations of the past and future climate (Meyssignac et al., 2017; Loeb et al., 2018). This is one of the reasons that motivated space agencies to build up a continuous and accurate observing system of the sea level since 1993, with the constellation of satellite altimeters. Another reason that motivated space agencies was to provide the observational basis for the study of regional and coastal impacts of SLR through erosion and flooding (Cazenave and Le Cozannet, 2013) and also of changes in extreme events (Woodworth et al., 2011). In 2014, the sea-level variable was identified as an Essential Climate Variable (ECV, Bojinski et al., 2014) that should be monitored with enough accuracy and stability to report the GMSL variability at monthly to multidecadal time scales. In this context, the role of climate services (and marine services for ocean variables) is to use all information available (including the space data from satellite altimeters) to produce, validate and distribute sea level products that respond to the ECV requirements, and which can be used, in the end, by policy makers and stakeholders to elaborate adaptation and mitigation strategies.

The Copernicus program of the European Union provides Earth Observation information for the benefit of European citizens and consists of different services. The program plays a key role in the production and distribution of the different ECV products. The information delivered by the different Copernicus services include measurements of the sea level evolution on a global and regional scale and also added-value information that contribute to a better understanding of the SLR and to adapt to the associated impacts. The global strategy of the Copernicus program related to adaptation to sea level rise is presented in a dedicated article in this special issue (Melet et al., 2021).

Among the different services, the Copernicus Climate Change Service (C3S) and Copernicus Marine Environment Monitoring Service (CMEMS) provide a wide range of information related to the Earth system based on satellite measurements, *in situ* observations, model reanalyses and climate projections. The sea level evolution is one piece of this information. Within the CMEMS and C3S Copernicus services, the objectives of the production center in charge of the sea level satellite ECV product are to fit to the target requirements as described by the Global Climate Observing System (GCOS), to provide a high level of maturity of datasets and metadata and to answer the users needs (Copernicus users, meteo and climate organizations, data assimilation, research, climate model projections among others).

International cooperation has been at the origin of satellite altimetry with the joint effort of the NOAA and CNES French space agency together with the European Space Agency (ESA), leading to a 28-year long sea level time series starting in 1993 with the launch of the TOPEX-Poseidon mission and 14 other altimetry missions since then (see **Figure 1**). In Europe, the CNES/CLS DUACS (Data Unification and Altimeter Combination System) production system has processed the altimeter sea level measurements of the different missions since 2001[1] to provide multi-mission gridded sea surface heights and derived variables. The altimeter products have been distributed since 2003 through the AVISO CNES Satellite Altimetry Data portal.[2] Since 2015, the whole processing, operational production and distribution of the DUACS along-track (Level 3, L3) and gridded (Level 4, L4) altimeter sea level products have been taken over by the European Copernicus Programme (with the support of EUMETSAT, ESA and CNES for the Sentinel missions). The AVISO portal still includes ocean monitoring indicators (such as the GMSL evolution), added value and pre-operational research products.[3] In the current context of the Copernicus sea level data production, EUMETSAT is in charge of the production and distribution of the altimeter observations of the European Sentinel missions and CNES and ESA are responsible for the other altimeter missions in collaboration with NASA/NOAA as well as the Indian and Chinese space agencies for some of the missions (see **Figure 1**).

These observational products build on the validated Level 2 Plus (L2P) altimeter datasets produced in-house by the different space agencies. They are also maintained up-to-date and at the highest level of quality thanks to the R&D activities funded by CNES and ESA. **Figure 1** illustrates that a large number of new missions are expected to be included in the altimeter constellation during the next decade and they will contribute to ensure the long-term monitoring of sea level evolution.

The present paper is a review paper that intends to describe all the activities required to ensure the quality of the satellite-based sea level products developed by Copernicus services and to explain why and to which extent these products are appropriate to face the challenge of understanding and adapting to SLR. The paper does not aim at explaining the full methodology related to the sea level production system since the details are provided online with the datasets, together with the user manuals and the validation procedures. The interested readers are invited to access the documentation (see **Table 1**). The paper rather focuses on the presentation of the key processing steps that ensure the quality of the final product. These include the sea surface height computation, the calibration/validation activities, the use of homogeneous and validated along-track (L2P) altimeter standards from all missions, the role of the reference missions to ensure stability and the production of cross calibrated multi-mission L3 and gridded gap-free L4

[1] duacs.cls.fr

[2] www.aviso.altimetry.fr/en

[3] www.aviso.altimetry.fr/en/data/products

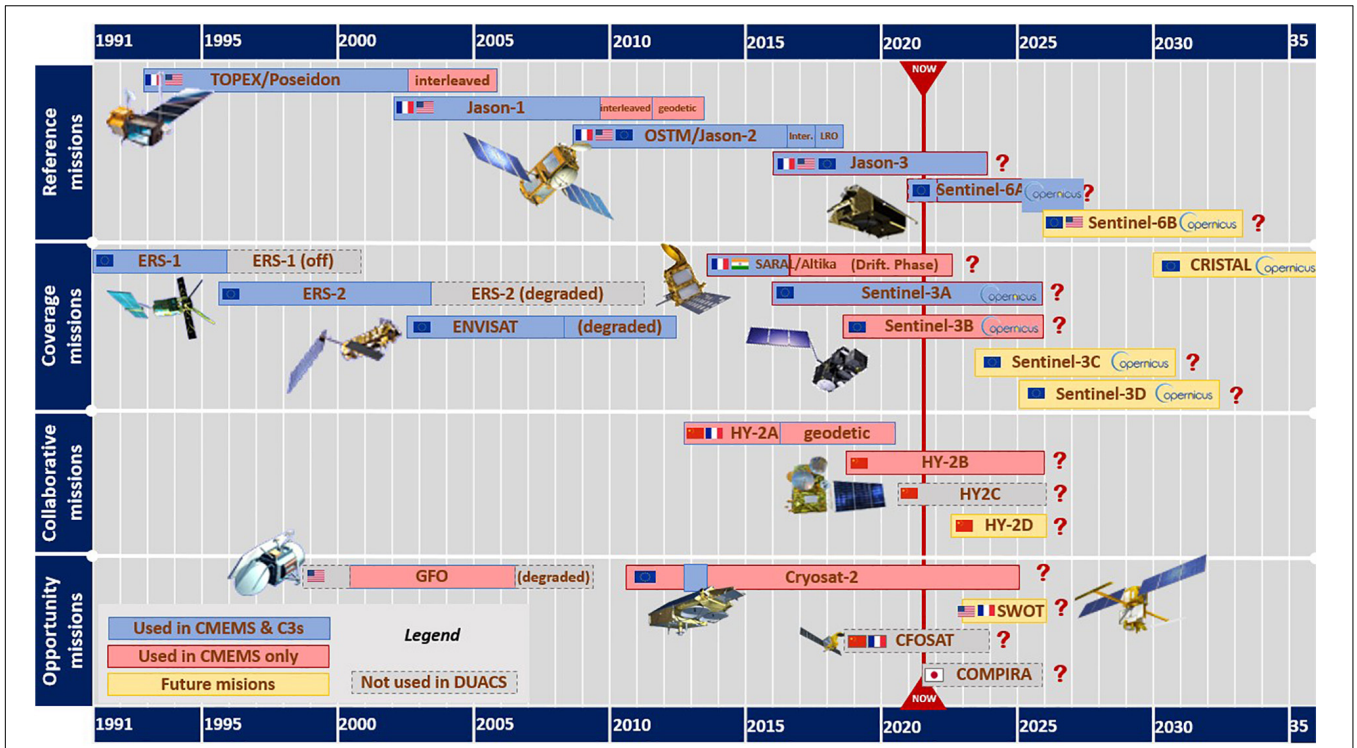

FIGURE 1 | Timeline of modern radar altimetry missions. Reference missions are used to ensure the stability of the sea level products and are distinguished from the coverage, collaborative and opportunity missions. The color of the labels of the different missions depends on their use in the different Copernicus altimeter sea level products (see section "Building Ready to Use Altimeter Sea Level Products").

TABLE 1 | Details of the delayed-time altimeter sea level products and their accesses in the Copernicus catalogs.

Altimeter products	Recommended applications	Access to Copernicus catalogs
C3S	Long-term evolutive, climate applications, ocean monitoring indicators	https://cds.climate.copernicus.eu/cdsapp#!/dataset/satellite-sea-level-global?tab=overview https://resources.marine.copernicus.eu/?option=com_csw&view=details&product_id=SEALEVEL_GLO_PHY_CLIMATE_L4_REP_OBSERVATIONS_008_057
CMEMS	Ocean modeling, analyses of the ocean circulation, and mesoscale signals	https://resources.marine.copernicus.eu/?option=com_csw&view=details&product_id=SEALEVEL_GLO_PHY_L4_REP_OBSERVATIONS_008_047

Further information on the user manuals and quality information are available in the respective documentation tabs.

sea level data (presented in section "Building Ready To Use Altimeter Sea Level Products"). All these activities contribute to the quality of the different Copernicus altimeter sea level products distributed to the users. A technical description of these products is provided, and the general maturity of the service is highlighted (section "The Copernicus Altimeter Sea Level Products and Ocean Monitoring Indicators"). These added-value products are then used to determine the mean sea level indicators and derive the sea level trend and acceleration at global and regional scales, which are key information to elaborate adaptation and mitigation strategies. At last, section "Remaining Gaps and Recommendations" provides discussion on the remaining gaps and recommendations related to the altimeter observing system and the associated uncertainties and it includes an illustration of a downstream project that contributes to define adaptation strategies to SLR.

BUILDING READY TO USE ALTIMETER SEA LEVEL PRODUCTS

In the following, we present the main processing steps required to ensure the high quality of the altimeter sea level products distributed to the users and especially the ones that contribute to the MSL stability.

Sea Surface Heights Computation

On the one hand, the raw sea level estimates are derived from the difference between the satellite altitude and the radar altimeter range. The former is derived from the Precise Orbit Determination (POD) which provides the altitude of the satellite above the reference ellipsoïd. The accuracy of this orbit determination directly affects the sea level estimates. The

consolidated POD is made available in delayed-time for the different missions within 90 days in the geophysical data records. The multi-technique solution based on GPS, laser and DORIS techniques contribute to the accuracy of the satellite positioning and of the associated individual sea level estimates, which reaches about 1.5 cm (Escudier et al., 2017). However, at a decadal time scale, the POD errors remain one of the main contributors to the sea-level rise uncertainty at the global scale (e.g., Couhert et al., 2018; Ablain et al., 2019) and at the regional scale (Prandi et al., 2021).

On the second hand, the sea level estimates rely on the L2 ocean retracking of the radar altimeter waveforms, which provides the altimeter range (at the origin of the raw sea surface height), and other altimeter parameters such as the Sigma-0 roughness coefficient and Significant Wave Heights (Chelton et al., 2001). A stable retracking algorithm thus contributes to the stability of the mean sea level. The MLE4 retracking algorithm is the solution used in the Geophysical Data Records distributed to the users for each altimeter mission (Amarouche et al., 2004). The evolution of the instrumental characteristics (given by the mean of its Point Target Response, PTR) is continuously monitored and static Lookup Tables are used to correct range estimates from the differences between a true instrument PTR and the Gaussian approximation. The drift of the PTR (Internal Path Delay) is thus accounted for to produce the estimates of the range. However, the asymmetry of the PTR is not considered in the MLE4-based range nor the temporal evolution of this asymmetry. Note that recent work has led to the development of a numerical adaptive retracking solution for which the actual PTR is numerically introduced in the algorithm (Thibaut et al., 2020, 2021). With this solution, all drifts or instabilities of the PTR are thus « natively » accounted for (without any approximation), which further improves the mean sea level stability. The adaptive retracking is currently distributed in the Geophysical Data Records of the Jason-3 mission. Note that the impact of the retracking on the sea level uncertainties is relatively reduced and this source of error has not been specifically identified in the existing error budgets.

Calibration and Validation Activities

Calibration and validation (Cal/Val) activities (funded by the space agencies) are essential to ensure the quality of the Copernicus sea level products (previously known as "AVISO products") and in particular, the sea-level stability strongly relies on these L2P activities. These activities include the assessment of the instrument performances in order to detect any anomaly that may affect the range estimates (Quartly et al., 2020). In addition, the monitoring of all geophysical and environmental altimeter corrections used to compute the sea level anomalies (Escudier et al., 2017) is a vital part of the Cal/Val activities so that any drift can be detected in the sea level observations. Indeed, some of the geophysical corrections are one of the main contributors to the altimeter sea-level rise uncertainty, such as the wet tropospheric correction derived from the microwave on-board radiometers (Legeais et al., 2014; Ablain et al., 2019). The Cal/Val activity is of particular importance for the missions currently in operation for which this activity is performed routinely.

Quality assessment of altimeter data can be performed thanks to internal comparisons (analyses of performances at crossover points between ascending and descending tracks) and cross-calibration with other altimeter missions flying at the same time. A third approach is to compare with external independent measurements derived from numerical models or *in situ* instruments. In particular, tide gages are extensively used (Mitchum, 1998; Valladeau et al., 2012; Watson et al., 2015) since they provide continuous high frequency sea level measurements over long periods although they are only located in the coastal ocean and the instruments are not homogeneously distributed over the coasts (hemispheric bias, see for example Prandi et al., 2015). Sea level dynamic heights derived from the *in situ* temperature and salinity profiles from the global Argo network are also of interest for Cal/Val activities (Valladeau et al., 2012; Legeais et al., 2016). Indeed, even if the physical content (steric height) cannot be directly compared to the altimeter observations of the total water column, the *in situ* observations can be used to detect geographically correlated altimetry errors (like hemispheric biases or other regional biases) and to assess the performances of orbit solutions at regional scale, as illustrated on **Figure 2** with the impact of an updated orbit standard on the sea level regional consistency from Jason-1 mission (see also Couhert et al., 2015). At last, absolute calibration of the different altimeter missions is also performed in different sites located along a few tracks of the satellites (Watson et al., 2011; Mertikas et al., 2018; Bonnefond et al., 2019). This also contributes to the quality assessment of the altimeter MSL estimates.

L2P Altimeter Standards

The L2P altimeter data used as input to the DUACS production system are homogeneous along-track datasets of validated sea level anomalies for all past and present missions (see example on the top panel of **Figure 3**). These products also include all corrections used for the computation of these sea level anomalies as well as a validity flag (spurious measurements impacted by rain cells, sea ice or the coast are identified) and inter-mission biases (see next subsection). These datasets are key elements to ensure that the sea level ECV derived from the Copernicus products follows as much as possible the GCOS requirements.[4] The L2P datasets used for the production of the current version (vDT2018) of the delayed-time Copernicus sea level products (Taburet et al., 2019) follow the recommendations made by the sea level project of the ESA Climate Change Initiative (SL_cci).[5] Within this project, optimized altimeter algorithms have been developed, tested and selected through a dedicated "round robin" approach in order to improve the homogeneity and stability of the sea level record. This led to the production of a delayed-time gridded monthly sea level product covering the period 1993–2015 (Ablain et al., 2015; Quartly et al., 2017; Legeais et al., 2018). The L2P products benefit from regular full reprocessing from space agencies (CNES and EUMETSAT). They include the latest L2 reprocessing from

[4] gcos.wmo.int/en/essential-climate-variables/about/requirements

[5] climate.esa.int/en/projects/sea-level/

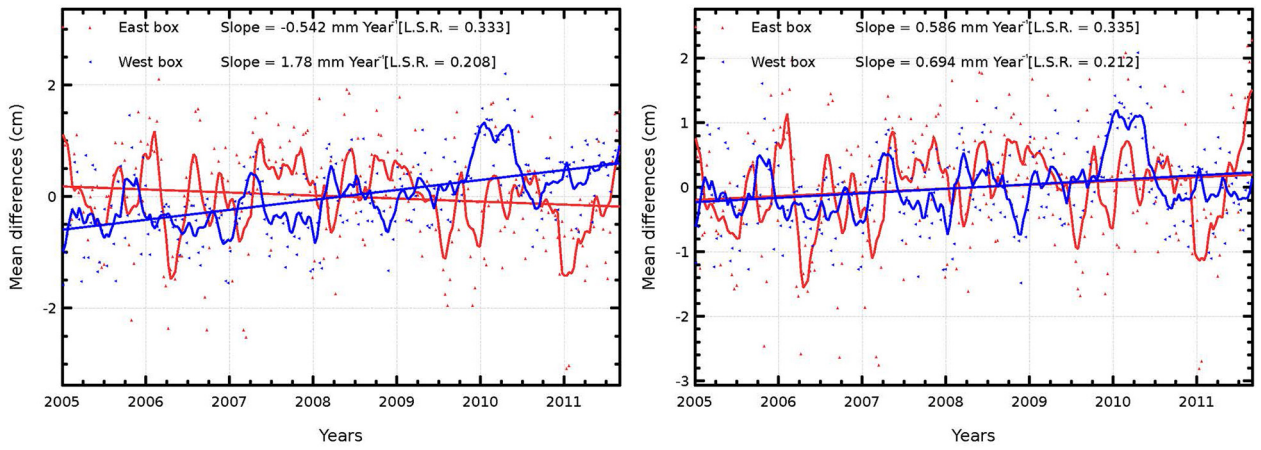

FIGURE 2 | Sea Surface heights differences (cm) between Jason-1 altimeter data (cycles 1–355) and dynamic height anomalies derived from the Argo *in situ* measurements (referenced to 900 dbar) computed with GDR-D (left) and GDR-E orbit solution (right), separating east box (Long: 60°/120°, Lat: –30°/30°, in red) and west box (Long: –150°/–190°, Lat: –50°/10°, in blue). Corresponding annual and semi-annual signals are removed. Trends of raw data (dots) are indicated, and the 2-month filtered signal is added (curves). The hemispheric trend bias is reduced from 2.32 to 0.1 mm/yr. Adapted from Legeais et al. (2016).

individual missions and the latest geophysical and instrumental corrections recommended by the ocean science topography community, aiming at providing unified and up-to-date datasets for all past and present altimetry missions. The next version (vDT2021) of the Copernicus L4 sea level products is derived from the new 2021 release of the L2P product, produced by CNES/AVISO (Lievin et al., 2020).

The Altimeter Reference Missions

The long-term stability of the sea level record is ensured by the TOPEX-Poseidon, Jason-1, Jason-2, and Jason-3 reference missions (and soon Jason-CS/Sentinel-6 MF mission). They are thus essential for the computation of the sea level trends (Ollivier et al., 2012; Ablain et al., 2015). They cover the ± 66° latitude band and have a repeat cycle of 10 days. Other complementary and opportunity missions (ERS-1, ERS-2, Envisat, SARAL/AltiKa, HY-2A and 2B, Sentinel-3A and 3B, and CryoSat-2) are homogenized with respect to the reference missions (with the reduction of the intermission sea surface heights differences at crossover locations) (Ducet et al., 2000; Pujol et al., 2016). These missions improve the geographical sampling of mesoscale processes by improving the spatiotemporal resolution, they provide high-latitude coverage (up to ± 82°) and increase the sea level accuracy.

Another crucial step required to compute the long-term sea level record is the reduction of the inter-mission biases at the transition between two successive missions. During these periods (e.g., between Jason-2 and Jason-3), calibration phases are planned for a few months during which the two successive satellites fly in tandem on the same ground track a few tens of seconds apart and thus observe the same ocean, allowing the computation of global and regional sea level biases between both missions. Despite the available measurements during the tandem phase, there are remaining uncertainties on these inter-mission biases, which directly affect the uncertainty of the trend of the GMSL evolution. The impact can reach 0.2 mm/yr of uncertainty during a 25-year-long period (SL_cci CECR, 2016; Zawadzki and Ablain, 2016; Guerou et al., 2020). Note that the estimates of the inter-mission biases strongly depend on the altimeter standards used in the sea level computation and thus, they have to be computed every time reprocessed sea level measurements are available.

L3 and L4 Production

In the context of the Copernicus activities, the DUACS system is used for the operational production of the inter-calibrated along-track (L3) mono-mission sea level products (ready to be assimilated in ocean models) and the multi-mission merged gridded 1/4° products (L4). After removing the biases between the different missions, long wavelength errors (e.g., orbit errors) are removed thanks to multi-mission crossover minimization (Dibarboure et al., 2011) and remaining aliased short scale signals are also filtered out (see middle of **Figure 3**). Measurements from all missions are merged in the gridded products with an objective analysis approach (Ducet et al., 2000; Le Traon et al., 2003; see bottom of **Figure 3**). The present paper does not aim at providing the details of the methodology related to the altimeter processing and production system. Readers interested in more information on the specification of the Copernicus altimeter sea level products are invited to consult the product user manuals of the respective Copernicus services (see **Table 1** for the accesses to the documentation) as well as Pujol et al. (2016) and Taburet et al. (2019).

The delayed time DUACS products are regularly reprocessed (every ∼4 years) in order to consider the latest progress achievements in the upstream data (e.g., improved geophysical corrections, homogenization of the time series, new retrackings, etc.) and evolutions in the L3/L4 processing (e.g., improved parameters of the mapping technique). Since the beginning of the Copernicus service, the altimeter sea level Climate Data Record

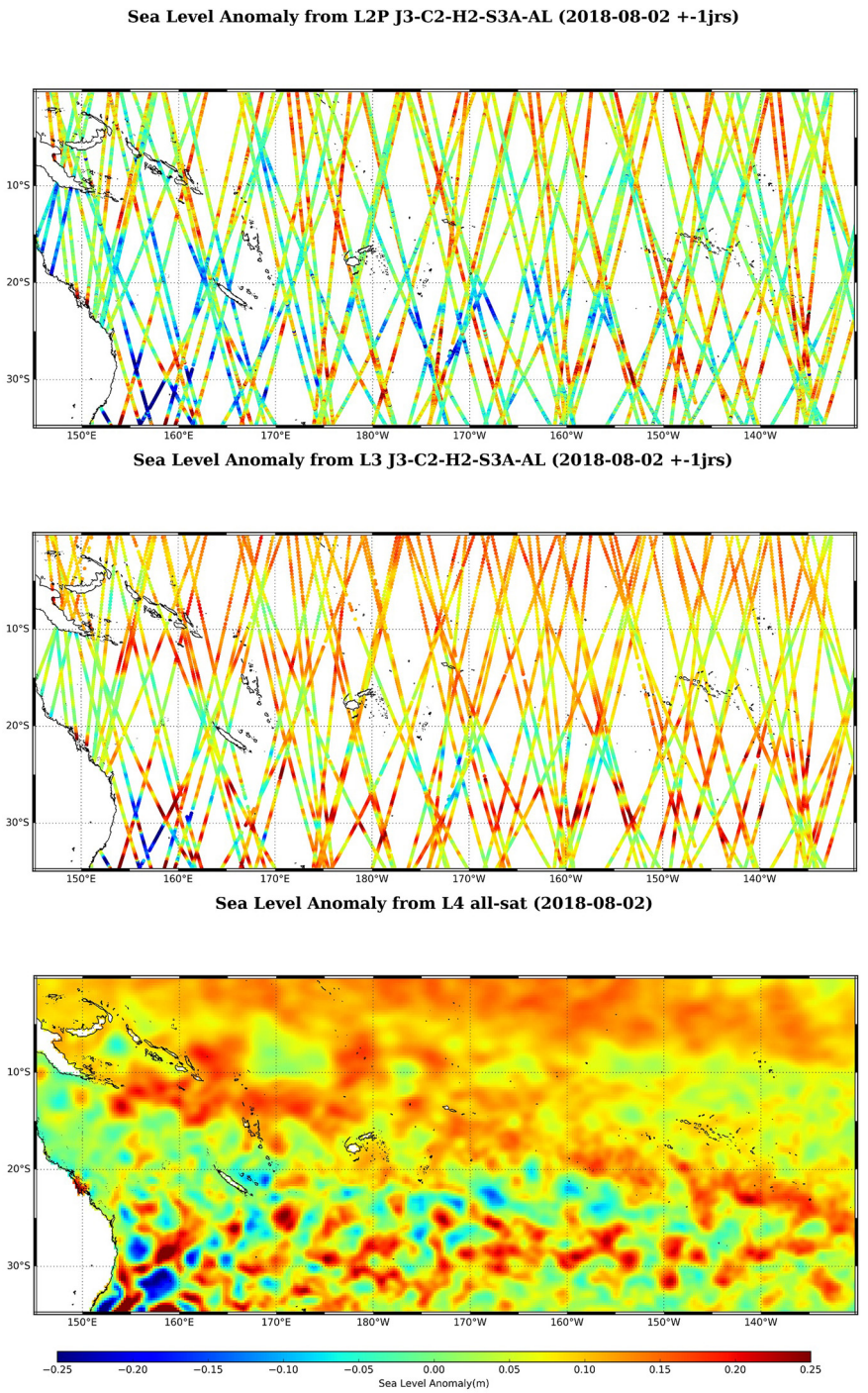

FIGURE 3 | Sea level anomalies L2P input data processed by the DUACS production system from Jason-3, CryoSat-2, HY-2A, Sentinel-3A, and SARAL/AltiKa missions on 02/08/2028 (± 1 day) in the South-West Pacific Ocean (top). The corresponding along-track cross-calibrated L3 and merged L4 data are shown in the middle and bottom panels, respectively.

has benefited from three consecutive full reprocessing, named DUACS DT2010 (Dibarboure et al., 2011), DT2014 (Pujol et al., 2016), and DT2018 (Taburet et al., 2019). Each version benefits from regular temporal extensions (∼3 times per year) with the production of the Interim Climate Data Record, to keep the time series close to present time. This production is made possible thanks to the availability of the upstream input L2P datasets distributed by the different space agencies (see above).

The DUACS production system is regularly upgraded to ensure the best quality of the products. Implementation of

a fully reprocessed version usually requires evolutions of the different processing parameters. System's evolutions are also required to ensure the routine production and take into account the different changes in the constellation (see **Figure 4**): new missions are introduced in the system while past missions are deactivated, and specific evolutions may be required to avoid any impact of measurements with a reduced quality on the DUACS output products.

An extensive quality assessment is performed before disseminating the products. A large spectrum of metrics are used to check the sea level time series integrity (no missing values; no corrupted file, etc.) as well as the quality of the various parameters delivered. The validation approach is based on different type of information, varying from the most simple (e.g., along-track statistics of the different variables) to more complex (e.g., statistics at altimeter cross-over positions), implying independent measurements (e.g., tide gauges, drifters, independent altimeter data not used in the processing) and other internal data for validation purpose (see **Table 1** for the accesses to the quality information document and product quality assessment report distributed by the Copernicus services).

THE COPERNICUS ALTIMETER SEA LEVEL PRODUCTS AND OCEAN MONITORING INDICATORS

The processing steps presented above are integrated in the sea level production center of the Copernicus program, and we present here the different sea level products available for the users and discuss their maturity. They allow the estimate of added-value ocean monitoring indicators (L4P) such as the mean sea level evolution. The associated trend and acceleration are presented, and we highlight the importance of the determination of the associated uncertainties.

Two Copernicus Altimeter Sea Level Products

The DUACS altimeter production system delivers two different types of delayed-time sea level datasets. In the first one, all the altimeter missions are processed to optimize the ocean sampling at each moment, allowing the retrieval of a large range of wavelengths, as required for ocean modeling and ocean circulation analyses. This dataset is produced by the Copernicus Marine Environment Monitoring Service (CMEMS).[6] A second sea level dataset focuses on the monitoring of the long-term evolution of sea level for climate applications and the analysis of ocean/climate indicators. This climate-oriented dataset ensures the homogeneity and stability of the record (mainly based on the ESA SL_cci legacy) and it is produced by the Copernicus Climate Change Service (C3S).[7] Numerous altimeter algorithms are required for the sea level production, and it is complex to ensure both the retrieval of high-resolution mesoscale signals and the stability of the large-scale wavelengths. This has led to the production and distribution of two altimeter sea level datasets available for the users in the climate (C3S) and marine (CMEMS) datastores (see **Table 1** for accesses to the documentation and data; note that the C3S sea level dataset is also distributed in the CMEMS catalog). Both delayed-time datasets are available as daily 1/4° global gridded files derived from optimal interpolation and available from January 1993 with a ∼6 months timeliness. Temporal extensions are provided ∼3 times per year and a full reprocessing is performed every 4 years (the latest version vDT2021 will be released in 2021). The same L2P input data are used for both datasets and the main differences between the CMEMS and C3S altimeter sea level datasets concern the two following elements:

(i) The number of altimeters used in the satellite constellation: all available altimeters are considered in the CMEMS products whereas a steady number (currently two) of altimeters are included in the C3S products (see **Figure 4**). Previous studies (Pascual et al., 2006; Dibarboure et al., 2011) underscored the necessity of a minimum of a two-satellite constellation for the retrieval of mesoscale signals. The total number of satellites strongly varies during the altimetry era and this varying number has currently no impact on the global MSL estimate. However, when focusing on a regional/basin scale, the introduction of a new satellite in the constellation can be at the origin of some bias in the MSL time series, affecting the stability of the sea level record. To illustrate this, **Figure 5** presents the impact of the change of the number of satellites in the constellation in the vDT2018 CMEMS dataset in terms of MSL averaged in the Black Sea area. The MSL derived from the all-satellite merged CMEMS product is compared to the MSL derived from the same product where only two satellites are used in the computation of the sea level anomalies, highlighting the impact of the number of satellites considered. A 1.5 cm increase of the MSL difference is observed in early 2012 (right axis, in red), corresponding to the change from Envisat to CryoSat-2 in the two-satellite merged dataset and to the Envisat mission termination (CryoSat-2 was already included) and the change of Jason-1 from a repeat to a drifting geodetic orbit in the all-satellite merged dataset (cf **Figure 1**). The observed MSL differences (red curve, of the order of ± 1 cm) contribute to the uncertainties in the MSL trend value [estimated here to be 0.3 mm/yr during the period (2009, 2016) considered for this figure].

The risk of introducing a bias remains with the integration of a future mission. This explains why a stable number of satellites (two) has been preferred for the design of the C3S product. Indeed, even if the spatial sampling is reduced with less satellites, such a choice contributes to the MSL stability (the bias introduction is more related to missions experiencing a change of orbit and these missions are usually not included in the C3S product). In the CMEMS product, the stability is provided by the reference missions and the mesoscale errors are reduced due to the improved ocean surface sampling thanks to the use of all satellites available in the constellation. Note that the varying number of satellites in the constellation also affects mesoscale signals, especially the number of eddy detections (Pegliasco et al., 2021). It is pointed out that both CMEMS and C3S sea level datasets are of interest for eddy detection

[6] marine.copernicus.eu/

[7] climate.copernicus.eu/

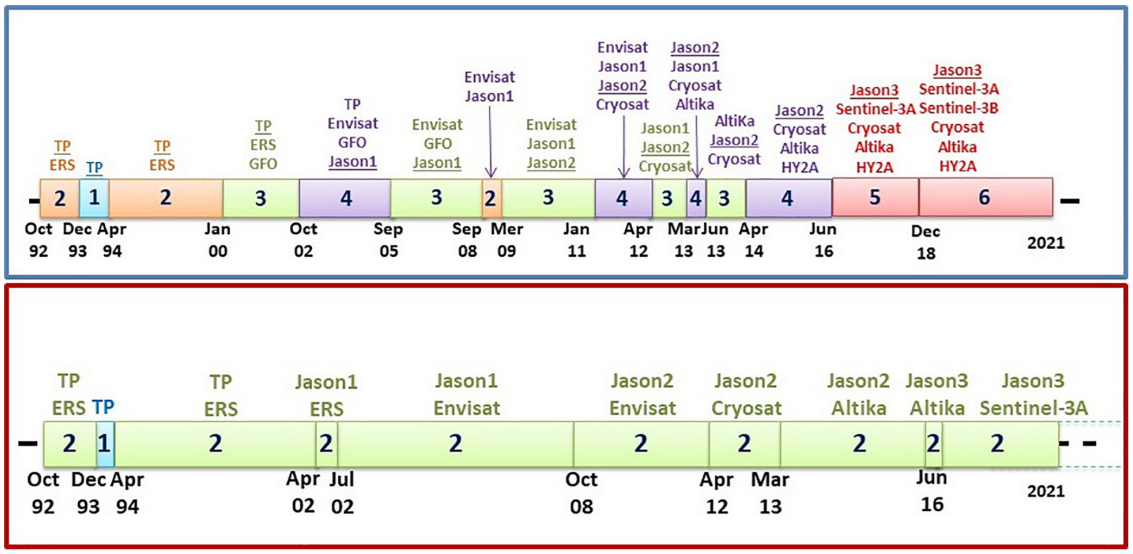

FIGURE 4 | Number of altimeter missions considered in the constellation of both CMEMS and C3S altimeter sea level datasets.

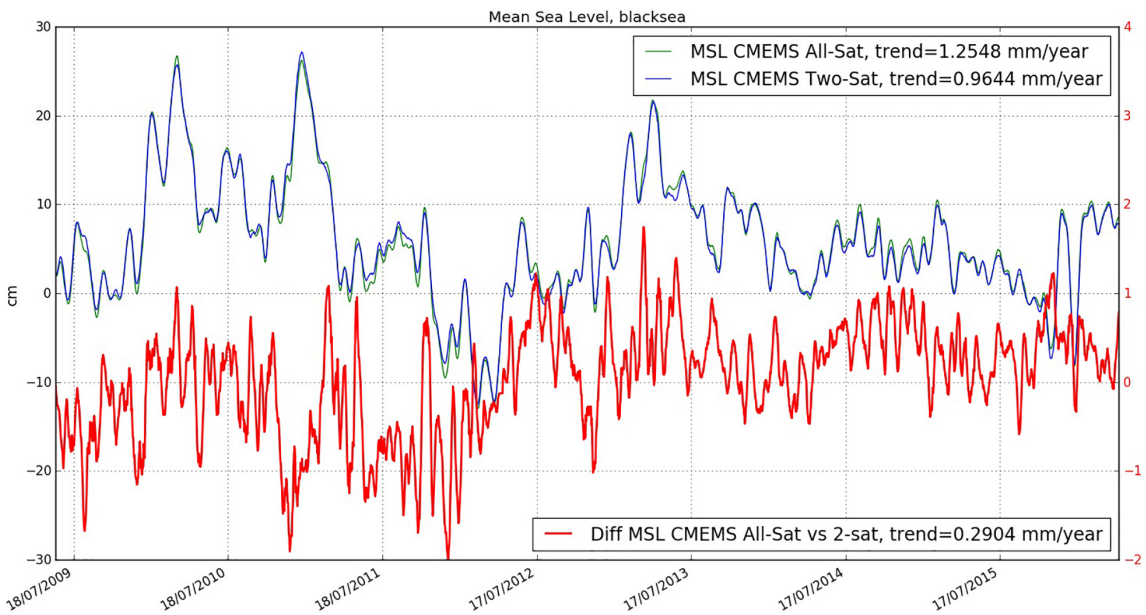

FIGURE 5 | Area-averaged mean sea level in the Black Sea: impact of the difference of constellation between the all-satellite merged dataset (CMEMS vDT2018, in blue) and the corresponding dataset in a two-satellite merged configuration (in green), in terms of mean sea level in the Black Sea and their difference (in red, in cm).

and tracking application, depending on the final goal of the study: the C3S dataset rather ensures a stability in the retrieved mesoscale activity (EKE, number of detections through the time) whereas the CMEMS dataset provides a higher resolution and thus improved location and other characteristics (e.g., amplitude, size, shape) of the eddies.

(ii) The reference field used to compute sea level anomalies: an optimized reference field (mean along-track profiles of sea surface heights) is used for missions with a repetitive orbit in CMEMS to provide the best sea level estimates, especially in coastal areas. The use of a mean profile is, however, not possible for all missions (e.g., CryoSat-2, or more generally missions with a geodetic orbit). In these cases, a gridded Mean Sea Surface must be used and the merging of the sea level anomalies computed with the two different methods can introduce large scale errors affecting the MSL stability. Even if this has no impact on a global scale (with respect to the uncertainty on an interannual timescale), the MSL stability can be impacted on a regional scale. In the C3S sea level product, the gridded mean sea surface is used for all missions (as in the ESA SL_cci product), which can introduce

errors at short wavelengths but ensures optimal estimates of the large-scale signals.

Figure 6 shows the difference of MSL in the Black Sea area between two altimeter datasets: they are both based on a stable two-satellite merged constellation but one is computed with a homogeneous mean sea surface reference field for all missions (i.e., the C3S product) whereas a mix of reference fields is used in the other dataset. Some jumps of up to 1 cm are observed in the difference of area-averaged sea-level in the Black Sea, corresponding to changes from a mission using a mean profile of sea surface heights or a mean sea surface (introduction of CryoSat-2 in 2011 and SARAL/AltiKa in 2013 and the change of this latter mission to a drifting orbit in 2015). This illustrates some remaining inhomogeneities between these two types of mean references, which should be reduced in the next version of the product (vDT2021). The associated impact in terms of MSL trend reaches almost 0.5 mm/yr during a 15-year long period [2002, 2016] (note that this impact varies according to the period considered and the date of the events within this period). Thus, the systematic use of a homogeneous reference field for the computation of sea level anomalies of all missions contributes to ensure the stability of the altimeter regional sea-level in the C3S dataset. On the other hand, the use of mean sea surface height profiles for repetitive missions remains of interest to increase the accuracy of the product at short scales (as requested for the CMEMS dataset).

Product Maturity

The production of these sea level datasets (previously known as "AVISO products") is mature enough to be implemented operationally within the E.U. Copernicus services. However, the operational production requires some good practices in order to ensure the quality of the service for a vast range of users. Among its wider activities, the World Meteorological Organisation (WMO) fosters collaboration to develop technical guidance and standards for the collection, processing and management of data and forecast products. Part of this process aims at providing a tool that enables data providers to assess and rate their datasets quantifiably based on internationally validated data stewardship best practices. A dedicated stewardship maturity matrix is used to evaluate if the production of a data record follows best practices for specific aspects and facilitation of usage (with a maximum grade of 5). The tool is an essential part of ensuring and improving the way datasets are documented, preserved, and disseminated to users (Peng et al., 2019; Dunn et al., 2021). It also enables data providers to determine a roadmap for future development and improvement, as well as compare their process against other data providers. Note that the maturity assessment is only related to aspects of process maturity and does not guarantee the scientific reliability of a given climate data record.

The WMO stewardship maturity matrix has been used to assess the altimeter sea level Climate Data Record produced and distributed by C3S (Dunn et al., 2021). In terms of "Data Access" (ability to find and obtain the dataset), the grade is 5 for the "Discoverability" aspect since the dataset is searchable and easily available through the online institutional C3S catalog and 4.5 for "Accessibility" due to the Climate Data Store interface and the associated toolbox (no spatial subsetting is possible when downloading the data and all variables have to be downloaded together). Regarding the "Usability and Usage" (easy to use and impact of its usage), the attributed grade for "Data Portability" is 4.5 since the data are distributed as NetCDF (Network Common Data Form) files, compliant with the Climate and Forecast (CF) convention, but no other format is available. A grade

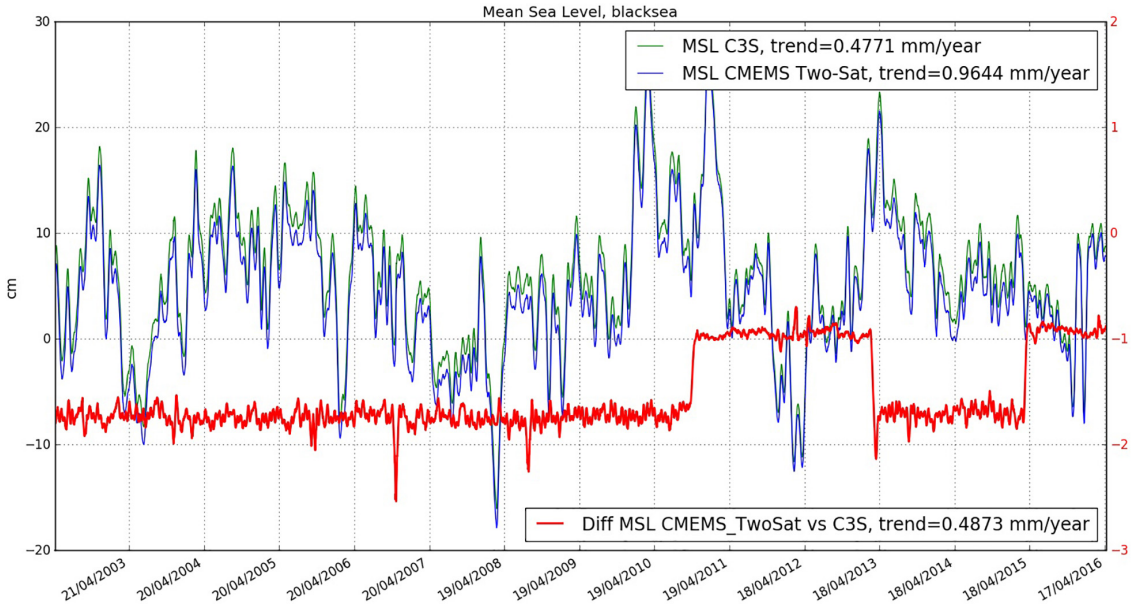

FIGURE 6 | Area-averaged mean sea level in the Black Sea computed with two-satellite merged gridded global datasets including a homogeneous mean sea surface reference field for all missions (in green) and a combined use of a mean sea surface and mean profile of sea surface heights for missions with a drifting or repeat orbit, respectively (in blue). The difference between both regional mean sea level is shown in red (y-axis on the right, in cm).

of 5 is given for "Documentation" and "Usage" aspects since the dataset is fully documented and has been referenced in international climate assessment and published reports. In terms of "Quality Management," the quality assurance procedure is fully documented with an additional independent evaluation and quality control performed by the Copernicus service. Target requirements and a detailed gap analysis are available, and details of the error budget have been published in peer-reviewed journals, leading to a grade of 5 for both "Quality Assurance and Assessment" aspects. The same grade of 5 is given for "Data Integrity," which is systematically verified with a standard approach to ensure that the distributed data are the same as the initial data files. Finally, regarding the "Data Management" category, a grade of 4 is attributed for "Data Preservation" since the data are distributed on an institutionally maintained platform and are archived following a defined and implemented procedure which agrees with community standards. A grade of 5 is given for both "Metadata" and "Governance" aspects since the dataset is distributed with comprehensive metadata, detailed documentation and versioning system, and governance aspects are well-defined within the E.U. Copernicus programme and are compliant with international standards.

Mean Sea Level Indicators: Key Information for Adaptation and Mitigation Strategies

As presented earlier, the GMSL is a key ocean monitoring indicator that can be derived from satellite altimetry. It can either be computed by directly averaging the validated along-track data of the reference missions (as distributed by AVISO; see also Ablain et al., 2017)[8] or averaging the multi-mission merged gridded Copernicus datasets (as distributed by Copernicus).[9] The associated GMSLs are considered to be identical since the same altimeter standards are used to compute the sea level anomalies, and the long-term stability is ensured by the same reference missions. The remaining observed GMSL differences are not significant given the uncertainty considered on different scales (Ablain et al., 2015, 2019; Prandi et al., 2021).

The GMSL shows a significant rise over the 26-years of altimetry data record (1993–2021) of + 3.1 ± 0.4 mm/yr (at the 90% confidence level) (**Figure 7**; WCRP Global Sea Level Budget Group, 2018; Ablain et al., 2019). This means that over these 26 years, the sea level has risen by ∼8 cm on average, globally. At the regional scale, the SLR distribution ranges between 0 and 6 mm/yr (**Figure 8**), with uncertainties ranging from ± 0.8 to ± 1.2 mm/yr depending on the location. On the overall, sea level is rising almost everywhere over the globe (Prandi et al., 2021). Not only is the sea level rising, but it is accelerating (Dieng et al., 2017; Nerem et al., 2018; Ablain et al., 2019). This acceleration has been quantified at 0.12 ± 0.06 mm/yr^2 (90% confidence level) at the global scale (Ablain et al., 2019) once the TOPEX/Poseidon drift is empirically corrected for (WCRP Global Sea Level Budget Group, 2018). At regional scales, the sea-level accelerations range between −1 mm/yr^2 and + 1 mm/yr^2 with uncertainties between 0.057 and 0.12 mm/yr^2 (Prandi et al., 2021). A strong added value to the sea-level ECV is the provision of its uncertainties. They are essential to characterize the reliability of the observing systems and avoid misinterpretation of signals that could potentially come from observational errors. Quantifying the error at each level of the observational systems (instrumental, processing) is a difficult task and has been addressed by any group. An alternative approach based on error budgets has been proposed by Ablain et al. (2019) at the global scale, and recently adapted to the regional scale by Prandi et al. (2021). Such approach allows to specify *a posteriori* the different sources of errors contained in the data records. Different types of errors are provided such as inter-mission biases, correlated errors at different time scales (typically 2-months, 1 and 5 years), and linear drifts (orbits, ITRF, GIA). A variance-covariance matrix has been derived from this error budget and, combined with an ordinary least square estimation method to derive uncertainties on the trend and acceleration of sea level (see Ablain et al., 2019; Prandi et al., 2021 for more details).

[8] www.aviso.altimetry.fr/en/data/products/ocean-indicators-products/mean-sea-level.html

[9] marine.copernicus.eu/science-learning/ocean-monitoring-indicators/catalogue/

REMAINING GAPS AND RECOMMENDATIONS

As mentioned in the last IPCC report (chapter 4 of IPCC, 2019), the knowledge of the GMSL estimate as well as the determination of the regional and coastal sea level changes are of major importance for understanding SLR, validating climate model simulations of past and future SLR and for societal applications. In this section we identify the remaining gaps so that the sea level ECV products keep on answering the users needs and contributes to support public policies to adapt to and mitigate SLR. The first key element is to ensure the continuity of the sea level record. In terms of observing system, the long-term production of the Copernicus altimeter sea level products relies on the continuity of the Copernicus satellite missions. This continuity of altimeter measurements is essential for climatology, oceanography, hydrology and also marine glaciology. Sentinel-6A MF will be soon used as a reference mission (ensuring the stability of the record) and in the future, Sentinel-3C, 3D and Sentinel-6B as well as the SWOT prototype will be launched before 2025. However, most other missions are expected to reach their end of life before this date (CryoSat-2, HY-2A, B and C, Jason-3, Sentinel-3 A and B, CFOSat), which makes the future of the altimeter time series uncertain. Only Sentinel-3 Next Generation (NG) mission (after 2025) and Sentinel-6 NG mission (after 2030) are planned to be launched (and probably the HPCM Cristal mission, providing an improved resolution and spatial coverage at high latitudes). It is thus of major importance that these future Sentinel NG missions are launched to guarantee the long-term continuity of the sea level measurements and that Sentinel-6 NG flies on the same orbit as its predecessors so that the climate continuity is provided. A second major objective is to maintain the homogeneity and consistency of the altimeter sea level record. This requires the reprocessing of the past missions so

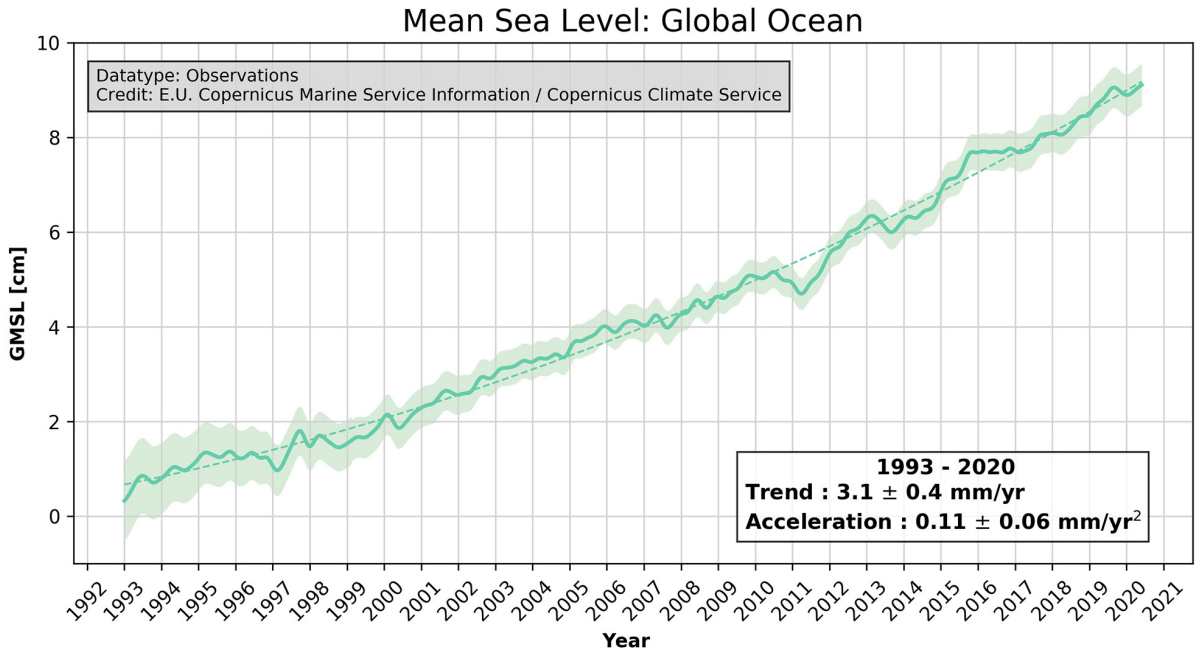

FIGURE 7 | Global Mean Sea Level derived from the altimeter C3S multi-mission gridded sea level product (DUACS vDT2018) from January 1993 to June 2020. The global average is derived from box-averaged gridded sea level maps weighted by the cosine of the latitude. The timeseries is low-pass filtered, the annual and semi-annual periodic signals are adjusted. The curve is corrected for TOPEX-A instrumental drift during 1993–1998 (WCRP Global Sea Level Budget Group, 2018) and is corrected for the GIA effect. Quoted uncertainties are within a 90% confidence level (adapted from Ablain et al., 2019).

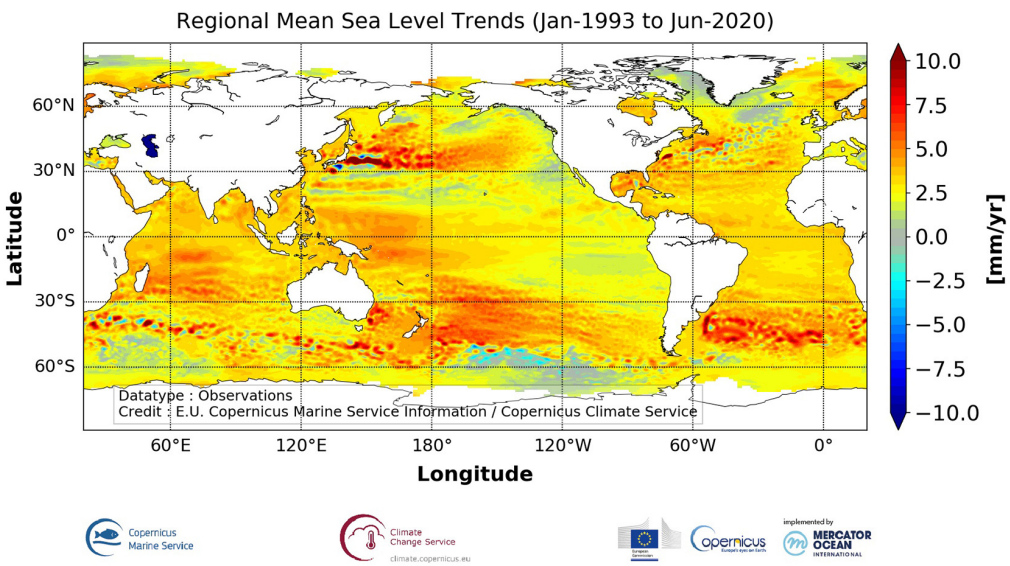

FIGURE 8 | Regional distribution of the trends of the satellite altimeter sea level observations (in mm/yr) from January 1993 to June 2020. The trends are derived from the altimeter C3S multi-mission gridded sea level product (DUACS vDT2018). The trends are not corrected for the TOPEX-A instrumental drift nor for the GIA effect.

that they remain up-to-date by space agencies (e.g., the on-going TOPEX-Poseidon L2 reprocessing by CNES/JPL) and the use of homogeneous algorithms for all missions (e.g., ERA-5 forcing for atmospheric altimeter corrections in the CNES 2021 L2P reprocessing) with adequate inter-mission calibration.

Another crucial element is to reduce altimeter sea level errors and to better characterize the associated uncertainties. Indeed, the GMSL estimate provides an essential source of information for several key questions of the World Climate Research Programme such as the detection and attribution of the sea level forced response to climate change, the detection of changes in the contributions to SLR (e.g., acceleration in ice mass loss, terrestrial water storage evolution, etc.; see IPCC, 2019), the detection of potential new contributions to SLR (e.g.,

the permafrost thawing, decrease of persistent snow cover or the increase of water vapor content, etc.; see WCRP Global Sea Level Budget Group, 2018), or the estimates of the energy imbalance at the top of the atmosphere that is responsible for climate change (Meyssignac et al., 2019). Different amplitudes and time scales are involved in these different physical processes. The current GCOS requirement on the stability of the GMSL (of ± 0.3 mm/yr over a decade) is probably enough to detect the current total GMSL rise and acceleration due to greenhouse gases (GHG) emissions but it is not enough to detect a potential contribution of the permafrost thawing or to help understand the change of Earth energy imbalance during Hiatus periods (of the order of 0.1 $W.m^{-2}$ over 15 years; see Hedemann et al., 2017), which will rather require a ± 0.1 mm/yr accuracy over a decade (Meyssignac et al., 2019). On time scales longer than a decade, the acceleration and the trend in forced sea level may change in response to climate change mitigation policies. These evolutions are slow and may not exceed a few tenth of mm/yr over 20-year windows (see the difference in SLR between the RCP2.6 scenario and the RCP 8.5 scenario along the twenty-first century in IPCC, 2019). If we want to monitor these changes to support mitigation policies we will need an accuracy of the order of ± 0.1 mm/yr over 20-year windows which is beyond the current GCOS requirements. Reaching such a level of accuracy is a major challenge and we will have to make the most of future altimeter missions to go in this direction.

At regional scale, the accuracy in the altimeter SLR estimates is above ± 1 mm/yr over 10 years for regions of 1,000 square km and larger (Prandi et al., 2021). This is clearly not sufficient because the expected sea level signal forced by the anthropogenic GHG emissions is at the level of [0.5–0.8] mm/yr over 10 year and longer time scales for regions of 1 000 square km and larger (see for example Palanisamy et al., 2015; Fasullo and Nerem, 2018). Thus, the detection of the regionally forced signal requires the reduction of all sources of uncertainty in sea level estimates below this level of 0.5 mm/yr over regions of 1,000 square km. In order to reduce the uncertainty due to the altimeter instrument, Ablain et al. (2020) have suggested to plan a second 2 to 3 month tandem calibration phase (approximately 1.5–2 years after the first tandem phase) between Jason-3 and Sentinel-6A. Simulations show that this second tandem phase would allow linking the MSL from both missions with an accuracy below ± 0.5 mm/yr regionally and thus identify any issues or error between missions that lead to higher signals.

Another remaining gap is related to the improvement of the sea level estimates in some key regions. In ice-covered areas at the poles, the uncertainty on the sea level estimates remains relatively high due to the deteriorated conditions of retroflexion of the radar echo. The efforts made to better retrieve the sea level evolution in these regions should be encouraged to better understand its contribution to the global SLR. In coastal areas, it remains unclear if the sea level increases at the same rate as the SLR as seen by altimetry in the open ocean. The Climate Change Initiative Coastal Sea Level Team (2020) suggests that global gridded sea level products provide enough information to assess coastal sea level trends but this is not the case in some specific sites. More studies are required on the altimeter sea level products to understand the different processes involved in coastal SLR. At the coast, the altimeter observing system provides the sea surface height of the total water column whereas the information of interest is rather the sea level relative to the shore (Wöppelmann and Marcos, 2016). Indeed, vertical land motions remain the main source of uncertainty in the relative sea level and efforts should be made on their improved characterization involving available information (tide gauges and GNSS measurements, InSAR technique). The risk assessment at the coast related to SLR is also made more difficult due to the complexity to determine a common reference level between digital elevation models over land and the mean sea surface reference level. The relative sea level is a combination of the global MSL, the regional variability and the result of small-scale processes (shelf currents, changes in wind and waves, modification of the sea water density due to freshwater input from estuaries etc.). Additional observations (from *in situ* networks) and high-resolution models would be a great asset to contribute to the understanding of all these processes and their impact on the coastal sea level changes.

Working on solutions to face the rising MSL challenges a wide range of disciplines (e.g., climate science, geosciences, social sciences). Scientists are working on estimating the local impacts of sea-level rise at the shore to help policy makers define mitigation and/or adaptation strategies. As the impacts and adaptation needs are a response to relative SLR including vertical land movements (rather than global SLR), they require the knowledge of all processes involved at the coast, and the potential of all techniques (as the ones listed earlier) should be optimized in interaction with other expert communities. Understanding the processes and assessing the societal consequences remains difficult due to the partitioning of the research community and an integrated and interdisciplinary approach is thus needed (see for instance the JPI 2020 Knowledge Hub on SLR,[10] and the Copernicus support to public policies).[11] In addition, engagement with coastal stakeholders and showcasing the already existing Earth observation products and associated services should be strengthened to enhance these products and further improve decision making (see for instance the CEOS Coastal Observations, Applications, Services, and Tools).[12] Satellite measurements are of major interest to provide concrete evaluation of the impact of climate change on coastal territories in various areas such as flooding, bathymetry and coastline mapping, coastal eutrophication, turbidity and sedimentation. Today, these satellite Earth observations provide the framework that further allow the elaboration of adaptation strategies and efforts should be made so that adaptation decisions can be directly supported by these observations. This is one of the objectives of the CLS/CNES Space Climate Observatory "Littoscope" project, which investigates the capacity of satellite-derived high resolution Digital Elevation Model (DEM) to be used in climate modeling studies or early warning tools, in

[10] www.jpi-climate.eu/joint-activities/sealevelrise.knowledgehub

[11] marine.copernicus.eu/support-public-policies/

[12] earthobservations.org/geo_blog_obs.php?id=521

combination with the Copernicus altimeter regional sea level trends to help in the anticipation and mitigation of coastal flood hazards. The risk assessment is made further possible by crossing the hazard intensity with social, economic, natural and cultural exposures derived from a multi-sources approach (datasets from geographical information systems combined with land use information derived from HR optical satellite imagery). In the near future (∼5 years), depending on the accuracy of the satellite-derived information (DEM, regional sea level changes, etc.) and considering the associated uncertainties, such an approach will contribute to the development of adaptation strategies to SLR.

DATA AVAILABILITY STATEMENT

The datasets presented in this study can be found in online repositories. The names of the repository/repositories and accession number(s) can be found below: cds.climate.copernicus.eu/cdsapp#!/dataset/satellite-sea-level-global?tab=overview; https://resources.marine.copernicus.eu/?option=com_csw&view=details&product_id=SEALEVEL_GLO_PHY_L4_REP_OBSERVATIONS_008_047.

AUTHOR CONTRIBUTIONS

J-FL has written the article with contributions provided by AG (on "Ocean Monitoring Indicators"), M-IP (on "L3 and L4 production") and CD (Littoscope project description). BM, YF, MA, and GD contributed to the improvement and finalization of the article. All authors contributed to the article and approved the submitted version.

FUNDING

The development of the DUACS altimeter production system has been supported by CNES since 2001 and the operational production has been funded by Copernicus since 2015 (CMEMS SL-TAC, C3S_312a_Lot2 and C3S_312b_Lot3 contracts).

ACKNOWLEDGMENTS

The authors thank Guillaume Taburet for his contribution to the preparation of a figure.

REFERENCES

Ablain, M., Cazenave, A., Larnicol, G., Balmaseda, M., Cipollini, P., Faugère, Y., et al. (2015). Improved sea level record over the satellite altimetry era (1993–2010) from the climate change initiative project. *Ocean Sci.* 11, 67–82. doi: 10.5194/os-11-67-2015

Ablain, M., Jugier, R., Marti, F., Dibarboure, G., Couhert, A., Meyssignac, B., et al. (2020). Benefit of a second calibration phase to estimate the relative global and regional mean sea level drifts between Jason-3 and Sentinel-6a. *Earth Space Sci. Open Arch.* 1, 1–10 doi: 10.1002/essoar.10502856.2

Ablain, M., Legeais, J. F., Prandi, P., Fenoglio-Marc, L., Marcos, M., Dieng, H. B., et al. (2017). Satellite altimetry-based Sea level at global and regional scales. *Surv. Geophys.* 38, 7–31. doi: 10.1007/s10712-016-9389-8

Ablain, M., Meyssignac, B., Zawadzki, L., Jugier, R., Ribes, A., Cazenave, A., et al. (2019). Uncertainty in satellite estimate of global mean sea level changes, trend and acceleration. *Earth Syst. Sci. Data* 11, 1189–1202. doi: 10.5194/essd-11-1189-2019

Amarouche, L., Thibaut, P., Zanife, O. Z., Dumont, J.-P., Vincent, P., and Steunou, N. (2004). Improving the Jason-1 ground retracking to better account for attitude effects. *Mar. Geod.* 27, 171–197. doi: 10.1080/01490410490465210

Bojinski, S., Verstraete, M., Peterson, T. C., Richter, C., Simmons, A., and Zemp, M. (2014). The concept of essential climate variables in support of climate research, applications, and policy. *Bull. Am. Meteor. Soc.* 95, 1431–1443. doi: 10.1175/BAMS-D-13-00047.1

Bonnefond, P., Exertier, P., Laurain, O., Guinle, T., and Féménias, P. (2019). Corsica: a 20-Yr multi-mission absolute altimeter calibration site. *Adv. Space Res.* 68, 1171–1186. doi: 10.1016/j.asr.2019.09.049

Cazenave, A., and Le Cozannet, G. (2013). Sea Level rise and its coastal impacts. *Earths Future* 2, 15–34. doi: 10.1002/2013EF000188

Chelton, D. B., Ries, J. C., Haines, B. J., Fu, L.-L., and Callahan, P. S. (2001). "Chapter 1: satellite altimetry," in *Satellite Altimetry and Earth Sciences – A Handbook of Techniques and Applications International Geophysics*, Vol. 69, eds L.-L. Fu and A. Cazenave (San Diego, CA: Academic Press), 1–131. doi: 10.1016/s0074-6142(01)80146-7

Couhert, A., Cerri, L., Legeais, J. F., Ablain, M., Zelensky, N., Haines, B., et al. (2015). Towards the 1 mm/y stability of the radial orbit error at regional scales. *Adv. Space Res.* 55, 2–23. doi: 10.1016/j.asr.2014.06.041

Couhert, A., Mercier, F., Moyard, J., and Biancale, R. (2018). Systematic error mitigation in DORIS-derived geocenter motion. *JGR Solid Earth* 123, 10142–11061. doi: 10.1029/2018JB015453

Dibarboure, G., Pujol, M.-I., Briol, F., Le Traon, P. Y., Larnicol, G., Picot, N., et al. (2011). Jason-2 in DUACS: updated system description, first tandem results and impact on processing and products. *Mar. Geod.* 34, 214–241.

Dieng, H. B., Cazenave, A., Meyssignac, B., and Ablain, M. (2017). New estimate of the current rate of sea level rise from a sea level budget approach. *Geophys. Res. Lett.* 44, 3744–3751, https://doi.org/10.1002/2017GL073308, 2017.

Ducet, N., Le Traon, P. Y., and Reverdin, G. (2000). Global high resolution mapping of ocean circulation from the combination of TOPEX/POSEIDON and ERS-1/2. *J. Geophys. Res.* 105, 19477–19498.

Dunn, R., Lief, C., Peng, G., Wright, W., Baddour, O., Donat, M., et al. (2021). Stewardship maturity assessment tools for modernization of climate data management. *Data Sci. J.* 20:1. doi: 10.5334/dsj-2021-007

Escudier, P., Couhert, A., Mercier, F., Mallet, A., Thibaut, P., Tran, N., et al. (2017). "Satellite radar altimetry: principle, geophysical correction and orbit, accuracy and precision," in *Satellite Altimetry Over Oceans and Land Surfaces*, eds D. Stammer and A. Cazenave (Boca Raton, FL: CRC Press).

Fasullo, J. T., and Nerem, R. S. (2018). Altimeter-era emergence of the patterns of forced sea-level rise in climate models and implications for the future. *Proc. Natl. Acad. Sci. U.S.A.* 115, 12944–12949. doi: 10.1073/pnas.1813233115

Guerou, A., Zawadzki, L., Raynal, M., Ablain, M., and Jugier, R. (2020). *Revised Uncertainties of the Global Mean Sea Level Biases Between the TOPEX and Jasons Reference Mission*. OSTST. Available online at: meetings.aviso.altimetry.fr/fileadmin//user_upload/tx_ausyclsseminar/files/OSTST2020_GMSL_Bias_Uncertainties_01.pdf (accessed Nov 04, 2020).

Hedemann, C., Mauritsen, T., Jungclaus, J., and Marotzke, J. (2017). The subtle origins of surface-warming hiatuses. *Nat. Clim. Change* 7, 336–339. doi: 10.1038/nclimate3274

IPCC. (2019). *Special Report on the Ocean and Cryosphere in a Changing Climate*, eds H.-O. Pörtner, D. C. Roberts, V. Masson-Delmotte, P. Zhai, M. Tignor, E. Poloczanska, et al. (Geneva: IPCC).

Le Traon, P. Y., Faugère, Y., Hernandez, F., Dorandeu, J., Mertz, F., and Ablain, M. (2003). Can we merge GEOSAT follow-on with TOPEX/Poseidon and ERS-2 for an improved description of the ocean circulation? *J. Atmos. Ocean. Technol.* 20, 889–895.

Legeais, J.-F., Ablain, M., and Thao, S. (2014). Evaluation of wet troposphere path delays from atmospheric reanalyses and radiometers and their impact on the altimeter sea level. *Ocean Sci.* 10, 893–905. doi: 10.5194/os-10-893-2014

Legeais, J.-F., Ablain, M., Zawadzki, L., Zuo, H., Johannessen, J. A., Scharffenberg, M. G., et al. (2018). An improved and homogeneous altimeter sea level record from the ESA Climate Change Initiative. *Earth Syst. Sci. Data* 10, 281–301. doi: 10.5194/essd-10-281-2018

Legeais, J.-F., Prandi, P., and Guinehut, S. (2016). Analyses of altimetry errors using Argo and GRACE data. *Ocean Sci.* 12, 647–662. doi: 10.5194/os-12-647-2016

Lievin, M., Kocha, C., Courcol, B., Philipps, S., Denis, I., Guinle, T., et al. (2020). *Reprocessing of Sea Level L2P Products for 28 Years of Altimetry Missions*. OSTST. Available online at: meetings.aviso.altimetry.fr/fileadmin//user_upload/tx_ausyclsseminar/files/OSTST2020_Reprocessing_L2P_2020.pdf (accessed Nov 04, 2020).

Loeb, N. G., Thorsen, T. J., Norris, J. R., Wang, H., and Su, W. (2018). Changes in Earth's energy budget during and after the "Pause" in global warming: an observational perspective. *Climate* 6:62. doi: 10.3390/cli6030062

Melet, A., Buontempo, C., Mattiuzzi, M., Salamon, P., Bahurel, P., Breyiannis, G., et al. (2021). European Copernicus services to inform on sea-level rise adaptation – current status and perspectives. In this research topic issue: climate services for adaptation to sea level rise. *Front. Mar. Sci.* 8:703425. doi: 10.3389/fmars.2021.703425

Mertikas, S. P., Donlon, C., Féménias, P., Mavrocordatos, C., Galanakis, D., Tripolitsiotis, A., et al. (2018). Fifteen years of Cal/Val service to reference altimetry missions: calibration of satellite altimetry at the permanent facilities in Gavdos and Crete, Greece. *Remote Sens.* 10:1557. doi: 10.3390/rs10101557

Meyssignac, B., Boyer, T., Zhao, Z., Hakuba, M. Z., Landerer, F. W., Stammer, D., et al. (2019). Measuring global ocean heat content to estimate the earth energy imbalance. *Front. Mar. Sci.* 6:432. doi: 10.3389/fmars.2019.00432

Meyssignac, B., Slangen, A. B. A., Melet, A., Church, J. A., Fettweis, X., Marzeion, B., et al. (2017). Evaluating model simulations of twentieth-century sea-level rise. Part II: regional sea-level changes. *J. Clim.* 30, 8565–8593. doi: 10.1175/JCLI-D-17-0112.1

Mitchum, G. T. (1998). Monitoring the stability of satellite altimeters with tide gauges. *J. Atmos. Ocean. Tech.* 15, 721–730.

Nerem, R. S., Beckley, B. D., Fasullo, J., Hamlington, B. D., Masters, D., and Mitchum, G. T. (2018). Climate change driven accelerated sea level rise detected in the altimeter era. *Proc. Natl. Acad. Sci. U.S.A.* 115, 2022–2025. doi: 10.1073/pnas.1717312115,2018

Ollivier, A., Faugere, Y., Picot, N., Ablain, M., Femenias, P., and Benveniste, J. (2012). Envisat ocean altimeter becoming relevant for mean sea level trend studies. *Mar. Geod.* 35 (Supp. 1), 118–136, doi: 10.1080/01490419.2012.721632.

Palanisamy, H., Meyssignac, B., Cazenave, A., and Delcroix, T. (2015). Is anthropogenic sea level fingerprint already detectable in the Pacific Ocean? *Environ. Res. Lett.* 10:8. doi: 10.1088/1748-9326/10/8/084024

Pascual, A., Faugere, Y., Larnicol, G., and Le Traon, P.-Y. (2006). Improved description of the ocean mesoscale variability by combining four satellite altimeters. *Geophys. Res. Lett.* 33, L02611. doi: 10.1029/2005GL024633

Pegliasco, C., Delepoulle, A., Morrow, R., Faugère, Y., and Dibarboure, G. (2021). META3.1exp : a new Global Mesoscale Eddy trajectories atlas derived from altimetry. *Earth. Syst. Sci. Data Discuss.* [preprint]. doi: 10.5194/essd-2021-300.

Peng, G., Wright, W., Baddour, O., Lief, C., and The SMM-CD Work Group (2019). The guidance booklet on the WMO-Wide Stewardship Maturity Matrix for Climate Data. *Figshare.* 1:1. doi: 10.6084/m9.figshare.7002482

Prandi, P., Meyssignac, B., Ablain, M., Spada, G., Ribes, A., and Benveniste, J. (2021). Local sea level trends, accelerations and uncertainties over 1993-2019. *Sci. Data* 8:1. doi: 10.1038/s41597-020-00786-7

Prandi, P., Valladeau, G., Ablain, M., Picot, N., and Desjonquères, J.-D. (2015). *Desjonquères: Accuracy of global Comparisons Between Altimetry and Tide Gauges*. OSTST. Available online at: meetings.aviso.altimetry.fr/fileadmin/user_upload/tx_ausyclsseminar/files/OSTST2015/SC1-03-Pres_OSTST2015_AltiTgComparisons_Prandi.pdf (accessed Nov 03, 2020).

Pujol, M.-I., Faugère, Y., Taburet, G., Dupuy, S., Pelloquin, C., Ablain, M., et al. (2016). DUACS DT2014: the new multi-mission altimeter data set reprocessed over 20 years. *Ocean Sci.* 12, 1067–1090. doi: 10.5194/os-12-1067-2016

Quartly, G. D., Legeais, J. F., Ablain, M., Zawadzki, L., Fernandes, M. J., Rudenko, S., et al. (2017). A new phase in the production of quality-controlled sea level data. *Earth Syst. Sci. Data* 9, 557–572. doi: 10.5194/essd-9-557-2017

Quartly, G. D., Nencioli, F., Raynal, M., Bonnefond, P., Nilo Garcia, P., Garcia-Mondéjar, A., et al. (2020). The roles of the S3MPC: monitoring, validation and evolution of sentinel-3 altimetry observations. *Remote Sens.* 12:1763. doi: 10.3390/rs12111763

SL_cci CECR (2016). *Comprehensive Error Characterisation Report, CLS-DOS-NT-13-100, SLCCI-ErrorReport-030*. Available online at: https://climate.esa.int/media/documents/SLCCI-ErrorReport-030-2-2.pdf (accessed Nov 04, 2020).

Taburet, G., Sanchez-Roman, A., Ballarotta, M., Pujol, M.-I., Legeais, J.-F., Fournier, F., et al. (2019). DUACS DT2018: 25 years of reprocessed sea level altimetry products. *Ocean Sci.* 15, 1207–1224. doi: 10.5194/os-15-1207-2019

The Climate Change Initiative Coastal Sea Level Team (2020). Coastal sea level anomalies and associated trends from Jason satellite altimetry over 2002–2018. *Sci. Data* 7:357. doi: 10.1038/s41597-020-00694-w

Thibaut, P., Piras, F., Roinard, H., Guerou, A., Boy, F., Maraldi, C., et al. (2021). "Benefits of the "Adaptive retracking solution" for the Jason-3 GDR-F reprocessing campaign," in *Proceedings of the 2021 IEEE International Geoscience and Remote Sensing Symposium IGARSS*, Brussels.

Thibaut, P., Roinard, H., Piras, F., Guerou, A., Bignalet-Cazalet, F., Dibarboure, G., et al. (2020). *Benefit of the Adaptive Retracker for Improving Jason-3 GMSL Estimations*. OSTST. Available online at: meetings.aviso.altimetry.fr/fileadmin//user_upload/tx_ausyclsseminar/files/Thibaut_Benefits_of_Adaptive_For_GMSL_01.pdf (accessed October, 2020).

Valladeau, G., Legeais, J. F., Ablain, M., Guinehut, S., and Picot, N. (2012). Comparing altimetry with tide gauges and argo profiling floats for data quality assessment and mean sea level studies. *Mar. Geod.* 35(Suppl. 1), 42–60. doi: 10.1080/01490419.2012.718226

von Schuckmann, K., Cheng, L., Palmer, M. D., Hansen, J., Tassone, C., Aich, V., et al. (2020). Heat stored in the Earth system: where does the energy go? *Earth Syst. Sci. Data* 12, 2013–2041. doi: 10.5194/essd-12-2013-2020

Watson, C., White, N., Church, J., Burgette, R., Tregoning, P., and Coleman, R. (2011). Absolute calibration in Bass Strait, Australia: TOPEX, Jason-1 and OSTM/Jason-2. *Mar. Geod.* 34, 242–260. doi: 10.1080/01490419.2011.584834

Watson, C. S., White, N. J., Church, J. A., King, M. A., Burgette, R. J., and Legresy, B. (2015). Unabated global mean sea-level rise over the satellite altimeter era. *Nat. Clim. Chang.* 5, 565–568. doi: 10.1038/NCLIMATE2635

WCRP Global Sea Level Budget Group. (2018). Global sea-level budget 1993–present. *Earth Syst. Sci. Data* 10, 1551–1590. doi: 10.5194/essd-10-1551-2018

Woodworth, P. L., Menéndez, M., and Roland Gehrels, W. (2011). Evidence for century-timescale acceleration in mean sea levels and for recent changes in extreme sea levels. *Surv. Geophys.* 32, 603–618. doi: 10.1007/s10712-011-9112-8

Wöppelmann, G., and Marcos, M. (2016). Vertical land motion as a key to understanding sea level change and variability. *Rev. Geophys.* 54, 64–92. doi: 10.1002/2015RG000502

Zawadzki, L., and Ablain, M. (2016). Accuracy of the mean sea level continuous record with future altimetric missions: Jason-3 vs. sentinel-3a. *Ocean Sci.* 12, 9–18. doi: 10.5194/os-12-9-2016

Conflict of Interest: The authors declare that the research was conducted in the absence of any commercial or financial relationships that could be construed as a potential conflict of interest.

Publisher's Note: All claims expressed in this article are solely those of the authors and do not necessarily represent those of their affiliated organizations, or those of the publisher, the editors and the reviewers. Any product that may be evaluated in this article, or claim that may be made by its manufacturer, is not guaranteed or endorsed by the publisher.

Copyright © 2021 Legeais, Meyssignac, Faugère, Guerou, Ablain, Pujol, Dufau and Dibarboure. This is an open-access article distributed under the terms of the Creative Commons Attribution License (CC BY). The use, distribution or reproduction in other forums is permitted, provided the original author(s) and the copyright owner(s) are credited and that the original publication in this journal is cited, in accordance with accepted academic practice. No use, distribution or reproduction is permitted which does not comply with these terms.

frontiers in Marine Science

ORIGINAL RESEARCH
published: 16 December 2021
doi: 10.3389/fmars.2021.620570

Local Sea-Level Rise Caused by Climate Change in the Northwest Pacific Marginal Seas Using Dynamical Downscaling

*Yong-Yub Kim[1], Bong-Gwan Kim[1], Kwang Young Jeong[2], Eunil Lee[2], Do-Seong Byun[2] and Yang-Ki Cho[1]**

[1] School of Earth and Environmental Sciences/Research Institute of Oceanography, Seoul National University, Seoul, Republic of Korea, [2] Ocean Research Division, Korea Hydrographic and Oceanographic Agency, Busan, Republic of Korea

Global climate models (GCMs) have limited capacity in simulating spatially non-uniform sea-level rise owing to their coarse resolutions and absence of tides in the marginal seas. Here, regional ocean climate models (RCMs) that consider tides were used to address these limitations in the Northwest Pacific marginal seas through dynamical downscaling. Four GCMs that drive the RCMs were selected based on a performance evaluation along the RCM boundaries, and the latter were validated by comparing historical results with observations. High-resolution (1/20°) RCMs were used to project non-uniform changes in the sea-level under intermediate (RCP 4.5) and high-end emissions (RCP 8.5) scenarios from 2006 to 2100. The predicted local sea-level rise was higher in the East/Japan Sea (EJS), where the currents and eddy motions were active. The tidal amplitude changes in response to sea-level rise were significant in the shallow areas of the Yellow Sea (YS). Dynamically downscaled simulations enabled the determination of practical sea-level rise (PSLR), including changes in tidal amplitude and natural variability. Under RCP 8.5 scenario, the maximum PSLR was ∼85 cm in the YS and East China Sea (ECS), and ∼78 cm in the EJS. The contribution of natural sea-level variability changes in the EJS was greater than that in the YS and ECS, whereas changes in the tidal contribution were higher in the YS and ECS. Accordingly, high-resolution RCMs provided spatially different PSLR estimates, indicating the importance of improving model resolution for local sea-level projections in marginal seas.

Keywords: sea level rise, climate change, Northwest Pacific marginal seas, numerical model, dynamical downscaling, tidal amplitude change

OPEN ACCESS

Edited by:
Roderik Van De Wal, Utrecht University, Netherlands

Reviewed by:
Tim Hermans, Royal Netherlands Institute for Sea Research (NIOZ), Netherlands
Jessie Louisor, Bureau de Recherches Géologiques et Minières, France

***Correspondence:**
Yang-Ki Cho
choyk@snu.ac.kr

Specialty section:
This article was submitted to Coastal Ocean Processes, a section of the journal Frontiers in Marine Science

Received: *23 October 2020*
Accepted: *29 November 2021*
Published: *16 December 2021*

Citation:
Kim Y-Y, Kim B-G, Jeong KY, Lee E, Byun D-S and Cho Y-K (2021) Local Sea-Level Rise Caused by Climate Change in the Northwest Pacific Marginal Seas Using Dynamical Downscaling. Front. Mar. Sci. 8:620570. doi: 10.3389/fmars.2021.620570

INTRODUCTION

Global mean sea-level has risen over past decades (WCRP Global Sea Level Budget Group, 2018), with a significant acceleration in sea-level rise [SLR; (Chen et al., 2017; Dangendorf et al., 2019)]. Satellite altimetry has revealed a $\sim 3.0 \pm 0.4$ mm·year^{-1} increase in global mean sea-level from 1993 to 2017 (Nerem et al., 2018). Accordingly, projected SLR and its effects on coastal zones have garnered the attention of the scientific community and public (Cazenave and Le Cozannet, 2014).

Sea-level rise, however, is not globally uniform, and local sea-level changes (SLCs) can substantially deviate from global averages due to different processes (Stammer et al., 2013). For example, dynamic SLCs driven by water density and currents are one primary cause of non-uniform SLR (Gregory et al., 2019). Changing ocean currents can result in the redistribution of mass, heat, and salt, resulting in substantial sea-level variability (Stammer et al., 2013). In particular, ocean temperatures are crucial for calculating thermosteric SLCs and dynamic sea-level distribution (Griffies et al., 2016).

Projections of SLCs by global climate models (GCMs) are available from the Coupled Model Intercomparison Project Phase 5 (CMIP5) database (Taylor et al., 2012). However, their coarse grid resolutions (∼100 km × 100 km) may not accurately predict eddy-scale variability in coastal regions (Jones et al., 1995; Grose et al., 2020). Furthermore, GCMs lack relevant local shelf processes controlling SLCs due to tides and buoyancy input from rivers. The water exchange between marginal seas and the open ocean is likely an essential factor for simulating accurate regional SLCs (Hermans et al., 2020); yet, the coarse resolution of GCMs confines this relationship to transport through straits (Seo et al., 2014a).

The Northwest Pacific (NWP) marginal seas have a complex topography and narrow straits (**Figure 1**). Accordingly, most coarse-resolution GCMs are incapable of resolving such complicated topographies, nor can they reproduce the currents of the NWP marginal seas. Previously, regional models with dynamical downscaling have been used to project local climate change in the NWP (Seo et al., 2014b; Liu et al., 2016; Sasaki et al., 2017; Jin et al., 2021; Nishikawa et al., 2021). For example, Seo et al. (2014b) assessed the predicted changes in ocean temperature, salinity, and circulation in the NWP marginal seas, whereas Liu et al. (2016) projected regional SLCs using dynamical downscaling with a regional model based on three GCMs. Sasaki et al. (2017) examined sea-level variability around Japan from 1906 to 2010 using a regional model with observational data and CMIP5 historical simulations. However, the local SLCs of the NWP marginal seas were beyond the scope of these previous studies. More recently, Jin et al. (2021) studied the SLC around China, but this study did not consider tidal influence.

The ability of sea-level rise to alter tidal regimes has been well documented (Pickering et al., 2012; Pelling and Green, 2014; Passeri et al., 2015; Idier et al., 2017), potentially intensifying extreme sea levels (Smith et al., 2010; Warner and Tissot, 2012; Arns et al., 2015). The effect of SLR on tidal amplitudes has also been investigated for the NWP marginal seas (Gao et al., 2008; Yan et al., 2010; Pelling et al., 2013; Zhang and Ge, 2013; Kuang et al., 2017), with larger changes observed in shallow coastal regions rather than deeper regions.

We defined practical sea-level rise (PSLR) here as the sum of relative sea-level rise, the change in tidal amplitude and the change in natural variability, as the evaluation of this parameter may help identify localities with more severe SLCs. More detailed future SLC projections can also help with local risk assessments, mitigation, and adaptation planning. In this study, local SLR was simulated according to increasing spatiotemporal resolutions of the downscaled regional model, and with the inclusion of tidal influences for the NWP marginal seas. Downscaled SLCs were projected using regional ocean climate models (RCMs) driven by four different GCMs. The data and model configuration used are introduced in Section 2, comparisons between GCMs and RCMs using historical data are presented in Section 3, the projections of SLCs by GCMs and RCMs under two climate change scenarios are discussed in Section 4, and conclusions are provided in Section 5.

DATA AND METHODS

Global Climate Models

Global climate models driven by observed greenhouse gas concentrations until 2005, and subsequently by intermediate

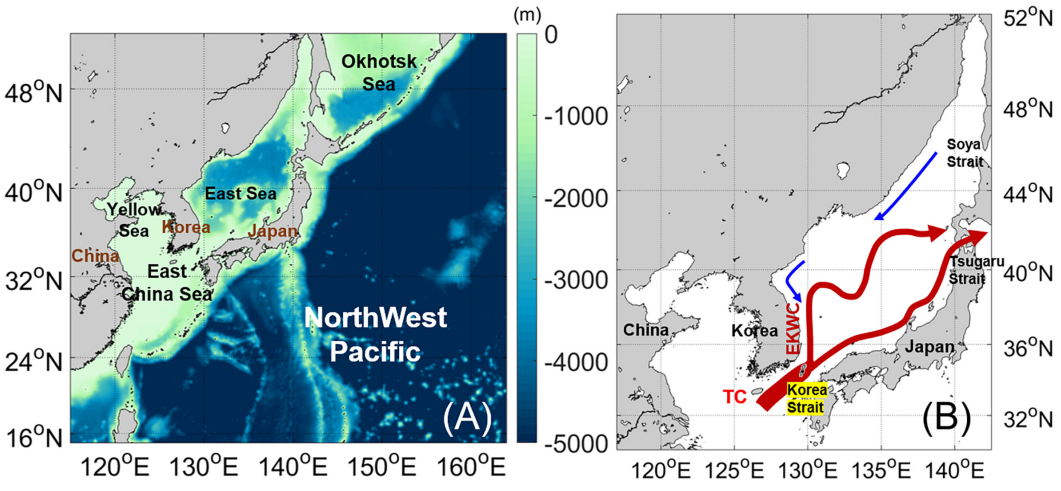

FIGURE 1 | (A) Bottom topography (unit: m) of the NWP in the RCM. **(B)** Main currents present in the study area: Tsushima Current (TC) and the East Korean Warm Current (EKWC).

(RCP 4.5) or high-end emissions (RCP 8.5) scenarios from 2006 to 2100, were selected for analysis (Church et al., 2013). All GCM simulations were acquired from the CMIP5 database (Taylor et al., 2012), and 13 of the 48 models available provided all oceanic and atmospheric variables required for deriving boundary values of the RCM.

Following performance evaluations of sea-level and sea surface temperature (SST) predictions based on observations from the NWP, four CMIP5 GCMs were selected for regional downscaling. The spatial mean sea surface heights (SSHs) along the lateral boundaries of the RCM from 1976 to 2005 were compared with reconstructed sea-level data created using cyclostationary empirical orthogonal functions derived from satellite altimetry and sea-level measurements from tidal gauges (Hamlington et al., 2011). Spatial mean SST along the lateral boundary grid was compared with a combination of the climatological mean from the World Ocean Atlas 2009 (WOA09) (Levitus et al., 2010) and anomaly data (Levitus et al., 2012). The corrected SSH (*zos_c*) was calculated for direct comparison with the reconstructed sea-level data according to Equation (1):

$$zos_c\,(x, y, t) \;=\; zos\,(x, y, t) - zos_m(t) \;+\; zostoga\,(t) \;+\; bary_sle(t) \tag{1}$$

where the SSH above the geoid (*zos*) is the dynamic sea-level reflecting fluctuations from the geoid (Griffies et al., 2014). The global mean SSH (*zos_m*) was removed from *zos* to exclude spurious model drift in each GCM. Global mean SLCs due to thermosteric effects (*zostoga*), and the correlated change in ocean mass (i.e., mass effect; *bary_sle*) were then added. Different values for the thermosteric sea-level were used depending on the GCM, and the mass effect on sea-level was calculated as the sum of the contributions from glaciers, ice sheets, and land water storage (Church et al., 2013). For all GCMs, annual mass effects were linearly interpolated to monthly. GCM model performance was evaluated in two ways: The performance index (*PI*) to evaluate GCMs can be defined according to Equations (2, 3):

$$PI_{SSH} = \frac{X_{SSH}/\overline{X_{SSH}} + E_{SSH}/\overline{E_{SSH}}}{2} \tag{2}$$

$$PI_{SSH\&SST} = \frac{X_{SSH}/\overline{X_{SSH}} + E_{SSH}/\overline{E_{SSH}} + X_{SST}/\overline{X_{SST}} + E_{SST}/\overline{E_{SST}}}{4} \tag{3}$$

where X is the root mean square error (RMSE) of the annual variables, and E is the absolute difference in trends between GCMs and observations. The overall RMSE and trends of SSH between GCMs and the observations were evaluated from the spatial mean along the lateral boundary (PI_{SSH}). The RMSE and trends of SSH and SST were also evaluated simultaneously ($PI_{SSH\&SST}$). The numbers of selected grids for calculating spatial mean along the lateral boundary were approximately 200 and 800 for the observations and GCMs, respectively.

Performance evaluation results are shown in **Table 1**. To select the most reasonable number of GCMs for dynamical downscaling, the *PI*s for each multi-model ensemble (*EPI*) were ranked by increasing ensemble size. Both EPI_{SSH} and $EPI_{SSH\&SST}$ were best with two ensemble members, as these values increased when ensemble size $\geq$ 3. Four GCMs were selected for our experiment. The top 2 models, IPSL-CM5A-LR and IPSL-CM5A-MR, were selected based on minimum EPI_{SSH}. NorESM1-M and MPI-ESM-LR which showed minimum $EPI_{SSH\&SST}$, were also selected. IPSL-CM5A-LR and IPSL-CM5A-MR have a coarser horizontal grid resolution (∼2.0°; Dufresne et al., 2013), whereas NorESM1-M and MPI-ESM-LR have resolutions of ∼1.1° and 1.5°, respectively. **Figure 2** shows topography of selected GCMs in the NWP.

TABLE 1 | GCMs results based on PI_{SSH} and $PI_{SSH\&SST}$ (see Equations 2, 3, respectively).

Model ID	PI_{SSH}	EPI_{SSH}	Model ID	$PI_{SSH\&SST}$	$EPI_{SSH\&SST}$
IPSL-CM5A-LR	*0.58*	*0.58*	*NorESM1-M*	*0.73*	*0.73*
IPSL-CM5A-MR	*0.66*	*0.39*	*MPI-ESM-LR*	*0.81*	*0.61*
MIROC-ESM-CHEM	0.74	0.47	CNRM-CM5	0.81	0.63
CNRM-CM5	0.77	0.52	CSIRO-Mk3-6-0	0.84	0.62
MPI-ESM-LR	0.78	0.47	CanESM2	0.87	0.65
CanESM2	0.81	0.51	IPSL-CM5A-MR	0.94	0.68
NorESM1-M	0.89	0.55	bcc-csm1-1-m	0.98	0.67
CSIRO-Mk3-6-0	1.12	0.58	MPI-ESM-MR	1.00	0.69
bcc-csm1-1-m	1.18	0.64	MIROC-ESM-CHEM	1.10	0.61
MRI-CGCM3	1.28	0.69	GFDL-ESM2G	1.14	0.65
GFDL-ESM2G	1.35	0.73	IPSL-CM5A-LR	1.15	0.67
MPI-ESM-MR	1.36	0.77	MIROC5	1.23	0.66
MIROC5	1.48	0.80	MRI-CGCM3	1.40	0.62

EPI_{SSH} and $EPI_{SSH\&SST}$ represent the performance index (PI) of the multi-model ensemble according to increasing the ensemble size from the best (lowest PI) to worst models (highest PI). The four top performing models employed for all further analyses are italicized.

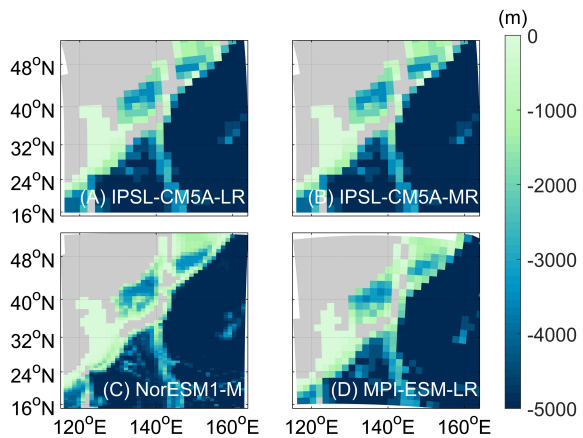

FIGURE 2 | Bottom topography (unit: m) of: **(A)** IPSL-CM5A-LR (GCM-IPSL-L), **(B)** IPSL-CM5A-MR (GCM-IPSL-M), **(C)** NorESM1-M (GCM-Nor), and **(D)** MPI-ESM-LR (GCM-MPI) with gray land mask.

Regional Ocean Climate Models

The Regional Ocean Modeling System (ROMS) was employed to downscale and project long-term SLCs in the NWP marginal seas (Shchepetkin and McWilliams, 2005). The ROMS has a free-surface and uses a Boussinesq approximation. This model uses

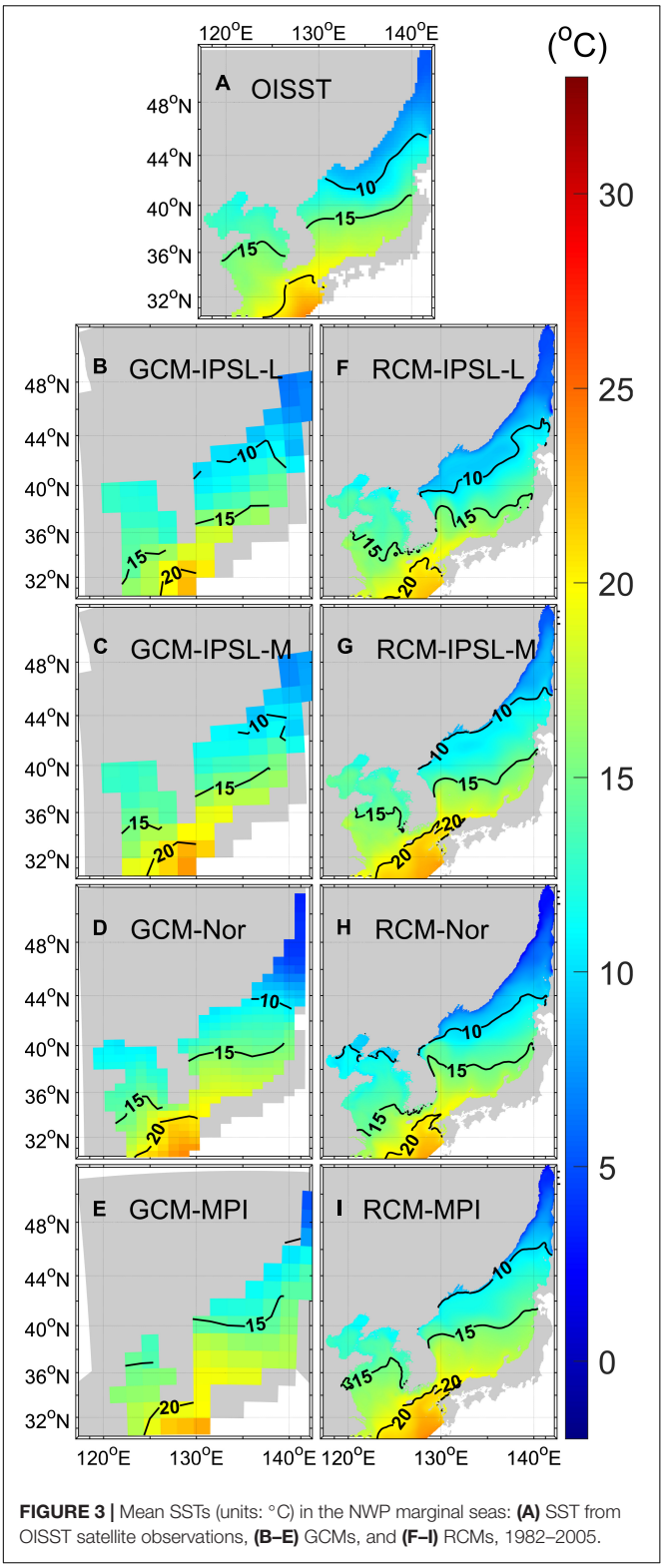

FIGURE 3 | Mean SSTs (units: °C) in the NWP marginal seas: **(A)** SST from OISST satellite observations, **(B–E)** GCMs, and **(F–I)** RCMs, 1982–2005.

the hydrostatic primitive equation, and is discretized based on the Arakawa-C staggered grid in the horizontal direction. The RCM domain (15°–52° N, 115°–164° E) covered the NWP and its marginal seas (**Figure 1A**), with a horizontal grid size of 1/20°. In the vertical direction, 40 layers were applied according to the scheme of Song and Haidvogel (1994), and resolution varied according to topography, increasing in shallower marginal seas. The employed scheme minimized the pressure gradient error at the slope. The RCM was initialized with temperature and salinity data from the World Ocean Atlas 1998 (WOA98) (Antonov et al., 1998; Boyer et al., 1998), and included a spin-up period of 10 years, beginning with the initial conditions in 1976. Subsequently, the RCMs were continuously simulated from 1976 to 2100.

Daily mean atmospheric surface variables of GCMs, such as mean sea-level pressure, 10-m wind, 2-m air temperature, specific humidity, and shortwave radiation were used for surface forcing. A bulk formula was employed to calculate surface heat flux (Fairall et al., 2003), and monthly GCM temperature, salinity, sea-level, and velocities were applied to the ocean lateral boundary in the RCMs. Chapman conditions were adopted for the sea-level (Chapman, 1985), Flather radiation conditions for barotropic velocities (Flather, 1976), and clamped (Dirichlet) conditions for baroclinic velocities, ocean temperature, and salinity. Chapman and Flather conditions allow surface gravity waves generated within the model domain to propagate out through the open boundary with minimal impedance or reflection, while simultaneously imposing tidal sea-levels and currents from the GCMs to the RCMs (Solano et al., 2020). Clamped conditions were applied for all other variables to directly reflect the oceanic forcing of GCMs. All monthly variables were linearly interpolated at every model time step, and applied to the lateral boundaries. RCM sea-levels increased over time to mimic the SLR at the lateral boundary by incorporating the corrected SSH (*zos_c*).

Tides were included at the oceanic lateral boundary using 10 tidal components (M_2, S_2, N_2, K_2, K_1, O_1, P_1, Q_1, M_f, M_m) provided by the TPXO7 ocean tide model (Egbert and Erofeeva, 2002). Tidal amplitudes and phases at the boundary were assumed to be constant for historical simulations and future projections, as changes in the tides caused by SLR are comparatively small along the boundary of the RCM in the open ocean (Pickering et al., 2017). Monthly freshwater discharge data from the Yangtze was used for historical simulations. The mean discharge across the historical period for each river was used for future projections. We used the climate monthly mean data from the Global River Discharge Database (Vörösmarty et al., 1996) for eleven other rivers around the Yellow Sea (YS) and Bohai Sea for both historical simulation and future projection. Topography

TABLE 2 | The root mean square error (RMSE; units: °C) between the satellite-derived SST and modeled SST in the shallow (YS-ECS) and deep seas (EJS).

Model ID (Region)	GCM (YS-ECS)	RCM (YS-ECS)	GCM ('EJS)	RCM (EJS)
IPSL-L	2.93	2.74	3.13	3.25
IPSL-M	2.48	2.57	2.72	2.83
Nor	2.66	2.63	3.28	2.58
MPI	2.17	2.17	3.47	2.89
Mean	2.56	2.53	3.15	2.89

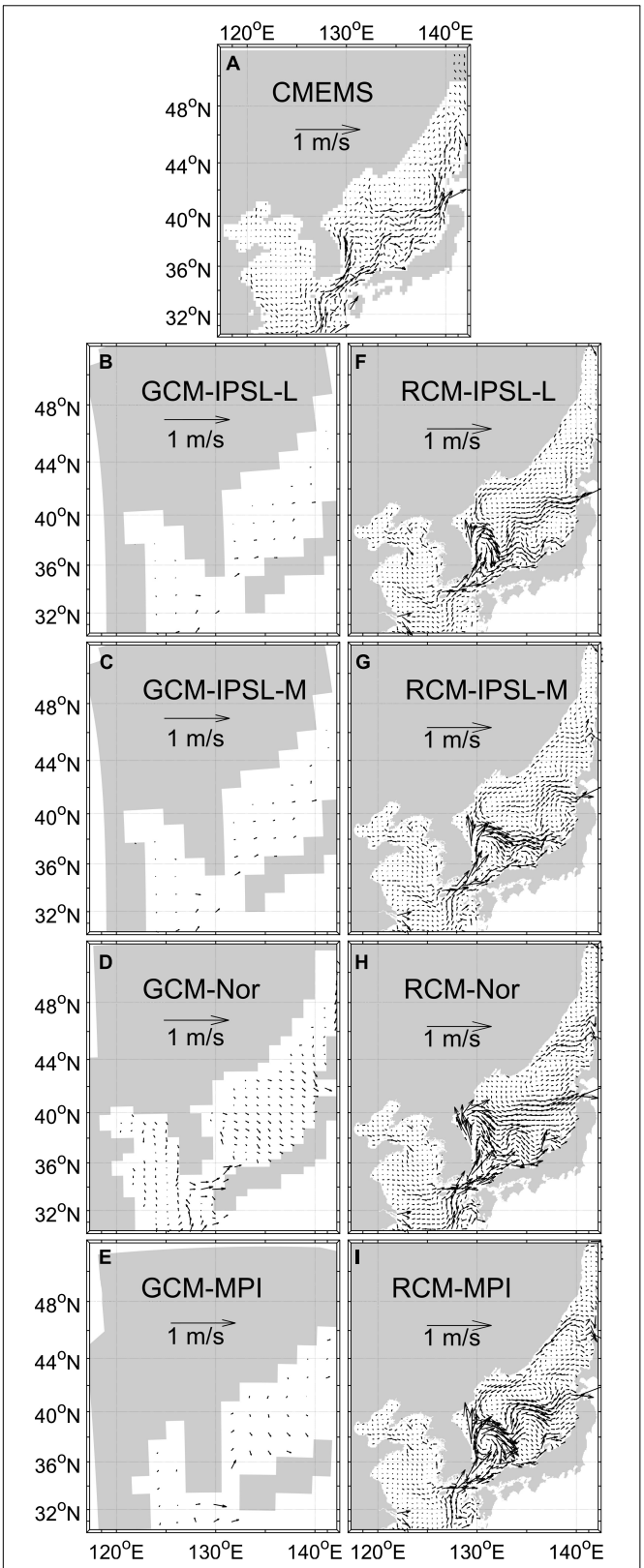

FIGURE 4 | Mean surface currents in the NWP marginal seas: **(A)** Satellite-derived geostrophic current from CMEMS, and mean surface currents of panels **(B–E)** GCMs and **(F–I)** RCMs, 1993–2005.

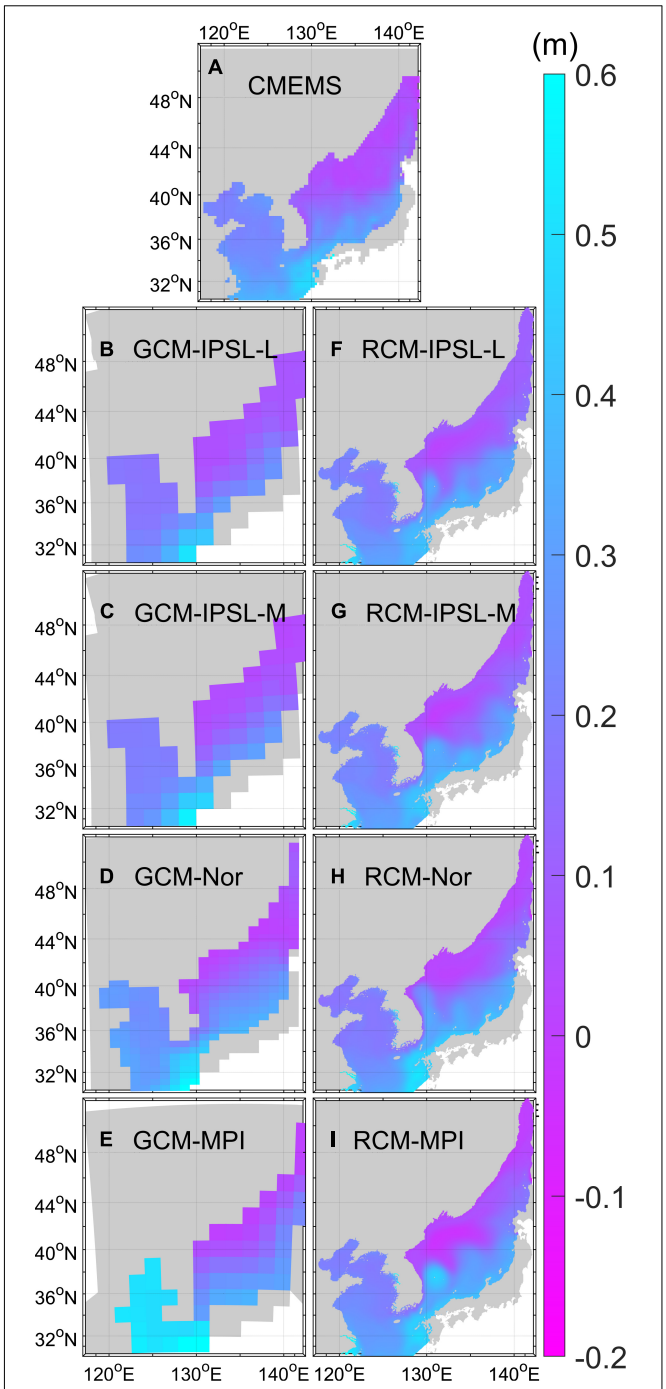

FIGURE 5 | Horizontal distribution of the mean sea-level (unit: m) in the NWP marginal seas: **(A)** Mean sea-level calculated from CMEMS absolute dynamic topography, and those of the **(B–E)** GCMs and **(F–I)** RCMs, 1993–2005.

data were obtained from the Earth Topography 1 arc minute (ETOPO1) dataset and interpolated into the RCM grid points (Amante and Eakins, 2009).

For clarity, the simulations of IPSL-CM5A-LR, IPSL-CM5A-MR, NorESM1-M, and MPI-ESM-LR are hereafter referred to as GCM-IPSL-L, GCM-IPSL-M, GCM-Nor, and GCM-MPI,

respectively; whereas the respective downscaled simulations from the RCM are referred to as RCM-IPSL-L, RCM-IPSL-M, RCM-Nor, and RCM-MPI.

HISTORICAL SIMULATIONS

Surface Temperature

Sea surface temperature is a fundamental indicator of climate change and has a significant correlation with thermal expansion and steric SLC (Casey and Adamec, 2002). Accordingly, SST has increased in the NWP as well (Levitus et al., 2000). GCM and RCM SSTs were compared with averaged satellite observations averaged from 1982 to 2005 (**Figure 3**). The optimum interpolation sea surface temperature (OISST), which uses satellite SST data from the Advanced Very High-Resolution Radiometer (Reynolds et al., 2007), was employed to compare with model simulations. **Figure 3A** shows the satellite-based SST observations for the NWP marginal seas. The Kuroshio supplies warm water (>20°C) to the East China Sea (ECS). The Tsushima Current (TC), through the Korea Strait, separates into the nearshore branch along the Japanese coast and the East Korean Warm Current (EKWC) along the Korean coast. Surface temperatures > 15°C in the East/Japan Sea (EJS) were defined as the path of the TC and EKWC. The warm EKWC flows northward as a western boundary current along the Korean coast and separates from the coast at 37 ∼ 38° N. Surface temperatures in the EJS where the TC and EKWC supply heat is notably higher than the YS at the same latitude.

Latitudes of the 15 °C isotherms showed a large difference among the GCMs, but were more similar among the RCMs. The SSTs of GCM-IPSL-L and GCM-IPSL-M were underestimated in the TC and EKWC paths. The absence of the EKWC decreases the SST. The latitudes of the 10 °C isotherm in the EJS showed a large difference between both the GCMs and RCMs. The GCMs expressed spatial SST patterns correlating to different surface atmospheric forcing, whereas the 10°C isotherm latitudes in the RCMs were similar despite employing the different surface atmospheric forcing variables. The RMSE was improved in RCM-Nor and RCM-MPI because of a considerable improvement in the warm bias of the northern EJS. The average RMSE of the RCM in the EJS was 0.26°C lower than that of the GCM (**Table 2**). Further, only RCM-IPSL-L and RCM-Nor showed improvements in modeling the YS and ECS (YS-ECS), where spatial SST differences were relatively small (**Table 2**).

Surface Current

Dynamic sea-levels are closely related to oceanic currents (Couldrey et al., 2021); thus, the surface currents of GCMs and RCMs were compared with satellite-derived surface geostrophic currents averaged across 1993–2005 (**Figure 4**). The geostrophic currents calculated using altimeter data from the Copernicus Marine Environment Monitoring Service (CMEMS) were used for comparison. **Figure 4A** shows the satellite-derived currents in the NWP marginal seas, and pattern correlation coefficients (PCCs) were calculated for the geostrophic velocities in the YS and ECS (**Supplementary Table 1**). GCM-Nor (**Figure 4D**) most closely resembled the observed coastal currents, while GCM-IPSL-L (**Figure 4B**) and GCM-IPSL-M (**Figure 4C**) performed worse. All RCMs yielded improved PCCs, especially

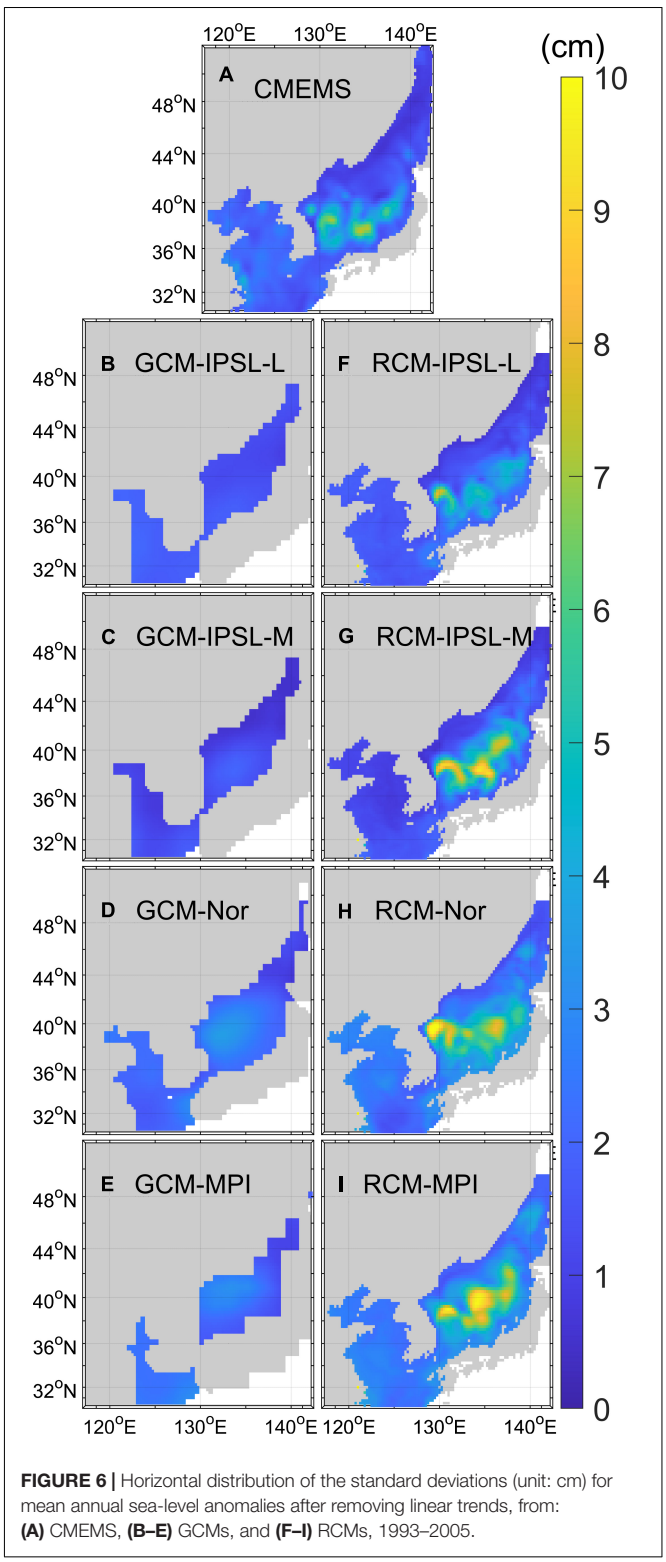

FIGURE 6 | Horizontal distribution of the standard deviations (unit: cm) for mean annual sea-level anomalies after removing linear trends, from: **(A)** CMEMS, **(B–E)** GCMs, and **(F–I)** RCMs, 1993–2005.

in RCM-IPSL-L and RCM-IPSL-M, where the mean value across all RCMs (0.49) was 0.30 greater than that of GCMs (0.19).

GCM-IPSL-L and GCM-IPSL-M, which have the coarser resolutions, did not effectively resolve the TC and EKWC (Hogan and Hurlburt, 2000) in the EJS, whereas the RCMs were able to simulate the paths of these currents distinctly. The PCCs in the EJS supported a distinct difference between the GCMs and RCMs (**Supplementary Table 2**). GCM-IPSL-L and GCM-IPSL-M showed negative PCCs of northward velocities, as they were unable to simulate the currents' detailed structure (including the EKWC in the EJS). Conversely, the PCCs of RCM-IPSL-L and RCM-IPSL-M increased by 0.26 and 0.31, respectively. Specifically, the RCMs simulated the northeastward TC along the Japanese coast and the northward EKWC along the Korean coast (**Figures 4F–I**). However, the separation latitudes of the EKWC varied among the RCMs. RCM-Nor shows the northernmost separation latitude among the RCMs because of the overshooting EKWC (**Figure 4H**).

Sea Surface Height

The SSHs from each model simulation were compared with satellite-derived observations provided by the CMEMS (**Figure 5**). The observational SSH products computed using sea-level anomaly and mean dynamic topography data were averaged for 1993–2005, and the modeled SSH values were similarly averaged across the same period. Sea-level observations were higher in the southeastern area where the Kuroshio passes and lower in the YS (**Figure 5A**). All RCMs had high PCCs (0.97) with the CMEMS for horizontal sea-level distributions in the YS-ECS (**Supplementary Table 3**), whereas the mean PCC of the GCMs (0.88) was lower. The PCC of GCM-MPI was the lowest due to the high sea-level in the YS (**Figure 5E**). The oversimplified topography of the GCM-MPI (**Figure 2D**), which fails to resolve the Taiwan Strait and allocates a single cell to the Korea Strait, may be causing a weak circulation and high sea-level in the YS-ECS, as these estimates were improved with the more accurate topographic conditions of the RCMs.

Satellite-derived SSHs in the EJS were higher in the southern warm waters along the paths of the TC and EKWC, and lower in the northern cold-waters (**Figure 5A**). GCM-IPSL-L and GCM-IPSL-M showed similar SSH distributions, and could not resolve the higher SSHs in the EKWC path (**Figures 5B,C**), resulting in relatively low PCCs of 0.76 and 0.85 in the EJS, respectively (**Supplementary Table 3**). Conversely, all RCMs captured the high SSHs in the path of the EKWC (**Figures 5F–I**), yielding slightly improved PCCs over GCMs. RCM-Nor maintained the best performance in the EJS (0.93), whereas RCM-IPSL-M and RCM-MPI PCCs (0.82 and 0.80) were slightly lower than GCM-IPSL-M and GCM-MPI (0.85 and 0.92). The low PCCs of two RCMs occur in the northern EJS.

Comparisons of sea-level variability between the model and the observation highlighted the differences between the GCMs and RCMs (**Figure 6**). Interannual sea-level variability was defined here as the standard deviation after annual signals and linear trends from 1993 to 2005 had been removed. Satellite-derived SSHs showed large variations (>5 cm) in the warm water region of the EJS likely due to the strong currents and active eddy motions, whereas weak variations (<2 cm) were observed in the northern cold-water region. The calculated variabilities in the YS-ECS were between 1 and 5 cm. Further, only the RCMs were able to resolve the spatial differences in the variability of the EJS. The satellite-based sea-level variation in the EKWC (near 38° N, 131° E) was 5.47 cm, notably more similar to those recorded in the RCMs (5.78 cm) compared to the GCMs (2.00 cm).

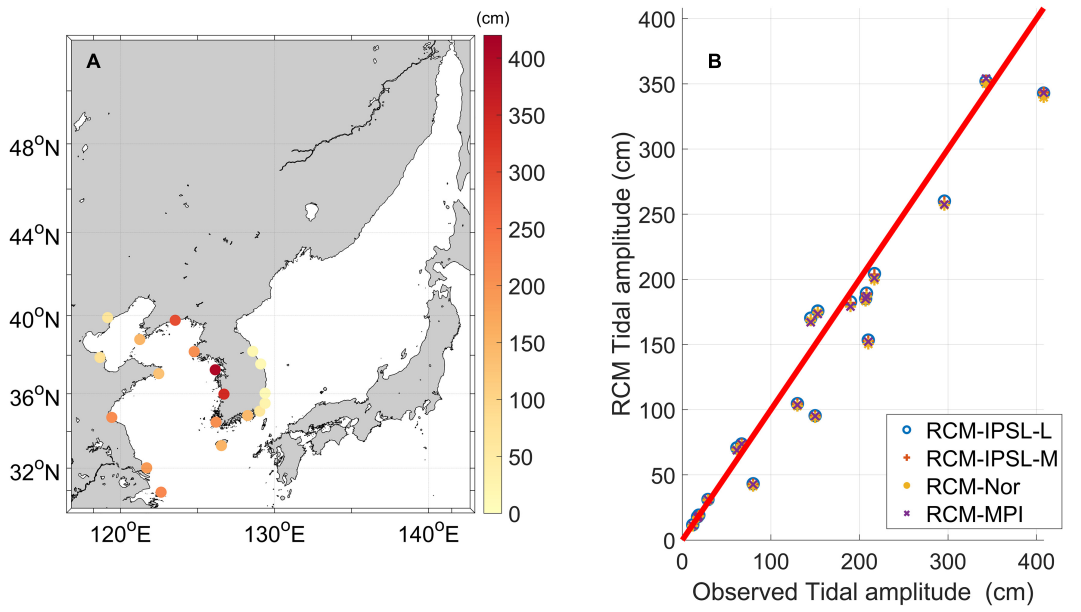

FIGURE 7 | (A) Sum of the amplitudes (unit: cm) for four major tidal constituents (M_2, S_2, K_1, and O_1) at the observation station from Choi (1980). Point colors represent the tidal amplitude at the station. **(B)** Comparison of observed and 2005 RCM tidal amplitudes.

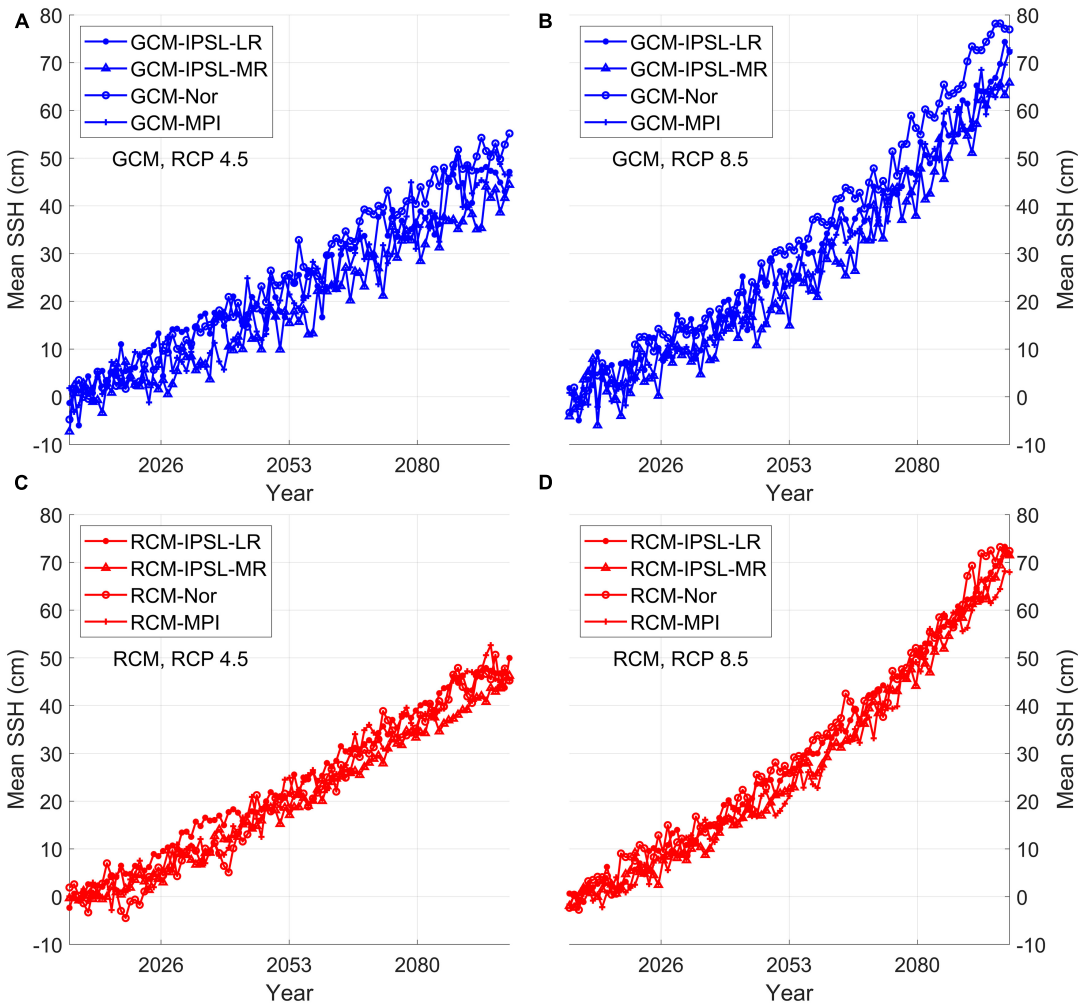

FIGURE 8 | Timeseries of sea-level changes (unit: cm) from 2006 to 2100, for two representative concentration pathway (RCP) scenarios: **(A)** GCMs—RCP 4.5, **(B)** GCMs—RCP 8.5, **(C)** RCMs—RCP 4.5, and **(D)** RCMs—RCP 8.5.

To validate the tidal simulations, the sums of the modeled amplitudes for four major tidal components (M_2, S_2, O_1, and K_1) were compared between the RCMs and the observations at 14 selected points along the YS (Choi, 1980), in addition to 5 tidal stations operated by the Korea Hydrographic and Oceanographic Administration (KHOA) in the EJS. The observed sum of the tidal amplitudes was large (>3 m) along the Korean coast in the YS, but only < 0.5 m in the EJS (**Figure 7A**). The spatial distribution of the simulated tidal amplitudes in 2005 was comparable to the observations, yielding correlation coefficients of 0.97 for all RCMs (**Figure 7B**), with an average absolute error of 0.15 m.

PROJECTIONS FOR THE 21ST CENTURY

Projection of Sea-Level Changes

Timeseries of the mean annual data showed the projected SLR according to the warming signal under future climate scenarios for both the GCMs and RCMs (**Figure 8**). The data represent the spatial means of the NWP marginal seas (**Figure 1B**). In addition to the gradual increase due to the warming signal, annual mean sea-level also showed the interannual variation due to the internal natural variability and external variation from the lateral boundary sea-level. The mean correlation coefficient values between the sea-levels of GCMs and RCMs in the NWP were both 0.99 under RCP 4.5 and 8.5 scenarios, respectively. The direct response of RCMs to the sea-level change of GCMs forced at the lateral boundary might result in this high correlation. The ensemble mean SLR estimates of the RCMs from 2081–2100 relative to that in 1976–2005 for RCP 4.5 and 8.5 scenarios in the NWP marginal seas were 46 and 65 cm, respectively. The ensemble spreads of annual sea-levels among the GCMs were 4.3 and 4.5 cm under RCP 4.5 and RCP 8.5 scenarios, respectively, whereas those of the RCMs were 2.6 under both scenarios.

Figure 9 shows the projected mean SLR between 1986–2005 and 2081–2100. The coarse resolution GCMs could not simulate SLR near the coastal area, and the mean SLR for the highest

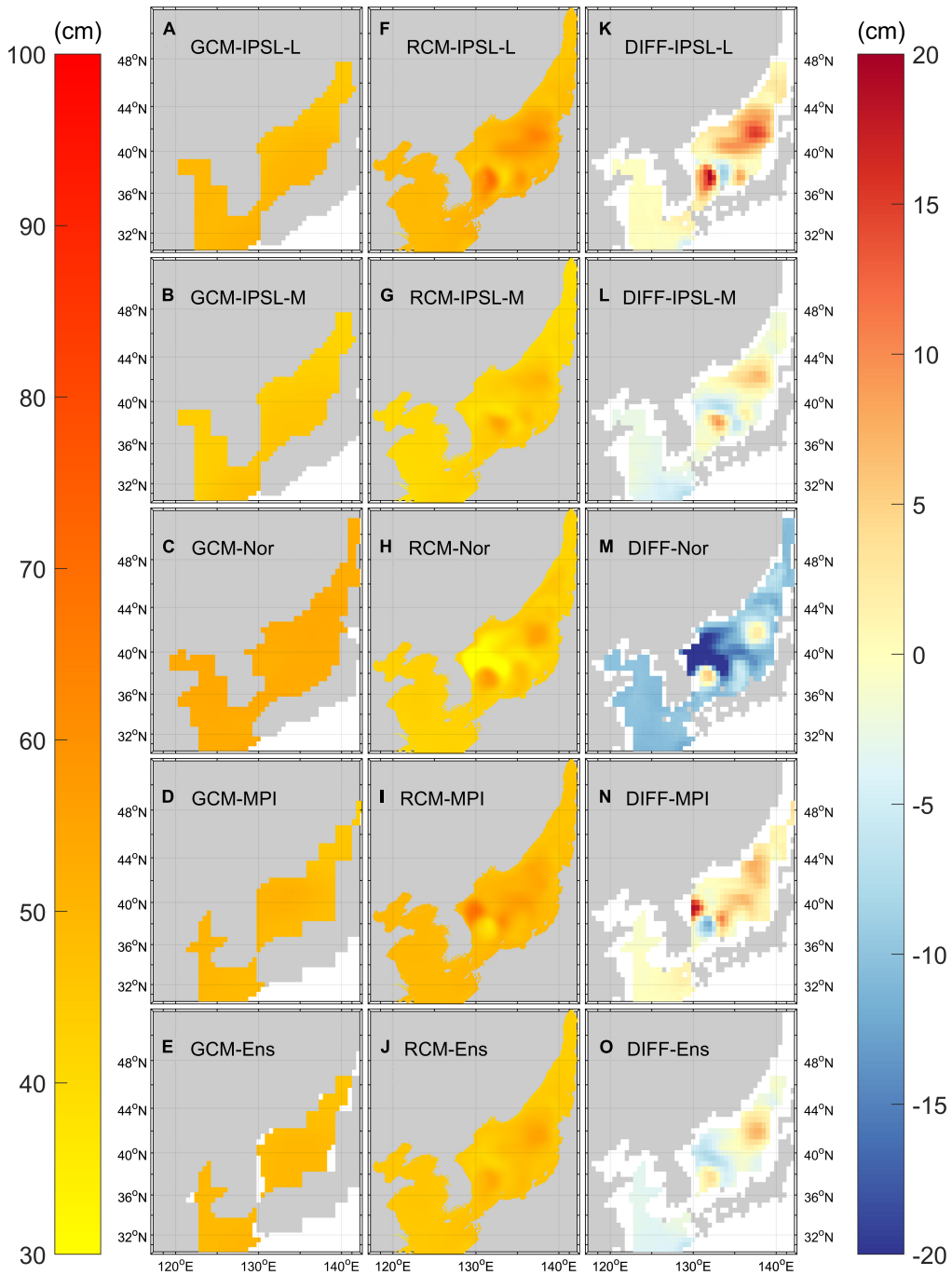

FIGURE 9 | Sea-level rise (unit: cm) between 1986–2005 and 2081–2100 in the NWP marginal seas under RCP 4.5 scenario according to panels **(A–D)** GCMs, and **(F–I)** RCMs. **(E)** and **(J)** represent the ensemble means of the GCMs and RCMs, respectively. Differences between the two modeling methods (RCM-GCM) are shown in panels **(K–O)**.

(GCM-Nor) and lowest models (RCM-IPSL-M) were 53.3 cm and 41.4 cm, respectively (**Table 3**). The RCMs showed relatively high SLR in the paths of the EKWC (near 38°N, 131°E) and TC (near 42°N, 138°E) where non-seasonal variations of the SSH are predominant (Choi et al., 2004). The maximum spatial differences in the SLR of the EJS were 5.5, 4.4, 2.0, and 9.6 cm for GCM-IPSL-L, GCM-IPSL-M, GCM-Nor, and GCM-MPI, respectively, whereas those for RCM-IPSL-LR, RCM-IPSL-MR, RCM-Nor, and RCM-MPI were 29.1, 17.8, 39.6, and 31.4 cm, respectively. Further, these spatial differences in SLR were three times higher than the maximum natural variability observed throughout the historical period (**Figure 6**). High SLR in the

TABLE 3 | Sea-level rise (SLR; unit: cm) of GCMs and RCMs between 1986–2005 and 2081–2100 (**Figures 9**, **10**) in the shallow (YS-ECS) and deep seas (EJS), under RCP 4.5 and RCP 8.5 scenarios.

Model ID	GCM-RCP4.5 (YS-ECS)	RCM-RCP4.5 (YS-ECS)	GCM-RCP4.5 (EJS)	RCM-RCP4.5 (EJS)	GCM-RCP8.5 (YS-ECS)	RCM-RCP8.5 (YS-ECS)	GCM-RCP8.5 (EJS)	RCM-RCP8.5 (EJS)
IPSL-L	50	49	48	51	63	63	62	65
IPSL-M	45	41	44	43	64	61	64	65
Nor	53	43	53	42	72	66	70	66
MPI	50	49	49	50	66	66	66	67
Mean	50	46	49	47	66	64	66	66

EJS is related to sea-level variations caused by the north-south migration of the polar front, meandering of the EKWC and TC, and active motions of the semi-permanent Ulleung Warm Eddy (Choi et al., 2004; Hogan and Hurlburt, 2006), none of which could be resolved in the coarse resolution GCMs.

We calculated the local steric SLC (**Supplementary Figure 1**) following Griffies et al. (2016), and subsequently the manometric SLCs (**Supplementary Figure 2**) by subtracting steric SLC from SLR. The steric SLCs were high in the deep regions, and lower in the shallow locations. However, the inverse patterns were observed for manometric SLC. These dependences of the local steric and manometric SLC patterns on water depth are consistent with those reported in the Northwestern European shelf seas (Hermans et al., 2020). The mean steric SLC differences between GCMs and RCMs were 4.19 and 15.00 cm in the YS-ECS and EJS, respectively.

The projected SLRs under RCP 8.5 were predictably higher than those under RCP 4.5 (**Figure 10**), reaching its maximum in GCM-Nor (71.6 cm), and minimum in GCM-IPSL-L (63.3 cm) for the YS-ECS (**Table 3**). Higher levels of SLR appeared along the EKWC and TC paths as in RCP 4.5 scenario models. The spatial differences in SLR for the EJS ranged from 5.9 to 13.9 cm (GCM-Nor–GCM-MPI). The differences between RCMs were larger than that of GCMs (39.3, 24.1, 34.4, and 38.4 cm for RCM-IPSL-LR, RCM-IPSL-MR, RCM-Nor, and RCM-MPI, respectively).

Under RCP 8.5, steric (**Supplementary Figure 3**) and manometric SLC (**Supplementary Figure 4**) followed water depth (like RCP 4.5). The mean steric SLC difference between the GCMs and RCMs was 4.48 and 16.26 cm in the YS-ECS and EJS, respectively. RCM-Nor showed a slightly higher steric sea-level among the RCMs because of the smaller predicted temperature changes than other models in either RCP scenario.

Changes in Tidal Amplitude

The changes in the sum of the tidal amplitudes between 2006 and 2100 under RCP 4.5 and RCP 8.5 scenarios are shown in **Figure 11**. Four major constituents (M_2, S_2, K_1, and O_1) were selected for summation, revealing that the tidal amplitude increase in the shallow region was $>$ 5 cm under RCP 4.5, and $>$ 10 cm under RCP 8.5, comparable to the findings of Kuang et al. (2017) in the YS. Although the changes for all RCMs (**Supplementary Figure 5**) were calculated, only the ensemble mean in **Figure 11** is presented here, due to the overall similarity between the models. The horizontal mean standard deviations among the RCMs were 0.21 and 0.14 cm under RCP 4.5 and RCP 8.5 scenarios, respectively. The different tidal amplitude changes within the same scenario may result from the differences in SLR among the RCMs, as the increase of tidal amplitude was roughly proportional to the SLR. SLR increases tidal wave speed, leading to the movement of amphidromic points. However, the shift of these points is not a simple function of SLR, as its movement is two-dimensional, and the curvature of corange lines creates a complex response (Pickering et al., 2017). Thus, changes in tidal amplitude were not simply proportional to the SLR in the YS (Feng et al., 2015).

As tides are shallow-water ocean waves, tidal wave speed (c) can be approximated by Equation (4) if bottom friction is neglected:

$$c = \sqrt{gH} \tag{4}$$

where g is gravitational acceleration, and H is water depth. As tidal wave speed is positively correlated with depth, increasing sea-levels will cause tidal waves to propagate more quickly. At that time, wavelength ($\lambda = c \times T$) also increases with SLR, and displacement of the amphidromic point due to the increase in wavelength significantly affects tidal amplitude (Kuang et al., 2017), and thus the redistribution of tidal energy (Song et al., 2013; Feng et al., 2019).

The tidal amplitude changes for each major constituent (M_2, S_2, K_1, or O_1) are presented in **Supplementary Figures 6–9**. Amplitude changes were more remarkable in shallower waters under both RCP 4.5 and RCP 8.5 scenarios. Tidal amplitude changes in this study showed different patterns between diurnal and semidiurnal tidal constituents, expressing large differences in period and wavelength consistent with previous study in the YS (Feng et al., 2019).

Practical Sea-Level Rise

The projections indicated SLR under future climate scenarios. However, the PSLR may differ due to spatially non-uniform changes in natural variability and tidal amplitude. Accordingly, the estimation of PSLR may be beneficial and help inform local risk assessments of climate change.

Practical sea-level rise is defined as according to Equation (5):

$$PSLR = SLR + a_{tide} + \delta(\sigma_{SSH}) \tag{5}$$

where a_{tide} is the tidal amplitude change (**Supplementary Figure 5**), and $\delta(\sigma_{SSH})$ is the difference in natural sea-level variability between the future and the past [2081–2100 (minus) 1986–2005] after removing trends which are

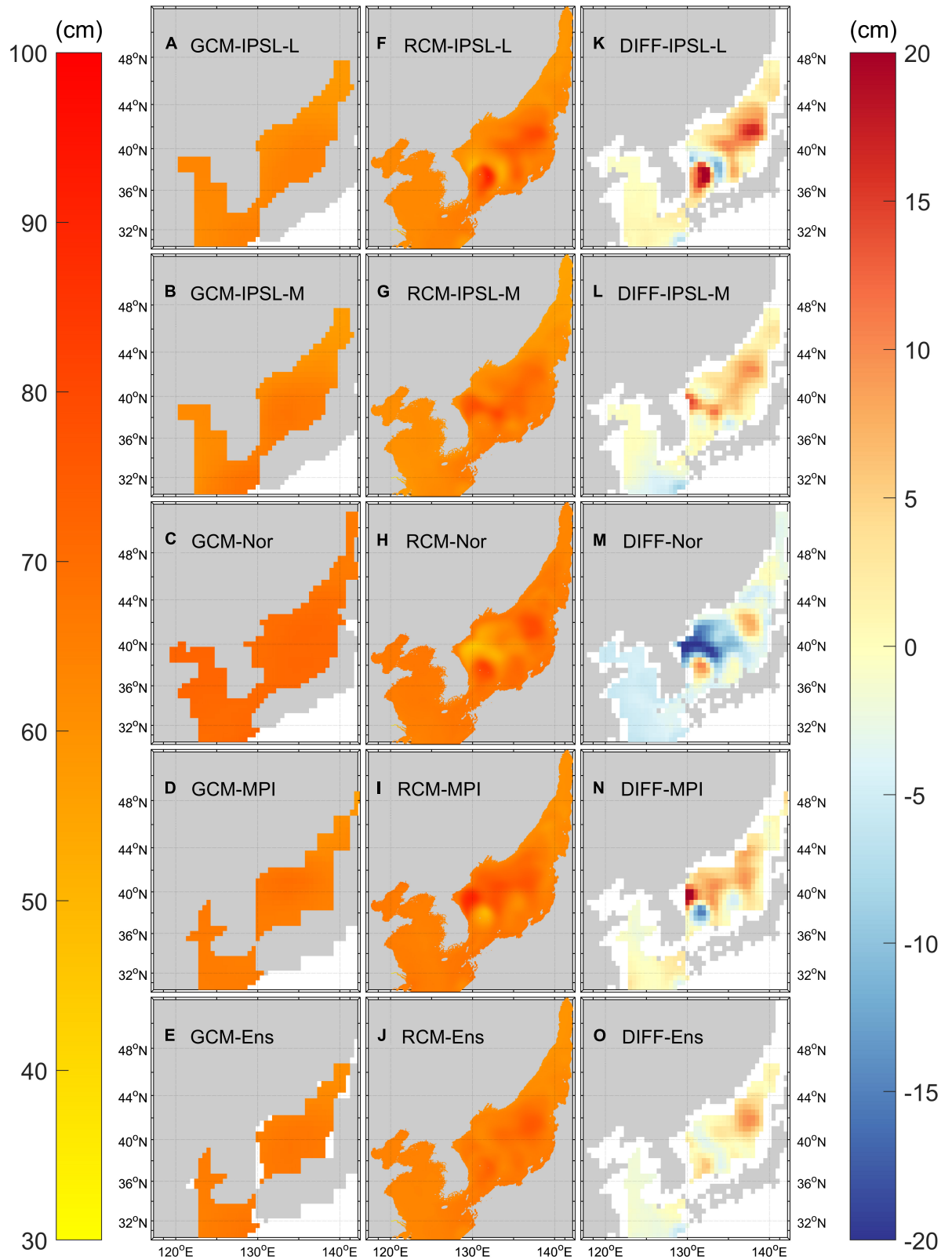

FIGURE 10 | Sea-level rise (unit: cm) between 1986–2005 and 2081–2100 in the NWP marginal seas under RCP 8.5 scenario according to panels **(A–D)** GCMs, and **(F–I)** RCMs. **(E)** and **(J)** represent the ensemble means of the GCMs and RCMs, respectively. Differences between the two modeling methods (RCM-GCM) are shown in panels **(K–O)**.

linear in the historical period and exponential in RCP scenarios (**Supplementary Figure 10**). The natural variability is represented by the standard deviation of annual mean sea-level anomalies during each period, and shows large changes (>5 cm) in the EKWC path. Mean spatial natural variability under RCP 8.5 was 1.14 cm greater than that during the historical period.

Although all calculated changes in the PSLR for all RCMs can be seen in **Supplementary Figure 11**, the ensemble mean is presented in **Figure 12**. Under RCP 8.5 (RCP 4.5), the PSLR was 66 (47) cm for the YS-ECS. Notably, PSLR reached its maximum in the Jiangsu coastal area [82 (58)] cm and the Gyeonggi Bays [83 (58)] cm near 32.8° N, 121.2° E and 37.3°N, 126.5°E, respectively, due to the increase in tidal amplitude. Furthermore, the PSLR was approximately 21 (13) cm higher than SLR in both regions. Other shallow regions with substantial tidal amplitude changes also displayed higher PSLR values than the surrounding areas.

The PSLR of the EJS was 67 (47) cm under RCP 8.5 (RCP 4.5) scenario, and the contributions of the natural sea-level variability changes in the EJS were higher than that in the YS-ECS, whereas tidal contributions were higher in the latter seas. The PSLR was

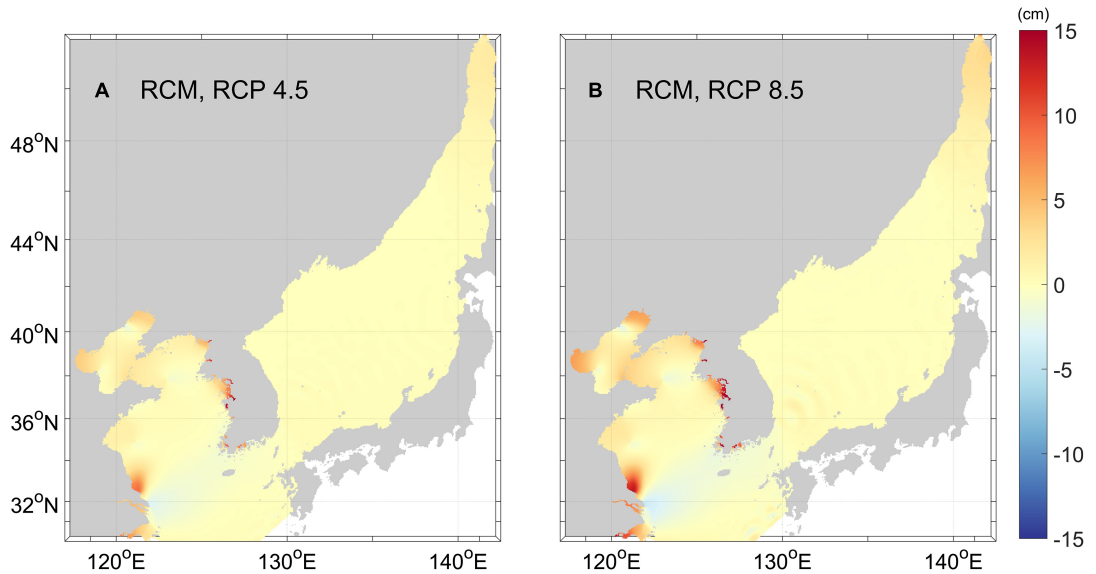

FIGURE 11 | Changes in the sum of the mean ensemble tidal amplitudes (unit: cm) for four major tidal constituents (M_2,S_2,K_1, and O_1) of the RCMs between 2006 and 2100, for: **(A)** RCP 4.5, and **(B)** RCP 8.5 scenarios.

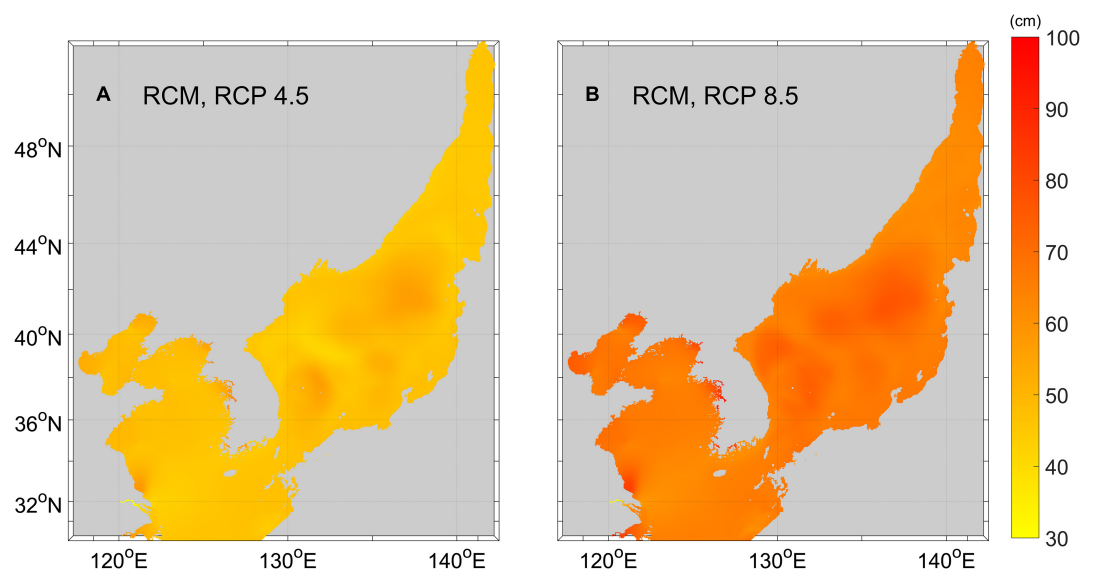

FIGURE 12 | Horizontal distributions of the practical sea-level rise (PSLR; unit: cm) for the RCMs between 1986–2005 and 2081–2100, under: **(A)** RCP 4.5 and **(B)** RCP 8.5 scenarios.

73 (46) cm near the EKWC path (near 39°N, 130°E), ∼5 (2) cm higher than SLR in the same region.

CONCLUSION AND DISCUSSION

In this study, we projected the SLR including barystatic and sterodynamic components considered in lateral boundary sea-level. The projected SLR and local PSLR in the NWP marginal seas were evaluated under intermediate and high-end climate change scenarios using dynamically downscaled RCMs. Climate change signals of the GCMs were directly applied at the lateral model boundaries, and the results showed significant predictive improvements in SST, currents, and SSH compared with coarser resolution GCMs. The high-resolution RCMs used in this study were able to resolve detailed currents and simulated PSLR, having considered changes in sea-level variability and tidal amplitude under two RCP scenarios.

The higher-resolution RCMs could resolve SLCs driven by eddy motions, capturing greater SLR in the EKWC and TC paths of the EJS resulting from strong currents and active eddy motions, whereas the GCMs maintained a limited ability to simulate spatially non-uniform SLR due to their coarse resolution. The RCMs also showed higher steric SLR in the deeper regions of the EJS, supporting the importance of resolving topographic features in SLR projections, as in other downscaled SLR projections (Hermans et al., 2020).

Tidal changes resulting from climate change were also examined using the RCMs, showing an increase in the tidal amplitude by > 15 cm in the shallow region of the YS, consistent with the results of Kuang et al. (2017). Moreover, tidal amplitude changes caused by different SLR values were simulated depending on the RCMs, where previous studies had assumed arbitrary SLR at the open boundary (Kuang et al., 2017; Feng et al., 2019; Jiang et al., 2021). The results suggested that the climate-induced changes in tidal amplitude conventionally missed by GCMs should be considered when estimating extreme sea levels for future coastal flood risk assessments in the marginal seas which is dominated by tides. Flood risks may increase due to the mean SLR, in addition to changes in the magnitude of extreme events, such as tides. Extreme sea level is also affected by storm surges, waves, and a combination of these processes (van de Wal et al., 2019). Besides that, the vertical ground motion may affect the local relative sea-level rise (Raucoules et al., 2013; Palanisamy Vadivel et al., 2021).

Practical sea-level rise, which is defined by the sum of the SLR, tidal amplitude changes, and natural variability changes, was proposed here to estimate the effective SLR. The PSLR suggested that the coastal areas where the tidal amplitude changes were largest in the YS-ECS were likely to be more vulnerable to the effects of SLR due to climate change under RCP scenarios. Dynamical downscaling was important for PSLR simulation in the NWP marginal seas containing a narrow strait, complex coastlines, and are affected primarily by tidal forcing. Most GCMs were unable to consider tidal forcing, and simulated low sea-level variability due to the limitations of capturing active eddy motions. Thus, GCM accuracy was limited when calculating PSLR in the NWP marginal seas. The RCMs resolved eddies, but may be limited in simulating the exact paths of the EKWC. Hogan and Hurlburt (2000) suggested a 1/16° resolution for the improved simulation of the EKWC path, and a 1/32° resolution for an accurate simulation of baroclinic instability along the EKWC. Accordingly, a higher-resolution model grid may further improve the results of RCMs in future studies. Higher-resolution topography provided recently by the General Bathymetric Chart of the Oceans (doi: 10.5285/c6612cbe-50b3-0cff-e053-6c86abc09f8f) may improve the model performance in the future simulation.

The downscaled RCMs more accurately simulated PSLR by resolving changes in local variability, and incorporating tidal changes not previously considered in GCMs. Thus, the PSLR may help decision-makers in planning for SLR and coastal flood management. The results also indicated the importance of improving model resolution for local sea-level projections in marginal seas, and providing PSLR for determining SLR vulnerability in coastal regions.

Only four GCMs were selected here based on a comparison of historical GCM results with the observations due to the limitations of computational resources and time. However, historical performance may not ensure future performance. Accordingly, more ensembles for downscaling may be desirable for improving local projections in future studies.

DATA AVAILABILITY STATEMENT

The original contributions presented in the study are included in the article/**Supplementary Material**, further inquiries can be directed to the corresponding author/s.

AUTHOR CONTRIBUTIONS

Y-YK and Y-KC: conceptualization. Y-YK and B-GK: methodology. Y-YK: writing draft and visualization. D-SB and Y-KC: review and editing. Y-KC: supervision. KJ and EL: project administration. All authors contributed to the article and approved the submitted version.

FUNDING

This research was a part of the project titled "Analysis and Prediction of Sea-Level Change in Response to Climate Change Around Korean Peninsula (5)" funded by the Korea Hydrographic and Oceanographic Agency (KHOA), and "Deep Water Circulation and Material Cycling in the East Sea (0425-20170025)" funded by the Ministry of Oceans and Fisheries, Republic of Korea.

SUPPLEMENTARY MATERIAL

The Supplementary Material for this article can be found online at: https://www.frontiersin.org/articles/10.3389/fmars.2021.620570/full#supplementary-material

REFERENCES

Amante, C., and Eakins, B. W. (2009). *ETOPO1 1 arc-minute global relief model: procedures, data sources and analysis". Technical Memorandum NESDIS NGDC-24. 19. National Geophysical Data Center*. Washington, DC: NOAA.

Antonov, J., Levitus, S., Boyer, T., Conkright, M., O'Brien, T., and Stephens, C. (1998). *World Ocean Atlas 1998 Vol. 2: temperature of the Pacific Ocean, NOAA Atlas NESDIS 28*. Washington, DC: US Government Printing Office.

Arns, A., Wahl, T., Dangendorf, S., and Jensen, J. J. C. E. (2015). The impact of sea level rise on storm surge water levels in the northern part of the German Bight. *Coast. Eng.* 96, 118–131.

Boyer, T., Levitus, S., Antonov, J., Conkright, M., O'Brien, T., and Stephens, C. (1998). *World Ocean Atlas 1998 Vol. 5: salinity of the Pacific Ocean, NOAA Atlas NESDIS 31*. Washington, DC: US Government Printing Office.

Casey, K. S., and Adamec, D. (2002). Sea surface temperature and sea surface height variability in the North Pacific Ocean from 1993 to 1999. *J. Geophys. Res. Oceans* 107, 14–11.

Cazenave, A., and Le Cozannet, G. (2014). Sea level rise and its coastal impacts. *Earths Future* 2, 15–34. doi: 10.1002/2013ef000188

Chapman, D. C. (1985). Numerical treatment of cross-shelf open boundaries in a barotropic coastal ocean model. *J. Phys. Oceanogr.* 15, 1060–1075. doi: 10.1175/1520-0485(1985)015<1060:ntocso>2.0.co;2

Chen, X., Zhang, X., Church, J. A., Watson, C. S., King, M. A., Monselesan, D., et al. (2017). The increasing rate of global mean sea-level rise during 1993–2014. *Nat. Clim. Chang.* 7, 492–495.

Choi, B. H. (1980). *A Tidal Model Of The Yellow Sea And The Eastern China Sea*. Seoul: Korea Ocean Research and Development Institute, 73.

Choi, B. J., Haidvogel, D. B., and Cho, Y. K. (2004). Nonseasonal sea level variations in the Japan/East Sea from satellite altimeter data. *J. Geophys. Res. Oceans* 109:C12028.

Church, J. A., Clark, P. U., Cazenave, A., Gregory, J. M., Jevrejeva, S., Levermann, A., et al. (2013). "Sea level change," in *Climate Change 2013: the Physical Science Basis. Contribution of Working Group I to the Fifth Assessment Report of the Intergovernmental Panel on Climate Change*, ed. T. F. Stocker (Cambridge: Cambridge University Press), 1137–1216.

Couldrey, M. P., Gregory, J. M., Dias, F. B., Dobrohotoff, P., Domingues, C. M., Garuba, O., et al. (2021). What causes the spread of model projections of ocean dynamic sea-level change in response to greenhouse gas forcing? *Clim. Dyn.* 56, 155–187.

Dangendorf, S., Hay, C., Calafat, F. M., Marcos, M., Piecuch, C. G., Berk, K., et al. (2019). Persistent acceleration in global sea-level rise since the 1960s. *Nat. Clim. Chang.* 9, 705–710. doi: 10.1038/s41558-019-0531-8

Dufresne, J.-L., Foujols, M.-A., Denvil, S., Caubel, A., Marti, O., Aumont, O., et al. (2013). Climate change projections using the IPSL-CM5 Earth System Model: from CMIP3 to CMIP5. *Clim. Dyn.* 40, 2123–2165.

Egbert, G. D., and Erofeeva, S. Y. (2002). Efficient inverse modeling of barotropic ocean tides. *J. Atmos. Ocean. Technol.* 19, 183–204. doi: 10.1175/1520-0426(2002)019<0183:eimobo>2.0.co;2

Fairall, C., Bradley, E. F., Hare, J., Grachev, A., and Edson, J. (2003). Bulk parameterization of air–sea fluxes: updates and verification for the COARE algorithm. *J. Clim.* 16, 571–591. doi: 10.1175/1520-0442(2003)016<0571:bpoasf>2.0.co;2

Feng, M., Hendon, H. H., Xie, S. P., Marshall, A. G., Schiller, A., Kosaka, Y., et al. (2015). Decadal increase in Ningaloo Niño since the late 1990s. *Geophys. Res. Lett.* 42, 104–112.

Feng, X., Feng, H., Li, H., Zhang, F., Feng, W., Zhang, W., et al. (2019). Tidal responses to future sea level trends on the Yellow Sea shelf. *J. Geophys. Res. Oceans* 124, 7285–7306. doi: 10.1029/2019jc015150

Flather, R. A. (1976). A tidal model of the north-west European continental shelf. *Mem. Soc. R. Sci. Liege* 10, 141–164.

Gao, Z., Han, S., Liu, K., Zhrng, Y., and Yu, H. (2008). Numerical Simulation of the Influence of Mean Sea Level Rise on Typhoon Storm Surge in the East China Sea. *Mar. Sci. Bull.* 10, 36–49.

Gregory, J. M., Griffies, S. M., Hughes, C. W., Lowe, J. A., Church, J. A., Fukimori, I., et al. (2019). Concepts and terminology for sea level: mean, variability and change, both local and global. *Surv. Geophys.* 40, 1251–1289. doi: 10.1007/s10712-019-09525-z

Griffies, S. M., Danabasoglu, G., Durack, P. J., Adcroft, A. J., Balaji, V., Böning, C. W., et al. (2016). OMIP contribution to CMIP6: experimental and diagnostic protocol for the physical component of the Ocean Model Intercomparison Project. *Geosci. Model Dev.* 9, 3231–3296.

Griffies, S. M., Yin, J., Durack, P. J., Goddard, P., Bates, S. C., Behrens, E., et al. (2014). An assessment of global and regional sea level for years 1993–2007 in a suite of interannual CORE-II simulations. *Ocean Model.* 78, 35–89.

Grose, M. R., Narsey, S., Delage, F., Dowdy, A. J., Bador, M., Boschat, G., et al. (2020). Insights from CMIP6 for Australia's future climate. *Earths Future* 8:e2019EF001469. doi: 10.1038/s41558-021-01173-9

Hamlington, B., Leben, R., Nerem, R., Han, W., and Kim, K. Y. (2011). Reconstructing sea level using cyclostationary empirical orthogonal functions. *J. Geophys. Res. Oceans* 116:C12015.

Hermans, T. H., Tinker, J., Palmer, M. D., Katsman, C. A., Vermeersen, B. L., and Slangen, A. B. (2020). Improving sea-level projections on the Northwestern European shelf using dynamical downscaling. *Clim. Dyn.* 54, 1987–2011. doi: 10.1007/s00382-019-05104-5

Hogan, P. J., and Hurlburt, H. E. (2000). Impact of upper ocean–topographical coupling and isopycnal outcropping in Japan/East Sea models with 1/8° to 1/64° resolution. *J. Phys. Oceanogr.* 30, 2535–2561.

Hogan, P. J., and Hurlburt, H. E. (2006). Why do intrathermocline eddies form in the Japan/East Sea? A modeling perspective. *Oceanography* 19, 134–143. doi: 10.5670/oceanog.2006.50

Idier, D., Paris, F., Le Cozannet, G., Boulahya, F., and Dumas, F. (2017). Sea-level rise impacts on the tides of the European Shelf. *Cont. Shelf Res.* 137, 56–71. doi: 10.1016/j.csr.2017.01.007

Jiang, C., Kang, Y., Qu, K., Kraatz, S., Deng, B., Zhao, E., et al. (2021). High-resolution numerical survey of potential sites for tidal energy extraction along coastline of China under sea-level-rise condition. *Ocean Eng.* 236:109492. doi: 10.1016/j.oceaneng.2021.109492

Jin, Y., Zhang, X., Church, J. A., and Bao, X. (2021). Projected sea-level changes in the marginal seas near China based on dynamical downscaling. *J. Clim.* 34, 7037–7055.

Jones, R., Murphy, J., and Noguer, M. (1995). Simulation of climate change over Europe using a nested regional-climate model. I: assessment of control climate, including sensitivity to location of lateral boundaries. *Q. J. R. Meteorol. Soc.* 121, 1413–1449.

Kuang, C., Liang, H., Mao, X., Karney, B., Gu, J., Huang, H., et al. (2017). Influence of potential future sea-level rise on tides in the China Sea. *J. Coast. Res.* 33, 105–117.

Levitus, S., Antonov, J. I., Boyer, T. P., Baranova, O. K., Garcia, H. E., Locarnini, R. A., et al. (2012). World ocean heat content and thermosteric sea level change (0–2000 m), 1955–2010. *Geophys. Res. Lett.* 39:L10603.

Levitus, S., Antonov, J. I., Boyer, T. P., and Stephens, C. (2000). Warming of the world ocean. *Science* 287, 2225–2229.

Levitus, S., Locarnini, R. A., Boyer, T. P., Mishonov, A. V., Antonov, J. I., Garcia, H. E., et al. (2010). *World ocean atlas 2009". NOAA atlas NESDIS*. Washington, DC: U.S. Government Printing Office.

Liu, Z.-J., Minobe, S., Sasaki, Y. N., and Terada, M. (2016). Dynamical downscaling of future sea level change in the western North Pacific using ROMS. *J. Oceanogr.* 72, 905–922. doi: 10.1007/s10872-016-0390-0

Nerem, R. S., Beckley, B. D., Fasullo, J. T., Hamlington, B. D., Masters, D., and Mitchum, G. T. (2018). Climate-change–driven accelerated sea-level rise detected in the altimeter era. *Proc. Natl. Acad. Sci. U. S. A.* 115, 2022–2025. doi: 10.1073/pnas.1717312115

Nishikawa, S., Wakamatsu, T., Ishizaki, H., Sakamoto, K., Tanaka, Y., Tsujino, H., et al. (2021). Development of high-resolution future ocean regional projection datasets for coastal applications in Japan. *Prog. Earth Planet. Sci.* 8, 1–22.

Palanisamy Vadivel, S. K., Kim, D.-J., Jung, J., Cho, Y.-K., and Han, K.-J. (2021). Monitoring the vertical land motion of tide gauges and its impact on relative sea level changes in Korean peninsula using sequential SBAS-InSAR time-series analysis. *Remote Sens.* 13:18. doi: 10.3390/rs13010018

Passeri, D. L., Hagen, S. C., Medeiros, S. C., and Bilskie, M. V. (2015). Impacts of historic morphology and sea level rise on tidal hydrodynamics in a microtidal estuary (Grand Bay, Mississippi). *Cont. Shelf Res.* 111, 150–158.

Pelling, H. E., and Green, J. M. (2014). Impact of flood defences and sea-level rise on the European Shelf tidal regime. *Cont. Shelf Res.* 85, 96–105. doi: 10.1016/j.csr.2014.04.011

Pelling, H. E., Green, J. M., and Ward, S. L. (2013). Modelling tides and sea-level rise: to flood or not to flood. *Ocean Model.* 63, 21–29. doi: 10.1016/j.ocemod.2012.12.004

Pickering, M., Horsburgh, K., Blundell, J., Hirschi, J.-M., Nicholls, R. J., Verlaan, M., et al. (2017). The impact of future sea-level rise on the global tides. *Cont. Shelf Res.* 142, 50–68. doi: 10.1016/j.csr.2017.02.004

Pickering, M., Wells, N., Horsburgh, K., and Green, J. (2012). The impact of future sea-level rise on the European Shelf tides. *Cont. Shelf Res.* 35, 1–15.

Raucoules, D., Le Cozannet, G., Wöppelmann, G., De Michele, M., Gravelle, M., Daag, A., et al. (2013). High nonlinear urban ground motion in Manila (Philippines) from 1993 to 2010 observed by DInSAR: implications for sea-level measurement. *Remote Sens. Environ.* 139, 386–397. doi: 10.1016/j.rse.2013.08.021

Reynolds, R. W., Smith, T. M., Liu, C., Chelton, D. B., Casey, K. S., and Schlax, M. G. (2007). Daily high-resolution-blended analyses for sea surface temperature. *J. Clim.* 20, 5473–5496. doi: 10.1175/2007jcli1824.1

Sasaki, Y. N., Washizu, R., Yasuda, T., and Minobe, S. (2017). Sea Level Variability around Japan during the Twentieth Century Simulated by a Regional Ocean Model. *J. Clim.* 30, 5585–5595.

Seo, G.-H., Cho, Y.-K., and Choi, B.-J. (2014a). Variations of heat transport in the northwestern Pacific marginal seas inferred from high-resolution reanalysis. *Prog. Oceanogr.* 121, 98–108.

Seo, G. H., Cho, Y. K., Choi, B. J., Kim, K. Y., Kim, B. G., and Tak, Y. J. (2014b). Climate change projection in the Northwest Pacific marginal seas through dynamic downscaling. *J. Geophys. Res. Oceans* 119, 3497–3516. doi: 10.1002/2013jc009646

Shchepetkin, A. F., and McWilliams, J. C. (2005). The regional oceanic modeling system (ROMS): a split-explicit, free-surface, topography-following-coordinate oceanic model. *Ocean Model.* 9, 347–404. doi: 10.1029/2007JC004602

Smith, J. M., Cialone, M. A., Wamsley, T. V., and McAlpin, T. O. (2010). Potential impact of sea level rise on coastal surges in southeast Louisiana. *Ocean Eng.* 37, 37–47. doi: 10.1016/j.oceaneng.2009.07.008

Solano, M., Canals, M., and Leonardi, S. (2020). Barotropic boundary conditions and tide forcing in split-explicit high resolution coastal ocean models. *J. Ocean Eng. Sci.* 5, 249–260. doi: 10.1016/j.joes.2019.12.002

Song, D., Wang, X. H., Zhu, X., and Bao, X. (2013). Modeling studies of the far-field effects of tidal flat reclamation on tidal dynamics in the East China Seas. *Estuar. Coast. Shelf Sci.* 133, 147–160. doi: 10.1016/j.ecss.2013.08.023

Song, Y., and Haidvogel, D. (1994). A semi-implicit ocean circulation model using a generalized topography-following coordinate system. *J. Comput. Phys.* 115, 228–244. doi: 10.1006/jcph.1994.1189

Stammer, D., Cazenave, A., Ponte, R. M., and Tamisiea, M. E. (2013). Causes for contemporary regional sea level changes. *Ann. Rev. Mar. Sci.* 5, 21–46. doi: 10.1146/annurev-marine-121211-172406

Taylor, K. E., Stouffer, R. J., and Meehl, G. A. (2012). An overview of CMIP5 and the experiment design. *Bull. Am. Meteorol. Soc.* 93, 485–498. doi: 10.1175/bams-d-11-00094.1

van de Wal, R., Zhang, X., Minobe, S., Jevrejeva, S., Riva, R., Little, C., et al. (2019). Uncertainties in long-term twenty-first century process-based coastal sea-level projections. *Surv. Geophys.* 40, 1655–1671. doi: 10.1007/s10712-019-09575-3

Vörösmarty, C., Fekete, B., and Tucker, B. (1996). *Global river discharge database, Version 1.0 (RivDIS v1. 0), A contribution to IHP-V Theme 1.* Paris: UNESCO Press.

Warner, N. N., and Tissot, P. E. (2012). Storm flooding sensitivity to sea level rise for Galveston Bay, Texas. *Ocean Eng.* 44, 23–32.

WCRP Global Sea Level Budget Group (2018). Global sea-level budget 1993-present. *Earth Syst. Sci. Data* 10, 1551–1590. doi: 10.5194/essd-10-1551-2018

Yan, Y.-F., Zuo, J.-C., and Chen, M.-X. (2010). Influence of the long-term sea level variation on tidal waves in the eastern China Sea. *Period. Ocean Univ. China* 40, 19–28.

Zhang, Y., and Ge, E. (2013). Temporal scaling behavior of sea-level change in Hong Kong—Multifractal temporally weighted detrended fluctuation analysis. *Glob. Planet. Change* 100, 362–370. doi: 10.1016/j.gloplacha.2012.11.012

Conflict of Interest: The authors declare that the research was conducted in the absence of any commercial or financial relationships that could be construed as a potential conflict of interest.

Publisher's Note: All claims expressed in this article are solely those of the authors and do not necessarily represent those of their affiliated organizations, or those of the publisher, the editors and the reviewers. Any product that may be evaluated in this article, or claim that may be made by its manufacturer, is not guaranteed or endorsed by the publisher.

Copyright © 2021 Kim, Kim, Jeong, Lee, Byun and Cho. This is an open-access article distributed under the terms of the Creative Commons Attribution License (CC BY). The use, distribution or reproduction in other forums is permitted, provided the original author(s) and the copyright owner(s) are credited and that the original publication in this journal is cited, in accordance with accepted academic practice. No use, distribution or reproduction is permitted which does not comply with these terms.

frontiers in Marine Science

ORIGINAL RESEARCH
published: 16 December 2021
doi: 10.3389/fmars.2021.728687

Global Climate Services: A Typology of Global Decisions Influenced by Climate Risk

Alexander Bisaro[1], Jochen Hinkel[1,2], Gonéri Le Cozannet[3], Thomas van der Pol[1] and Armin Haas[4]*

[1] Global Climate Forum, Berlin, Germany, [2] Division of Resource Economics, Humboldt-Universität zu Berlin, Berlin, Germany, [3] Bureau de Recherches Géologiques et Minières, French Geological Survey, Orléans, France, [4] Institute for Advanced Sustainability Studies, Potsdam, Germany

Climate services are ideally co-developed by scientists and stakeholders working together to identify decisions and user needs. Yet, while climate services have been developed at regional to local scales, relatively little attention has been paid to the global scale. Global climate services involve decisions that rely on climate information from many locations in different world regions, and are increasingly salient. Increasing interconnections in the global financial system and supply chains expose private companies and financial institutions to climate risk in multiple locations in different world regions. Further, multilateral decisions on greenhouse gas emission reduction targets, disaster risk finance or international migration should make use of global scale climate risk assessments. In order to advance global climate service development, we present a typology of decisions relying on global (i.e., non-local) climate risk information. We illustrate each decision type through examples of current practice from the coastal domain drawn from the literature and stakeholder interviews. We identify 8 types of decisions making use of global climate information. At a top-level, we distinguish between "multilateral climate policy decisions," and "portfolio decisions involving multiple locations." Multilateral climate policy decisions regard either "mitigation targets" or "multilateral adaptation" decisions. Portfolio decisions regard either "choice of location" or "choice of financial asset" decisions. Choice of location decisions can be further distinguished as to whether they involve "direct climate risks," "supply chain risks" or "financial network risks." Our survey of examples shows that global climate service development is more advanced for portfolio decisions taken by companies with experience in climate risk assessment, i.e., (re-)insurers, whereas many multilateral climate policy decisions are at an earlier stage of decision-making. Our typology thus provides an entry-point for global climate service development by pointing to promising research directions for supporting global (non-local) decisions that account for climate risks.

Keywords: climate services, sea-level rise, adaptation, finance, climate risk

OPEN ACCESS

Edited by:
João Canning-Clode, Center for Marine Environmental Sciences (MARE), Portugal

Reviewed by:
Adam Peter Hejnowicz, Newcastle University, United Kingdom
Rachel Gjelsvik Tiller, SINTEF, Norway

****Correspondence:***
Alexander Bisaro
sandy.bisaro@globalclimateforum.org

Specialty section:
This article was submitted to Global Change and the Future Ocean, a section of the journal Frontiers in Marine Science

Received: *29 June 2021*
Accepted: *23 November 2021*
Published: *16 December 2021*

Citation:
Bisaro A, Hinkel J, Le Cozannet G, van der Pol T and Haas A (2021) Global Climate Services: A Typology of Global Decisions Influenced by Climate Risk. Front. Mar. Sci. 8:728687. doi: 10.3389/fmars.2021.728687

INTRODUCTION

Climate services provide stakeholders with "usable" climate information and tools in order to assist decision-making (Hewitt et al., 2012), and are being promoted by leading institutions in the United States and Europe, e.g., National Research Council, the European JPI-Climate, or the global Climate Services Partnership (Brasseur and Gallardo, 2016). Climate services however exhibit "usability gap" (Lemos et al., 2012). Uptake of climate services has been limited by the science-driven, as opposed to demand-driven, climate service development (Lourenço et al., 2016). Indeed, barriers to uptake include low climate risk awareness among some stakeholders, a lack of tailored communication formats of the services, or lack of salience of climate service products (Brasseur and Gallardo, 2016). To overcome these barriers, co-development approaches to climate services that involve stakeholders working directly with scientists to identify decisions, user needs, and thus climate service products needed (Bremer et al., 2019). Indeed, at local and regional scales, climate service co-development has led to seasonal forecasting tools for agricultural sector stakeholders, local flood risk assessment tools (Soares et al., 2018), and coastal risk assessment (Van der Pol et al., 2019).

Yet global climate services have hardly been addressed to date. Global climate services refer to climate information or tools that are non-local, and thus support specific global decisions by delivering coherent information for many locations, regions or countries around the globe. This is a significant gap as there are a number of salient decisions with global dimensions that are exposed to climate risks. Multilateral decisions on greenhouse gas emission mitigation action, disaster risk finance or international migration rely in part on global scale climate risk assessments (Hedlund et al., 2018). Further, decisions on trade policy, food security and macro-economic policy (e.g., sovereign risk) can be usefully informed by global scale information on climate risks (Benzie et al., 2019). More broadly, both the global financial system and global supply chains have become increasingly interconnected, exposing private companies and financial institutions to direct and indirect climate risks in multiple locations around the world (SEI, 2020).

This paper aims to fill the gap in the literature regarding climate services addressing global decisions. We do so by identifying different types of decisions that rely on information on climate risks at the global scale. We thus develop a typology of decisions relying on global, i.e., non-local, climate risk information, and explore the current state-of-the-art in global climate services to address these decisions. Our analysis is aligned with a co-development approach, as we identify global decisions through analysis of real-world decisions through both stakeholder interviews and literature review. Further, we characterize these global decisions and the need for global climate services they give rise to.

Our paper is thus exploratory presenting a typology of global decisions in order to explore the state-of-the-art in the global climate service development. We note that political scientists have studied global governance arrangements and contexts emerging in transnational climate governance for more than a decade (Pattberg and Stripple, 2008; Biermann et al., 2009; Dzebo and Stripple, 2015). Our paper presents a complementary view to the governance one, which describes governance contexts and involve actors. Our paper focuses on describing global decisions and influence of climate risk upon these in order to identify salient climate information needs. Governance contexts also influence these information needs (discussed in section "Characterizing global decisions and decision contexts"), however, understanding these contexts in not the main focus of our analysis.

Our examples of global climate services are mostly drawn from real-world approaches to decision-making incorporating global (i.e., non-local) information on coastal risks and sea-level rise (SLR). We focus on coastal risk and SLR, as one of the most critical areas for climate service development (Kopp et al., 2019), and because this domain is relatively well-developed for aspects important to global decisions, i.e., indirect economic impacts (Parrado et al., 2020) and financial system impacts (Mandel et al., 2021) of coastal flooding. Indeed, SLR is a salient issue because of the severe consequences of high-end SLR for Small Island States (Nurse et al., 2014), and because of the prevalence of population and economic assets in coastal flood plains globally (Lincke and Hinkel, 2018). Further, SLR increases flood exposure key economic hubs of ports and exclusive economic zones (EEZ), which have can have disproportionally large indirect impacts globally due to supply chain linkages (Haraguchi and Lall, 2015). Our typology illustrated with examples from the relatively advanced coastal domain thus enables an assessment of the state-of-the-art in global climate services development, to identify gaps and discuss salient directions of future research for developing global climate services.

MATERIALS AND METHODS

Approach to Global Climate Services

Climate services have been defined by the WMO Global Framework for Climate Services as "the provision of climate information in such a way as to assist decision-making" (Hewitt et al., 2012). More precisely, under climate service, we understand any effort to deliver information and tools that support addressing the specific decision-problems users face (Hinkel et al., 2019). Global climate services, a sub-set of climate services, deliver climate information and tools at a global scale to support specific global decisions users face. Such global decisions make use of global scale information on climate risk, i.e., coherent information for many locations, regions or countries around the globe.

The aim of this paper is to explore the state-of-the-art in global climate services and our approach to doing so is as follows. First, we build a typology of global decisions requiring climate information. The typology is based on several distinctions regarding the number of actors involved, whether decisions involve mitigation or adaptation, as well as the types of assets and risks at issue. Second, in the spirit of the co-development approach, we identify real-world examples of such decisions mostly from the coastal domain based on stakeholder interactions

and literature review. We further characterize the decisions based on decision-analysis and context variables in order to highlight the relevance of global climate and SLR information to the decisions. This further characterization of decisions provides insight into directions for the future development of global climate services by identifying appropriate decision-making methods, and identifying constraints or enablers (e.g., institutions or norms) for global climate service development.

Characterizing Global Decisions and Decision Contexts

Global decisions can be further characterized according to typical decision-analysis variables, e.g., decision objectives, available alternatives, time horizon of options, and presence of uncertainty (Kleindorfer et al., 1993). Characterizing decisions along these variables can inform the choice of appropriate decision-making methods and the climate information needs they give rise to, which in turn is key to climate service development (Hinkel et al., 2019). For example, if a decision involves only costly, long-term and inflexible options, in which there is high risk adversity regarding negative outcomes, it is important to identify options that are effective under a wide range of scenarios, and the climate information needed to do so should be developed as climate services (Lempert et al., 2012). In contrast, when the set of options considered include short-term or flexible options, climate services can focus on monitoring and re-evaluating options over time (Hinkel et al., 2016). For global climate services, examples that involve costly, long-term, inflexible options because climate and SLR information is salient for these decisions (see Section "Results").

The decision context may also influence global climate service development. Relevant decision context variables include, e.g., risk aversion, legal and regulatory rules, norms and practices. For example, national laws may influence which objectives (e.g., efficiency, equality, loss avoidance, etc.) or which options are deemed appropriate in coastal protection decisions (Bisaro et al., 2020). For instance, in France, coastal planning regulations became stricter following Cyclone Xynthia, leading to more coastal hazard and SLR impact assessments to inform coastal land use planning and set-back zones (Le Cozannet et al., 2017).

Further, for multilateral climate policy decisions, where collective decision-making is required, an important decision context variable is the "empirical status of the decision," which describes the extent to which a decision-making process has been institutionalized. This variable has an indication on climate services development, as multilateral speculative decisions may require scoping assessments that identify major knowledge gaps or provide rough order of magnitude estimates of impacts. In contrast, institutionalized multilateral decisions require more precise information on climate impacts, for example, on the costs and benefits of the measures being considered. In section "Results," we highlight in examples any decision context aspects that influence global climate service development, for example, by presenting barriers to supporting a particular decision.

Table 1 lists variables characterizing decisions and their contexts, and describes their influence on climate service development and SLR information needs in the coastal domain. The list is not exhaustive, but reflects those often discussed for adaptation decision-making (Kwadijk et al., 2010; Haasnoot et al., 2012).

Data Collection

Data collection for identifying real-world global decisions was carried out in the INSeaPTION project, a collaborative research project, which had, among others, the aim of co-developing coastal climate services at the global scale. To this end, two workshops (September 2018 and June 2020) were conducted with global stakeholders. The initial workshop ($n = 22$) included stakeholders from governments ($n = 8$), and private companies ($n = 4$), as well as coastal domain experts and researchers ($n = 10$). Participants were asked to present current decisions they faced that were influenced by climate risks, and these were discussed among the wider group with the aim of distilling key characteristics and information needs. Based on the results of the initial workshop, interview candidates were identified and in-depth semi-structured interviews ($n = 6$) were conducted to further elaborate decisions and climate services. A literature review, based on suggestions of interviews and workshops, and the domain knowledge of the author group, was then conducted, to further characterize the specific real-world examples and global climate services identified (see **Supplementary Materials**). Finally, a second workshop was conducted ($n = 27$) with stakeholders from government ($n = 6$), private companies ($n = 2$), and research ($n = 19$). IN the workshop, the authors of the present paper presented a description of the identified decisions and climate services in order to collect further feedback and validate the description of decisions and climate services developed. The results of this workshop were then integrated into the typology and examples (see **Supplementary Materials** for details).

RESULTS

A Typology of Global Decisions Making Use of Climate Information

At a top-level, global decisions that make use of climate information involve either: multilateral climate policy decisions – multiple countries deciding on climate policy measures that affect many or all of them; or portfolio decisions involving multiple regions/locations – single decision-making entities (e.g., countries, companies, etc.) exposed to climate risk across many and diverse locations around the world.

Multilateral climate policy decisions are generally public decisions that consider aggregate outcomes, e.g., damages, fatalities, macroeconomic effects, in many different locations. The involvement of multiple countries' governments is key to the global character of these decisions because when multiple countries are involved and affected by a climate policy decision, information needs increase beyond the local or regional scale. For instance, for a single country deciding on coastal protection options, a local-scale impact assessment may be sufficient. In contrast, for multiple countries considering

TABLE 1 | Decision and decision context variables.

	Variable	Description	Indication on global climate service development
Decision	Cost/flexibility of all options	Cost of changing from one option to another. High cost of changing options indicates inflexibility of an option.	Inflexibility (high cost of changing options) increases salience of SLR information, when the options considered are also long-term.
	Time horizon	Period of time over which outcomes of a decision are evaluated.	Long time horizon increases salience of SLR information.
	Risk aversion	Preferences of decision-makers for certain over uncertain outcomes.	High risk aversion increases salience of SLR information.
Decision context	Empirical status of decision	Extent to which decision-making processes and institutions are established and agreed.	More established processes require more precise information on costs and benefits of measures being considered.
	Laws and regulations	Existing laws, regulations or other rules that determine, e.g., acceptable risk, types of measures to be considered, etc.	Laws, regulations influence which SLR information is relevant, and can drive or constrain climate services development.

large-scale geoengineering measures to adapt to SLR, global (or regional/continental) SLR impact assessments would be required.

Portfolio decisions involving multiple regions/locations consider selected physical or financial assets at specific locations or world regions. In contrast to multilateral climate policy decisions, portfolio decisions can have a global character without the involvement of multiple actors in decision-making. Rather, the global distribution of assets, supply chains or financial networks affected by climate impacts give this type of decision its global character. For example, a multinational company designing its global supply chain requires information on climate risks in multiple locations around the globe when selecting its suppliers and transportation hubs.

At a next level, different distinctions are relevant for each of these two top-level decision types. For multilateral climate policy decisions, a subsequent distinction is between decisions involving mitigation (i.e., greenhouse gas emission reduction) and those involving multilateral adaptation. The former generally involves countries weighing up the costs and benefits of different emission pathways with respect to various outcome metrics, e.g., GDP, extreme event damages, fatalities, biodiversity losses, etc. For the latter, i.e., decisions on multilateral adaptation options, several further sub-types can be distinguished based on the stage of the decision-making, and types of measures considered (e.g., insurance versus protection measures) (see section "Choosing mitigation policy options").

For portfolio decisions, a distinction can be made between decisions that involve choosing physical assets (i.e., direct investments) and those that involve choosing financial assets (e.g., indirect investments) (Bisaro and Hinkel, 2018). Physical assets are tangible and thus can depreciate through wear and tear. Financial assets, in contrast, are not tangible. Thus, a parcel of land and any building on it are physical assets. In contrast, a mortgage on the same parcel of land and building is a financial asset, and derives its value through the stream of revenues it generates, i.e., interest and capital repayments.

For each of these portfolio decision sub-types, a further distinction can be made regarding whether the decision is impacted by direct climate risks, supply chain risks or financial network risks. Direct climate risks refer to direct impacts of climate change, e.g., rising temperatures, droughts, floods, storms, forest fires, etc. Supply chain risks refer to climate impacts that propagate through supply chains thus impacting a physical or financial asset. For example, a company producing and selling cars in Europe may be exposed to climate-related supply chain risks due to its production or transport centers being located in the coastal flood plains in other world regions. Financial network risks only apply to financial assets, and arise due to the risk that the issuer of the financial asset (i.e., the counterparty) cannot meet its obligations due to climate impacts on its balance sheet or due to broader financial system impacts (see section "Choice of financial asset such that financial network risk is minimized"). A prominent example of financial network risk is climate-induced sovereign risk, namely, the risk that a given country's government bonds will lose their value because the government in question is not able to meet their financial obligations due to climate impacts (Kling et al., 2018).

Combining these distinctions, results in 8 types of global decision influenced by climate risk (see **Table 2**). We note that there is no one-to-one relationship between decision type and global climate services needed. Global climate service development requires in-depth decision and contextual analysis (together with stakeholders) to choose appropriate decision-making methods and identify climate information needs (Vincent et al., 2018). For each of the decision types, we elaborate real-world examples and describe decision characteristics that make global SLR information relevant to the decision. Further, we describe the current state-of-the-art in terms of global climate services addressing these decisions. In doing so, we identify gaps in current global climate services and some of the barriers identified by stakeholders to addressing these gaps.

Table 2 presents the typology of global decisions, which combines each of the three dimensions and presents real-world examples for each, identified mostly from the coastal domain. We note that the decision types are "ideal types" and in practice decisions may encompass more than one decision type. For instance, adaptation and mitigation are complementary responses to climate change. Thus, decisions on mitigation targets depend on the outcomes of decisions on adaptation measures and vice versa. Further, some portfolio decisions may need to consider several types of risk, i.e., direct climate risk, supply chain risk, and financial network risk. Here, we however,

TABLE 2 | A typology of decisions requiring global climate information with examples from the coastal domain.

Type	**Multilateral climate policy decisions**				**Portfolio decisions involving multiple regions/locations**			
Sub-types	**Choice of mitigation options**	**Choice of multilateral adaptation options**			**Choice of physical assets locations or design such that.**		**Choice of financial assets such that**	
		Scoping adaptation decisions	**Choice of multilateral flood risk pools**	**Choice of multilateral coastal protection measures**	**. . .adaptation benefits are maximized**	**. . . supply chain risks are minimized**	**. . . direct SLR risk is minimized**	**. . . SLR-induced financial network risk is minimized**
Examples	• Global community of countries negotiating on global mitigation targets	• Global community of countries deciding on adaptation financing targets • Re-insurers deciding on strategy regarding entering a regional market	• Multilateral European Solidarity Fund deciding on risk pool design • Multilateral Caribbean Cat. Risk Pool deciding on risk pool design	• European countries choosing coastal adaptation options from a set of alternatives including a North European Enclosure Dam • Global community of countries choosing coastal adaptation options from a set of alternatives including geoengineering Antarctica	• Coastal engineering companies identifying adaptation business opportunities • Global community of countries deciding on location of adaptation investments to reduce large-scale migration risk	• Automaker choosing assembly plants and suppliers • Country deciding on food supply chains to ensure national food security • Ratings agencies assessing credit risk • Green bond certifier assessing benefits of adaptation projects	• Institutional investor illiquid portfolio manager choosing an investment • Banks issuing mortgages on coastal real estate • Institutional investor liquid portfolio manager choosing an investment	• Investor choosing a financial asset linked to a coastal real estate market • Investor choosing a government-backed financial asset (e.g., bond)

discuss each decision type separately. In section "Discussion: global climate service development," we discuss our results and implications for global climate service development, including examples that address multiple decision types (see **Table 2**).

Multilateral Climate Policy Decisions

Choosing Mitigation Policy Options

A first type of multilateral climate policy decision involves governments choosing mitigation targets. Generally, this involves countries assessing different emission pathways with respect to various social, economic and environmental outcome metrics, e.g., GDP changes, extreme event damages, fatalities, biodiversity losses, etc.

An *example* is the collective choice of GHG emission targets involving the global community of states in the international climate negotiations, perhaps the longest established global climate policy decision. The decision context has evolved over time formalized in 1992 by the United Nations Framework Convention on Climate Change (UNFCCC) with the objective to stabilize greenhouse gas concentrations "at a level that would prevent dangerous anthropogenic interference with the climate system" (Article 2 UNFCCC, 1992). More recently, with the 2015 Paris Agreement countries committed to National Determined Contributions toward global goals, which were agreed as "well below" 2 degrees Celsius increase in global mean temperatures over pre-industrial levels.

Global climate services supporting these decisions are provided foremost through the Intergovernmental Panel on Climate Change (IPCC), which synthesizes the scientific knowledge on climate change and its impacts through its Assessment and Special Reports. The IPCC has thus informed the design of international treaties, including the UNFCCC and the Paris Agreement, that specify global GHG targets. For example, an IPCC Special Report assessed the impacts of 1.5°C of global warming, and thus provided support to the decision on the ambitious goal of the Paris Agreement to limit warming to 1.5°C (IPCC, 2018). Another example of global climate services comes from the Intersectoral Impact Modeling Intercomparison Project (ISIMIP) project, a global climate impact modeling effort finding that coastal impacts produce among the highest expected costs of all sectors from climate change (Lange et al., 2020). For the coastal domain specifically, global coastal flood damages by 2100 are much more sensitive to coastal adaptation strategies than to differences in climate and socioeconomic scenarios, showing that long-term adaptation strategies are key complements to any mitigation targets that may be achieved (Hinkel et al., 2014).

Choosing Multilateral Adaptation Options

Overview

A second type of multilateral climate policy decision involves governments choosing multilateral adaptation options. Multilateral adaptation measures are defined as adaptation measures that affect more than one country through direct or indirect impacts (e.g., avoided damages). Multilateral adaptation measures that require global climate services are not often considered in the literature, as adaptation is generally considered a local responsibility (Nalau et al., 2015). While transboundary coastal risk management is taking place in, for example, the low-lying west-European North Sea flood plain (Zagonari, 2013; Kuiper, 2020), these initiatives are largely at local scale.

Sub-types of decisions regarding multilateral adaptation options can be distinguished based on the stage of the decision-process at issue, i.e., scoping versus choosing options. Scoping is a common stage in decision-making aimed at identifying options and generating information on the impacts of these (Kleindorfer et al., 1993). For choosing adaptation options, further sub-types can be distinguished based on whether they involve "soft" options (e.g., flood insurance) or hard structural options (e.g., coastal protection measures).

Scoping Adaptation Decisions

Scoping adaptation decisions is a broad decision type that involves decision-makers seeking to generate information on climate impacts prior to formalizing the decision by specifying decision objectives, criteria and alternatives. Order of magnitude estimates of climate and SLR impacts are often sufficient for scoping decisions. Global (or multi-regional) climate impact assessment that are too coarse in scale for local formal decision-making are often sufficient for generating such estimates (Patt et al., 2005).

A *first example* involves the global community scoping global adaptation financing targets for support to developing countries. This is a scoping decision because deciding on adaptation financing targets requires an understanding of adaptation objectives and needs in developing countries, which are also not yet clearly defined (UNEP, 2020). While the Paris Agreement includes a global adaptation goal, it does not define a/the level of adaptation needed or metrics for measuring progress toward this goal. Further, Article 2.1c of the Paris Agreement stipulates to make "finance flows consistent with a pathway toward low greenhouse gas emissions and climate-resilient development." Yet several decades of scholarship have shown that measuring adaptation, or climate-resilient development, is often contested and varies across different national and socio-economic contexts (Adger et al., 2009). Indeed, the 2020 Adaptation Gap Report finds difficulties in estimating the current adaptation finance gap (and thus related adaptation finance targets to fill this gap) because of problems in estimating both current adaptation finance flows as well as current and future adaptation costs (UNEP, 2020).

A *global climate service* supporting the scoping of this decision in the coastal domain is a recent World Bank global assessment of coastal adaptation infrastructure investment needs (Nicholls et al., 2019). The assessment scopes aggregate investment needs for reducing climate risks under alternative adaptation strategies, such as constant protection levels, constant flood risk, or cost-benefit analysis.

The study shows that there is high uncertainty regarding future SLR impacts. Importantly, for scoping global adaptation financing decisions it shows that the key driver of future adaptation costs is the type of adaptation strategy applied, though other factors also contribute including socio-economic development, national development priorities and SLR scenarios. Such indicative information on global protection needs and costs provides an entry-point for supporting decision-making on global coastal adaptation finance needs, and key knowledge gaps to address.

A *second example* involves re-insurers taking a strategic decision regarding entering or leaving regional coastal insurance markets. Generally, re-insurance policies (e.g., property, business interruption, etc.) are issued for only 1 year. Thus, climate change information does not play a significant role in re-insurers' core business decisions of risk pool design or setting re-insurance premiums, because climate change does not significantly influence insured risks on annual time scales. However, strategic decisions regarding entering a particular regional market or sector may involve longer time horizons, e.g., 10–15 years, because of the time and resources needed to establish a risk pool by marketing and selling re-insurance policies. This is a scoping decision because rough estimates of coastal risk and how it is likely to develop over the relevant timescale are sufficient for informing the decision. Whereas subsequent decisions, e.g., on risk pool design, will require a more precise and detailed risk assessment.

A *global climate service* supporting this decision involves reinsurers current practices of assessing climate change and SLR influence on regional coastal risks. Generally, (re-)insurer risk assessment methodologies apply statistical approaches based on historical data, e.g., storm losses, to support their core business decisions regarding flood risk pool design, and insurance underwriting. However, in order to assess how risks in coastal regions will develop beyond the short-term, (re-)insurers are now considering how to integrate climate change projections into risk assessment methodologies. To this end, one major European reinsurer has an established internal process for reviewing developments in climate science in order to assess whether scientific knowledge on climate change can provide information on how risks are changing. Currently, the scientific evidence, e.g., on the magnitude and direction of changes in hurricane incidence, remains too uncertain for use in medium-term decision-making, and thus they rely on a historical datasets and statistical modeling approaches.

Choice of Multilateral Flood Risk Pool Design

The choice of multilateral flood risk pool design involves a (re-)insurer choosing an appropriate design for a flood risk pool covering multiple countries. When designed appropriately, flood risk pools are an adaptation measure because they provide the insured with incentives for *ex ante* flood risk reduction, and

needed liquidity that can enable faster recovery from disasters (Hudson et al., 2016). Multilateral flood risk pool design must consider, first, capital requirements to ensure solvency in the case of major hazards events (Gurenko, 2006). For instance, the Solvency II Directive requires European (re-)insurers have sufficient capital to cover claims from a 1-in-200 years event. Second, flood risk pool design must consider premium affordability particularly in developing countries, where flood insurance is often heavily subsidized, e.g., through development assistance (Surminski and Oramas-Dorta, 2014).

A *first example* involves EU Member States deciding on capital allocation to the European Union Solidarity Fund (EUSF). The EUSF is a core disaster financing instrument in the EU, providing a risk pooling mechanism between EU member states that supplements national disaster risk financing, and disperses disaster risk finance to Member States in the case of triggering events, such as, natural hazards. EU Member States must decide on EUSF capital requirements, which determine the level of risk up to which the Fund can provide coverage for. Further, it must decide the contributions (i.e., premiums) of each Member State to participate in the EUSF. These contributions can be differentiated by Member State and thus may include cross-subsidies according to relative exposure or ability-to-pay.

A *global climate service* is provided by Jongman et al. (2014), who estimate river flood damages for Europe by developing a model that calculates the joint probabilities of flood events across all of Europe's 1,007 river basins. Further, they estimate damages from these events by including known and estimated flood protection standards in place. They find that the EU Solidarity Fund of €1 billion had a 5% chance of exceedance in 2013, which will rise to 9% in 2050. Thus, capital allocation to EUSF under future climate change will need be increased substantially to maintain the same level of coverage.

A *second example* is the decision on the design of the risk pool managed by the Caribbean Catastrophic Risk Insurance Facility (CCRIF), which provides disaster risk financing for Caribbean countries. The Caribbean Climate Risk Insurance Facility (CCRIF) has been operating for more than a decade. It is a parametric risk finance instrument, which means that pay-outs are triggered by pre-defined values of climate variables, e.g., extreme water levels, max. wind speed and duration, rather than damages thresholds, which lowers the monitoring cost associated with pay-outs.

Key for the long-term sustainability of CCRIF is an appropriate assessment of the current and future frequency and severity of hurricanes. This is a complex issue as one of its determinants is the Atlantic Multidecadal Variability (AMO) and its two alternating phases, plus the quite complex issue of how climate change is going to impact both the AMO pattern and the respective hurricane dynamics in each of them (O'Reilly et al., 2019). Moreover, organizing a risk pool is completely different a business than re-insurance as it involves building up trust among governments and finding a scheme that is economically and politically sustainable long-term.

Choice of Multilateral Adaptation Measures

The choice of multilateral adaptation measures involves large regional or global-scale adaptation measures that have direct impacts (i.e., reducing climate risk) in multiple countries. Such measures are of a much greater scale than local adaptation measures typically considered in the adaptation literature. Indeed, while many coastal adaptation measures have an international dimension because, for example, they affect sediment transport, related decisions generally are not global because they require only regional scale information. In contrast, multilateral adaptation measures with a global dimension are much larger in terms of engineering works and the geographical extent of their impacts.

A *first example* involves countries along the North and Baltic Sea Coasts choosing from a set of coastal adaptation measures that include a North European Enclosure Dam (NEED), a measure that entails enclosing the North Sea with 576 km of dams between France, the United Kingdom, and Norway. The NEED would reduce coastal flood and erosion risk along the coast of 14 countries over the long term (100+ years). Alternatives to NEED include another major enclosure of only the Baltic Sea. Finally, countries could also choose to implement coastal adaptation nationally or at sub-national scales through a mix of protection, accommodation and retreat measures, as is the current practice.

A *global climate service* supporting this decision is provided in the literature by a feasibility and costs assessment of NEED in the context of SLR (Groeskamp and Kjellsson, 2020). NEED appears to be technologically feasible because the maximum depth of sea-floor the dam would cross is ca. 300 m, while currently stationary oil rigs can be built at 500 m depth. Costs are estimated at €300 to €600 billion, including the 40,000 m^3 of pumping capacity needed to balance the incoming water flow from rivers in the new enclosure. Total costs annualized over 20 years amount to around 0.2% GDP of countries involved, which may be less than the cost of protection the Netherlands alone for 2 m SLR (Lincke and Hinkel, 2018). NEED would, however, also have major adverse impacts for ecosystems both within and outside the barrier (Groeskamp and Kjellsson, 2020). A similar project has been proposed for the Mediterranean (Gower, 2015), with the caveat, also applicable to NEED, that the proposed solution only addresses SLR and would accelerate marine ecosystem decline and related services.

A *second example* involves the global community choosing geoengineering measures in Antarctica to slow ice sheet loss and reduce coastal food and erosion risk along the entire global coastline over the long term (100+ years) (Feldmann et al., 2019). This decision affects coastal risk along the entire global coastline. Alternatives to geoengineering Antarctica include geoengineering of Greenland, which also would have impacts of global extent, and other multilateral adaptation measures including those discussed above.

A *global climate service* supporting this decision is provided by the feasibility and impact assessments of various measures to geoengineer polar glaciers, and particularly those in Antarctica (Moore et al., 2018; Gürses et al., 2019). Various authors have assessed measures designed to slow ice flow in West

Antarctica, which is of greatest concern for high-end global sea level rise scenarios. These include constructing islands in front of the glaciers, berms to prevent warm water from flowing underneath glacial sea-ice, and cooling or removing water underneath glaciers. Moore et al. (2018) find that all of these measures appear to be effective in slowing glacial flow into the sea. In contrast, Gürses et al. (2019) apply a global sea-ice ocean model to assess impacts of an underwater wall in West Antarctica to prevent the inflow of warm water underneath sea-ice. They find that warm waters diverted by the sea-wall to other parts of Antarctica reduce its overall effectiveness, with ice loss for Antarctica as a whole being reduced by only 10% with the wall in place. Thus, ambiguity remains regarding the engineering effectiveness of these measures. Further, such a project requires major energy consumption with extremely large environmental impacts (Feldmann et al., 2019), and only addresses SLR and not other climate change impacts (Mora et al., 2017). Future climate service development could focus on further resolving both engineering effectiveness and environmental impact ambiguities and thus scoping decisions to support multilateral decision-making processes (see section "Discussion: global climate service development").

Portfolio Decisions Involving Multiple Countries

Choice of Physical Asset Location

A first type of portfolio decision involves actors choosing the location of physical assets. This decision type can be distinguished into three sub-types. A first sub-types involves decisions on location that maximize adaptation benefits. A second sub-type involves decisions on location that minimize supply chain risks. A third sub-type involves decisions on location that minimize direct climate risks (Note that for this third sub-type, the decision may involve either the choice of physical or financial assets, see **Table 2**).

Choice of Physical Asset Location Such That Adaptation Benefits Are Maximized

Decisions on location that maximize adaptation benefits in the coastal domain involve identifying locations in which an adaptation intervention can significantly reduce climate risks compared to alternative locations. It is important to note that for this decision type, location selection is for a prospective asset or adaptation measures, which must be subsequently designed and implemented. Thus, the location decision involves identifying "hot-spots" of climate vulnerability as entry point for deeper analysis to develop specific adaptation measures under various criteria (e.g., cost-efficiency, cost-effectiveness, robustness, etc.).

A *first example* involves a multinational coastal engineering company that operates at a global scale seeking to identify new business opportunities through scoping coastal impacts and adaptation measures. Coastal engineering companies, whose core business involves dredging and construction, want to identify coastal areas or regions for future business development regarding coastal engineering solutions. Currently, such companies are particularly interested in identifying areas attractive for nature-based solutions (NBS) due to the potential to attract additional investors (e.g., development banks or foundations) to such projects (Kok et al., 2021). Locations that are attractive and feasible for coastal NBS present significant opportunities for partnerships that can attract investment needed to make a project viable. Identifying locations (hot spots) that are attractive for coastal NBS involves identifying locations where the benefit-cost ratio of coastal adaptation projects is likely to be high, and coastal NBS are feasible.

A *global climate service* supporting this decision is being developed by a multinational coastal engineering company. For this company, their coastal risk assessment experts have developed a global assessment tool, the Climate Risk Overview, that integrates climate, SLR and flood and erosion hazard data with socio-economic data in order to identify coastal locations that are most "at risk," and thus have high adaptation benefits potential (Van Oord, 2021). The tool also seeks to identify coastal segments well- suited for NBSs, and has been made available in the public domain, as a tool to attract public investment and catalyze public-private partnerships for coastal adaptation.

Choice of Physical Asset Location Such That Supply Chain Risk Is Minimized

Portfolio decisions on physical asset locations may also aim to minimize supply chain risks. A company or government's supply chain risk is determined by the physical locations of its production and inventory management sites (and those of its suppliers) as well as the structural characteristics of the supply chain. Structural characteristics include the diversity of suppliers, and asset specificity of production processes or locations (i.e., substitutability of assets or production processes) (Haraguchi and Lall, 2015). While supply chain decisions are common, only when they involve physical assets that have high costs, long lifetimes, and high asset specificity (low substitutability) is SLR information relevant. In such cases, supply chains are inflexible and SLR should be considered in decision-making because it is a significant driver of coastal risks over long time horizons (Weaver et al., 2013). This decision type generally involves large companies with global supply chains spanning many countries and world regions. Public actors, however, may also face supply chain decisions regarding the supply of public goods, e.g., food security, vaccines or other pharmaceuticals, etc.

A *first example* involves an automaker choosing assembly plant and inventory management locations in their supply chain such that SLR risk is minimized. Large automakers cannot entirely avoid coastal risk because, as automobiles are relatively large and heavy, assembly plants and storage facilities are generally located close to ports to minimize overland transportation costs (Haraguchi and Lall, 2015). Moreover, automakers make asset specific supply chain investments and are generally not able to shift key production processes, i.e., assembly and inventory hubs, quickly at low cost to other locations. Indeed, following the 2011 floods in Thailand that severely impacted the auto industry, surveys of affected companies found that most would not change the location of existing facilities due to financial constraints (Haraguchi and Lall, 2015). Automakers must choose supply chain locations such that exposure to SLR is tolerable, while their production processes remain efficient.

Examples of *global climate service* supporting such decisions are scarce, as the literature largely addresses port and supply chain implications for the perspective of macro-economic impacts. For example, a recent study assesses how global port infrastructure will be affected by SLR under different socio-economic and climate scenarios until 2050 (Hanson and Nicholls, 2020). The authors find that the costs of building new ports to meet global demand due to increasing trade will be much greater than the cost of adapting existing ports. While this provides relevant information regarding SLR exposure of existing ports, for multinational companies making supply chain location decisions global climate services development could be extended by including more precise information on their supply chains.

A *second example* involves a national government choosing agricultural production and inventory management locations in order to ensure domestic food security. Many developing countries are net food importers, and are thus exposed to supply chain risks from SLR impacts on food transport infrastructure. Moreover, agricultural trade depends on critical transport hubs in ports with exceptional large trade volumes that are exposed to coastal risk. For example, 53% of global wheat, rice, maize and soybean exports pass through two hubs in Brazil and the United States (Bailey and Wellesley, 2017). Food importing countries concerned with food security decision-making should account for coastal risks at major transportation hubs in their food supply chains.

A *global climate service* supporting this decision is the assessment of "chokepoints" in global food trade (Bailey and Wellesley, 2017). Chokepoints are transportation hubs that pass through significant shares of trade volume in a basic agricultural commodities or food stuff. For food importing countries, food security risks arise because disruption at a chokepoint can directly interrupt imports or indirectly increase global food market prices. Currently, there are three major coastal chokepoints in global agricultural trade: US Gulf Coast Ports, Brazil's southern ports, and Black Sea ports. For example, Black Sea ports are a major coastal wheat chokepoint, passing through 12% of global wheat trade and 60% of Ukrainian and Russian exports (Bailey and Wellesley, 2017).

Future global climate service development could combine chokepoint analysis with global SLR impact analysis to assess SLR impacts at key chokepoint locations. This could support governments to integrate choke-point analysis and SLR information into food supply chain decisions, and would also be relevant for systemic actors concerned with food security, e.g., development aid organizations, UNCHR, etc. (Hedlund et al., 2018; Benzie et al., 2019).

Choice of Physical Asset Location Such That Direct Sea-Level Rise Risk Is Minimized

Portfolio decisions on physical asset locations may also aim to minimize direct climate risk. This decision type differs from the previous one in that only the direct risk at particular location is considered, and not the role of the asset or location in a broader production process (i.e., supply chain).

For these location decisions, as for other portfolio decision types, SLR information is only useful when the decisions involve physical assets with high costs, long lifetimes, and high asset specificity (low substitutability) (Hinkel et al., 2019). These characteristics mean that location decisions are relatively inflexible, and thus SLR should be considered over the medium to long-term.

We note however that asset specificity is a decision characteristic that depends also on the decision-maker. Consider portfolio decisions on physical real estate assets. While real estate assets can generally be exchanged at low transaction costs (e.g., cost of information collection, negotiation, contracting), the relative importance of these transaction costs (and thus asset specificity) differs for different investors. For instance, for institutional investors (i.e., insurers and pension funds) transaction costs associated with individual real estate transactions may be prohibitively high because of the large volume of assets they hold. They prefer "buy and hold" investment strategies with investment horizons of 10–50 years, over which time SLR information is increasingly relevant (Ameli et al., 2020). In contrast, smaller volume investors (e.g., individual investors or single market real estate companies) may be less constrained by the transaction costs of trading real estate assets, and such transactions may even be part of their core business model and competitive advantage. For these investors, SLR information is less salient because price dynamics in the real estate markets may be affected by other factors that vary on much shorter time scales.

A *first example* involves an institutional investor, a European re-insurer, choosing physical asset investment locations within their direct investment portfolio. Broadly, re-insurers make direct (illiquid) and indirect (liquid) investments with the objective of managing overall assets and liabilities, including those from the insurance side of their business. For this European re-insurer, direct investments make up around 10% of their equity portfolio, and for these investments they prefer "buy and hold" strategies in choosing physical assets in order to minimize transaction costs, which include physical risk assessments. The time horizon of such direct investments is thus at least 10–15 years, and typically longer. For specific investments, detailed local information is needed to conduct risk assessments and thus global climate information is not strictly required. However, for the illiquid investment portfolio more broadly, the reinsurer assesses their exposure to particular natural catastrophe scenarios, particularly considering the (re-)insurance policies they have issued. Thus, similar to the examples of multilateral risk pools above, re-insurers require assessments of current and future frequency and severity of hurricanes to assess their overall exposure.

A *global climate service* supporting this decision is generally provided internally by such investors through their own experts making use of experience and datasets from the insurance side of their business. Re-insurers core business involves assessing physical climate-related risks, and thus they make use of this expertise in risk assessments for investment decisions. The investment arm of a major European re-insurer convenes an internal expert group that is involved in due diligence for every major investment decision in physical assets. Further, where relevant, the due diligence process of the re-insurer makes use of historical databases, e.g., on storm or flood events, claims,

etc, from the insurance side of business to conduct the physical risk assessments. However, the re-insurer identifies a salient gap in their risk assessments. Their current approaches focus only on historical data sets, whereas equity "buy and hold" investors require assessments of how risks will develop under climate change over much longer time horizons, i.e., 50+ years.

Future global climate service development could focus on addressing this gap in terms of integrating climate change impacts with long-term natural catastrophe modeling. However, generally, re-insurers indicate that they will seek to address this gap internally with their own experts. This is not surprising as private investing is a competitive arena, and improved risk assessments can lead to profitable investments for companies that development them. This raises an interesting issue for global climate service development as supporting private investment decisions may lead to adaptation benefits that are almost entirely private.

Choice of Financial Assets

A second type of portfolio decision involves choosing financial assets. This decision type can be distinguished into two sub-types. A first sub-type involves decisions on financial assets such that direct SLR risks to the underlying physical assets are minimized. A second sub-type involves decisions on financial assets such that climate-induced financial network risks are minimized.

Choice of Financial Assets Such That Direct Physical Risk Is Minimized

A first sub-type of financial asset decisions involves choosing financial assets such that direct SLR risk is minimized. This decision type is similar to that described in section "Choice of physical asset location such that direct SLR risk is minimized." The risks addressed (i.e., direct physical SLR risk) are the same, only the type of asset and its related decision context differ (see **Table 2**). One key difference between physical assets and financial assets is that the latter are often tradeable at lower transaction costs compared to physical assets. Financial assets thus exhibit low asset specificity and SLR is generally not salient to such decisions. However, there are some exceptions, when financial asset choice requires considering long time horizons.

A *first example* is a bank deciding on issuing mortgages on coastal real estate. Mortgages are financial assets tied to underlying physical real estate assets that may be exposed to coastal risk and SLR. Typical mortgage terms in many countries can range up to 30 years or more, time horizons over which SLR information is useful. Mortgage-issuing banks are often concentrated lenders making many loans in few markets, and thus making use of detailed local information, e.g., on environmental amenities and risks, individual credit worthiness, etc. Given their local knowledge and concentrated lending practices, such banks do not need to make use of global SLR information. However, concentrated lenders often make many loans in disaster recovery periods and sell them on to larger more diversified investors (Keenan and Bradt, 2020). There is thus a related decision of an investor choosing mortgage-backed securities containing bundled coastal real estate mortgages. Keenan and Bradt (2020) report information asymmetry between concentrated local lenders who issue mortgages, and then sell them on to large diversified investors. The information asymmetry arises out of the local knowledge of flood risk that local lenders have, and that is not reflected in national flood maps.

A *global climate service* supporting this decision of large investors choosing bundled mortgage securities is generally provided by regulations such as, those enacted through National Flood Insurance Program flood maps in the US. However, current evidence shows that these maps do not adequately reflect property level flood risks for investment decision, as they are largely only elevation based, and do not incorporate local hydrology, adaptations, etc. (Keenan and Bradt, 2020). Relying on national flood maps can lead to investment decisions based on somewhat arbitrary "bluelines" from national flood maps that increase exposure to SLR. Future global climate service development can address this gap, and information asymmetry between local and more diversified investors, by incorporating SLR information in flood maps.

A *second example* involves an institutional investor, a re-insurer, choosing a financial asset (e.g., a stock or bond), such that physical risks are minimized. As discussed in section "Choice of physical asset location such that direct SLR risk is minimized," these decisions are generally taken by the investment arm of reinsurers within the overall framework of seeking to balance assets and liabilities including the insurance side of the business. Decisions involving financial assets are taken by managers of the "liquid" asset portfolio and generally make up a larger share (e.g., 90%) of the overall re-insurer investment portfolio. These managers generally act within an Environment, Social and Governance (ESG) investing framework in which they seek to identify physical risks to the financial assets they invest in, and to the companies issuing them. However, while initiatives such as the Task Force on Climate-Related Financial Disclosures (TCFD) launched in 2015 are driving increased disclosure of both climate policy and physical risks, there are still major gaps, and information on physical climate risks is not available for many financial assets.

A *global climate service* supporting such decisions is currently provided by third-party data providers and ratings agencies. However, for institutional investors, there are a number of barriers to assessing physical risks associated with financial assets. First, third-party data providers and ratings agencies do not generally focus on physical risks as key performance indicators for financial assets, and thus often do not provide this information at all. Second, companies or governments issuing financial assets are not under pressure to produce data on physical risks, as the focus of disclosure initiatives as to date has been on climate policy risks. Third, producing this information is itself challenging and costly because physical risks to financial assets can change on short time scales. For example, company that issuing a bond may change its production site from an inland to a coastal area, which would require a new assessment of physical risk associated with the bond. Finally, a comprehensive risk assessment would also require information on insurance coverage of a given company, e.g., against Atlantic hurricanes, but such information is generally not publicly available, and coverage may also change annually.

Choice of Financial Asset Such That Financial Network Risk Is Minimized

A second sub-type of financial asset decision involves choosing financial assets such that climate-related financial network risk is minimized. Financial network risks arise with respect to the counterparty in a financial asset (e.g., risks to a bond issuer's balance sheet) as well as with respect to the financial system more broadly. The latter aspect entails "transition risks," whereby financial assets are at risk of being dramatically re-priced following a triggering event. While transition risks most often refer to climate policy risks and stranded assets related to the sustainability transition, transition risks may also arise from physical risks. For instance, slow onset SLR combined with a triggering event, e.g., a major flood, could significantly affect perceptions of coastal risk leading to an abrupt mass exit of the coastal real estate market (herd behavior) that threatens financial system stability (Ortega and Taşpınar, 2018).

A *first example* involves an institutional investor choosing a financial asset, such as a mortgage-backed security or an equity stake in a real estate investment trust (REIT) and considering financial network or "transition risks," i.e., the risk that climate change causes a disruptive shift in real estate market conditions. We note that this example is similar to the second example in "Choice of financial assets such that direct physical risk is minimized," however, here we consider broader financial network risks, rather than only direct physical risks. We note that such transition risks may be particularly acute in real estate markets that have not already priced in SLR exposure (Bakkensen and Barrage, 2017).

A *global climate service* supporting this decision is provided by recent research analyzing whether SLR is accounted for in real estate prices, and the conditions under which these risks are priced in. Evidence from the US shows that real estate markets are beginning to account for SLR, discounting residential property prices exposed to SLR by 7% compared to non-exposed properties (Bernstein et al., 2019). However, owner-occupant dominated markets may be susceptible to financial network and transition risks. In such markets, SLR risk is less likely to impact real estate prices (Bernstein et al., 2019). Further, owner-occupied dominated markets may be more susceptible to financial network and transition risks, as owner-occupants are more likely to update their beliefs regarding SLR following flood events. Research in the US coastal housing market shows that accounting for changing beliefs, i.e., increased risk perception, after flood events leads to a fourfold increase in expected coastal housing market declines and increased price volatility (Bakkensen and Barrage, 2017).

A *second example* involves an institutional investor choosing a government bond and seeking to minimize financial network risk. Government bonds are generally attractive to institutional investors as low-risk assets. However, government-backed financial assets, including government bonds, are exposed to financial network risk in the form of sovereign risk, i.e., the risk that a government cannot meet its financial obligations. Climate change can impact sovereign risk, as direct climate impacts can damage a government's physical assets or increase its liabilities, e.g., through damages to individuals or companies that it has committed to compensate. Thus, assessing sovereign risk involves assessing not only direct climate impacts, but also the resilience of a countries' financial system, e.g., whether it has disaster risk finance in place, and if so, whether its disaster risk finance is sufficiently sustainable.

To date, *global climate service* supporting the decision on choosing a government bond though assessing sovereign risk is somewhat lacking. There are effects of ratings agencies or other third-party data providers to assess sovereign risk, but these largely focus on carbon footprint approaches and sovereign risk related to climate policy risks and stranded assets. Physical risks have yet to be systematically incorporated into sovereign risk ratings by ratings agencies. In the scientific literature, there have been efforts to assess financial system resilience under climate change and SLR. For instance, Schinko et al. (2017) assess sovereign risk in Austria posed by natural disasters under climate change until 2050 by comparing projected disaster losses and national disaster risk financing arrangements. They find that sovereign risk will increase as the National Disaster Fund, capitalized at €260 million, approximately covers current expected annual disaster losses, but will be insufficient in the near future as expected losses increase due to climate change and socio-economic development.

Future global climate service development could build on approaches in the scientific literature to provide more differentiated assessment of sovereign risk based on not only direct climate impacts assessed by Schinko et al. (2017), but also climate risks that propagate through the financial system due to international lending arrangements (see Mandel et al., 2021).

DISCUSSION: GLOBAL CLIMATE SERVICE DEVELOPMENT

Empirical Status of Decisions

Our typology presents eight decision types and real-world examples mostly for the coastal domain together with the current-state of-the-art in global climate services supporting these decisions. We note that the decision types identified, and associated example provide an entry-point for developing global climate services, and that in practice decisions (and decision types) may be combined, leading to synergies or trade-offs between different objectives. We have not been able to address such combinations here. Our discussion illustrates that global decision-making on climate risks is salient, as both public and private stakeholders are becoming increasingly aware of the need to incorporate global scale information on climate risks into their decision-making.

The examples presented further illustrate that both decision-making processes and related global climate service development vary widely in terms of how advanced they are. On one hand, for decisions on multilateral adaptation, we observe that decisions' "empirical status" (**Table 1**) is often in early stages. Moreover, because of the absence of institutionalized decision-making processes driving demand for knowledge, scientific knowledge may be lacking for these decisions. For example, multilateral adaptation measures involve geoengineering at a scale that

exceeds most engineering works in world history. Decision-making processes on such measures remains highly speculative and often controversial (Leane and McGee, 2019). Global climate services development in such settings can focus on "decision identification" approaches (Kleindorfer et al., 1993) that generate information on likely impacts of particular measures (e.g., costs, effectiveness) and identify knowledge gaps to be addressed at a later stage for more formal decision-analysis. Such global climate services may inform public and policy discussions on whether such measures merit being considered, given the high stakes and risk aversion regarding the decisions.

On the other hand, for portfolio decisions, decision-making is driven by private actors' own business models and incentives, and multi-actor processes are not generally required. Indeed, portfolio decisions are generally taken in a competitive market environment and create largely private adaptation benefits (Pauw, 2017). Further, complementary to these private incentives are regulations related to climate risk in the financial sector, such as, financial disclosure regulations proposed by the Task Force on Climate Disclosure (Ameli et al., 2020). Examples of portfolio decisions thus show greater consideration of climate risks. For example, most institutional investors, including those interviewed for this paper, consider ESG requirements in their portfolio decisions, which includes considering both climate policy and physical climate risk components. Further, the COVID-19 pandemic has demonstrated the salience of global supply chain risks and is likely to reinforce the considering of global climate information in portfolio decisions.

Private investors that are most advanced in considering global climate risks in portfolio decisions are experienced with climate risks from their core business, i.e., (re-)insurers. For these stakeholders, global climate service development should be complementary to approaches they are developing internally, e.g., integrating climate modeling with historical extreme event data, and focus on co-development tailored to gaps in existing knowledge and data sets in the financial sector. Even for stakeholders not experienced with climate risk analysis, e.g., automakers, co-development approaches are also needed. In this case, combining private supply chain data with climate change impact projections could improve decision-making providing private benefits to the concerned stakeholders, as well as positive indirect benefits for the global economy. Finally, co-development approaches can also support portfolio decisions of governments related to national security, e.g., to minimize climate risks to critical national defense infrastructure. While such decisions are generally highly sensitive and thus difficult to obtain information, there is evidence that governments are beginning to consider climate risks in this context, and may be an important direction for global climate service (co-) development (DRGIS, 2020).

It should be noted that future development of global climate services will be influenced by approaches to respective public and private roles in managing climate risks, and appropriate sharing of costs and benefits of such adaptation. Further, approaches to cost and benefit sharing between governments and the private sector are shaped at the global level by power asymmetries between actors in the Global North and Global South. Such power asymmetries can be manifested both in interactions between governments, as well as, between multinational corporations and developing country governments (Vogel et al., 2019). The salience of power asymmetries for cost and benefit sharing between public and private actors in climate risk management can be illustrated through the issue of private versus open access data. Large multinational companies may make use of data to facilitate their own adaptation, and seek to protect this data on competition grounds. Yet open access to this data, which is often particularly scarce in developing countries, may also facilitate adaptation more broadly with wider collective or public benefits. How such data protection issues are managed in the development of global climate services is strongly shaped by power relations, and attention to such issues is needed to ensure both efficient and equitable adaptation in developing global climate services.

Global Scale Knowledge Gaps and Implications for Global Climate Service Development

In addition to differences in the focus of global climate service development for multilateral and portfolio decisions noted above, other knowledge gaps emerge that cut across multiple decision types and should be addressed by global climate service development.

One knowledge gap involves climate-related financial network risk, which can affect portfolios decisions regarding both physical and financial assets as well as multilateral climate policy decisions. This is because financial network risks can affect individual asset prices, but also financial system stability adding to the overall global costs of climate change (Batten, 2018). While emerging efforts to integrate climate risks into sovereign risk assessments capture financial network risks to an extent, these activities do not address climate-related risk to financial system stability more broadly. A few recent studies have begun to address the question of climate-related risks to financial stability. For example, Lamperti et al. (2019) apply an agent-based macro-economic model linked to climate impact functions finding that climate change may increase the frequency of banking crises and contribute to financial instability through weakening of banks' balance sheets. Another example is Mandel et al. (2021) who apply a global SLR impact model together with financial system network analysis, finding that direct flood losses can be amplified by a factor 10 in terms of financial losses depending on the centrality in the global financial system and leverage of the country that is directly impacted. While these studies begin to address questions relevant to the global decisions presented here, further global service development should focus on co-developing financial network risk analysis to specific decisions faced by stakeholders, e.g., investors or governments.

Another knowledge gap relates to decisions that address more than one decision type. As noted in section "A typology of global decisions making use of climate information," real-world decisions often involve more than one decision type, and global climate services to address such decisions are lacking. Prominent examples from the financial services sector address multiple decision types and are promising directions for global climate service development.

One example involves ratings agencies that currently aim to integrate climate risk into their ratings activities. Such credit ratings are in principle comprehensive assessments and thus should consider all types of climate-induced risk (i.e., direct physical, supply chain, and financial network). While ratings agencies are currently directing efforts toward integrating physical climate risk into sovereign risk assessment (Kling et al., 2018), they face several limitations, e.g., lack of data, lack of access to propriety data on productive assets, etc., and do not yet comprehensively assess climate risk.

Another example involves financial services companies certifying "Green Bonds" linked to adaptation projects. Currently, certification decisions are supported by "Green Bond taxonomies," which define activities and benefit thresholds that qualify a bond for certification (EC, 2019). While conducting detailed local assessments for individual projects is too resource intensive to implement at the scale required for the large and growing Green Bond market (CPI, 2019), Green Bond taxonomy activities could be extended by global scale SLR impact assessments. Such assessments would be particularly valuable outside of the US and Western Europe, where data needed to assess coastal risk is often scarce. Moreover, these assessments could also address all types of climate-induced risk (i.e., physical, supply chain and financial network risk), and the adaptation benefits produced from reducing this risk.

Finally, beyond these specific knowledge gaps, we note that developing "usable" science for global climate services requires co-development between scientists, policy-makers and private companies, and these interfaces are influenced by the norms, institutions and preferences in specific decision contexts (Haasnoot et al., 2020). Of particular relevance for developing such "usable" science at the global level is the global sustainable development agenda, as articulated in international agreements, most prominently through the UNFCCC, Convention on Biodiversity, Sustainable Development Goals and Agenda 2030. Developing global climate services requires understanding and addressing specific decisions and the relevant context in which they are taken, of which the sustainable development agenda makes up a significant part. At the global level, understanding of how to address these specific decisions, within the context of the sustainable development agenda, is underdeveloped (Kopp et al., 2019). Our typology provides a differentiated set of entry-points toward advancing understanding of the governance challenges involved in global climate service development. It is worth noting in the post-COP26 context that such global decisions, because of their transnational and multilateral character, may be particularly challenging to integrate with current calls for locally led adaptation. Resolving such tensions is a salient challenge for the future development of global climate services.

CONCLUSION

This paper has presented a typology of global decisions affected by climate risk. The aim has been to bring a focus onto global climate services from the perspective of decisions that users are currently facing. This perspective has currently been neglected at the global level in the literature, and this paper contributes to filling this gap. The presented typology shows that there are many salient global decisions currently being addressed by governments and private companies around the world. Further, we found that global climate service development should address very different aspects for multilateral (and generally public) decisions, as compared to portfolio (and largely private) decisions. For the former, scoping assessments and decision identification are needed, in order to advance discussion and research on impacts of large-scale global climate policy measures. For the latter, private investors are already beginning to address climate risk in their own decisions, and global climate service development can further support this through co-developed tailored approaches that respond to the specific decision contexts and knowledge gaps encountered by these stakeholders.

DATA AVAILABILITY STATEMENT

The raw data supporting the conclusions of this article will be made available by the authors, without undue reservation.

ETHICS STATEMENT

Ethical review and approval was not required for the study on human participants in accordance with the local legislation and institutional requirements. The patients/participants provided their written informed consent to participate in this study. Written informed consent was obtained from the individual(s) for the publication of any potentially identifiable images or data included in this article.

AUTHOR CONTRIBUTIONS

AB, JH, and GL designed the research. AB, AH, JH, and GL organized and carried out the research. AB wrote the manuscript, with AH contributing sections of the manuscript. All the authors contributed to revising and editing the manuscript.

FUNDING

We acknowledge funding from the project INSeaPTION as part of ERA4CS, an ERA-NET initiated by JPI Climate, and funded by BMBF (DE), MINECO (ES), NWO (NL), and ANR (FR) with co-funding by the European Union (Grant 690462). This publication was also supported by PROTECT. This project has received funding from the European Union's Horizon 2020 Research and Innovation Program under grant agreement no. 869304. This is PROTECT contribution number 24.

SUPPLEMENTARY MATERIAL

The Supplementary Material for this article can be found online at: https://www.frontiersin.org/articles/10.3389/fmars.2021.728687/full#supplementary-material

REFERENCES

Adger, W. N., Dessai, S., Goulden, M., Hulme, M., Lorenzoni, I., Nelson, D. R., et al. (2009). Are there social limits to adaptation to climate change? *Clim. Change* 93, 335–354. doi: 10.1007/s10584-008-9520-z

Ameli, N., Drummond, P., Bisaro, A., Grubb, M., and Chenet, H. (2020). Climate finance and disclosure for institutional investors: why transparency is not enough. *Clim. Change* 160, 565–589. doi: 10.1007/s10584-019-02542-2

Bailey, R., and Wellesley, L. (2017). *Chokepoints and Vulnerabilities in Global Food Trade*. London: Chatham House.

Bakkensen, L. A., and Barrage, L. (2017). *Flood Risk Belief Heterogeneity and Coastal Home Price Dynamics: Going Under Water? (Working Paper No. 23854)*. Cambridge: National Bureau of Economic Research. doi: 10.3386/w23854

Batten, S. (2018). *Climate Change And The Macro-Economy: A Critical Review*. London: Bank of England.

Benzie, M., Carter, T. R., Carlsen, H., and Taylor, R. (2019). Cross-border climate change impacts: implications for the European Union. *Reg. Environ. Change* 19, 763–776.

Bernstein, A., Gustafson, M. T., and Lewis, R. (2019). Disaster on the horizon: the price effect of sea level rise. *J. Financ. Econ.* 134, 253–272. doi: 10.1016/j.jfineco.2019.03.013

Biermann, F., Pattberg, P., Van Asselt, H., and Zelli, F. (2009). The fragmentation of global governance architectures: a framework for analysis. *Glob. Environ. Polit.* 9, 14–40. doi: 10.1162/glep.2009.9.4.14

Bisaro, A., de Bel, M., Bouwer, L. M., Hinkel, J., Kok, S., Stojanovic, T. A., et al. (2020). Multilevel governance of coastal flood risk reduction: a public finance perspective. *Environ. Sci. Policy* 12, 203–212. doi: 10.1016/j.envsci.2020.05.018

Bisaro, A., and Hinkel, J. (2018). Mobilising private finance for coastal adaptation: a literature review. *Wiley Interdiscip. Rev. Clim. Change* 9:e514. doi: 10.1002/wcc.514

Brasseur, G. P., and Gallardo, L. (2016). Climate services: lessons learned and future prospects. *Earths Fut.* 4, 79–89. doi: 10.1002/2015ef000338

Bremer, S., Wardekker, A., Dessai, S., Sobolowski, S., Slaattelid, R., and van der Sluijs, J. (2019). Toward a multi-faceted conception of co-production of climate services. *Clim. Serv.* 13, 42–50. doi: 10.1016/j.cliser.2019.01.003

CPI (2019). *Global Climate Finance Landscape 2019*. Washington: Climate Policy Initiative.

DRGIS (2020). *Climate security in the Western Indian Ocean - Septembre 2020*. Washington: Direction Générale des relations internatinales et de la strategie.

Dzebo, A., and Stripple, J. (2015). Transnational adaptation governance: an emerging fourth era of adaptation. *Glob. Environ. Change* 35, 423–435. doi: 10.1016/j.gloenvcha.2015.10.006

EC (2019). *TEG Report on EU Green Bond Standard*. Brussels: European Commission.

Feldmann, J., Levermann, A., and Mengel, M. (2019). Stabilizing the West Antarctic Ice Sheet by surface mass deposition. *Sci. Adv.* 5:eaaw4132. doi: 10.1126/sciadv.aaw4132

Gower, J. (2015). A sea surface height control dam at the Strait of Gibraltar. *Nat. Hazards* 78, 2109–2120. doi: 10.1007/s11069-015-1821-8

Groeskamp, S., and Kjellsson, J. (2020). NEED: the Northern European Enclosure Dam for if climate change mitigation fails. *Bull. Am. Meteorol. Soc.* 101, E1174–E1189.

Gurenko, E. (2006). *Earthquake Insurance in Turkey: History of the Turkish Catastrophe Insurance Pool*. Washington: World Bank Publications.

Gürses, Ö., Kolatschek, V., Wang, Q., and Rodehacke, C. B. (2019). Brief communication: a submarine wall protecting the Amundsen Sea intensifies melting of neighboring ice shelves. *Cryosphere* 13, 2317–2324. doi: 10.5194/tc-13-2317-2019

Haasnoot, M., Biesbroek, R., Lawrence, J., Muccione, V., Lempert, R., and Glavovic, B. (2020). Defining the solution space to accelerate climate change adaptation. *Reg. Environ. Change* 20:37. doi: 10.1007/s10113-020-01623-8

Haasnoot, M., Middelkoop, H., Offermans, A., Beek, E., and van Deursen, W. A. (2012). Exploring pathways for sustainable water management in river deltas in a changing environment. *Clim. Change* 115, 795–819. doi: 10.1007/s10584-012-0444-2

Hanson, S. E., and Nicholls, R. J. (2020). Demand for Ports to 2050: climate policy, growing trade and the impacts of sea-level rise. *Earths Fut.* 8:e2020EF001543. doi: 10.1029/2020EF001543

Haraguchi, M., and Lall, U. (2015). Flood risks and impacts: a case study of Thailand's floods in 2011 and research questions for supply chain decision making. *Int. J. Disaster Risk Reduct.* 14, 256–272.

Hedlund, J., Fick, S., Carlsen, H., and Benzie, M. (2018). Quantifying transnational climate impact exposure: new perspectives on the global distribution of climate risk. *Glob. Environ. Change* 52, 75–85. doi: 10.1016/j.gloenvcha.2018.04.006

Hewitt, C., Mason, S., and Walland, D. (2012). The global framework for climate services. *Nat. Clim. Change* 2, 831–832. doi: 10.1002/wcc.290

Hinkel, J., Bisaro, A., and Swart, R. (2016). *Towards a Diagnostic Adaptation Science*. Berlin: Springer. doi: 10.1007/s10113-015-0850-x

Hinkel, J., Church, J., Gregory, J., Lambert, E., Le Cozannet, G., Lowe, J., et al. (2019). Meeting user needs for sea-level rise information: a decision analysis perspective. *Earths Fut.* 7, 320–337. doi: 10.1029/2018ef001071

Hinkel, J., Lincke, D., Vafeidis, A. T., Perrette, M., Nicholls, R. J., Tol, R. S. J., et al. (2014). Coastal flood damage and adaptation costs under 21st century sea-level rise. *Proc. Natl. Acad. Sci. U. S. A.* 111, 3292–3297. doi: 10.1073/pnas.1222469111

Hudson, P., Botzen, W. J. W., Feyen, L., and Aerts, J. C. J. H. (2016). Incentivising flood risk adaptation through risk based insurance premiums: trade-offs between affordability and risk reduction. *Ecol. Econ.* 125, 1–13. doi: 10.1016/j.ecolecon.2016.01.015

IPCC (2018). "Summary for Policymakers," in *Global Warming of 1.5°C. An IPCC Special Report on the Impacts of Global Warming of 1.5°C Above Pre-Industrial Levels and Related Global Greenhouse Gas Emission Pathways, in the Context of Strengthening the Global Response to the Threat of Climate Change, Sustainable Development, and Efforts to Eradicate Poverty*, eds V. Masson-Delmotte, P. Zhai, H.-O. Pörtner, D. Roberts, J. Skea, P. Shukla, et al. (Geneva: World Meteorological Organization).

Jongman, B., Hochrainer-Stigler, S., Feyen, L., Aerts, J. C., Mechler, R., Botzen, W. W., et al. (2014). Increasing stress on disaster-risk finance due to large floods. *Nat. Clim. Change* 4, 264–268. doi: 10.1038/nclimate2124

Keenan, J. M., and Bradt, J. T. (2020). Underwaterwriting: from theory to empiricism in regional mortgage markets in the U.S. *Clim. Change* 162, 2043–2067. doi: 10.1007/s10584-020-02734-1

Kleindorfer, P. R., Kunreuther, H. G., and Schoemaker, P. J. (1993). *Decision Sciences: An Integrative Perspective*. Cambridge: Cambridge University Press.

Kling, G., Lo, Y. C., Murinde, V., and Volz, U. (2018). *Climate Vulnerability and the Cost of Debt (SSRN Scholarly Paper No. ID 3198093)*. Rochester: Social Science Research Network, doi: 10.2139/ssrn.3198093

Kok, S., Bisaro, A., de Bel, M., Hinkel, J., and Bouwer, L. M. (2021). The potential of nature-based flood defences to leverage public investment in coastal adaptation: cases from the Netherlands, Indonesia and Georgia. *Ecol. Econ.* 179:106828. doi: 10.1016/j.ecolecon.2020.106828

Kopp, R. E., Gilmore, E. A., Little, C. M., Lorenzo-Trueba, J., Ramenzoni, V. C., and Sweet, W. V. (2019). Usable science for managing the risks of sea-level rise. *Earths Fut.* 7, 1235–1269. doi: 10.1029/2018EF001145

Kuiper, C. J. (2020). *The Regulation of Flood Risk Management of Transboundary Rivers in the Dutch-German Border Area*. Available Online at: http://essay.utwente.nl/82390/ (accessed July16, 2021).

Kwadijk, J. C. J., Haasnoot, M., Mulder, J. P. M., Hoogvliet, M. M. C., Jeuken, A. B. M., van der Krogt, R. A. A., et al. (2010). Using adaptation tipping points to prepare for climate change and sea level rise: a case study in the Netherlands. *Wiley Interdiscip. Rev. Clim. Change* 1, 729–740. doi: 10.1002/wcc.64

Lamperti, F., Bosetti, V., Roventini, A., and Tavoni, M. (2019). The public costs of climate-induced financial instability. *Nat. Clim. Change* 9, 829–833. doi: 10.1038/s41558-019-0607-5

Lange, S., Volkholz, J., Geiger, T., Zhao, F., Vega, I., Veldkamp, T., et al. (2020). Projecting exposure to extreme climate impact events across six event categories and three spatial scales. *Earths Fut.* 8:e2020EF001616. doi: 10.1029/2020EF001616

Le Cozannet, G., Nicholls, R. J., Hinkel, J., Sweet, W. V., McInnes, K. L., Van de Wal, R. S. W., et al. (2017). Sea level change and coastal climate services: the way forward. *J. Mar. Sci. Eng.* 5:49. doi: 10.3390/jmse5040049

Leane, E., and McGee, J. (2019). *Anthropocene Antarctica: Perspectives From The Humanities, Law And Social Sciences*. London: Routledge. doi: 10.4324/9780429429705

Lemos, M. C., Kirchhoff, C. J., and Ramprasad, V. (2012). Narrowing the climate information usability gap. *Nat. Clim. Change* 2, 789–794. doi: 10.1038/nclimate1614

Lempert, R., Sriver, R. L., and Keller, K. (2012). *Characterizing Uncertain Sea Level Rise Projections to Support Investment Decisions*. Sacramento: California Energy Commission.

Lincke, D., and Hinkel, J. (2018). Economically robust protection against 21st century sea-level rise. *Glob. Environ. Change* 51, 67–73. doi: 10.1016/j.gloenvcha.2018.05.003

Lourenço, T. C., Swart, R., Goosen, H., and Street, R. (2016). The rise of demand-driven climate services. *Nat. Clim. Change* 6, 13–14.

Mandel, A., Tiggeloven, T., Lincke, D., Koks, E., Ward, P., and Hinkel, J. (2021). Risks on global financial stability induced by climate change: the case of flood risks. *Clim. Change* 166:4. doi: 10.1007/s10584-021-03092-2

Moore, J. C., Gladstone, R., Zwinger, T., and Wolovick, M. (2018). Geoengineer polar glaciers to slow sea-level rise. *Nature* 555, 303–305. doi: 10.1038/d41586-018-03036-4

Mora, C., Dousset, B., Caldwell, I. R., Powell, F. E., Geronimo, R. C., Bielecki, C. R., et al. (2017). Global risk of deadly heat. *Nat. Clim. Change* 7, 501–506. doi: 10.1038/nclimate3322

Nalau, J., Preston, B. L., and Maloney, M. C. (2015). Is adaptation a local responsibility? *Environ. Sci. Policy* 48, 89–98. doi: 10.1016/j.envsci.2014.12.011

Nicholls, R. J., Hinkel, J., Lincke, D., and van der Pol, T. (2019). *Global Investment Costs for Coastal Defense through the 21st Century*. Washington: The World Bank. doi: 10.1596/1813-9450-8745

Nurse, L. A., Mclean, R. F., Agard, J., Briguglio, L. P., Duvat-magnan, V., Pelesikoti, N., et al. (2014). "Small islands," in *Climate Change 2014: Impacts, Adaptation, and Vulnerability. Part B: Regional Aspects. Contribution of Working Group II to the Fifth Assessment Report of the Intergovernmental Panel on Climate Change*, eds V. R. Barros, C. B. Field, D. J. Dokken, M. D. Mastrandrea, K. J. Mach, T. E. Bilir, et al. (Cambridge: Cambridge University Press), 1613–1654.

O'Reilly, C. H., Zanna, L., and Woollings, T. (2019). Assessing external and internal sources of Atlantic multidecadal variability using models, proxy data, and early instrumental indices. *J. Clim.* 32, 7727–7745. doi: 10.1175/JCLI-D-19-0177.1

Ortega, F., and Taşpınar, S. (2018). Rising sea levels and sinking property values: hurricane Sandy and New York's housing market. *J. Urban Econ.* 106, 81–100. doi: 10.1016/j.jue.2018.06.005

Parrado, R., Bosello, F., Delpiazzo, E., Hinkel, J., Lincke, D., and Brown, S. (2020). Fiscal effects and the potential implications on economic growth of sea-level rise impacts and coastal zone protection. *Clim. Change* 160, 283–302. doi: 10.1007/s10584-020-02664-y

Patt, A. G., Klein, R. J. T., and de la Vega-Leinert, A. C. (2005). Taking the uncertainty in climate change vulnerability assessment seriously. *Comptes Rendus Geosci.* 337, 411–424. doi: 10.1016/j.crte.2004.11.006

Pattberg, P., and Stripple, J. (2008). Beyond the public and private divide: remapping transnational climate governance in the 21st century. *Int. Environ. Agreem.* 8, 367–388. doi: 10.1007/s10784-008-9085-3

Pauw, W. P. (2017). Mobilising private adaptation finance: developed country perspectives. *Int. Environ. Agreem.* 17, 55–71. doi: 10.1007/s10784-016-9342-9

Schinko, T., Mechler, R., and Hochrainer-Stigler, S. (2017). A methodological framework to operationalize climate risk management: managing sovereign climate-related extreme event risk in Austria. *Mitig. Adapt. Strateg. Glob. Chang.* 22, 1063–1086. doi: 10.1007/s11027-016-9713-0

SEI (2020). *Climate-Resilient Trade and Production: The Transboundary Effects of Climate Change and Their Implications for EU Member States*. Oaks: SEI.

Soares, M. B., Alexander, M., and Dessai, S. (2018). Sectoral use of climate information in Europe: a synoptic overview. *Clim. Serv.* 9, 5–20. doi: 10.1016/j.cliser.2017.06.001

Surminski, S., and Oramas-Dorta, D. (2014). Flood insurance schemes and climate adaptation in developing countries. *Int. J. Disaster Risk Reduct.* 7, 154–164. doi: 10.1016/j.ijdrr.2013.10.005

UNEP (2020). *Adaptation Gap Report 2020*. Nairobi: UNEP.

UNFCCC (1992). *United Nations Framework Convention On Climate Change. United Nations, FCCC/INFORMAL/84 GE.05-62220 (E) 200705*. Bonn: Secretariat of the United Nations Framework Convention on Climate Change, 24.

Van der Pol, T., Hinkel, J., Merkens, J., and Macpherson, L. (2019). *A Comparison of Economic Decision-Support Methods for the Efficient and Robust Protection of the German Baltic Sea Coast Against Flooding*. Lisbon: ECCA.

Van Oord (2021). *Climate Risk Overview*. Rotterdam: Van Oord.

Vincent, K., Daly, M., Scannell, C., and Leathes, B. (2018). What can climate services learn from theory and practice of co-production? *Clim. Serv.* 12, 48–58. doi: 10.1016/j.cliser.2018.11.001

Vogel, C., Steynor, A., and Manyuchi, A. (2019). Climate services in Africa: re-imagining an inclusive, robust and sustainable service. *Clim. Serv.* 15:100107. doi: 10.1016/j.cliser.2019.100107

Weaver, C. P., Lempert, R. J., Brown, C., Hall, J. A., Revell, D., and Sarewitz, D. (2013). Improving the contribution of climate model information to decision making: the value and demands of robust decision frameworks. *Wiley Interdiscip. Rev. Clim. Change* 4, 39–60. doi: 10.1002/wcc.202

Zagonari, F. (2013). Implementing a trans-boundary flood risk management plan: a method for determining willingness to cooperate and case study for the Scheldt estuary. *Nat. Hazards* 66, 1101–1133. doi: 10.1007/s11069-012-0538-1

Conflict of Interest: The authors declare that the research was conducted in the absence of any commercial or financial relationships that could be construed as a potential conflict of interest.

Publisher's Note: All claims expressed in this article are solely those of the authors and do not necessarily represent those of their affiliated organizations, or those of the publisher, the editors and the reviewers. Any product that may be evaluated in this article, or claim that may be made by its manufacturer, is not guaranteed or endorsed by the publisher.

Copyright © 2021 Bisaro, Hinkel, Le Cozannet, van der Pol and Haas. This is an open-access article distributed under the terms of the Creative Commons Attribution License (CC BY). The use, distribution or reproduction in other forums is permitted, provided the original author(s) and the copyright owner(s) are credited and that the original publication in this journal is cited, in accordance with accepted academic practice. No use, distribution or reproduction is permitted which does not comply with these terms.

frontiers in Marine Science

PERSPECTIVE
published: 20 January 2022
doi: 10.3389/fmars.2021.709595

Sea-Level Rise: From Global Perspectives to Local Services

Gaël Durand[1], Michiel R. van den Broeke[2], Goneri Le Cozannet[3], Tamsin L. Edwards[4], Paul R. Holland[5], Nicolas C. Jourdain[1], Ben Marzeion[6], Ruth Mottram[7], Robert J. Nicholls[8], Frank Pattyn[9], Frank Paul[10], Aimée B. A. Slangen[11], Ricarda Winkelmann[12,13], Clara Burgard[1], Caroline J. van Calcar[2,14], Jean-Baptiste Barré[1], Amélie Bataille[1] and Anne Chapuis[1]*

[1] Université Grenoble Alpes, CNRS, IRD, Grenoble INP, IGE, Grenoble, France, [2] Institute for Marine and Atmospheric Research, Utrecht University, Utrecht, Netherlands, [3] Coastal Risks and Climate Change Unit, Risk and Prevention Department, French Geological Survey, BRGM, Orléans, France, [4] Department of Geography, King's College London, London, United Kingdom, [5] British Antarctic Survey, Cambridge, United Kingdom, [6] Institute of Geography and MARUM, Center for Marine Environmental Sciences, University of Bremen, Bremen, Germany, [7] Danish Meteorological Institute, Copenhagen, Denmark, [8] Tyndall Centre for Climate Change Research, University of East Anglia, Norwich, United Kingdom, [9] Laboratoire de Glaciologie, Université Libre de Bruxelles, Brussels, Belgium, [10] Department of Geography, University of Zurich, Zurich, Switzerland, [11] Department of Estuarine and Delta Systems, NIOZ Royal Netherlands Institute for Sea Research, Yerseke, Netherlands, [12] Potsdam Institute for Climate Impact Research (PIK), Member of the Leibniz Association, Potsdam, Germany, [13] Institute of Physics and Astronomy, University of Potsdam, Potsdam, Germany, [14] Faculty of Aerospace Engineering, Delft University of Technology, Delft, Netherlands

OPEN ACCESS

Edited by:
Riccardo Briganti, University of Nottingham, United Kingdom

Reviewed by:
Francesco De Leo, Cal Poly San Luis Obispo College of Engineering, United States
Giovanni Besio, University of Genoa, Italy

***Correspondence:**
Gaël Durand
gael.durand@univ-grenoble-alpes.fr

Specialty section:
This article was submitted to Coastal Ocean Processes, a section of the journal Frontiers in Marine Science

Received: *14 May 2021*
Accepted: *22 December 2021*
Published: *20 January 2022*

Citation:
Durand G, van den Broeke MR, Le Cozannet G, Edwards TL, Holland PR, Jourdain NC, Marzeion B, Mottram R, Nicholls RJ, Pattyn F, Paul F, Slangen ABA, Winkelmann R, Burgard C, van Calcar CJ, Barré J-B, Bataille A and Chapuis A (2022) Sea-Level Rise: From Global Perspectives to Local Services. Front. Mar. Sci. 8:709595. doi: 10.3389/fmars.2021.709595

Coastal areas are highly diverse, ecologically rich, regions of key socio-economic activity, and are particularly sensitive to sea-level change. Over most of the 20th century, global mean sea level has risen mainly due to warming and subsequent expansion of the upper ocean layers as well as the melting of glaciers and ice caps. Over the last three decades, increased mass loss of the Greenland and Antarctic ice sheets has also started to contribute significantly to contemporary sea-level rise. The future mass loss of the two ice sheets, which combined represent a sea-level rise potential of ∼65 m, constitutes the main source of uncertainty in long-term (centennial to millennial) sea-level rise projections. Improved knowledge of the magnitude and rate of future sea-level change is therefore of utmost importance. Moreover, sea level does not change uniformly across the globe and can differ greatly at both regional and local scales. The most appropriate and feasible sea level mitigation and adaptation measures in coastal regions strongly depend on local land use and associated risk aversion. Here, we advocate that addressing the problem of future sea-level rise and its impacts requires (i) bringing together a transdisciplinary scientific community, from climate and cryospheric scientists to coastal impact specialists, and (ii) interacting closely and iteratively with users and local stakeholders to co-design and co-build coastal climate services, including addressing the high-end risks.

Keywords: sea-level rise, Antarctic, Greenland, glaciers, local impact

INTRODUCTION

Coastal zones (regions less than 10 m above mean sea level) are ecologically rich, diverse and productive, but highly sensitive to changes in sea level (Wong et al., 2014; Oppenheimer et al., 2019). They concentrate population, being home to more than 600 million people, of which about 300 million live in flood-prone areas. Coastal zones are key engines of the global economy and sites of significant urbanization, hosting 65% of the world's largest and numerous smaller cities. If current trends continue, the coastal population will roughly double by 2060 (Neumann et al., 2015), while the coastal economy will grow even more – plausibly by an order of magnitude – greatly increasing the exposure of humans and infrastructure to the hazards caused by sea-level rise (SLR). From an environmental and socio-economic point of view, improving decadal to centennial projections of regionally resolved SLR and making them available to coastal stakeholders has the highest priority.

This study aims to consider how we can most effectively enhance global understanding of sea level, and translate this into coastal climate services to provide useful information for local impact and adaptation needs assessment. This involves considering the science of global sea-level change, translation of global information to potential local sea-level change, as well as user and stakeholder engagement to co-produce projections appropriate to the decisions being made. These three points are outlined in more detail below and in the following sections.

In the 20th century, SLR was mainly caused by mass loss of glaciers and ice caps, henceforth simply referred to as glaciers,[1] and by ocean thermal expansion (IPCC, 2019, 2021). However, since 1990, both the Antarctic Ice Sheet (AIS) and Greenland Ice Sheet (GrIS), which combined represent a sea-level rise *potential* of ∼65 m, have increasingly contributed to SLR (Bamber et al., 2018; Shepherd et al., 2018, 2021). As highlighted in the last three assessment reports of the Intergovernmental Panel on Climate Change (IPCC) (IPCC, 2007, 2013, 2021) and the Special Report on the Ocean and Cryosphere in a Changing Climate (BR001), the main uncertainty in projections of future SLR is the limited ability to model the future melt dynamics of the AIS and GrIS. Uncertainty quantification is further complicated by the fact that both ice sheets have been estimated to have tipping points at, or slightly above, 1.5–2.0°C warming compared to the pre-industrial epoch (Pattyn et al., 2018; Pattyn and Morlighem, 2020; Noël et al., 2021). Crossing these tipping points might lead to self-sustained demise of large parts of both ice sheets with a multi-meter contribution to SLR within a couple of centuries as a consequence. Though the relative contribution of ice sheet mass loss to SLR is expected to increase further over the 21st Century (Marzeion et al., 2018; Goelzer et al., 2020; Seroussi et al., 2020), glaciers will continue to contribute significantly to SL, a contribution that must also be better quantified (IPCC, 2021). Clearly, future SLR is a global problem that is mainly controlled by the future losses of land ice masses. This aspect is further detailed in Section "Components of Global Mean Sea-Level Rise."

It is important to recognize that SLR is highly non-uniform in space and time and this needs to be understood to provide useful sea-level scenarios and coastal climate services. While in mitigation we consider global changes, impacts and adaptation need to reflect local changes. Ocean warming causes thermal expansion which leads to an increase in ocean volume. Water exchange between the land and the ocean, for instance by the melting of land ice, causes a change in ocean mass. Superimposed on these global processes are regional variations resulting from changes in ocean currents and density, as well as gravitational, rotational and deformational effects resulting from changes in the loading of ice and water masses and all components of vertical land movement. To make an inventory of potential coastal impacts and adaptation needs thus requires SLR projections that are essentially regional (Slangen et al., 2014) and local (Wöppelmann and Marcos, 2016; Woodworth et al., 2019; Nicholls et al., 2021a). This is detailed in Section "Sea-Level Rise Impacts: The Need for Local Information."

There are multiple approaches to quantify SLR uncertainty, yet none of these can fully embrace the wide variety of user needs for sea level information. Individual user needs depend strongly on the value of exposed assets, their level of risk aversion, the relevant timescale and the wider context set by other stakeholders such as national governments, regional/local authorities, coastal conservation agencies, insurance/investment companies, etc (Hinkel et al., 2019; Kopp et al., 2019; Nicholls et al., 2021a). As a consequence, improving and adjusting SLR projections to the needs of our society can only be achieved through a broad and multidisciplinary collaboration in close and iterative interaction with users and stakeholders. This is discussed in Section "Interactions With Stakeholders and Co-design of Sea-Level Rise Projections."

COMPONENTS OF GLOBAL MEAN SEA-LEVEL RISE

Sea-level rise contributions from thermal expansion (due to ocean warming) and changes in ocean dynamics (due to changes in ocean currents and density) can be quantified by global climate and related models. Between 2006 and 2018, thermal expansion contributed to increase mean SLR by 1.39 mm/yr and for 2100 is projected to contribute to SLR in the range between 0.12 (0.09–0.15) m under the high mitigation SSP1-1.9 scenario to 0.30 (0.24–0.36) m under the highly pessimistic SSP5-8.5 scenario, accounting for 30–40% of the total SLR (Fox-Kemper et al., 2021). Thermal expansion is a relatively well understood process, and uncertainties mainly reflect differences between scenarios.

The remainder of the projected 21st century total SLR mainly constitutes the melting of land ice. Apart from glaciers and increasingly the GrIS, this represents continued mass loss from specific regions in Antarctica, notably the West Antarctic Ice

[1]Here, we follow the definition of glaciers as used in the 5th assessment report of the Intergovernmental Panel on Climate Change (IPCC, 2013): "*A glacier is a perennial mass of land ice that originates from compressed snow, shows evidence of past or present flow (through internal deformation and/or sliding at the base) and is constrained by internal stress and friction at the base and sides. A glacier is maintained by accumulation of snow at high altitudes, balanced by melting at low altitudes and/or discharge into the sea. An ice mass of the same origin as glaciers, but of continental size, is called an ice sheet. For the purpose of simplicity, all ice masses other than ice sheets are referred to as glaciers.*"

Sheet and the Antarctic Peninsula. Evidence of mass loss in these regions of the AIS has become clear with the advent of widespread remote sensing measurements in the early 1990s, and their rate of mass loss has steadily increased since the early 2000s. In contrast, the mass balance of the much bigger East Antarctic Ice Sheet remains highly uncertain (Shepherd et al., 2018; Rignot et al., 2019). Overall, Antarctica contributed 0.37 (0.24–0.50) mm/yr to SLR between 2006 and 2018 (Fox-Kemper et al., 2021). The mass balance of the AIS currently has two major components: a positive contribution made by the annual accumulation of ∼2500 Gt of snow at the ice sheet surface and a negative contribution of similar magnitude made by the flow of ice streams and outlet glaciers toward the ocean, where they form extensive floating ice shelves which lose mass by basal melt at the ocean-ice interface and iceberg calving at the ice shelf front. Assumed smaller (<10%) but poorly understood contributions to the AIS mass balance are basal melt at the ice-bedrock interface, (drifting snow) sublimation and the runoff of meltwater (van Wessem et al., 2018; Agosta et al., 2019).

The primary driver of current AIS mass loss is the acceleration of outlet glaciers, notably those feeding the Amundsen Sea Embayment (ASE) in West Antarctica. Here, ice discharge increased by about 77% from 1973 to 2013 (Mouginot et al., 2014). Acceleration of ice flow in the ASE occurs in response to incursions of warm Circumpolar Deep Water, thinning the ice shelves from below (Dutrieux et al., 2014). The thinning of ice shelves reduces the buttressing they exert on upstream grounded glaciers and consequently enhances the ice flow, causing mass loss of grounded ice and SLR (Gagliardini et al., 2010). The ASE is of particular concern because the grounding line, the transition between grounded and floated ice, rests on bedrock generally sloping downwards toward the interior of the ice sheet (Morlighem et al., 2020). In such a topographic configuration, the grounding line may be unstable whereby an initial retreat reinforces the ice outflow, leading to thinning and further retreat, etc. This process, known as the Marine Ice Sheet Instability (MISI), has been discussed for decades (Weertman, 1974; Vaughan, 2008) and it is nowadays acknowledged that unconfined ice shelves are indeed unstable (Schoof, 2007), although ice-shelf buttressing and/or rapid bedrock uplift might in some situations stabilize the glacier (Gudmundsson et al., 2012; Barletta et al., 2018). It has been proposed that MISI could be engaged in the ASE once a 1.5–2°C global warming compared to preindustrial has been exceeded (Pattyn et al., 2018; Rosier et al., 2021).

The retreat of Antarctic outlet glaciers that are currently confined by ice shelves might be further accelerated if intense surface melting leads to meltwater ponding and subsequent ice shelf disintegration. This process of hydro-fracturing is thought to be responsible for the catastrophic disintegration of Larsen A (1995), Larsen B (2002), and Wilkins (2008) ice shelves in the Antarctic Peninsula (Scambos et al., 2009). It has also been proposed that the collapse of ice shelves could expose ice cliffs high enough to produce stresses exceeding the strength of ice and leading to consecutive ice cliff collapses and rapid retreat of the ice shelf front (DeConto and Pollard, 2016). This process, named Marine Ice Cliff Instability (MICI), remains as yet unproven (Edwards et al., 2019). Current median projections of the contribution of the AIS to SLR from 1995–2014 baseline to 2,100 range from 0.10 to 0.12 m independent of the considered Shared Socioeconomic Pathways (SSP) (Fox-Kemper et al., 2021). However, the poorly understood MISI and MICI and the subsequent dynamical responses could introduce a considerably higher contribution (Bamber et al., 2019; DeConto et al., 2021; Fox-Kemper et al., 2021).

The mass balance of the GrIS is very different from that of the AIS. Apart from iceberg calving in narrow fjords -the GrIS does not have extensive ice shelves-, an additional significant negative mass balance component is meltwater runoff. Until the mid 1990s, mass losses from the GrIS were probably modest (Mouginot et al., 2019), but a series of strong melt years since the mid 2000s, together with the rapid acceleration and retreat of multiple major outlet glaciers (King et al., 2020), tipped the annual ice sheet budget into a persistent negative state (Shepherd et al., 2018). With a contemporary mass loss equivalent of 0.63 (0.51–0.74) mm per year between 2006 and 2018, the GrIS is currently the largest single net contributor to increased ocean mass leading to SLR (Fox-Kemper et al., 2021). At the same time, interannual variability of mass loss also appears to have increased (Simonsen et al., 2021), mainly owing to highly variable surface processes. The increase in surface melt and runoff since the late 1990s is in part due to the increased occurrence and persistence of atmospheric blocking over Greenland, leading to clear skies, higher air temperatures and higher melt rates notably on the southwestern GrIS (Hanna et al., 2018). However, this effect varies between years.

By storing and refreezing liquid water, the layer of firn (compressed snow) that covers 90% of the GrIS currently prevents nearly half of the percolating meltwater to run off. Strong melt events, particularly in the summers of 2012 and 2019, measurably increased the extent of impermeable ice layers that reduce percolation into the deeper firn in subsequent years, enhancing runoff (MacFerrin et al., 2019). The increase in GrIS mass loss from acceleration and increased submarine melting of marine-terminating outlet glaciers was likely, at least in part, initiated by increased ocean temperatures (Straneo and Heimbach, 2013). Notably, the retreat of glaciers in southeast and west Greenland concurred with warm ocean waters becoming entrained into the fjord environments and eventually melting the glacier fronts. In spite of the continuously improved understanding of dynamic behavior of marine-terminating outlet glaciers, the wide range of factors that determine this behavior, including bed topography, makes it complicated to generalize the response of outlet glacier dynamics to future climate warming.

In a long term perspective, the GrIS might enter a self-sustained melting state, due to positive feedbacks such as the melt-elevation feedback (a lower ice sheet surface faces a warmer atmosphere and melts even faster, etc.) and the melt-albedo feedbacks (as the ice sheet melts its surface gets darker and melts even faster). Once meltwater runoff exceeds the accumulation of snow, mass loss becomes quasi-irreversible; Pattyn et al. (2018) estimated that such a threshold could be crossed at about 2°C warming above pre-industrial, which could be reached already around 2055 under a high-end warming scenario (Noël et al., 2021). Current main projections of the contribution of the GrIS to SLR from 1995–2014 baseline to 2100 range from

0.05 (0.00–0.09) m (SSP1-19) to 0.13 (0.09–0.18) m (SSP5-85) (Fox-Kemper et al., 2021).

While glaciers store less than 1% of the global ice mass (Farinotti et al., 2019), their increasing mass loss rates (Zemp et al., 2019; Hugonnet et al., 2021) exceeded those of the GrIS or AIS in recent years. For the period 2006 to 2018, Fox-Kemper et al. (2021) estimated the glacier contribution (excluding glaciers in the periphery of the ice sheets) to SLR to be 0.62 (0.57–0.68) mm/yr. In the past two decades, all regions that harbor glaciers have contributed to SLR (Hock et al., 2019a; IPCC, 2019). Because the geometric adjustment of glacier extent in response to climate change is delayed, glacier mass loss during the first half of the 21st century is already committed and to a large degree independent of future greenhouse gas emissions (Marzeion et al., 2018). The evolution of glacier mass during the second half of the 21st century depends strongly on the considered emission scenario, but also on the combination of climate and glacier models used for the projection (Hock et al., 2019b; Marzeion et al., 2020). Current main projections of the contribution of the glaciers to SLR from 1994–2015 baseline to 2100 range from 0.08 (0.06–0.10) m (SSP1-19) to 0.18 (0.15–0.20) m (SSP5-85) (Fox-Kemper et al., 2021).

Given (i) the leading contribution to SLR of land ice melt and the associated future SLR commitment, (ii) its huge potential to further contribute to future SLR with tipping points that could be crossed in the coming decades by both the AIS and the GrIS, combined with (iii) the deep uncertainties attached to poorly understood processes controlling the possible self-sustained demise of large regions of both ice sheets, we must intensify in-depth research into glacier and ice sheet mass balance. The complexity of the system under study requires an interdisciplinary team with numerical/observational experts from the following research disciplines: (i) meteorology and surface mass balance of ice sheets and glaciers, (ii) oceanography and ice shelf basal melting, (iii) ice sheet and glacier processes (including calving) and dynamics, (iv) the coupling of these components, and (v) uncertainty quantification.

SEA-LEVEL RISE IMPACTS: THE NEED FOR LOCAL INFORMATION

Although global-mean SLR is a useful climate metric, multiple processes cause large spatial and temporal variations in sea-level change on a wide range of scales, which must be considered if we wish to develop information relevant to impacts, adaptation needs, and wider climate services in sea level (**Figure 1**). At the regional scale (∼100 km), changes in dynamic sea level reflect changes in ocean water density (temperature and salinity) as well as changes in the wind-driven and density-driven ocean circulation, e.g., forced by El Niño Southern Oscillation. A second driver for regional sea-level changes are the gravitational, rotational and deformational effects resulting from mass redistribution between land and ocean. When an ice sheet loses mass, its gravitational pull on the ocean is reduced, leading to a sea-level fall close to the ice sheet itself, but greater than average SLR in the far field, i.e., more than 2,000 km away from the mass source (Mitrovica et al., 2001). The resulting pattern is often referred to as a sea-level 'fingerprint' and typically shows an above-average SLR in the Northern Hemisphere for mass loss from the AIS, and an above-average SLR in the Southern Hemisphere for mass loss from the GrIS. Vertical land movement is also of particular importance, as in some coastal locations its magnitude is equal to or even larger than the long-term SLR, amplifying local relative SLR (Nicholls et al., 2021b). Possible causes are natural or human-induced subsidence (through e.g., compaction of sedimentary layers due to groundwater extraction), glacial isostatic adjustment, and tectonics. Glacial isostatic adjustment is estimated using global models (e.g., Peltier et al., 2015), while other components can be derived from *in situ* measurements such as in deltas and cities (Nicholls et al., 2021b) and at tide gauges (e.g., Kopp et al., 2014).

Sea-level rise is also affected by processes acting on a local scale (∼10 km or less) such as ocean and coastal dynamic (geomorphological) processes (Zhang et al., 2017). Of particular relevance to coastal risk management are changes in the frequency and height of sea-level extremes, for instance from tides, storm surges or waves and their combinations, including mean SLR (Allison et al., 2021). Although these processes typically occur on short timescales (hours to days) and only have a local to regional effect on the coast, their impacts are magnified by long-term SLR (Oppenheimer et al., 2019). There is also evidence that tide and surge propagation is being affected by SLR, as well as human modifications to bathymetry, and this has the potential to enhance extreme events more than SLR alone (Arns et al., 2015; Haigh et al., 2020; Talke and Jay, 2020). Further, such extreme events cause most floods and damage, so stakeholders strongly focus on adaptation to them while often raising the consideration of adaptation to mean SLR as well (e.g., Rosenzweig et al., 2011; Ranger et al., 2013). Adding appropriate allowance, **Figure 1** summarizes crucial processes influencing change in sea level and their associated spatial and temporal scales.

As SLR will have a local impact, and decisions on adaptation and mitigation are also made on a local scale, it is essential that coastal climate services provide local sea-level projections that include the downscaling of all relevant processes; considering only global mean projections will seriously misdirect adaptation efforts and may lead to maladaptation. Therefore, producing reliable and sensible SLR projections requires that climate and sea-level scientists interact with specialists in the field of geodesy, earth science and ocean dynamics. Further, the context of use and application of the local (or relative) sea-level rise information needs to be considered so the relevant coastal impacts, adaptation needs and societal context needs to be considered as discussed in the next section.

INTERACTIONS WITH STAKEHOLDERS AND CO-DESIGN OF SEA-LEVEL RISE PROJECTIONS

The processes and methods described above contain uncertainties that differ in both nature and magnitude

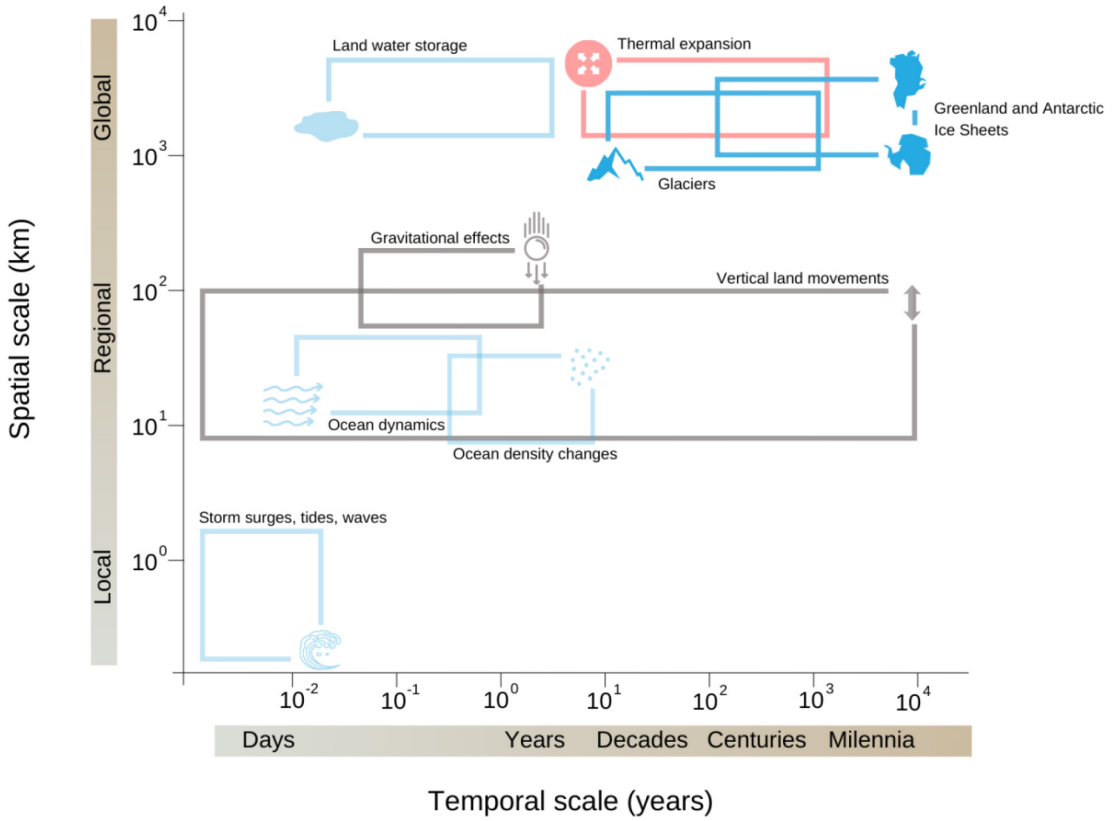

FIGURE 1 | Illustration of the processes that contribute to sea level change with respect to their temporal and spatial scales.

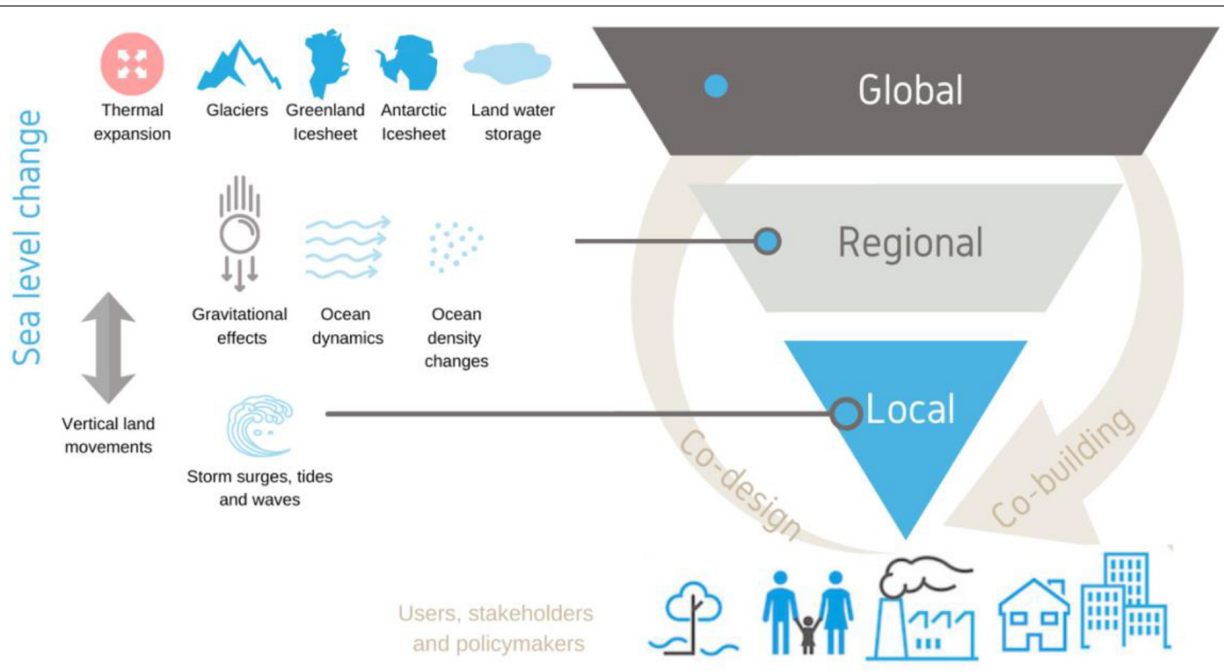

FIGURE 2 | Providing reliable coastal adaptation services requires considering a large variety of processes on a wide range of scales. It should be iteratively co-designed and built with local users stakeholders, and policymakers.

(e.g., Bakker et al., 2017), accumulate across scales (e.g., Rohmer et al., 2019) and ultimately affect coastal impact and adaptation assessments (Toimil et al., 2020; Rohmer et al., 2021). Historically, the IPCC has delivered sea-level projections with uncertainties described using quantitative metrics (likelihood) associated with qualitative confidence statements reflecting the quality of the evidence and the degree of agreement (Mastrandrea et al., 2011). This may not be sufficient from an adaptation perspective, particularly where users have a high risk aversion (Hinkel et al., 2019). In these cases, the emerging practice is to deliver a high-end scenario together with likely or probable scenarios (Ranger et al., 2013; Stammer et al., 2019; Nicholls et al., 2021a). High-end in this context means a scenario well above the likely projected SLR that cannot be excluded with present (limited) understanding of ice-sheet mass loss processes. Other uncertainty frameworks which consider probabilistic models or semi-quantitative information (Le Cozannet et al., 2017) might also be considered to deliver consistent sea-level information suited to the needs of various users. In its latest assessment report (AR6), the IPCC for the first time presented a "low likelihood high impact" scenario attached to the SSP5-8.5, showing that a sea level rise of 1.7 m by 2100 and more than 15 m by 2300 could not be excluded under high emissions (Fox-Kemper et al., 2021).

The impacts caused by SLR are wide-ranging – increased flooding, erosion, salinization and ultimately submergence – and there are many approaches to adaptation from planned or forced retreat, accommodation, hard and/or soft protection and even advance (Oppenheimer et al., 2019). The selected adaptation strategy will depend strongly on the local situation and decision context (Hinkel et al., 2019; Nicholls et al., 2021a). Some decisions such as beach nourishment operate at a decadal timescale and are easily adjusted over time, e.g., adding more or less sand (assuming sand resources are readily available). Hence these approaches can be easily adjusted to improved understanding as sea levels rise. In contrast, decisions such as building a nuclear power station or raising low-lying islands for urban development have long lead times, i.e., a century or more, and high risk aversion means there is strong interest in high-end SLR projections (e.g., Wilby et al., 2011; Brown et al., 2020): as the rate of SLR considered increases, the ability to protect may be overwhelmed for extreme cases linked to ice sheet collapse (Haasnoot et al., 2020). There are so many local situations that we do not *a priori* know the best approach to adaptation or the SLR information needs: the sea-level and adaptation scientists need to work together to understand the adaptation problem and what SLR science can presently provide that is relevant. Hence, the most useful SLR projections should be co-designed with users. This implies an iterative process in which all parties have to understand the needs, the possibilities to address these needs and the range of potential changes, and then jointly envision a future coastal adaptation service before elaborating projections (**Figure 2**).

CONCLUSION

This paper has considered how we can most effectively translate global understanding of sea level, including the major ice sheets and their uncertainties, to effective local climate services and coastal adaptation. It can be concluded that there are two important factors to consider: (i) to provide local sea-level projections, information from many different research disciplines needs to be transparently exchanged and combined, and (ii) to ensure usability for local stakeholders, sea-level information needs to be tailored to local requirements. Following these principles, as also adopted in the EU project "Projecting sea-level rise: from projections to local implications" (PROTECT), we encourage the formation of research consortia that cover the entire knowledge chain, ranging from ice sheet and ocean modeling, global, regional and extreme SLR projections, through to the analysis of SLR risks and adaptation needs and the co-design of sea-level information across the range of stakeholder needs. In this way global sea-level science can be linked to effective coastal climate services at the scale of risk and adaptation.

DATA AVAILABILITY STATEMENT

The original contributions presented in the study are included in the article, further inquiries can be directed to the corresponding author.

AUTHOR CONTRIBUTIONS

All authors contributed to the establishment of the concept defended here and applied in the PROTECT project. They also contributed to the writing of the manuscript and the design of the figures.

FUNDING

This publication was supported by PROTECT. This project has received funding from the European Union's Horizon 2020 Research and Innovation Programme under grant agreement No 869304, PROTECT contribution number 27.

REFERENCES

Agosta, C., Amory, C., Kittel, C., Orsi, A., Favier, V., Gallée, H., et al. (2019). Estimation of the Antarctic surface mass balance using the regional climate model MAR (1979–2015) and identification of dominant processes. *Cryosphere* 13, 281–296. doi: 10.5194/tc-13-281-2019

Allison, I., Paul, F., Colgan, W., and King, M. (2021). "Chapter 20 – Ice sheets, glaciers, and sea level," in *Snow and Ice-Related Hazards, Risks, and Disasters (Second Edition)*, eds W. Haeberli and C. Whiteman (New York, NY: Elsevier), 707–740. doi: 10.1016/B978-0-12-817129-5.00013-5

Arns, A., Wahl, T., Dangendorf, S., and Jensen, J. (2015). The impact of sea level rise on storm surge water levels in the northern part of the german bight. *Coast. Eng.* 96, 118–131. doi: 10.1016/j.coastaleng.2014.12.002

Bakker, A. M. R., Louchard, D., and Keller, K. (2017). Sources and implications of deep uncertainties surrounding sea-level projections. *Climat. Change* 140, 339–347. doi: 10.1007/s10584-016-1864-1

Bamber, J. L., Oppenheimer, M., Kopp, R. E., Aspinall, W. P., and Cooke, R. M. (2019). Ice sheet contributions to future sea-level rise from structured expert judgment. *Proc. Natl. Acad. Sci. U.S.A.* 116, 11195–11200. doi: 10.1073/pnas.1817205116

Bamber, J. L., Westaway, R. M., Marzeion, B., and Wouters, B. (2018). The land ice contribution to sea level during the satellite era. *Environ. Res. Lett.* 13:063008. doi: 10.1088/1748-9326/aac2f0

Barletta, V. R., Bevis, M., Smith, B. E., Wilson, T., Brown, A., Bordoni, A., et al. (2018). Observed rapid bedrock uplift in amundsen sea embayment promotes ice-sheet stability. *Science* 360, 1335–1339. doi: 10.1126/science.aao1447

Brown, S., Wadey, M. P., Nicholls, R. J., Shareef, A. A., Khaleel, Z., Hinkel, J., et al. (2020). Land raising as a solution to sea-level rise: an analysis of coastal flooding on an artificial Island in the Maldives. *J. Flood Risk Manag.* 13:e12567. doi: 10.1111/jfr3.12567

DeConto, R. M., and Pollard, D. (2016). Contribution of Antarctica to past and future sea-level rise. *Nature* 531, 591–597. doi: 10.1038/nature17145

DeConto, R. M., Pollard, D., Alley, R. B., Velicogna, I., Gasson, E., Gomez, N., et al. (2021). 'The Paris climate agreement and future sea-level rise from Antarctica'. *Nature* 593, 83–89. doi: 10.1038/s41586-021-03427-0

Dutrieux, P., De Rydt, J., Jenkins, A., Holland, P. R., Ha, H. K., Lee, S. H., et al. (2014). Strong sensitivity of pine island ice-shelf melting to climatic variability. *Science* 343, 174–178. doi: 10.1126/science.1244341

Edwards, T. L., Brandon, M. A., Durand, G., Edwards, N. R., Golledge, N. R., Holden, P. B., et al. (2019). Revisiting Antarctic ice loss due to marine ice-cliff instability. *Nature* 566, 58–64. doi: 10.1038/s41586-019-0901-4

Farinotti, D., Huss, M., Fürst, J. J., Landmann, J., Machguth, H., Maussion, F., et al. (2019). A consensus estimate for the ice thickness distribution of all glaciers on earth. *Nat. Geosci.* 12, 168–173. doi: 10.1038/s41561-019-0300-3

Fox-Kemper, B., Hewitt, H. T., Xiao, C., Aðalgeirsdóttir, G., Drijfhout, S. S., Edwards, T. L., et al. (2021). *Ocean, Cryosphere and Sea Level Change*. *Climate Change 2021: The Physical Science Basis. Contribution of Working Group I to the Sixth Assessment Report of the Intergovernmental Panel on Climate Change*, Cambridge University Press.

Gagliardini, O., Durand, G., Zwinger, T., Hindmarsh, R. C. A., and Le Meur, E. (2010). Coupling of ice-shelf melting and buttressing is a key process in ice-sheets dynamics. *Geophys. Res. Lett.* 37:L14501. doi: 10.1029/2010GL043334

Goelzer, H., Nowicki, S., Payne, A., Larour, E., Seroussi, H., Lipscomb, W. H., et al. (2020). The future sea-level contribution of the greenland ice sheet: a multi-model ensemble study of ISMIP6. *Cryosphere* 14, 3071–3096. doi: 10.5194/tc-14-3071-2020

Gudmundsson, G. H., Krug, J., Durand, G., Favier, L., and Gagliardini, O. (2012). The stability of grounding lines on retrograde slopes. *Cryosphere* 6, 1497–1505. doi: 10.5194/tc-6-1497-2012

Haasnoot, M., Kwadijk, J., van Alphen, J., Le Bars, D., van den Hurk, B., Diermanse, F., et al. (2020). Adaptation to uncertain sea-level rise; how uncertainty in Antarctic mass-loss impacts the coastal adaptation strategy of the Netherlands. *Environ. Res. Lett.* 15:034007. doi: 10.1088/1748-9326/ab666c

Haigh, I. D., Pickering, M. D., Green, J. A. M., Arbic, B. K., Arns, A., Dangendorf, S., et al. (2020). The tides they are A-Changin': a comprehensive review of past and future nonastronomical changes in tides, their driving mechanisms, and future implications. *Rev. Geophys.* 58:e2018RG000636. doi: 10.1029/2018RG000636

Hanna, E., Fettweis, X., and Hall, R. J. (2018). Brief communication: recent changes in summer greenland blocking captured by none of the CMIP5 models. *Cryosphere* 12, 3287–3292. doi: 10.5194/tc-12-3287-2018

Hinkel, J., Church, J. A., Gregory, J. M., Lambert, E., Le Cozannet, G., and Lowe, J. (2019). Meeting user needs for sea level rise information: a decision analysis perspective. *Earths Future* 7, 320–337. doi: 10.1029/2018EF001071

Hock, R., Bliss, A., Marzeion, B., Giesen, R. H., Hirabayashi, Y., Huss, M., et al. (2019a). GlacierMIP – a model intercomparison of global-scale glacier mass-balance models and projections. *J. Glaciol.* 65, 453–467. doi: 10.1017/jog.2019.22

Hock, R., Rasul, G., Adler, C., Cáceres, B., Gruber, S., Hirabayashi, Y., et al. (2019b). *High Mountain Areas: IPCC Special Report on the Ocean and Cryosphere in a Changing Climate. The Intergovernmental Panel on Climate Change*. Geneva: IPCC, 2019.

Hugonnet, R., McNabb, R., Berthier, E., Menounos, B., Nuth, C., Girod, L., et al. (2021). Accelerated global glacier mass loss in the early twenty-first century. *Nature* 592, 726–731. doi: 10.1038/s41586-021-03436-z

IPCC (2007). *Climate Change 2007: The Physical Science Basis. Contribution of Working Group I to the Fourth Assessment Report of the Intergovernmental Panel on Climate Change*. Cambridge: Cambridge University Press.

IPCC (2013). *Climate Change 2013: The Physical Science Basis: Working Group I Contribution to the Fifth Assessment Report of the Intergovernmental Panel on Climate Change*. Cambridge: Cambridge University Press, 2014.

IPCC (2019). "Polar Regions," in *IPCC Special Report on the Ocean and Cryosphere in a Changing Climate* (Geneva: IPCC).

IPCC (2021). *Climate Change 2021: The Physical Science Basis. Contribution of Working Group I to the Sixth Assessment Report of the Intergovernmental Panel on Climate Change*. Cambridge: Cambridge University Press, 2021.

King, M. D., Howat, I. M., Candela, S. G., Jeong, S., Noh, M. J., Noël, B., et al. (2020). Dynamic ice loss from the Greenland ice sheet driven by sustained glacier retreat. *Commun. Earth Environ.* 1:1. doi: 10.1038/s43247-020-0001-2

Kopp, R. E., Gilmore, E. A., Little, C. M., Lorenzo-Trueba, J., Ramenzoni, V. C., and Sweet, W. V. (2019). Usable science for managing the risks of sea-level rise. *Earths Future* 7, 1235–1269. doi: 10.1029/2018EF001145

Kopp, R. E., Horton, R. M., Little, C. M., Mitrovica, J. X., Oppenheimer, M., Rasmussen, D. J., et al. (2014). Probabilistic 21st and 22nd century sea-level projections at a global network of tide gauge sites. *Earths Future* 2, 383–406. doi: 10.1002/2014EF000239

Le Cozannet, G. L., Manceau, J., and Rohmer, J. (2017). Bounding probabilistic sea-level projections within the framework of the possibility theory. *Environ. Res. Lett.* 12:014012. doi: 10.1088/1748-9326/aa5528

MacFerrin, M., Machguth, H., van As, D., Charalampidis, C., Stevens, C. M., Heilig, A., et al. (2019). Rapid expansion of Greenland's low-permeability ice slabs. *Nature* 573, 403–407. doi: 10.1038/s41586-019-1550-3

Marzeion, B., Hock, R., Anderson, B., Bliss, A., Champollion, N., Fujita, K., et al. (2020). Partitioning the uncertainty of ensemble projections of global glacier mass change. *Earths Future* 8:e2019EF001470. doi: 10.1029/2019EF001470

Marzeion, B., Kaser, G., Maussion, F., and Champollion, N. (2018). Limited influence of climate change mitigation on short-term glacier mass loss. *Nat. Climate Change* 8, 305–308. doi: 10.1038/s41558-018-0093-1

Mastrandrea, M. D., Mach, K. J., Plattner, G. K., Edenhofer, O., Stocker, T. F., Field, C. B., et al. (2011). The IPCC AR5 guidance note on consistent treatment of uncertainties: a common approach across the working groups. *Climat. Change* 108:675. doi: 10.1007/s10584-011-0178-6

Mitrovica, J. X., Tamisiea, M. E., Davis, J. L., and Milne, G. A. (2001). Recent mass balance of polar ice sheets inferred from patterns of global sea-level change. *Nature* 409, 1026–1029. doi: 10.1038/35059054

Morlighem, M., Rignot, E., Binder, T., Blankenship, D., Drews, R., Eagles, G., et al. (2020). Deep glacial troughs and stabilizing ridges unveiled beneath the margins of the Antarctic Ice Sheet. *Nat. Geosci.* 13, 132–137. doi: 10.1038/s41561-019-0510-8

Mouginot, J., Rignot, E., Bjørk, A. A., van den Broeke, M., Millan, R., Morlighem, M., et al. (2019). Forty-six years of Greenland ice sheet mass balance from 1972 to 2018. *Proc. Natl. Acad. Sci. U.S.A.* 116, 9239–9244. doi: 10.1073/pnas.1904242116

Mouginot, J., Rignot, E., and Scheuchl, B. (2014). Sustained increase in ice discharge from the Amundsen Sea embayment, West Antarctica, from 1973 to 2013. *Geophys. Res. Lett.* 41, 1576–1584. doi: 10.1002/2013GL059069

Neumann, B., Vafeidis, A. T., Zimmermann, J., and Nicholls, R. J. (2015). Future coastal population growth and exposure to sea-level rise and coastal flooding – a global assessment. *PLoS One* 10:e0118571. doi: 10.1371/journal.pone.0118571

Nicholls, R. J., Hanson, S. E., Lowe, J. A., Slangen, A. B. A., Wahl, T., Hinkel, J., et al. (2021a). Integrating new sea-level scenarios into coastal risk and adaptation assessments: an ongoing process. *WIREs Climate Change* 12:e706. doi: 10.1002/wcc.706

Nicholls, R. J., Lincke, D., Hinkel, J., Brown, S., Vafeidis, A. T., Meyssignac, B., et al. (2021b). A global analysis of subsidence, relative sea-level change and coastal flood exposure. *Nat. Climate Change* 11, 338–342. doi: 10.1038/s41558-021-00993-z

Noël, B., van Kampenhout, L., Lenaerts, J. T. M., van de Berg, W. J., and van den Broeke, M. R. (2021). A 21st century warming threshold for sustained greenland ice sheet mass loss. *Geophys. Res. Lett.* 48:e2020GL090471. doi: 10.1029/2020GL090471

Oppenheimer, M., Glavovic, B. C., Hinkel, J., van de Wal, R., Magnan, A. K., Abd-Elgawad, A., et al. (2019). *Sea Level Rise and Implications for Low-Lying Islands,*

Coasts and Communities. IPCC Special Report on the Ocean and Cryosphere in a Changing Climate, Vol. 126, Geneva: IPCC.

Pattyn, F., and Morlighem, M. (2020). The Uncertain Future of the Antarctic Ice Sheet. *Science* 367, 1331–1335. doi: 10.1126/science.aaz5487

Pattyn, F., Ritz, C., Hanna, E., Asay-Davis, X., DeConto, R., Durand, G., et al. (2018). 'The Greenland and Antarctic ice sheets under 1.5 °C global warming. *Nat. Climate Change* 8, 1053–1061. doi: 10.1038/s41558-018-305-308

Peltier, W. R., Argus, D. F., and Drummond, R. (2015). Space geodesy constrains ice age terminal deglaciation: the global ICE-6G_C (VM5a) model. *J. Geophys. Res. Solid Earth* 120, 450–487. doi: 10.1002/2014JB011176

Ranger, N., Reeder, T., and Lowe, J. (2013). Addressing "Deep" uncertainty over long-term climate in major infrastructure projects: four innovations of the Thames Estuary 2100 Project. *EURO J. Decis. Process.* 1, 233–262. doi: 10.1007/s40070-013-0014-5

Rignot, E., Mouginot, J., Scheuchl, B., van den Broeke, M., van Wessem, M. J., and Morlighem, M. (2019). 'Four decades of Antarctic Ice sheet mass balance from 1979–2017. *Proc. Natl. Acad. Sci. U.S.A.* 116, 1095–1103. doi: 10.1073/pnas.1812883116

Rohmer, J., Le Cozannet, G., and Manceau, J.-C. (2019). Addressing ambiguity in probabilistic assessments of future coastal flooding using possibility distributions. *Climatic Change* 155, 95–109. doi: 10.1007/s10584-019-02443-4

Rohmer, J., Lincke, D., Hinkel, J., Le Cozannet, G., Lambert, E., and Vafeidis, A. T. (2021). Unravelling the importance of uncertainties in global-scale coastal flood risk assessments under sea level rise. *Water* 13:774.

Rosenzweig, C., Solecki, W. D., Blake, R., Bowman, M., Faris, C., Gornitz, V., et al. (2011). Developing coastal adaptation to climate change in the New York City infrastructure-shed: process, approach, tools, and strategies. *Climat. Change* 106, 93–127. doi: 10.1007/s10584-010-0002-8

Rosier, S. H. R., Reese, R., Donges, J. F., De Rydt, J., Gudmundsson, G. H., and Winkelmann, R. (2021). The tipping points and early warning indicators for Pine Island Glacier, West Antarctica. *Cryosphere* 15, 1501–1516. doi: 10.5194/tc-15-1501-2021

Scambos, T., Fricker, H. A., Liu, C.-C., Bohlander, J., Fastook, J., Sargent, A., et al. (2009). Ice shelf disintegration by plate bending and hydro-fracture: satellite observations and model results of the 2008 Wilkins Ice shelf break-Ups. *Earth Planet. Sci. Lett.* 280, 51–60. doi: 10.1016/j.epsl.2008.12.027

Schoof, C. (2007). Ice sheet grounding line dynamics: steady states, stability, and hysteresis. *J. Geophys. Res. Earth Surf.* 112:F03S28. doi: 10.1029/2006JF000664

Seroussi, H., Nowicki, S., Payne, A. J., Goelzer, H., Lipscomb, W. H., Abe-Ouchi, A., et al. (2020). ISMIP6 Antarctica: a multi-model ensemble of the Antarctic Ice sheet evolution over the 21st Century. *Cryosphere* 14, 3033–3070. doi: 10.5194/tc-14-3033-2020

Shepherd, A., Ivins, E., Rignot, E., Smith, B., van den Broeke, M., Velicogna, I., et al. (2018). Mass balance of the Antarctic Ice sheet from 1992 to 2017. *Nature* 558, 219–222. doi: 10.1038/s41586-018-0179-y

Shepherd, A., Ivins, E., Rignot, E., Smith, B., van den Broeke, M., Velicogna, I., et al. (2021). *Antarctic and Greenland Ice Sheet Mass Balance 1992-2020 for IPCC AR6'. Text/Plain,Text/CSV*. London: UK Polar Data Centre, Natural Environment Research Council, UK Research & Innovation. doi: 10.5285/77B64C55-7166-4A06-9DEF-2E400398E452

Simonsen, S. B., Barletta, V. R., Colgan, W. T., and Sørensen, L. S. (2021). Greenland Ice sheet mass balance (1992–2020) from calibrated radar altimetry. *Geophys. Res. Lett.* 48:e2020GL091216. doi: 10.1029/2020GL091216

Slangen, A. B. A., Carson, M., Katsman, C. A., van de Wal, R. S. W., Köhl, A., Vermeersen, L. L. A., et al. (2014). Projecting twenty-first century regional sea-level changes. *Climat. Change* 124, 317–332. doi: 10.1007/s10584-014-1080-9

Stammer, D., van de Wal, R. S. W., Nicholls, R. J., Church, J. A., Le Cozannet, G., Lowe, J. A., et al. (2019). Framework for high-end estimates of sea level rise for stakeholder applications. *Earths Future* 7, 923–938. doi: 10.1029/2019EF001163

Straneo, F., and Heimbach, P. (2013). North Atlantic warming and the retreat of Greenland's outlet Glaciers. *Nature* 504, 36–43. doi: 10.1038/nature12854

Talke, S. A., and Jay, D. A. (2020). Changing tides: the role of natural and anthropogenic factors. *Annu. Rev. Mar. Sci.* 12, 121–151. doi: 10.1146/annurev-marine-010419-010727

Toimil, A., Camus, P., Losada, I. J., Le Cozannet, G., Nicholls, R. J., Idier, D., et al. (2020). Climate change-driven coastal erosion modelling in temperate sandy beaches: methods and uncertainty treatment. *Earth Sci. Rev.* 202:103110. doi: 10.1016/j.earscirev.2020.103110

van Wessem, J. M., van de Berg, W. J., Noël, B. P. Y., van Meijgaard, E., Amory, C., Birnbaum, G., et al. (2018). Modelling the climate and surface mass balance of polar Ice sheets using RACMO2 – Part 2: Antarctica (1979–2016). *Cryosphere* 12, 1479–1498. doi: 10.5194/tc-12-1479-2018

Vaughan, D. G. (2008). West Antarctic Ice sheet collapse – the fall and rise of a Paradigm. *Climat. Change* 91, 65–79. doi: 10.1007/s10584-008-9448-3

Weertman, J. (1974). Stability of the junction of an Ice Sheet and an Ice Shelf'. *J. Glaciol.* 13, 3–11. doi: 10.3189/S0022143000023327

Wilby, R. L., Nicholls, R. J., Warren, R., Wheater, H. S., Clarke, D., and Dawson, R. J. (2011). Keeping nuclear and other coastal sites safe from climate change. *Proc. Inst. Civil Eng.* 164, 129–136. doi: 10.1680/cien.2011.164.3.129

Wong, P. P., Losada, I. J., Gattuso, J.-P., Hinkel, J., Khattabi, A., McInnes, K. L., et al. (2014). Coastal systems and low-lying areas. *Climate Change* 2104, 361–409.

Woodworth, P. L., Melet, A., Marcos, M., Ray, R. D., Wöppelmann, G., Sasaki, Y. N., et al. (2019). Forcing factors affecting sea level changes at the coast. *Surv. Geophys.* 40, 1351–1397. doi: 10.1007/s10712-019-09531-1

Wöppelmann, G., and Marcos, M. (2016). Vertical land motion as a key to understanding sea level change and variability. *Rev. Geophys.* 54, 64–92. doi: 10.1002/2015RG000502

Zemp, M., Huss, M., Thibert, E., Eckert, N., McNabb, R., Huber, J., et al. (2019). Global glacier mass changes and their contributions to sea-level rise from 1961 to 2016. *Nature* 568, 382–386. doi: 10.1038/s41586-019-1071-0

Zhang, X., Church, J. A., Monselesan, D., and McInnes, K. L. (2017). Sea Level projections for the Australian region in the 21st century. *Geophys. Res. Lett.* 44, 8481–8491. doi: 10.1002/2017GL074176

Conflict of Interest: The authors declare that the research was conducted in the absence of any commercial or financial relationships that could be construed as a potential conflict of interest.

Publisher's Note: All claims expressed in this article are solely those of the authors and do not necessarily represent those of their affiliated organizations, or those of the publisher, the editors and the reviewers. Any product that may be evaluated in this article, or claim that may be made by its manufacturer, is not guaranteed or endorsed by the publisher.

Copyright © 2022 Durand, van den Broeke, Le Cozannet, Edwards, Holland, Jourdain, Marzeion, Mottram, Nicholls, Pattyn, Paul, Slangen, Winkelmann, Burgard, van Calcar, Barré, Bataille and Chapuis. This is an open-access article distributed under the terms of the Creative Commons Attribution License (CC BY). The use, distribution or reproduction in other forums is permitted, provided the original author(s) and the copyright owner(s) are credited and that the original publication in this journal is cited, in accordance with accepted academic practice. No use, distribution or reproduction is permitted which does not comply with these terms.

frontiers | Frontiers in Marine Science

ORIGINAL RESEARCH
published: 11 May 2022
doi: 10.3389/fmars.2022.710086

Coastal Flood Modeling to Explore Adaptive Coastal Management Scenarios and Land-Use Changes Under Sea Level Rise

Jessie Louisor[1], Olivier Brivois[1], Paloma Mouillon[2], Aurelie Maspataud[3], Patrice Belz[2] and Jean-Michel Laloue[2]*

[1] Risks and Prevention Department, Bureau de Recherches Géologiques et Minières (BRGM), Orléans, France,
[2] Conservatoire du Littoral, Corderie Royale, Rochefort, France, [3] BRGM, Parc technologique Europarc, Pessac, France

In a Climate Change (CC) context, low-lying areas like marshes are more vulnerable to Sea Level Rise (SLR) or extreme climate events leading to coastal flooding. The main objective of this study is to help local stakeholders determine the best coastal management strategy for the Moëze marsh (France) that can contribute to adapt to SLR in this zone. To do so, we used the MARS hydrodynamic model to simulate coastal overflowing in the zone for different scenarios. We first calibrated the model based on data from the Xynthia storm which occurred on February 28th 2010. Our focus is on modeling the high astronomical tide-induced flooding, taking into account regional SLR projections by 2030 and 2050 under the pessimistic RCP 8.5 CC scenario. Several Coastal management configurations proposed by local decision-makers, as well as different land-use projections were considered. The results highlight that the implementation of closed defenses around human and economic stakes do not lead to significant reductions in flooding (surface extent and maximum water height) compared to the case where the sea-dikes are no longer maintained and the coastline is unconstrained. This can be explained by the fact that these stake zones were historically built on higher points of the marsh. We have also shown that land-use changes have an influence on flooding in the Moëze marsh, especially an increase greater than 0.25 m in the maximum simulated height when considering a new land-use by 2030. The increase is less pronounced (under 0.25 m) when considering a new land-use by 2050. These results do not take into account the possible future evolution of the topography due, for example, to the presence of new habitats that would trap the sediments.

Keywords: coastal flooding, numerical modeling, sea level rise (SLR), adaptation, Moëze marsh, land-use changes

OPEN ACCESS

Edited by:
Roderik Van De Wal,
Utrecht University, Netherlands

Reviewed by:
Charlotte Lyddon,
Bangor University, United Kingdom
Liqin Zuo,
Nanjing Hydraulic Research Institute, China

****Correspondence:***
Jessie Louisor
j.louisor@brgm.fr

Specialty section:
This article was submitted to Coastal Ocean Processes, a section of the journal Frontiers in Marine Science

Received: *15 May 2021*
Accepted: *11 April 2022*
Published: *11 May 2022*

Citation:
Louisor J, Brivois O, Mouillon P, Maspataud A, Belz P and Laloue J-M (2022) Coastal Flood Modeling to Explore Adaptive Coastal Management Scenarios and Land-Use Changes Under Sea Level Rise. Front. Mar. Sci. 9:710086. doi: 10.3389/fmars.2022.710086

INTRODUCTION

It is well known that extreme events such as storms or tropical cyclones can lead to coastal flooding (Haigh et al., 2016; IPCC, 2021). One of the most well known storms in France, having led to the last permanent actions of the state services, is storm Xynthia (French Ministry of Environment, 2017). This storm occurred the 27-28th February 2010 and affected the entire Vendée and Charente-

Maritime on the Atlantic coast of mainland France, and also impacted other countries in Europe (Belgium, Swiss, Spain, Portugal, Germany, Luxembourg). The flooding led to dramatic consequences, 59 human casualties over Europe (Vu et al., 2019). The combination of high spring tide and low pressure (977 hPa) led to an important storm surge along the coast of the Bay of Biscay for example (Vu et al., 2019). The La Rochelle-La Pallice tide gauge recorded the largest storm surge (1.53 m) ever recorded in France in the last 150 years (Pineau-Guillou et al., 2012). In addition, according to Bulteau et al. (2015), storm Xynthia had a ~200-year return period.

Moreover, many studies have highlighted that Sea Level Rise (SLR), could significantly alter coastal flooding in the future (Hallegatte et al., 2013; Arns et al., 2015; Haigh et al., 2016; Idier et al., 2020; Rocha et al., 2020). As sea level is rising, it becomes possible that in low-lying areas, flooding occurs for high spring tides, without any stormy conditions leading to storm surges or wave setup (Ezer and Atkinson, 2014; Moftakhari et al., 2015; Ray and Foster, 2016). Kirezci et al. (2020) assessed that by 2100, at global scale, 63% of the coastal area flooded will be caused by tide and storm surges, 5% by wave setup and 32% due to projected regional SLR. Indeed, as SLR is not uniform at spatial scale, regionalized SLR projections are needed (Kopp et al., 2014; Melo et al., 2020). As a comparison, considering the pessimistic Representative Concentration Pathways RCP 8.5 by 2100, the SLR likely-range is assessed to [0.61–1.10 m] at global scale (IPCC, 2019), whereas these values could potentially be doubled along the France coastline for a high-end scenario (Thiéblemont et al., 2019).

In addition, it is interesting to note that according to Vousdoukas et al. (2016), projected storm surge level changes along the Bay of Biscay show a small decrease, under the RCP 8.5 scenario by 2040 and 2100. The same trend is observed when considering not only storm surges, but the Extreme Sea Level (ESL) composed by Mean Sea Level + Tide + Waves + Storm Surges (Imani et al., 2021).

With storms and SLR, flooding may become chronic, and could change former inland habitats to new ecosystems. Indeed, coastal flooding may cause direct or indirect changes to habitats established in the marshes, over the short and the long term. For example, Yu Mo et al. (2020) have shown that in some conditions, long-term nutrient enrichment (by seawater penetration) may impair the resilience of marshes. Martinez et al. (2014) also showed that the combination of SLR and human coastal infrastructures might cause a coastal squeeze that exposes the ecosystems and species to local extinction. More generally, the vulnerability of coastal ecosystems to SLR depends on their ability to adapt through enhanced sediment trapping to grow upward with SLR (Timmerman et al., 2021).

At local scales, decision-makers have to deal with the legislation, their knowledge of the field and studies conducted by researchers or design offices in order to adapt or to become more resilient to SLR and extreme events leading to coastal flooding. The options proposed are mainly sea-front dikes (Rosenzweig et al., 2011; Ezer and Atkinson, 2014), or nature-based actions such as dune revegetation or habitat restoration (Fernández-Montblanc et al., 2020; Grothues and Able, 2020), and dike retreat (Bongarts Lebbe et al., 2021). In order to help local stakeholders in their strategy to protect human activities and improve the resilience, an adaptive coastal management project named Adapto has been initiated by the Conservatoire du Littoral (coastal conservatory), hereinafter CDL. Note that one of the main missions of this public institution is to purchase coastal threatened or degraded lands, in order to restore and develop the ecosystems. The Adapto project is supported by the European Union through the LIFE program and explores solutions in order to reduce the impacts of climate change on the coasts. Thus, 10 pilot sites with various coastal issues are studied in mainland France, Corsica and French Guiana (See **Supplementary Material** for more information). The implementation of these solutions is at different phases depending on the sites. For example, study sites such as Ile Nouvelle and the Mortagne-sur-Gironde polders (Gironde estuary, France), which have both been depoldered since 1999 and 2010 respectively, provide feedback and lessons that can be transferred to other sites. For other sites, a multidisciplinary support is proposed in order to develop a strategy taking into account the identified issues. The originality of this approach is that it cross-references key findings of studies on coastal flood risk, biodiversity, economic activities and social perception in order to identify their impact on local issues and help decision-makers to define an integrated coastal management strategy. For this reason, many stakeholders are involved in the project, such as oyster farmers, local decision-makers, coastal engineers, landscape designers, biologists, etc. In this paper, we focus on the Moëze Brouage marsh, hereinafter Moëze marsh. In this region, local stakeholder expectations are high because this area was impacted by extreme storms in the past, e.g storm Xynthia, (Breilh et al., 2013; Bertin et al., 2014; Breilh et al., 2014b), and the marsh is affected by chronic flooding due to high spring tides. The protection against coastal flooding has been breached, and according to the local stakeholders, its maintenance is becoming more and more difficult. The main focus is whether to rebuild and maintain the existing dikes, add new defenses, or adopt an ecosystem-based process and let the marsh reconnect to the sea. In order to try to determine the best strategy for coastal management in this area, we used flood modeling under regional SLR projections by 2030 and 2050, taking into account several coastline management scenarios.

In this paper, we first describe the site studied, the data used and the methods applied in Section 2. In section 3, we present our results considering SLR and land-use projections by 2030 and 2050. Finally, we conclude and give some perspectives to our work in the last section.

STUDY SITE, AND DATA USED

The Moëze Marsh

The Moëze marsh is located in Charente-Maritime (France), facing the Marennes-Oléron Bay (**Figure 1A**). The area is a tidal dominant area connected to the Atlantic Ocean (Chaumillon et al., 2003). This macrotidal zone is affected by semi-diurnal

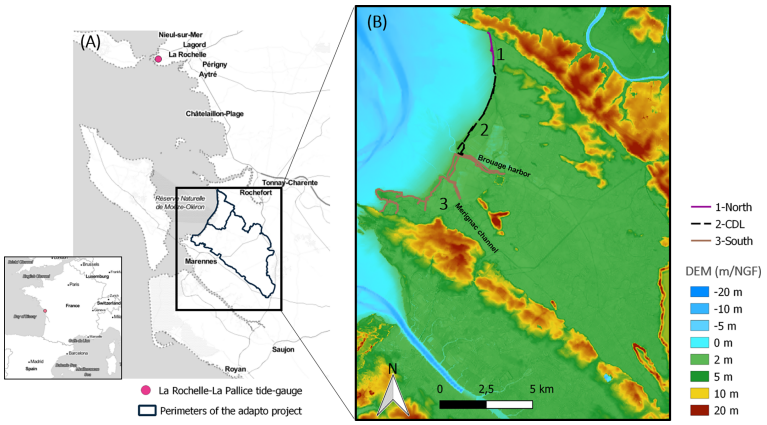

FIGURE 1 | 2**(A)** Study site location. The black perimeter represents the immediate study area and the extended study area in the Adapto project; **(B)** Topo-bathymetric data used with a 20 m × 20 m resolution. The coastal defenses are represented in purple (1), black (2), and brown (3).

tides with a theoretical range between -3.3 m for the lowest astronomical tide (LAT) and 3.37 m for the highest astronomical tide (HAT) at the La Rochelle-La Pallice reference tide gauge (Shom, 2017). Note that in this paper, all data are presented in NGF/IGN69, the official French leveling reference.

The Moëze marsh is also a low-lying area polderized over the centuries (Bento and Blanc, 2017), and exposed to extreme events leading to large coastal flooding events. Severe storms like Martin (December 27th 1999) and Xynthia (February 27-28th 2010) in the last decade, have impacted the whole area. Several coastal defenses have been raised since the 1970s against the assaults of flooding. Indeed, the site presents a coastal protection composed by three embankment dikes belonging to different property owners (**Figure 1B**). The central dike (2-CDL on **Figure 1B**) is a patchwork of heterogeneous materials, sometimes set against the dune, (Bento and Blanc, 2017). This coastal protection presents breaches in several points due to successive storms (DDTM-17, 2011).

Forcing Conditions

In our study, several tidal conditions are taken into account: high spring tide close to HAT, and stormy conditions leading to high water levels. Under stormy conditions, the water level that includes the storm surge, is derived from the nearest reference tide gauge, located at La Rochelle - La Pallice (**Figure 1A**), and applied to the model as a boundary condition. In the present case, we used the time series from 02/26/10 22:00 UTC to 03/01/10 08:00 UTC during storm Xynthia, with a 10-minute temporal resolution. Other tide gauges exist close to the Moëze marsh but their measurements were not available (not yet in operation or experienced power failures) for the storm tested. Note that most of the tide gauges in the zone belong to the RONIM network operated by the Shom. Moreover, in the rest of the study, we also used the tidal signal coming from the La Rochelle – La Pallice tide gauge because: i) it is the reference tide gauge, with the longest time series in the zone; ii) the regional SLR projections used in the next sections have been computed with the sea levels coming from this tide gauge.

In a prospective approach, we looked at high spring tide, especially in conditions close to the HAT that is 3.37 m at La Rochelle - La Pallice. The analysis of tidal predictions provided by the Shom over the period 1996-2015 shows that conditions close to the HAT occur about twice a year (see **Supplementary Material**). **Table 1** summarizes the different offshore conditions used as boundary conditions in the paper. We also analyzed the time series of the Ile d'Aix tide gauge closer to our zone of interest. A comparison between the tide predictions at La Rochelle– La Pallice and Ile d'Aix between 2012 and 2016 shows a good agreement between the 2 tide gauges (see **Supplementary Material**). However, the storm surges are greater at La Rochelle than at Ile d'Aix when exceeding 1 m (this point cannot be verified for Xynthia because there is a lack of data at Ile d'Aix).

Topo-Bathymetric Data, DEM Building and Surface Roughness

In order to build a Digital Elevation Model (DEM) representing the nearshore domain, the land areas and the sea-land continuum without any discontinuities, we gathered several topo-bathymetry datasets. This led to the building of a so-called composite DEM.

The bathymetric data are derived from the HOMONIM dataset, provided by the French Hydrographic Office (Shom, 2015). This full DEM extends over a large area (not shown here) from the coast to about 60 m depth with a 0.0002° (~ 22 m at this latitude) resolution. The topographic data used, including the intertidal zone, come from both RGE ALTI® 1 m and RGE ALTI® 5 m products made available by IGN. Note that the RGE ALTI® product is initially composed of data issued from the BD ALTI® at 25 m, resampled at 1 m (or 5 m depending on the product), and is updated with more accurate data when they are available. Once the different datasets were homogenized, and set to the same vertical reference, we

TABLE 1 | Summary of offshore conditions presented in the paper.

	Offshore conditions	Source	SLR	Use
Xynthia storm (02/28/2010)	SWL time series	Shom (RONIM network)	–	Model calibration
2030	Tide prediction + SLR	Shom (SHOMAR)	+ 0.18 m	Test of coastal management scenarios
2050	Tide prediction + SLR	Shom (SHOMAR)	+ 0.36 m	Test of coastal management scenarios

performed an interpolation in order to fill gaps and get a continuous and regular surface. We used a spline function adapted to topo-bathymetric data, as suggested by Amante and Eakins (2016). We performed visual controls in order to ensure consistency and gradual topographic/bathymetric transitioning along limits of the datasets composing the DEM (slope, cross-section and 3D views). This highlighted the presence of local artifacts (vertical discontinuities of tens of centimeters in the intertidal zone), corrected by interpolation (see **Supplementary Material**). The final DEM covers the entire marsh, and nearshore domain with a 20 m×20 m resolution (**Figure 1B**). Since the original datasets used have broadly a 20 m resolution, we decided to keep this resolution as it combines a reasonable computational time and resources model, with an accurate DEM on coastal defenses (i.e using the features of the high-resolution RGE ALTI® for the coastal defenses). Indeed, we performed some treatment on the DEM, in order to take accurately into account infrastructures, such as road dikes, or to erase them depending on the scenario considered (see **Supplementary Material**).

To ensure that flows are properly represented, it is necessary to consider the land-use in the hydrodynamic model. Indeed, the impact of land-use on flows is usually represented using a bottom-friction parameter characterizing the roughness of each type of soil (concrete, grass, sand, etc.). The surface roughness is usually parameterized in terms of Manning or Strickler coefficients, as presented in **Table 2**. A spatialized representation of roughness can be obtained from a synthetic land cover classification. As a first approximation, we used the Corine Land Cover (European Environment Agency, 2012) database. This classification was then interpreted in terms of Strickler coefficient values as exposed in Papaioannou et al. (2018). **Table 2** gives a simplified classification, adapted from Papaioannou et al. (2018), based on Corinne land cover data and Strickler coefficients associated. The values taken for the Strickler coefficients in the different simulations vary from 10 $m^{1/3}s^{-1}$ in high friction areas (small and non-dense urbanized areas) to 50 $m^{1/3}s^{-1}$ for low friction areas (water area). The values used are those recommended by different sources and are applicable for studies in coastal domains (Brown et al., 2007; Bunya et al., 2010; Papaioannou et al., 2018).

Finally, we checked if the land cover and roughness coefficient associated was consistent with recent orthophographs (taken after February 2010) and with the BD TOPO® Hydrographie product (providing the hydrographic network), made available by IGN. This qualitative step highlighted a good agreement between the information provided by the land use and hydrographic databases and the recent orthophotographs. **Table 3** gives a summary of topo-bathymetric and land-use products used in this study.

METHODS

Modeling Method

In this study, we used the hydrodynamic model MARS (Model for Applications at Regional Scale) developed by IFREMER (Lazure and Dumas, 2008). This model is particularly well suited to simulating flows in coastal regions, from the regional scale to the estuary (Bruneau et al., 2014; Nicolae-Lerma et al., 2018; Lemoine and Le Hir, 2021). The MARS code is a free-surface hydrodynamic model, solving the classical equations of fluid mechanics (Navier-Stokes equations) under the Boussinesq approximation, the quasi-hydrostatic approximation as well as the dispersion-diffusion equation of a transported element, in the horizontal plane. The momentum conservation and mass conservation of the system are described by the shallow-water equations. These equations are solved by a finite difference method. In its MARS-FLOOD version, the code can take into account the dike breaches and rupture of structures, treatment of singularities such as culverts, weirs, and other incoming flows from rivers. The model also manages part-time dry areas (tidal flats, flood-plains). It allows the spatialization of bottom-friction

TABLE 2 | Simplified classification based on Corinne land cover data and Strickler coefficients associated. Adapted from Papaioannou et al. (2018).

Land cover class	Strickler coefficient Ks ($m^{1/3}.s^{-1}$)
Pastures	28
Annual crops associated with permanent crops	25
Complex cultivation patterns	25
Small and non-dense urbanized areas	10
Land principally occupied by agriculture, with significant areas of natural vegetation	20
Beaches, dunes, sands	40
Sparsely vegetated areas	37
Inland marshes, Peat bogs	25
Salt marshes, Salines, Intertidal flats	25
Sea and ocean	50

TABLE 3 | Summary of topo-bathymetric and land-use datasets used in the study.

	Variable	Product	Source	Spatial Resolution
Topo-bathymetric data for numerical simulation	Bathymetry	HOMONIM	Shom	0.0002° (~22 m)
	Topography	RGE ALTI®	IGN	5 m; 1 m
Land-use	Land unit	Corine Land Cover 2012; BD Ortho®; BD TOPO®	Copernicus; IGN	Min. mapping unit/width= 25 ha/100 m; 0.1 m

(see section 2.3) and effects of meteorological phenomena. Here, the model covers the whole Moëze marsh and includes a single structured computational grid with a spatial resolution of 20 m × 20 m over the domain (1419 × 1213 elements).

Figure 2 summarizes the modeling method. The first step of our model set up has consisted in a calibration/validation. To do so, we have tried to reproduce the flooding extension of storm Xynthia over the marsh, by forcing the MARS-FLOOD model with a Still Water Level (SWL) time series (**Figure 2A**).

Figure 3 shows the flooded area observed a few days following the storm Xynthia (delimited by the black line) and the maximum heights (colors) obtained by simulating the event from 26th February to 1st March 2010. The observed extension has been derived from aerial pictures a few days after the storm, and provided by DDTM 17 (local state services). Based on a criterion of elevation, we identify some additional elements that would have an influence on the hydraulic behavior of the flood. Namely, the main rivers and the channels, the second row dikes, and other embankments that constrain the flow. A sensitivity test phase allowed the implementation of the DEM taking into account structural elements such as dikes, embankments, roads (see **Supplementary Material**). It also permits testing the influence of the formation of breaches in the sea-dikes. The sensitivity test phase has highlighted a flooded area of 30.09 km² against 28.75 km² observed (i.e. a relative error of 4.7%) for the best configuration. In comparison, Breilh (2014a) found a flooded area of 41.16 km² applying a static GIS-based approach. Bertin et al. (2014) also showed an overestimation of the flooded area of this marsh after the implementation of a hydrodynamic modeling chain built with unstructured nested grids. The difference between the observed and simulated areas can be explained by the fact that the DEM used refers to post-Xynthia data (possible backfilling of some areas after the storm), or by the fact that some hydraulic connections and the rain that are not integrated in the model have obviously played a role on the flooding. Many uncertainties remain: the breach dynamics, the rainfall infiltration, the exact elevation of dikes in 2010, the lack of measurements or quantitative information regarding the water heights observed during the flooding. Furthermore, the modeled flooded area, very close to the observation without breaches integration in the dikes (not shown), tends to confirm that it would rather be a flood by overflow. Breilh et al. (2013), also suggest this.

Breilh et al. (2014b) also showed that several past storms in this region had a significant wave setup, i.e wave-induced increase of the mean water level due to breaking waves. As an example, a storm in 1924 had generated a setup estimated at 0.5 m in our area of interest. Breilh et al. (2014b) identified three types of storm conditions that can lead to marine submersion in the central Bay of Biscay: moderate storm surge and extreme tidal range; moderate tidal range and large storm surge, (confirmed by Dodet et al., 2019); extreme waves which induce very large setup that can propagate in sheltered zones. In order to explore all these conditions, a dynamical approach that includes overflowing,

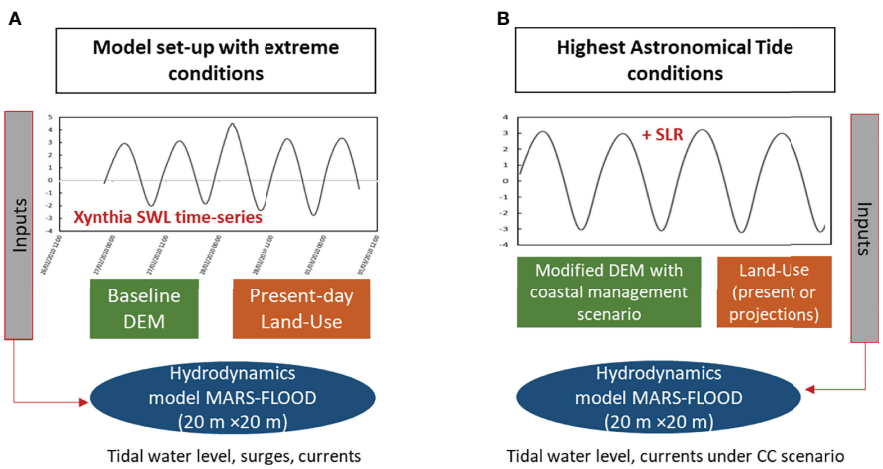

FIGURE 2 | Model set-up: **(A)** under stormy conditions, using storm Xynthia Still Water Level time series and the baseline DEM; **(B)** for highest astronomical tide conditions, using the modified DEM.

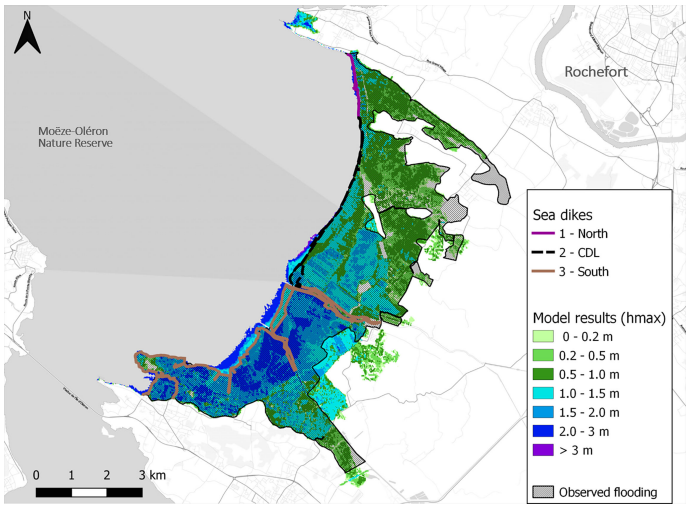

FIGURE 3 | Flooding extension area observed during storm Xynthia (2010) delimited in black and maximum heights simulated for storm Xynthia conditions.

potential overtopping, and river flows (e.g a modeling chain as proposed by Bertin et al. (2014) or Filippini et al., 2018) could be set up. However, this approach can limit the number of coastal management scenarios and land-use tested, as it is more expensive in computer time and resources compared to our strategy. Hence, such a type of modeling chain is not included in the study, as the next parts we focused on high spring tides and SLR-induced overflowing without stormy conditions (**Figure 2B**).

Propositions From Local Stakeholders

One of the strengths of this study is the consultation of local decision-makers about coastal management scenarios such as coastal dikes location, new land-use by the establishment of a flood expansion area, or other defenses they thought useful in order to adapt to SLR. Indeed, this first collaborative phase was crucial because it builds i) credibility; ii) legitimacy; and iii) decision-makers' involvement in the study. These three components are, according to Leitch et al. (2019), indicators of an effective transition between the technique (here flooding risk assessment by numerical modeling) and the pragmatic decision. We have presented preliminary simulation results during a local mayors' workshop. The participants were able to propose adaptation actions for their municipalities. During the workshop, small groups tried to identify the human, the economic, and the immaterial issues based on their knowledge of the field and the documents provided. They were helped by a map of the marsh (similar to **Figure 1A**); a map presenting the topo-bathymetry (similar to **Figure 1B**); a map with the flooding extension caused by storm Xynthia and some simulation results shown in the **Supplementary Material**. With these elements, they were asked to answer the following questions: Q1/*According to you, what are the important issues to preserve/protect in this area, now and in the future? Identify them on the map and explain them.* Q2/*What kind of development(s) would you consider to protect/preserve them? Draw them and explain them.*

Their propositions are summarized on **Figure 4**. The **Figure 4** highlights that they consider several possibilities:

i. The first proposition P1 consists of the total embankment of the marsh (**Figure 4A**), with two hydraulic connections represented by a red star. According to the workshop participants, the hydraulic connections are set up in order to reduce flooding coming from the rivers. These solutions can be locks, nozzles, culverts, etc., and have to be assessed by a civil engineering office if such a coastal management scenario is retained.
ii. The proposition P2: An unconstrained coastline with the reinforcement of two road-dikes backwards, close to three villages (**Figure 4B**).
iii. The third proposition (**Figure 4C**), hereinafter P3, leaves an unconstrained coastline and implements coastal defenses around identified stakes. These locations, composed of villages or isolated houses, are vulnerable according to the workshop participants.

Moreover, they considered that economic activities (shellfish farming, cereal crop) have to be relocated in configurations B and C (**Figure 4**). They also have represented a moving coastline (blue arrows) that may be advancing or retreating in their perception of the evolution of this area.

As the Adapto project explores adaptive coastal management, we here focus on the scenario P3 that proposes a hybrid solution with reduced embankment, and managed retreat. In addition to the P3 provided by the local decision-makers, we also proposed a scenario without any coastal defenses, hereinafter P4 proposition. The P4 is a scenario with an assumption of generalized ruin of all defenses. In this scenario, coastal structures are not maintained over the long term, and the coastline is not constrained, as suggested by the Coastal risks and prevention plan guideline (DGPR, 2014). Moreover, note

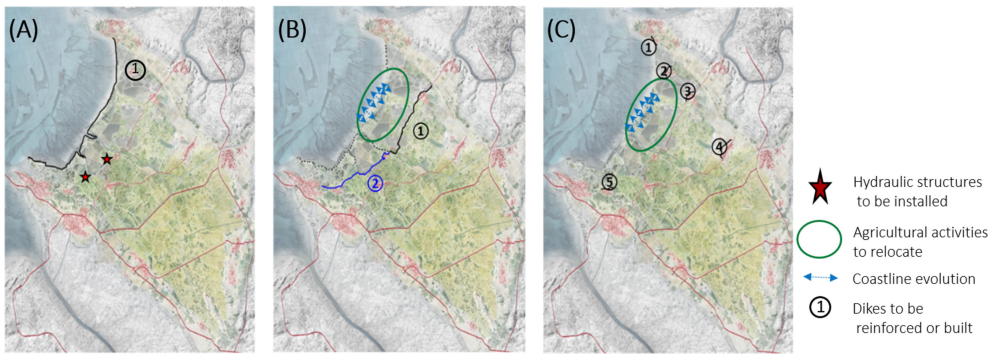

FIGURE 4 | Adapted from the local stakeholders workshop. **(A)** Proposition P1: reinforcement of the sea-dike and hydraulic infrastructures identified by red stars; **(B)** P2: Reinforcement of a road-dike (represented by the black and blue lines n°1 and n°2), without maintenance or reinforcement of the existing sea-dikes; **(C)** P3: Proposition of coastal defenses located around identified issues, without maintenance or reinforcement of the existing sea-dikes. Agricultural activities to relocate are identified by a green circle and blue arrows represent the coastline evolution.

that the propositions P1 and P2 were also proposed by the local decision-makers in order to assess the cost of such dikes (height, materials and culverts or other required hydraulic connections, maintenance), and in order to know if this solution would protect the population and the activities in the long term. These propositions were simulated and discussed with stakeholders but are not presented in this research paper.

Taking Into Account the Sea Level Rise and Future Land Use

With SLR, a tidal condition close to the HAT could maybe have a similar impact to coastal flooding caused by severe storms. As a comparison, the sea level should rise by about 1.20 m to reach the conditions observed during Xynthia at La Rochelle. For example, Thiéblemont et al. (2019) presented such value along the French coasts by 2100, for the high-end prediction under the RCP 8.5 scenario. In order to consider tidal conditions close to the HAT, we tried to assess the coastal flooding under future change conditions. To do so, we have considered two SLR projections: i) corresponding to a regional SLR projection by 2030; ii) corresponding to a regional SLR projection by 2050. These regional projections were computed by Le Cozannet et al. (2019), using the stable La Rochelle-La Pallice tide gauge. Basically, these authors used projections provided by Kopp et al. (2014) to which they apply a subsidence correction. They assumed that the probabilistic SLR projections at La Rochelle were consistent for the Aquitaine coast, once corrected from the local vertical ground motions (we invited the reader to report to Le Cozannet et al. (2019) for more details on their methods). Thus, we used the following values to integrate SLR within the hydrodynamical model: +0.18 m by 2030 and +0.36 m by 2050. These values correspond to the upper bound of the "likely-range", built for the pessimistic RCP 8.5 (Church et al., 2013). During the study, we assumed that the values proposed by Le Cozannet et al. (2019) could be more consistent with those that would be derived from the SROCC (IPCC, 2019) and lastly by the 6th IPCC report (IPCC, 2021), compared to those provided by the 5th IPCC report (Church et al., 2013). Based on the recent literature, our assumption is in accordance with the regional projections derived from the SROCC (Thiéblemont et al., 2019). Indeed, considering the SROCC projections, the likely-range is assessed between [0.15-0.17 m] by 2030 for the scenario RCP 8.5 in the Bay of Biscay, whereas the values are between [0.12-0.13 m] when derived from the AR5-IPCC report. In the same way, the values are assessed between [0.31-0.34 m] by 2050 in the Bay of Biscay for the scenario RCP 8.5, whereas there are between [0.24-0.26 m] when derived from the AR5-IPCC report. In accordance with the stakeholders, we applied the most conservative approach using the regional values proposed by Le Cozannet et al. (2019). However, it is important to note that these regional values are greater than global projections of SLR. Indeed, Global Mean Sea Level (GMSL) rises between [0.15-0.26 m] for 2031–2050 under RCP 8.5 (SROCC, 2019). When considering the pessimistic scenario Shared Socioeconomic Pathway SSP5 8.5, the GMSL rises between [0.2-0.29 m] by 2050 (IPCC, 2021).

The hydrodynamic simulations and field observations can provide frequency and duration of flooding, height and speed flow, as many elements that can allow the assessment of possible evolutions or establishment of some habitats. Based on our preliminary results (see **Supplementary Material**), Fouin et al. (2020) have assessed land-use projections by 2030 and 2050 for a scenario where the CDL-dike (black dike in **Figure 1**) was no longer maintained. Their method for assigning new habitats and land-use is shown in **Figure 5A**. Such type of land-use changes has a consequence in terms of Strickler coefficients governing the bottom-friction in the model. For example, a land principally occupied by agriculture (Strickler coeff. Ks = 20 $m^{1/3}.s^{-1}$) becoming a salted meadow (Ks = 29 $m^{1/3}.s^{-1}$) will experience a decrease in surface roughness. Therefore, we used their land-use projections to assign new Strickler coefficients to the bottom-friction parameter in the model as presented at **Figures 5B, C**.

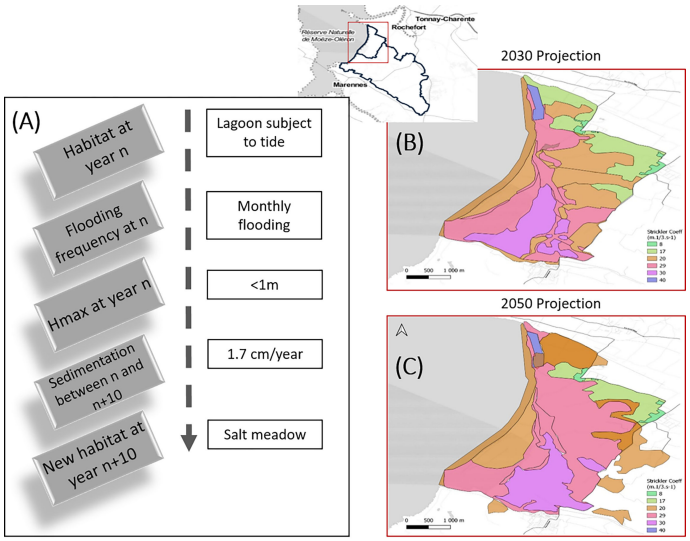

FIGURE 5 | Land-use projections: **(A)** method for assigning new habitats (grey boxes), and example (white boxes), adapted from Fouin et al. (2020); **(B)** translated into Strickler coefficients by 2030; **(C)** translated into Strickler coefficients by 2050.

RESULTS AND DISCUSSION

Results for Different Coastal Defenses and Sea Level Rise Scenarios

Here we present the results obtained by simulating the local decision-makers proposition to build defenses around some villages (see **Figure 4C**). Based on their proposal, we have taken into account coastal defenses of lengths between 300 m and 2500 m with a height preventing the overflow (>10 m). We simulated the P3 scenario, taking into account the regional SLR projections by 2030 and 2050. **Table 4** summarizes the different scenarios presented in this section.

Figure 6 presents the maximum heights simulated taking into account: (A) $P3_{_2030}$ scenario; (B) $P3_{_2050}$ scenario; (C) $P4_{_2030}$ scenario; (D) $P4_{_2050}$ scenario; (E) Difference $P4_{_2030} - P3_{_2030}$ by 2030; and (F) Difference $P4_{_2030} - P3_{_2030}$ by 2050. The results highlight that the maximum heights are greater when considering 2050 SLR projection (**Figures 6B, D**) compared to 2030 (**Figures 6A, C**). The areas most affected by flooding in terms of maximum heights (about 1.5 m by 2030 and 2 m by 2050) also correspond to those identified by local decision-makers as agricultural activities to relocate (see **Figures 4B, C**). In addition, the flooding extension is larger by 2050 than by 2030. Especially, the extension is closer to Saint-Frou, Moëze and Hiers villages by 2050 than by 2030. There are the expected results, but we can see that adding 0.18 m of sea level between 2030 and 2050 projections can induce higher maximum water heights, around 0.5 m in some zones close to the Brouage harbour and its channels.

It further appears that the villages embanked by the defenses proposed by local decision-makers in the P3 scenario are not affected by flooding when there are no defenses (P4 scenario). **Figures 6E, F** confirm that the difference between P4 and P3 is very limited (< 0.02 m). This can be explained by the fact that the potentially vulnerable areas were historically built on higher points of the marsh (Bento and Blanc, 2017).

Finally, comparing our results to a "bathtub approach", i.e based on land elevation relative to the selected shoreline water level and GMSL rising, the entire area demarcated as the large Adapto project perimeter (**Figure 1A**) is projected to be below annual flood level in 2050 according the sea-level rise tool by Kulp and Strauss (2019) called Climate Central. This approach may be more conservative, but it does not take into account physical processes as we do, such as tides or surface roughness.

TABLE 4 | Summary of coastal management scenarios presented.

Combinations	Projection	Strickler coefficient Ks ($m^{1/3}.s^{-1}$)
$P3_{_2030}$	2030	Unconstrained coastline + coastal defenses around villages
$P3_{_2050}$	2050	Unconstrained coastline + coastal defenses around villages
$P4_{_2030}$	2030	Complete reconnexion to the sea, no defenses maintained
$P4_{_2050}$	2050	Complete reconnexion to the sea, no defenses maintained
$Diff_{_2030}$	2030	Difference between $P4_{_2030}$ - $P3_{_2030}$
$Diff_{_2050}$	2050	Difference between $P4_{_2050}$ - $P3_{_2050}$

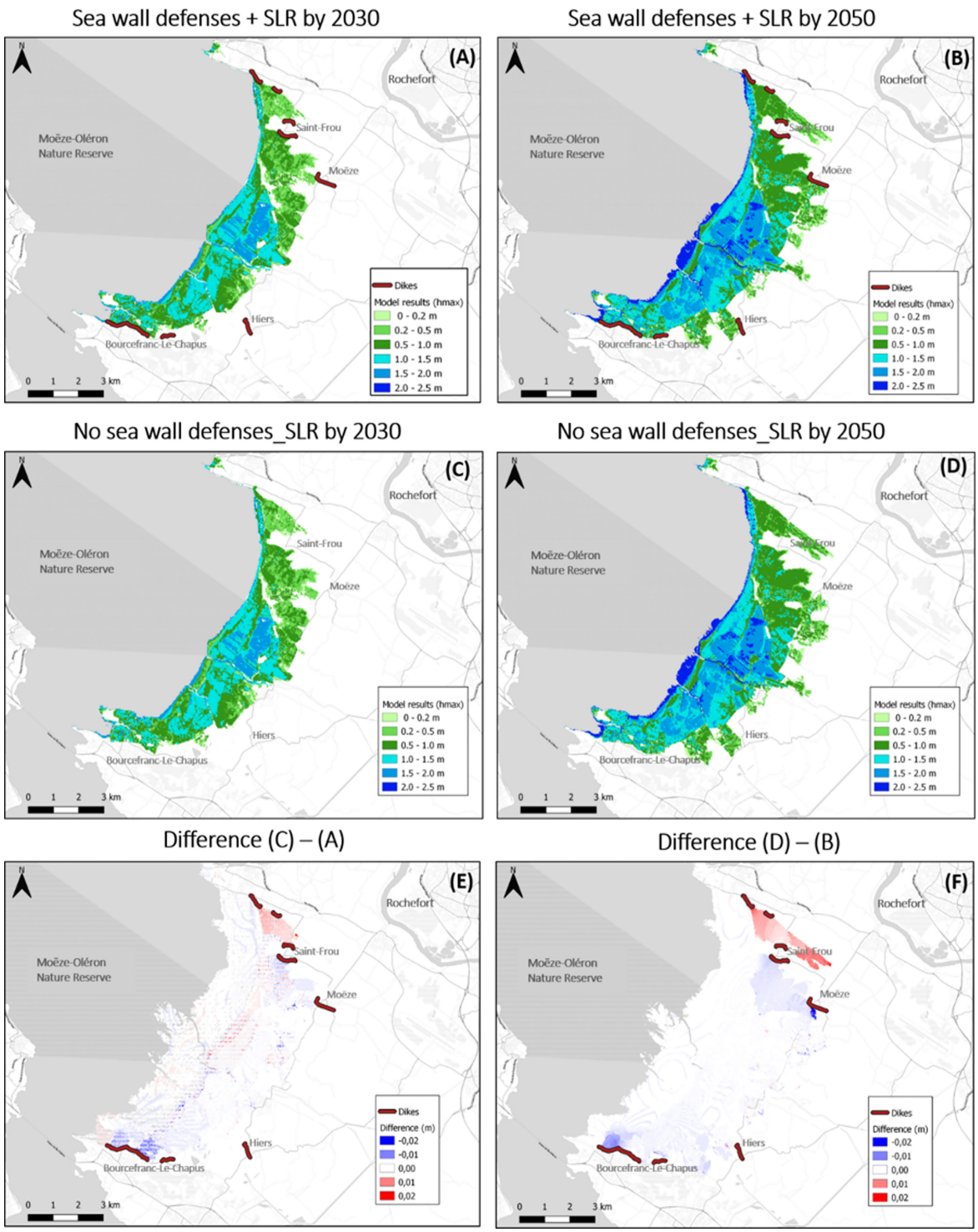

FIGURE 6 | Maximum heights simulated taking into account: **(A)** $P3_{2030}$ scenario; **(B)** $P3_{2050}$ scenario; **(C)** $P4_{2030}$ scenario; **(D)** $P4_{2050}$ scenario; **(E)** Difference $P4_{2030} - P3_{2030}$; **(F)** Same as **(E)** by 2050.

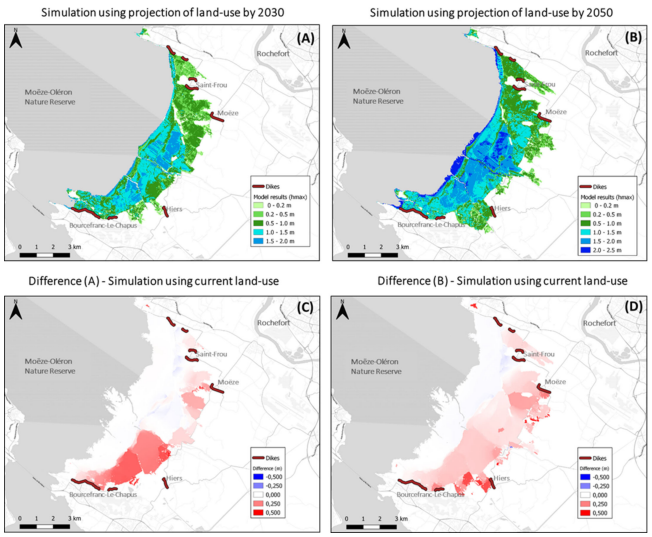

FIGURE 7 | Maximum heights simulated taking into account: **(A)** regional SLR projection by 2030, the P3 proposition and land-use projection by 2030; **(B)** same as **(A)** by 2050; **(C)** difference between **(A)** and simulations using current land-use by 2030; **(D)** same as **(C)** by 2050.

In-Situ Effect of Land-Use Changes on Flooding

Figure 7 presents the maximum heights simulated taking into account: (A) the regional SLR projection by 2030 + P3 + land-use projection by 2030; (B) regional SLR projection by 2030 + P3 + land-use projection by 2050. **Figure 7** also presents: (C) the difference between the results on panel (A) and simulations using current land-use by 2030; the difference between the results on panel (A) and simulations using current land-use by 2050. It highlights no significant changes by 2030 in the zone identified by the local decision-makers as agricultural activities to be relocated (see **Figures 4B, C**). **Figure 5C** also shows an increase of more than 0.25 m in the maximum height when considering a new land-use by 2030. We can see that in the north of Bourcefranc-Le-Chapus and Hiers villages, the increase is particularly apparent. This could be explained by the fact that the new habitats in this area are less "rough". Therefore, water flows more easily in the 2030 projection compared to the 2012 land use. Moreover, even if the land-use projections are limited to the small perimeter of the Adapto project (see **Figure 1A** and **Figure 5B**), the change seems to have an effect on the Bourcefranc/Hiers area. The increase is less pronounced (less than 0.25 m) when considering a new land use by 2050, as the habitats are rougher, in sea front compared to 2030. Finally, we bring to your attention to the fact that the Strickler coefficients classification does not have the same level of details in its typology, as the new land-use classification proposed. As an example, Salicornia, obione, or other halophilous species are classified as the same type in the Strickler coefficient classification, whereas in the land-use projection each species has its feature on the habitat evolution.

Here, we did not take into account the possible change of elevation in the topography with new habitats that would trap the sediments. However, Bertin and Chaumillon (2006) have shown that at a regional scale, the accretion of tons of sediments under the oyster beds constitute 30% of the sediments accreted in Marennes-Oléron Bay since 1824. They have also shown that the tons of sediments accreted since that time have reduced by 20% the water volume infilling the bay. As many oyster farms are located inside the Réserve Naturelle of Moëze-Oléron (**Figure 1A**), it would be interesting to simulate their impact on flooding not only in terms of surface roughness (i.e by changing the Strickler coefficients), but also in terms of sediment sources.

More generally, in case of complete depolderization of the area, it seems crucial to take into account morphologic changes induced by marine sources (sediments, waves, SLR, currents, tide), using numerical modeling and *in-situ* monitoring (topo-bathymetric survey, suspended matter measurements, site monitoring after storms, etc.).

CONCLUSION

The main objective of this study was to help local stakeholders determine the best coastal management strategy for the Moëze marsh (France) that can contribute to the adaptation to SLR in this zone. For this purpose different coastal management scenarios were studied using numerical modelling, in order to assess: i) the areas submitted to coastal flooding for future sea level conditions; ii) the potential effects of land-use changes on flooding. We have first calibrated and validated the model allowing a good assessment of the extension of the observed flooding during a reference event: storm Xynthia, occuring on February 28th 2010. We then focused on the high astronomical tide-induced flooding, taking into account regional SLR

projections by 2030 and 2050 for different coastal management scenarios, and different land-use projections. Some major conclusions can be drawn:

1) The implementation of close defenses around potentially vulnerable areas (P3 proposition) does not lead to significant changes in flooding (surface extent or maximum water height) compared to the case where the dikes are no longer maintained (P4 proposition).
2) Land-use changes have a non-negligible influence on flooding in the Moëze marsh. Especiallywith an increase of more than 0.25 m in the maximum height when considering a new land-use by 2030, and an increase less pronounced (under 0.25 m) when considering a new land-use by 2050. This result is nuanced because the possible change of elevation in the topography due to new habitats that would trap the sediments is not taken into account.

To go further in the adaptive coastal management strategy, historical extreme sea level events are additional components to take into account (Vousdoukas et al., 2016). Indeed, recent studies (including ours), mainly consider recent extreme storms in the zone. This is due to the fact that these are still very present in the collective memory, and also by the French regulation that has resulted. However, Breilh et al. (2014b) showed that since 1900, 46 severe storms had affected this region. Among these storms, several had a significant wave setup that increased the total water level close to the coast due to wave breaking. A perspective to this work is to simulate extreme conditions using such historical data combined to contemporary topo-bathymetric data (or projections), SLR and future land-use projections Future extreme sea levels could also be considered in our further work. (Vousdoukas et al, 2017).

Although we have not addressed this topic in the present paper, the potential cost of the facilities (construction and/or maintenance) required to protect to SLR is a key element in the coastline management strategy and choices made by the decision-makers. At this point, no coastal management scenario has been decided yet for the Moëze marsh, but local stakeholders now have more knowledge, based on land-use projections in a context of SLR. It is interesting to note that the decision-makers and technicians of the Moëze marsh were able to meet stakeholders from other pilot sites and discover their territories (Lancieux Bay and Orne estuary). They were able to share their experience and learn about regulations, financial levers, public perception, difficulties and possible solutions, as well as get feedback from other stakeholders who have started a managed retreat or ecosystem-based adaptation to SLR. Through these different actions, the multidisciplinary approach used in the Moëze marsh, and broadly in the Adapto project, removes several barriers identified by authors in terms of habitat restoration and adaptation (Lorie et al., 2020; Bongarts Lebbe et al., 2021; Cortina-Segarra et al., 2021). In our case, we can mention the motivation in decision-makers to incorporate innovation, the integrated land-use planning, and the collaboration between different stakeholders, and different expertise domains as barriers removed. Finally, the approach presented can be adapted to other coastal sites exposed to SLR.

DATA AVAILABILITY STATEMENT

The raw data supporting the conclusions of this article may be made available by the authors made available by the authors, without reservation.

AUTHOR CONTRIBUTIONS

Conceptualization, JL, OB, PM, PB, and J-ML. Methodology, JL, OB, PM, AM, PB, and J-ML. Software, JL and AM. Validation, JL. Investigation, JL, OB, PM, AM, PB, and J-ML. Data curation, JL and AM. Writing-original draft preparation, JL. Writing-review and editing, JL, OB, PM, AM, PB, and J-ML. All authors have read and agreed to the published version of the manuscript.

FUNDING

This research was funded by the EU LIFE (Climate Change Adaptation) Adapto project (LIFE16 CCA/FR/000131). http://www.lifeAdapto.eu/.

ACKNOWLEDGMENTS

The authors are grateful to the local mayors' comity, all local stakeholders involved in the project, the RNNMO-LPO. We thank A. Martinet for project administration. The following data providers are acknowledged: Shom, IGN, and Copernicus. We also thank G. Le Cozannet for making available regionalized SLR projections. We thank F. Paris for his support and recommendations on the preliminary phase of this study, and C. Capderrey, X. Philippenko, L. Guan and A. Loil for fruitful discussions. We thank J. Challis for his careful proofreading. The authors are very grateful to the reviewers for their comments and expert advice.

SUPPLEMENTARY MATERIAL

The Supplementary Material for this article can be found online at: https://www.frontiersin.org/articles/10.3389/fmars.2022.710086/full#supplementary-material

REFERENCES

Amante, C. J., and Eakins, B. W. (2016). "Accuracy of Interpolated Bathymetry in Digital Elevation Models," in *Brock, J.C.; Gesch, D.B.; Parrish, C.E.; Rogers, J.N., and Wright, C.W. (Eds.), Advances in Topo-Bathymetric Mapping, Models, and Applications. Journal of Coastal Research, Special Issue, No. 76*, vol. pp. (Florida: Coconut Creek), 123–133. doi: 10.2112/SI76-011

Arns, A., Wahl, T., Dangendorf, S., and Jensen, J. (2015). The Impact of Sea Level Rise on Storm Surge Water Levels in the Northern Part of the German Bight. *Coastal Eng.* 96, 118–131. doi: 10.1016/j.coastaleng.2014.12.002

Bento, C., and Blanc, M. (2017). *Les Paysages Du Marais De Brouage, Technical Report* (ENSP Versailles). Available at: https://issuu.com/cb935/docs/apr_marais_de_brouage_all_g_.

Bertin, X., and Chaumillon, E. (2006). The Implication of Oyster Farming in Increasing Sedimentation Rates in a Macrotidal Bay: The Marennes-Oléron Bay, France. *Cah. Biol. Mar.* 47, 19–22. doi: 10.21411/CBM.A.6E675E7B

Bertin, X., Li, K., Roland, A., Breilh, J. F., Zhang, Y. L., and Chaumillon, E. (2014). A Modeling-Based Analysis of the Flooding Associated With Xynthia, Central Bay of Biscay. *Coastal Eng.* 94, 80–89. doi: 10.1016/j.coastaleng.2014.08.013

Bongarts Lebbe, T., Rey-Valette, H., Chaumillon, É, Camus, G., Almar, R., Cazenave, A., et al. (2021). Designing Coastal Adaptation Strategies to Tackle Sea Level Rise. *Front. Mar. Sci.* 8. doi: 10.3389/fmars.2021.740602

Breilh, J.-F. (2014a). *Les Surcotes Et Les Submersions Marines Dans La Partie Centrale Du Golfe De Gascogne : Les Enseignements De La Tempête Xynthia. (PhD Thesis)* (La Rochelle, France: Université de la Rochelle). Available at: https://tel.archives-ouvertes.fr/tel-01174997.

Breilh, J.-F., Bertin, X., Chaumillon, E., Giloy, N., and Sauzeau, T. (2014b). How Frequent is Storm-Induced Flooding in the Central Part of the Bay of Biscay? *Global Planetary Change* 122, 161–175. doi: 10.1016/j.gloplacha.2014.08.013

Breilh, J.-F., Chaumillon, E., Bertin, X., and Gravelle, M. (2013). Assessment of Static Flood Modeling Techniques: Application to Contrasting Marshes Flooded During Xynthia (Western France). *Natural Hazards Earth System Sci.* 13, 1595–1612. doi: 10.5194/nhess-13-1595-2013

Brown, J. D., Spencer, T., and Moeller, I. (2007). Modelling Storm Surge Flooding of an Urban Area With Particular Reference to Modelling Uncertainties: A Case Study of Canvey Island, United Kingdom. *Water Resour. Res.* 43, W06402. doi: 10.1029/2005WR004597

Bruneau, N., Bertin, X., Castelle, B., and Bonneton, P. (2014). Tide-Induced Flow Signature in Rip Currents on a Meso-Macrotidal Beach. *Ocean Modelling* 74, 53–59. doi: 10.1016/j.ocemod.2013.12.002

Bulteau, T., Idier, D., Lambert, J., and Garcin, M. (2015). How Historical Information can Improve Estimation and Prediction of Extreme Coastal Water Levels: Application to the Xynthia Event at La Rochelle (France). *Nat. Hazards Earth Syst. Sci.* 15, 1135–1147. doi: 10.5194/nhess-15-1135-2015

Bunya, S., Deitrich, J. C., Westerink, J. J., Ebersole, B. A., Smith, J. M., Atkinson, J. H., et al. (2010). A High-Resolution Coupled Riverine Flow, Tide, Wind, Wind Wave, and Storm Surge Model for Southern Louisiana and Mississippi. Part I: Model Development and Validation. *Monthly Weather Rev.* 18, 345–377. doi: 10.1175/2009MWR2906.1

Chaumillon, E., Bertin, X., Weber, N., and Tesson, M. (2003). "Internal Architecture and Sedimentary Facies of a Macrotidal Bay: Implication in Terms of Morphodynamics (The Marenne-Oléron Bay, Atlantic Coast of France)," in *Proceedings of the 3rd IAHRD Symposium on River, Coastal and Estuarine Morphodynamics (RCEM 2003)*. Eds. A. Sanchez-Arcilla and A. Bateman (Madrid, Spain: IAHRD publication), 423–432.

Church, J. A., Clark, P. U., Cazenave, A., Gregory, J. M., Jevrejeva, S., Levermann, A., et al. (2013). "Sea Level Change," in *Climate Change 2013: The Physical Science Basis. Contribution of Working Group I to the Fifth Assessment Report of the Intergovernmental Panel on Climate Change*. Eds. T. F.,. D. Qin, G.-K. Plattner, M. Tignor, S. K. Allen, J. Boschung, A. Nauels, Y. Xia, V. Bex and P. M. Midgley (Cambridge, United Kingdom and New York, NY, USA: Cambridge University Press), 1137–1216. doi: 10.1017/CBO9781107415324.026

Cortina-Segarra, J., García-Sánchez, I., Grace, M., Andrés, P., Baker, S., Bullock, C., et al. (2021). Barriers to Ecological Restoration in Europe: Expert Perspectives. *Restor. Ecol.* 29, e13346. doi: 10.1111/rec.13346

Kulp, S. A., and Strauss, B. H. (2019). New Elevation Data Triple Estimates of Global Vulnerability to Sea-Level Rise and Coastal Flooding. *Nat. Commun* 10, 5752. doi: 10.1038/s41467-019-13552-0

DDTM-17. (2011). *Éléments De Mémoire Sur La Tempête Xynthia Du 27 Et 28 Février 2010 En Charente-Maritime*. Available at: http://www.charente-maritime.gouv.fr/layout/set/print/Politiques-publiques/Environnement-risques-naturels-et-technologiques/Risques-naturels-et-technologiques/Generalites-sur-la-prevention-des-risques-naturels/Elements-de-memoire-Xynthia/Elements-de-memoire-sur-la-tempete-Xynthia-du-27-et-28-fevrier-2010.

DGPR. (2014). *Guide Méthodologique : Plan De Prévention Des Risques Littoraux*. Available at: https://www.ecologie.gouv.fr/sites/default/files/Guide%20PPRL%20-%20version%20finale%20mai%202014.pdf.

European Environment Agency. (2012). *CORINE Land Cover Project. Commission of the European Communities*. Available at: http://land.copernicus.eu/pan-european/corine-land-cover/clc-2012/view.

Ezer, T., and Atkinson, L. P. (2014). Accelerated Flooding Along the U.S. East Coast: On the Impact of Sea-Level Rise, Tides, Storms, the Gulf Stream, and the North Atlantic Oscillations. *Earth's Future* 2, 362– 382. doi: 10.1002/2014EF000252

Fernández-Montblanc, T., Duo, E., and Ciavola, P. (2020). Dune Reconstruction and Revegetation as a Potential Measure to Decrease Coastal Erosion and Flooding Under Extreme Storm Conditions. *Ocean Coastal Manage.* 188, 105075. doi: 10.1016/j.ocecoaman.2019.105075

Filippini, A., De Brye, S., Perrier, P., Marche, F., Ricchiuto, M., Lannes, D., et al. (2018). UHAINA: A Parallel High Performance Unstructured Near-Shore Wave Model. *Journées Nationales Génie Côtier - Génie Civil* (France) 15, 47–56. doi: 10.5150/jngcgc.2018.006

Fouin, M., Travichon, S., and Mouillon, P. (2020) *Quelles Evolutions De La Biodiversité En Fonction De La Gestion Du Trait De Côte Dans Un Contexte D'élévation Du Niveau Marin? Analyse Sur Le Site De Moëze-Brouage: Prévisions a 2050*. Available at: https://www.lifeAdapto.eu/media/5772/Brouage_2021_Rapport%20LPO.pdf.

French Ministry of Environment (2017) *Actions Menées Par L'État a La Suite De La Tempête Xynthia*. Available at: https://www.ecologie.gouv.fr/sites/default/files/20170203_Bilan_Xynthia-v4.pdf.

Grothues, T. M., and Able, K. W. (2020). Shoreline Infrastructure Degradation and Increasing Littoral Naturalization Accommodates Juvenile Fish and Crab Assemblages in Heavily Urbanized Upper New York Harbor. *Restor. Ecol.* 28, 947–959. doi: 10.1111/rec.13163

Dodet, G., Bertin, X., Bouchette, F., Gravelle, M., Testut, L., and Woppelmann, G. (2019). Characterization of Sea-Level Variations Along the Metropolitan Coasts of France: Waves, Tides, Storm Surges and Long-Term Changes. *J. Coastal Res.* 88 (sp1), 10–24. doi: 10.2112/SI88-003.1

Haigh, I., Wadey, M. P., Wahl, T., Ozsoy, O., Nicholls, R. J., Brown, J. M., et al. (2016). Spatial and Temporal Analysis of Extreme Sea Level and Storm Surge Events Around the Coastline of the UK. *Sci. Data* 3, 160107. doi: 10.1038/sdata.2016.107

Hallegatte, S., Green, C., Nicholls, R. J., and Corfee-Morlot, J. (2013). Future Flood Losses in Major Coastal Cities. *Nat. Climate Change* 3 (9), 802. doi: 10.1038/nclimate1979

Idier, D., Rohmer, J., Pedreros, R., Le Roy, S., Lambert, J., Louisor, J., et al. (2020). Coastal Flood: A Composite Method for Past Events Characterisation Providing Insights in Past, Present and Future Hazards—Joining Historical, Statistical and Modelling Approaches. *Nat. Hazards* 101, 465–501. doi: 10.1007/s11069-020-03882-4

Imani, M., Kuo, C.-Y., Chen, P.-C., Tseng, K.-H., Kao, H.-C., Lee, C.-M., et al. (2021). Risk Assessment of Coastal Flooding Under Different Inundation Situations in Southwest of Taiwan (Tainan City). *Water* 13, 880. doi: 10.3390/w13060880

IPCC. (2019). *IPCC Special Report on the Ocean and Cryosphere in a Changing Climate*. Eds. H.-O. Pörtner, D. C. Roberts, V. Masson-Delmotte, P. Zhai, M. Tignor, E. Poloczanska, K. Mintenbeck, A. Alegría, M. Nicolai, A. Okem, J. Petzold, B. Rama and N. M. Weyer (In press). (Cambridge, UK: Cambridge University Press).

IPCC. (2021). *Climate Change 2021: The Physical Science Basis. Contribution of Working Group I to the Sixth Assessment Report of the Inter-Governmental Panel on Climate Change*. Eds. V. Masson-Delmotte, P. Zhai, A. Pirani, S. L.

Connors, C. Péan, S. Berger, N. Caud, Y. Chen, L. Goldfarb, M. I. Gomis, et al. (Cambridge, UK: Cambridge University Press).

Kirezci, E., Young, I. R., Ranasinghe, R., Muis, S., Nicholls, R. J., Lincke, D., et al. (2020). Projections of Global-Scale Extreme Sea Levels and Resulting Episodic Coastal Flooding Over the 21st Century. *Sci. Rep.* 10, 11629. doi: 10.1038/s41598-020-67736-6

Kopp, R. E., Horton, R. M., Little, C. M., Mitrovica, J. X., Oppenheimer, M., Rasmussen, D. J., et al. (2014). Probabilistic 21st and 22nd Century Sea-Level Projections at a Global Network of Tide-Gauge Sites. *Earths Future* 2, 383–406. doi: 10.1002/2014EF000239

Lazure, P., and Dumas, F. (2008). An External-Internal Mode Coupling for a 3D Hydrodynamical Model for Applications at Regional Scale (MARS). *Adv. In Water Resour.* 31 (2), 233–250. doi: 10.1016/j.advwatres.2007.06.010

Le Cozannet, G., Bulteau, T., Castelle, B., Ranasinghe, R., Wöppelmann, G., Roher, J., et al. (2019). Quantifying Uncertainties of Sandy Shoreline Change Projections as Sea Level Rises. *Sci. Rep.* 9, 42. doi: 10.1038/s41598-018-37017-4

Leitch, A. M., Palutikof, J. P., Rissik, D., Boulter, S. L., and Tonmoy, F. N. (2019). Co-Development of a Climate Change Decision Support Framework Through Engagement With Stakeholders. *Climatic Change.* 153, 587–605 doi: 10.1007/s10584-019-02401-0

Lemoine, J. P., and Le Hir, P. (2021). Maintenance Dredging in a Macrotidal Estuary: Modelling and Assessment of its Variability With Hydro-Meteorological Forcing. *Estuarine Coastal Shelf Sci.* 258, 107366 doi: 10.1016/j.ecss.2021.107366

Lorie, M., Neumann, J. E., Sarofim, M. C., Jones, R., Horton, R. M., Kopp, R. E., et al. (2020). Modeling Coastal Flood Risk and Adaptation Response Under Future Climate Condition. *Climate Risk Manage.* 29, 100233. doi: 10.1016/j.crm.2020.100233

Martínez, M. L., Mendoza-González, G., Silva-Casarín, R., and Mendoza-Baldwin, E.(2014). Land Use Changes and Sea Level Rise May Induce a "Coastal Squeeze" on the Coasts of Veracruz, Mexico. *Global Environ. Change 29*, 180–188. doi: 10.1016/j.gloenvcha.2014.09.009

Melo, W., Pinho, J., Iglesias, I., Bio, A., Avilez-Valente, P., Vieira, J., et al. (2020). Hydro- and Morphodynamic Impacts of Sea Level Rise: The Minho Estuary Case Study. *J. Mar. Sci. Eng.* 8, 441. doi: 10.3390/jmse8060441

Moftakhari, H. R., AghaKouchak, A., Sanders, B. F., Feldman, D. L., Sweet, W., Matthew, R. A., et al. (2015). Increased Nuisance Flooding Along the Coasts of the United States Due to Sea Level Rise: Past and Future. *Geophys. Res. Lett.* 42, 9846– 9852. doi: 10.1002/2015GL066072

Mo, Y., Kearney, M., and Turner, R. (2020). The Resilience of Coastal Marshes to Hurricanes: The Potential Impact of Excess Nutrient. *Environ. Int.* 138. doi: 10.1016/j.envint.2019.105409

Nicolae Lerma, A., Bulteau, T., Elineau, S., Paris, F., Durand, P., Anselme, B., et al (2018). High-Resolution Marine Flood Modelling Coupling Overflow and Overtopping Processes: Framing the Hazard Based on Historical and Statistical Approaches. *Nat. Haz. Earth Syst. Sci.* 18, 207–229. doi: 10.5194/nhess-18-207-2018

Papaioannou, G., Efstratiadis, A., Vasiliades, L., Loukas, A., Papalexiou, S. M., Koukouvinos, A., et al. (2018). An Operational Method for Flood Directive Implementation in Ungauged Urban Areas. *Hydrology* 5 (2), 24. doi: 10.3390/hydrology5020024

Pestana Almeida Pinto, R. (2014) *Floodplain Inundation Models and SAR Imagery Analysis. (Master's Thesis)*. Available at: https://fenix.tecnico.ulisboa.pt/cursos/meft/dissertacao/846778572210435.

Pineau-Guillou, L., Lathuiliere, C., Magne, R., Louazel, S., Corman, D., and Perherin, C. (2012). Sea Levels Analysis and Surge Modelling During Storm Xynthia. *Eur. J. Environ. Civ Eng.* 16, 943–952. doi: 10.1080/19648189.2012.676424

Ray, R. D., and Foster, G. (2016). Future Nuisance Flooding at Boston Caused by Astronomical Tides Alone. *Earth's Futur.* 4, 578–587. doi: 10.1002/2016EF000423

Rocha, C., Antunes, C., and Catita, C. (2020). Coastal Vulnerability Assessment Due to Sea Level Rise: The Case Study of the Atlantic Coast of Mainland Portugal. *Water* 12, 360. doi: 10.3390/w12020360

Rosenzweig, C., Solecki, W. D., Blake, R., Bowman, M., Faris, C., Gornitz, V., et al. (2011). Developing Coastal Adaptation to Climate Change in the New York City Infrastructure-Shed: Process, Approach, Tools, and Strategies. *Climatic Change* 106, 93– 127. doi: 10.1007/s10584-010-0002-8

Shom. (2015). *MNT Topo-Bathymétrique Côtier Des Pertuis Charentais (Projet Homonim). (diffusion Shom).* doi: 10.17183/MNT_COTIER_PERTUIS_HOMONIM_20m_WGS84

Shom. (2017) *Ouvrage De Marée. References Altimétriques Maritimes Ports De France Métropolitaine Et D'outre-Mer. Cotes Du Zéro Hydrographique Et Niveaux Caractéristiques De La Marée*. Available at: https://www.data.gouv.fr/fr/datasets/references-altimetriques-maritimes.

Thiéblemont, R., Le Cozannet, G., Toimil, A., Meyssignac, B., and Losada, I. J. (2019). Likely and High-End Impacts of Regional Sea-Level Rise on the Shoreline Change of European Sandy Coasts Under a High Greenhouse Gas Emissions Scenario. *Water* 11 (12), 2607. doi: 10.3390/w11122607

Timmerman, A., Haasnoot, M., Middelkoop, H., Bouma, T., and McEvoy, S. (2021). Ecological Consequences of Sea Level Rise and Flood Protection Strategies in Shallow Coastal Systems: A Quick-Scan Barcoding Approach. *In Ocean Coastal Manage.* 210, 105674). doi: 10.1016/j.ocecoaman.2021.105674

Vousdoukas, M. I., Mentaschi, L., Feyen, L., and Voukouvalas, E. (2017). Earth's Future Extreme Sea Levels on the Rise Along Europe's Coasts. *Earth's Futur.* 5, 304–323. doi: 10.1002/2016EF000505

Vousdoukas, M. I., Voukouvalas, E., Annunziato, A., Giardino, A., and Feyen, L. (2016). Projections of Extreme Storm Surge Levels Along Europe. *Climate Dynamics* 47 (9–10), 3171. doi: 10.1007/s00382-016-3019-5

Vu, P. L., Ha, M. C., Frappart, F., Darrozes, J., Ramillien, G., Dufrechou, G., et al. (2019). Identifying 2010 Xynthia Storm Signature in GNSS-R-Based Tide Records. *Remote Sens.* 11, 782. doi: 10.3390/rs11070782

Conflict of Interest: The authors declare that the research was conducted in the absence of any commercial or financial relationships that could be construed as a potential conflict of interest.

Publisher's Note: All claims expressed in this article are solely those of the authors and do not necessarily represent those of their affiliated organizations, or those of the publisher, the editors and the reviewers. Any product that may be evaluated in this article, or claim that may be made by its manufacturer, is not guaranteed or endorsed by the publisher.

Copyright © 2022 Louisor, Brivois, Mouillon, Maspataud, Belz and Laloue. This is an open-access article distributed under the terms of the Creative Commons Attribution License (CC BY). The use, distribution or reproduction in other forums is permitted, provided the original author(s) and the copyright owner(s) are credited and that the original publication in this journal is cited, in accordance with accepted academic practice. No use, distribution or reproduction is permitted which does not comply with these terms.

Advantages of publishing in Frontiers

OPEN ACCESS
Articles are free to read for greatest visibility and readership

FAST PUBLICATION
Around 90 days from submission to decision

HIGH QUALITY PEER-REVIEW
Rigorous, collaborative, and constructive peer-review

TRANSPARENT PEER-REVIEW
Editors and reviewers acknowledged by name on published articles

Frontiers
Avenue du Tribunal-Fédéral 34
1005 Lausanne | Switzerland

Visit us: www.frontiersin.org
Contact us: frontiersin.org/about/contact

REPRODUCIBILITY OF RESEARCH
Support open data and methods to enhance research reproducibility

DIGITAL PUBLISHING
Articles designed for optimal readership across devices

FOLLOW US
@frontiersin

IMPACT METRICS
Advanced article metrics track visibility across digital media

EXTENSIVE PROMOTION
Marketing and promotion of impactful research

LOOP RESEARCH NETWORK
Our network increases your article's readership